SOIL WATER MODELLING IN HILL COUNTRY,

NEW ZEALAND

A thesis presented in partial fulfilment of the requirements for the degree of

Doctor of Philosophy in Earth Science

At Massey University, Palmerston North, New Zealand

Istvan Hajdu

2019

"Despite the artistic pretensions, sophistication and many accomplishments of mankind, we owe our existence to a six-inch layer of topsoil and the fact that it rains"

Anonymous

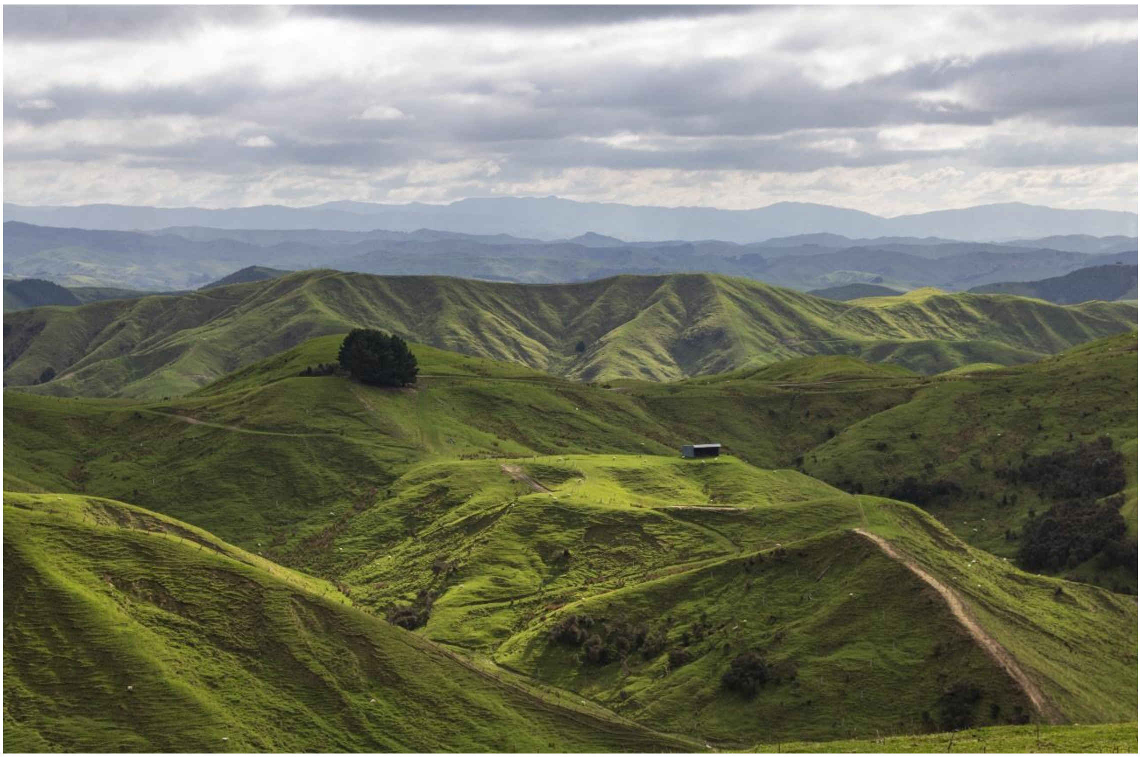

The photo was taken at the research area, "the farmland of extremities"

Patitapu Station, Wairarapa, North Island, New Zealand

Abstract

As the importance of environmental sustainability and increasing market demands have expressed pressure on New Zealand's hill country farming systems, the more effective use of available resources and additional inputs has become crucial. Pastoral hill country farms are critical components of New Zealand's economy, and precision agriculture solutions have been increasingly utilised to improve the sectors' financial stability and resilience, and to satisfy the elevated expectations in yield. Profitability is dependent on pasture productivity that is highly influenced by the availability of nutrients as well as the amount of soil moisture (θ_v, m^3 m^{-3}). However, high variability of soil and landscape factors that control productivity is the primary concept describing these diverse landscapes. Hence, a study was conducted on a 2600 ha dominantly beef and sheep farm in the southern east coast of the North Island of New Zealand representing typical hill country settings.

Some of the specific concerns of this research were the examination of the role of accurate, calibrated θ_v measurements via a wireless sensor network (WSN) (1) and the spatiotemporal variability of θ_v (2). Furthermore, the study investigates the potential of remote sensing for the mapping of near surface θ_v in sloping lands (3) and the characterisation of pasture yield patterns induced by the topography (4). These primary points were addressed to better understanding the complexity occurring behind the environmental factors governing pasture yield and to potentially achieving improvement in pasture growth simulations.

Systematic θ_v measurements have been used increasingly to inform decisions regarding fertiliser applications, feed supply and stock management in non-irrigated farming systems. To assist near real time θ_v and soil temperature (T_s) monitoring, 400 mm capacitance-based AquaCheck (AquaCheck, South Africa) probes (four θ_v and four T_s sensors per probe) were installed at 20 locations (hereinafter microsites) in predominantly silt loam soils. The spatially distributed probes were arranged into a WSN to capture data from various topographical positions. The application of manufacturer-provided calibration formula resulted in a mean root mean square error (RMSE) of 0.106 m^3 m^{-3}, a mean bias error of -0.099 m^3 m^{-3} (indicating underestimation), and a coefficient of determination (R^2) of 0.58 when correlated to directly measured reference $\theta_v$values. A single custom formula, relevant to the local soils resulted in an improved RMSE of 0.039 m^3 m^{-3}, while microsite-specific calibrations achieved an RMSE of 0.029 m^3 m^{-3} and R^2 of 0.77. The application of a sensor-specific calibration resulted in an RMSE of

0.019 m^3 m^{-3} with R^2 = 0.9. Sensor performance and accuracy errors were observed to vary as a function of soil wetness, bulk density (ρ_b, gcm^{-3}) clay and total organic carbon (TOC) content. These effects were significant (P value < 0.001) but eliminated by the sensor-specific custom calibration.

Sensor specifically calibrated θ_v was utilised the examine the effect of highly variable terrain attributes such as aspect, slope angle and soil physical properties on the θ_v patterns, stability and distribution both spatiotemporally and along the soil profile. Non-normal θ_v distribution was observed in the study period. The statistical analysis confirmed that the temporal stability of θ_v was higher in the deeper sections in both dry and wet seasons, while the spatial variability of θ_v increased with decreasing mean θ_v, although the greatest was in the rewetting stages. The degree of temporal persistence of the θ_v patterns varied with soil wetness conditions and seasons. Based on the temporal stability assessment, a representative location was selected based on a north-facing and open slope with silt loam soils. The θ_v distribution patterns were influenced by the topographic attributes showing that north-facing steep and moderately steep slopes were characterised with the highest variation, while east- and west-facing slopes showed similar trends.

Due to the significant variability, near surface θ_v mapping at a spatial resolution that would be useful for describing within farm heterogeneity has been challenging for researchers. The near surface θ_v modelling performance of a Random Forest (RF) ensemble learning method and the synergetic use of various remote sensing data with terrain attributes were investigated at 20x 20 m pixel size. The RF model was trained using a two-year reference dataset containing Sentinel-1 SAR backscatter data (i), normalized difference vegetation index (NDVI derived from Sentinel-2, Landsat 7 and Landsat 8 images) (ii), a number of landscape parameters (iii) and in situ near surface θ_v values obtained by the WSN (iv) as ground truth. The RF algorithm captured a significant amount of the complex relationships and the model predicted θ_v with a mean RMSE of 0.047 m^3 m^{-3} and adjusted R^2 of 0.76 at the point scale as given by the repeated cross validation. The fine-tuned RF regressor was trained using 15 microsites and a series of near surface θ_v maps was developed. The maps were validated using the five left out microsites resulting in 0.049 m^3 m^{-3} RMSE and 0.76 adjusted R^2 indicating good agreement between modelled and observed θ_v values. The general annual trend of θ_v was closely reflected in the developed maps.

The role of near surface and root zone θ_v, T_s, climatic variables and topographical attributes on the spatiotemporal pattern of pasture productivity was investigated at 13 selected microsites at which pasture herbage accumulation was monitored by the moveable exclusion cage method in

2016-2018. Considerable differences were found in the stored soil water response to significant rainfall events and climatic variables influencing pasture production. On the created multitable dataset, a multiple factor analysis was executed. As a result of this analysis, the role of various environmental parameters was defined highlighting the role of slope angle as the most significant determinant of pasture growth. The effect of landscape position was found to be more significant than aspect, which showed a seasonal dependence. Additionally, the contribution of terrain attributes was not consistent during the study period and changed from year to year. T_s and θ_v at a soil depth of 100 mm demonstrated the strongest governing effect on pasture production among the monitored parameters.

In conclusion, the outcomes of this study imply that an extended and improved version of the proposed methods have the potential to be a basis of more accurate water balance simulations in complex landscapes at the regional scale. The presented quantification and isolation of the influencing topographic factors on pasture production may assist in hill country intensification by adding value to the generation of regulatory nutrient management plans. Ultimately, these advancements will enable the better characterisation of the dynamic hill country pastoral systems, which will lead towards helping hill country sheep and beef farmers to grow more pasture and increase returns while reducing the degrading effects of fertiliser applications on the environment.

Acknowledgements

The completion of this thesis required great effort, dedication, teamwork and continuous interaction with many individuals in the last few years. To be completely honest, I really enjoyed the journey and the work with many scientists, colleagues, fellow students, farmers and technicians from various companies. As a result of this project and the collaboration, not only research output was produced but also many of us have become good friends making New Zealand feeling like home.

I wish to express my sincere gratitude to the four valuable members of my supervisory panel for providing support and constructive feedback on the presented work. First of all, I am thankful to my chief-supervisor, Professor Ian Yule, for giving me the opportunity to get involved with the Primary Growth Partnership (PGP) programme, thereby my PhD project at Massey University. His encouraging open-minded thinking, innovative ideas, stimulating creativity and faith allowed me to have access to modern technologies and develop numerous new skills. My sincere thanks also go to co-supervisors for providing much appreciated support. Dr. Ranvir Singh, his critical and thorough reviews and background in statistics helped me to complete this thesis with great care. Dr. Mike Bretherton, his knowledge about New Zealand's hill country, soil water dynamics, sensing methods and thoughtful feedback added significant amount of improvement to several chapters. Dr. Carolyn Hedley from Landcare Research, her soil science background and broad interest in New Zealand soils, sensor technologies and constructive, yet kind comments made valuable contribution to the thesis.

In terms of financial support, I would like to acknowledge the Ministry of Primary Industries, the PGP initiative, Ravensdown's "Pioneering to Precision" programme and Massey University for funding the scholarship and providing full sponsorship during my studies. I also appreciated the collaboration with Agri Optics New Zealand Ltd. and TAG I.T Technologies during the sensor network deployment and the professional support during the network maintenance. I would like to acknowledge the help of the staff of Ravensdown, especially Michel White, Alistair Metherell who were involved with my project and ensured that I was on the right track.

I am grateful for all the staff members of the New Zealand Centre for Precision Agriculture (NZCPA) for guiding the project and for their assistance in the office, in the field and in life. Special thanks go to Kate Saxton, Eduardo Sandoval, Matt Irwin, Sue Chok, Pip McVeagh, Federico Duranovich and Louise Hopkins. Eduardo, many thanks for your help in the field, those days were long, tiring and many times challenging.

I would like to express my kind regards to Anja Möbis, Ian Furkert and Roberto Calvelo who helped me with the laboratory work and taught me how to operate several instruments safely.

I wish to thank Doug and Jo McKenzie, the landowner partners who were willing to provide the stunning landscapes of "Patitapu Station" as research area for the completed work. Doug's local knowledge, human power, unlimited patience, friendly attitude and great interest in science were important contributors to the development of this fruitful connection between scientific research and practical implementations from the farmer's point of view.

I would like to thank Gabor Kereszturi, Angela "Gigi" Denes, Boglarka Nemeth, Szabolcs Kosik, Zsuzsa Szmolinka and Titusz for their friendship and help as well as for the many amazing times during the last few years we shared. I wish to thank Bogi and Szabolcs for helping me during the challenging fieldwork. I would particularly like to thank Gabor, a good friend, colleague, unofficial supervisor, adventure buddy for his invitation to New Zealand and his top-quality professional advices and guidance. That move has changed my life and has given me some of the best and most memorable life experiences besides the personal and scientific growth.

A huge thank-you to the "Thursday Dinners" a very special group of people, the previous and current flatmates, the previous and recent members of the Volcanic Risk Solutions for their international friendship, love and the tremendous great moments that have made my life in Palmerston North unforgettable and enjoyable.

The generous efforts of Emily (M ;)), Stuart, Megan, Tommy, Mohammad and Reddy for helping me improving the shape and presentation of this thesis and our inspirational conversations are highly acknowledged and appreciated.

Most importantly, my family…I am deeply indebted to them and I would like to express my heartfelt thanks to my parents and my brother whose consistent, unconditional love and care helped me through the difficult times and enabled me to achieve one of my dreams and complete this work.

Istvan Hajdu

April 2019
Palmerston North, New Zealand

Table of contents

Preface

The main body of the thesis

List of tables

List of figures

List of Acronyms

AAE	Absolute Accuracy Error
ANN	Artificial Neural Networks
ANOVA	Analysis of Variance
ASC	Ascending orbit
AWHC	Available Water Holding Capacity
CV	Coefficient of variation
DEM	Digital Elevation Model
DES	Descending orbit
DM	Dry Matter
DSM	Digital Surface Model
ECHC	East Coast Hill Country
EM	Electromagnetic
ESA	European Space Agency
FC	Farm-specific Calibration
FD	Frequency Domain
FDR	Frequency Domain Reflectometry
FSL	Fundamental Soil Layers
GEE	Google Earth Engine
GIS	Geographic Information System
ISMN	International Soil Moisture Network
ISR	Incoming Solar Radiation
ITS	Index of Time Stability
LDM	Laser Diffraction Method
LINZ	Land Information New Zealand
LUC	Land Use Capability
LUCAS	Land Use and Carbon Analysis System
MAE	Mean Absolute Error
MBE	Mean Bias Error
MC	Manufacturer Calibration
MFA	Multiple Factor Analysis
MRD	Mean Relative Difference
NDVI	Normalised Difference Vegetation Index
NIR	Near Infrared
NIWA	National Institute of Water and Atmospheric Research
NZSC	New Zealand Soil Classification
PAW	Plant Available Water
PCA	Principle Component Analysis
PGP	Primary Growth Partnership
PGR	Pasture Growth Rate
R^2	Coefficient of Determination
RAW	Readily Available Water Holding Capacity
RF	Random Forest
RMSE	Root Mean Square Error
SAR	Synthetic Aperture Radar
SD	Standard Deviation
SDRD	Standard Deviation of the Relative Difference
SEC	Sensor-specific Calibration
SF	Scaled Frequency
SIC	Microsite-specific Calibration
SMAP	Soil Moisture Active Passive
SMOS	Soil Moisture and Ocean Salinity
SNAP	Sentinel Application Platform
SVM	Support Vector Machine
SWI	SAGA Wetness Index
SWIR	Shortwave Infrared
TDR	Time Domain Reflectometry
TIR	Thermal Infrared
TOA	Top of Atmosphere
TOC	Total Organic Carbon
TPI	Topographic Position Index
TRI	Terrain Ruggedness Index
USDA	U.S. Department of Agriculture
WSN	Wireless Sensor Network

Chapter 1

GENERAL INTRODUCTION

This introductory chapter establishes the project background and the position of the study in the "big picture". Chapter 1 provides the scientific rational of the research and informs the reader about the importance of hill country farming systems and their economic contribution. Based on the given general information the role and advantages of environmental monitoring is presented that guides the chapter towards to the problem statement and the potential research gaps where improvements can be achieved with the aim of higher pasture production rates. Afterwards, the chapter defines the specific directions of the study and the methodology used for addressing the research questions. Finally, Chapter 1 depicts the outline of the entire thesis with brief summaries given about the structure and the key concepts of each chapter.

1 Chapter 1 - General introduction

1.1 Project background

The conducted research is associated with the innovation project, “Transforming Hill Country Farming”, running under the ‘Pioneering to Precision: Application of Fertiliser in Hill Country ‘- Primary Growth Partnership (PGP) programme. The initiative was funded by Ravensdown Fertiliser Cooperative and Ministry of Primary Industries to target the development of hill country farming from a new perspective. The outcome of the PGP project aimed to enable hill country sheep and beef farmers to grow more pasture and increase returns while reducing the degrading effects of fertiliser applications on the environmental systems.

One of the main limiting factors of pasture growth is the soil water content, thus, one slice of the PGP project is looking at the ways of better estimation and spatial mapping of soil water content for the potential improvement of the simulation accuracy of a commercial pasture growth forecaster. As the availability of nutrients for pasture growth is highly dependent on soil water content influencing the amount and quality of yield, thereby making the timely decisions for feed budgeting crucial in dry hill country farming. Hill country is an iconic part of New Zealand’s farming and variability is a key concept describing these terrains. The interaction of climate, topography, parent materials and time has resulted in many different soil types with varying soil properties, nutrient levels, and soil depths that has led to high diversity in pasture cover and production rates.

The main challenge of the programme is to find answerers for the following questions:

- Is it possible to find a way for better fertiliser placement so famers will be able to grow more pasture without increasing the pressure on the environment?
- Is it possible to capture the environmental variability existing in hill country landscapes and use that information for better predictions, management and more efficient, sustainable exploitation of natural resources and external inputs?

1.2 Hill country farming and its economic contribution

A simplified definition of hill country in New Zealand is given by Cameron (2016) and Kerr (2016) stating that hill country is classified as land with slopes greater than 15° and below an altitude of 1000 metres above mean sea level. Beef and sheep pastoral systems, dominantly situated on hill country landscapes, represents the majority (70-75 %) of New Zealand’s agricultural land use. Beef and sheep farms are distributed among approximately 5500-6000 holdings, from which ~80 % is located in the North Island (Kerr, 2016). Approximately 4 million ha of the North Island under pastoral land use is hill country which is 43 % of the total pastoral land area of New Zealand (Fraser and Vesely, 2011, Kerr, 2016). Hill country is a major annual contributor to the New Zealand economy and agricultural primary production accounts for nearly 50 % of New Zealand's export earnings (Statistics New Zealand, 2015). Through the export of various products such as sheep meat, lamb, beef, venison, velvet and wool, hill country farms produced $2.8 billion value of exports in 2012 (Kemp and López, 2016).

Based on these measures, the weight of hill country in the primary industries is evident making these farms critical components of New Zealand's economic activity. Therefore, this sloping land has been in the centre of attention as a main breeding platform in the last 40 years and its importance has been increasing with a research focus on higher yield rates, resilience and adaptation (Kerr, 2016). The most distinguishing feature of hill country and the associated land management is the variability due to the contour and sloping nature of the soil surface coupled with generally low fertility soils (Gillingham, 1973). In the last decades, noticeable productivity growth has been achieved as a result of improved grazing and pasture species, livestock-breeding and the slowly increasing adaptation of sensor technologies (Fraser and Vesely, 2011).

The systematic observation of pasture production affecting variables, for example soil moisture, can assist in better operational decisions and optimising feed over time. The benefits of soil moisture observations have been recognised for many years. However, hill country soils have not been studied in sufficient detail in terms of soil water variability and spatiotemporal patterns at the paddock (i.e. an enclosed pastoral grazing management unit). Most hill country farmers do not measure these variables regularly or if they do, they will monitor them at a single point like location not capturing the existing variability. Some might use regional, coarse resolution predictions or simply their experience and the "look and feel" method (Johnson, 1962) for evaluating the land conditions. The recognition and characterisation of soil water regimes and pasture yield distribution in time and spatially at least at the paddock scale could be considered as a "game changer" in fertiliser input distribution planning as well as in farm management.

1.3 The importance of the monitoring of production influencing variables concerning the future of hill country farming

Hill country farmers are used to dry summer conditions and extended dry autumns stretching into early May but not to dry springs, which strongly influences yield by creating periods of soil water stress. Their land and grazing management decisions are not only dependent upon experience and historical data but also on predictions regarding yield and weather, which are also functions of soil moisture input.

New Zealand has experienced clear upward trends in historical temperature, with 0.09 ± 0.03 °C temperature rise per decade since 1909. In the 21st century, virtually certain further warming combined with considerable changes in extreme events have been projected with increasing number of hot days (T_{max} > 25 °C). According to the National Institute of Water and Atmospheric Research (NIWA), these indicated drifts in climate are likely to cause change in rainfall patterns, more frequent and increased runoff, flood and drought events in several regions of New Zealand. Recent droughts on the East Coast of the North Island (Eastern Wairarapa) in 2008 and 2010 caused significant soil moisture stress and heavily affected grass and plant growth with the driest April monitored since 1956 (Greater Wellington Regional Council, 2012). According to NIWA, January 2018 was the hottest month and obviously the hottest January on record in New Zealand breaking the previous record of January observed in 1956. Due to the combined impact of extreme temperatures and the relative lack of rainfall, soil moisture levels were lower or much lower than normal at certain parts of the country including the eastern and southern parts of the North Island.

Considering the potential impacts of the projected climate change, a substantial contribution can be anticipated to economic losses and pasture production may be influenced by the changing environmental conditions (Pearce et al., 2017). Moreover, the issues around preserving water quality and the consideration of several environmental and political limitations will make farmers to operate within certain boundaries. Adapting to the forecasted changes can increase costs and the pressure on producing more output for the same or reduced physical inputs (Fennessy et al., 2016). These issues and the related consequences will possibly shape the introduction of innovative ideas and technology to develop a solid, sustainable future for hill country farming and to ensure the financial stability of the hill country farming sector.

Profitability is underpinned by the productivity of the land that is highly dependent on the soil fertility, feed quantity and quality, water supply and the most effective strategic exploitation of the available resources (Shadbolt and Martin, 2005, Lieffering et al., 2012, Fennessy et al., 2016). The generally variable spatial pattern of soil moisture and feed supply are further complicated by changes in slope, aspect and relief of the terrain in hill country (Bretherton, 2012). The monitoring of farming systems and defining the variations in soil water content, pasture yield, the vegetation’s biophysical parameters and soil characteristics can provide farmers with key information for operational decisions and optimising feed over time (Schrimgeour, 2016).

Pastoral hill country farms are operated under a wide range of micro-climatic conditions and various management regimes typically with low inputs (i.e. fertiliser, feed from external sources). The dynamic nature of hill country and the interaction among numerous environmental factors, e.g. climate, high variation in relief, soil properties, soil type patterns, stock and grazing management, results in highly diverse production rates and pasture composition (Radcliffe et al. 1968, Murray et al. 2007, Chapman and Macfarlane, 1985, Bretherton, 2012). For these reasons, the spatial mapping and assessment of pasture growth characteristics are still challenging and labour-intensive tasks. While soil conversation, water quality and the mitigation of environmental pressure are among the highest priorities, fertiliser applications are essential and will remain the key for the future of hill country farming (Schrimgeour, 2016).

Considering the location-specific irregularities in environmental conditions, the precisely targeted management practises and fertiliser inputs can significantly improve the farms' yield and the general efficiency of the farming system (Judd et al., 1990). To balance out the differences in pasture productivity caused by the hilly landscape the farm-specific planning of fertiliser applications is built on pasture growth simulations.

To facilitate improved yield and water management strategies in non-irrigated farming systems the integration of soil moisture data into the decision making and forecasting systems and a detailed description of yield affecting factors will enable a better understanding of feed supply patterns. Hill country farming can benefit from both near surface and rooting zone soil moisture estimation that can also provide an information on the amount of plant available water. Furthermore, soil water content controls the soil infiltration rate, runoff and evapotranspiration influencing the water storage and thereby the water uptake by plants (Rodriguez-Iturbe et al., 1999, Woodward et al., 2001).

Thus, soil moisture monitoring is rapidly developing across different types of soil-plant systems over many landscape features and scales at a time of increasing food demand and the forecasted more extremities in weather patterns (Howell, 2001, Charlesworth, 2005, Trenberth et al., 2013). Systematic and frequent soil moisture information allow farmers and agronomists to better inform pre- and in-crop strategic inputs, pasture management (Matson et al., 1997), and nutrient cycling (Dougill et al., 1998) at the farm scale. Consequently, obtaining accurate, frequent and non-destructive soil water data is significantly advantageous, if not fundamental.

The importance of soil water content and pasture growth distribution patterns suggests that quantification of their spatiotemporal behaviour needs to be studied from the global scale to the small watersheds, paddocks and hill slopes. Most environmental variables are out of the human control, but the perception and quantification of their effect on pasture growth patterns enable farmers to maximise their land resources and optimise the production as well as the consumption. It can be concluded that better-designed yield forecasters, advanced model parameterisation, improved fertiliser application planning, more efficient, timely land management and budgeting decisions are some of the key aspects that need to be addressed by further research.

1.4 Problem statement – The soil water balance module

Pasture growth simulation models have been increasingly used for assessing the effects of the controllable and fixed variables of the pastoral system (Li et al., 2011). Some standard units of these commercial models are well understood, such as the seasonal distribution of feed demand (Holmes et al., 1987), bringing together the existing knowledge of pastoral systems.

An ideal pasture growth forecaster algorithm would be able to predict yield spatially and temporally. Additionally, it should take into account the effects of topography (slope angle, aspect and altitude), climate variables (temperature, rainfall, incoming solar radiation, ventilation effect), soil fertility (fertiliser history) and had a detailed water balance module calculating daily soil water deficit considering the sub-paddock variations.

The modules accounting for soil hydrology, a critical component of agriculture, are still lacking improvement for complex terrain and it is assumed that one of the weakest points of these models lies in this component. The water balance module often fails to represent the variability due to the complicated flow processes occurring on and under the rolling surface with heterogeneous soil types.

The soil water balance for flat land in New Zealand has been extensively studied and it is quite well understood (Scotter et al., 1979, McAneney and Judd, 1983, Woodward et al., 2001). In contrast, relatively few studies have been published on the soil water balance in hill country (Bircham and Gillingham, 1986, Bretherton et al., 2010, Bretherton et al., 2018), despite its significant role in the primary sector. In general, soil water content predictability and variability are not yet fully understood on rugged terrain, especially near the surface and within the root-zone; these being the layers of high interest for most agricultural activities (Wilson et al., 2004, Petropoulos et al., 2014).

In New Zealand, the spatial water balance model of one of the major commercially utilised, real-world yield forecasting applications is fed by water-holding capacity values generated from national, low spatial resolution soil layers, containing soil textural and water-holding capacity estimations. Although, the sub-farm variability is dominantly much larger than that of the existing and utilised input layers would be able to describe. Due to the interaction of numerous environmental parameters, soil water content is generally considered as a spatiotemporally highly changeable environmental variable (Vachaud et al., 1985, Vanderlinden et al., 2012, Brocca et al., 2017).

Due to the lack of highly detailed soil cover information and water holding parameters obtained by actual field surveys, a significant amount of uncertainty is introduced to the pasture yield predictions and consequently to the farm-specific input applications. Moreover, soil water content is too laborious and expensive to measure systematically that makes their incorporation into these models rather difficult (Woodward, 2001).

Hence, the need for improved soil moisture monitoring is critical to support the planning of fertiliser applications. Particularly, a more reliable soil water balance estimation would have a considerable effect on the accuracy of pasture growth predictions. Apart from better, more efficient and targeted fertiliser placement, there are several key advantages of soil water information. These include the early prediction and recognition of declined pasture growth, which reduces the risk behind the timing of significant land management practices and financial decisions, such as selling stock or purchasing feed.

1.5 Specific directions of the study

As the productivity of hill country will come under increased pressure, being or becoming resilient to climate change, more frequent dry periods and high intensity rainfall events, is crucial for farmers (Kenny, 2001, Cameron, 2016). To be able to meet the growing demand, farmers need to react to these environmental changes. As most of the environmental parameters are not controllable, management and adaptation to the changes can be the only way to resilience and sustainable future farming. Such situations and forecasts coupled with the above-mentioned uncertainties in yield predictions raise numerous issues to solve and questions to answer in the field of framing and scientific research. The questions listed below have set some of the specific directions of this study.

I. How can the soil water content be measured effectively, systematically and accurately without regular fieldwork in hill country to represent the diverse terrain conditions?
II. How does the complex landscape of hill country affect the spatial distribution patterns and temporal evolution of the near surface and the root zone soil water?

III. What are the possible ways to obtain or predict soil water information spatially on hilly landscapes utilising various data sources?
IV. How could it be mapped at a spatial and temporal resolution, which is practically useful for decision making, farming and pasture growth forecasting?
V. What are the main driving factors of pasture growth in hill country and how could their understanding be further improved for better pasture growth simulations?

1.6 Proposed methodology and its background

The future of pasture management, the sustainable production and the concept of optimising returns and preserving resources requires research at various scales. This study aims to provide useful, practical, transferable and understandable information at the farm scale and target the within farm environmental heterogeneity including pasture growth and soil moisture. An approximately 2600 ha hill country farm was chosen as research area, providing a good representation of the heterogeneity of static (topographical features, soil types) and dynamic (climate, vegetation) variables in the Wairarapa region of the North Island of New Zealand. Ideally, the generated knowledge will be valuable for improving, refining and validating yield predictions and soil water simulations in hilly landscapes.

In order to achieve more realistic water balance modelling outputs and therefore better yield predictions, the incorporation of actual, systematic water content estimations on a spatial basis seems to be an innovative and promising approach. Therefore, the input data would be required regularly at least at medium spatial resolution (10-100 m pixel size) (Gao et al., 2010) to account for the previously highlighted variability.

Soil moisture can be monitored by several methods, although field campaigns using classic methods on hill country pastures have traditionally been cost-prohibitive due to the time- and labour-intensive in situ (and mainly point scale) field measurements required for accurate description of the landscape. On the other hand, in the geospatial sense, interpolation and extrapolation based on point-scale like measurements are rather complex over rugged terrain (Crow et al., 2012b). Consequently, a method for the determination of soil moisture without the necessity for labour-intensive measurements would be beneficial for characterising soil moisture patterns instantly at low cost.

Remote sensing missions equipped with microwave sensors, such as Soil Moisture Active Passive (SMAP), Soil Moisture and Ocean Salinity (SMOS) have demonstrated their capability to measure soil moisture under different environmental conditions near the surface (Kerr et al., 2001, Entekhabi et al., 2010a). To date, the spatial resolution of soil water products has not yet reached the paddock scale (10-100 m) with reliable accuracy in an operational manner. Although, that level of detail would be necessary to make a difference in the agriculture related applications, water resource and land management decisions as well as in the improvement of pasture growth models in hill country. Synthetic Aperture Radar (SAR) images from different satellite missions (ENVISAT, RADARSAT-1 and ERS-2, etc.) have also been widely used for soil moisture retrieval at finer spatial scales (10-20m) showing good agreement with in situ measurements in the top soil (Baghdadi et al., 2012). However, they provide relatively low temporal coverage and these sensors are sensitive to soil moisture as well as vegetation and surface roughness (Paloscia et al., 2013). In hilly landscapes, the additional influence of topography needs to be considered as well (Baghdadi et al., 2007, Bertoldi et al., 2014).

Optical (0.4-2.5 µm) and thermal infrared (3.5-14 µm) domains have been used for soil moisture estimations (Schmugge et al., 1980, Kerr et al., 2010, Petropoulos, 2013). Optical soil moisture retrieval methods take advantage of various water absorption wavelength regions and that of reflectance generally drops with increasing soil moisture over bare soils (Anne et al., 2014, Fabre et al., 2015). Over vegetation, the change in plant biophysical and biochemical characteristics are sensed that are strongly dependent on water, indirectly indicating soil moisture conditions (Gao et al., 2013). Soil moisture estimation methods utilising the thermal infrared wavelengths can capture information from the slightly deeper soil layers. Thermal inertia, (Price, 1977), the generation of crop water stress index, water deficiency index and temperature vegetation index (Gao et al., 2013) are common approaches.

Some of the main limitations of these techniques are the coarse temporal resolutions, atmospheric effects, daylight dependence, the cloud cover, the presence of vegetation, and the effect of soil properties. In addition, the reflectance for optical remote sensing is received directly from the soil or vegetation surface (Petropoulos et al., 2015, Sabaghy et al., 2018). Despite these drawbacks, there is a real interest in estimating soil water content from such sensors and the demand for high to medium resolution satellite-derived information for agricultural and land-based predictions is rising steadily (Petropoulos et al., 2015).

The synergetic use and the fusion of data captured in the optical, thermal infrared and microwave domain have been representing a new, promising direction in soil moisture mapping by the advances of high performing computers. The increasing abundance of freely available satellite images with higher spatial resolution and shorter revisit intervals than in the past, such as the Sentinel-1, Sentinel-2 missions, raised the number of possibilities in soil moisture retrieval research, especially in the last decade (Baghdadi et al., 2017, Bousbih et al., 2017, Gao et al., 2017). Combining images that are taken at various sections of the electromagnetic spectrum, e.g. in the optical, thermal infrared and microwave domains, numerous limitations can be reduced or eliminated. The integration of data from multiple, comparable, optical satellites can improve the temporal coverage. However, the pre-processing and analysis of a long, time series type of dataset containing hundreds of images is associated with significantly longer processing time and high computing power requirements.

To address this issue, cloud-based computing tools, such as Google Earth Engine, Amazon, etc., enable the processing and manipulation of large image collections (Gorelick et al., 2017, Hird et al., 2017). Advanced statistical methods, such as machine learning, plays a crucial role in these experiments since they are capable of handling large datasets and high number of variables as well as complex relationships (Ali et al., 2015). Machine learning has the capability to integrate data from various sources and link extracted values from remotely sensed images to ground-based reference observations as it has been shown in previous studies (Ali et al., 2015, Alexakis et al., 2017, Kumar et al., 2018). To complete an efficient learning process, highly accurate historical reference datasets are required that ideally cover the full range of the targeted. Consequently, these models are often valid only over the training area and their extension for generic use is challenging.

To target the above-mentioned scopes, the study utilised a combination of modern and traditional approaches to exploit the benefits of the currently available innovative techniques and the advantages of well known, broadly used data collection and statistical data analysis methods in one, compound research.

During the monitoring period, a wide range of data collection techniques were utilised across a variety of spatial scales including field-based, in situ soil and pasture sampling, the precise laboratory work and the analysis of remotely sensed imagery from various sources acquired over the research area. The field-based sample collection comprised of in situ soil sampling, soil moisture and soil temperature measurements and pasture yield accumulation observations through traditional pasture cuts. The laboratory work included the processing of the collected soil samples for soil particle size analysis, soil bulk density and gravimetric water content determination as well as total organic carbon content measurements. The pasture samples were used for accumulated dry matter and daily average pasture growth rate estimations.

In situ, ground-based measurements consist of pasture production sampling at pasture, and soil moisture and soil temperature recordings at the monitoring sites (i.e. microsites) by an effectively designed observation network. The use of Wireless Sensor Networks (WSN) is a promising new in situ measurement technology for monitoring the spatial and temporal variability of soil moisture in agricultural soils (Bogena et al., 2010, Hedley et al., 2012, Majone et al., 2013, Rawat et al., 2014).

From the remote sensing perspective, the study utilises a high number of remotely sensed images captured by spaceborne sensors mounted on Sentinel-1, Sentinel-2, Landsat 7 and Landsat 8 satellites. The remotely sensed scenes were derived from the Google Earth Engine (GEE) platform and the near surface soil moisture modelling was conducted using the Random Forest (Breiman, 2001) ensemble machine learning method. The two types of datasets were linked to each other based on the geographical location, i.e. the image pixels that corresponds to the microsites. Several types of statistical and comparative analyses was carried out on the final dataset, which was created as a combination of ground-based and remotely sensed data.

1.7 Research objectives and thesis outline

As a result of this study, an effective soil moisture and soil temperature monitoring network will be deployed and the importance of sensing accuracy assessment as well as the role of site-specific calibration will be highlighted. Secondly, the aim of the research is to characterise the spatiotemporal behaviour of soil moisture and soil temperature as a function of topography. Furthermore, an ensemble machine learning approach will be utilised and coupled with Geographic Information Systems (GIS) to develop a prediction tool. The algorithm will be capable of spatially modelling and predicting near surface soil moisture over the selected research area for pasture growth throughout the year. The model will take, process, collate and analyse point like and spatial data inputs from various sources and it will provide a better picture of land-surface interactions and micro-topographic variability on farms. The study aims to improve our understanding of the factors driving soil moisture distribution and their limiting effects on pasture yield in this environment. To evaluate the correlation among these variables, multivariate statistical approaches are accommodated. Medium resolution soil moisture maps will be obtained by the aid of remote sensing technologies. Eventually, these methods and the results will lead to the incorporation of the findings into pasture growth prediction models to better explain and predict pasture production and response to fertiliser in hill country. Based on the results of this study, critical pasture management decisions, such as species selection, grazing strategy, feed budgeting and fertiliser placement can be made, contributing to the increasing focus on the development of hill country pastoral systems.

This thesis is divided into 8 Chapters (including **Chapter 1** as Introduction). The thesis follows the paper-based format; thus Chapter 4-7 are considered as individual research papers representing the basis for publications. Due to the thesis structure and the limited space for background information and methodology description in the individual papers, separated literature review (Chapter 2) and methodology (Chapter 3) sections were necessary. The status of the publishing process is summarised in Table 1.1 at the end of this chapter. Additionally, DRC 16 forms can be found in Appendix 1 to comply with Massey University's policy on the "Thesis by Publication" format.

Chapter 2 - It contains the review of the relevant literature focusing on the wide range of scientific fields touched upon in this study. It aims to provide sufficient background information and the current state of the supporting knowledge beginning with the overview of basic soil water related terms. A general introduction to pastoral agriculture management is given and the relevance of the study is linked with the key concepts of hill country, such as diversity. This section is followed by the brief discussion of the recent issues of pasture yield simulations and the main driving factors of soil moisture distribution in complex landscapes. Then, the reader is introduced to the available soil moisture observation methods starting from the traditional approaches and moving on to the state-of-the-art technologies including both ground-based and remote sensing technologies. The presentation of soil moisture retrieval methods from satellite images and its difficulties is followed by focusing on the currently available, global soil moisture products.

Chapter 3 – This chapter specifically focuses on the research site located near Alfredton on the East Coast of the North Island by providing details on its environmental characteristics, i.e. geographical situation, geological settings and soil types. It is followed by reporting information on the experiment design, instrumentation, microsite selection, the WSN deployment procedure and the data collection. Furthermore, this chapter describes the steps of the conducted field-based soil and pasture sampling as well as the applied methods for laboratory work. The last section describes the generated dataset obtained by remote sensing including the data source, access and the relevant data processing tools.

Chapter 4 – This chapter reports results on the site-specific calibration of the AquaCheck capacitance-based soil probes arranged into a wireless sensor network. The calibration formulas are developed by the relation of sensor readings and a high number of field-based gravimetric soil moisture measurements. The generated conversion formulas are assessed, and the soil moisture sensor accuracy is tested with the examination of the effects of some of the measured soil properties potentially influencing the error distribution.

Chapter 5 - An understanding of spatial and temporal soil moisture patterns in the root zone and their driving factors in hill country is of great importance but has yet to emerge. This chapter investigates the spatiotemporal variability, temporal variation and stability of the soil moisture patterns and their profile characteristics. Temporal persistence and the most representative site is defined. The study uses several statistical measures to quantify the variability and the driving power of topography on the wetness conditions.

Chapter 6 – This chapter investigates the potential of a machine learning algorithm (Random Forest) for the spatial modelling of near surface soil moisture by the synergetic use of ground-based information and remotely sensed products at medium resolution. In addition, the sensitivity of radar signal captured from different orbits to soil moisture is explored. The dataset contains information extracted from an image series created from Sentinel-1, Sentinel 2, Landsat 7 and Landsat 8 satellite acquisitions. Training and test datasets are generated, and the accuracy of the predictions is assessed through cross validation at each microsite. Furthermore, an independent validation is carried out on a series of predicted soil moisture maps along the study period.

Chapter 7 – The factors driving the spatiotemporal patterns of pasture productivity are studied in this chapter to provide a better understanding of the interrelations for hill country pasture management. Yield measurements collected from 13 locations are subjected to comparative and multivariate statistical analyses to disaggregate the controlling role of selected environmental variables. The spatial organisation and temporal trends of total herbage accumulation and pasture growth rate are examined concerning the sites' varied topographic settings. Heat accumulation, soil temperature and soil water storage dynamics are related to pasture production and the limiting role of these parameters as well as their optimal range for the best growth conditions are described. In addition, a hypothesised hill concept was used for visualising the difference as a function of slope angle and aspect in the polar space.

Chapter 8 – The final chapter of this thesis starts with highlighting the key concepts and the motivation behind the conducted research with a brief description of the thesis structure and study methods. The main part of the discussion is governed by four specified scopes and the research questions or objectives raised within each scope. The four scopes contain brief introductions to each topic, briefly describing the applied methods and their limitations, and summarising the relevant findings of the study with their potential implications. Suggestions for future work are made and possible ways are recommended for improving the outcome of the thesis and utilising the generated valuable dataset.

Table 1.1 The status of paper-based chapters in terms of publications process

Chapter	Journal (or potential journals)	Status	Year
3	▪ Water Resource Research ▪ Sensors	About-to-be-submitted	2020
4	▪ Agricultural Water Management	Published	2019
5	▪ Journal of Hydrology ▪ Agricultural Water management	About-to-be-submitted	2020
6	▪ Remote Sensing	About-to-be-submitted	2020
7	▪ New Zealand Journal of Agricultural Research ▪ Plant and Soil	About-to-be-submitted	2020

Chapter 2

REVIEW OF RELEVANT LITERATURE

The second chapter aims to provide a focussed overview of the relevant topics touched upon in Chapter 1. It starts by several definitions related to soil water, the various ways for its expression and the relevance of soil moisture in global environmental systems. This chapter also describes basic principles and significance of pastoral farming in hill country and its associated driving factors. These include pasture productivity, yield simulation methods and the highly important role of plant available water. A detailed description is given on soil water variability in relation to several environmental parameters. The review continues with a presentation of the various ground-based methods available for soil moisture data acquisition. Afterwards, the focus is placed on the potential of spaceborne remote sensing applications related to soil water content retrieval. A summary regarding the key points and conclusions of the literature review completes the chapter.

2 Chapter 2 - Review of relevant literature

2.1 Basic concepts of soil moisture

2.1.1 Relevant soil moisture and soil water storage definitions

The term 'soil moisture' has been approached in many ways by agronomists, climatologists, hydrologists and researchers belonging to various disciplines (Seneviratne et al., 2010). It is generally referred to as the amount of water present in the soil, and expressed as a weight or volume per soil material. Alternative definitions occur depending on whether it is expressed in absolute, relative or indirect terms (Seneviratne et al., 2010, Petropoulos et al., 2014). Soils are considered as three phase systems, comprised of the solid phase (organic matter and mineral components), the liquid phase (soil solutions) and the gaseous phase (dominantly air) (Hillel, 1998).

The liquid phase, consisting of soil water carrying dissolved minerals, is the main source for plant water and nutrient uptake in the unsaturated zone, i.e. the portion of subsurface above the groundwater table. The fractional content of soil water can be defined as the amount of water in a soil, expressed as volume (or weight) of water to the total volume (or weight) of oven-dry soil, which can be reported as decimal fractions or percentages (Petropoulos et al., 2015). Gravimetric water content (θ_g, g g^{-1}), the ratio of soil water mass and dry soil mass is a frequently employed mass-based soil water content expression. The computation of θ_g is given as per Eq. (2.1) as follows:

$$\theta_g = \frac{(m_{ws}) - (m_{ds})}{(m_{ds})} = \frac{m_{aq}}{m_{ds}} \tag{2.1}$$

Where m_{ws} = weight of wet soil, m_{ds} = oven dried weight of soil sample and m_{aq} = weight of water. The computation of water fluxes in water balance models, land-surface simulations and irrigation management often requires volumetric soil water content (θ_v, m^3 m^{-3}), which is calculated as per Eq. (2.2):

$$\theta_v = \frac{(V_w)}{(V_{ts})} \tag{2.2}$$

Where V_w is the volume of water and V_{ts} is the volume of the known total soil sample (including solids, water and air). Additionally, it is often converted to θ_v in (mm mm^{-1}) and referred to as soil water storage S_i of a particular soil profile per unit area. The quantity of S_i can be described as per Eq. (2.3):

$$S_i = \sum_{i=1}^{n} b_i \bullet \theta_{v\,i} \tag{2.3}$$

Here n indicates the number of layers, whereas b_i and θ_{vi} are the depth and θ_v content for layer i, respectively. Via the determination of soil bulk density (ρ_b, gcm^{-3}), θ_v can also be obtained (Gardner et al., 2000, Shukla, 2013). In agriculture, ρ_b is defined as the ratio of the mass of oven dried soil to a unit volume of soil (Grossman and Reinsch, 2002) as per Eq. (2.4):

$$\rho_b = \frac{m_{ds}}{V_{ts}} \tag{2.4}$$

These parameters are related as per Eq. (2.5) (Gardner, 1986) to convert θ_g to θ_v.

$$\theta_v = \frac{m_{aq}}{m_{ds}} \bullet \frac{\rho_b}{\rho_{aq}} = \theta_g \bullet \frac{\rho_b}{\rho_{aq}} \tag{2.5}$$

Where, ρ_{aq} refers to the density of water. In this thesis, the phrase "soil moisture" will generally refer to the soil water content expressed in volumetric basis, i.e. θ_v, if not specified otherwise.

To inform practical agriculture-specific and water management applications such as irrigation scheduling, and to understand the soils' water storage capability, four key soil water-holding states are needed that express water status across various water potentials. Soil water content at or near the level of saturation (i) (θ_{SAT}) expresses approximately 0 – 0.0001 MPa matric potential and it is considered a state, when all pores are filled with water (Seneviratne et al., 2010). Field capacity (ii) (θ_{FC}) represents the soil water content retained against free drainage by matric forces at approximately -0.01 - 0.033 MPa tension. Soil water at the refill point (iii) (θ_{RF}) ranges from -0.04 to -0.06 MPa and marks the point above which the evapotranspiration rate is not affected by water stress. At ca. -1.5 MPa tension the water adheres too strongly to mineral particles to be extractable for plants, thus this state is highly dependent on vegetation type and defined as permanent wilting point (iv) (θ_{PWP}) (Sperry J. S. et al., 2002, Kirkham, 2014). These parameters can be derived from soil moisture release curves, estimated from field measurements or through pedo-transfer functions.

The maximum volume of plant available water (PAW) is generally described as the difference between θ_{FC} and θ_{PWP} (Cassel and Nielsen, 1986). The maximum amount of water the soil can hold onto during a rain-free period is defined as θ_{FC} (Petropoulos et al., 2014, Horne and Scotter, 2016) which usually indicates the upper limit of PAW. The lower limit of PAW is commonly associated with the θ_{PWP}. However, only a certain portion of the PAW can be easily taken up for unrestricted growth since the water held among larger pores is more readily available than water found in the smaller pores (Horne and Scotter, 2016). Plants experience water stress below a nominated θ_{RF} level that depends on species, climatic conditions, soil types and rooting depth. Therefore, the amount of water held between the root zone storage upper limit or θ_{FC} and θ_{RF} is referred to as readily available water holding capacity (RAW).

Available water holding capacity (AWHC) is determined by integrating PAW over the root-zone depth where water extraction occurs (Zotarelli et al., 2010, Horne and Scotter, 2016). The concepts of θ_{FC} and θ_{PWP}, therefore PAW, RAW as well as AWHC have been objects of arguments as various definitions exist in the literature (Kirkham, 2014). This is due to the dynamic nature of soil water and the lack of agreement on the exact soil matric potential or value range used during the retention-based determination (Horne and Scotter, 2016). The previously mentioned terms relate soil water content to plant growth and are widely used in modern numerical models, although, various water potential thresholds and terms have been employed by the scientific community. This thesis accepts and refers to the definitions of the main soil water parameters as they were described above.

2.1.2 Soil moisture, an environmental state variable

Soil moisture is a spatially and temporally highly variable environmental parameter and its fundamental role in the hydrological cycle has been studied extensively (Brocca et al., 2017). Although, the overall quantity of soil moisture is relatively small, ~0.001 % of total water reserves (Dingman, 2002); hydrology, agronomy, geomorphology, bio-geography, ecology and climatology heavily rely on soil moisture observations (Romano, 2014). Point-, field-, catchment-, regional-, continental- and global-scale soil water content data obtained at various temporal resolution have been utilised in a broad range of applications. Soil moisture data is crucial for numerical weather prediction, climate simulations, flood monitoring, drought assessment, water and energy budget calculations, greenhouse gas accounting, land-atmosphere-biosphere interactions, estimation of land-surface fluxes, natural hazards forecasting, optimising agricultural management and crop yield predictions (Dugua and Pietroniro, 2005, Entekhabi et al., 2010b, Li and Rodell, 2013, Ochsner et al., 2013, Romano, 2014, Vereecken et al., 2014, Bogena Heye R. et al., 2015, Dorigo and de Jeu, 2016).

Soil moisture is also considered as energy storage due to its dynamic long- and short-term effects on the climate system by regulating heat and water fluxes (Pan et al., 2001, Teuling et al., 2007b). Because of its well-established importance and that it can be globally monitored by remote sensing, soil moisture was recognised as an Essential Climate Variable in 2004. In 2010, it was added to the terrestrial Essential Climate Variables group by the Global Climate Observing System program (Bojinski et al., 2014, Dorigo et al., 2015).

Above all, soil moisture provides the plant-available water for vegetative life. In agriculture, soil moisture is essential for crop and pasture yield improvements, irrigation scheduling and extending the period of unstressed transpiration (Hillel, 2003a). The most crucial phases of the life and growth of vegetation, such as photosynthesis, biomass production, the rates of transpiration, organic matter cycle and nutrient uptake are often limited by soil water content (Porporato et al., 2002, Rodríguez-Iturbe and Porporato, 2007). Thus, soil moisture is the principal limiting resource for pasture growth and agricultural production in New Zealand (Woodward et al., 2001, Bittelli, 2011). Accurate information about soil moisture at a few cm to tens of km scales are essential to improve the reliability and precision of many applications. Measuring soil water content in a consistent and spatially comprehensive manner is challenging, due to its spatiotemporal variability and environmental heterogeneity (Entin et al., 2000, Rodríguez-Iturbe and Porporato, 2007).

2.2 The relevance of soil moisture studies in the pastoral agriculture in New Zealand's hill country

2.2.1 Geographical extent and definition of hill country

Slightly different definitions have been published in the literature regarding 'hill country'. A broadly accepted, generalised definition of hill country was presented by Basher et al. (2008) in their erosion process report. The authors defined hill country as *`all lowland and montane hill and steeplands (slope > 15 °), classified as Land Use Capability (LUC) class 5, 6 or 7, and being described in the unit descriptions in the New Zealand Land Resource Inventory as hill country'.* 'Lowland' and 'montane' categories follow the altitude/temperature-related bioclimatic zones of Wardle (1991). A simplified definition was followed by Cameron (2016) and Kerr (2016) stating that hill country is classified as land with slopes greater than 15° and below an altitude of 1000 metres above mean sea level. It is worth noting that there will be hill slopes with lower steepness and flat lands in these complex landscapes.

For the purposes of the study, the latter, simplified version of hill country definition is adequate and will be applied hereinafter. According to the above criteria, 63% (6.3 million ha) of New Zealand's hill country area occurs in the North Island and 37% (3.7 million ha) in the South Island that constitutes over 75% of New Zealand pastoral land (Bretherton, 2012). Around 5 million ha of the total 10 million ha is designated as pastoral hill country farmland from which 4 million ha is located in the North Island (Kemp and López, 2016, Kerr, 2016).

The presented research was conducted in the East Coast Hill Country (ECHC) region of the North Island. ECHC is a significant contributor to the national economy and covers the majority of

North Island's hill country area. To approximate the spatial extent of grazed pastures in the North Island, the Land Use and Carbon Analysis System (LUCAS) dataset was chosen (Ministry for the Environment, 2012). The study site and its surroundings are depicted on Figure 2.1 and the low-producing grassland area that contains mostly hill country land is superimposed on a Sentinel-2 satellite image mosaic (Land Information New Zealand, LINZ).

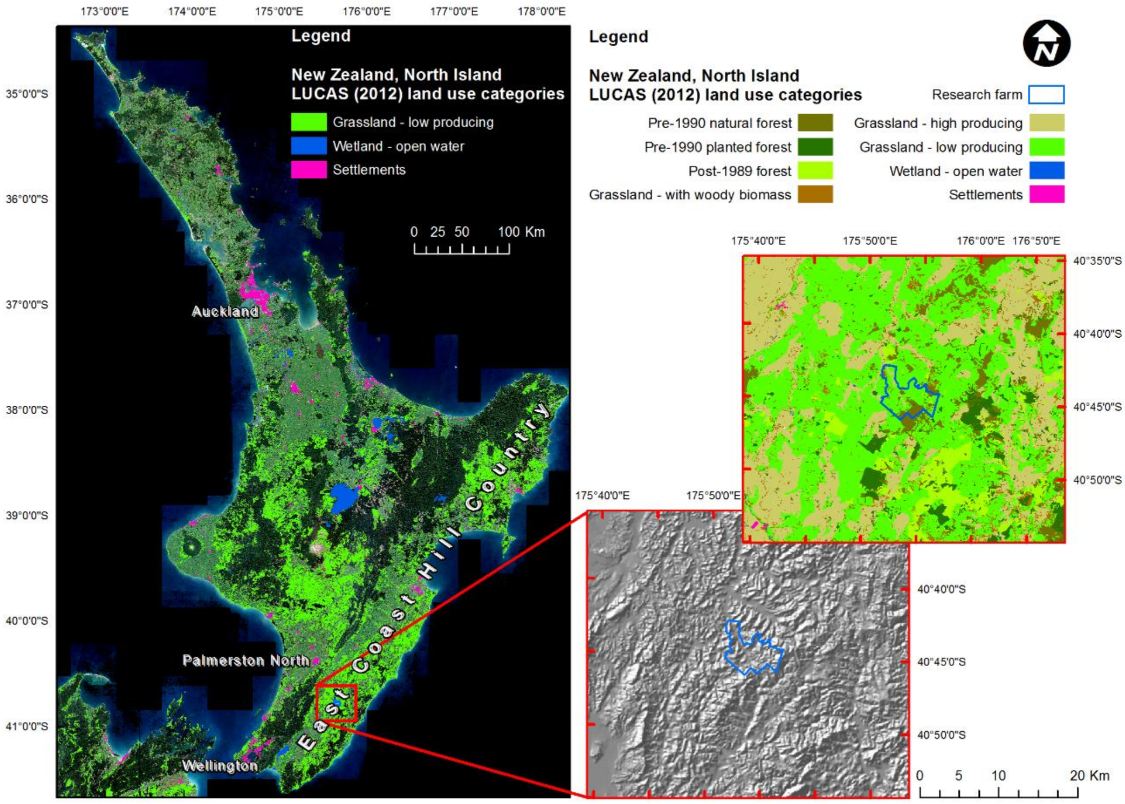

Figure 2.1 Spatial distribution of pastoral hill country land in the North Island extracted from LUCAS land use maps. On the right, a closer view the research area is shown. A detailed map of LUCAS land use classes is provided along with a shaded relief map that illustrates the rugged, hilly terrain conditions (Ministry for the Environment, 2012, LINZ, 2017).

2.2.2 Hill country farming and its economic value

The history of hill country pastoral farming and the establishment of pastures started with the clearance of the indigenous forest about 100-150 years ago (Kemp and López, 2016). This agricultural expansion happened intensively and had a large effect on the environment and economy. Hill country pasture development reached a milestone in the 1950's when the introduction of effective and affordable aerial spreading of fertilisers and seeds allowed significant increases in production (Moot et al., 2009). Since then, the flatter and generally better land has been lost dominantly to the dairy farming and partly to the urbanisation. In the last few decades, the importance of hill country farming has been increasing and it has been in an enhanced focus of research as a productive platform (Kerr, 2016).

In 2017, more than $38 billion of New Zealand's annual export earnings benefitted from primary industrial production and a positive economic outlook with strong increase in export revenue was expected for 2018 and 2019 (MPI, 2018). Pastoral farming contributes $20-25 billion towards annual exports; this is approximately 75% of all agricultural exports (Morrison, 2017). In terms of contributions to gross domestic products (GDP), the agriculture sector accounted for 3.1% of total GDP in 2016; hill country farming was a major annual contributor generating $7-7.5 billion through the export of various products, such as meat and wool (Kemp and López, 2016, Statistics New Zealand, 2018, updated April 2018). Over 90% of the production was exported to more than 120 countries making the red meat, mainly originating from hill country, the second most imported product. The North Island accounts for 71% (2.485 million) of the total amount of beef cattle and 50% (13.8 million) of sheep stock (Beef + Lamb New Zealand, 2017, Ministry for Primary Industries, 2018). Based on the above-mentioned economic indicators and the weight of hill country in the primary industries, it is evident that hill country farms are critical components of New Zealand's economic activity.

2.2.3 Pasture management in hill country

New Zealand's predominantly moist temperate climate, soil characteristics and its vegetation species makes hill country farming unique and allows the development and operation of efficient year round grazing systems (Hodgson et al., 2005). An essential requirement is matching the pasture growth with the animals' demand by producing the best quality feed and fully utilising the local resources. As a consequence of growing food demand and quality requirements of the international marketplace, future farming will likely involve further management intensification (Mackay et al., 1993, Shadbolt and Martin, 2005, Mackay, 2008, Hoogendoorn et al., 2016).

A large proportion of moderately intensive pastoral production is carried out on low-altitude hill country farms where sheep and beef farming predominates. These farms are operated under a range of climatic conditions and various management regimes typically with low inputs (i.e. fertiliser, feed from external sources). Consequently, sustainability and profitability rely on adapting to changing environmental conditions and the strategic exploitation of the available biophysical, human and financial resources (Shadbolt and Martin, 2005, Lieffering et al., 2012). Precisely targeted management practises that considers site-specific irregularities can significantly improve the hill country farmers' responsiveness, yield and the general efficiency of their pastoral system (Judd et al., 1990).

2.2.3.1 Diversity, a key concept in hilly landscapes

The most distinguishing feature of hill country land management are the contouring and sloping nature of its soil surface coupled with generally low fertility soils (Gillingham, 1973). The geologically young highly broken landscape - both at macro and micro topographical levels, the variable climate and degree of erosion all affect soil development; in turn, this determines the spatiotemporal heterogeneity and diversity of production rates (Phillips et al., 2016). Due to these reasons and the differences in pasture composition and soil development, yield estimation and improvement are challenging tasks (Radcliffe et al., 1968, Murray et al., 2007). A good understanding of the complex soil/plant/animal/environment system is key to appropriate farm management in order to convert forage into a profitable animal product. Certain pasture growth affecting factors are natural or fixed and others are controllable (Shadbolt and Martin, 2005).

2.2.3.2 Role of natural factors in non-irrigated pastoralism

Some of the physical characteristics of a land are given by its geographical location, underlying geology, geomorphology, natural soil fertility and climate. Such variables are mostly out of human control, but the perception and quantification of their effect on pasture growth patterns enable farmers to maximise their land resources. Parameterisation is also necessary for accurate yield predictions and assessment of pasture production. According to Scott et al. (1985), temperature, soil moisture, soil fertility and pasture managament are the four most important influencing factors of hill country farming, although these factors are somewhat functions of the terrain. Harris et al. (1985) concluded that temperature and PAW are the two most important enviromental factors influencing pasture production as the majority of hilly country is non-irrigated. Since all of the above-mentioned factors are linked to the terrain, it can be concluded that specific management challenges are associated with the micro-climatic and landscape features (i.e. slope and aspect) that govern the amount of PAW and yield potential.

2.2.3.2.1 Soil moisture

Water supply is a critical regulator of plant growth as they require water to transport nutrients and to perform cellular processes (Rodrigez-Iturbe, 2000, Robbins and Dinneny, 2018). The fact that pasture production in hill country is strongly related to soil water content received early recognition. Booth and Gibbs (1969) reported that many farmers are drought-conscious and the provision of sufficient water management is top priority in the development of ECHC. According to Card (1977) and Rodrigez-Iturbe (2000) moisture supply is probably the most important environmental control of vegetation diversity and the attainment of production potentials.

Salinger (1979) attributed much of the growth of the pastoral industry in 1950-69 to the below average occurrence of drought in those years compared to the drier 1970's. Furthermore, Maunder (1979) observed that significant fluctuations in soil moisture deficits between years had considerable effect on pasture and animal production. The annual pattern of soil moisture change and deficit are crucial in grazing management and many regions of the North Island, including the ECHC, are regularly influenced by water shortage during summer and autumn (Chapman and Macfarlane, 1985, Bircham and Gillingham, 1986, Bretherton et al., 2011).

2.2.3.2.2 Topography

There is a strong relationship between pasture composition, distribution, growth, soil properties and topography (Radcliffe, 1982, Kemp and López, 2016). Topographic features such as altitude, slope angle and aspect play important roles in hill pasture ecosystems; hence their effects on pasture production have been investigated in several studies (Gillingham, 1973, Gillingham and Bell, 1977, Lambert and Roberts, 1978, Radcliffe, 1982, López et al., 2003, Moot et al., 2009, Kemp and López, 2016). Zhang et al. (2005) observed that slope angle and spring rainfall were the two dominant variables limiting pasture growth. Production usually declines as slope increases (mainly due to PAW limitations), whereas nutrient transfer and runoff losses increase (Roberts and White, 2016). Slope angle and position differentiate the soil depth and soil physical properties, soil fertility and the supply of water for plants, that is generally reduced by increasing steepness (Radcliffe and Lefever, 1981, López et al., 2003, Zhang et al., 2005).

Hill slopes modify the distribution of incoming solar radiation and heat budget that effects soil and air temperature, as well as the rate of photosynthesis (McAneney and Noble, 1976). In addition, if the slopes are steep enough, stock tracks may develop and exert further impact on soil nutrient levels and pasture variability (Gillingham, 1973, Sheath and Boom, 1985).

The role of slope angle in pasture productivity is better defined, than that of aspect. The presence of a seasonal pattern makes the interpretation of aspect effects sometimes controversial and it varies from region to region (Suckling, 1959, Lambert et al., 1983). The largest contrast has been found between north- and south-facing aspects. Northerly aspects often produce more winter growth, while southerly aspects yield more herbage during moisture stress in summer, although the length of the seasons has a major effect on the annual productivity of both aspects (Lambert et al., 1983). White et al. (1972), Lambert and Roberts (1978) and Radcliffe (1982) reported that annual pasture growth was higher on shady aspects, than on northerly slopes, however, Gillingham (1973) and Suckling (1975) found the opposite.

2.2.3.2.3 Ground temperature

Plant development is strongly influenced by soil temperature as plant species have different requirements for optimal growth (Baars and Waller, 1979). Soil temperature is partly determined by season, latitude, altitude, slope angle and aspect conditions in hill country (Scott et al., 1985). Some legumes and grass species prefer the sunnier, warmer north aspects, while southerly faces suit other species. Gillingham (1973) observed 10 % higher total pasture production from northern aspects than southerly faces. Increased slope angle with reduced pasture cover are associated with greater diurnal variation (Sheath and Boom, 1985).

A limiting temperature exists for each species, called base temperature (T_b), below which their development technically stops, for instance, the perennial ryegrass (*Lolium perenne*) displays significantly higher leaf elongation above 4-5 °C, which is close to its T_b (Peacock, 1975, Nagelmüller et al., 2016). Growth rate and soil temperature are most likely linked by a combination of linear and non-linear relationships (Voorend et al., 2014).

High temperatures rarely cause limitations if there is no moisture stress, in contrast, low temperatures are common constraints of potential yield in hill country (Harris et al., 1985). Moreover, the regrowth of common temperate grasses is strongly dependent on temperature (Baars and Waller, 1979) and the species selection process needs to take into account how different plant species tolerate the temperature fluctuations over seasons (Chapman and Macfarlane, 1985).

2.2.3.3 The role of controllable soil management factors

Fertiliser management and grazing system are the main controllable factors in hill country that have the potential to enhance the land's production capability (Kemp and López, 2016). The natural fertility of the soil is fixed, but it can be modified by fertiliser applications and can be exploited in a sustainable way by correct management practises. Grazing management (structure, duration and intensity) highly depends on the level of knowledge regarding feed requirements, the available pasture and the incorporated animals (Hodgson et al., 2005). A solid understanding of growth patterns, feed surplus and deficiencies are parts of the grazing strategy that a farmer needs to apply to accumulate pasture for the low producing periods.

In hill country, the main input is fertiliser as irrigation is currently not a feasible option in many cases. Pasture growth and herbage accumulation can be stimulated through fertiliser applications that also has effects on soil biological activity, botanical composition and organic matter content, therefore, indirectly on soil water holding properties (López et al., 2003, Kemp and López, 2016). Pastures rely on the nitrogen input fixed by legumes and supplied to associated grasses that usually generates deficiencies in phosphorus, sulphur and sometimes lime. Thus, required correction of these constituents are dependent on the spatially heterogeneous soil properties that makes fertiliser inputs location and climate specific (Scott et al., 1985). Moreover, an adequate amount of soil water is required for the successful interaction within the legume-grass-fertiliser-soil system (Gillingham et al., 1998), suggesting that input placement and timing are critical components of pasture management.

2.2.3.4 Production quality and pastoral system management efficiency

Pasture management practises play a key role in the improvement of pasture quality that determines animal productivity and performance (Gray et al., 2004). In New Zealand, pasture quality is commonly characterised by the nutritive value that is estimated by two main indicators, i.e. digestibility and metabolisable energy (Lambert and Litherland, 2000). These parameters are strongly linked to feed allocation systems and the rate of intake that is constrained by the amount of pasture available for the animals. To achieve quality increase, farmers have been improving their management, introducing better quality species, attempting to maximise legume content and green material while minimising dead matter (Hodgson et al., 2005).

Land management development and operation efficiency are related to the stocking rate that is a function of soil fertility, the vegetative cover, the amount and distribution of rainfall, soil water-storing capabilities, the grazing system and the type of animal grazed. Two other major measures of the performance of grazed pasture systems and animal production are the herbage accumulation rate and herbage mass. In non-irrigated lands, productivity can be frequently limited by moisture stress altering the strategic control on the paddock level (Lambert et al., 1983, Harris et al., 1985, Bluett et al., 1998). Management decision are made by comparing herbage mass distribution with a target value (Van Bysterveldt and Christie, 2007, Romera et al., 2010).

Traditionally, farmers collected pasture growth data from their land on a regular basis, during the so called 'farm walk' and sorted their paddocks considering the herbage mass and a target line (Romera et al., 2013). To eliminate the time consuming data collection and to exploit more information from the pastures, a collection of environmental variables and soil parameters have been used to model potential yield (Scott et al., 1985, Romera et al., 2013). Although, these models are prone to errors and uncertainties despite their key role in pasture management.

2.2.4 Simulating pasture productivity

Pasture growth simulation models have been increasingly used by agronomists for assessing the effects of the controllable and fixed variables of the pastoral system (Li et al., 2011). Some standard units of these models are well-understood, such as the seasonal distribution of feed demand (Holmes et al., 1987). However, pasture growth depends on a large number of variables that are too laborious to measure or require a long-term data collection, making their incorporation into these models rather difficult (Woodward, 2001).

Deterministic and process-based models are commonly applied and integrated into whole farm and pastoral system simulations (Johnson et al., 2003, McCall and Bishop-Hurley, 2003, Barrett et al., 2004, Romera et al., 2010, Li et al., 2011). However, most of these models were originally designed for flat conditions such as the climate-driven Pasture Growth Simulation Using Smalltalk (PGSUS) algorithm introduced by Romera et al. (2010). Consequently, modifications and additional modules have been developed to make these models applicable on sloping lands.

In hill country, an ideal pasture growth forecaster application would be able to estimate the potential pasture growth rate on various landscape features with spatiotemporally high resolution for farming activities. Such a forecaster would take into account the topography (slope, aspect, and altitude), climate variables (temperature, rainfall, incoming solar radiation, ventilation effect), soil fertility (fertiliser history) and have a detailed water balance module calculating daily RAW or soil water deficit considering the sub-paddock variations.

2.2.5 The water balance model

The soil water balance for flat land has been extensively studied and is quite well understood in New Zealand. For instance, Woodward et al. (2001) provided an analysis of the work by Scotter et al. (1979), leading to a validated daily time-step, two soil-layer model. In contrast, relatively few studies have been published on the water balance in hill country, despite its significant role in New Zealand's primary sector. Bircham & Gillingham (1986) and Bretherton et al. (2010) provided in-depth studies on the water balance modelling on New Zealand's pastoral hill country soils. Bretherton (2012) conducted a research on repellency-induced runoff and its consequences in hill country environment, where he used a modified and refined version of the water balance model described by Bircham and Gillingham (1986).

Commercial versions of these models are in operation, although it is assumed that one of the weakest points of these models lies in the soil moisture balance estimations. The water balance module often fails to represent the variability in hill country due to the complex water dynamics under rolling surfaces and heterogeneous soil types. To overcome some of the issues encountered by the single-layer models (under-prediction of transpiration and growth in prolonged dry periods), a two-layer water balance model for flat-lands was developed by Scotter et al. (1979) and modified by Woodward et al. (2001). The two-layer Scotter model is illustrated on Figure 2.2.

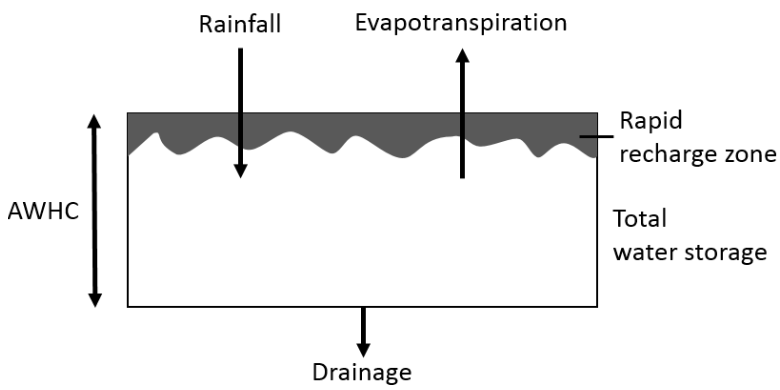

Figure 2.2 The simple two-zone, Scotter water balance model, depicting the division of the soil profile into a preferentially recharged and depleted zone near the surface and a deeper soil section (Scotter et al., 1979). AWHC-available water holding capacity.

The model derives the soil water deficit (W) for the deeper zone and soil water deficit for the rapid recharge surface zone (W_s) on a daily basis t. The formula requires the calculation of potential evapotranspiration (PET) and soil-specific parameters i.e. AWHC for both layers. PET can be estimated by using existing models that take into account the climatic data, such as temperature, sunshine hours or radiation (Smith et al., 1998). The Woodward water balance model is given as per Eq. (2.6).

$$W_{t+1} = min(0, W_t + rain_t - AET_t) \quad (2.6)$$

$$\mathrm{W_{s\,(t+1)}} = \min(0, \mathrm{W_{s\,(t)}} + \mathrm{rain_t} - \mathrm{AET_{s\,(t)}})$$

Where $\mathrm{W_t}$ is soil moisture deficit (negative), $rain_t$ is the daily precipitation and $\mathrm{AET_t}$ is actual evapotranspiration on day t. The AET model is expressed as:

$$AET \ = min(PET, \sigma\, RAW) \quad (2.7)$$

$$AET_s \ = min(PET, \sigma\, RAW_s)$$

Where σ is the proportion of RAW taken up by plants in one day. Woodward et al. (2001) proposed that RAW can be calculated as the sum of available water in the surface zone $\mathrm{RAW_s}$, and the remainder of available water in the deeper zone as per Equation 8.

$$RAW \ = RAW_s + \alpha PET[(AWHC + W) - \ RAW_s] \quad (2.8)$$

$$RAW_s = AWHC_s + W_s$$

Where $\alpha\mathrm{PET}$ is the availability of soil water, whereas $\mathrm{AWHC_s}$ and $\mathrm{W_s}$ represents the water holding capacity and soil water deficit of the surface zone, respectively.

In the real-world applications, the spatially extended water balance model is fed by AWHC values generated from national, low spatial resolution soil layers. Dominantly, the sub-farm spatial variability is much larger than the utilised input layers would suggests, therefore the improvement of the soil water balance part of the simulations would have a considerable effect on the prediction accuracy of the pasture growth forecasters.

2.3 Factors driving soil moisture availability and distribution in hill country

Soil moisture is part of a complex environmental system, where static and dynamic controlling factors may be distinguished according to Reynolds (1970) . Static or slowly changing parameters include mainly the physical soil properties and topographical features. Climatic variables, vegetation properties, soil organic matter, depth to water table and time since last rainfall event are classified as dynamic factors. Many of these are interrelated and most of them vary spatially and/or temporally, therefore the time and spatial scale are critical points (Crow et al., 2012b).

Changes in soil moisture levels can generally occur via precipitation, evapotranspiration, net lateral flow, or vertical drainage over a variety of timescales (Wilson et al., 2004). Consequently, soil moisture is generally considered as a spatiotemporally highly changeable parameter (Korres et al., 2013, Vereecken et al., 2014) that is particularly true at the soil surface, the interface of energy and water exchange (Wilson et al., 2004, Petropoulos et al., 2014, Bretherton et al., 2018).

On the other hand, Grayson et al. (1997) grouped the various affecting factors into local and non-local controls. Local controls, such as soil properties, vegetation and possibly the radiation (if the terrain is complex) determine the vertical fluxes, i.e. drainage and evapotranspiration during dry periods. In contrast, under wet conditions, surface and subsurface lateral fluxes govern the soil moisture distribution where the non-local controls dominate. These mechanisms switch from one to the other when evapotranspiration increases/decreases and precipitation decreases/increases. That is explained by the dominance of lateral flow over vertical fluxes or vice versa (Grayson et al., 1997). In general, isolating the effects of the listed factors (or group of factors) are difficult (Vereecken et al., 2014). A brief description is given about their impacting magnitude regarding soil moisture variability.

2.3.1 Meteorological forcing

Incoming solar radiation, air and soil temperature, wind, humidity and precipitation exert their effects on the space-time dynamics of soil moisture (Petropoulos et al., 2014). A number of studies have shown that precipitation is the most important of all meteorological factors influencing soil water, runoff and subsurface flow characteristics (Chen et al., 2005), although it is scale dependent (Crow et al., 2012b). The rate of evaporation is mainly controlled by incoming solar radiation. Additionally, radiation also contributes to the rate of transpiration, consuming a remarkable ~65-80% of rainfall (Bretherton et al., 2010). Climatic factors are often studied from a cumulative, multi-parameter point of view due their complex interrelationships a (Bell et al., 1980, Famiglietti et al., 1998).

2.3.2 Topography

The patterns of soil variation are strongly related to the topographical features of hill country. Slope angle, aspect, curvature, specific contributing area and relative elevation strongly affect the distribution of soil moisture (Crow et al., 2012b). It has been established that the direction and angle of a slope can have a significant influence on surface temperature as they directly control the amount of solar irradiation received (Petropoulos et al., 2014). The amount of infiltration, drainage and runoff is influenced by the slope angle; steeper slopes have been observed to be generally drier than flat areas (Famiglietti et al., 1998). As a general rule in the southern hemisphere it is accepted that northern aspects are warmer and drier than south-facing aspects (Radcliffe and Lefever, 1981). Radcliffe and Lefever (1981) also observed that the moderately steep (25°) north-facing slopes exerted higher evapotranspiration rates and received 80 % more radiation than the south-facing slopes on a grazed pasture over a year period.

Curvature provides information on the convexity or concavity of the landscape that showed significant correlation to soil moisture patterns (Moore et al., 1988, Sulebak et al., 2000, Kaleita et al., 2007, Shi et al., 2012). It quantifies the rate of change of a first derivative such as slope or aspect in a given direction that defines lateral flow characteristics (Gallant and Wilson, 2000).

Representing the catchment area, specific contributing area (also called upslope area) controls the volume of subsurface moisture and lateral fluxes (Nyberg, 1996, Grayson et al., 1997). It is defined as the upslope area above a certain length of contour line segment or grid cell that drains to the given element or contributes to the flow across the element (Famiglietti et al., 1998, Rieger, 1998, Gallant and Wilson, 2000). Larger upslope areas usually lead to higher soil water contents on hillslopes whereas slopes with a smaller contributing area are likely to be drier (Famiglietti et al., 1998).

An inversely proportional relationship has been found between soil moisture and slope position, also known as relative elevation (Hawley et al., 1983, Jacobs et al., 2004, de Rosnay et al., 2009). It was observed that sites at higher relative elevation tend to lose more water and can have less water received from the upslope areas (Qiu et al., 2001b). Exposed slopes and hilltops are most likely to present drier conditions due to higher evapotranspiration rates (Qiu et al., 2001b). The presence of topographic control on soil moisture variability is generally accepted, although it may be a poor indicator during drying stages (Western et al., 2003).

2.3.3 Soil properties

Variations in soil texture, structure, organic matter and macro-porosity have been documented to influence soil moisture distribution (Petropoulos et al., 2014). Gao et al. (2011) found strong correlation between soil texture and moisture content. Infiltration, permeability, and water-holding capacity are affected by the characteristics of soil texture and structure (Moore et al., 1988). The proportion of clay, silt, and sand can also intensify the soil moisture deficit, since the smaller the soil particle the greater its ability to retain water, meaning that clay soils have greater water holding capacity than silt and sand (Younis and Iqbal, 2015). Water and air storage capabilities, drainage and drying processes depend on the porosity, where macro-pores ($\varnothing > 30$ μm) influence the rate of water drainage and vertical penetration (Niemann and Edgell, 1993, McLaren and Cameron, 1996).

The presence of soil organic matter (decomposed organic material) can improve the AWHC (McLaren and Cameron, 1996). Additionally, soil albedo (reflectance) is partly a function of organic matter content, which controls the amount of energy absorbed by the evaporating surface of a bare soil (Kurucu et al., 2009).

2.3.4 Vegetation

The bidirectional relationship was investigated between soil moisture and vegetative cover by Hawley et al. (1983) and Liancourt et al. (2012). Vegetation related controls are mainly linked to the alteration of infiltration and evapotranspiration rates. These processes include canopy throughfall, land surface shading, the generation of turbulence enhancing evapotranspiration, the addition of organic matter and root activity which influence hydraulic conductivity and water extraction (Famiglietti et al., 1998). The contribution of vegetation amount, type, density and uniformity to soil moisture spatial variability has been documented to be a more dynamic variable than soil and topographic factors (Crow et al., 2012a, Petropoulos et al., 2014). Hawley et al. (1983) also observed that variations caused by topography tend to be diminished by the vegetative cover.

2.3.5 Land use and management

Soil physical properties, top soil structure and vegetation cover can be significantly affected by land use and related practises that can have a significant effect on soil moisture patterns (Qiu et al., 2001a). Unsuitable land management may lead to soil degradation, decreased soil organic matter content, lower infiltration rate and PAW as well as enhanced erosion processes. Studies have shown that differences in land management history can have a high impact on the hydraulic properties of soils and can negatively influence soil productivity (Sonneveld et al., 2003, Haghighi et al., 2010). Gao et al. (2014) observed that different land uses resulted in differing spatial variations in soil water content. On farmed lands, the water pathways are subject to change by the establishment of roads, terraces and ditches thereby modifying the hydrological continuity and the spatial variation of soil moisture (Hébrard et al., 2006).

2.4 Observed soil moisture data

The benefits of reliable soil moisture data has been recognised for many decades as it governs numerous key environmental processes at various spatial and temporal scales. From the traditional 'look and feel' approach (Johnson, 1962) through to non-invasive, ground-based approaches (Bogena Heye R. et al., 2015) to satellite-based observations (Wagner et al., 2007, Wang and Qu, 2009), several techniques have been developed to estimate soil moisture.

Figure 2.3 depicts an illustration of several soil moisture observation methods as a function of spatial extent and on what scale they are mostly applied. A combination of various observation techniques is frequently utilised in soil moisture research and applications, therefore Figure 2.3 aims to give an understanding of how methods can be synergised.

Various ways exist to group soil moisture measuring and estimation methods. The available techniques are often divided into three main approaches such as in-situ measurements, soil-water models and remote sensing. Robinson et al. (2008b) and Romano (2014) categorised the field techniques based on whether direct contact is required with the soils, i.e. contact-based(invasive) and contact free (non-invasive) techniques.

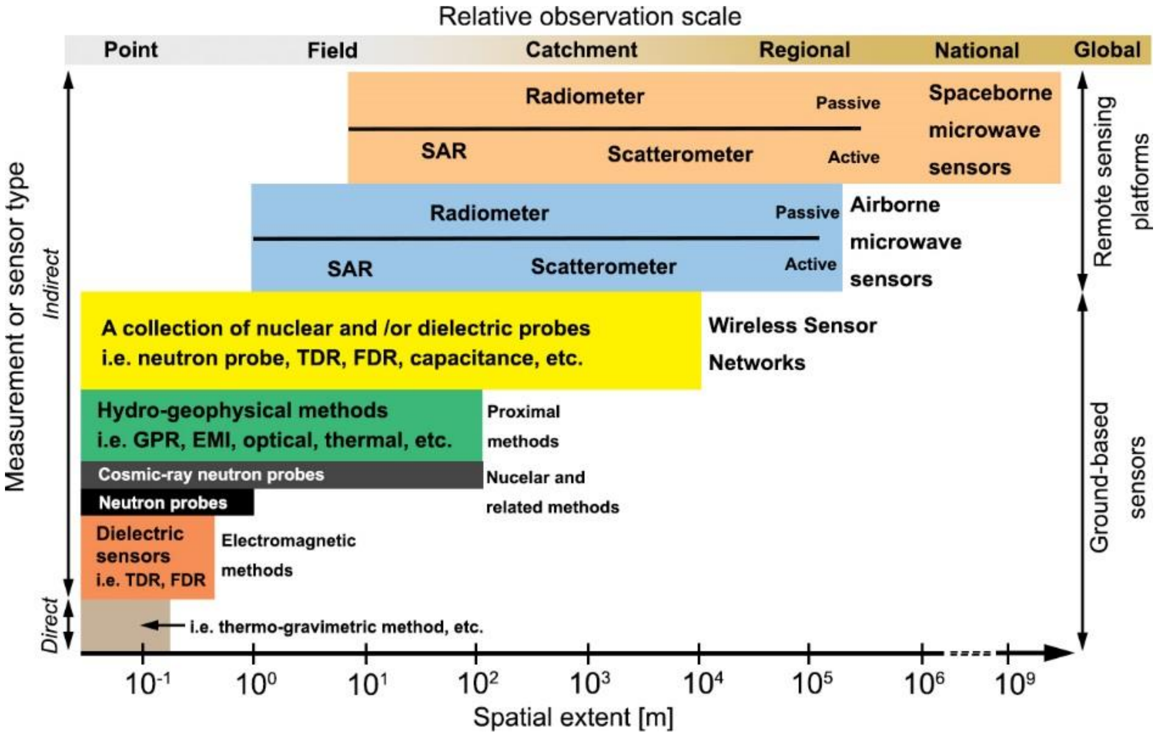

Figure 2.3 Summary of the discussed ground-based and microwave remote sensing soil moisture observation techniques. The methods are related to the spatial extent as well as the relative spatial scale of observations (modified after Vereecken et al. (2008).

In the overview of Dobriyal et al. (2012) ground-based techniques and remote sensing methods were discussed. Seneviratne et al. (2010) assessed the available soil moisture datasets from ground-based measurements (direct, indirect), remote sensing, atmospheric-terrestrial water balance and land-surface models. This thesis will discuss the methods by dividing them into ground-based and remote sensing techniques.

2.4.1 Ground-based measurement methods

2.4.1.1 Direct methods

Direct methods are considered as the most accurate techniques, although they involve invasive soil sampling and the removal of soil moisture by evaporation or chemical reaction. Despite being a classical approach, the thermo-gravimetric technique is the most commonly applied direct soil water determination method (Schmugge et al., 1980, Lekshmi et al., 2014). Due to its unprecedented accuracy for all soil types, it is often referred to as the reference technique in comparisons with soil moisture estimations using other methods (Johnson, 1962, Lal and Shukla, 2004, Dobriyal et al., 2012). The procedure consist of taking soil samples (100-200g) from the site of interest, weighing the wet samples and placing them in a forced draft oven for drying to a constant weight at 105 °C. The process ends when the sample weight becomes stable and as a result, θ_g on dry basis can be calculated as per Eq. (2.1) and then converted to θ_v according to

Eq. (2.5) if ρ_b is known. Thermo-gravimetric observations are often required for calibration and validation purposes, although the method is labour-intensive and time-consuming. The method has limitations and disadvantages in obtaining a temporally dense dataset from the same location. Therefore, indirect techniques have been established that are more cost and time effective and can sense soil moisture with a higher temporal resolution.

2.4.1.2 Indirect methods

Several indirect methods measure a physico-chemical property of the soil to estimate soil water content (Evett and Parkin, 2005). Strictly speaking, they are not able to measure soil water content; thus, empirical calibrations are used to convert the measurements to soil moisture values. Most of these methods require contact with the soil medium (Julien et al., 2011).

2.4.1.2.1 Nuclear techniques

The radioactive technology and idea of the neutron moisture probe published by Gardner and Kirkham (1952) introduced a breakthrough in modern soil moisture estimation, which was developed after the significantly improved knowledge about nuclear physics in the 1940s. The most widely applied radioactive techniques are neutron scattering, nuclear magnetic resonance (Zazueta and Xin, 1994) and gamma-ray attenuation. The latter has the capability to sense soil water content in the top 1-2 cm of soil layer. The method uses the principle that gamma-ray scattering and absorption are affected by the changes in soil wetness density (Schmugge et al., 1980). Even though the gamma attenuation have some advantages over the neutron moisture meters, the neutron scattering method remained the standard indirect method until the age of dielectric sensors arrived in the 1980s (Ochsner et al., 2013).

The concept of neutron scattering is partly based on the physical fact that fast neutrons slow down to the thermal stage through collision with common soil elements. Secondly, hydrogen is the most effective element in the neutron thermalisation, which is mostly present in the form of water molecules (Evett, 2000a). Neutron moisture meters are equipped with a high-energy neutron source and a detector to sense the scattered and thermalized neutrons. Since the portion of slow neutrons is mainly controlled by the amount of water present, the instrument can estimate soil water content on the volume basis (Greacen, 1981). Neutron moisture meters have been frequently used as reference techniques among the indirect, non-destructive methods due to their high accuracy (Evett and Steiner, 1995, Chanasyk and Naeth, 1996). The technique is extremely costly and it has special requirements for installation and operation. Additionally, its sphere of influence varies in dry and wet conditions (Keys, 1990).

2.4.1.2.2 Dielectric soil moisture sensing methods

The next set of θ_v sensing are the dielectric techniques or electromagnetic (EM) methods as they operate based on the measurements of EM properties. A broad spectrum of instruments makes use of the dielectric parameters of the sensed media from the sample scale to remotely sensed several km^2 area, which will be discussed outside of the ground-based methods. Each technique produces one of the following outputs: travel time, impedance, capacitor charge time, oscillation frequency or frequency shift depending on the sensor type. The raw acquisitions are then converted to θ_v through calibration functions (Blonquist et al., 2005). Dielectric methods have been increasingly applied due to their non-destructive and reliable soil moisture estimations that can be delivered rapidly and repeatedly from the same location via automation (Robinson et al., 2003, Stacheder et al., 2009).

In general, dielectric instruments sense soil water content by measuring the apparent soil bulk permittivity Ka that determines the velocity of an EM wave emitted into the surrounding soil media. The theoretical relative permittivity ε_r describes how a given medium interacts with the electric field compared to the effect of vacuum on the same electric field. The ε_r, also called dielectric constant, is defined as the ratio of absolute permittivity of the substance to the permittivity of a vacuum (=1). ε_r is a complex quantity with a real and imaginary component, although the imaginary part can be neglected concerning the field of study and its small contribution (Topp et al., 1980).

Since the soil is a composite material, the measured permittivity is made up by the relative contribution of minerals, air and water. The relative permittivity of liquid water Ka_w (=81) is considerably larger than that of the other soil constituents Ka_s (=2–13 for most soil minerals) and air Ka_a (= 1), thus, the Ka is mainly governed by the amount of liquid water (Jones et al., 2002, Chandler et al., 2004). The terms relative permittivity and relative dielectric constant are used interchangeably in this study, although they can have different meanings in certain aspects. Commonly, the relationship between Ka and θ_v is established by an empirical equation (Eq. 2.9) of Topp et al. (1980) that provides estimations of θ_v < 0.5 m^3 m^{-3} in most soils with a θ_v error of ±0.02 m^3 m^{-3} (Evett and Parkin, 2005):

$$\theta_v = -5.3 \bullet 10^{-2} + 2.29 \bullet 10^{-2} Ka - 5.5 \bullet 10^{-4} Ka^2 + 4.3 \bullet 10^{-6} Ka^3 \qquad (2.9)$$

The relationship between Ka and θ_v has been re-established in numerous studies by using physical approaches, such as dielectric mixing and composite sphere models to enhance the general applicability of dielectric sensors and standardise their characteristics (Dobson et al., 1985, Friedman, 1998, Jones et al., 2005). A range of dielectric methods are available on the market, but this review will focus only on the time domain reflectometry (TDR), frequency domain reflectometry (FDR) and capacitance-based techniques due their relevance in this thesis.

2.4.1.2.2.1 Time domain reflectometry (TDR)

TDR is a widely accepted EM method, which was developed to sense soil water content and made operational in the 1980s by Hoekstra and Delaney (1974) and Topp et al. (1980). In an operating TDR device, very short, precisely timed EM pulses are generated and sent along metallic rods (length L), at a bandwidth of 0.02-3 GHz, which are part of the so called transmission lines (Fig. 2.4 (A)) (Robinson et al., 2003, Romano, 2014).

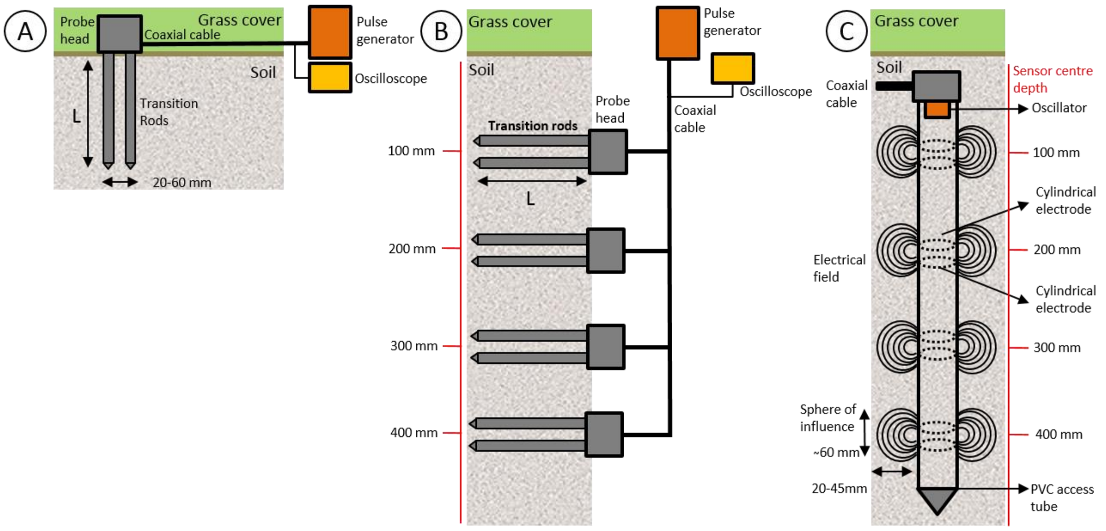

Figure 2.4 Schematic design of a rod type TDR installed vertically (L = rod length) (A), multiple TDR sensors for soil profile monitoring placed horizontally (B) and a multi-sensor capacitance-based probe with ring electrodes.

By measuring the travel time of the propagating EM wave along the probe inserted in the soil, the soil Ka can be determined (Dobriyal et al., 2012). The propagation velocity of the travelling pulse is strongly controlled by the soil moisture content; hence, it can be related to θ_v. The instrument is equipped with 2-3 rods that are inserted in the soil, and a digitiser detects changes in the energy levels along the transmission lines. The use of high frequency pulses provides a less susceptible response to soil specific properties (Robinson et al., 2008b). However, soil salinity or highly conductive heavy clay contents may affect TDR, as it contributes to attenuation of the reflected pulses (Ferrara and Flore, 2003) and the rods need to be installed horizontally from a soil pit which is a considerable disadvantage of the technique (Fig. 2.4 (B)).

2.4.1.2.2.2 Frequency Domain (FD) techniques

Frequency domain (FD) sensors have been favoured in agricultural applications, such as real-time, feedback based irrigation control systems (Stacheder et al., 2009). Although they are less precise than the neutron probes (Gabriel et al., 2010, Wendroth et al., 2013), FD probes offer a low cost alternative (Paltineanu and Starr, 1997). FD reflectometry (FDR) and capacitance methods are often discussed simultaneously since both belong to the frequency domain (FD) group (Romano, 2014). The basic idea behind FD methods is that a capacitor can be formed between two or more electrodes (metal rods, spikes or rings) and the surrounding soil medium, therefore the electrical capacitance is dictated by Ka. FDR techniques differ from the TDR in that the former measures the variation in frequency of the returned EM pulses. FDR instruments detect the swept frequency, i.e. it records data over a range of frequencies (Lekshmi et al., 2014).

Capacitance-based sensing devices also make use of the FD, although they measure the charging time of the generated capacitance field that extends into the soil medium (Mittelbach et al., 2012). An oscillator is often connected to the circuit, that converts the changes in Ka to the variation in the frequency of the transmitted signal between the electrodes (Leib et al., 2003, Lekshmi et al., 2014). If circular shaped electrode configuration is used, the electric components (electrodes, oscillator) are often inserted into a PVC access tube (Fig. 2.4 (C)).

The frequencies used in FD devices (20-300MHz) are lower than that of TDR, which causes sensitivity to soil properties (Romano, 2014), therefore FD sensors require the development of soil-specific calibration curves (Blonquist et al., 2005). The sphere of influence is relatively small (radius up to 5-6 cm) (Gabriel et al., 2010) making the correct installation crucial to ensure optimal sensor to soil contact for accurate data acquisition. Despite these drawbacks, obtaining multi-depth θ_v data by field-calibrated FD instruments has been receiving growing interest especially in the field of precision agriculture.

2.4.1.2.3 Other indirect methods

Since several further indirect techniques have been developed, a brief overview is given without any intention to provide a complete synopsis. Describing each technique in detail is beyond the scope of this thesis, therefore the reader is referred to the cited material for further information.

Additional indirect methods include amplitude domain reflectometry (Muñoz-Carpena et al., 2004), soil resistance sensors, time domain transmission (Blonquist Jr et al., 2005) thermal dissipation block technique (Dias et al., 2011), tensiometers, gypsum block method, pressure plate method (Dobriyal et al., 2012), free line sensing (Stacheder et al., 2009), gamma-ray scanners and hygrometric techniques (Zazueta and Xin, 1994).

The popularity of non-invasive, contactless sensing of soil moisture has been growing, along with an increasing demand for large scale, regular, high spatial resolution products. Bogena Heye R. et al. (2015) summarised the sensing of soil moisture by cosmic-ray neutron probes, Global

Navigation Satellite System reflectometry, ground-based microwave radiometry, gamma-ray intensity monitoring, terrestrial gravimetry and low frequency EM surface waves. In recent years, cosmic-ray probes have been emerging, as they are able to sense the integrated soil moisture from a profile down to approximately 75 cm (depending on wetness) and with a horizontal footprint of about 330m. The probes make use of secondary fast neutrons generated by the incoming, primary cosmic-ray particles. As the neutrons make their way back to the soil surface, the amount of escaping particles is a function of the soil water content (Vereecken et al., 2014).

Proximal methods, such as electrical resistivity tomography, ground penetrating radar (GPR) (Lunt et al., 2005), EM induction (EMI) and optical (Vis-NIR) field-spectroscopy (Adamchuk and Rossel, 2010) are referred to as non-invasive, hydro-geophysical approaches. Their soil moisture outcome is commonly compared or combined with TDR or neutron probe estimations (Huisman et al., 2002). Proximal techniques offer promising alternatives to occasional surveys with high spatial resolution to map the spatial distribution of soil properties filling the gap between the point like and remote sensing methods (Robinson et al., 2012, Romano, 2014).

2.4.1.3 Ground-based wireless soil moisture data management

The above-mentioned methods have limitations regarding the spatial scale or the temporal density of data collection. With the development of micro-electro-mechanical systems and computer science, the wireless sensor network (WSN) technology has advanced and can offer new, promising possibilities besides the initially prevalent military applications (Romer and Mattern, 2004, Yick et al., 2008). WSNs provide a wireless communication protocol to send sensor data to remote end users. These networks aim to bridge the gap between the small (point to field) and the larger spatial scale (catchment-regional) terrestrial environmental observations.

A WSN is composed of a collection of spatially distributed, autonomous devices, called sensor nodes, organised into a cooperative network that communicates wirelessly and forwards data to the gateway (also known as base station or centre connecting point) (Verdone et al., 2010, Rawat et al., 2014). These nodes are usually equipped with a processor, a radio interface, an analog-to-digital converter, sensors, memory and a power supply. Sensors are connected to the wireless nodes that are linked to the gateway unit via radio communication. Wireless internet connection is established between the gateway's modem and a server, which hosts the data.

Once the WSN has been deployed, the network can operate without continuous supervision and perform data acquisition, logging and reporting functions (Yick et al., 2008). WSNs are commonly deployed for soil moisture monitoring as they allow near-real time data access at increased temporal, spatial and vertical resolutions, thus eliminating some of the limitations caused by conventional ground sampling. Due to the advantages offered by WSNs, observing networks are utilised in precision irrigation scheduling (Hedley et al., 2012, Ekanayake and Hedley, 2018), characterisation of hydrological fluxes, calibration and validation of remote sensing data (Dorigo et al., 2015) and soil moisture variability investigations (Kerkez et al., 2012, Majone et al., 2013).

2.4.1.3.1 Topologies, deployment strategies and node architectures

In this study, a "one of a kind" WSN was deployed for ground-based θ_v data collection in hilly environment that required a well-planned design to ensure unobstructed communication and data transfer. Therefore, a basic review is provided to understand the main issues during a WSN installation and its various structures for environmental observation.

For most WSNs the critical design step is the selection of representative sensor locations of the targeted region. Sensor nodes can be deployed randomly, in an ad hoc manner, or installed at pre-planned locations depending on the application, the environment and the sensor types (Buratti et al., 2009, Abdollahzadeh and Navimipour, 2016). A well-designed network is flexible and it is possible to increase the number of nodes or to replace devices without disturbing the data collection (Bogena et al., 2010).

There are many factors influencing the WSN design comprising failure probability, scale dependency, installation and maintenance costs, environmental conditions, topology, hardware, transmission media and power supply (Akyildiz et al., 2002). The WSN topology (i.e. the geometric properties and spatial relations of the WSN) determines major network characteristics, such as data routing and processing, diameter and robustness (Romer and Mattern, 2004). Logical topologies characterise how a sensor node communicates with other nodes. Townsend & Arms (2005) described three topologies (star, mesh and hybrid) commonly utilised in WSNs.

A star network (1) is a simple communication structure, where the remote nodes are connected wirelessly to a single gateway. Sending and receiving data are only permitted between a single base station and a remote node (a.k.a. single-hop communication). However, this topology is prone to single point failure and there is no alternative routing path.

In contrast, a mesh network (2) setup allows for any node to transmit to any other node in the WSN that is within its radio range, enabling multi-hop communications among the sensor nodes. Therefore, if a device is set to transfer data to an out of range node, or there is a communication barrier (topography, buildings, trees, etc.), it can use any node as relay to forward the message to the desired destination. Mesh networks may form an arbitrary and self-healing structure with several message paths.

A hybrid star-mesh network (3) is the combination of the previous two types and provides a robust and versatile communication network while maintaining the ability to keep the wireless sensor node power consumption to a minimum. It is also known as partial mesh topology, meaning that some nodes are enabled to operate in a multi-hop manner and the rest of the nodes are only connected to those nodes they most frequently communicate to. The hybrid topology utilises all the advantages of the star and mesh networks (Romer and Mattern, 2004, Townsend and Arms, 2005, Sharma et al., 2013a, Sharma et al., 2013b, Rawat et al., 2014).

2.4.1.4 Global ground-based in situ soil moisture observations

Remote sensing techniques and land-surface models have been serving several environmental simulation systems by providing operational global soil moisture products (Rodell et al., 2004, Drusch and Viterbo, 2007, Dorigo et al., 2011b). The required input data varies with applications; satellite missions would only sense soil moisture in the top soil layer depending on the sensor type. Land-surface models usually operate on a layer-based manner and require input data from the near-surface as well as the deeper sections of the soil profile (Bruckler et al., 1988, Wagner et al., 1999a, Albergel et al., 2012, Choi and Hur, 2012).

Systematic soil moisture data acquisition was started in the 1930s using mainly repeated direct, gravimetric methods at weather stations (Robock et al., 2000b). In the following decades, more and more countries were interested in soil moisture monitoring and deployed their own research stations to establish observation networks. However, the datasets suffered from inconsistent techniques and protocols that led to significant variation in the data. In the 1990s, in situ soil moisture data from around the globe was made available through the Global Soil Moisture Data Bank (Robock et al., 2000a). This database served as a starting point for the revolutionary international cooperation and resulted in the establishment of the International Soil Moisture Network (ISMN) in 2009. ISMN is a centralised data hosting facility, which collects and harmonises the in situ soil moisture data acquired by a large variety of individually operating networks. ISMN makes the data available for the geoscientific community through their data portal at https://ismn.geo.tuwien.ac.at/data-access/ (Dorigo et al., 2011a, Dorigo et al., 2011b, Dorigo et al., 2013).

2.4.2 Remote sensing of soil moisture

While soil moisture information is still of great importance at the point scale, the opportunities lying behind large-scale observations from satellites (i.e. catchment, region, continent or global) have turned scientists to the rapidly evolving remote sensing or Earth observation techniques. In the context of remote sensing, the information about physical objects is carried by the long-range EM and gravitational fields (Robinson et al., 2008a). Consequently, remote sensing can be defined as the science of physical information obtained by a device from a determined distance through the analysis of the received EM or gravimetric signal after interaction with the object, area or phenomenon of interest (Sharkov, 2003, Lillesand et al., 2014). Satellite gravimetry is still among the emerging methods and can only be applied on an irrelevant large scale considering the aim of this study (Tapley et al., 2004, Rodell, 2012). Thus, only the methods that make use of the EM energy will be discussed here.

On this basis, remote sensing of soil moisture refers to those non-invasive, contact free techniques that acquire observations via the EM spectrum from a remote position without getting in direct contact with the soils. Sensors for remote observation of the Earth surface are dominantly mounted airborne and spaceborne platforms but can also be installed on towers providing a footprint range of m^2 to thousands of km^2 (Wagner et al., 2007). Spaceborne platforms are frequently preferred as they provide global coverage on a regular basis offering consistent datasets and quality.

Remote sensing methods are subdivided into two groups primarily distinguished based on the source of EM energy used (Mladenova et al., 2014). Passive methods (1) provide only reception of the variation in the EM field reflected or emitted from a natural source, while active techniques (2) emit energy from their own illumination source and receive the reflected signal from the investigated objects (Sharkov, 2003). The main components of the remote sensing process are illustrated in Figure 2.5 for passive and active methods.

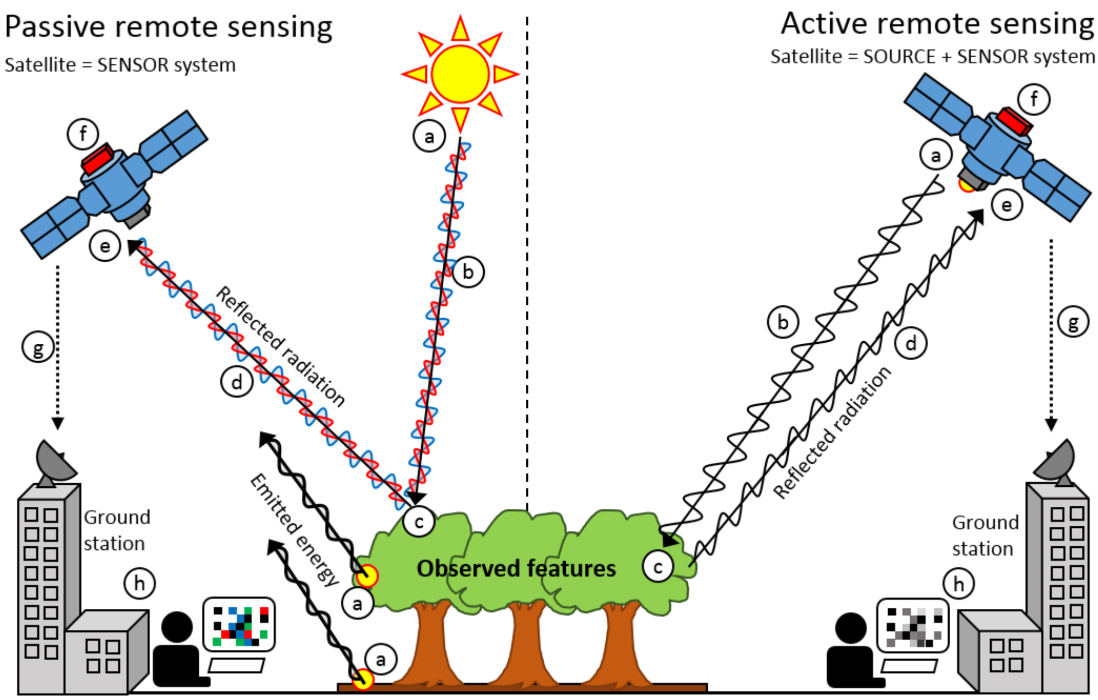

Figure 2.5 Components of remote sensing processes: source of energy (a), propagation of energy through the atmosphere (b), interaction (c), radiation towards sensor (d), detection of electromagnetic signal (e), generation of sensor data (f) and transmission of data to Earth (g) and interpretation of data (h) (Lillesand et al., 2014).

Since the 1970s, remote sensing approaches for soil moisture observations have drawn the researchers' attention and the potential of large-scale soil moisture observation has been investigated intensively (Ulaby et al., 1986c, Schmugge and Jackson, 1994, Wagner et al., 1999b, Chen et al., 2012, Ochsner et al., 2013). The considerable role of soil moisture in environmental systems triggered many attempts to retrieve surface soil water content information using various regions of the EM spectrum. Changes in the EM field can be detected and related to a number of soil parameters (Robinson et al., 2008a). The highest potential for soil moisture retrieval was found in the application of the optical (Vis, NIR, SWIR), thermal infrared (TIR) and microwave regions (Maltese et al., 2013, Rahimzadeh-Bajgiran et al., 2013).

Optical remote sensing of soil moisture uses the 0.4-2.5 μm domain of the EM spectrum and measures the solar energy reflected back from the land surface (Petropoulos, 2013). The early optical remote sensing over bare soil surfaces made use of the fact that wet soil is darker than dry soil (Kerr et al., 2010). Optical spectral reflectance at various water absorption wavelength regions (around 1.2, 1.4 and 1.9 μm) was observed to be sensitive to soil water content, showing that reflectance generally drops with increasing soil moisture (Anne et al., 2014, Fabre et al., 2015). Over vegetation, the Vis-NIR-SWIR bands are able to sense the change in plant biophysical and biochemical characteristics which are strongly dependent on water (Gao et al., 2013). Thus, vegetation indices, such as Normalized difference Vegetation Index (NDVI) and Normalized

Difference Water Index (NDWI) have been developed to indicate the physiological state of the vegetation and indirectly the soil moisture (Peters et al., 2002).

TIR remote sensing proved its capability to map soil moisture in deeper depth than optical methods by using the 3.5-14 μm wavelength range (Schmugge et al., 1980, Behari, 2006, Anderson et al., 2007). The most commonly applied technique is the thermal inertia approach (Price, 1977), the generation of crop water stress index, water deficiency index and temperature vegetation index (Gao et al., 2013). The thermal inertia method is built upon the diurnal cycle of land surface temperature and the principle that heat capacity and heat conductivity of the land surface is impacted by the soil water content. By knowing the amplitude of diurnal temperature change, a model function can be developed to predict soil moisture, because the increase in soil water content reduces the diurnal temperature fluctuation, thus the thermal inertia proportionally increases (Petropoulos, 2013, Zhao and Li, 2013, Zhang and Zhou, 2016).

Optical and TIR approaches have numerous limitations due to the coarse temporal resolution and the atmospheric effect, night effect, vegetation, soil properties, surface roughness and cloud cover (Behari, 2006, Kerr et al., 2010, Zhang and Zhou, 2016). Moreover, optical bands can interact only with the top few millimetres of bare soil or the surface of the plant leaves and stems which allows only the indirect retrieval of soil water content (Petropoulos et al., 2015, Sabaghy et al., 2018).

By using specific sections of the microwave region of the EM spectrum (0.1-100 cm), numerous limitations related to the optical and TIR methods can be eliminated, placing the active and passive microwave sensing among the preferred methods for spatial soil moisture mapping.

Furthermore, synergistic methods are able to derive soil moisture from a combination of several remotely sensed information obtained at various regions of the EM spectrum. Common fusion-based methods include the synergistic use of optical and thermal earth observation data (i), the combination of active and passive microwave observations (ii) and the fusion of microwave and optical or thermal infrared acquisitions (iii) (Petropoulos et al., 2015).

2.5 Microwave-based soil moisture remote sensing

2.5.1 Physical background

The EM waves applied in soil moisture remote sensing covers an extensive range from the short, 400 μm to long, 1 m wavelengths. The shortest wavelengths of the radio spectrum, the microwaves, refer to the approximate frequency range of 0.3-300 GHz corresponding to a wavelength range between 1 m and 1 mm shown (Fig 2.6) (Behari, 2006, Petropoulos, 2013).

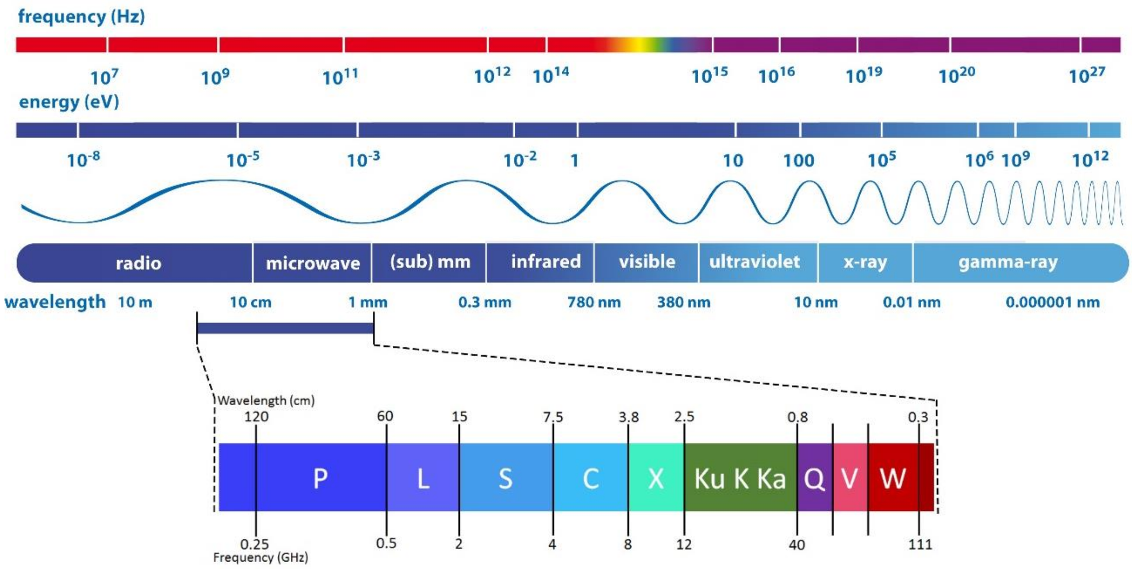

Figure 2.6 The electromagnetic spectrum (European Space Agency, 2012) and the band designation of the microwave region used in microwave remote sensing (Ouchi, 2013).

This region is effectively independent of solar illumination and the sensed intensity depends on the objects' radiative, dielectric, physical, chemical, geometrical and thermal characteristics (Sharkov, 2003). The microwave domain can be subdivided into several bands (Fig. 2.6). Most studies found the low-frequency (X, C and L band) microwave sensing the most suitable for quantifying soil moisture (Behari, 2006, Calvet et al., 2011, Dobriyal et al., 2012). These findings made use of the large contrast between the Ka of dry and wet soils (Schmugge et al., 2002). L-band has been the preferred choice for many satellite missions, but C and X bands carry useful information regarding soil moisture if the vegetation is not too dense (Calvet et al., 2011).

2.5.2 Passive microwave remote sensing

Passive instruments usually detect the intensity of the naturally reflected or emitted energy from the land surface. This energy either travels in the form of reflected solar radiation in the Vis and NIR regions or emitted energy in the TIR or microwave regions (Schmugge et al., 2002, Petropoulos et al., 2015). Every object that has a temperature higher than the absolute zero (-273.15 °C) emits EM waves (thermal bands). Passive microwave remote sensing (radiometry) is able to detect the radiated energy in the 1-30 cm region which is usually expressed in the form of brightness temperature (Petropoulos, 2013). The thermally generated radiation is less sensitive to surface roughness, soil parameters and land cover (Das and Paul, 2015a), although it is largely influenced by soil water (Njoku and Entekhabi, 1996, Behari, 2006, Rees, 2013). Passive sensors require large antennas to detect the thermal radiation that limits the spatial resolution.

2.5.3 Active microwave remote sensing

Active microwave platforms (radars) measure the magnitude of artificially generated energy that is reflected, scattered back from the land surface or the targeted objects in the radio region (Schmugge et al., 2002, Seneviratne et al., 2010, Lillesand et al., 2014). Radars may or may not produce images. Radars mounted on satellites are mainly imaging systems that use the synthetic aperture radar (SAR) technology producing continuous strips of imagery from a side-looking position (Rees, 2013, Lillesand et al., 2014). SAR systems utilise an advanced signal processing technique to synthesise the antenna length and a large aperture (Warner et al., 2009, Rees, 2013). The coherency of the emitted signal allows the creation of aperture synthesis and when combined with the time history of radar echoes results in the high spatial resolution of SAR images (Sharkov, 2003, National Academies of Sciences and Medicine, 2015). SAR imagery is a major contributor to the objectives of this thesis.

2.5.4 Spaceborne missions for microwave-based soil moisture observations

Both passive and active microwave remote sensing have been of great importance in terms of remotely sensed soil moisture retrieval in the past four decades (Ochsner et al., 2013, Wagner et al., 2013, Mohanty et al., 2017). Hence, several space missions have been used for deriving soil moisture even though they have initially not been foreseen to observe soil water (Table 2.1) (Brocca et al., 2010b, Liu et al., 2011, Mladenova et al., 2014). These missions are characterised by approximately 25-150 km spatial resolution with varied revisit time, which are the cause of several limitations. Nonetheless, promising correspondences were found between satellite derived and ground-based data, closely reproducing the temporal dynamics of in situ soil moisture (Brocca et al., 2010a, Dorigo et al., 2015).

Table 2.1 Overview of spaceborne, microwave-based missions relevant for soil moisture applications (λ - frequency, EOL - End of Life, A-active, P - passive, rad - radiometer, scat -scatterometer, con - constellation).

Type	*Satellite*	*Agency*	*Launch*	*EOL*	*Instrument*	*Band / λ (GHz) / polarisation*	*Revisit (d)*	*Spatial res.*
P	SKYLAB	NASA	1973	1977	S-194 rad.	L /1.4 / HH	NA	*110km*
P	NIMBUS 7	NASA	1978	1994	SMMR rad.	C-Ka / 6.6. 10.7. 18.0. 21.0. 37.0 / V. H	2	*22-120km*
A/P	SEASAT	NASA	1978	1987	SAR	L / 1.275 / HH. VV	2	*25m*
				1987	SMMR rad	C-Ka / 6.6. 10.7. 18.0. 21.0. 37.0 / V. H	2	*22-120km*
P	DMSP	USDD	1987		SSM/I	K / 19.4 / V. H	0.5	*13-69km*
A	ERS 1	ESA	1991	2000	AMI in SAR or SCAT	SAR: C / 5.3 / VV: SCAT: C / 5.3	3-4	*50km*
A	JERS-1	JAXA	1992	1998	SAR	L / 1.275 / HH	44	*18m*
A	ERS 2	ESA	1995	2011	AMI in SAR or SCAT	SAR: C / 5.3 / VV: SCAT: C / 5.3	3-4	*50km*
A	RADARSAT 1	CSA	1995	2013	SAR	C / 5.3 / HH	24	*10-100m*
P	TRMM	NASA/JAXA	1997	2015	TMI	X-W / 10.7. 19.4. 21.3. 37. 85.5 / V.H	1	*25-38km*
P	OCEANSAT-1	ISRO	1999	2001	MSMR rad	C-Ka / 6.6. 10.7. 18. 21 / HH. VV	2	*50-150km*
A	ENVISAT	ESA	2002	2012	ASAR	C / HH. VV. HV. VH	5	*30-1000m*
P	AQUA	NASA	2002		AMSR-E rad	C-W/ 6.9. 10.6. 18.7. 23.8. 36.5. 89 / V. H	2	*25-50km*
A	CORIOLIS	NASA/DOD	2003		WINDSAT	C-Ka / 6.8. 10.7. 18.7. 23.8. 37 / full	1.5-8	*8-71km*
A	ALOS	JAXA	2006	2011	PALSAR	L / 1.27 / full	46	*10-100m*
A	METOP A	ESA	2006		ASCAT scat	C / 5.25 / VV	2	*25-50km*
A	RADARSAT 2	CSA/MDA	2007		SAR	C / 5.4 / multi	24	*10m*
A	TERRASAR X	DLR	2007		SAR	X / 9.65 / HH. VV. VH. HV	4-11	*1-40m*
A	COSMO-SKYMED con. (4)	ASI	2007-2010		SAR-2000	X / 9.65 / multi	0.5-14	*1-100m*
P	SMOS	ESA	2009		MIRAS rad	L / 1.4 / full	3	*30-50km*
A	TANDEM X	DLR	2010		SAR	X / 9.65 / HH. VV. VH. HV	2.5	*1-16m*
A/P	AQUARIUS SAC-D	NASA/GSFC	2011	2015	AQUARIUS scat	L / 1.26 / full	7-8	*100-150km*
P	GCOM-W1	JAXA	2012		AMSR-2 rad	C-W/ 6.9. 7.3. 10.6. 18.7. 23.8. 36.5. 89 / V. H	2	*25-50km*
A	METOP B	ESA	2012		ASCAT scat	C / 5.25 / VV	1.5	*25-50km*
				2015	AQUARIUS rad	L / 1.41 / full	7-8	*100-150km*
A	SENTINEL-1 con. (2)	ESA	2014. 2016		SAR	C / 5.405 / multi	6-12	*10m*
A	ALOS-2	JAXA	2014		PALSAR-2	L / 1.2 / HH. VV + HV. VH	14	*10-100m*
A/P	SMAP	NASA	2015	2015	SMAP SAR	L / 1.26 / VV. HH. HV	2-3	*3km*
			2015		SMAP MW rad	L / 1.41 / full	2-3	*40km*

Dedicated satellite missions designed for global soil moisture measurements appeared relatively late. First, the Soil Moisture and Ocean Salinity (SMOS) mission was launched in 2009 by the European Space Agency (ESA) (Mecklenburg et al., 2012) which was followed by NASA's Soil Moisture Active Passive (SMAP) program in 2015. The SMOS satellite is equipped with and L-band radiometer recording the surface's brightness temperature at a spatial resolution of 50 km with an accuracy of ±0.04 m^3 m^{-3} every three days. The basic idea behind the SMAP mission was to merge the coarse resolution but highly sensitive passive and high-resolution active microwave observations for the first time, and achieve an improvement in resolution and accuracy (Entekhabi et al., 2010b). Unfortunately, a component of the L-band radar instrument failed in the same year leaving only the radiometer operational, generating 36 km pixel size passive soil moisture products (Ming et al., 2016, Das et al., 2018).

Potential future missions, summarised in Table 2.2, will be able to provide soil moisture retrievals at higher spatial and temporal resolution and will open a market for new applications (Mohanty et al., 2017). The number of SAR missions are on the rise and already either in the planning or developmental phase. The commonly followed open data policy will allow more widely available datasets for research and educational purposes.

Table 2.2 Overview of the future space borne missions that will open new possibilities for soil moisture retrieval and global applications (λ - frequency, EOL - End of Life, A-active, P - passive, rad - radiometer, scat -scatterometer, con - constellation (number of satellites).

Type	*Satellite / Mission*	*Agency*	*Planned launch*	*Planned EOL*	*Instrument*	*Band / λ (GHz) / polarisation*	*Revisit (d)*	*Spatial res.*
A	RADARSAT con. (3)	CSA and more	2018	2025	SAR	C / 5.4 / multi	4-12	3-100m
A	METOP C	ESA	2018	2024	ASCAT	C / 5.3 / VV	1.5	12.5-50km
A	METOP SG	ESA	2021		SCAT	C / 5.3 / VV , VH		15-20km
A	SAOCOM con. (4)	CONAE/ASI	2018	2023	SAR	L / 1.27 / multi	8-16	10-100m
A	NISAR	NASA/ISRO	2020		SAR	L, S / polarimetric	12-60	0.1-50km
A	TERRASAR-X NG	DLR	2020-2022		SAR	X / 9.65 / multi	2.5	1-16m
A	PAZ	INTA	2018		SAR	X / 9.65 / multi	11	1-15m
A/P	WCOM	CAS	2020		FPIR	L, S, C / ~1.41, ~2.65, ~6.7 / full	2-3	15-50km
A	TANDEM L	DLR	2022		SAR	L / 1.2 / full	8-16	50-500m
A	COSMO-SKYMED SG con. (2)	ASI	2018	2026	SAR 2000 SG	X / 9.6 / multi	1.5-10	1-35m

2.5.5 Main characteristics of Synthetic Aperture Radar (SAR) remote sensing

A SAR image pixel represents measurements of physical processes, expressed as digital numbers. The fundamentals of radar backscattering was presented by Ulaby et al. (1982a) providing the relationship between the received and the transmitted power. A common form of the 'radar equation' is given by Eq. (2.10) (Ulaby et al., 1981) that establishes the relationship between received power on the antenna P_r (W) and power reradiated by a single target:

$$P_r = \frac{P_t G_t G_r \lambda^2}{(4\pi)^3 \eta R^4}\sigma \tag{2.10}$$

Where P_t is the transmitted power (W), G_t is the power gain on transmit, G_r is the power gain on receive, λ is the wavelength (m), R is the distance between the radar and the target (m), η is the efficiency of the antenna and σ is the scattering cross section (m^2). SARs measure an infinite collection of statistically identical signals from a target volume. Therefore, Eq. (2.10) is extended to gain the backscattering coefficient or cross-section per unit surface area σ^0 ($m^2\,m^{-2}$) (Ulaby et al., 1996). The value of σ^0 quantifies the signal intensity and represents the power loss caused by the interaction mechanisms. The σ^0, for a given SAR configuration, can be expressed by dividing the mean σ with the illuminated area A_0 (m^2) as per (Eq. 2.11).

$$\sigma^0 = \frac{\langle\sigma\rangle}{A_0} = \frac{4\pi R^2 \langle|E_s|^2\rangle}{A_0 |E_i|^2} \tag{2.11}$$

Where E_s is the scattered electromagnetic field and E_i is the incident EM wave intensity.

Due to its wide dynamic range, σ^0 is usually converted to decibels (dB) (Rees, 2013) by Eq. (2.12) presented in (Ulaby et al., 1996), where *i, j* = transmit and receive signal polarisation.

$$\sigma^0_{i,j}(dB) = 10\,log\,\sigma^0_{i,j}(m^2\,m^{-2}) \tag{2.12}$$

2.5.5.1 The side-looking SAR geometry

The basic geometry of an operating, spaceborne SAR imaging system is shown in Figure 2.7 (A). As the SAR platform moves along the flight path, short, high-frequency pulses are transmitted from an antenna perpendicular to the SAR propagation direction (azimuth direction) at an off nadir angle (look angle) θ_{off} at the order of microseconds (Ouchi, 2013, Rees, 2013). The θ_i is defined as the angle between the illumination direction (slant range direction) and the vertical direction at the point of interaction. Ground range direction is the projected slant range direction to the ground. The intersection of the radar beam (characterised by the azimuth beamwidth) and the surface defines the width of an image swath (Rees, 2013). Range resolution is the function of the bandwidth of the radar pulse and it allows the separation of ground features located close to each other. The azimuth resolution depends on the azimuthal beamwidth, slant range and the signal-processing algorithms. The deterioration of azimuth resolution is eliminated by SAR, (Warner et al., 2009, Lillesand et al., 2014).

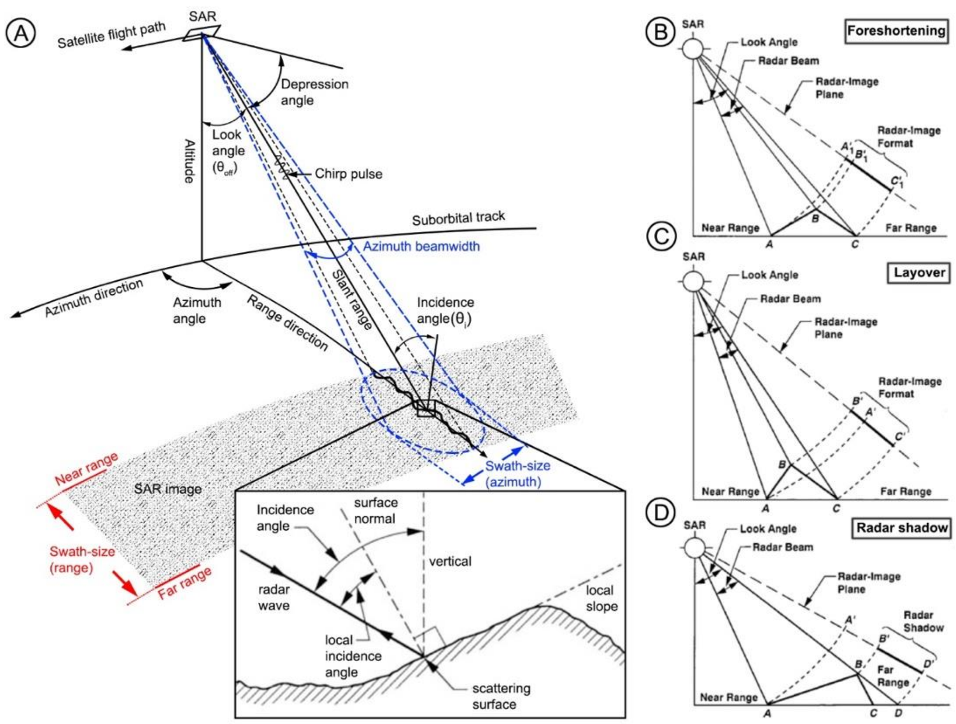

Figure 2.7 Illustration of a side-looking SAR system geometry in operation (A) and the main geometric distortions (B, C, D). Modified after Ouchi (2013) and Ford et al. (1993).

The collectively utilised side-looking geometry allows high spatial resolution images, although the configuration induces geometric distortion effects (Fig. 2.7 (B) and (D)), especially over undulating terrain (Jensen, 2009). As SARs measure travel time and the backscattered signals are projected to an image reference plane, the process can lead to the phenomena of foreshortening and layover. In case of foreshortening, the slopes oriented towards the SAR appear compressed along the range direction (Fig. 2.7 (B)) while the backslope is extended by the temporal shift of the signal (Braun and Hochschild, 2017).

Steep slopes may result in layover effects, if the valley has a larger slant range than the top of the slope, thus the image will show a reversed order of the observed points compared to their real position (Fig. 2.8 (C)). Due to topographic effects, radar shadow (zero returned signal) may appear on the images (Fig. 2.8 (D)) if the slopes oriented away from the sensor are steeper than the SAR's depression angle (Warner et al., 2009, Lillesand et al., 2014). These effects are taken into account during the image processing by using a digital elevation model (Bayer et al., 1991).

2.5.5.2 Basic scattering processes

The nature of interaction and the magnitude of the σ^0 upon contact with the target object are dependent mainly on sensor and target properties (Mahdavi et al., 2017). Polarisation, θ_i and frequency are the primary sensor properties, whereas target parameters include surface roughness, topography, soil properties (Ka, soil texture) and vegetation cover (biomass, geometry, structure, orientation and dielectric features) (Ogilvy and Merklinger, 1991, Moran et al., 2004, Patel et al., 2006, Anguela et al., 2010, Kornelsen and Coulibaly, 2013, Braun and Hochschild, 2017). The radar beam can be absorbed, scattered, reflected, double-bounced and it can penetrate into the objects and become further absorbed or scattered (Fig. 2.9) (Kornelsen and Coulibaly, 2013). In general, three main scattering processes are discussed, i.e. surface scattering, volume scattering and double-bounce scattering (Zou et al., 2015).

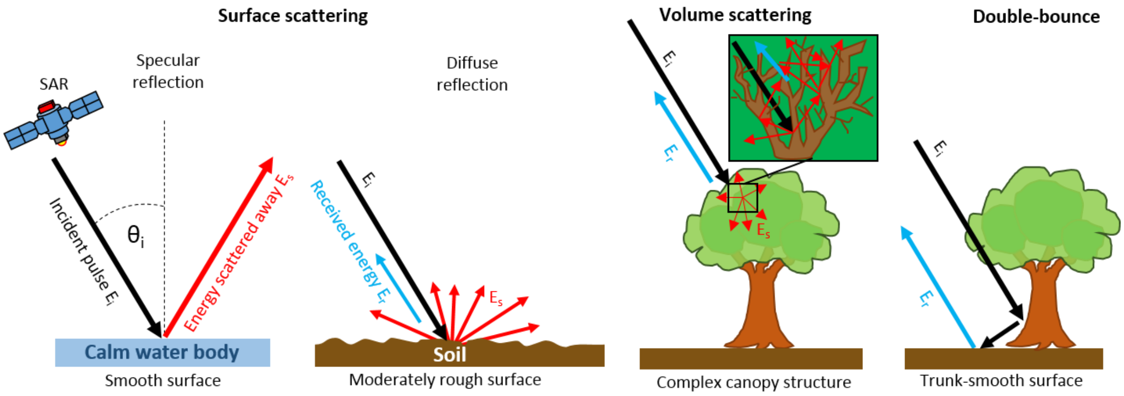

Figure 2.8 Schematised elementary scattering processes of an incident radar signal over smooth, rough surfaces and vegetated land (E_s - scattered electromagnetic field, E_i - incident electromagnetic wave intensity, E_r - received energy).

In a specific case of surface scattering, a smooth surface can act similar to a mirror and reflect the incident radiation away from the SAR. The process is known as specular scattering and it commonly occurs over calm, smooth water surfaces, flooded soils, sealed roads and it can be present over very smooth bare soils (Lillesand et al., 2014). Diffused surface reflection occurs if the transmitted energy pulse interacts with a homogenous media such as soil scattering the incoming wave in all directions (incoherent component) mainly governed by the surface roughness (Moreira et al., 2013).

Volume scattering is the process, when the incident illumination enters an inhomogeneous medium, such as vegetation and the discrete elements (leaves, stems, branches) scatter the incident wave in multiple directions.

In the particular situation whereby the incident radar pulse is reflected away from the sensor direction by a horizontal (or vertical) surface but it bounces back from a vertical (or horizontal) structure (i.e. tree chunks, trunks, high buildings, smooth surfaces), double-bounce scattering occurs. Thus, manmade features adjacent to smooth surfaces usually appear with particularly high σ^0 on SAR images (Warner et al., 2009, Lillesand et al., 2014).

2.5.5.3 SAR configuration

High θ_i, can cause little or no energy return because of the specular reflection on smooth surfaces, whereas high depression angles, i.e. low θ_i, may be received by the SAR resulting in stronger backscatter (Dobson and Ulaby, 1986, Sabins, 2007). Due to the side-looking geometry, radars are extremely sensitive to the θ_i and terrain relation (Toselli, 1987).

The illumination frequency determines the wavelength; hence, it affects the backscattering properties defining which parts of the target take part in the interaction (Chen et al., 2014). The long P-waves are able to penetrate the vegetation canopy providing more information about the soils, while L-band is more sensitive to vegetation cover and plant density (Patel et al., 2006, Moreira et al., 2013). Shorter wavelengths are optimal for vegetation canopy and biomass sensing, since they are not able to penetrate the canopy completely (Lillesand et al., 2014).

To obtain more information from images, SARs apply multiple polarisation modes, such as co-polarised VV or HH, and cross-polarised VH or HV (Ulaby et al., 1996, Robinson et al., 2008a). The first letter denotes to the polarisation of the transmitted wave whereas the second letter refers to the polarisation of the received wave (V-vertical, H-horizontal) (Robinson et al., 2008a). However, due to the geometric structure and dielectric properties of the target, a portion of the radar signal is depolarised creating cross-polarised σ^0 (Toselli, 1987). Cross-polarisation was observed to be more sensitive to vegetation parameters than co-polarisation (Patel et al., 2006).

2.5.5.4 Effect of target characteristics on SAR scattering and the inherent noise

The scattering behaviour over natural surfaces is highly dependent on the relative concept of roughness. Surface roughness is often expressed as the root mean square height RMS_h (cm) (Gupta and Jangid, 2011, Bousbih et al., 2017). In remote sensing, the application of the Rayleigh Criterion can estimate whether the surface is rough or smooth (Sabins, 2007, Lillesand et al., 2014). Increasing degree of roughness generally results in increased σ^0, although its effect varies depending on sensor parameters (Ulaby and Batlivala, 1976, Ulaby et al., 1982b, Sano et al., 1998, Wagner et al., 2007, Baghdadi and Zribi, 2016).

The soil and the vegetation dielectric properties, often referred to as complex ε_r and their effects on the radar waves need to be considered (Lillesand et al., 2014). The value ε_r is proportional to the number of water dipoles present (Dobson and Ulaby, 1986). ε_r increase with increasing water content. Free water has the largest effect on the ε_r, although bound water can also impact soil moisture estimates (Njoku and Entekhabi, 1996). If other factors are not taken into account, increasing soil moisture results in increasing Ka that is followed by increasing σ^0 until an insensitivity threshold (Ulaby et al., 1986c, Kornelsen and Coulibaly, 2013).

Vegetation exerts a significant effect on the σ^0 by causing a complex scattering and two-way attenuation of the signal. Consequently, the total σ^0 of a vegetated land-surface is a result of several contributions from surface, volume and multiple scattering and double-bounce (Hajnsek et al., 2009, Wagner et al., 2013). C-band σ^0 is a result of combined scattering and soil-vegetation interaction, suggesting that it can penetrate through the canopy to a certain extent (Ulaby et al., 1986b, Bouman and Hoekman, 1993). The vegetation ε_r, the size, shape and orientation of canopy elements, the growth stage and biomass are the main controlling factors of σ^0 (Ulaby et al., 1986a, Mattia et al., 2003). Ferrazzoli et al. (1992) and Toan et al. (1992) both found that σ^0 increases with increasing amount biomass until a saturation point.

An additional amount of uncertainty is added to the image interpretation as SAR remote sensing (and active systems in general) inherently suffers from a phenomenon called speckle or noise. The active nature and the coherent data processing of SAR imagery introduce seemingly random noise (speckles) to the images resulting in a grainy image appearance (Verhoest et al., 2008, Rees, 2013, Braun and Hochschild, 2017). The interference introduces seemingly random bright and dark pixels. The effect can be reduced by statistical noise modelling or averaging and filtering techniques (Lee, 1981, Rees, 2013).

2.5.6 Soil moisture retrieval from SAR observations

Satellites equipped with SAR are considered as the most successful platforms for the monitoring of soil moisture in an operational manner (Verhoest et al., 2008, Barrett et al., 2009, Petropoulos et al., 2015). Although many affecting factors are present, the backbone of SAR-based soil moisture estimation is the measurement's sensitivity to the contrast between dielectric properties of the soils and water, which acts as a proxy for soil moisture (Barrett et al., 2009, Das and Paul, 2015b, Petropoulos et al., 2015).

The three microwave bands dominantly utilised for soil moisture estimation with ranging sensitivity are the L-band (1-2 GHz, 30-15 cm), C-band (4-8 GHz, 7.5-3.8 cm) and X-band (8-12 GHz, 3.8-2.5 cm) (Wagner et al., 2007, Gao et al., 2017). Due to the diversity of the developed approaches, the methods can be categorised in different ways. In the work of Barrett et al. (2009), model-based approaches, change detection-based approaches and polarimetry are investigated. Kornelsen and Coulibaly (2013) discriminated among empirical, semi-empirical, theoretical (physical), numerical and analytical techniques. Karthikeyan et al. (2017) summarised the main milestones and improvements made in remotely sensed soil moisture research and classified the available active methods as physical, semi-empirical, empirical and change detection models (Fig. 2.9). In this review, only the retrieval methods applicable on vegetated soils are discussed.

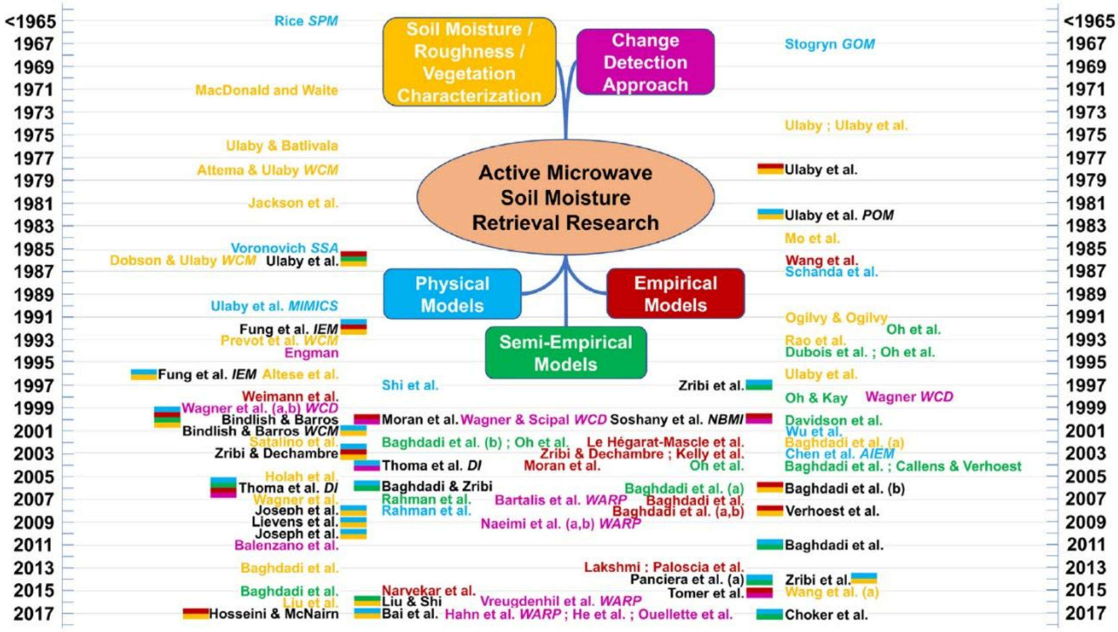

Figure 2.9 Overview of the developed soil moisture retrieval approaches with color-coded citations and algorithms. Citations in black have provided multiple algorithms; the contribution to two or more different approaches is indicated by colour streaks (Karthikeyan et al., 2017).

2.5.6.1 Soil moisture retrieval over bare soil and with vegetation cover

Over bare soil surfaces, the σ^0 can be thought of as a simplified function of the SAR configuration $conf$, including polarisation, wavelength and θ_i, and two main ground-based components, i.e. θ_v, and surface roughness R_s as shown by Eq. (2.13) (Barrett et al., 2009, Aubert et al., 2013, Ouchi, 2013).

$$\sigma^0_{conf} = f_{conf}(\theta_v,\ R_s) \tag{2.13}$$

One of the most problematic tasks is to disentangle the individual effects of roughness and soil water content that usually requires a priori knowledge of the surface parameters (Ouchi, 2013). The soil moisture retrieval is more complicated over vegetated areas partly due to volume scattering. The vegetation cover tends to reduce the sensitivity of σ^0 to soil water content (Ulaby and Batlivala, 1976), as the radar response is influenced by the biomass water content and structure (Vereecken et al., 2012). Therefore, the dependencies of the received radar signal can be described as per Eq. (2.14):

$$\sigma^0_{conf} = f_{conf}\left(\theta_v, R_s, V_{p1}, V_{p2} \dots V_{pn}\right) \tag{2.14}$$

Where $V_{p1}, V_{p2} \dots V_{pn}$ refers to the additional parameters introduced by of vegetation.

Several studies attempted to decompose the σ^0 and gain the contributions from vegetation and surface properties to reduce the bias on θ_v estimations (Freeman and Durden, 1998, Hajnsek et al., 2009, Jagdhuber et al., 2013, Ullmann et al., 2016). The σ^0 can be defined as a composition of three main components as per Eq. (2.15) (Ulaby et al., 1996):

$$\sigma^0 = \tau^2 \sigma_s^0 + \sigma_{dv}^0 + \sigma_{int}^0 \qquad (2.15)$$

Where σ_s^0 represents the contribution from bare soil, τ^2 is the two-way attenuation factor of vegetation, σ_{dv}^0 is the direct contribution of the vegetation layer, while σ_{int}^0 accounts for the interaction between the soil surface and vegetation caused by multiple scattering mechanisms. Eq. (2.17) introduces the basic concept of the semi-empirical Water Cloud Model developed by Attema and Ulaby (1978). The model treats the vegetation canopy as a collection of randomly distributed spherical droplets and models the soil σ^0 affected by vegetation (Barrett et al., 2009). Since most of the real world applications are interested in soil moisture dynamics under vegetation, many attempts have been made to improve the Water Cloud Model parameterisation (Joseph et al., 2008, Kumar et al., 2012, He et al., 2014, Liu and Shi, 2016, Chauhan et al., 2017).

2.5.6.1.1 Change detection methods

If multi-temporal images are available, the effect of surface roughness and vegetation on σ^0 can be assumed constant in time between two acquisitions and there is no need for a priory information of the study area (Gao et al., 2017). This concept is employed by several change detection based soil moisture retrieval approaches such as image differencing and rationing (Engman, 1994, Wagner et al., 1999a, Shoshany et al., 2000, Thoma et al., 2004).

Change detection techniques rely on the assumption that changes in extraneous factors such as vegetation, surface roughness and soil texture occur in a longer time scale than changes in near surface Ka. Consequently, the σ^0 becomes dominantly a function of θ_v variations between two image observation dates (Barrett et al., 2009). By the application of most change detection methods, the relative change in θ_v (if not absolute θ_v content) can be obtained and represented by soil moisture indices (Karthikeyan et al., 2017). Shoshany et al. (2000) presented the Normalised Radar Backscatter Soil Moisture Index (NBMI) for the generalisation of the relationship between σ^0 and θ_v within the 0-40% range, expressed by Eq. (2.16).

$$NBMI = \frac{\sigma_{t1}^0 + \sigma_{t2}^0}{\sigma_{t1}^0 - \sigma_{t2}^0} \qquad (2.16)$$

Where σ_{t1}^0 and σ_{t2}^0 are the backscattered signal at different times t_1, t_2.

In contrast, when a multi-year σ^0 series is available, the acquisitions taken at the historically driest and wettest soil moisture level can be analysed. The operationally used TU-Wien change detection method estimates the relative soil moisture content $m_{s,t}$ by comparing the σ^0 on that particular day t with the historically driest σ^0_{dry} and wettest σ^0_{wet} reference values measured at a reference incidence angle $\vartheta_{i\,ref}$ as per Eq. (2.17) (Wagner et al., 1999b, Moran et al., 2006).

$$\theta_{v,t} = \frac{\sigma^0(t,\vartheta_{i\,ref}) - \sigma^0(t,\vartheta_{i\,ref})}{\sigma^0_{wet}(t,\vartheta_{i\,ref}) - \sigma^0_{dry}(t,\vartheta_{i\,ref})} * 100 \tag{2.17}$$

The product $\theta_{v,t}$ indicates the degree of saturation of the surface soil layer expressed as a percentage. The method has been used in operational global soil moisture retrieval from ASCAT sensors onboard METOP satellites (Wagner et al., 2013, Hahn et al., 2017, Karthikeyan et al., 2017). The primary limitations of the change detection are the temporal resolution of imagery and the constant surface roughness assumption (Lievens and Verhoest, 2011, Kornelsen and Coulibaly, 2013).

2.5.6.1.2 Machine learning

In the past two decades, the research and remote sensing community has made a turn towards more sophisticated techniques regarding the complex, non-linear retrieval problems. Advanced statistical learning functions, implemented in so-called machine learning, can capture this complexity. Several studies reported their success (Kashif et al., 2006, Notarnicola et al., 2008, Paloscia et al., 2008, Ahmad et al., 2010, Ali et al., 2015, Alexakis et al., 2017) in modelling the non-linear, multi-variable relationships among the parameters interacting with the incident radar signal, without having a detailed knowledge about the input parameters' distribution and probability density. Machine learning is commonly used similarly to the conventional inversion methods as the algorithms can be trained to extract information about surface parameters based on various remotely sensed input data (Notarnicola et al., 2008). The dominant machine learning algorithms include the Artificial Neural Networks (ANN) (Baghdadi et al., 2002, Satalino et al., 2002, Pierdicca et al., 2008, Paloscia et al., 2013, Santi et al., 2013) and the Support Vector Machine (SVM) (Lin et al., 2009, Ahmad et al., 2010, Pasolli et al., 2011, Khedri et al., 2017). ANN methods have been found to be more accurate than conventional regression and Bayesian approaches (Notarnicola et al., 2008, Pierdicca et al., 2008). To obtain geophysical and biophysical parameters, including soil moisture, from various land cover types, the non-parametric ANN, SVM and Random Forest (RF) methods have been commonly chosen showing great potential (Lakhankar et al., 2009, Ali et al., 2015, Park et al., 2017, Kumar et al., 2018).

Machine learning is able to ingest data from ground-based and remote sensing sources, as well as taking into account multiple radar configurations, frequently achieving shorter operation time and higher accuracy than conventional methods (Ali et al., 2015). However, as machine learning is a data-driven approach, it usually requires robust and extensive training datasets (Paloscia et al., 2013). Moran et al. (2006) and Barrett et al. (2009) presented a summary and review of several other retrieval techniques along with their advantages and disadvantages.

2.6 Conclusions

This comprehensive survey of the literature demonstrates that soil moisture is a spatially and temporally highly variable environmental and essential climate parameter having a fundamental role in the hydrological cycle. Agronomists, geomorphologists, hydrologist, bio-geographers and climatologist heavily rely on soil moisture data, utilised in a broad range of applications from point to global scale. The key is to understand which scale is appropriate to study for specific purposes, e.g. precision management requires high spatiotemporal resolution, but regional planning can be performed on lower resolution soil moisture information. To meet the objectives of the study, the spatiotemporal behaviour of soil moisture would ideally be examined and modelled on the so-called paddock scale (10-100 m).

Soil moisture is the single most important factor in hill country pastoral agriculture that is responsible for a major part of New Zealand's economic performance. Hill country is principally characterised by high heterogeneity due to the complex landscape, soil and climatic features. The complexity of the land, the lack of detailed soil information and the non-irrigated hill country creates challenges in sustainable land management. Pastoral farming has been under increasing pressure due to the growing food demand and quality requirements. Improved land management can be achieved by the more efficient use of natural and controllable resources such as land, water and fertiliser input. Well timed and better decision making supported by more accurate data acquisitions, fertiliser input strategy and pasture yield predictions are crucial in the enhancement of resilience and sustainable productivity in hill country that can also reduce the environmental impact.

The rugged terrain results in varied pasture growth rates and distribution patterns that make predictions prone to errors on account of the variability caused by topography, soil cover and meteorological forces. An essential part of the simulations is the water balance module, which is well understood for flat surfaces, although only a few studies have approached the challenge of modelling soil water dynamics in the hillslope environment. Therefore, it is one of the weakest points in the algorithms. As environmental heterogeneity within a farm or within the paddocks is significant, the low spatial resolution of the modelled output is subject to uncertainties that are carried along to the fertiliser application planning.

Ground-based methods can provide accurate soil moisture measurements and reliable estimations; although in situ techniques are time consuming, costly, equipment intensive and not feasible to conduct on the required spatial and temporal scale when it comes to real-world applications. WSN technologies have been attempting to fill the gap between small and large-scale applications and finding an optimal way for soil moisture monitoring with practically and spatiotemporally useful resolution. Compared to conventional data collection, WSNs offer a scale independent, reliable, and technically feasible solution with rapid deployment. The main drawbacks are the cost of the installation, equipment and operation if a large number of sensors are employed and the point like nature of the observations. On the other hand, in situ soil moisture measurements play an important role in validating soil moisture data retrieved from other methods, such as remote sensing.

Remote sensing techniques have demonstrated their capability to acquire surface soil water content values under a variety of vegetation cover and topographical conditions. SAR measurements are weather and daylight independent offering a possible solution for near-surface soil moisture monitoring over frequently cloudy areas. The retrieval of accurate, high-resolution soil moisture measurements has been of great interest and it has been a difficult task for researchers.

Given the importance of soil moisture, there have been numerous studies on remotely sensed soil moisture mapping and modelling at global, regional and watershed scale, leaving an obvious gap for research at the sub-watershed, i.e. paddock and farm scale. The current state of research suggests that the combination of modern machine-learning methods, remotely sensed and ground-based systematic measurements integrated into a GIS framework is a promising selection of tools for spatial soil moisture modelling on heterogeneous landscapes, such as New Zealand’s hill country. Therefore, these methods and resources are used in the present study that aims to investigate the possibilities regarding the soil moisture retrieval and modelling from satellite imagery.

Chapter 3

MATERIALS AND METHODS

Chapter 3 aims to describe the methodology related mainly to the data collection. Since the paper-based chapters contain only brief descriptions on the chosen methods, more details are given here. A thorough summary is provided regarding the research site and its geographical settings. This chapter presents the site-specific soil characteristics and describes the utilised laboratory approaches. Fieldwork constitutes a core part of this research that included the deployment of a wireless sensor network, regular pasture growth data collection and occasional soil sampling. This section summarises the fieldwork with a strong focus on the sensor network installation procedure. Additionally, the chapter introduces imagery obtained by the radar-based remote sensing, the related data access and the satellite mission.

3 Chapter 3 - Materials and methods

3.1 Research site and soil characterisation

3.1.1 Geographical and geological settings

A non-irrigated hill country farm (~2600 ha) was selected as the research site, called Patitapu Station situated in the southern part of the ECHC (40.745020 S, 175.887320 E). Lang (2015) described the east coast region as "an extensive stretch of land from southern Wairarapa to the top of the East Cape, predominantly pastoral farmland and forestry, on rolling to steep hills, from the coast to the inland ranges, interspersed with flat terraces and fertile plains". Rock forming processes, soil development and geomorphological processes are partly the consequences of the underlying geology. The Wairarapa coast is located 65-125 km northwest of the Hikurangi Trough, which is the southern end of a subduction zone, the boundary between the Australian and Pacific plates (Suggate et al., 1978). The subducting Pacific Plate dips gently north-westwards beneath the Australian Plate to reach a depth of about 10-15 km beneath the eastern Wairarapa coast. The research site is situated within the Eastern Uplands, where the subsurface consists of deformed sandstone, mudstone, greywacke, argillite and limestone with river flats filled by alluvium. Intense long- and short-term geomorphological processes resulted in an area of undulating and rolling topography, where slumping is common and much of the region is prone to unstable slopes and landslides (Lee and Begg, 2002).

ECHC is renowned for its low fertility soil types with their complex spatial patterns. As the underlying rock types differ widely, the expected variations are reflected in the soil patterns representing weakly to moderately developed, shallow silt loam, silty clay loam, sandy loam and sandy silt loam textures. The most extensive soil types are Argillic Pallic Soils and Orthic Brown Soils in the southern ECHC while Orthic Recent Soils can be found in the northern regions of the coastal area (Hewitt, 2010).

Patitapu Station is situated in the Manawatu-Wanganui region in southern Wairarapa, within the Manawatu River's catchment (Fig. 3.1) where beef and sheep farming dominates (> 50 % of the area). The river drains an approximately 5850 km^2 watershed and its headwaters are located between the Southern Ruahine Ranges and the northern end of the Tararua Ranges, with hill country on the east, and the Manawatu Plains and sand country on the west.

Much of the Wairarapa's climate parameters represent high variability through the year, with common heavy rainfall events, regular summer dry periods and semi-regular droughts (Murray, 1982, Lang, 2015). The ECHC area receives most rainfall during winter with annual values ranging between 800-1600 mm. Low, unreliable precipitation and frequent seasonal lack of water characterise the late spring and summer periods (Zhang et al., 2005). Historical climate data was extracted from a NIWA weather station (Wairere, Ihuraua), located 4.3 km southwest of the farm's meteorological station. Sixty-four year average annual rainfall of 1144 mm ranging from 721-1735 mm was received by the research site while the thirty-year (1961-1990) mean daily temperature normals ranged between 6.4 °C in July and 18 °C in January (NIWA CliFlo, 1953-2017, Tomlinson and Sansom, 1994). A permanent weather station (40.750032° S, 175.887493° E) was installed at the property in 2015, from where meteorological parameters were obtained and used in the following chapters.

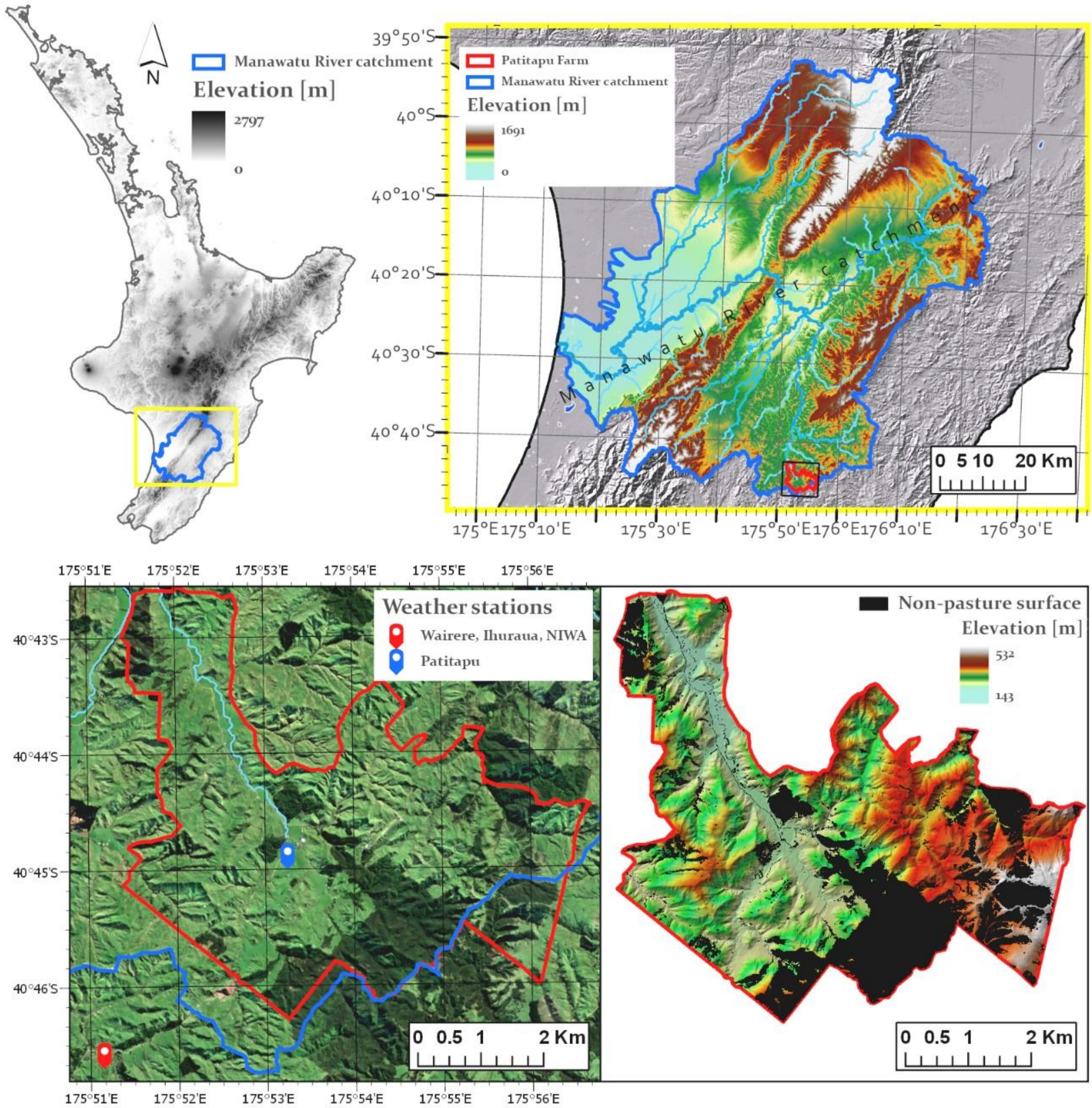

Figure 3.1 Location of the Manawatu River catchment (top left) and the research site situation (top right), land cover (bottom left) and topography with elevation and non-pasture mask (bottom right).

In New Zealand, Land Resource Inventory and LUC have been used to assist long-term, sustainable land and resource management from the individual farm to the national level since the 1950s (Lynn et al., 2009). LUC *Class VI* land covers 85 % of the farm, indicating that the land is not suitable for arable use, but suitable for pastoral grazing where erosion is a common limitation. Along the main water way in the middle of the property *Class III* land can be found that is suitable for cultivation and cropping to a certain extent. Considering the potential utilisation of the collected field-based datasets, the study adopted the slope groups recognised by LUC, except the 'very steep' and 'steep' groups were merged into one 'steep' class. By the application of LUC slope groups, 8.2 % of the research area is flat (0-3°), 8.8 % is undulating (3-8°), 35.5 % is rolling (7-15°), 25.6 % is strongly rolling (15-20°), 14.9 % is moderately steep (20-25°), 7 % is steep (>25°). The slope distribution closely agrees with the parameters of a typical hill country property where significant variability is present at both macro- and micro-topographical level as well as in the soil resources. Elevation ranges from 143-532 m above mean sea level.

3.1.2 General soil description of Patitapu Station using available digital databases

Two main digital, geospatial datasets were available for Patitapu Station in terms of soil resources at the time of the study. The nationwide, New Zealand Soil Portal held by Manaaki Whenua, Landcare Research provides access to coarse resolution soil information based on the New Zealand Soil Classification (NZSC). The most recent, national scale spatial soil information system, S-map, is being developed by Landcare Research which has not covered the research area to date (24/11/2017). Thus, the publicly available Fundamental Soil Layers (FSL) (now being updated and incorporated into S-map) were used as a guideline for the research. Those layers are built upon the spatial join of National Soils Database and New Zealand Land Resource Inventory. The FSL is composed of 16 key spatial soil attribute layers from which the soil physical properties were retrieved.

Hewitt (2010) defined the top three classes of the hierarchical NZSC. The majority of the property is covered by Brown Soils in terms of soil order (Fig. 3.2 (A)) which also represents the most extensive category in New Zealand covering 43% of the land. *Soil orders* are divided into *soil groups* and those are further divided into *subgroups*. A common soil in the east side of the North Island, the Pallic Orthic Brown (BOP) soil dominates over the study site at the subgroup level. Typic Firm Brown (BFT) soils can be found in the generally steep, eastern side of the farm at the highest altitudes within the property. Between BOP and BFT covered areas Mottled Orthic Brown (BOM) soils were mapped. Brown soils are commonly found on slopes and young land surfaces (Hewitt, 2010). The topsoil is typically described as dark grey-brown while the subsoil is often brown or yellow-brown. This type of soil typically occurs in places where summer drought is uncommon and which are not water logged in winter (Hewitt, 2010, Landcare Research, 2017). The flat middle sections of the farm have Typic Orthic Gley (GOT) soils along the streams where waterlogging due to a persistent high water table are frequently observed. Mottled Immature Pallic (PIM) soil can be found in the north-west corner of the property covering a small extent. Regarding particle size, according to the FSL database (Fig. 3.2 (B)), the silt is the primary texture class over the farm along with some loam and loam over sand.

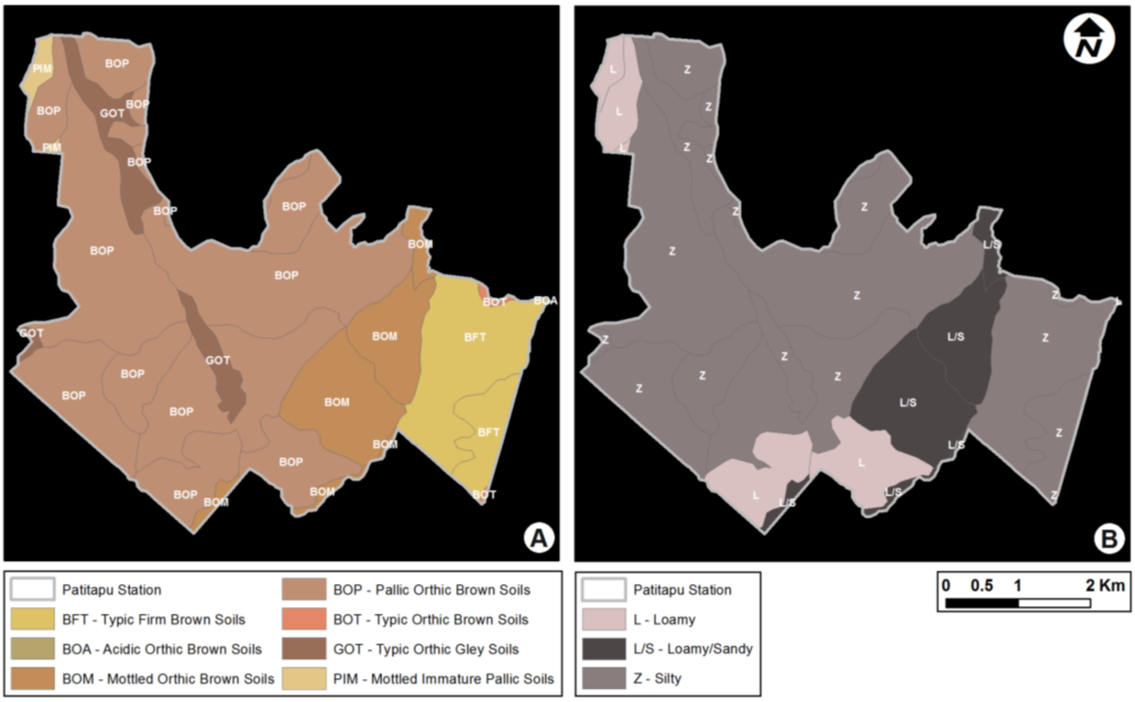

Figure 3.2 Soil classification map (A) and soil particle size map (B) extracted and adapted from the FSL digital database (Landcare Research, 2017).

A more detailed soil survey was carried out by the Horizons Regional Council (Palmerston North, New Zealand) at the Patitapu Station in 2009. It provides information at the paddock scale including the soil parent materials, rock class, texture, soil depth, stone content, upper and lower textures, and drainage as well as functional horizon attributes detailing horizon stone content, texture, structure size, and consistence (Fig. 3.3). Dominant soil textures are the variations of silt loam, silty clay loam, sandy loam and sandy silt loam with different drainage properties and ranging from weakly to moderately developed status.

Concerning the main soil types and units, the soil maps from different sources displayed broad agreement. Both maps indicate a distinguishable soil unit along the main waterway, which formed on the plain surfaces from sediments strongly affected by waterlogging. Another good agreement can be seen in the eastern part of the farm with the highest relief. Here, the Mottled Orthic Brown (MOB) soils were displayed on the FSL and dark yellow silt loam was dominantly observed by the Horizon's soil survey.

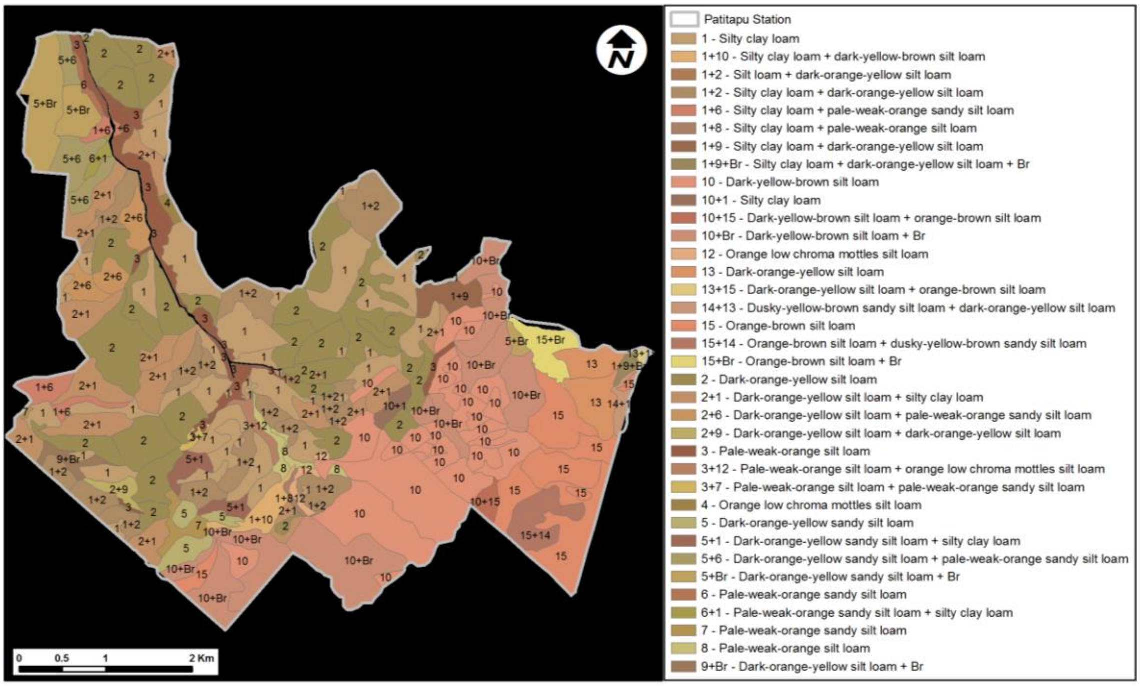

Figure 3.3 Soil resource map of Patitapu Station, adapted from the Horizons Regional Council (Landvision Ltd., 2009).

The rest of the farm area, the mostly rolling land surface is characterised with dark-orange yellow silt loam according to the Horizons' soil survey, whilst Pallic Orthic Brown (BOP) soils were defined by the FSL. In terms of soil texture, both soil layers demonstrate that the study area is dominantly covered by silt loam soils or its varieties. The Horizon's soil layer was used as the most recent resource during the sensor network design and microsite selection.

3.2 Wireless sensor network deployment

3.2.1 Network description and design

In August 2016, twenty AquaCheck Classic subsurface, capacitance sensor probes were installed at the Patitapu Station and these microsites were arranged into a WSN. A pre-determined deployment strategy was applied, meaning that the sensor nodes were placed at specified locations (Halder et al., 2011). After deployment, a two-month period was allowed for the soils to equilibrate and to develop an optimal soil to sensor contact, thereby starting the data collection on 1 November 2016. Each probe is equipped with soil moisture and soil temperature sensor placed at four fixed, consecutive depths (100, 200, 300 and 400 mm). The WSN covers an approximately 3 km x 4.6 km area (~13.8 km^2) giving an average spacing density of ~0.69 km^2 per microsite. The mean distance between microsites and the permanent local climate station varies between 0.34 - 2.9 km giving a mean distance of 1.8 km.

Consequently, the representative microsite selection was a challenging task and a crucial design step to optimise sensor distribution, ensure easy access for installation and maintenance purposes. To deploy the WSN, a criteria set was created that included macro- and micro-topographical features, soil information, land cover type, land use, microsite accessibility, equipment protection and foreseeable farm management plans.

In terms of wireless communication, the microsite selection was limited by an optimal, ~1.7 km radio range recommended by the manufacturer. Each of the sensor nodes required line-of-sight visibility to the gateway, or another sensor node, or alternatively, to the relay station. The above-mentioned requisites had to be met without exceeding the cost constraints and by ensuring sufficient equipment protection as the research area is an operating farm with livestock and other activities associated with general farm operation. The deployment process considered the concept that soil moisture and soil temperature measurements should be applicable for validating products retrieved from land-surface models or remote sensing applications.

3.2.2 A GIS-supported network deployment approach

The WSN deployment posed a three dimensional problem due to the heterogeneous field that contains obstacles mainly in the form and relief of the terrain, man-made (buildings) and natural (tree lines) objects, which can prevent communication between the nodes. To address the variability of the terrain, GIS platforms can provide powerful tools in sensor network planning over complex environments (El Emary and Ramakrishnan, 2014). The Patitapu WSN deployment was divided into three main tasks, including the identification of potential positions for the gateway (1), finding an optimal location for the relay node (2) and preselecting suitable, representative areas for sensor nodes (3) while fulfilling the line-of-sight visibility criteria. To accomplish these tasks, GIS capabilities were used to support the decision-making and to integrate the available environmental and auxiliary information. The GIS-assisted spatial methodologies included raster- and vector-based examination, such as land cover classification, terrain analysis, conditional evaluation and intervisibility analysis (line-of-sight and viewshed) as illustrated on Figure 3.4. Prior to the WSN deployment, several network variations and scenarios were generated taking into account the number of sensor nodes, limitations and the study objectives.

The input dataset consisted of a group of raster layers, i.e. a Digital Elevation Model (DEM), aerial orthophoto collection and a hyperspectral image; and a group of vector based data layers, i.e. fence lines, farm tracks, soil resources, cellular coverage and fencelines. The land cover classification was executed in ENVI (Exelis Visual Information Solutions, Boulder, Colorado), the terrain analysis was conducted in ESRI ArcGIS ArcMap (ESRI Inc. Redlands, CA, USA, version 10.4) and System for Automated Geoscientific Analysis (SAGA) (Conrad et al., 2015) software environments.

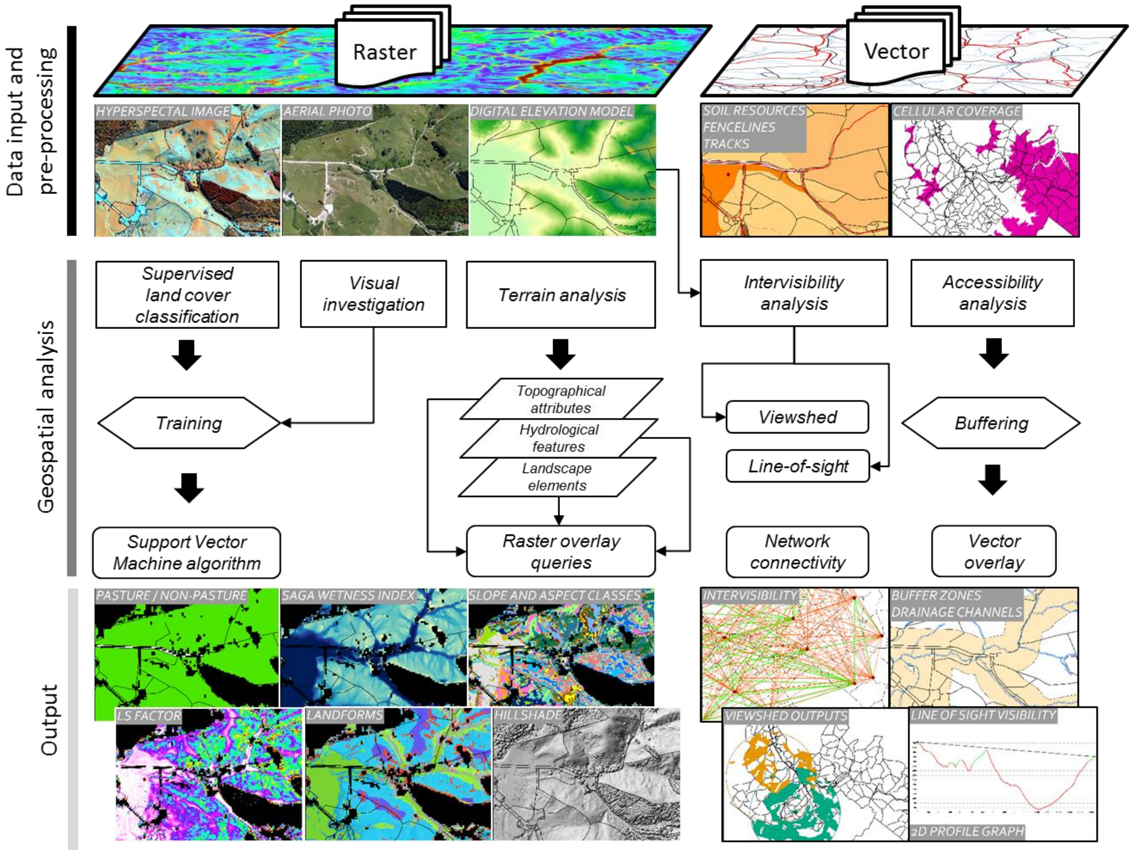

Figure 3.4 The available raster and vector layers and the executed GIS-assisted spatial analysis methods to support decision making in the network deployment. The derived datasets were analysed to delineate the potential areas for the sensor installation that satisfy the predetermined requirements.

3.2.2.1 Land cover classification

The objective of the study required that the sensors were placed under pastoral vegetation coverage; therefore, the delineation of grass surfaces was needed as part of the WSN planning stage. Ground features have specific reflection signatures that characterises the radiance values obtained from the object pixel by pixel, allowing the identification of a large variety of surface types. Hyperspectral imagery demonstrated its capability in detailed thematic urban mapping consisting of a wide range of surface classes (Goetz et al., 1985, Pullanagari et al., 2017).

The study area is comprised of several land cover types, such as buildings, manmade surfaces, gravel roads, bare soil, vegetation (pasture surfaces, native bush and trees), waterways and ponds. For the purpose of the study, pasture and non-pasture land cover classes were discriminated through image classification. The hyperspectral image was acquired by a full-spectrum, pushbroom AisaFENIX (Specim Ltd., Oulu, Finland) full spectrum, imaging system mounted on a fixed-wing aircraft. The sensor measures upwelling radiance between the visible (Vis) and SWIR spectral regions (370-2500 nm) with a total of 448 bands that make it suitable for remote, high-resolution spatial mapping of various surfaces (Pullanagari et al., 2018).

The image pre-processing included the following steps: correction for boresight effects, correction for bad detector, geometric and radiometric calibration, atmospheric correction, georectification, mosaicking, spatial and spectral smoothing. A detailed description of the applied image processing and classification procedure can be found in Pullanagari et al. (2017).

Land cover types were identified by using high-resolution RGB imagery from which training polygons were collected for a total of 13 land-cover classes (eight vegetation types, water, wetland, bare soil, shadows and manmade surfaces) that were considered in the supervised classification scheme. A commonly used classification method, the so-called Support Vector Machines (Camps-Valls and Bruzzone, 2009, Camps-Valls et al., 2014), was chosen to link the input training data to the corresponding reflectance spectrum of the underlying picture elements. After validation and accuracy assessment, the number of classified land-cover types were reduced to pasture and non-pasture classes.

3.2.2.2 Terrain analysis

At the time of the WSN planning stage, an 8x8 m resolution DEM was available through Land Information New Zealand (LINZ) (LINZ, 2012). This national scale DEM contains only ground-surface elevation data originally generated from contour lines providing information about the terrain morphology. The DEM was sufficient for the WSN planning to gain insight into the terrain, although shortly after the WSN installation, a high-resolution digital surface model (DSM) of the research area was provided by Massey University and Ravensdown Ltd. The DSM was generated using structure-from-motion technology (Micheletti et al., 2015), originally acquired at 0.2x0.2 m pixel size. Focal statistics, resampling and smoothing were applied to create a 5x5 m spatial resolution dataset, which was used for extracting the topographic attributes of the microsites.

For the quantitative description and characterisation of the terrain, geomorphometric derivatives can be computed in a GIS environment (Evans, 1972, Mark, 1975). The terrain descriptors can be divided into zero order (i.e. elevation), first order (slope angle, aspect) and second order (compound) derivatives (e.g. wetness index, curvature, etc.) (Kienzle, 2004, Minar and Evans, 2008). For exploratory spatial data analysis and for the evaluation of the geographic suitability of an area for WSN deployment, several fundamental terrain attributes were derived.

To develop an overall impression of the topography, the relief forms were emphasised by the use of analytical hill shading that simulates the effect of natural light on the terrain surface to depict light and shadow. The terrain analysis included the mapping of slope angle (the degree of incline of a surface) and aspect (the orientation of the slope) in degrees by the transformation of the elevation data. These two first order derivatives played a key role in the microsite deployment due to their dominating effect on soil moisture patterns in hill country.

The DEM was reclassified by overlaying the slope angle and aspect layers to distinguish flat areas and to group each pixel into one of the five slope angle categories using the LUC categories (Lynn et al., 2009) on each aspect. A more thorough investigation was achieved by calculating the second derivatives of these initial metrics. To avoid erosion prone surfaces, the modified slope length and steepness factor was computed as key attribute for predicting erosion potential within a landscape (Desmet and Govers, 1996). The combination of slope steepness and specific catchment area effects were used to delineate the areas of risk of soil erosion.

The geomorphological characterisation of the terrain was further examined by automated landform classification to identify topographic units or principle landform elements and slope positions. The analysis was performed on the basis of Topographical Position Index computation (Guisan et al., 1999, Wilson and Gallant, 2000) and the study area was divided into 10 macro-landform classes. The process defined stream, upland drainage, plain, valley, open slope, upper slope, local ridge, midslope drainage, midslope ridge and high ridge categories. Landforms and geomorphic features can be an indication of numerous factors related to water distribution and soil conditions (Evans et al., 2016). Soils tend to be deeper and often mixed at lower slopes and shallower on crests, having an impact on the sensor deployment.

Prior to the computation of compound hydrological metric outputs, the DEM was pre-processed to fill the sinks or depressions that would capture the flow of water. At the small catchment and hillslope scales, soil moisture distribution can be reasonably well indicated by the Topographic Wetness Index developed by Beven and Kirkby (1979) and its modified version, the SAGA Wetness Index (SWI) (Beven and Kirkby, 1979, Moore et al., 1991, Böhner et al., 2001). In this study, the SWI was used to map organised spatial fields of soil moisture and to identify potentially extremely wet or dry areas. Moreover, drainage channels, upslope contribution area (flow accumulation) and flow directions were mapped as part of the watershed analysis including the delineation of catchments and the stream network. Drainage channels and farm tracks were used as inputs in the buffer zone generation to limit the distance to stream lines, and to ensure that the microsites will be accessible as installation and maintenance are labour-intensive, especially on steep terrain.

3.2.2.3 Intervisibility analysis

The chosen telemetry system required line-of-sight visibility for stable communication between nodes. To ensure connectivity within the telemetry range, an intervisibility analysis was undertaken in a three-dimensional space, as two nodes cannot connect to each other if the terrain or other type of obstacles break the signal. The sightline visibility and viewability was assessed over a functional surface, namely the DEM, taking into account the relief and the effective communication range. The analysis was carried out by using the geoprocessing tools built in the Esri ArcGIS software package version 10.4. Tree lines were generally avoided, given the unknown height of the vegetation cover during the planning stage. To conduct the intervisibility analysis, 4 m height was chosen as offset from the surface considering the radio antenna position.

The line-of-sight analysis produced line features between each pair of nodes and labelled with a value of intervisibility, one or zero, visible or not visible. Visibility profiles were extracted between the potential locations and coupled with aerial imagery to ensure the connecting line was not positioned too close to the surface concerning the presence of vegetation. The spatial visualisation of radio coverage from a given location was produced by the viewshed analysis workflow. Viewability grids were generated to predict the visible and not visible grid cells from a specific location of the landscape. Due to the omnidirectional capabilities of the radio transceivers, the operation attributes were selected regardless of the direction.

3.2.3 Gateway and relay station deployment

Once the required data layers had been generated, a thorough visual interpretation was carried out to preselect various candidate locations for the gateway, relay node and the sensor nodes. Firstly, the datasets were assessed to find potential gateway locations, which was mainly governed by the cellular network coverage and suitable land surface conditions. The gateway unit provides a connection between a computing device-based user platform and the physical world via a cellular network. The ideal position was characterised with strong and sound cellular reception, good accessibility, 360° clear visibility, free of obstacles, shade and potential risk sources such as trees, power lines, and erosion prone surfaces. During an earlier field visit, cellular coverage was generally found above 300 m altitude, thus these areas were queried from the DEM and superimposed on multiple spatial layers. The final location was chosen on a stable, outstanding hill top position at 320 m altitude.

The relay node had to be placed within 1.7 km radius to the gateway to provide a direct link. A similar approach to the described above was taken to find candidate relay node positions, except the need for cellular reception. As the relay node aims to balance out data traffic and increase the number of alternative communication paths, such a centric position was chosen that is visible from every block of the farm and has a direct link to the gateway. The relay station was placed on a hilltop elevated between two wide and open valleys at 287 m altitude nearby the permanent weather station.

3.2.3.1 Sensor node locations

Considering the number of probes (20) available, the microsite locations were chosen with the aim of establishing an adequate spatial distribution on a variety of topographic positions, land use suitability categories and representing the agriculturally important soils of the pastoral area. The microsite selection was driven by a two-step, conditional decision approach consisting of candidate area pre-selection supported by GIS tools. This was followed by an on-site area evaluation and validation of the potential sites. Each of the provided 20 sensor probes were assigned to one of the slope angle and aspect classes adapting the modified LUC (Lynn et al., 2009) categories. Figure 3.5 depicts the selection process for *Site i,* for a given slope angle and aspect class.

A location was considered highly suitable if the attributes of a selected location or grid cell passed through a series of specific conditional statements with TRUE values. Land cover, terrain, visibility and accessibility contained the most important criteria sets. In terms of environmental GIS data layers, a selected sensor location was situated over pastoral land surface class, positioned farther than 5 m from stream edges. The cell needed to represent the given slope and aspect class derived from overlay operation by combining the slope angel and aspect thematic layers, and situated on a surface with low erosion risk as it was defined by the length and slope factor layer.

To satisfy the effective communication range, 1.7 km distance was given as the longest distance from either the gateway, the relay node or another sensor node. Additionally, the line-of-sight visibility criteria had to be met without obstruction by tree lines or buildings. If any of these conditions were evaluated as FALSE, a new location was placed under investigation. In case the location satisfied these requirements, it was further examined for accessibility. Ideally, the highly suitable site was located within 100 m to the closest track, as each node required the installation of a robust fencepost and drilling applications for the radio and sensor placement.

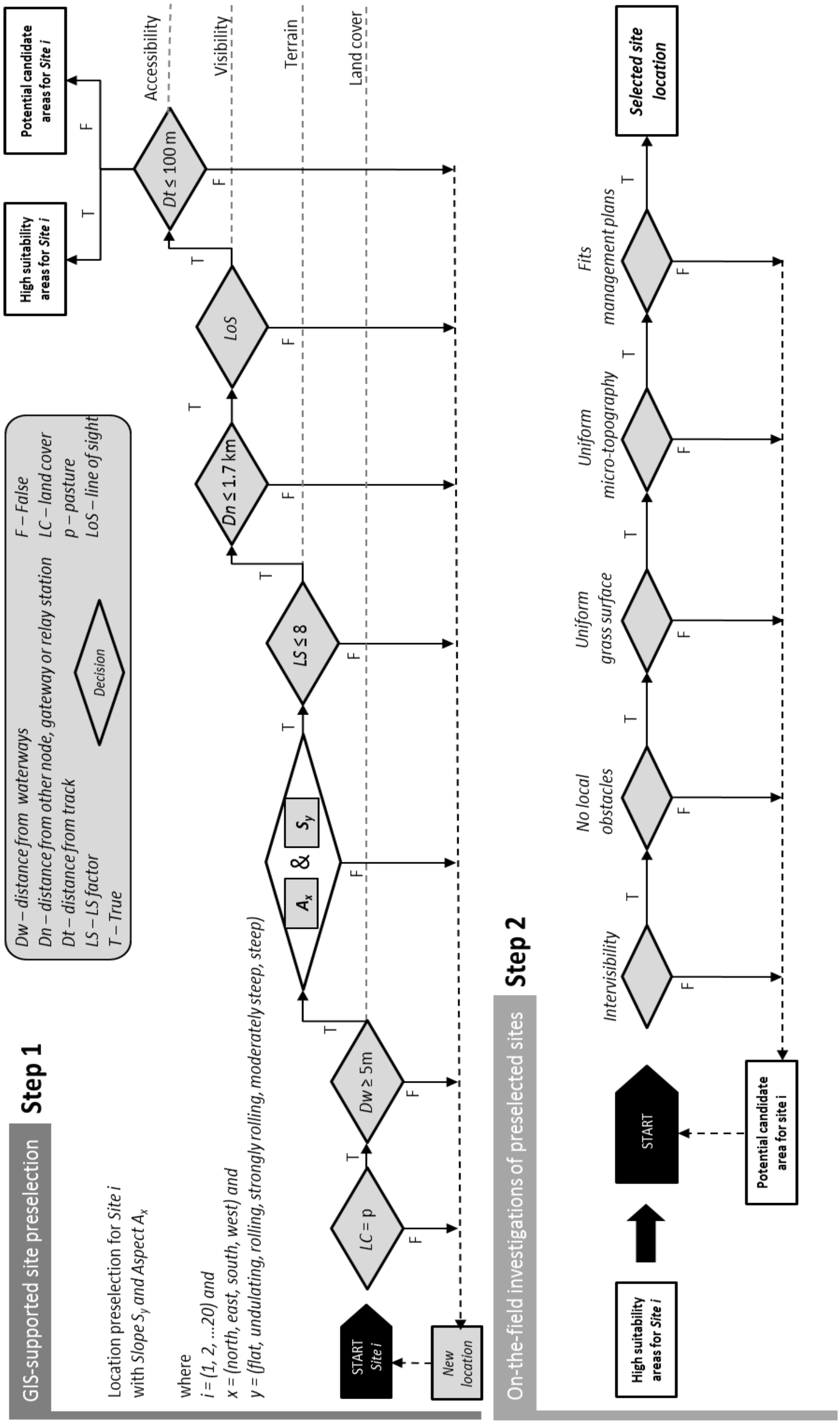

Figure 3.5 Flowchart of the pre-selection and field-based validation of suitable sensor node locations.

If the logical condition was FALSE, then the location was classified as a potential candidate area for the *Site i*. These areas were taken into account if the high suitability areas did not pass the on-site validation criteria. Figure 3.6 illustrates the raster and vector layers explored in the suitability analysis related to terrain and accessibility features.

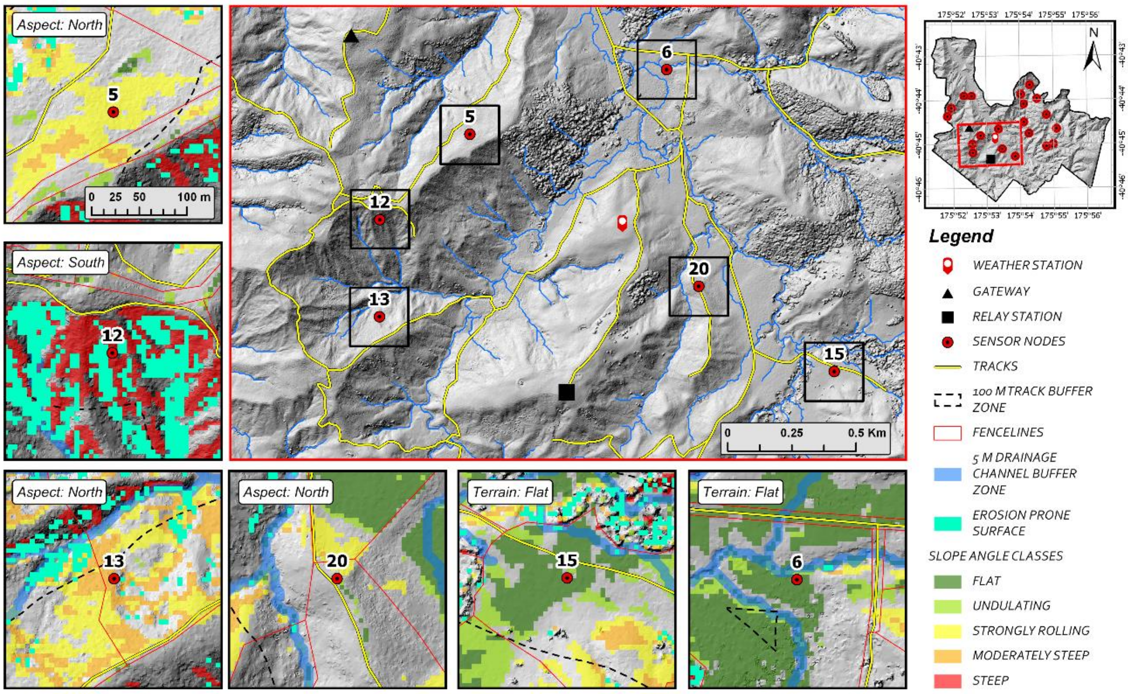

Figure 3.6 The central part of the research area illustrating the terrain (slope angle and aspect) and accessibility characteristics for 6 selected sensor nodes along with the position of the gateway, relay node and weather station.

Once every sensor node location went through the conditional pre-selection process, the high suitability areas were visited in the field by finding the GPS coordinates extracted from the GIS data set. The on-site procedure involved the confirmation of intervisibility and that the microsites were situated on well-grown, uniform pasture surfaces free of obstacles and frequent shade. Figure 3.7 shows the architecture of the WSN including the established line-of-sight connections among the gateway, relay station and sensor nodes from a three-dimensional point of view. The land surface cover is represented by a high-resolution orthophoto that was superimposed on the original, 0.2x0.2 m pixel size, DSM for an improved pasture surface visualisation.

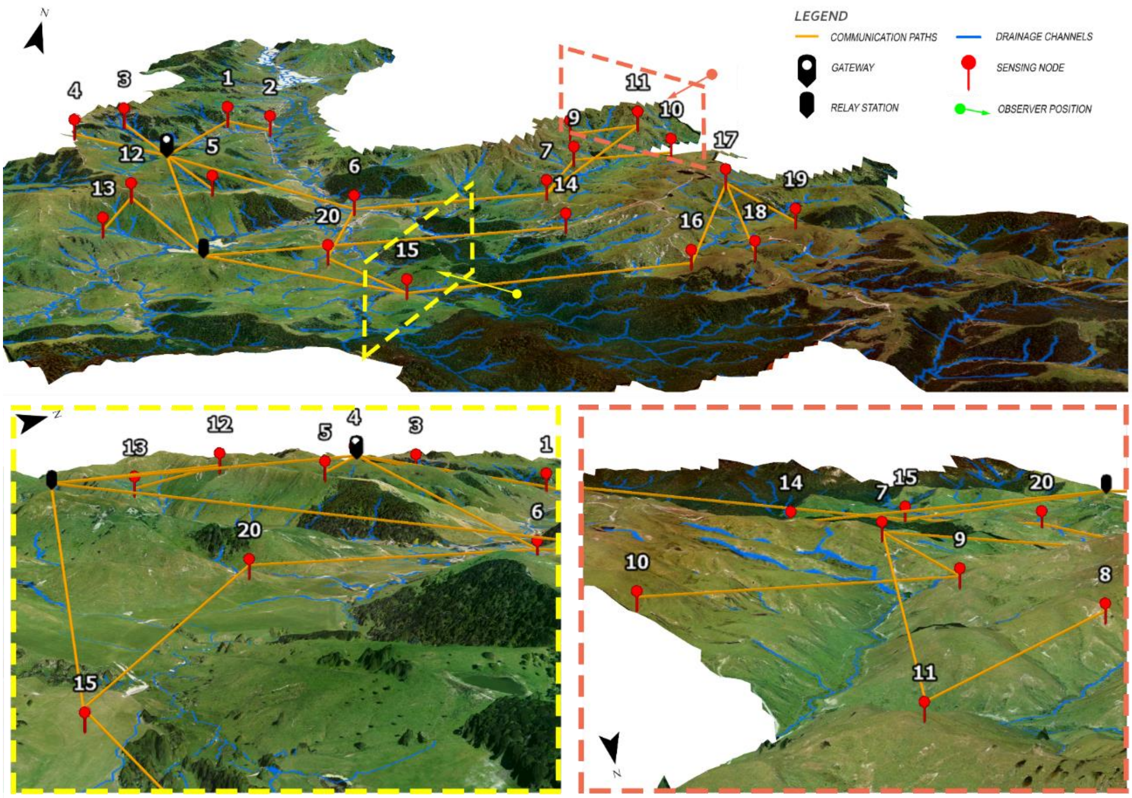

Figure 3.7 A three dimensional demonstration of the deployed WSN with line-of-sight intervisibility and vegetation cover overlaid on a high-resolution DSM.

Sufficient soil depth was inspected and micro-topographical features were examined to avoid local water accumulating depressions and irregularities, i.e. stock tracks, soil erosion surfaces. Accessibility was reassessed and farm management plans were reviewed during the field-based validation to ensure that the assorted microsite locations were not subject to changes in management plans, such as cultivation.

Table 3.1 contains the summary of the terrain parameters of each selected microsite extracted from the 5x5 m pixel size DSM. In terms of land cover, the microsites were chosen from mostly uniform pastoral grassland surfaces where the predominant plant communities are ryegrass and clover species. Three probes were placed on flat areas spread over the plains along the main waterway draining the farm area. Concerning slope angle classes, two nodes were placed on undulating, three on rolling, four on strongly rolling, four on moderately steep and four on steep surfaces. To capture the high contrast between south- and north-facing aspects, five nodes were installed on each of these two classes, while four sensor probes were deployed on west and three on east aspects. The geographical position of the gateway, relay station and sensor nodes were surveyed by using a high accuracy (few cm) real-time kinematic global positioning system (RTK GPS).

Table 3.1 Main topographical characteristics of the selected microsites locations at the Patitapu Station.

Site ID	*Landscape element*	*Slope (degree and class)*		*Aspect (degree and class)*		*Elevation (m)*
1	Upper slope	13	Rolling	175	South	196.7
2	Plain	-	Flat	-	Flat	160.6
3	Open slope	16	Strongly rolling	115	East	249.0
4	Open slope	23	Moderately steep	94	East	279.0
5	Open slope	16	Strongly rolling	1	North	282.5
6	Plain	-	Flat	-	Flat	173.3
7	Open slope	14	Rolling	305	West	309.9
8	Midslope ridge	35	Steep	35	North	307.8
9	High ridge	5	Undulating	187	South	292.9
10	Open slope	22	Moderately steep	298	West	318.6
11	Upper slope	26	Steep	257	West	314.8
12	High ridge	32	Steep	178	South	301.8
13	Open slope	23	Moderately steep	22	North	232.8
14	Upper slope	23	Moderately steep	157	South	287.8
15	Plain	-	Flat	-	Flat	196.4
16	Open slope	17	Strongly rolling	283	West	373.6
17	High ridge	20	Strongly rolling	224	South	362.3
18	Open slope	26	Steep	46	East	400.7
19	Open slope	14	Rolling	15	North	380.7
20	High ridge	7	Undulating	355	North	199.5

The Patitapu WSN deployment followed a comprehensive manually guided approach with a significant amount of visual interpretation that relied on datasets from various sources. The microsite selection procedure was not automated mainly because of the poor knowledge regarding soil moisture variability in hill country, the complex topography and the uncertainty induced by the low-resolution soil information. Moreover, most of the automated statistical methods and algorithms require a significant amount of input data. Additionally, microsite localisation was influenced by the farm management plans and foreseeable land use changes, which required an effective collaboration with the farm owner.

In the literature, there exist several, advanced approaches for designing soil sampling campaigns and establishing sensor networks for observing environmental variables. Minasny and McBratney (2006) applied the Latin hypercube method as a sampling strategy that is based on a high amount of a priori knowledge of the targeted area. Some other approaches for generating spatial sampling schemes have been based on the estimation of variograms (Pettitt and McBratney, 1993) and the spatial interpolation of the variables using geostatistical tools, such as kriging and the optimisation of kriging (Van Groenigen et al., 1999). Robertson et al.

(2013) developed the balanced acceptance sampling algorithm for selecting spatially balanced sampling locations that takes into account the spatial distribution of the resource.

3.2.4 WSN instrumentation and deployment

Due to the long-term nature of the research project, the terrain conditions, and the fact that the microsites are located on an operating farm with livestock and other daily activities associated with farm operation, the instrument selection was a crucial part of the planning stage. The sensor nodes needed to withstand harsh outdoor conditions for several years; therefore, robust, solid sensors and stable, long-range telemetry system with firm protection were required.

The chosen telemetry unit was provided by TAG I.T Technologies Ltd (Hamilton, New Zealand) with capabilities of near real-time data logging and reporting at adjustable time intervals. The HALO Farm System, an online service developed by the same company was responsible for monitoring and visualising the data received from the sensors as it was sent to the web via cellular 3G connection. The secure online dashboard can be accessed from smart computing devices, allowing flexible display of time series data and the receiving of fault alerts, which enabled prompt reaction to operational issues.

Once the sensor node, gateway and relay station locations were finalised, fence posts were placed into the ground to provide a stable and secure base for the radio unit. Figure 3.8 (A) illustrates the sensor node design on a hill slope position. The enclosure was installed on a 3 m galvanised pole extension attached to the fence post. A high range antenna was placed into a weatherproof PVC tube and mounted on the top end of the pole at ~4 m height. This position improved visibility and connectivity attributes for the radio communication. The solar panels were orientated to the north to ensure efficient battery recharging.

The sensing unit (Fig. 3.8 (B)) is connected to the telemetry device by a cable running through a durable Alkathene pipe suitable for below ground installation. The flexible pipe was buried in an ~10 cm deep trench from the fencepost base to the head of the probe, protecting the wiring from damage. Both ends of the Alkathene pipe were sealed to avoid water intrusion. The pipe was guided along the galvanised pole and zip tied to it to protect it from stock. In the last stage, the topsoil turves were placed back into the trench and the gaps were filled back with fine-grained soil material.

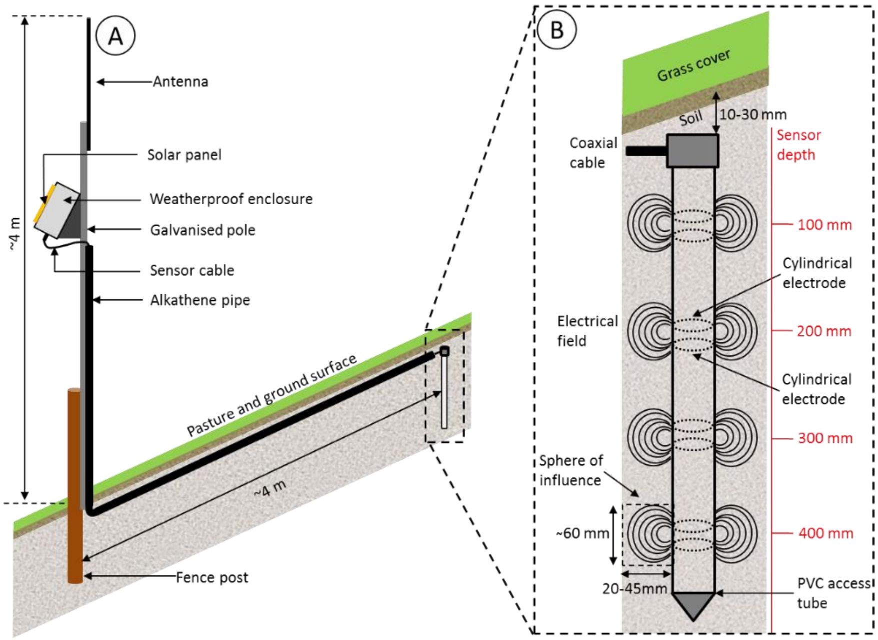

Figure 3.8 Schematic diagram depicting the design of a typical example of a microsite (A) and the configuration of a 400 mm AquaCheck Sub-surface multi-sensor probe (B).

For root-zone soil moisture monitoring, 400 mm long subsurface type, the AquaCheck (AquaCheck Soil Moisture Management, Durbanville, South Africa) multi-sensor probe was chosen. A single AquaCheck probe was connected to a single radio unit reporting soil moisture and soil temperature readings simultaneously at every 15 minutes. The solid-state, capacitance-based probe is equipped with four sensors spaced at intervals of 100 mm and with a right hollow cylindrical shaped sampling range. The sphere of influence can be approximated with geometric parameters of h = 60 mm (cylinder height), r = 16 mm (internal radius) and R = 20-45 mm (external radius). The probes are designed to be completely buried with an attached wire for data transmission to a logger (Fig. 3.8 (A)). The probe measures the variation in the capacitance of pairs of pieces of metal inside the probe as a proxy for soil moisture. The soil forms the dielectric of the capacitor, with changes in moisture content altering the relative permittivity of the soil. Most often, the capacitance is measured by forming an oscillator whose frequency is dependent on the unknown capacitance. The frequency is then easily measured by the microprocessor in the probe. The sensor transforms the frequency readings to Scaled Frequency (SF) as raw output. The SF values range from 0-100 %, where 0 % is equal to a reading in open air and 100 % when the sensor is immersed in distilled water. The SF readings are automatically corrected for possible inherent temperature change by embedded compensation functions.

To calculate θ_v (%), SF values need to be converted using an empirical, laboratory-based calibration curve. The conversion is not a built-in function; therefore, the device is offered with factory calibration equations for six soil textures, e.g. sand, clay, silt loam, loam, clay and generic (composited from sand, silt loam and clay soils) (Agri Optics, 2017). For the purpose of this study, the resulting θ_v (%) output was converted to θ_v ($m^3\,m^{-3}$).

Soil temperature data is collected at the four depths by a Resistant Temperature Detector. The temperature sensors are able to read data between 0-51 °C with 0.2 °C steps.

3.2.4.1 AquaCheck probe installation

The probe installation was a crucial part of the WSN deployment; therefore, the sensor installation followed a standard procedure provided by precision agriculture technicians at Agri Optics New Zealand Ltd. After the selection of the desired location, an approx. 25x25 cm square shaped and 1-3 cm thick topsoil turf was removed. In order to allow the snug insertion of a sensor probe, an installation auger (⌀ 40 mm) was used to bore a slightly wider hole than the probe shaft body. The hole was drilled in increments and the soil was removed from the auger at each section and kept separately after a visual check of the variation within the profile. Great care was taken to ensure that the holes were as vertical as possible at each site as it was recommended during the training and by the installation guide.

As the correct depth was reached, soil slurry was made from the soil material obtained from the hole by using a cordless driller and paint mixer. The homogenous, milk shake consistency was made to ensure an optimal sensor-to-soil contact. After the removal of organic material, and coarse soil components, such as gravels, an adequate amount of slurry was poured into the hole. As the diameter of the auger was only slightly larger than the probe shaft diameter, the sphere of influence is much larger than the thickness of the slurry, therefore the information is dominantly collected from the soils occurring at the sensor depths. At the time of the experiment, there was no published studies available on the effect of the installation method on AquaCheck sensor readings. The next step was the careful insertion of the probe until only the probe cap was visible on the fresh surface. Some slurry was forced out from the hole and it surrounded the plastic cap. This slurry overflow was not removed, as it helps to improve the snug fit by preventing additional water running down along the access tube and the formation of air gaps. In the final step, the topsoil turf block was placed back to its original position and the gaps were filled with finely screened soil material in order to assist soil recovery. The main steps of the field-based probe placement process are shown in Figure 3.9.

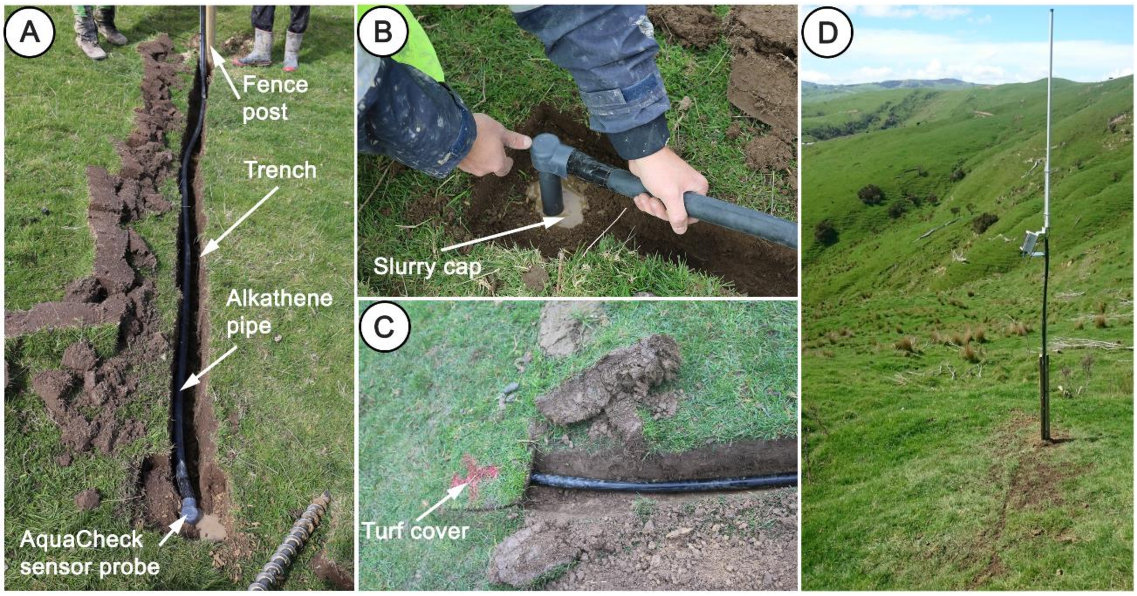

Figure 3.9 An example of the main steps of the sensor node installation process on site. A) Underground wiring with an Alkathene pipe running to the radio device in a trench. B) Probe insertion that creates the slurry cap surrounding the device. C) A block of turf cover placed on the top of the probe. D) Complete and connected sensor node.

3.2.5 WSN communication and architecture

The proposed WSN architecture consists of a gateway, a repeater station and twenty sensor nodes arrayed in a mesh topology. The mesh feature enables multi-hop communication in an arbitrary structure with numerous message paths, meaning that the nodes are allowed to communicate with every other node in line-of-sight and within radio distance without any restriction in the protocol (Townsend and Arms, 2005). A sensing node has a dual role, collecting and sensing of data from its own sensor or acting as a relay for neighbouring nodes. The network was considered homogenous as each of the sensor nodes have identical power, hardware, transmitting and receiving capabilities. The employment of homogenous networks may lead to the phenomenon known as the energy hole issue. Larger power consumption frequently occurs in the nodes closer to the gateway or sink node, due to the increased data traffic received from the more distant sensor nodes (Olariu and Stojmenovic, 2006, Halder et al., 2011, Abdollahzadeh and Navimipour, 2016). The result is a non-uniform dissipation of energy leading to drained batteries, data loss and communication issues. The application of non-uniform sensor topology, energy-balanced network models or the deployment of relay nodes to forward data packages can save energy for the nodes with sensing units attached (Al-Turjman et al., 2013, Huang et al., 2013). The integration of a relay node ensures data load balancing, extra storage capacity, increases the number of backup routes, extends the spatial network coverage and reduces the risk of network disconnection due to unexpected failures and natural hazards. At Patitapu, a relay node was added to the network architecture and installed on a farm centric position from where a direct radio link was provided towards the gateway and several sensing nodes.

The sensor readings are passed through underground wires from the sensors to the telemetry units among which the data is transmitted via radio connection until they reach the gateway. The information is uploaded to a server via cellular network ensuring near real-time access to the data. Figure 3.10 illustrates the WSN workflow in respect to the main operational steps (A) the related physical units (B) and the type of connectivity (C).

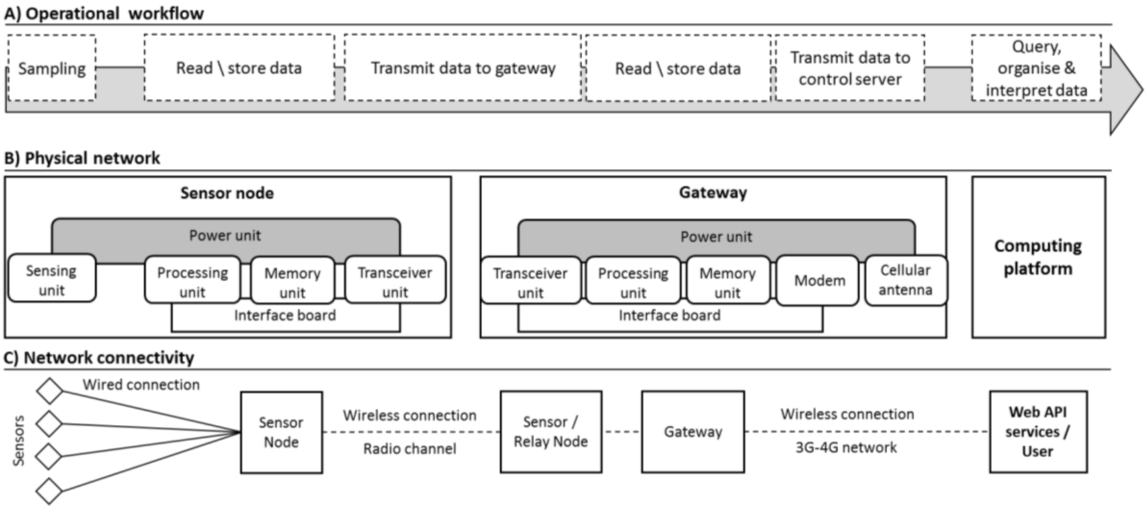

Figure 3.10 Main operational workflow for the sensor network at Patitapu Station coupled with the responsible physical units and the nature of connectivity among the nodes.

The radio protocol uses 15 channels in the 2.4 GHz band that implements a self-healing tree structure for routing. The gateway device is the root of the network, with other nodes connecting to parent nodes so that every node has a single route back to the root. Nodes select a parent to connect to by scanning for nodes already connected to the network, and then rank them by signal strength and distance from the root. If they need to send data to a node that is not reachable by one of their children, they forward it up the chain to their parent. Such packets will travel up the tree until they reach a node that knows how to reach the destination. Links between each node use a channel hopping protocol, with discrete time slots allocated for communication by the parent node. Each time slot is assigned a pseudo-random channel generated by a seed known to both nodes. Carrier-sense multiple access with collision detection is used to avoid interfering with ongoing transmissions from other nodes. If a node is unable to transmit in a time slot due to contention, it backs off and attempts again in its next time slot.

Connectivity (or adjacency) matrices and node-link network diagrams can be used to visualise the possible links among nodes. The node-link diagram generated for the Patitapu WSN used line features to represent the sightlines from each node towards every other visible node that was not obstructed by topography, vegetation or other manmade objects. In the finite simple matrix form, each column and row represents a node and the binary (i.e. 0 or 1) elements indicate whether the pairs of sensor nodes are visible or not. Figure 3.11 demonstrates the network organisation and connectivity in a graphical, i.e. node-link diagram on the left, and in a matrix form without taking into account the effective radio range on the right.

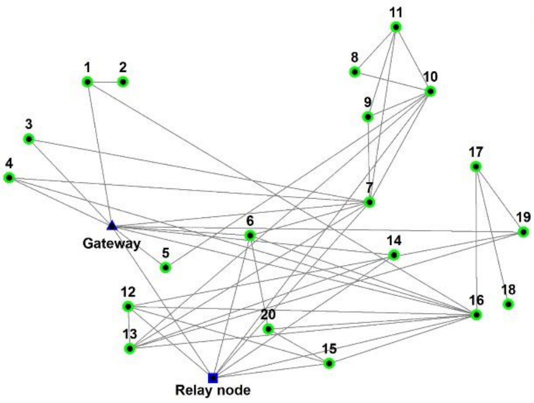

Node	1	2	3	4	5	6	7	8	9	10	11	12	13	14	15	16	17	18	19	20	G	R	MD [m]	VN
1	0	1	0	0	0	0	0	0	0	0	0	0	0	0	0	1	0	0	0	0	1	0	1891	3
2	1	0	0	0	0	0	0	0	0	0	0	0	0	0	0	0	0	0	0	0	0	0	316	1
3	0	0	0	0	0	0	1	0	0	0	0	0	0	0	0	0	0	0	0	0	1	0	2087	2
4	0	0	0	0	0	0	1	0	0	0	0	0	0	0	0	1	0	0	0	0	1	0	2862	3
5	0	0	0	0	0	0	0	0	0	1	0	0	0	0	0	0	0	0	0	0	1	0	1722	2
6	0	0	0	0	0	0	1	0	0	0	0	0	0	0	0	1	0	0	0	1	1	1	1330	5
7	0	0	1	1	0	1	0	0	1	1	1	0	1	0	0	0	0	0	0	0	1	1	2391	9
8	0	0	0	0	0	0	0	0	0	1	1	0	0	0	0	0	0	0	0	0	0	0	620	2
9	0	0	0	0	0	0	1	0	0	1	1	0	0	0	0	0	0	0	0	0	0	0	736	3
10	0	0	0	0	1	0	1	1	1	0	1	0	1	0	0	0	0	0	0	0	0	1	1809	7
11	0	00	0	0	0	0	1	1	1	1	0	0	0	0	0	0	0	0	0	0	0	0	904	4
12	0	0	0	0	0	0	0	0	0	0	0	0	0	0	1	1	0	0	1	0	0	1	1988	4
13	0	0	0	0	0	0	1	0	0	1	0	0	0	1	0	1	0	0	1	0	0	0	2616	5
14	0	0	0	0	0	0	0	0	0	0	0	0	1	0	0	0	0	0	0	0	1	1	2329	3
15	0	0	0	0	0	0	0	0	0	0	0	1	0	0	0	1	0	0	0	1	0	1	1230	4
16	1	0	0	1	0	1	0	0	0	0	0	1	1	0	1	0	1	0	0	1	1	1	2710	10
17	0	0	0	0	0	0	0	0	0	0	0	0	0	0	0	1	0	1	1	0	0	0	1103	3
18	0	0	0	0	0	0	0	0	0	0	0	0	0	0	0	0	1	0	0	0	0	0	1264	1
19	0	0	0	0	0	0	0	0	0	0	0	1	1	0	0	0	1	0	0	0	1	0	2914	4
20	0	0	0	0	0	1	0	0	0	0	0	0	0	0	1	1	0	0	0	0	0	0	1113	3
G	1	0	1	1	1	1	1	0	0	0	0	0	0	1	0	1	0	0	1	0	0	1	1944	10
R	0	0	0	0	0	1	1	0	0	1	0	1	0	1	1	1	0	0	0	0	1	0	1833	8

Figure 3.11 The Patitapu WSN represented by its geometry (left) and its respective connectivity or adjacency matrix (right, 1 – visible, 0 – not visible). Each grey line in the graph and each element of the adjacency matrix represent a connection between two nodes. The mean distance (MD) among the visible nodes and the number of visible nodes (VN) from each location are shown regardless the effective radio range (G – gateway, R – relay node).

Once the network was in operation, network communication layouts were pulled out multiple times from the system on various dates (06/12/2016, 17/06/2017, 08/09/2017). A reversed tree diagram was used to visualize network connectivity that shows the WSN communication at a specific time stamp (Fig. 3.12). The trees were generated from ASCII art trees provided by TAG IT and the plots revealed the important role of the relay node and the parent-children relationships. As the communication-protocol is self-healing and flexible, the WSN communication structure changes depending on radio signal strength and node availability.

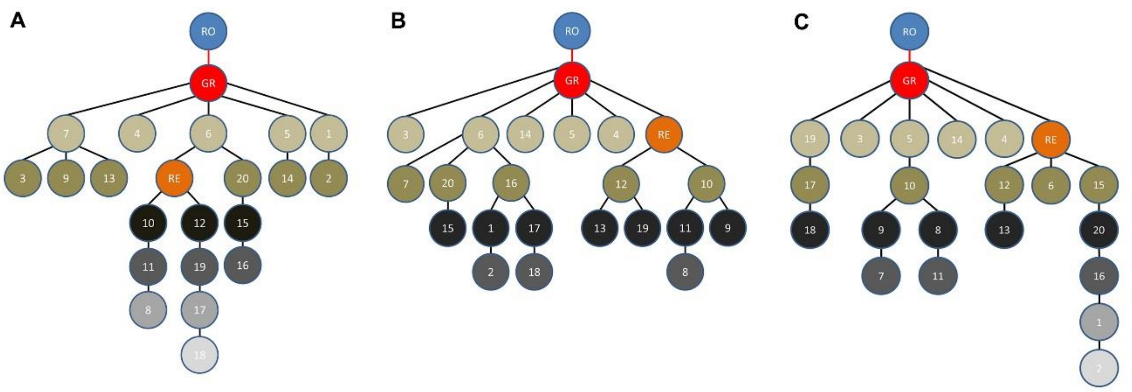

Figure 3.12 Examples of WSN communication layouts are shown on 6 October 2016 (A), on 17 June 2017 (B) and on 8 September 2017 (C) generated from ASCII art trees. The data transmission is dynamic and it restructurers itself to maintain connectivity (RO: Root, GR: Gateway Radio, RE: Relay node). The colours indicate various levels of the parent children relationships.

3.2.6 AquaCheck probe calibration

Due to the distance among sensors, topography and soil conditions vary between microsites, and this can effect sensor readings. Factory provided calibration functions were assessed and they were observed to significantly underestimate the true soil water content (Hajdu et al., 2019). Consequently, the accuracy of the probes were improved by performing a multi-level, farm-, microsite or probe- and sensor-specific calibration depending on the required precision and available soil information. Chapter 4 provides a detailed description of the calibration procedure and accuracy assessment.

3.3 Determination of microsite-specific soil properties

The research required soil samples for gravimetric (θ_g, gg^{-1}) and volumetric soil water content (θ_v, m^3 m^{-3}), bulk density (ρ_b, gcm^{-3}), particle size analysis (soil texture) and total organic carbon (TOC, %) measurements.

3.3.1 Gravimetric soil water content

The soil sampling events were carried out during dry ($\theta_v \approx 0.25$ m^3 m^{-3}), moderately wet ($\theta_v \approx$ 0.35 m^3 m^{-3}) and wet ($\theta_v \approx 0.45$ m^3 m^{-3}) stages of θ_v conditions over five sampling events (on 21/11/2016, 23/02/2017, 24/04/2017, 31/10/2017 and 18/11/2017). During four sampling events, the gravimetric samples were taken using a soil auger (⌀ 5 cm) approximately 0.6-0.8 m away from the multi-sensor probe location avoiding the upper slope areas (Fig. 3.13 (A)). Three soil cores were collected at each location and the cores divided into four depths (70-130, 170-230, 270-330 and 370-430 mm) corresponding to the depth of the soil volume sampled by each sensor (Fig. 3.13 (B and C)).

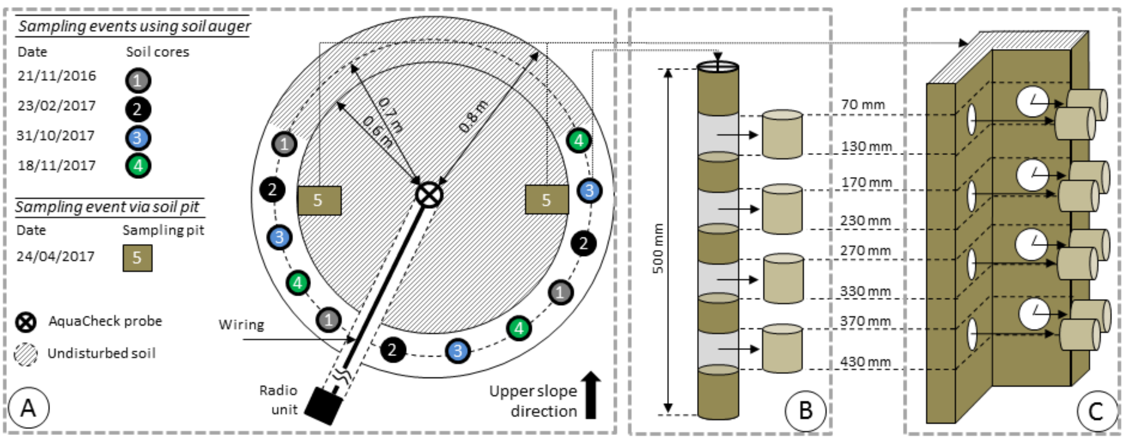

Figure 3.13 **Soil sampling design illustrating the soil core locations arranged in a circle surrounding the sensor probe (A). The four soil depth increments obtained from soil cores for gravimetric analysis are shown in (B) and the sampling method for soil bulk density measurements from soil pits is shown in (C).**

The samples were immediately placed in sealed containers inside a cooling box and taken directly to the laboratory to be processed. For one sampling event, the three soil cores were kept separate to ascertain variability caused by the sampling method. For the other three sampling events, the samples were composited for each depth and treated as one sample in the laboratory.

To obtain reference soil water content values used in the sensor calibration, θ_g was measured by the thermo-gravimetric technique (oven drying). Despite being an old technique, this approach has been the most widely used for the direct determination of soil moisture (Schmugge et al., 1980, Lekshmi et al., 2014). Therefore, it is often required for calibrating soil moisture measuring equipment (Johnson, 1962, Lal and Shukla, 2004, Dobriyal et al., 2012). The procedure involves taking representative soil specimens from the site of interest, and placing the samples in a forced draft oven for drying at a constant temperature of about 105 °C. The process ends if the sample weight becomes constant, and as a result, θ_g on dry basis can be calculated as per Eq. (2.1). Soil cores were used for obtaining samples for θ_g measurements and they were subsampled for particle size analysis and TOC estimation. Sampling pits provided opportunity to examine the soil media surrounding the sensor probes down to 50 cm depth.

3.3.2 Bulk density measurements

For most purposes, water content based on volume fraction (i.e. θ_v) is required and more useful. Through the determination of ρ_b of the soil sample, θ_v can be obtained (Gardner et al., 2000, Shukla, 2013). Soil compaction is indicated by ρ_b that affects infiltration, rooting depth, plant available water, nutrient extraction by plants, soil porosity and aeration. In agriculture, ρ_b is defined as the ratio of the mass of oven dry soil to a unit volume of soil (Grossman and Reinsch, 2002) as per Eq. (2.4). The relationship between ρ_b and θ_g was used to compute θ_v as presented by Eq. (2.5).

During one sampling event, soil samples for both ρ_b and θ_g measurements were acquired by opening two narrow, 0.5 m deep pits approximately 0.4 m from the AquaCheck probe (Fig. 3.13 (A and C)). The ρ_b samples were obtained horizontally using 84.76 cm^3 steel cylinders within which the soil material was retained for subsequent drying and analysis. The steel cylinders with the samples were dried in an oven at 105 °C for 24 h.

Soil variability tends to be greater near the soil surface in hill country. This is mainly due to the interrelated effects of grazing livestock, soil organic matter, land use, topsoil downslope movement, rooting characteristics, and the presence of soil organisms (Stavi et al., 2008, Chaudhari et al., 2013). Hence, five replicates were taken from 100 mm soil depth while three replicates were obtained for all other soil depths. Mid-points of the sampling depths corresponded to those of the sensing volume of each sensor. Sampling holes were subsequently infilled with soil from the same horizon, preserving the compaction.

3.3.3 Particle size distribution analysis

The relative size distribution of the primary particles in a soil, referred to as soil texture, plays a fundamental role in most pedogenic processes (Gee and Bauder, 1986). Soil water holding capabilities, nutrient retention, the exchange of air and water parameters, effective rooting depth and the overall physical behaviour of the soils are highly influenced by its mechanical composition and clay content (Kettler et al., 2001, Eshel et al., 2004, Bronick and Lal, 2005). Furthermore, the ground-based soil monitoring sensing units are usually sensitive to soil texture and require soil-specific calibration. In case of the AquaCheck product utilised in this study, the manufacturer provides 6 calibration equations for volumetric water content calculations depending on the soil textural classes, namely sand, clay, silt-loam, generic, loam, and clay-loam (Aquacheck, 2008). The following chapters of the study heavily rely on accurate soil moisture readings. This requires detailed information on soil texture at the microsites at multiple depth.

Several methods are employed to determine the particle size distribution and to separate the textural fractions. Field texturing, the hydrometer method, pipette method, sedimentation technique, sieving, dynamic light scattering, image analysis and laser diffraction are some of the various techniques applied for a wide range of sample types (Kettler et al., 2001). The overall textural designation is determined based on mass ratios of the three separates, i.e. sand, silt and clay using one of the standard soil textural classifications.

In this study, a laser scattering particle size distribution analysis or laser diffraction method (LDM) was performed using a Horiba LA-950 (HORIBA Scientific, Kyoto, Japan) machine and an attached slurry sampler extension (Fig. 3.14). The method was chosen based on the number of samples under investigation and the accuracy required for the purpose of the study. It was observed by Fisher et al. (2017) that LDM is a reliable approach for routine soil particle size analysis. In the same study, the LDM results were also compared to grain size distribution obtained from sedimentation method and showed strong agreement. The LDM offers acceptable time effectiveness, reliability, precision and reproducibility parameters for soil particle sizing, as well as continuous size information between the sensing ranges (Miller and Schaetzl, 2012).

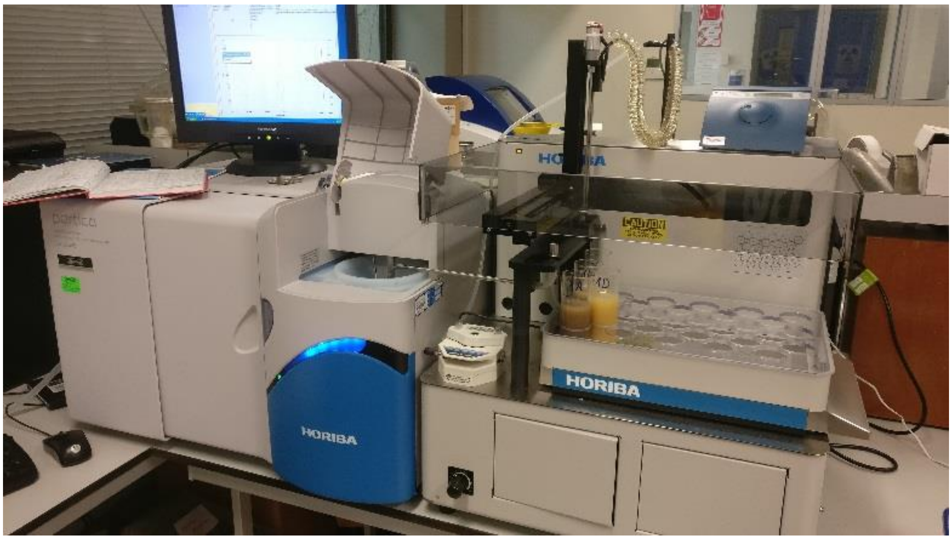

Figure 3.14 The Horiba LA-950 laser particle size analyser with the attached slurry sampler extension during operation.

The Horiba LA-950 unit is a sophisticated laser particle size distribution analyser that uses 2 beams of light of different wavelengths (LED: λ = 405 nm, Laser: λ = 650 nm) to determine the distribution of grain size classes in fluid-solids dispersions. The grain size range of particles compatible with the instrument is 10 nm to 3 mm. The internal circulation system uses deionised water as dispersion medium. A double array of sensors detects light rays passing through or scattered by solid particles of specific refractive indices (RI) in relation to deionised water. It works on the principle that the angle of scattered light beam is inversely proportional to the interacting object size. A collection of particles will produce a recognisable pattern of scattered light defined by intensity and angle, providing information that can be converted into a particle size distribution and visualised through the Horiba Software. The Horiba particle size distribution analyser is calibrated by commercially available, traceable standard particles (polymer micro spheres). This process guarantees a high accuracy of ±0.6 % or less and a reproducibility of ±0.1 % or less (Horiba Scientific, 2017).

In this research, only the fine earth class of soil granulometry was in interest, covering a particle size range of 0-2000 µm. Fine earth is usually divided into three particle size classes: clay (fine particles < 2 µm), silt (medium size particles between 2-50 µm) and sand (coarser particles between 50-2000 µm). The diameter range of the individual size groups were defined by the U.S. Department of Agriculture (USDA) (Gee and Bauder, 1986) and their size limits were accepted in this analysis since it widely applied globally and also generally accepted in New Zealand. Taking into account the predefined size limits by the Horiba particle size distribution analyser, the size intervals were chosen as 0-1.953 µm for the clay, 1.953-44.19 µm for the silt and 441.9-2000 µm for the sand fraction.

3.3.3.1 Sample processing

Each collected soil increment was sub-sampled into two sets, from which only one was chosen for the particle size analysis. 3-4 grams of material was separated taking care that subsamples reflect the entire sample as much as possible. It has been observed that in the case of LDM the difference between using or not using chemical pre-treatment was not statistically apparent neither for topsoil or subsoil (Fisher et al., 2017). On the other hand, ultrasound treatment was observed to be a faster method for breaking down the particle aggregates than applying chemical solutions such as Na-hexametaphosphate (Ryżak and Bieganowski, 2011). Additionally, the samples were not treated for fine organic matter removal since the Aquacheck probes also measure the original, intact soil material containing organic matter.

Prior to analysis, the samples were air-dried and the roots and coarse fragments (> 3 mm) were separated since the Horiba LDM is not able to detect these elements. The samples were placed in glass cylinders to achieve efficient dispersion through physical procedures (Fig. 3.15). The tubes were filled with deionised water up to three quarter level for dilution and the samples were stirred with a rod until homogenous suspensions were formed. Afterwards, a 16-hour end-to-end rotational mixing was applied which was followed by a 10 min ultrasonic bath treatment to improve the disintegration of the agglutinated particles.

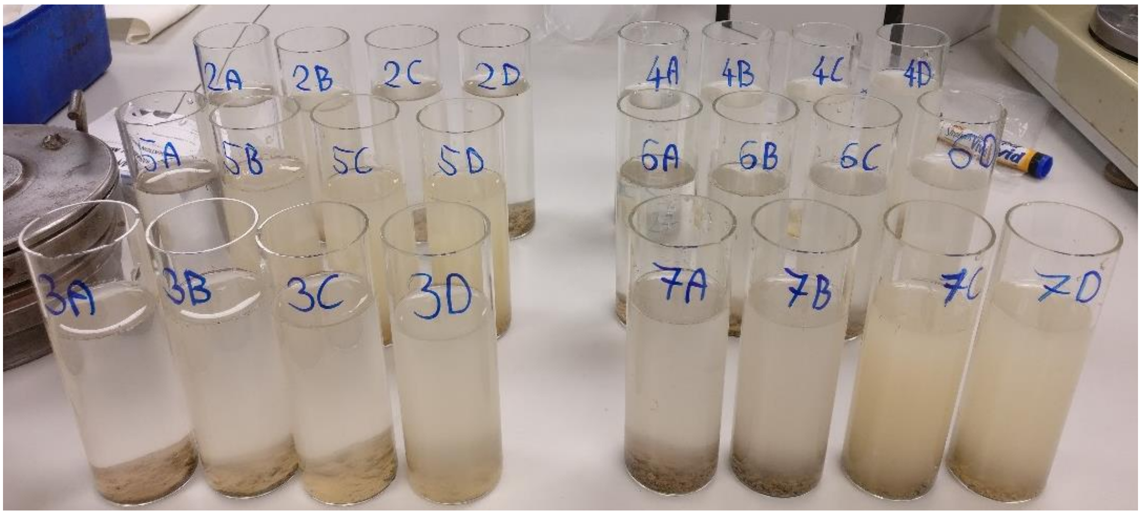

Figure 3.15 Sample dispersions with added deionised water prior to the stirring as first step of the preparation process.

Prior to the measurements, the suspensions were thoroughly mixed once again by a rod to dislodge the sediment from the bottom of the cylinder.

3.3.3.2 Laboratory measurements

The LDM method quantitatively determines the physical proportions of various sizes of primary soil particles falling somewhere within the 38 predefined grain size bins. The slurry sampler extension was used to run the samples in suspension and in batches of 30 samples. The Scheduler part of the controlling software was set up to automate and simplify the analysis by executing a pre-defined series of steps using the slurry sampler tray. The sequence includes feeding, debubbling, aligning, blank measurement and rinsing multiple times to ensure consistent reading and to mitigate contamination. The sample is taken from the glass beakers after a high rpm mechanical stirring controlled by the Horiba software. Each sample was analysed three times and the mean of the three measurements were taken to define soil texture. Volume-based particle size distribution was calculated by utilising the Mie scattering theory as standard, modern procedure for specimens with all fine grain sizes (Sperazza et al., 2004, Ozer et al., 2010). Input parameters, such as particle RI and particle absorption index were determined by the statistical method (considering R parameter and X square) suggested by Horiba (Bodycomb, 2013) whereas the RI of the dispersant (i.e. deionised water) was set to 1.33.

3.3.4 Total organic carbon (TOC) measurements

The TOC encompasses a wide range of organic compounds in soils, therefore its quantification in soil horizons provides essential information for scientific research, agricultural activities and management practices (Matejovic, 1993). TOC is a vital component of the complex soil-water-atmosphere system, influencing numerous biological and physical processes that are in continuous interaction with nutrient cycles. Microbiological activity, biomass accumulation, organic matter decomposition and mineralisation are governed by soil water content that affects yield production (Linn and Doran, 1984, Amador et al., 2005, Tulina et al., 2009).

Furthermore, TOC plays an important role in the characterisation of soil water storage and hydraulic properties and there exists an optimum level of TOC that is required to hold adequate amount of moisture and nutrients (Post and Kwon, 2000). Soil water holding capacity is strongly limited by soil water retention that is impacted by TOC, hence driving soil moisture redistribution, water availability, evaporation rates and several ecological processes (Yang et al., 2014). Moreover, soil moisture spatial variability is strongly related to TOC as it was shown by Baumann et al. (2009) on alpine grasslands.

TOC, particle size distribution and ρ_b are the main parameters in most pedotransfer functions that predict soil water holding properties including field capacity, saturation, plant available water and permanent wilting point (Yang et al., 2014, Minasny and McBratney, 2018).

Although, various methods are available to measure TOC content in soils, such as the wet oxidation techniques, the popular dry (or heat) combustion method was chosen in the present study. It is one of the most commonly applied techniques for measuring TOC in soils and agricultural products due to its precise and accurate automated operation that is able to measure the quantity of C, H, N and S content from one weighed sample rapidly and simultaneously (Sleutel et al., 2007).

3.3.4.1 Sample processing and preparation

As it was mentioned above, for particle size distribution analysis, 80 soil samples were collected in the field and subdivided into two subsets in the laboratory. One set was used for the particle size distribution analysis, whereas the second subset was used for the TOC analysis. The samples were taken from the depth intervals corresponding to the soil moisture sensors' position at 100, 200, 300 and 400 mm. The samples were air-dried, crushed and sieved using a 2 mm sieve before they were homogenised. As a last step, the particle size was reduced to < 250 µm by gentle grinding.

The subsamples were packed in aluminium foils and WO_3 powder was used as additive to increase the efficiency of the combustion. The samples were wrapped and closed gas tight avoiding the loss of substance, before the capsules were weighed. Afterwards, the compressed and folded sample packets were placed in the carousel sample magazine and were covered by a plastic ring during the automated measurement process. To calculate the daily factor and calibrate the instrument, conditioning samples were prepared that included blank samples and daily factor samples using the factory recommended Sulphanilamide.

3.3.4.2 Sample analysis

The analysis was conducted by a Vario MACRO Cube CHNS elemental analyser (Elementar Analysensysteme GmbH, Hanau, Germany) that operates on a catalytical, dry-combustion principle (Fig. 3.16). The samples are combusted in a furnace at 950 °C to 1200 °C when lowered in a combustion tube and oxygen is jet injected over the sample. The elevated temperature and the use of accelerants ensure the complete combustion of all carbon forms present in the soils. During combustion, the targeted sample elements are converted into simple gases, the desired components are separated and moved to the detectors by carrier gases. The TOC is estimated from the evolved CO_2 by a thermal conductivity detector (Sleutel et al., 2007). For the purposes of the study, a single soil subsample was used for both total C and N content estimation.

Figure 3.16 The Vario Macro Cube elemental analyser used in the study (A) and an example of the prepared, grinded samples just before subsampling (B). The WO_3 powder was added to the subsamples as combustion aid and Sulphanilamide was used for instrument conditioning.

3.4 Pasture growth measurements

3.4.1 The cage technique

In New Zealand, a commonly used method to measure herbage production is the application of the exclosure cage-technique or "Cut method". The method has been applied successfully, providing valuable information in a number of studies where relative pasture production differences were the main focus (Devantier et al., 1998). It involves the collection of re-growth from a trimmed quadrat (Radcliffe, 1974a).

In this study, to assess the accumulated dry matter (DM), three moveable livestock exclusion cages were positioned at 13 microsites to exclude stock from grazing that specific area. The cage-protected surface was trimmed down to 10 mm height by using a grass shear and re-trimmed every 4-6 weeks within a standard 320x320 mm quadrat. The cages were moved around the AquaCheck probe and placed back on freshly cut surfaces making sure that the previously measured spots were avoided.

The fresh pasture cuts were stored in chilled polystyrene boxes until they were weighed. The selected 3 m diameter sampling areas were considered to represent a stand of more or less homogenous pasture cover with relatively consistent pasture composition, terrain attributes and soil parameters.

The samples were cleaned from soils and placed in paper bags for the determination of the accumulated DM. The measurement was achieved through the evaporation of water from the feed in a forced air oven with a drying time of 24-48 hours, leaving only the DM behind. The effects of the cage technique on growth rate have been studied by Marsh (1978) who did not observe any significant effect caused by the presence of exclosure cages. Slight change in micro-climate under cages and increased growth rate was recorded by Heady (1957) inside the caged area during the cold season with slow growth. The differences in growth rate between caged and not caged sampling sites seemed to disappear in spring with fast growth and there was no difference detected in composition. Therefore, in the present study, the effect of cages have not been taken into account. A comparison of cage and model techniques can be viewed in Devantier et al. (1998).

3.4.2 The sampling sites and field data collection

The 13 microsites were distributed on flat areas as well as north-, east-, south- and west-facing slopes, which were subdivided, based on slope angle. Each aspect class contains microsites on steep and gently rolling slopes. These microsites were established to determine the effect of soil physical properties, climatic parameters and topographical attributes on pasture production.

Pasture growth sampling was conducted 16 times during the experiment, covering the period between 01/11/2016 and 20/06/2018. At every site, the total herbage accumulation was calculated by averaging the DM data from the three sampling points. Yields were calculated as kg DM/ha for each harvest date. Growth per day was computed by dividing the total yield by the number of days separating two cuts.

3.5 Remote sensing data

The study aimed to synergistically use spaceborne radar (Sentinel-1) and multispectral (Sentinel-2, Landsat 7 and Landsat 8) data for the spatial prediction of near-surface soil water content at the Patitapu Station. The Materials and Methods section of Chapter 6 provides a brief description of the Sentinel-2 and Landsat satellite missions and the characteristics of the utilised image collections. After a brief summary of the science program and objectives behind the Sentinel missions, the focus will be placed on the Sentinel-1 satellites, their characteristics and currently available products due to the increasing role of radar data in soil moisture research. A short description is given on how the remote sensing data is generally accessed in this study. Finally, the section ends with a brief report detailing the specifications of the used radar dataset over the research area.

3.5.1 The Copernicus Earth observation program

The Copernicus initiative, headed by the European Commission and the ESA was designed to provide easily accessible information about the environment and to obtain data for civil services and applications. Within the program’s lifetime, ESA is developing and placing into orbit a fleet of new satellites, called Sentinels, to serve the requirements of the European Commission and the European Union (Torres et al., 2012). The Sentinels will capture images of the land, oceans and the atmosphere through currently seven satellite missions. At the time of the study, three operating, two-satellite constellations were in orbit, including the Sentinel-1, Sentinel-2 and Sentinel-3 launched in the years of 2014-2018. The data is made available via a range of information services to provide imagery for researchers, policy makers, civil services and numerous other humanitarian needs (ESA, 2018b). These missions are considered as "game changers" due to their operational configuration and improved instrumentation in the field of land management, dynamic hydrological processes, marine environment, atmosphere, emergency response, security and climate change.

3.5.2 The Sentinel-1 mission

The Sentinel-1 is a radar-imaging mission for land and ocean services generating systematic, high quality products with quick data delivery. The Sentinel-1 mission, particularly Sentinel-1A satellite represents the first dedicated component of the European Copernicus program that was placed into orbit. The Sentinel-1A was sent to space on 3 April 2014 whereas Sentinel-1B was launched on 25 April 2016. The constellation was designed to take images over landmasses, coastal zones, sea-ice, polar areas and the global ocean to ensure data continuity after the age of the first reliable and operational ERS 1 and 2 radar-imaging systems. The Sentinel-1 imaging radar mission aimed to provide microwave-based observations with improved resolutions with weather and daylight independent image collection capabilities. Taking into account these advantages and the global coverage, the Sentinel-1 mission has the potential to be used for operational soil moisture monitoring at a finer scale than previous space missions could achieve (Wagner et al., 2009b, Hornacek et al., 2012, Paloscia et al., 2013).

Both satellites were placed on the same polar orbital plane at an altitude of 693 km but with a phase difference of 180 degree. These conditions allow the formation of interferograms and the maximum 12-day revisit time that applies to each satellite individually, can be shortened. Therefore, the Sentinel-1 constellation is able to cover the main landmasses every six days at the Equator and even shorter revisit times are given for areas with higher latitudes. The mission offers regular, frequent image acquisition and a ground resolution of 5m x 20 m in the main, 250 km wide swath operation mode over landmasses (Attema et al., 2008, Torres et al., 2012). ESA specified the life time of the individual satellites as 7 years, with consumables allowing the extension of the mission up to 12 years, while the life cycle of a satellite generation is planned to be in the order of 15–20 years (Torres et al., 2012).

3.5.2.1 Instruments and operational modes

The Sentinel-1 satellite pair was mounted with identical C-band SAR instruments working at 5.405 GHz frequency (λ = 5.6 cm) and with 1dB radiometric accuracy. The C-band radar signal can penetrate through clouds and most rain events without major impact on the signal giving a significant advantage over optical imagery for time series and change detection analysis (Muro et al., 2016) in land surface monitoring. The C-SAR instrument is supplemented by an active phased array antenna (length of 12 m) with dual channel transmit and receive modules. The SAR is able to provide images with single or dual polarisation i.e. HH or VV for single and HH+HV and VV+VH for dual channels (Hornacek et al., 2012). Four exclusive acquisition modes are available, namely Stripmap, Interferometric Wide swath, Extra-Wide swath and Wave (Fig. 3.17).

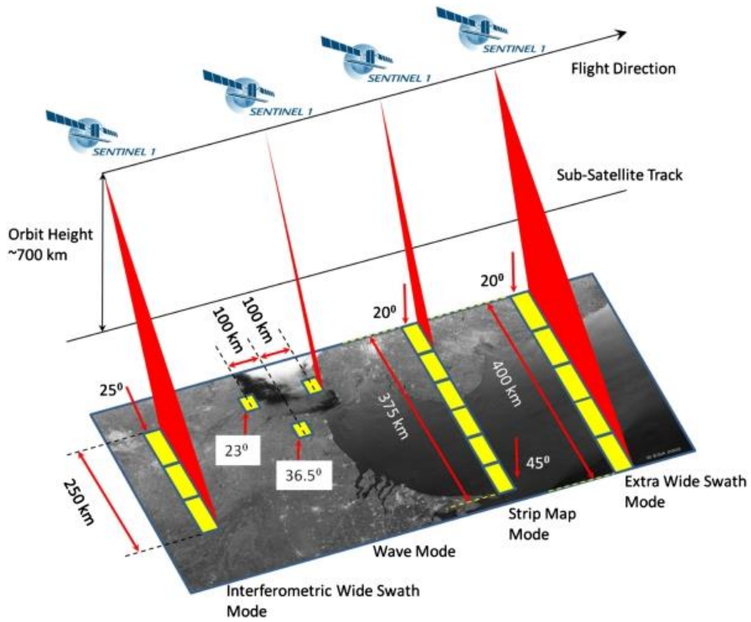

Figure 3.17 Sentinel-1 image acquisition modes. Out of the four operational modes, the Interferometric Wide swath mode satisfies the most requirements for numerous environmental applications (ESA, 2018c).

While the Stripmap, Extra-Wide swath and Wave modes are used only over specific areas and specific applications, the Interferometric Wide swath option with VV+VH polarisation is the primarily used mode over landmasses that serves most applications (ESA, 2018c).

There are three product types, Level 0, Level 1 and Level 2 depending on the level of processing. Level 0 products contain the raw data with noise that is compressed and unfocused. The Level 1 and Level 2 data are produced from the Level 0 products. Most data users are interested in the images derived by the Level 1 processing chain as it is transformed from raw data via various algorithms to an easier to handle product. The processing can result in Single Look Complex images or Ground Range Detected (GRD) images (ESA, 2018d). Single Look Complex products contain the phase and backscattering information, which is required for the generation of the coherency matrix for interferometry. In this study, the Level 1 GRD images were used that have been detected, multi-looked (5 x 1 looks) and projected to the ground range by the application of the Earth ellipsoid model WGS84, on which additional terrain correction was carried out. It carries less information and the file size is significantly smaller compared to the Single Look Complex data. The focussed SAR GRD images used in this study were acquired in Interferometric Wide swath operational mode at both VV (vertical transmit and vertical receive) and VH (vertical transmit and horizontal receive) polarisations were available for most of the experimental period. The pixel spacing was 10 x 10 m in range and azimuth directions.

3.5.3 Data access

Sentinel-1, Sentinel-2, Landsat 7 and Landsat 8 products are made freely available systematically through the Copernicus Open Access Hub (Copernicus Open Access Hub, 2018) to all data users including general public, researchers and commercial users. The ESA provides a freely accessible, open software environment, called Sentinel Application Platform (SNAP), within which the open source Sentinel-1 Toolbox is equipped with the essential tools for the pre-processing, visualisation and analysis of the Sentinel-1 data (SNAP, 2018).

However, the ever-growing amount of available Earth observation data has been reforming the concepts of how the data can be delivered to users and how the data is analysed (Hird et al., 2017, Esch et al., 2018). Individual, standard workstations are no longer able to process the data volume with improved spatial and temporal resolution acquired by the increasing number of satellites. In this study, the need for high computational power, storage capacity and the time series type of dataset meant that an alternative data platform was chosen to extract Sentinel-1 SAR data as well as Sentinel-2, Landsat 7 and Landsat 8 data. The high number of remote sensing images used in this thesis suggested the application of a cloud-based geoinformation service to access consistent and continuous image collections.

3.5.3.1 Google Earth Engine (GEE)

One of the modern cloud-computing platforms for accessing and processing large amount of Earth observation and geospatial data collections was developed by Google. Google's GEE offers a platform where researchers, scientists and developers have the possibility to conduct analysis from the local to the planetary scale. The combination of thirty years of satellite imagery, already existing or newly developed algorithms and real world applications makes GEE a powerful tool in the field of Earth observation. Monitoring the dynamic changes on the Earth surface is of great interest especially in the field of environmental applications such as the tracking of changes in natural resources, deforestation, agricultural practices and climate.

GEE allows users to execute various geospatial processes on Google's infrastructure and run the computations on high performance, intrinsically parallel services. The interaction between the user and the platform is provided in several ways, although a commonly used option is the Code Editor, a web-based integrated development environment. This environment supports the use of Python and JavaScript application programming interfaces that allows users to reach an analysis-ready, Internet accessible data catalogue. A large repository of pre-processed datasets are made available from several satellite missions containing optical and non-optical image collections (Gorelick et al., 2017, Google Earth Engine, 2018a). An advantage of using a cloud-computing platform is the consistent datasets that can be analysed by multiple users. Another benefit of the cloud-based approach is that the processing is done online and the data is not downloaded to the local desktop computer during processing.

3.5.3.2 Sentinel-1 image collection and pre-processing

The GEE catalogue contains all processed GRD Sentinel-1 scenes at Level 1 since Oct 2014 with weekly update. The dataset can be filtered to generate a homogenous image collection since images at three resolutions, in three instrument modes and with various band combinations of polarisation modes are all included. To be able to work with the SAR data and to create a GIS ready image collection, several pre-processing steps need to be executed.

The pre-processing procedure implemented is built upon the algorithms applied in the Sentinel 1 Toolbox that is also employed in SNAP. The description below is mainly based on the documentation available on GEE application programming interfaces (Google Earth Engine, 2018b). The standard workflow consists of six main steps that satisfy the data need for most applications and assure the quality of the results retrieved from the imagery. First, an orbit file refinement is performed to apply the most accurate satellite position and velocity information. The second step removes the GRD border noise and invalid data from the scene edges that is followed by the thermal noise removal as the third step to reduce discontinuities between sub-swaths and the additive background energy (Carsey, 1992). Fourth, radiometric calibration is conducted to derive backscatter intensity from digital numbers by the application of sensor-specific calibration parameters. In the fifth step, also knowns as terrain correction, the data is transformed from ground range geometry to backscatter coefficient σ^0 represent the target backscattering area (radar cross section) per unit ground area as it is explained in more detail in **Chapter 2**, Section 2.5.5. To correct for the geometric distortions and to generate orthorectified images, a 30 m DEM data from the Shuttle Radar Topography Mission (SRTM) is utilised. As a last step, the unitless σ^0 is converted to dB, i.e. from linear scale to logarithmic scale as it can vary across several orders of magnitude. The steps described above result in images with 10 m pixel spacing. The pre-processed images are stored in a pyramid type of tile database with optimal tile size for online data reading and visualising the dataset effectively (Gorelick et al., 2017).

3.5.4 Sentinel-1 imagery over New Zealand and the Patitapu Station

Over New Zealand, the available polarisations are VV and VH in both ascending and descending modes. GRD products were chosen for this study, as the objectives needed backscattering intensity and incidence angle data and did not require phase information. As the satellites carry the same type of instrument, combinations of descending and ascending modes are generally possible. Sentinel-1A passes over the research area in the evening, whereas Sentinel-1B flies over in the morning hours. Figure 3.18 depicts the Sentinel-1 acquisition segments and sensor view directions over New Zealand as well as the image positions that cover the Patitapu Station in both orbit types. The σ° and incidence angle information were obtained by creating an image collection within GEE and extract SAR data at the points of interests, i.e. at the twenty microsites. The information was extracted from 150 Level-1, GRD images acquired in Interferometric Wide swath mode between 01/11/2016 and 01/07/2018 in the available dual polarisation.

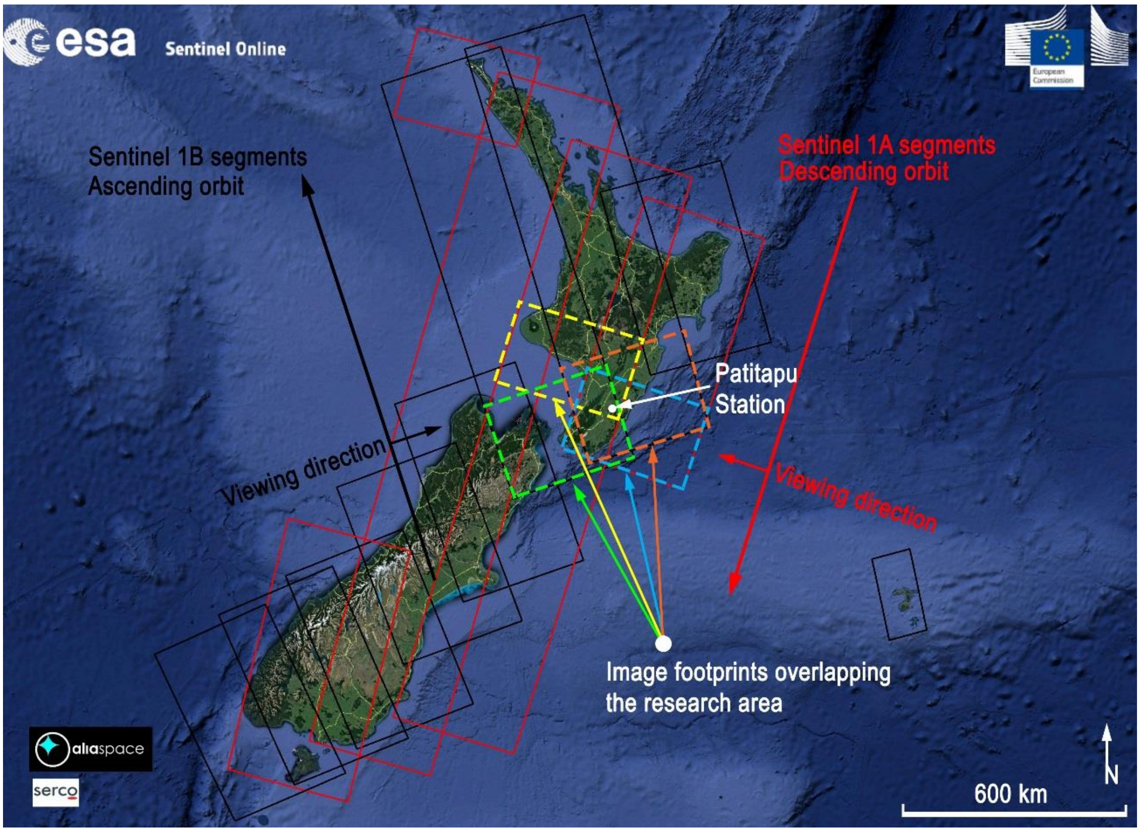

Figure 3.18 Illustration of the Sentinel-1A (red) and -1B (black) image acquisition segments over New Zealand and the image tiles as presented in Google Earth Engine specifically over the research area, Patitapu Station, located in the North Island (background image generated in Google Earth Pro and Sentinel 1 segments were accessed through ESA (2018a).

Chapter 4

Field performance assessment and calibration of multi-depth AquaCheck capacitance-based soil moisture probes

*The contents of **Chapter 4** was submitted as an original research article on 25 June 2018 and accepted for publication on 1 March 2019 in the peer-reviewed journal of Agricultural Water Management (impact factor of 3.182 in 2017). Some parts of the published paper were modified to fit in the thesis outline and to avoid repeating content and figures.*

The authors:

***Istvan Hajdu**[1*], Ian Yule[1], Mike Bretherton[1], Ranvir Singh[1], Carolyn Hedley[2]*

[1]*Massey University, Palmerston North*

[2]*Manaaki Whenua, Landcare Research, Palmerston North*

Citation:

HAJDU, I., YULE, I., BRETHERTON, M., SINGH, R. & HEDLEY, C. 2019. Field performance assessment and calibration of multi-depth AquaCheck capacitance-based soil moisture probes under permanent pasture for hill country soils. Agricultural Water Management, 217, 332-345.

4 Chapter 4 - Field performance assessment and calibration of multi-depth AquaCheck capacitance-based soil moisture probes

4.1 Introduction

Soil water content monitoring is rapidly developing across different types of soil-plant systems over many landscape features at a time of increasing food demand and more intense agricultural drought events (Howell, 2001, Charlesworth, 2005, Trenberth et al., 2013). Accurate measurements of real-time soil water contents allow farmers, agronomists and hydrologists to better inform pre- and in-crop strategic inputs, pasture production (Matson et al., 1997), irrigation management (Leib et al., 2003) and nutrient cycling (Dougill et al., 1998) at farm scale. Similarly it is essential for hydrological modelling (Western et al., 2002), meteorological applications (Rowntree and Bolton, 1983) and flood risk evaluation (Massari et al., 2014) at catchment scales. Soil water content controls the soil infiltration rate, runoff and evapotranspiration influencing plant water availability that plays an essential role in precision agriculture as the single most important natural resource for pasture production (Rodriguez-Iturbe et al., 1999, Woodward et al., 2001).

Due to the interaction of numerous environmental parameters, soil water content is generally considered a both temporally and spatially highly changeable soil physical state variable, although the spatial patterns have been observed to remain stable over time (Vachaud et al., 1985, Vanderlinden et al., 2012, Brocca et al., 2017). Soil water content predictability and variability are not yet fully understood, especially near the surface and within the root-zone; these being the layers of interest for most applications (Wilson et al., 2004, Petropoulos et al., 2014). Root-zone soil moisture is particularly useful for the evaluation of climate, land-surface and energy exchange models, while in-situ, near-surface soil moisture data is utilised in the validation and calibration of remotely sensed soil water products (Dorigo et al., 2011b, Liu et al., 2017). Consequently, obtaining accurate, frequent and non-destructive soil water data is significantly advantageous, if not essential, to facilitate improved yield and water management strategies in both irrigated and non-irrigated farming systems.

Several indirect methods measure a physico-chemical property of the soil to estimate soil water content (Evett and Parkin, 2005). The radioactive technology and the idea of the neutron moisture metre published by Gardner and Kirkham (1952) induced a breakthrough in modern soil moisture estimation. Calibrated neutron moisture meters are able to achieve high soil moisture sensing accuracy, although, the technique is extremely costly and it poses special requirements for installation and operation. The technique remained the standard until the age of dielectric sensors arrived in the 1980s (Ochsner et al., 2013). Since then, a wide range of electromagnetic soil water content sensing devices have been developed (Robinson et al., 2008b). State-of-the-art, continuous soil water measurement techniques make use of the dielectric property of the sensed soil matrix (Lekshmi et al., 2014). It has long been recognised that the measurement of the soils' apparent dielectric constant (Ka) can be directly related to volumetric soil water content (θ_v, m^3 m^{-3}) sensitivity (Dean et al., 1987).

Time Domain Reflectometry (TDR), Frequency Domain Reflectometry (FDR) and capacitance techniques are the most common methods to obtain soil water content by emitting electromagnetic energy pulses into the soil. The basics of TDR, FDR and capacitance techniques for soil water measurement were established by Topp et al. (1980) and Dean et al. (1987). The techniques rely on the physical principle that water in soil pores has a significantly higher Ka (~81 at 20 °C), than air in soil pores (~1), and higher than the typical mineral matrix of soils (3-12) (Dean et al., 1987, Noborio, 2001, Chandler et al., 2004). The TDR method relates soil water content to the travel time of the electromagnetic signal along a transmission line, since the propagation velocity of the electromagnetic energy impulse is mainly influenced by soil Ka (Blonquist et al., 2005). The generally expensive TDR sensors are commonly utilised as a reference (Bogena et al., 2007) due to their high accuracy and good agreement with observations obtained by neutron scattering (Serrarens et al., 2000). The FDR technique differs from TDR in that the former measures the variation of frequency of the returned electromagnetic pulses. Capacitance-based sensing devices are based on the frequency domain, although they make use of the charging time of the emitted electromagnetic field which is a function of soil Ka (Mittelbach et al., 2012). During measurement, a capacitor system is formed by two or more electrodes (metal rods, spikes or rings) inserted in the soil, which serves as the dielectric. An oscillator is often connected to the circuit - this converts the changes in soil Ka to the variation in the frequency of the transmitted signal between the electrodes (Leib et al., 2003, Lekshmi et al., 2014).

Soil Ka is influenced by factors other than soil water content, such as variation in soil bulk density (ρ_b), clay content, temperature, soil organic matter, and salinity (Topp et al., 1980, Roth et al., 1990, Tsheko and Savage, 2005). The sensing volume of FDR and capacitance techniques is relatively small and the operating frequency is generally below 100MHz. Therefore, these sensors have been observed to be sensitive to clay content, soil organic matter content, air gaps, temperature, amount of iron minerals and ρ_b (Robinson et al., 1994, Muñoz-Carpena et al., 2004, Dobriyal et al., 2012, Mittelbach et al., 2012, Visconti et al., 2014, Fares et al., 2016). In an attempt to circumvent this, calibrations provided by the manufacturer are generally developed under laboratory conditions by immersing the sensing units in solutions or in a soil medium with known parameters (Kizito et al., 2008).

Capacitance sensors have been proven to be accurate for effective soil water monitoring for either scientific or agronomic purposes, if a soil-specific calibration is provided (Matula et al., 2016, Singh et al., 2018), offering a significantly lower cost alternative to TDR (Evett, 2000b, Mittelbach et al., 2012, Visconti et al., 2014). However, their accuracy and dependency on soil properties have not been investigated extensively under field conditions, particularly not in New Zealand on diverse hill country landscapes and soils.

AquaCheck Ltd has more than 20,000 probes installed in more than 20 countries around the world, highlighting its key role among the industry's leading vendors in the rapidly growing global soil moisture sensor market space (Agri Optics, 2017). These numbers are expected to rise worldwide imposed by the increased pressure on sustainable agricultural productivity and the growing concern about climate, soil health and conservation. To date, AquaCheck Sub-surface sensor performance and the assessment of standard calibration functions have received little scientific attention, although they have been employed in several studies (Cronje and Mostert, 2008, Murungu et al., 2011). AquaCheck reported soil moisture data were compared to EnviroSCAN readings chosen as reference by Nolz (2013), however no comparisons were made against direct soil moisture measurements. Recently, Singh et al. (2018) presented a detailed evaluation of a variety of electromagnetic sensors in a loam soil in Nebraska, U.S, including the Aquacheck Classic probe. AquaCheck readings were related in reference to field calibrated neutron moisture meter observations. However, their study had a short timeframe (from 28 July to 6 September, 2016), and a narrow soil water content range. Additionally, the research was based on the statistical comparison of averaged soil moisture readings from two replicates at each of two selected depths, separately and combined. A criticism of the Singh et al. (2018) paper was published by Schwartz et al. (2018) questioning and commenting on the meaningfulness of the comparison between electromagnetic sensors and a neutron probe. In the reply of Rudnick et al. (2018), the authors reviewed the results in Singh et al. (2018) and rejected the claim proposed in Schwartz et al. (2018). Rudnick et al. (2018) clearly stated that their approach intended to generate a scientific review of the sensors available for customers rather than a comprehensive comparison.

Our study aims to evaluate the performance of 400 mm AquaCheck sub-surface multi-sensor, capacitance probes during a one-year period under field conditions in silt loam and silty clay loam soils. A comparison was made between sensor data collected from 20 spatially distributed probes and reference thermo-gravimetric observations. To achieve this aim, our objectives are to:

1. Assess the manufacturer-supplied calibration functions and establish new functions between raw sensor readings and reference observations to improve θ_v sensing accuracy at multiple depths. These custom calibrations will occur at three scales, i.e. farm (i.e. single calibration), probe (i.e. microsite-specific (20) calibrations) and sensor (i.e. sensor-specific (80) calibrations).
2. Investigate temporal θ_v patterns and compare differences in accuracy between the custom calibration methods and the manufacturer provided calibrations that were most suitable for the soil type at the research area.
3. Provide aspects about measurement accuracy for sensor users to help decision making on whether the complete (at sensor level) calibration is necessary for their applications.
4. Determine the effect of selected soil properties and soil wetness on sensor error distribution. Our intent is to inform future deployment of capacitance-based sensor probes for accurate predictions of multi-depth θ_v patterns on New Zealand hill country soils or in regions with similar soil characteristics.

4.2 Materials and methods

4.2.1 Experimental site and soil characterisation

The study was conducted on a ~2600 ha hill country property, Patitapu Station, located in the Wairarapa region of the North Island of New Zealand (40.745020 S, 175.887320 E, Fig. 4.1). The research site is primarily non-irrigated pastoral farmland mixed with native bush on rolling to steep hills, interspersed with fertile flat land. Sixty-four-year annual average rainfall is 1144 mm in this area with a range between 721-1735 mm (NIWA CliFlo, 1953-2017), although precipitation is often localised in hill country. Elevation ranges from 143-535 m above sea level. The microsites (Fig. 4.1) were selected from pastoral areas on the farm where the predominant plant communities are ryegrass and clover species. A permanent weather station (40.750032° S, 175.887493° E) was installed at the property, from where rainfall and air temperature observations were collected to investigate sensor response to climatic variables. The minimum, maximum and mean distance between the climate monitoring station and sensing probes were 0.34, 2.9 and 1.8 km, respectively.

Soil resource information was retrieved from the Fundamental Soil Layers that describes the spatial pattern of soil types defined by the New Zealand Soil Classification (Hewitt, 2010). The majority of the property is covered by Brown Soils as it is illustrated on Figure 4.1. At the group level, a common soil in the east side of the North Island, the Orthic Brown (BO) soil dominates over the study area, while patches of Orthic Gley (GO) soils occur along the main water ways and Firm Brown (BF) soils can be found in the eastern side of the property with higher altitudes. The topsoil is typically described as dark grey-brown while the subsoil is often brown or yellow-brown with generally well-drained characteristics and fine texture.

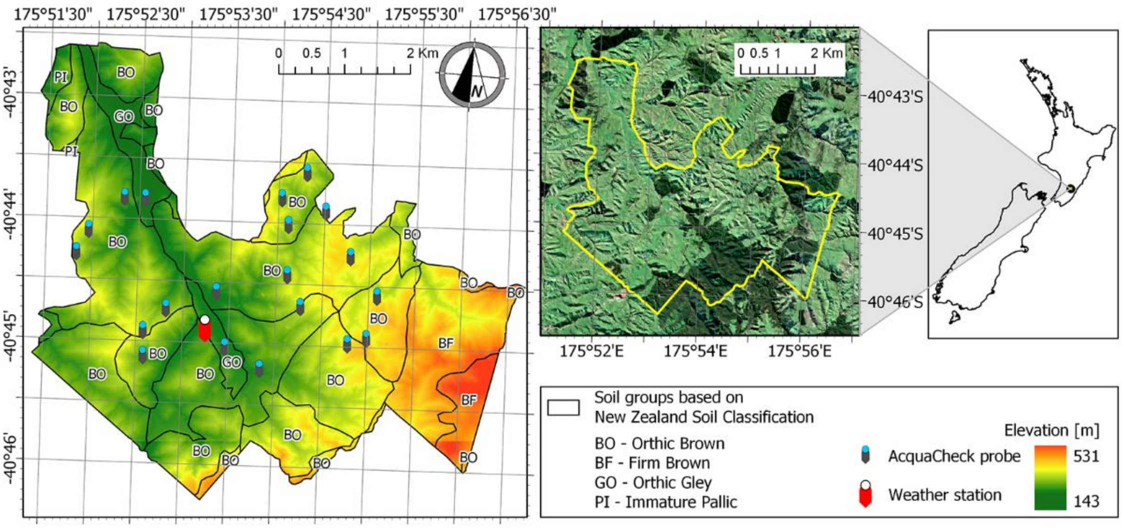

Figure 4.1 Location of the research area, land cover (LINZ, 2017), soil cover (New Zealand Soil Classification) and the distribution of the selected 20 microsites illustrated on a digital surface model.

4.2.2 Instrumentation and sensor data collection

4.2.2.1 AquaCheck multi-sensor probe specifications

The capacitance-based, 400 mm AquaCheck Sub-Surface probe is a robust multi-level device with four sensors spaced at intervals of 100 mm and with a right hollow cylindrical shaped sampling range. The sphere of influence can be approximated with geometric parameters of h = 60 mm (cylinder height), r = 16 mm (internal radius) and R = 20-45 mm (external radius). The probes are designed to be completely buried with an attached wire for data transmission to a logger (Fig. 2B). The sensor transforms the frequency readings to Scaled Frequency (SF) as raw output. The SF values range from 0-100 %, where 0 % is equal to a reading in open air, and 100 % when the sensor is immersed in distilled water. SF is calculated as per Eq. (4.1) as follows:

$$\boldsymbol{SF = \frac{F_{air} - F_s}{F_{air} - F_a}} \tag{4.1}$$

Where F_s is the frequency reading in the soil, F_{air} is the sensor frequency reading in air, and F_a is the sensor frequency reading in distilled water (Zettl et al., 2015). The SF readings are automatically corrected for possible inherent temperature change by embedded compensation functions. To calculate θ_v (%), SF values need to be converted using an empirical, laboratory-based calibration curve. The conversion is not a built-in function; therefore, the device is offered with factory calibration equations for six soil textures, e.g. sand, clay, silt loam, loam, clay and generic (composited from sand, silt loam and clay soils) (Agri Optics, 2017). The linear calibration equations provided by the manufacturer are in the form shown by Eq. (4.2):

$$\boldsymbol{\theta_v = b_0 + b_1 * SF} \tag{4.2}$$

where b_0 and $b_1$are the y-intercept and slope parameters of the generalised linear regression model and are dependent on the six determined soil textures. For the purpose of this study, the resulting θ_v (%) output was converted to θ_v ($m^3\ m^{-3}$).

4.2.2.2 Wireless sensor network based data collection and microsite design

At the Patitapu Station, a communication network utilising Wireless Sensor Network (WSN) technology was deployed for the investigation of soil water distribution and temporal change in the root-zone over a wide range of topographical positions on the farm. The WSN architecture is composed of 20 multi-sensor probes, a gateway unit (base station and connecting point to the cellular network) and a repeater station arrayed in a mesh topology. A typical example of a microsite is illustrated in Figure 3.8 (A) in Chapter 3. Each multi-sensor probe was connected to robust, long-range telemetry units for logging and transmission of data via radio connection to the gateway. Each multi-sensor probe was buried vertically (Fig. 3.8 (B)) and placed approximately 4 m away from the radio unit with a connecting cable running through a sealed underground Alkathene pipe. Manufacturer-provided instructions were followed during the probe installation to avoid preferential water flow and air gaps, as well as to ensure optimal sensor contact with the soil. The interface board and battery (recharged by a solar panel) were placed in a weatherproof enclosure mounted on a galvanised pole along with a long-range, omnidirectional antenna (Fig. 3.8 (A)). The HALO Farm System, an online service developed by Tag I.T Technologies Ltd (New Zealand, Hamilton), was used for web-based data collection and management via cellular network. The criteria associated with the research objectives and the farm management required the multi-sensor probes to be buried - this also provided equipment protection. A two-month period prior to the experiment was allowed for the sensors to equilibrate with the surrounding soil. For the purpose of this study, sensor readings were retrieved from the WSN database at the time closest to the time stamps of the sampling events at each microsite, giving a maximum of 7.5 min of time difference between sensor reading and sampling. There was no false or unusual reading in the analysis based on a comparison to the previous and the following three sensor readings.

4.2.3 Soil sampling and reference soil water content

The soil sampling events were carried out during dry ($\theta_v \approx 0.25$ m^3 m^{-3}), moderately wet ($\theta_v \approx 0.35$ m^3 m^{-3}) and wet ($\theta_v \approx 0.45$ m^3 m^{-3}) stages of θ_v conditions over five sampling events (on 21/11/2016, 23/02/2017, 24/04/2017, 31/10/2017 and 18/11/2017 as marked on Figure 4.8). The acquisition of gravimetric soil samples considered the variability in bulk density with depths, thus the number of replicates were chosen accordingly. Reference soil water content values were obtained from soil samples taken at multiple depths and the gravimetric water content (θ_g, gg^{-1}) was calculated by the standard gravimetric technique (Schmugge et al., 1980). For each sensor, the laboratory θ_g value was converted to θ_v by multiplying by the mean ρ_b value. These θ_v values were employed in comparisons and referred to as reference θ_v in the following sections of the chapter. The fieldwork, sampling scheme and the laboratory work related to the reference soil water content collection have been described in detail in Chapter 3, Section 3.3.

4.2.4 Soil description and soil texture

In this study, a laser scattering particle-size distribution analysis was performed on composited samples (three replicates at each depth) using a Horiba LA-950 (HORIBA Scientific, Kyoto, Japan) instrument to determine texture. The diameter range of the individual particle size classes were defined by the U.S. Department of Agriculture (USDA) (Gee and Bauder, 1986) and their size limits adopted in this analysis since it has been generally used in New Zealand for texture analysis. Figure 4.2 (A) and Figure 4.2 (B) summarise the results from the particle size analysis grouped by depth, along with the means and standard deviations (SDs) of the ρ_b values at each microsite. Most of the 300 and 400 mm soil increments exhibited fine-textured silty clay loam characteristics with 25 % and 28 % average clay content, respectively. Soil layers nearer the surface tend to fall in the silt loam class with increased proportions of sand fractions and less than 20 % clay content. Increasing ρ_b values were observed with increasing depth with a mean ρ_b of 1.1 gcm^{-3} for 100 mm, 1.22 gcm^{-3} for 200 mm, 1.32 gcm^{-3} for 300 mm, and 1.37 gcm^{-3} at 400 mm depth (Fig. 4.2 (B)).

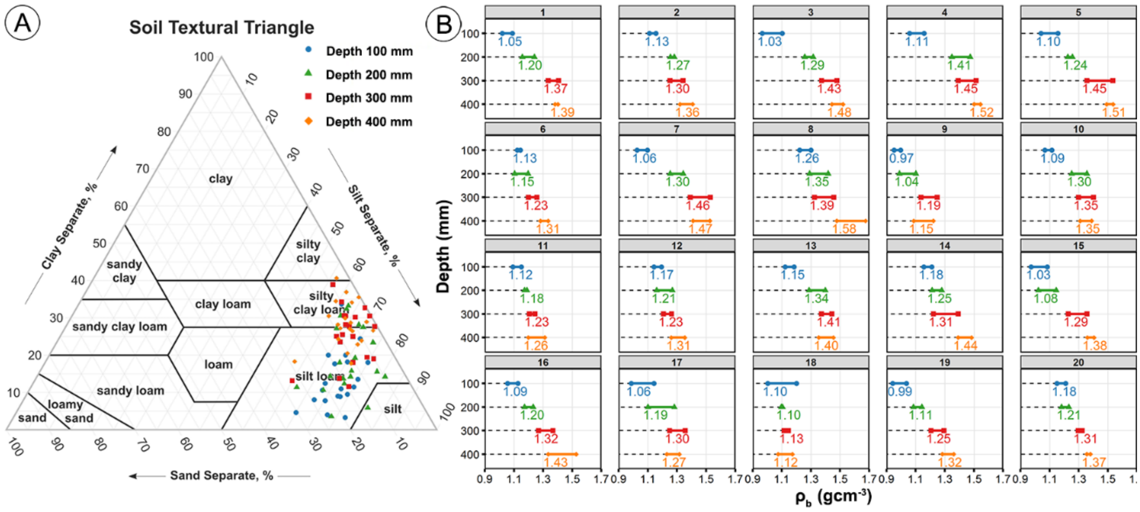

Figure 4.2 Soil textural properties based on USDA classification (A) and measured bulk density ρ_b (B) at each microsite (1-20) for each soil depth on the study farm. Mean ρ_b is labelled and the error bars indicate the mean ± standard deviation.

Apart from ρ_b, soil water holding properties are dependent on particle size distribution as well as total organic carbon (TOC) content, which are the main parameters in most pedotransfer functions that predicts field capacity, saturation, plant available water and permanent wilting point (Yang et al., 2014, Minasny and McBratney, 2018). Thus, TOC values were derived for each sensing depth at each microsite by a dry combustion method using a Vario MACRO Cube CHNS elemental analyser (Elementar Analysensysteme GmbH, Hanau, Germany). The soil samples taken on 31/10/2017 were used for the analysis providing a dominantly decreasing trend in TOC content with depth at most monitored locations. The TOC values ranged between 2.01-5.31 % (mean = 3.48 %) at 100 mm, 0.64-4.27 % (mean = 2.13 %) at 200 mm, 0.54-2.91 % (mean = 1.32 %) at 300 mm and 0.52-2.39 (mean = 0.99 %) at 400 mm soil depth.

4.2.5 Calibration methods and sensor evaluation

4.2.5.1 Custom calibration approach

Custom calibration was carried out at three levels of scale to provide options for users depending on their knowledge regarding the monitored soils. A farm-specific calibration (FC) used the entire dataset to provide a single linear relationship i.e. a single equation for the research area. At the next level of detail, microsite specific calibration (SIC), formulas were developed to provide a linear calibration for each microsite/probe (20 in total). These calibrations ignored the change in soil properties with depth. At the highest level of detail (SEC), a custom calibration formula was determined for each depth for each sensor, resulting in 80 individual calibration equations.

4.2.5.2 Statistical assessment of factory calibration and sensor accuracy

In this study, θ_v values computed by various factory calibration formulas were compared, the relationship between SF and reference θ_v was analysed, and sensor reported θ_v determined by three custom calibration and factory supplied functions were related to reference θ_v. A simple linear regression approach was followed to investigate how SF and reference θ_v were associated. The assessment was performed for different subsets based on depth and calibration type to identify errors and model fit for each group.

For the evaluation of sensor accuracy and the applicability of factory calibration functions, two primary statistical indicators were utilised, i.e. the degree of coincidence and the degree of association. The degree of coincidence was expressed by Absolute Accuracy Error (AAE, Eq. 4.3), Mean Bias Error (MBE, Eq. 4.4), Mean Absolute Error (MAE, Eq. 4.5) and Root Mean Square Error (RMSE, Eq. 4.6) to assess how well sensor measurements matched the reference water content values following the equations in Willmott (1982). AAE, MBE, MAE and RMSE are considered as best measures of overall accuracy, reliability and model performance. The simultaneous use of these metrics are often beneficial to assess model performance, thus their customised forms are commonly applied in evaluation studies (Willmott, 1982, Chai and Draxler, 2014).

$$\boldsymbol{AAE = y_{sen\,i} - y_{ref\,i}} \tag{4.3}$$

$$MBE = \frac{1}{n}\sum_{i=1}^{n}\left(y_{sen\,i} - y_{ref\,i}\right) \tag{4.4}$$

$$MAE = \frac{1}{n}\sum_{i=1}^{n}\left|y_{sen\,i} - y_{ref\,i}\right| \tag{4.5}$$

$$RMSE = \sqrt{\frac{1}{n}\sum_{i=1}^{n}\left(y_{sen\,i} - y_{ref\,i}\right)^2} \tag{4.6}$$

where i is the data pair index, n is the number of observations, y_{sen} is the sensor data and y_{ref} is the reference θ_v.

The simplest measure, AAE, was used to retrieve the magnitude of difference for each sample pair of sensor reported values and reference θ_v. AAE is the most useful when individual data pairs are examined. If the AAE values are averaged over multiple measurements, the MBE can be obtained that intends to measure average model bias. The MBE value can convey information on the degree of overestimation (positive) or underestimation (negative) (Sheiner and Beal, 1981) when calibration methods are compared to each other or to the reference θ_v measurements. The linear score of MAE was also calculated that measures accuracy by giving the average magnitude of the prediction errors regardless their direction and by weighing individual differences equally. Ideally, θ_v measurements are preferred within a certain threshold (depending on applications and sensor type) and large errors are not desirable, therefore RMSE was computed to penalise data pairs with large differences by giving them proportionally high weights. The coefficient of determination (R^2, the square of the Pearson correlation coefficient) was selected as a measure of the degree of association, indicating how well regression models can be fitted to raw sensor data, calibrated datasets, and to reference θ_v data.

A general linear model approach (two-way factorial analysis of variance (ANOVA)) was chosen to test the effect of soil physical properties, soil depth and calibration type on sensor response. Firstly, sensor readings at five SF levels (i.e. 40, 50, 60, 70, 80 % ± 0.5 %) and their corresponding reference θ_v values were selected to examine whether the sensors would produce the same SF values if either the soil texture or ρ_b was different.

Secondly, ANOVA offers a statistical means of assessing the influencing power of a measured variable (i.e. clay content /ρ_b) on a dependent continuous variable (i.e. sensor error) in addition to a secondary categorical variable (i.e. depth/calibration method that contain a finite number of categories). The influencing power of soil properties was expressed by statistical significance (P value) and mean measurement error. It is assumed that the measured soil variables have not been controlled by the experiment, but are considered to influence sensor performance. It is also assumed that the relationship between the measured soil properties and the sensor errors are linear based on previous findings regarding electromagnetic sensors types (Varble and Chávez, 2011, Parvin and Degré, 2016).

To help visualising these relationships, interaction plots are commonly used to analyse the interaction between categorical variables and a continuous response depending on the value of another factor (calibration method). For example, the effect of clay content and ρ_b on sensor error was visualised by displaying the levels of clay content / ρ_b on the x-axis with the means of the continuous variable for each factor level on the y-axis. Both ANOVA related analyses were conducted using the R statistical software version 3.4.1. (R Core Team, 2017).

4.3 Results and discussion

4.3.1 Assessment of manufacturer provided formulas

The sensors measured SF was converted to θ_v by the factory provided conversion equations and compared to 400 (80 samples per sampling event) corresponding reference θ_v. While the soils at the microsites are mainly silt loam or silty clay loam, five conversion formulas were selected for comparison. Table 4.1 provides a depthwise summary about the statistical measures of the various factory supplied calibration. Due to the linear nature of the factory calibration, R^2 values varied only with depth, giving a range of 0.74-0.49 through the observed soil profile. During the examination of the manufacturer calibration functions, the closest agreement with reference θ_v was achieved by the loam soil specific factory calibration, performing slightly better than the clay soil formula. The loam calibration resulted in a range of 0.038-0.043 $m^3\ m^{-3}$ for RMSE between the reference θ_v and the sensor reported θ_v across all depths providing the best overall accuracy.

Table 4.1 Statistical comparison of reference volumetric soil water content (θ_v) and five manufacturer calibrated θ_v at multiple soil depths. The values are presented in $m^3\ m^{-3}$.

	100 mm (R^2 = 0.74)			*200 mm (R^2 = 0.57)*			*300 mm (R^2 = 0.54)*			*400 mm (R^2 = 0.49)*		
Calibration	RMSE	MAE	MBE	RMSE	MAE	MBE	RMSE	MAE	MBE	RMSE	MAE	MBE
Loam	0.043	0.035	-0.015	0.043	0.037	0.011	0.038	0.030	0.017	0.038	0.030	0.013
Clay	0.061	0.051	-0.044	0.047	0.037	-0.015	0.040	0.032	-0.005	0.044	0.035	-0.007
Generic	0.104	0.096	-0.096	0.080	0.068	-0.068	0.071	0.062	-0.060	0.074	0.065	-0.063
Clay loam	0.109	0.101	-0.101	0.084	0.073	-0.073	0.075	0.066	-0.065	0.078	0.069	-0.067
Silt loam	0.125	0.118	-0.118	0.102	0.093	-0.093	0.095	0.089	-0.089	0.100	0.094	-0.094

The generic and clay loam calibration functions did not perform well providing very similar error levels with 0.071-0.109 $m^3\ m^{-3}$ RMSE. The loam type of factory calibration resulted in 0.163 $m^3\ m^{-3}$ root mean squared difference in loamy soils in comparison to neutron scattering observations according to Singh et al. (2018) which also highlights the uncertainty in the manufacturer calibrations and the need for soil- or microsite-specific formulas. The silt loam type of conversion significantly underestimated the θ_v, giving -0.0985 $m^3\ m^{-3}$ of MBE and RMSE between 0.095-0.125 $m^3\ m^{-3}$ depending on depth. In comparison with the other four texture-specific methods, the silt loam calibration showed the largest underestimation of the true θ_v. The assessment also showed generally higher error values in the top half of the profile than in the deeper sections regardless of the calibration method which was also observed by Nolz (2013) when comparing AquaCheck readings to EnviroSCAN estimations. Similar trends were reported by Mittelbach et al. (2012) during an evaluation of low-cost sensors to TDR measurements on loam and clay loam soils in Switzerland.

Taking into consideration the soil textural properties found at the majority of the microsites, AquaCheck probe users would apply the silt loam specific equation to compute θ_v for their applications. Therefore, the silt loam formula was selected and referred to as manufacturer calibration (MC) in the further analysis and various comparisons.

4.3.2 Regression calibration

4.3.2.1 Relating raw sensor readings to reference volumetric water content

Raw sensor outputs as a function of true θ_v were analysed by fitting a linear model on SF and reference θ_v. The relationship between SF and reference θ_v demonstrated significant positive linear correlations at every depth (Fig. 4.3 (A)). However, the slope and intercept of the fitted models differed for the various soil depth intervals (Fig. 4.3 (B)). The linear regression explained 58 % of the variability on the entire dataset and 74, 57, 54 and 58 % at 100, 200, 300, 400 mm depth, respectively. Since the correlation between raw AquaCheck SF and reference θ_v was characterised as positive moderate (R^2 between 0.5 - 0.7) and strong (R^2 > 0.7), a linear regression calibration approach was followed to develop custom calibration functions to improve the precision of θ_v predictions at different microsites and depths on the study farm. Since there is a saturation or plateau effect at the extremely wet end of the soil θ_v range (Fig. 4.8), a more complex model fit seems desirable for these conditions.

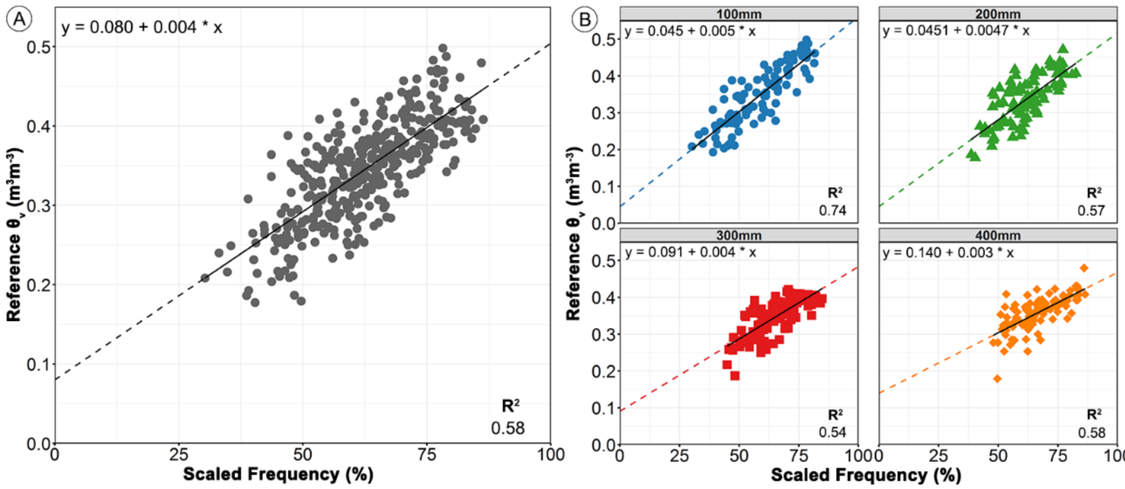

Figure 4.3 Graphical representation of linear fit between sensor reported scaled frequency SF and reference θ_v on the entire dataset (A) and depthwise (B).

A laboratory-based calibration process on site-specific soil samples could potentially improve the model fit between raw SF readings and high-resolution reference θ_v covering the entire sensing range and lead to the development of non-linear models. Considering the linear regression approach followed by the manufacturer and the main objectives of the study the linear calibration method seemed to be the most practical statistical approach that could be easily reproduced by individuals not belonging to the scientific community.

4.3.2.2 Development of the custom calibration functions and model fit analysis

Figure 4.4 presents the steps and results of an example how SIC (Fig. 4.4 (A)) and SEC (Fig. 4.4 (B)) equations were developed at a selected microsite (namely, Site 9).

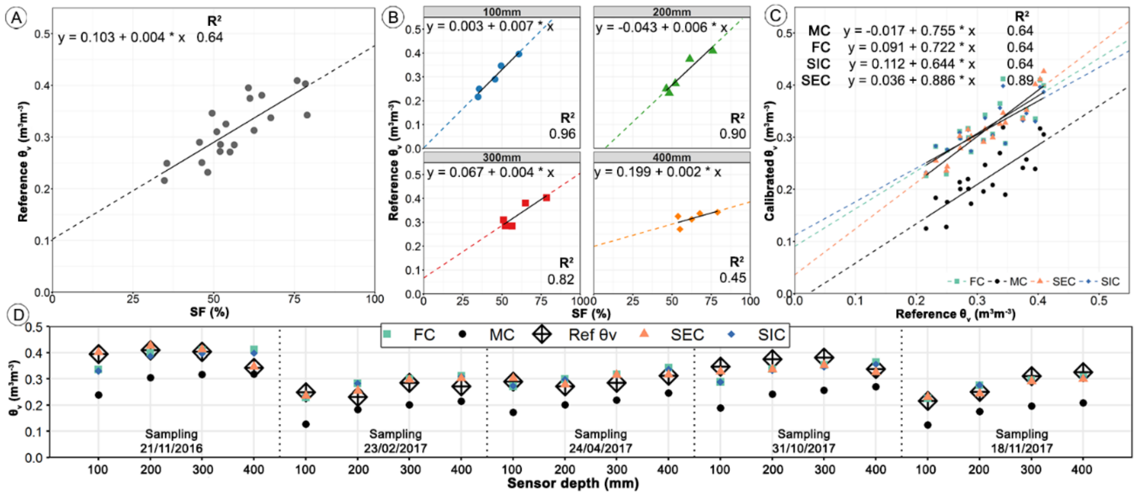

Figure 4.4 Linear regression at a selected microsite (Site 9) for creating the microsite-specific (A) and the sensor-specific (B) formulas. A comparison of reference θ_v, factory calibrated and custom calibrated θ_v (farm-specific: FC, manufacturer provided: MC, microsite-specific: SIC and sensor-specific: SEC, is presented in (C) while their correlation is shown in (D).

Notice, MC, FC and SIC methods use only one single equation for each probe at a particular location. The SIC model was fitted on reference θ_v and SF readings obtained from all four depths containing 20 data pair at each microsite. The SEC formula was generated from five data pair for every individual sensor. As a final step, θ_v computed by MC, FC, SIC, SEC were compared and correlated to the reference θ_v to assess the difference in the converted θ_v by various calibration functions (Fig. 4.4 (C) and (D)).

The general trend given by the reference θ_v was followed by both the MC and the custom calibration formulas (Fig. 4.4 (C)), although, it is clearly indicated that the custom linear regression coefficients are able to offer a better agreement between the sensor predictions and the reference θ_v. Figure 4.4 (D) plots the model fits after calibration, where SEC method evidently demonstrated an improved 0.89 R^2 as opposed to the 0.64 R^2 given by the other three calibration methods.

The calibration process and the computation of R^2 values were completed on every microsite at each depth for the four calibration methods. Figure 4.5 (A) summarises the results grouped by the methods and Figure 7B presents the statistical distribution of R^2 at each depth. The correlations between the sensor predictions and the reference θ_v obtained at the four soil depths (Fig. 4.5 (B)) were significantly different, indicating that one calibration formula for one microsite might not be sufficient, thus SEC for each soil depth may be used for applications where high accuracy is required.

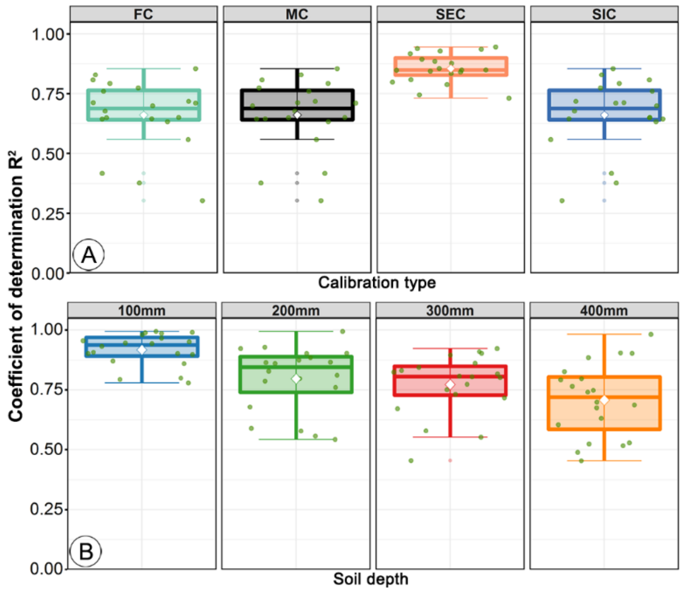

Figure 4.5 The linear model fit is represented by the distribution of the coefficient of determination (R^2) considering every microsite for each calibration method (farm-specific: FC, manufacturer provided: MC, microsite-specific: SIC and sensor-specific: SEC) (A) and for each soil depth (B). Upper extreme, upper quartile, median, mean, lower quartile and lower extreme are represented for each box.

The model fit for the 100 mm soil depth produced the highest mean R^2 of 0.91 and the 400mm soil depth demonstrated the lowest, 0.70 R^2 while 200 and 300 mm depth intervals performed similarly well, giving 0.8 and 0.77 of R^2. In terms of calibration methods, SEC method with 0.86 mean R^2 demonstrated considerably better fit than the MC, FC and SIC methods showing mean R^2 of 0.66 each.

4.3.2.3 Custom calibration accuracy and error assessment

To investigate the improvement in accuracy, θ_v values calculated by MC, FC, SIC and SEC were correlated to reference θ_v data and the change was examined both on the entire dataset (Fig. 4.6 (A)) and at each depth (Fig. 4.6 (B)). The custom regression calibrations FC, SIC and SEC led to substantial improvement in terms of accuracy of θ_v prediction considering the entire dataset. The overall regression developed for FC resulted in appreciable improvement compared to the MC method. The SIC method resulted in RMSE of 0.029 $m^3 m^{-3}$ compared to 0.039 $m^3 m^{-3}$ for FC and 0.106 $m^3 m^{-3}$ if the MC approach was utilised. The best performance was achieved by the SEC formulas with mean RMSE of 0.019 $m^3 m^{-3}$ (Table 4.2).

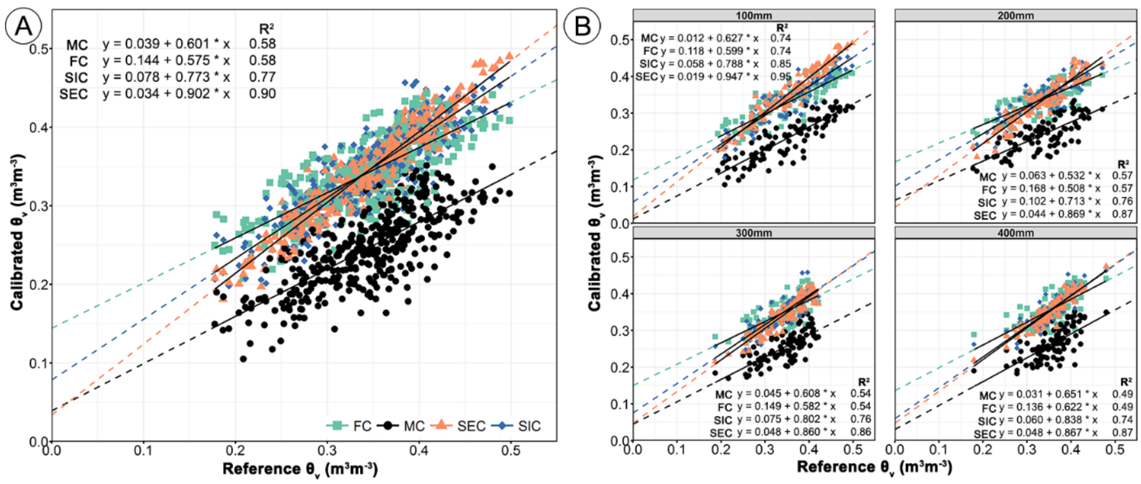

Figure 4.6 Graphical representation of linear model fit between corresponding reference θ_v and the custom calibrated values (farm-specific: FC, manufacturer provided: MC, site-specific: SIC and sensor-specific: SEC) for the entire dataset (A) and separately at four depths (B).

The MAE ranged from 0.09-0.118, 0.025-0.039, 0.019-0.029 and 0.013-0.019 $m^3 m^{-3}$ for MC, FC, SIC and SEC, respectively, meaning that the absolute error and the error range through four depths were reduced by moving towards the calibration at the sensor level. MBE varied between -0.089-(-0.118) for MC, -0.021-0.007 for FC, -0.016-0.027 for SIC and gave 0.000 $m^3 m^{-3}$ for SEC, suggesting that θ_v obtained by MC considerably underestimated the gravimetrically measured reference θ_v.

Table 4.2 Statistical comparison of reference θ_v, farm-specific (FC) manufacturer-calibrated (MC), microsite-specific (SIC) and sensor-specific (SEC) calibrated θ_v at four depths. The values are given in $m^3 m^{-3}$. Cal - calibration type

Depth	*100 mm*			*200 mm*			*300 mm*			*400 mm*			
Cal.	RMSE	MAE	MBE	RMSE	MAE	MBE	RMSE	MAE	MBE	RMSE	MAE	MBE	**Mean RMSE**
MC	0.125	0.118	-0.118	0.102	0.09	-0.093	0.095	0.09	-0.089	0.1	0.09	-0.094	**0.106**
FC	0.047	0.039	-0.021	0.042	0.036	0.003	0.034	0.027	0.007	0.034	0.025	0.001	**0.039**
SIC	0.034	0.029	-0.016	0.032	0.027	0.006	0.025	0.019	0.008	0.024	0.019	0.002	**0.029**
SEC	0.018	0.014	0.000	0.023	0.019	0.000	0.018	0.015	0.000	0.017	0.013	0.000	**0.019**

SEC was able to remove the presence of systematic over- or underestimation as the errors cancelled out (Table 4.2). These results show that even a single farm-specific calibration will perform better than the universal factory formulas. If the sensors are used in precision agriculture applications, a SEC calibration will produce accuracy beyond the single FC and SIC calibration, making perceivable difference on the long run in irrigation scheduling. Furthermore, fertiliser applications are strongly dependent on the right amount of θ_v (Monaghan et al., 2007, Ma and Herath, 2016), thus more precise timing of inputs (at least matter of days) can be chosen by using the most detailed, SEC method.

However, the distribution of errors in relation to reference θ_v was not uniform. The pattern of error distributions was examined by the correlation of reference θ_v and the calculated AAE for each custom and MC methods as plotted in Figure 4.7. To describe θ_v conditions during the five sampling events, the frequency distribution of reference θ_v was displayed in the bottom of Figure 4.7 for each depth. The histograms clearly demonstrate the wider range and higher variability of reference θ_v in the surface than in the deeper sections. At the 300 and 400 mm depths, the shape of the data is slightly skewed to the left showing that the deeper part of the soil profile was usually wetter than the surface on the date of sampling events.

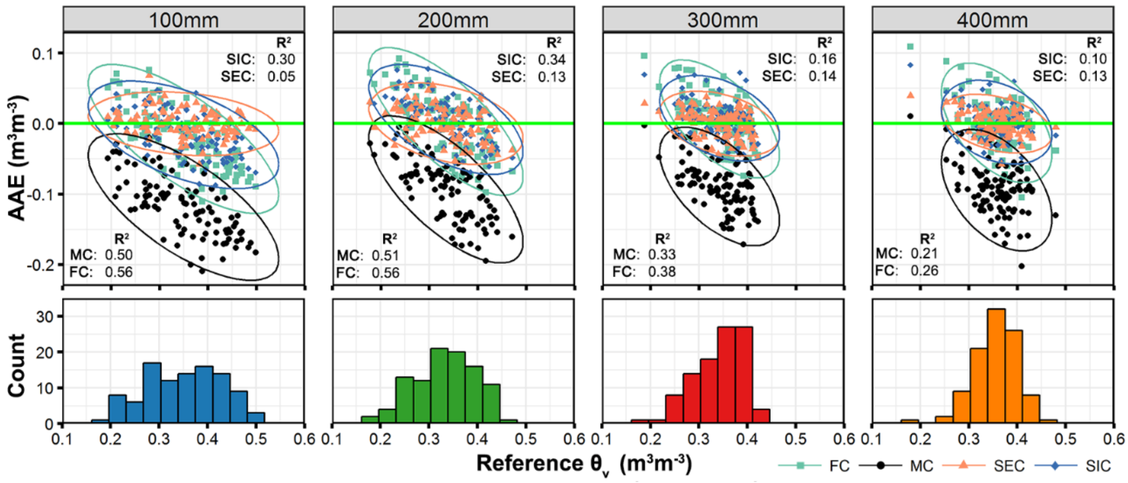

Figure 4.7 Absolute accuracy errors (AAE) of the AquaCheck reported data using the manufacturer and custom calibrations with frequency distribution of reference θ_v for each depth (farm-specific: FC, manufacturer provided: MC, microsite-specific: SIC and sensor-specific: SEC). AAE is calculated as the difference between calibrated sensor readings and reference θ_v.

In the upper section of Figure 4.7, normal confidence ellipsoids were added to the scatter plot matrix with 95% confidence level as a graphical representation of correlation between AAE and reference θ_v (Friendly et al., 2013). At every depth, the ellipsoids are stretched out diagonally from top left to bottom right indicating negative linear correlation.

The analysis revealed that sensor readings tend to overestimate the true θ_v at drier soil conditions (θ_v< 0.28-0.35 $m^3 m^{-3}$, depending on the depth and calibration type). On the other hand, underestimation occurred during the wetter soil stages, the largest AAE increased to 0.012 $m^3 m^{-3}$ if FC and to 0.009 $m^3 m^{-3}$ if SIC method was applied at 100 mm depth. The FC and SIC methods led to considerably reduced errors, SIC being more accurate than FC at every depth level. In general, the lowest AAE was observed if SEC calibration was used with less significant correlation, while the largest absolute differences were given by the MC. SEC was able to limit the AAE to around ±0.05 $m^3 m^{-3}$ for most observations at all depths.

The more elongated ellipses in the 100, 200 mm depths suggest higher correlation (R^2 of 0.56 for FC, 0.5 for MC, 0.30 for SIC and 0.05 for SEC at 100 mm) than the less elongated, nearly circular shaped ellipsoids, for the deeper parts of the monitored soil profile (R^2 of 0.26 for FC, 0.21 for MC, 0.1 for SIC and 0.13 for SEC at 400 mm). R^2 typically decreased as the scale of the calibration moved from FC towards the SEC, suggesting improvement and less sensitivity to high and low moisture conditions. These results depict that the effect can be minimised by calibration at the probe or sensor level, thus underestimation and overestimation can be diminished in comparison with MC. Furthermore, Mittelbach et al. (2011) and Mittelbach et al. (2012) found similar AAE trends for capacitance and FDR based sensors, who also emphasised the importance of site-specific calibration and the sensitivity to soil types that agree with the findings of this study.

A sensor-specific calibration might be an ideal option when the soils have variable physical properties within the monitored profile. The collected and analysed data indicates that the AquaCheck sensors can be effectively field calibrated using direct gravimetric measurements. Consequently, the new calibration coefficients developed in this study could be used for soils with similar textural properties. The key findings of this study is supported by other field-based evaluation experiments, stating that root mean square difference values dropped significantly when microsite-specific or sensor-specific equations were applied (Rudnick and Irmak, 2014, Singh et al., 2018). The generated custom calibration functions are expected to carry robust representations of accurate soil water measurements, since a wide spectrum of θ_v were used for the analysis along with sensor reported data acquired from 20 replicates. Therefore, the WSN deployed at Patitapu Station can be applied to validate soil moisture products from other sources, such as remote sensing.

4.3.3 Prediction of soil water temporal trends

Exploring the long-term behaviour of sensor response and general probe reliability through a time-series based comparison is of great importance since it can reveal hysteresis effects, reliability issues, technical problems and variation in measurement accuracy. It also highlights the relevance of soil or site-specific calibration development in capturing moisture sorption and desorption, especially when irrigation scheduling is guided by real-time soil water data from in situ sensors. On the other hand, in rainfed pastoral systems, timing of fertiliser application in relation to the received rainfall and the current state of θ_v can be crucial since untimely nutrient management can lead to nutrient loss and reduced amount of input taken up by plants (Beegle et al., 2000). Pasture growth rates are largely governed by soil water content; therefore, monitoring the temporal evolution of θ_v serves a valuable part in land management practices and sufficient exploitation of the uncontrollable land resources (Scott et al., 1985, Shadbolt and Martin, 2005).

Temporal evolution of climate variables is presented on Figure 4.8 including daily mean θ_v computed by MC at 100 mm depth with ± SD, total daily rainfall, daily mean near-surface soil temperature (obtained from 100 mm depth) ± SD, and daily maximum 2-m air temperature. Prior to trend analysis, the 15-min θ_v readings were converted to daily time series of θ_v and then the data obtained from 20 probes were averaged for each depth. The probes have a built-in compensation factor for correcting the effect of temperature, thus the effectiveness of correction functions are not discussed in this paper.

The θ_v monitoring started in the wet season (November 2016) which was followed by a drying out period for about 2 months. In late January, the soils began a rewetting stage leading towards near-saturated conditions in July and the θ_v levels remained high during the wintertime. In the second half of October 2017, a rapid drying period occurred which was significantly more intense than in the previous year. During the experiment, 1111.2 mm rainfall was recorded by property's weather station, showing an extremely heavy rainfall of 123.8 mm on 14 July 2017.

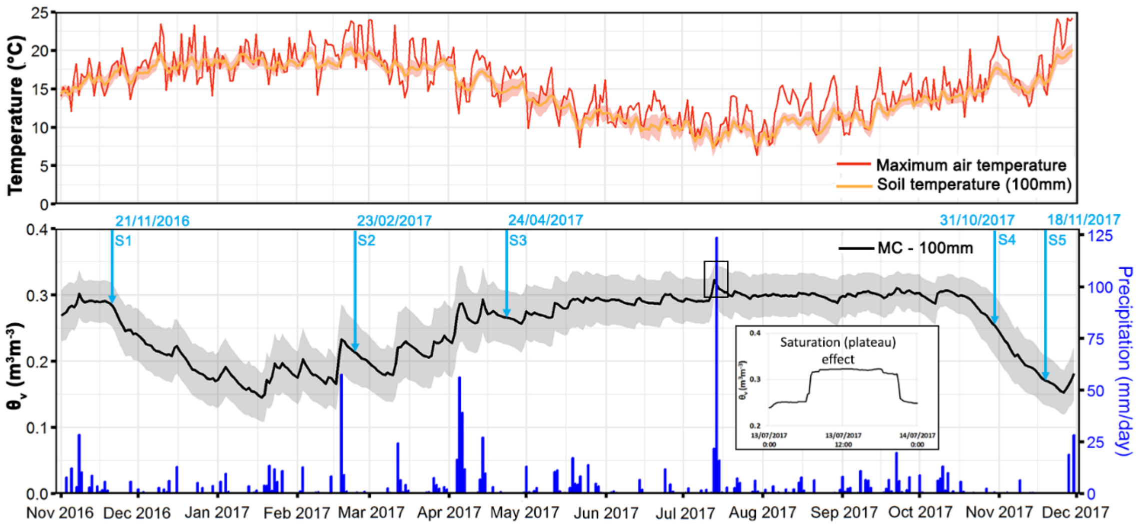

Figure 4.8 Temporal evolution of the main climate drivers, such as daily maximum 2-m air temperature, daily precipitation, near-surface soil temperature ±standard deviation (100 mm depth, n = 20) and mean volumetric soil moisture θ_v ± standard deviation (100 mm depth, n = 20) converted by the silt-loam factory formula (MC). The temporal distribution of sampling events (S1-S5) and a zoomed in view of the saturation (plateau) effect are depicted.

The dynamic sensor response to the timing and magnitude of rainfall events, drying cycles and the temporal trends of the climate variables were observed to be reasonable during the one-year observation period. It can be concluded, that the sensors demonstrated stable response to changes in soil Ka, i.e. indirectly to θ_v fluctuations making them reliable to use in non-irrigated farm management as well as in irrigation scheduling.

The differences of the continuous data between MC and custom calibrations and the variation among the four depths are illustrated on Figure 4.9. As it was expected the 100 mm, near-surface layer showed the highest rate of drying out process and the largest temporal variability of θ_v ranging from 0.24-0.47 $m^3 m^{-3}$ if the SEC method was applied. The lowest temporal θ_v variation was found in the deepest section of the observed soil profile, giving a range of 0.29-0.42 $m^3 m^{-3}$. Factory calibration and the custom calibration methods followed the same trend, although the θ_v variation and range among the 20 microsites decreased downwards the soil profile.

Sampling events were added to the timeline (marked with dotted lines) with the corresponding mean reference θ_v, so the temporal position of the collected gravimetric samples can be related to the evolution of θ_v through the experiment period. The SD was computed from the 20, composite samples at every sampling campaign for each depth. Overall, the 100 mm reference measurements exceeded the greatest spatial variability, whereas the reference set from 400 mm depth showed the smallest dispersion.

The interaction of numerous environmental parameters, such as incoming solar radiation, evapotranspiration, precipitation and wind causes higher variation in the surface layers than deeper in the soil profile. The comparison between MC and SEC exhibited more significant differences in the top layer than in the deeper sections. The MC approach presented underestimation over the entire observed timeframe at all depth, although a reduced difference was observed during the dry seasons. This result suggest that the measurement error tends to be larger when the θ_v is close to field capacity, while the sensor readings show closer agreement to reference θ_v in dry conditions. FC and SIC showed very similar behaviour through the profile and the study period except at the shallowest depth where the wet season exerted the greatest differences in θ_v between the MC and SEC. It was found that MC does not represent consistently the entire measurement range. The difference between MC and SEC began to increase at > 0.33 $m^3 m^{-3}$ θ_v levels especially in the 100 mm depth, although better agreement was observed in the low θ_v range (< 0.33 $m^3 m^{-3}$).

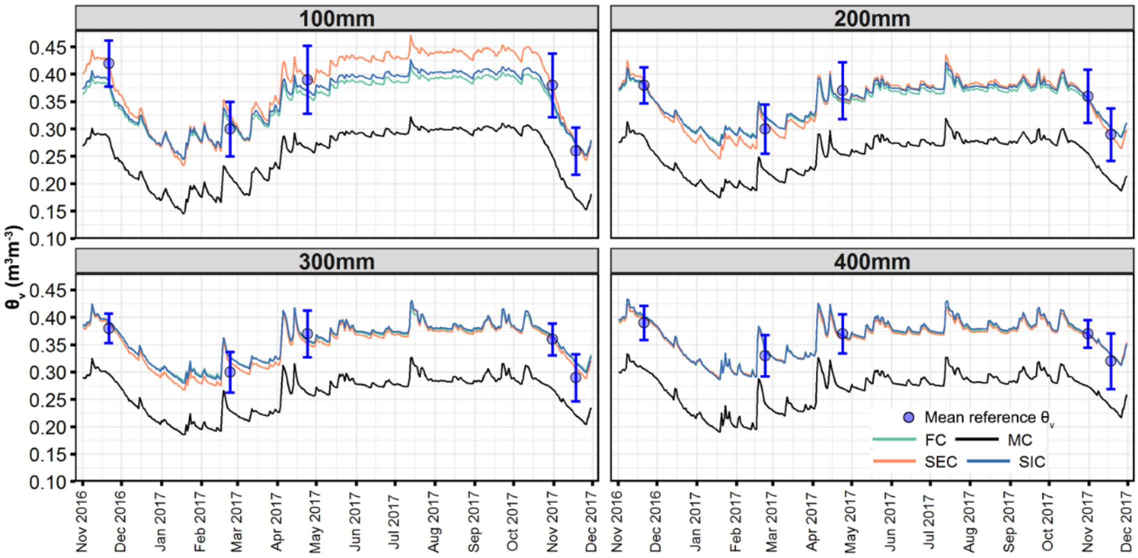

Figure 4.9 Temporal evolution of θ_v at four consecutive soil depths based on factory offered (MC), farm-specific (FC), microsite-specific (SIC) and sensor-specific (SEC) calibrations. Mean reference θ_v ±standard deviation (n = 20) corresponding to the sampling events are shown for each depth.

The application of factory provided and custom calibration functions to the time series output of the probes resulted in a visually more sensible representation of the importance of using the custom calibration functions. In case of irrigation scheduling, the improved prediction of daily water content will improve water usage and optimise water management as well as reduce the amount of water leaching below the root zone.

4.3.4 Effect of soil properties on sensor performance

4.3.4.1 Raw sensor output dependence on clay content, bulk density and total organic carbon content

Capacitance technique relies on the principle that θ_v is the main influencing factor of the change in soil Ka. Figure 4.10 (A), Figure 4.10 (B) and Figure 4.10 (C) present the sensor response at five predetermined SF levels with their corresponding reference θ_v as a function of soil clay content, ρ_b and TOC, respectively. Reference θ_v observations were selected corresponding to the SF output levels of 40, 50, 60, 70 and 80 % ±0.5 % to explore the potential impact of the clay content, ρ_b and TOC on the θ_v readings. At the 40, 50, 60 and 70 % SF levels, increasing clay content reflected lower reference θ_v, while the 80 % SF level expressed the opposite trend. A similar behaviour was observed for ρ_b at the same SF categories. However, an a reversed trend occurred in the case of TOC, i.e. decreasing TOC resulted in decreasing reference θ_v at a given SF level (Fig. 4.10 (C)) except at 80 % SF that showed the opposite trend.

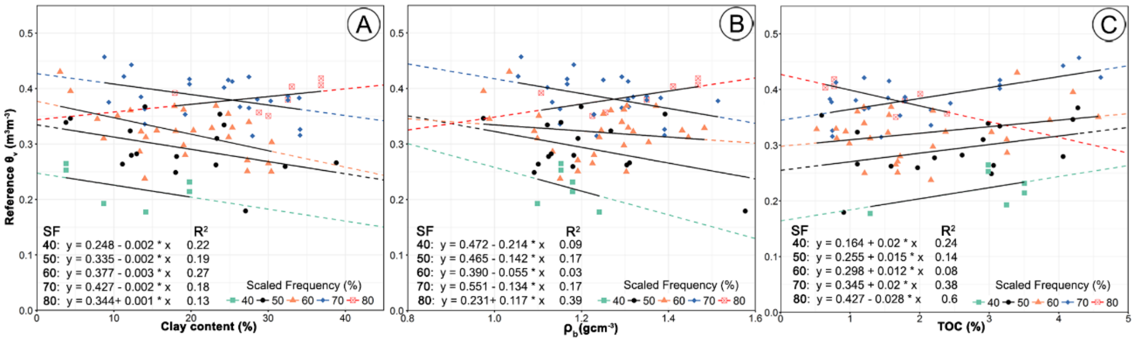

Figure 4.10 Reference θ_v at selected raw sensor scaled frequency SF output levels plotted against clay content (A), bulk density ρ_b (B) and total organic carbon (TOC) content (C).

By the utilisation of the factory-supplied conversion (i.e. not depth- specific calibration), our interpretation would suggest that at 40 % SF output, the predicted θ_v could fall anywhere between a relatively wide range of 0.27-0.17 m^3 m^{-3} depending on ρ_b or the amount of soil clay present. In other words, increasing clay content and ρ_b can lead to increase in raw sensor outputs at the same θ_v level. Dielectric sensors have been reported to overestimate θ_v with increasing clay content (Rüdiger et al., 2010, Sharma et al., 2017). Parvin and Degré (2016) reported increasing raw outputs for the layers with increasing clay content and ρ_b in case of capacitance sensors in contrast to Seyfried and Murdock (2001) who observed that increased bound water (i.e. increased clay content) resulted in decreased Ka, hence lower raw output values. In our study, the former has been observed, except in the very high θ_v range, i.e. at 80 % SF level. Since the clay content and ρ_b showed noticeable variation with soil depth at every microsite (Fig. 2), the SEC type is recommended to minimise these effects when AquaCheck products are chosen under similar soil conditions.

4.3.5 Summary of the analysis of variance (ANOVA)

Sensor errors were defined and computed as the difference between calibrated sensor readings and the reference θ_v and used as input of the statistical analysis. As a result of the two-way factorial ANOVA, it was observed that soils' clay content and the depth tend to have notable statistical effects on the sensor errors but their interaction is only significant on the 0.05 level (Table 4.3). Since the soil texture (including clay content) and ρ_b change with depth in a very similar manner (Fig. 4.2), the combination of their influencing power may be reflected by the depth as a factor.

The correlation between the sensor errors and soil clay content showed a P value < 0.001 and the soil depth exerted an important effect at the 0.001 level. The interaction of clay content and the calibration method factor was defined to be significant with P value < 0.001.

Table 4.3 A summary of the results from ANOVA using measurement error as dependent variable related to various factorial variables (Significance codes: 0 '*' 0.001 '**' 0.01 '*' 0.05 '.' 0.1 ' ' 1).**

Source	Degree of freedom	Sum of Squares	Mean Square	F value	P value	Significance
Clay	1	0.105	0.105	37.665	1.06e-09	***
Depth	3	0.046	0.015	5.440	0.00101	**
Clay : Depth	3	0.021	0.007	2.479	0.0596	.
Residuals	1592	4.457	0.003			
ρ_b	1	0.033	0.034	11.82	0.0006	***
Depth	3	0.069	0.023	8.101	2.35e-05	***
ρ_b : Depth	3	0.018	0.006	2.124	0.0952	.
Residuals	1592	4.508	0.003			
TOC	1	0.072	0.072	25.539	4.84e-07	***
Depth	3	0.036	0.012	4.256	0.00528	**
TOC : Depth	3	0.006	0.002	0.703	0.55	
Residuals	1592	4.514	0.003			
Clay	1	0.105	0.105	105.4	< 2e-16	***
Cal. type	3	2.871	0.957	956.2	< 2e-16	***
Clay : Cal. type	3	0.059	0.02	19.6	1.78e-12	***
Residuals	1592	1.593	0.001			
ρ_b	1	0.034	0.0335	31.113	2.86e-08	***
Cal. type	3	2.871	0.957	889.657	< 2e-16	***
Clay : Cal. type	3	0.012	0.004	3.606	0.0129	*
Residuals	1592	1.713	0.001			
TOC	1	0.072	0.072	69.535	< 2e-16	***
Cal. Type	3	2.871	0.957	918.967	< 2e-16	***
TOC : Cal. type	3	0.027	0.009	8.742	9.45e-06	***
Residuals	1592	1.658	0.001			

The high importance of ρ_b was also indicated by the ANOVA, giving a P value < 0.001. Calibration type and depth demonstrated strong influence on the sensor error distribution with a significant interaction between calibration method and ρ_b at the 0.05 level. According to the ANOVA table, soil clay content has statistically higher influencing power than the ρ_b, although they both represent the highest statistical significance category. The soils' TOC content demonstrated strong impact on sensor errors (P value < 0.001) while the interaction effect between TOC and soil depth was not significant (P value of 0.55). In contrast, the interaction between the calibration type and TOC was found significant with P value < 0.001.

The two-way interaction plots (Fig. 4.11) display the clay content (Fig. 4.11 (A)), ρ_b (Fig. 4.11 (B)) and TOC (Fig. 4.11 (C)) levels plotted against the mean of the θ_v errors at each level for each calibration method. The fitted regression lines with 95 % confidence intervals helped to identify the differences caused by the factors considered. The difference in the slopes of the linear functions indicates the rate of change, thus the effect of clay content, ρ_b and TOC is the most significant in the case of MC, less important for FC, hardly noticeable for SIC and completely eliminated by the SEC calibration. Furthermore, low clay content and ρ_b resulted in underestimation of θ_v, while increasing values of both variables showed overestimation when MC, SIC and FC were applied. In contrast, overestimation was observed with low TOC content and greater TOC values were associated with underestimation of θ_v. These findings represent defined influencing trends on sensor performance and error distribution (Fig. 4.11).

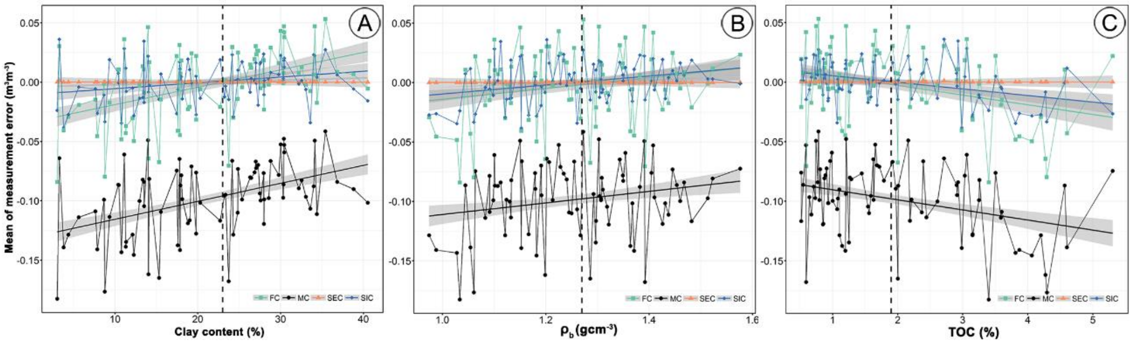

Figure 4.11 Interaction plots presenting the influencing effects of clay content (A), bulk density ρ_b (B) and total organic carbon (TOC) content on sensor performance with respect to measurement error distribution. The solid lines indicate linear model fits with 95% confidence intervals and the dashed lines mark the separation line between under- and overestimation.

With increasing depth, the ρ_b also increased and it shifted the sensor errors towards the positive side meaning that overestimation of θ_v could occur in soils with high ρ_b and underestimation may be observed in soils with lower ρ_b. The slopes' inflection points were found at 23 % clay content and 1.27 gcm^{-3} ρ_b (dashed vertical lines), respectively, indicating the observed boundary between under- and overestimation of θ_v at the study microsites. Interaction occurs mainly between MC, FC, SIC and SEC since the individually calibrated sensors acquired readings without sensitivity to the soil textural properties. Based on the results from ANOVA and the generated graphs shown, it is evident that the investigated soil physical properties have influencing power on the sensor readings, which should be taken into consideration.

4.4 Conclusions

We deployed and assessed capacitance-based AquaCheck subsurface multi-sensor probes in terms of performance and accuracy in monitoring θ_v at four depths, and at 20 locations. The 20 probes were organised into a WSN in order to collect high-temporal resolution data from soils with varying physical properties on a hill country farm in the southern east coast of the North Island of New Zealand. Our results clearly indicate the need for at least farm-specific calibration of the AquaCheck sensors since the application of factory-supplied formula for silt loam soils underestimated the true θ_v (mean RMSE of 0.106 m^3 m^{-3}). These findings were supported by the significant effects of soil texture, ρ_b and TOC (P value < 0.001) on the error distribution, thus on the conversion of SF readings to θ_v in the soil profile.

Compared to direct thermo-gravimetric $\theta_v$measurements, the farm-specific (RMSE of 0.039 m^3 m^{-3}, coefficient of determination of 0.58 R^2) and microsite-specific calibrations reduced the effect of the considered soil physical properties (i.e. wetness, clay content, ρ_b and TOC) resulting in a significant improvement in sensor measurement accuracy (RMSE of 0.029 $m^3 m^{-3}$, coefficient of determination of 0.77 R^2). In terms of absolute error distribution, positive errors were found in drier conditions (θ_v< 0.28-0.35 $m^3 m^{-3}$) while negative errors were observed in the wetter soil stages if absolute errors are related to reference θ_v. To eliminate the impact of these physical parameters, the sensor-specific calibration approach is recommended (RMSE of 0.019 $m^3 m^{-3}$, coefficient of determination of 0.9 R^2) that limited the absolute errors below ± 0.05 $m^3 m^{-3}$.

The suggested calibration method is limited in that it requires soil samples to be taken at dry, wet and intermediate θ_v levels, extending the time taken for this calibration procedure. The results of our study provides a quantitative awareness concerning the precision level that can be achieved by different levels of calibration methods and the amount of fieldwork required. Therefore, the paper aimed to provide valuable information and operational performance assessment for the application of the increasing number of AquaCheck sensors being installed around the globe. By taking into account the results of this study, and the presented soil properties, this type of sensor calibration may be applicable and useful for customers and researchers working with AquaCheck sensors on variable landscapes with similar soil characteristics in other regions of New Zealand or globally.

MASSEY UNIVERSITY
GRADUATE RESEARCH SCHOOL

STATEMENT OF CONTRIBUTION TO DOCTORAL THESIS CONTAINING PUBLICATIONS

(To appear at the end of each thesis chapter/section/appendix submitted as an article/paper or collected as an appendix at the end of the thesis)

We, the candidate and the candidate's Principal Supervisor, certify that all co-authors have consented to their work being included in the thesis and they have accepted the candidate's contribution as indicated below in the *Statement of Originality*.

Name of Candidate: Istvan Hajdu

Name/Title of Principal Supervisor: Prof. Ian Yule

Name of Published Research Output and full reference:

HAJDU, I., YULE, I., BRETHERTON, M., SINGH, R. & HEDLEY, C. 2019. Field performance assessment and calibration of multi-depth AquaCheck capacitance-based soil moisture probes under permanent pasture for hill country soils. Agricultural Water Management, 217, 332-345.

In which Chapter is the Published Work: Chapter 4

Please indicate either:

- The percentage of the Published Work that was contributed by the candidate: 90 %

  and / or

- Describe the contribution that the candidate has made to the Published Work:

  The candidate is recognised as first author. The chief and co-supervisors provided reviews and feedback on the published work.

Istvan Hajdu Digitally signed by Istvan Hajdu Date: 2019.04.30 20:31:04 +12'00'
Candidate's Signature

30/04/2019
Date

Principal Supervisor's signature

4/6/2019.
Date

Chapter 5

Analysis of field-scale, spatiotemporal soil moisture variability and its characteristics in a hill country terrain

5 Chapter 5 - Analysis of field-scale, spatiotemporal soil moisture variability and its characteristics in a steep hill country terrain

5.1 Introduction

Near surface soil moisture and the water content in the effective rooting-zone exert significant control on a wide spectrum of hydrological processes, soil water-plant relations and land-surface interactions (Bárdossy and Lehmann, 1998, Famiglietti et al., 1998). Although, numerous environmental processes are demonstrated non-linear relationships to soil moisture dynamics making the multicomponent system rather complex (Brocca et al., 2007). Hence, a solid understanding on the soil moisture spatial patterns is crucial for hydrologic modelling, remote sensing and indirectly for simulations, such as yield mapping, that utilises a spatially applied water balance module (Grayson et al., 1997, Western et al., 1998, Refsgaard, 2001). Climatic predictions, evaporation computations, watershed models, erosion control, runoff simulations, and soil nutrients cycle estimations all rely on the horizontal patterns and distribution of moisture vertically in the soil profile (Pachepsky et al., 2003, Zhu et al., 2009, Seneviratne et al., 2010).

In hill country pastoral farming systems, where irrigation is not possible (minor percentage is irrigated), plant growth is highly influenced by the management practices that take into account the variation in soil water availability in both space and time. As soil water is a vital component of yield forecaster algorithms for various fertiliser applications, it exhibits significant influences on the simulation accuracy. For these reasons, there have been an increasing interest to extend the body of our knowledge concerning the spatial and temporal variability of soil water content (Albertson and Kiely, 2001, Wilson et al., 2003, Famiglietti et al., 2008b).

Soil moisture is commonly characterised as a highly variable environmental parameter even in small catchments, due to the interaction of a multitude of factors (Vereecken et al., 2014). The heterogeneity in soil types, vegetation cover, land use type, climatic variables, subsurface and surface lateral flow processes and topographical attributes result in variable soil moisture patterns in the field scale (Hawley et al., 1983, Burt and Butcher, 1985, Gómez-Plaza et al., 2000, Vereecken et al., 2007). The interaction of static and dynamic controls can lead to various soil moisture patterns for a given area during wetting, draining and drying periods (Reynolds, 1970, Grayson et al., 1997).

Soil moisture spatiotemporal behaviour is strongly dependent on scale and it remains largely undocumented in complex landscapes such as the hill country of New Zealand. These rugged environments tend to enhance the spatiotemporal variations of soil moisture depending on the scale (Vanderlinden et al., 2012), introduce challenges and large uncertainties in accurate prediction of soil water fluxes.

Although, soil moisture changes with time, spatial soil moisture patterns have been observed to represent similar arrangements at different time steps at a given sampling location (Penna et al., 2013). This phenomena was defined as temporal stability by Vachaud et al. (1985) and it was described as ‘‘the time-invariant association between spatial location and classical statistical parameters of a given soil property’’. Kachanoski and Jong (1988) examined the temporal persistence of a spatial pattern of soil moisture as a function of spatial scale through successive time intervals. From a practical point of view, time stability analysis is commonly applied to find representative locations for long-term monitoring to avoid collecting biased measurements, i.e. records from consistently wetter or drier locations than the field mean, and represent the mean soil moisture for the entire study area (Grayson and Western, 1998, Penna et al., 2013).

A similar approach was followed by Martínez-Fernández and Ceballos (2005) to identify sampling stations in several networks that represent the mean soil moisture of the monitored area. Following this concept, it is assumed that a systematically surveyed location will keep its soil wetness characteristics with high probability on subsequent occasions (Hu et al., 2013). Therefore, time stability can be utilised to reduce the number of monitoring sites incorporated in a large network to a few representative sites as it suggests that spatial patterns persist through time (Vachaud et al., 1985, Wagner et al., 2008). Although, it has been noted that complex terrain driven hydrological processes and topographically routed soil moisture redistribution might diminish the time stable feature of soil moisture patterns in such landscapes (Kachanoski and Jong, 1988, Grayson and Western, 1998). The existing studies have been conducted on a variety of spatial extents ranging from a few meters (Jacques et al., 2001) to hundreds of meters (Famiglietti et al., 1998, Grayson and Western, 1998). Only a few studies have discussed soil moisture stability on fields larger than a km^2 (Grayson and Western, 1998). In addition, in terms of soil depth, most studies investigate the variability in the near surface, 0-20 cm layer (Gómez-Plaza et al., 2000, Cosh et al., 2008) and only a few papers refer to the deeper soil profile. Kachanoski and Jong (1988) examined temporal persistence down to 1.7 m and Hedley and Yule (2009) monitored soil moisture patterns to 60 cm.

The idea that soil moisture patterns are maintained over time for a specific field was investigated in various ways in this chapter. If such a pattern was proven existing for the given area, it could be used as advantage in several growing research fields, such as watershed scale studies and validation of remote sensing products (Grayson and Western, 1998, Cosh et al., 2004). Spaceborne radar (especially SAR) techniques have been increasingly used to generate remotely sensed soil moisture information (Wagner et al., 2008, Alexakis et al., 2017), although the retrieval methods are still only able to predict soil moisture on a large scale. The temporal resistance of soil moisture may be reflected in the spatiotemporal change in the radar signal, therefore it is of great interest to investigate this parameter (Wagner et al., 2008). The methods relate the spatial mean soil moisture and standard deviation (SD) on a selected day to the soil moisture measured at a given site within the field. However, the characterisation of soil moisture spatial distribution and the temporal stability of a spatial pattern has not been feasible at farm-scale due to the lack of reliable, accurate and high-resolution (between 10-100 m) soil moisture products e.g. from spaceborne observations. In addition, remotely sensed soil moisture products provide estimations in the near surface layer and need to be calibrated by ground-based measurements (De Lannoy et al., 2006). Therefore, it is a common approach to study the spatiotemporal distribution of soil water content by statistical methods using in situ, ground measurements at the field scale (Walker et al., 2004, Brocca et al., 2007).

The advent of remote automated measurement technologies, such as wireless sensor networks (WSN), enable customers, farmers and researchers to obtain data regularly without frequent field campaigns (Robinson et al., 2008a, Bogena et al., 2010, Ekanayake and Hedley, 2018). In addition, the sensor readings from numerous predetermined or randomly selected locations can be acquired simultaneously without inconsistency in the data. The combination of advanced multi-sensor probes and wireless communication technology allows the collection of temporally dense soil moisture datasets with improved spatial coverage. A WSN was deployed on a hill country property to collect frequent, point-based volumetric soil moisture measurements at multiple soil depths.

This chapter presents experimental outcomes from a farm-scale research (14-km^2) carried out on a hill country farm in the lower part of the North Island, New Zealand. The soil moisture data was collected from twenty locations distributed across various topographical positions with a range of slope angle and aspect parameters. Consequently, a detailed evaluation of soil moisture trends and its space-time variability on landscapes dominated by enhanced elevation gradients have been possible. Moreover, soil water holding properties estimated by pedotransfer functions (Saxton and Rawls, 2006) were briefly investigated by comparing the soil measurement distributions.

The ultimate aims of this analysis are to:

1. Develop new datasets and use novel techniques to investigate the temporal stability, dynamics and spatial variability of soil moisture at the farm-scale.
2. Contribute to the improvement of water management decisions of pastoral systems in dry, hill country landscapes.
3. Better understand the spatial and temporal patterns and trends on soil moisture organisation by revealing the degree of impact caused by the topography at farm-scale.
4. To identify representative locations that can explain most of the variability over the research area.
5. To characterise the individual microsites and the variability that occurred during the 22 months of recording time, which was divided into the sub-periods.

5.2 Materials and Methods

5.2.1 Study area and experimental microsites

The study site and the soil moisture data collection have been described previously in high detail in Chapter 2, Chapter 3 and Chapter 4, therefore only a brief description is given here.

The study was conducted on a non-irrigated hill country farm, namely Patitapu Station (Fig. 5.1) that is also the member of the farm group under research within the scope of the Ravensdown/Ministry of Primary Industries PGP project, “Pioneering to Precision”. The approximately 2600 ha, primarily beef and sheep farm is located in the East Coast Hill Country area of the North Island of New Zealand (Manawatu-Wanganui region), which is also home for a significant portion of the pastoral farmland in the country. The complex landscape can be described as a mixture of plain surfaces, and slopes from undulating to steep classes covered by approximately 1760 ha effective pastoral land for all year around grazing that is the focus of this study (Fig. 5.1 top).

In terms of environmental features, the windswept land is characterised with huge variability in physical resources including altitude, aspect, slope angle, soil type, and potentially rainfall distribution. Concerning climate, the landowners and their management decisions are confronted with highly heterogenic macro- and micro-climatic conditions that can result in not only extreme rainfall events but also summer dry periods with and average annual rainfall of 1144 mm (Murray, 1982, Lang, 2015). Based on New Zealand Soil Classification system, the area is mainly covered by Brown Soils (Hewitt, 2010). The dominant soil textures are the variations of weakly to moderately developed silt loam, silty clay loam, sandy loam and sandy silt loam with different drainage properties (Landvision Ltd., 2009).

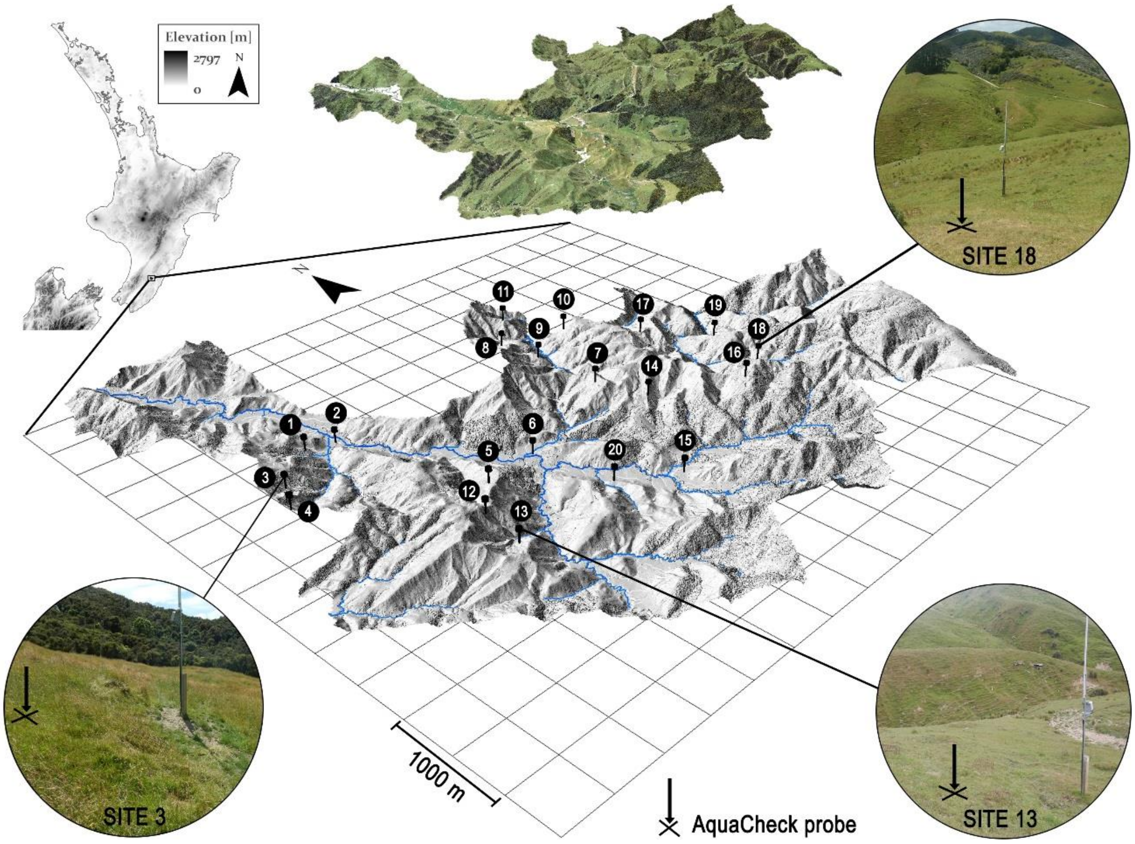

Figure 5.1 A 3D illustration of the study area by a hill shade model (centre) and an aerial photo superimposed on a high-resolution digital surface model (top middle). The distribution of the microsites is shown in the middle on a hill shade model. In addition, three examples of the microsites, the probe and the telemetry unit locations are illustrated by photos taken in the field.

5.2.2 Soil moisture data collection

Twenty microsite locations were selected at the Patitapu Station by a two-step, conditional decision approach developed for this research. The spatial distribution of the microsites are depicted on a hillshade model while a closer view of three microsites are illustrated by photos in Figure 5.1. The microsite selection procedure was mainly governed by a collection of geospatial information supported by field-based observations for validation. Several terrain attributes, soil types, land cover uniformity and land management were taken into account in the preselection stage along with the unique properties of the chosen instrumentation, with wireless communication and data transfer being subjects to special concerns due to the considerable difference in relief.

The microsites were equipped with AquaCheck (AquaCheck Soil Moisture Management, Durbanville, South Africa) sub-surface probes for the collection of multi-depth, temporally dense (15-min intervals) soil moisture observations. The 400 mm AquaCheck probes are supplied with four capacitance-based soil moisture sensors with sensing centre lines situated at 100, 200, 300 and 400 mm soil depths. The probes were attached to HALO telemetry units (Tag I.T Technologies Ltd, New Zealand, Hamilton) utilising radio-based data transfer as essential components of the Patitapu wireless sensor network. The raw AquaCheck sensor readings have been converted to soil moisture on the volumetric basis ($m^3 m^{-3}$) using sensor-specific calibration functions developed in Chapter 4 and reported by Hajdu et al. (2019). Thus, the expression "soil moisture" will be used to refer to volumetric soil water content hereinafter in this chapter.

5.2.3 Soil texture and soil water holding properties

To characterise the soils at each microsite and define soil texture, undisturbed soil cores were collected with three replicates using a soil auger. The relative size distribution of the primary particles (sand, silt and clay) was quantified by a laser scattering particle size distribution analysis or laser diffraction method using a Horiba LA-950 (HORIBA Scientific, Kyoto, Japan) instrument. Table 5.1 summarises the soil physical properties at the individual microsites at each soil depth.

To compute theoretical soil water holding properties, the Soil Water Characteristics Hydraulic Properties predictive system was used which was developed by Saxton and Rawls (2006). The improved soil water characteristics functions and hydrologic relationships were based on a previous, texture-based method developed by Saxton et al. (1986) and used in several studies (Saxton and Willey, 2005, Oyeogbe et al., 2012). The Soil Water Characteristics module is able to simulate soil water tension, conductivity and water holding capability by employing pedotransfer functions that take soil texture, gravel content, compaction, salinity and organic matter as input variables if available. In this study, the model was applied to estimate permanent wilting point and field capacity while saturation was estimated from the field measurements.

Table 5.1 The results of soil particle size distribution analysis for each microsite at four depths. Sa - Sand fraction > 50µm (%), Si - Silt fraction 50 - 2µm (%), Cl - Clay fraction < 2 µm (%).

Depths:	100 mm			200 mm			300 mm			400 mm		
Site ID	Sand	Silt	Clay	Sand	Silt	Clay	Sand	Silt	Clay	Sand	Silt	Clay
1	13.28	75.43	11.29	12.71	73.25	14.04	10.19	71.96	17.85	5.25	71.02	23.73
2	15.77	74.89	9.34	15.12	72.76	12.13	14.35	74.31	11.34	10.76	71.65	17.59
3	19.44	77.54	3.02	5.87	78.81	15.32	4.87	76.33	18.81	6.68	70.62	22.70
4	6.73	75.38	17.90	3.70	63.24	33.06	0.00	69.64	30.36	1.20	72.35	26.46
5	17.75	73.58	8.68	17.41	68.46	14.14	10.50	64.64	24.86	9.60	60.08	30.32
6	11.29	75.36	13.35	4.67	81.35	13.99	6.19	74.57	19.24	6.06	67.61	26.33
7	18.24	72.99	8.77	9.16	71.82	19.02	6.16	66.25	27.59	2.26	60.91	36.83
8	5.02	61.39	33.59	6.76	62.80	30.44	4.65	61.22	34.13	8.50	64.44	27.06
9	30.26	65.37	4.37	20.86	68.74	10.40	10.40	66.26	23.35	10.43	65.42	24.16
10	11.41	70.58	18.01	2.82	73.96	23.23	0.02	67.44	32.55	6.04	64.18	29.78
11	5.37	70.36	24.28	4.53	63.27	32.20	3.54	66.46	30.01	1.53	69.67	28.80
12	10.98	69.22	19.80	3.76	68.23	28.01	6.83	65.22	27.96	5.38	66.05	28.58
13	23.23	72.97	3.80	13.34	68.88	17.79	5.86	63.69	30.45	6.40	66.74	26.86
14	19.52	68.21	12.27	11.72	72.74	15.54	8.87	65.79	25.34	5.93	59.68	34.39
15	16.50	72.73	10.77	12.87	81.51	5.62	0.22	72.28	27.50	2.37	63.62	34.01
16	21.84	70.54	7.62	22.54	74.20	3.27	15.49	71.00	13.52	10.27	69.43	20.30
17	14.70	67.85	17.45	3.10	69.61	27.29	5.64	63.96	30.39	0.02	64.57	35.41
18	21.00	68.55	10.46	26.69	62.20	11.11	26.81	60.24	12.96	23.64	58.23	18.13
19	24.27	67.88	7.86	14.69	71.81	13.49	6.68	68.50	24.82	8.63	63.38	27.99
20	15.00	65.20	19.81	9.47	63.52	27.01	4.40	56.79	38.81	2.67	56.80	40.53
Ave	**16.08**	**70.80**	**13.12**	**11.09**	**70.56**	**18.35**	**7.58**	**67.33**	**25.09**	**6.68**	**65.32**	**28.00**

Silt	Silt loam	Silty clay loam	Silty clay

5.2.4 Data analysis

The collected soil moisture dataset was divided into two main time intervals considering the day when the wet period ended in 2017 October. By separating the data this way, full transition periods can be examined independently from the calendar year that was better suited the nature of the presented analysis. Therefore, a comparison of nearly two complete years (22 months) of soil moisture datasets was made possible. These two main data collection periods are referred to as Year 1 (01/11/2016-08/10/2017) and Year 2 (08/10/2017-31/08/2018) hereafter in this chapter. Within the two main time intervals, a series of drying and wetting cycles were identified covering a wide range of soil water content values.

The statistical analysis applied consists of three main approaches. First, the overall statistical behaviour of the dataset is characterised by descriptive statistics. As the second step, the temporal stability and variability of the collected data is investigated whereas the third approach examines the spatial variability of soil moisture and its behaviour through time.

5.2.5 Analysis of temporal changes in soil moisture content

Four methods were used to investigate the temporal and spatial behaviour of the soil moisture and find the most time stable soil moisture sensing locations. It has been shown that using only one single method might not be sufficient to describe the time stability and its controls (Lin, 2006). According to the review given by Vanderlinden et al. (2012), the literature reported contradictory results and the authors highlighted that some of the basic questions remained unanswered with respect to soil moisture time stability.

The first method (1) used the classic approach proposed by Vachaud et al. (1985) as a parametric test of relative differencing to reveal differences in constancy of temporal stability among the sampling stations. To assess the temporal stability, the mean relative difference (MRD or $\bar{\delta_i}$) and the standard deviation of the relative difference (SDRD or $\sigma(\delta)_{ij}$) were computed for all soil moisture measurements at each sampling time for four soil depths individually as well as for averaged depths. The property of $\bar{\delta_i}$ being positive or negative indicates whether a given microsite (i) is generally drier or wetter than the field mean soil moisture within the considered period. The temporal stability was described by the SDRD of the microsite, the lower the SDRD the more stable the microsite was during the experiment.

Following the equations suggested by the concept of Vachaud et al. (1985), the relative difference δ_{ij} was determined as per Eq. 5.1 as follows:

$$\delta_{ij} = \frac{S_{ij} - \bar{S_j}}{\bar{S_j}} \tag{5.1}$$

Where, $S_{ij}$is the soil moisture content at sampling microsite i on day j, and the spatial mean soil moisture $\bar{S_j}$ on day j can be calculated as per Eq. 5.2 as follows::

$$\bar{S_j} = \frac{1}{N}\sum_{i=1}^{N} S_{ij} \tag{5.2}$$

Where, N is the number of sampling locations. Therefore, the MRD for each location is computed as per Eq. 5.3 as follows:

$$\bar{\delta_i} = \frac{1}{m}\sum_{j=1}^{m} S_{ij} \tag{5.3}$$

Where, m is the number of observations or dates when the soil moisture was recorded during the study period. The microsite with the lowest MRD and SDRD values is generally considered the most time stable location and the most representative of the field mean. This method is efficiently used for identification of sampling locations that systematically show overestimation or underestimation of the field mean soil moisture (Vachaud et al., 1985). The SDRD was computed as per Equation 5.4 for each soil moisture recording station to describe the variability of MRD at the given location considering the study period, as per Eq. (5.4) as follows:

$$\sigma(\delta)_{ij} = \sqrt{\frac{1}{m}\sum_{j=1}^{m}\left(\delta_{ij} - \bar{\delta}_i\right)^2} \tag{5.4}$$

The second method (2) computed the index of time stability ITS or ITS_{ij} introduced by Zhao et al. (2010) based on the work of Jacobs et al. (2004). The ITS forms a single metric to quantify the time stability using the MRD and SDRD e.g. the variance of the relative difference at a given sampling location. The monitoring station with the lowest ITS is suggested to represent the point with the highest time stability and high values indicates either the wettest or the driest measurement sites (Jacobs et al., 2004, Penna et al., 2013). The formula for the calculation of ITS is given below as per Eq. (5.5) as defined by Zhao et al. (2010)

$$ITS_{ij} = \sqrt{\left(\bar{\delta}_{ij}^{\ 2} + \sigma(\delta)_{ij}^{\ 2}\right)} \tag{5.5}$$

The third method (3) included the time stable point assessment that was conducted by the calculation of the non-parametric, Spearman's rank correlation coefficient r_s as presented in Penna et al. (2013) to compute the total agreement between the spatial patterns captured on various dates. It can be used to determine if the soil moisture ranks at the sampling stations persists over the study period. The Spearman's rank correlation formula is given as per Eq. (5.6) as follows:

$$r_s = 1 - \frac{6 * \sum_{i=1}^{N}\left(R_{ij} - R_{ik}\right)^2}{N(N^2 - 1)} \qquad 5.6$$

Where, R_{ij} is the rank of variable i.e. volumetric soil moisture θ_{ij} at microsite i and day j, whereas R_{ik} is the rank of the same variable at the same location but on day k, and N is the number of microsites ($N = 20$). The higher value of r_s suggests higher time stability and $r_s = 1$ corresponds to the perfect agreement between the spatial patterns on different dates, i.e. it indicates the identity of the ranks on different sampling days (Penna et al., 2013). It should be considered only as a statistical tool that can be used for measuring the degree of concordance between rankings (Vachaud et al., 1985) for instance on selected days.

The fourth assessment (4), further investigated the stability of the spatial patterns, cumulative probability functions were computed for two extreme soil moisture stages e.g. the driest and wettest state. This aims to quantify whether a given monitoring location is able to maintain its rank on these two dates. The rank stability analysis was executed on all four depths combined and it was carried out by the application of cumulative probability plots similarly to Gao et al. (2011a) and Martínez-Fernández and Ceballos (2003). As a last step, Pearson correlation coefficients were determined to quantify the strength of the relationship between soil moisture acquired at successive observation times across all spatial locations. The temporal persistence of spatial patterns has been characterised by several authors by using this technique (Kachanoski and Jong, 1988, Lin, 2006, Heathman et al., 2009, Hedley and Yule, 2009).

5.2.6 Spatial variability analysis

The spatial variability of soil moisture was investigated by the calculation of spatial field mean, standard deviation (SD) and the coefficient of variation (CV) to describe relative variability (Famiglietti et al., 1999). Analysing the relationship between the spatial field mean, SD and CV has received considerable attention and it is a broadly used method for characterising spatial variance and defining the probability density functions of the obtained soil moisture data (Brocca et al., 2007, Molina et al., 2014). Additionally, these statistical parameters were computed on a daily basis that allowed the examination of the spatial pattern in terms of temporal stability (Peng et al., 2016) and made it comparable to other studies.

The SD and CV, calculated as the ratio of the SD of soil moisture to spatial field mean soil moisture, were related against the spatial field mean soil moisture to characterise the dynamics of the changing spatial variability through various wetness conditions and seasons following the work of Molina et al. (2014).

5.3 Results and discussion

5.3.1 Descriptive statistics and soil moisture distribution over time

The generation of Kernel density plots is usually a much more effective way for comparison purposes of continuous variables than histograms, as they are not affected by the number of bins (Vermeesch, 2012). Therefore, the non-parametric Kernel density estimation technique (Silverman, 1986) was employed to visually assess the nature of the distribution shape regarding the entire soil moisture data population by computing the probability density function without assuming normality (Fig. 5.2). In this case, the 15-min readings were taken and the years were plotted separately at each depth to be able to identify potential temporal stability trends and the peaks where values concentrated in each year. The comparison was completed to be able to explore the differences in the soil moisture pattern in similar wetness stages.

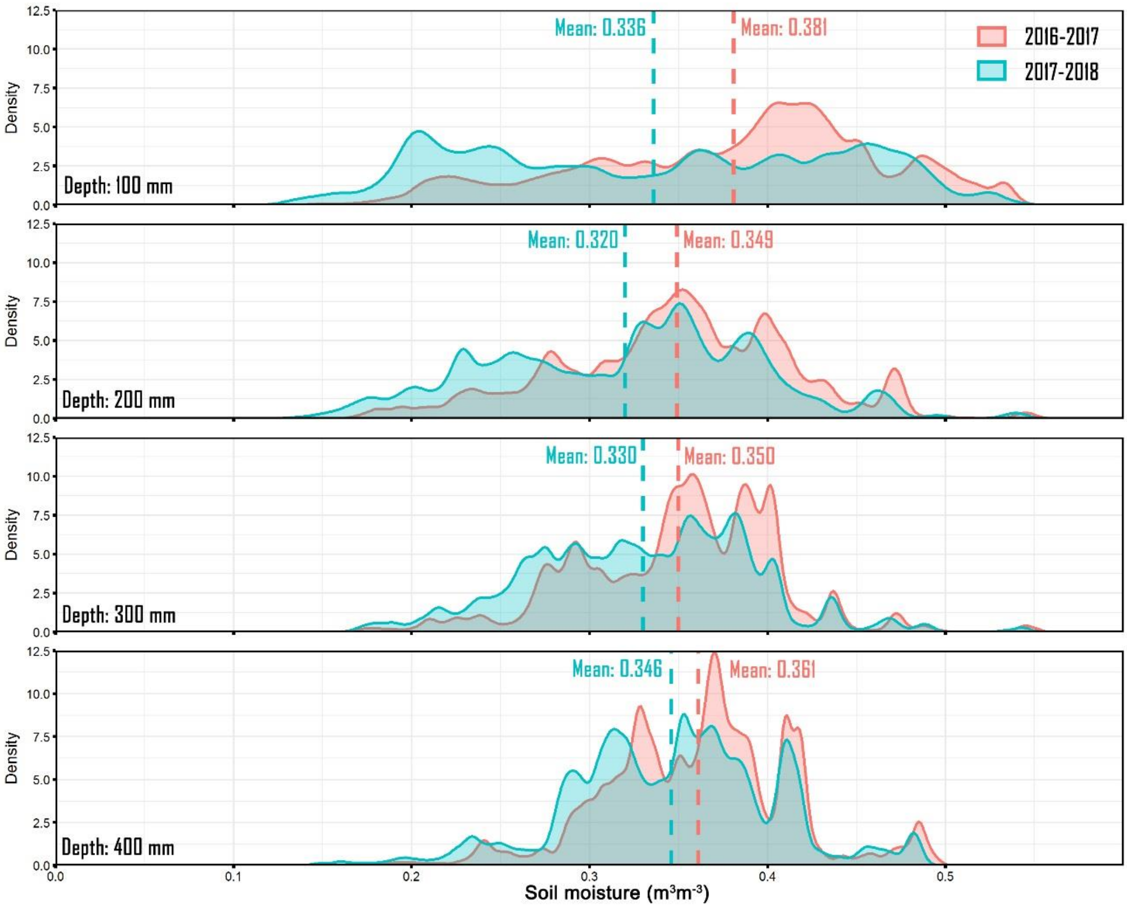

Figure 5.2 Kernel density plots visualising the 15-minute soil moisture content measurements collected from 20 probes at four depth for the year of 2016-2017 (red) and 2017-2018 (blue) with annual mean values indicated at the Patitapu Station.

The visual inspection was supported by the Shapiro-Wilk statistic that is a tool for testing significance and normality by comparing the sample distribution to a normally distributed set of scores (Ghasemi and Zahediasl, 2012). Table 5.2 contains the P values, and the test resulted in P value < 0.001 in all cases, meaning that the null hypothesis can be rejected and the soil moisture distribution can be characterised with non-normality.

The inspection of Figure 5.2 reveals the distinct differences in the mean soil moisture comparing the Year 1 and Year 2. The analysis of density curves showed that most distributions exhibited multimodal behaviour. The longer tail towards the left can be noticed in each depth that confirms the negative skewness, meaning that a large number of the soil moisture readings were lower than the average soil moisture. Furthermore, the length of the left tail increased in Year 2 compared to Year 1 due to the drier conditions in Year 2. Interestingly, some studies reported normal distribution for surface soil moisture, such as Francis et al. (1986) on a north-east facing slope in Spain and positively skewed distributions were also observed by Charpentier and Groffman (1992) in a valley, on flat and sloping land in Kansas, near Manhattan .

Table 5.2 summarises the descriptive statistical parameters of the spatially and temporally, i.e. daily averaged field data for each soil depth over the study period. The collected dataset contains readings from the 20 AquaCheck subsurface probes (i.e. at 80 depths as each probe is equipped with four sensors) to describe its overall behaviour and to conduct exploratory data analysis. To be able to compare the two years quantitatively, only the overlapping months were used for the descriptive, univariate statistical characterisation.

Table 5.2 Descriptive statistical parameters of the daily mean soil moisture (m^3 m^{-3}) data divided into two years (Year 1: 01/11/2016-01/09/2017, Year 2: 01/11/2017-01/09/2018) and grouped by the sensing depths at the Patitapu Station.

DEPTH	100 mm		200 mm		300 mm		400 mm	
PERIOD	Year 1	Year 2	Year 1	Year 2	Year 1	Year 2	Year 1	Year 2
NO. OF DAYS	305	305	305	305	305	305	305	305
NO. OF READINGS PER SITE	29286	29286	29286	29286	29286	29286	29286	29286
MEAN	0.374	0.331	0.345	0.316	0.347	0.327	0.359	0.344
MEDIAN	0.401	0.337	0.361	0.322	0.362	0.329	0.369	0.349
STANDARD DEVIATION	0.065	0.084	0.046	0.054	0.040	0.042	0.033	0.035
COEFFICIENT OF VARIATION (%)	17.35	25.37	13.24	17.07	11.41	12.90	9.11	10.15
SKEWNESS	-0.536	-0.029	-0.457	-0.166	-0.359	-0.131	-0.440	-0.271
EXCESS KURTOSIS	-1.213	-1.499	-1.119	-1.357	-1.044	-1.325	-0.808	-1.230
MINIMUM	0.233	0.201	0.246	0.225	0.268	0.258	0.290	0.284
25° P.	0.317	0.247	0.304	0.265	0.310	0.287	0.330	0.313
50° P.	0.401	0.337	0.361	0.322	0.362	0.329	0.369	0.349
75° P.	0.431	0.424	0.382	0.368	0.375	0.365	0.381	0.373
MAXIMUM	0.471	0.458	0.435	0.411	0.430	0.406	0.424	0.404
RANGE (TWO YEAR)		0.27		0.21		0.172		0.14
P VALUE	< 0.001	< 0.001	< 0.001	< 0.001	< 0.001	< 0.001	< 0.001	< 0.001

Therefore, in each year, 305 days' worth of data was considered that was about 30,000 soil moisture readings at one sensor in each year. Year 2 was relatively drier than Year 1 that is clearly indicated by the mean soil moisture content differences, particularly in the upper soil layers (100 and 200 mm). In Year 1, the near surface, 100 mm soil depth was generally the wettest (0.374 m^3 m^{-3}) while in Year 2 the soil at 400 mm held the highest amount of water (0.344 m^3 m^{-3}) (Table 5.2). The soil layers at 200 and 300 mm depths showed very similar mean soil moisture values in Year 1, while a 0.01 m^3 m^{-3} difference was observed in Year 2. The variance of soil moisture decreased with soil depth in both years, although larger CV and SD values occurred in Year 2 suggesting that higher soil moisture variability occurred during the drier year. The minimum and maximum mean daily soil moisture values were lower for every depth in Year

2 than in Year 1. As it was expected, the near surface layer dried out the most with soil moisture levels dropping from 0.431 to 0.233 $m^3 m^{-3}$ in Year 1 and from 0.458 to 0.201 $m^3 m^{-3}$ in Year 2 (Table 5.2).

In terms of kurtosis, platykurtic behaviour was observed for both years, although Year 2 was assessed to be closer to normal distribution than Year 1. The interquartile ranges at 200 and 300 mm soil depths showed similar values whereas the 100 mm soil depth measurements were the wettest except for the 25 percentile. The difference between Year 1 and Year 2 is also represented by the shape of the density curves. In general, the negative skewness was more apparent in Year 1 and the skewness values of Year 2 were closer to zero suggesting a more symmetric data distribution.

According to Famiglietti et al. (1999) and Vereecken et al. (2014) flat surfaces can often be characterised by normally distributed soil moisture probability density functions due to the less variable soil physical and hydraulic properties. On the other hand, the distribution of soil moisture on terrains with significant relief does not necessarily follow a normal pattern, i.e. it may be better described by non-normal distributions. Vereecken et al. (2014) noted that the normality of the probability density function of soil moisture is not an essential requirement for the application of geostatistical tools. In complex terrain, the lateral redistribution has an increased importance as it was shown by Western et al. (1998). During wet conditions, the most significant predictor for spatial soil moisture distribution was found to be the upslope contributing or specific area, whereas in dry conditions, aspect was the best predictor for soil moisture spatial patterns (Famiglietti et al., 1998, Western et al., 1999)

Towards the deeper sections in the soil profile, the density curves had very similar shape for Year 1 and Year 2. Figure 5.2 showed characteristic peaks occurring around certain soil moisture levels (for example at 0.35 $m^3 m^{-3}$ at 200 mm depth and 0.42 $m^3 m^{-3}$ at 400 mm depth) that can indicate that the spatial soil moisture patterns have a certain temporal stability at deeper soil depths. Therefore, temporal stability of the spatial patterns will be further investigated in the following sections.

5.3.2 Time stability analysis

5.3.2.1 Investigation of mean relative difference and index of time stability

Using Equation 5.4, MRD plots were developed following Cosh et al. (2008) at each depth separately and for combined soil depths. The MRD ± SDRD values were ranked from smallest to largest and shown on Figure 5.3 to assess soil moisture variability, time stability and bias at every individual microsite compared to the spatial field mean (represented by the green line). It is apparent that some microsites were consistently wetter and others consistently drier than the mean value. This mainly relates to the soil textural properties, topographic position of the microsites and the aspect and slope angle features of the terrain. Additionally, the ITS was computed based on Equation 5.5 and added to the ranked MRD plots for comparison. The most representative monitoring stations were defined considering the four soil depths and for an individual microsite if all soil depths are combined.

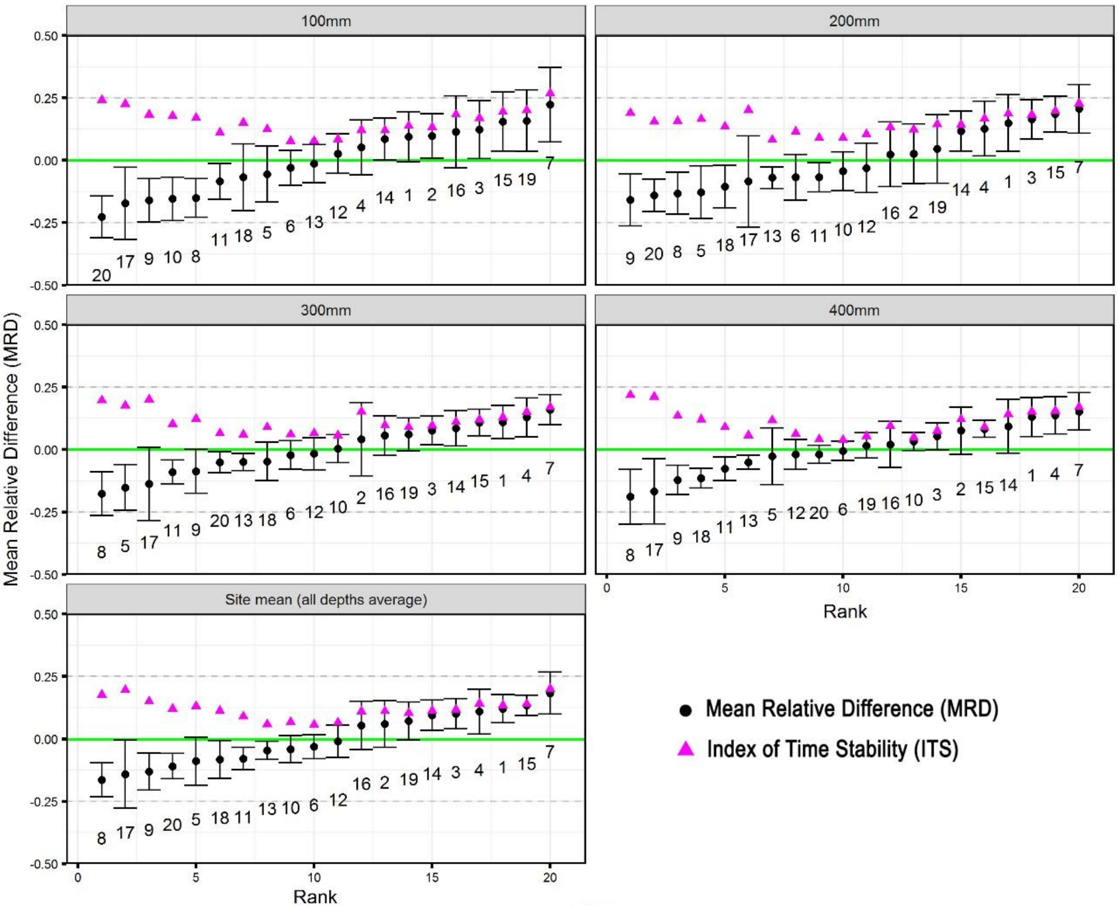

Figure 5.3 Ranked mean relative difference (MRD) of soil moisture and the index of time stability (ITS) for each sampling point and at each depth on the entire dataset in m^3 m^{-3} at the Patitapu Station. Vertical bars are associated with standard deviations of the relative differences (SDRD).

Figure 5.3 shows, that during the experiment, the temporal stabilities were not entirely consistent at various soil depths. Negative MRD values were found at each soil depth for four microsites on the north aspects (Site 5, Site 8, Site 13 and Site 20), two microsites on the west (Site 11) and east facing (Site 18) steep slopes, on a flat paddock (Site 6) and on an undulating, south-facing surface (Site 9). Their rank slightly changed along the soil profile, although their time stability can be considered moderate in general. The inspection of the ITS values confirmed these results and showed agreement in the position of the microsites that tend to be drier than the field mean soil water content. The ITS was generally high for Site 8, Site 17, Site 9, Site 15 and Site 7 while the lowest ITS values were observed at Site 6, Site 13 and Site 12 if all depths were combined.

Positive MRD values occurred at Site 19 on a rolling slope with north aspect, at a rolling (Site 16) and a strongly rolling (Site 7) west-facing stations, at locations on south aspect with rolling (Site 1) and moderately steep (Site 14) slopes, at two east-facing microsites on strongly rolling (Site 3) and moderately steep (Site 4) slopes and at two microsites situated on flat areas (Site 2 and Site 15). According to their rank and position, most of these locations would considerably overestimate the field mean soil moisture value, although their ranks were not consistent with soil depth. The ITS values showed a lower variability among these microsites with positive MRD values as compared to the microsites characterised with negative MRD values.

In terms of SDRD, the 100 and 200 mm soil depths demonstrated the greatest values as expected due to the higher sensitivity to the changes in the climatic parameters. It is apparent from Figure 5.3 that smaller SDRD values were represented by the 300 and 400 mm soil depth compared to the layers closer to the surface indicating significantly less variation.

5.3.2.2 Identification of a representative microsite

Similarly to other studies (Martínez-Fernández and Ceballos, 2003, Guber et al., 2008, Hu et al., 2010, Gao et al., 2011a, Lv et al., 2016), different time-stable microsites could be identified at various soil depths based-on the results given by the three considered statistical parameters, MRD, SDRD and ITS. Identifying representative locations can reduce the number of microsites necessary to describe the soil moisture characteristics of a given area (Brocca et al., 2007, Hu et al., 2010). In practical means, the representative sensor locations can be chosen through time-stability analysis for large scale, i.e. regional or national, monitoring network deployment. Since the average characteristics are captured by the representative microsites, they can be used to validate various remote sensing products. On the other hand, remote sensing and modelling applications require the knowledge of the temporal behaviour of soil moisture over multiple years. To select the most representative microsite, the results provided by the combined soil depth plot in Figure 5.3 was used that represents the time stability through the profile (0 - 400 mm).

Ideally, the locations with nearest zero MRD, lowest SDRD and ITS closest to zero can be referred to as representatives of the average soil water content for the given study area (Martínez-Fernández and Ceballos, 2005). Although, it has been found that MRD can carry inherent errors characterised by the SD, therefore, using only the MRD value closest to zero wouldn’t guarantee the highest temporal stability (Vanderlinden et al., 2012). Therefore, the main criteria in selecting the most time stable location was based on the lowest SDRD and MRD values close to zero as it was similarly used by Schneider et al. (2008) and Gao et al. (2011a). Due to this issue, the methods are commonly used simultaneously to identify the representative microsites (Jia and Shao, 2013, Liu et al., 2018).

In this study, none of the microsites were represented by the lowest values of all these three parameters used, therefore three potential microsites were selected for further investigation. The three potential representatives were Site 6 located on a flat paddock, Site 12 placed on a steep south-facing slope and Site 13 deployed on a moderately steep slope with north aspect (Table 5.3).

Table 5.3 Temporal stability parameters in $m^3\,m^{-3}$ for the three potential representative microsites are shown with main terrain attributes.

SITE	MRD	SDRD	ITS	SLOPE	ASPECT	LANDSCAPE ELEMENT	ELEVATION (m)
6	-0.031	0.048	**0.057**	Flat	Flat	Plains	173
12	**-0.009**	0.065	0.066	Steep	South	High ridge	301
13	-0.046	**0.004**	0.059	Moderately steep	North	Open slope	232

To validate the selection and to support the selection of the most time stable microsite, the time series of soil moisture collected at the selected three microsites were plotted along with the spatial field mean and the range considering all microsites (Fig. 5.4).

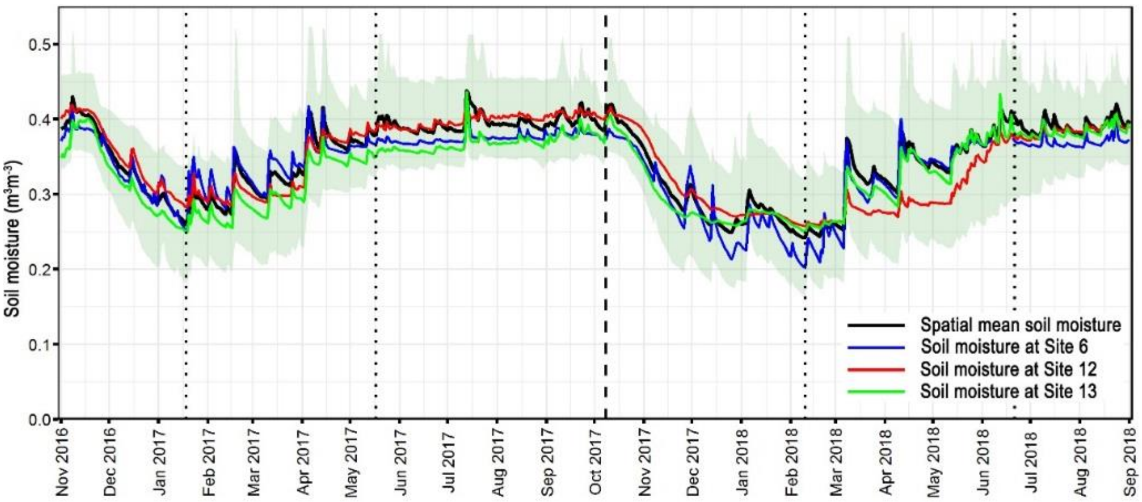

Figure 5.4 A time series based comparison of daily spatial mean soil moisture (considering all depth) and the evolution of soil moisture obtained from the three most representative microsites at the Patitapu Station. The ribbon illustrates the range between minimum and maximum over all microsites.

A linear regression was further carried out between the spatial field mean soil moisture and soil moisture readings collected from the three potential representatives, giving a coefficient of determination (R^2) of 0.94 for Site 13, 0.83 for Site 12 and 0.91 for Site 6. The root mean square errors (RMSE) between the field mean soil moisture, and soil moisture readings collected from the potential representatives were given as 0.056 $m^3 m^{-3}$ for Site 6, 0.022 $m^3 m^{-3}$ for Site 12 and 0.021 $m^3 m^{-3}$ for Site 13. This indicates that Site 13 is the most representative location at the Patitapu Station out of the 20 microsites. Site 13 showed a generally good agreement, i.e. low RMSE and high R^2 values when related to the spatial mean soil water content in every season during the entire data collection period (Fig. 5.4). Taking into account that Site 6 is located on a farm centric flat area near a waterway, it might be misleading to select that microsite as a representative for a complex, hill country landscape, although it had the lowest ITS and relatively low SDRD value. Based on the findings of Grayson and Western (1998) and Vivoni et al. (2008) the most representative microsites should be able to capture the soil moisture dynamics at mid slopes and mid elevation, which agrees with the selection of Site 13 as the most representative location. However, the idea of keeping multiple microsites as representatives of the farm will be further examined in the future which can be also linked to pasture growth accumulation.

5.3.3 Investigation of time stability of the spatial pattern

5.3.3.1 Frequency distribution analysis

To examine whether a soil moisture value derived from combined soil depths for a particular microsite can maintain its rank in the cumulative probability function at two extreme sampling dates, frequency distribution analysis was carried out following the approach by Brocca et al. (2009) and Martínez-Fernández and Ceballos (2003). The cumulative probability functions for the two selected dates in each year are given in Figure 5.4 with the aspect and slope angle classes indicated by various colours to investigate if the topographical position exhibits its effect on the rank stability over time.

Figure 5.5 (A) shows that only Site 1 and Site 8 maintained the same rank whereas Site 6 and Site 20 changed one rank only between the driest and wettest soil moisture conditions in Year 1. In Year 2, only Site 15 and Site 6 had the same rank under the extreme soil water levels. It is apparent that most of the microsites were not able to maintain their rank from the dry to the wet condition that suggests that the complex topography and the seasons affect the soil moisture spatial pattern. It can be concluded, that a WSN approach is useful in monitoring the variability so that it can be more effectively managed and interpreted. Looking at the aspect and slope angle classes, the microsites on north-facing aspects were mostly positioned on the bottom half of the plots in both years, while flat microsites were spread over the middle range. These findings suggest that these terrain attributes have a noticeable effect on the temporal stability of the spatial soil moisture pattern. In terms of slope angle classes, locations on steep and strongly rolling slopes typically situated near the bottom end of the cumulative probability function for both years. In addition, Figure 5.5 clearly shows that Site 13 was located near the 0.5 probability level in dry and wet conditions in both years, supporting the previous findings stating that Site 13 is the most representing microsite of the spatial field mean soil moisture at the research area.

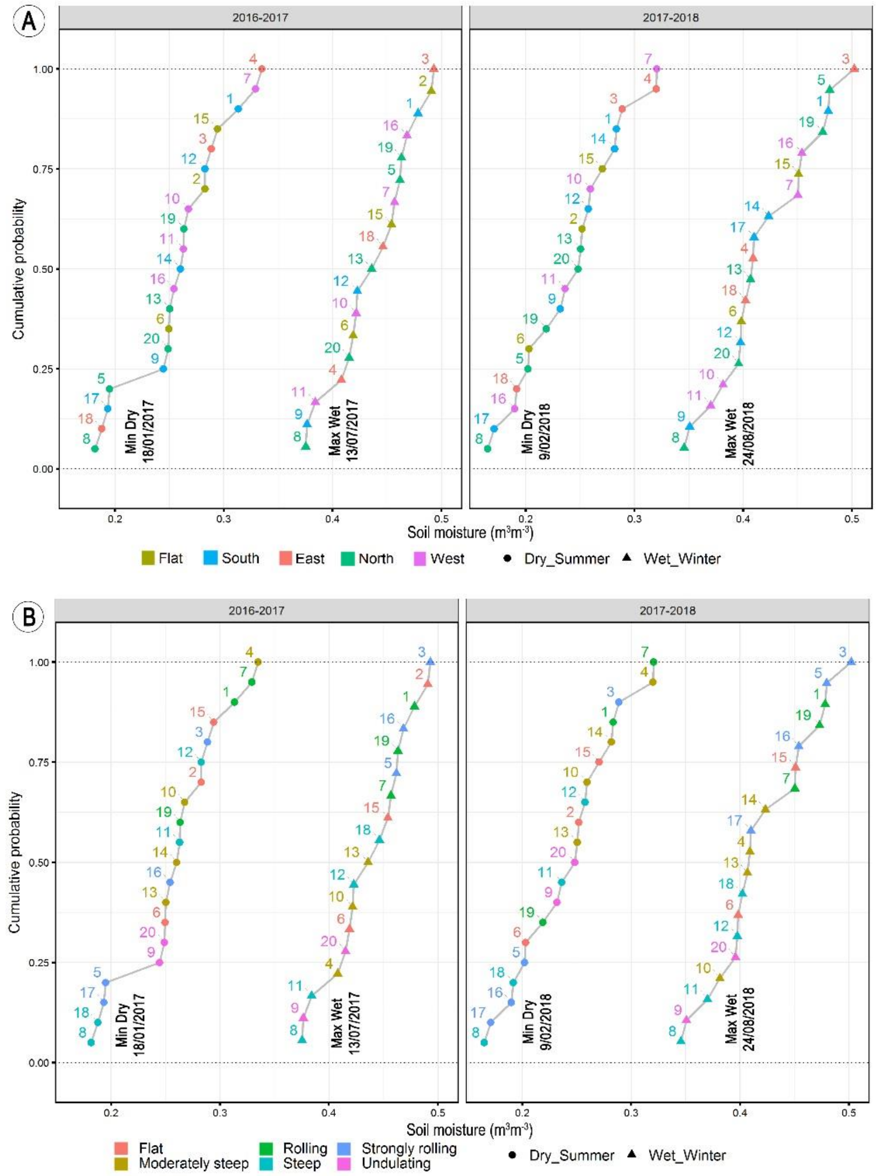

Figure 5.5 Comparisons of cumulative probability functions at two selected dates for various wetness (Min Dry and Max Wet) levels at the Patitapu Station. The data points are coloured based on aspect (A) and slope angle (B) classes.

5.3.3.2 Spearman's rank correlation

The behaviour of spatial patterns was further examined by comparing the r_s values on selected dates. Table 5.4 presents the matrix of r_s of the daily mean combined soil water content among 10 measurement days including dry, drying, wetting and wet conditions to represent extreme and transition wetness stages during the two-year time span. The dates were selected at minimum, 25th percentile, 75 percentile and maximum soil water content levels in both Year 1 and Year 2. The maximum water level, i.e. wet conditions were captured when the soils were near the saturation state.

The statistical significance was also determined and indicated next to the r_S. A P value < 0.001 was chosen as the condition to determine if the correlation was insignificant (Table 5.4). Blank fields are shown where statistically insignificant relationship was observed. The r_S ranges from 0.24 and 1, although only about 25% of the values were below 0.5. The lowest r_S (0.24) were shown between two dates with extreme soil moisture conditions i.e. between 18/01/17 and 13/07/17 in Year 1 and between 09/02/18 and 24/08/18 in Year 2, or between wet and wetting stages. The highest r_S values were observed between two dry (18/01/17 and 09/02/2018, r_S=0.88) and two wet days (13/07/17 and 24/08/2018, r_S=0.91). Although, days in the drying out and dry stages (14/12/16 and 18/01/17) also showed a high r_S of 0.85 between 14/12/16 and 18/01/17 (Table 5.4).

Table 5.4 Mean and standard deviation (SD) of daily mean soil moisture content (for all monitored positions) on the selected ten dates at the Patitapu Station. The matrix of Spearman's rank correlation coefficients is given for a series of sampling dates during the 2016-2018 study period (P value legend: 0 '*', 0.001 '**', 0.01 '*').**

	14/12/16	18/01/17	27/03/17	25/06/17	13/07/17	5/12/17	9/02/18	7/03/18	7/06/18	24/08/18
MEAN	0.324	0.259	0.325	0.395	0.437	0.283	0.242	0.292	0.380	0.420
SD	0.034	0.043	0.051	0.033	0.036	0.042	0.044	0.043	0.050	0.044
14/12/16	1	***	***	***		**	**	**	**	*
18/01/17	0.85	1	***	**		***	***	*	**	
27/03/17	0.78	0.74	1		*	**	*	***	***	*
25/06/17	0.78	0.64	0.77	1	*	*	*	*	***	*
13/07/17	0.38	0.39	0.53	0.5	1				***	***
5/12/17	0.63	0.84	0.6	0.52	0.31	1	***	*	**	
9/02/18	0.64	0.88	0.55	0.48	0.24	0.91	1	*	*	
7/03/18	0.65	0.55	0.74	0.53	0.29	0.52	0.48	1	***	
7/06/18	0.64	0.67	0.81	0.72	0.73	0.62	0.54	0.68	1	**
24/08/18	0.49	0.39	0.52	0.51	0.91	0.38	0.28	0.34	0.69	1

In most cases, the patterns were significantly correlated with relatively high r_S values, meaning that the spatial patterns can be preserved from one measurement time to another time to a certain extent. Several studies applied the method and confirmed time stability in the spatial distribution of soil moisture (Vachaud et al., 1985, Martínez-Fernández and Ceballos, 2003, Hu et al., 2009, Hu et al., 2013). In contrast, time instability was observed by Mohanty and Skaggs (2001) and Comegna and Basile (1994). In this study, the relationship generally became weaker with time. The relationship between the two extremes were shown to be not significant that might be due to the effect of slope angle and aspect that exerts its impact on the rate of drying and influences runoff and subsurface lateral flows.

The soil moisture spatial patterns were further examined from the perspective of temporal stability by relating the soil moisture levels against each other on different dates. For this analysis, the four depths were combined at each location. The scatterplot correlation matrix and the Pearson correlation coefficients (r) with significance levels are shown in Figure 5.6.

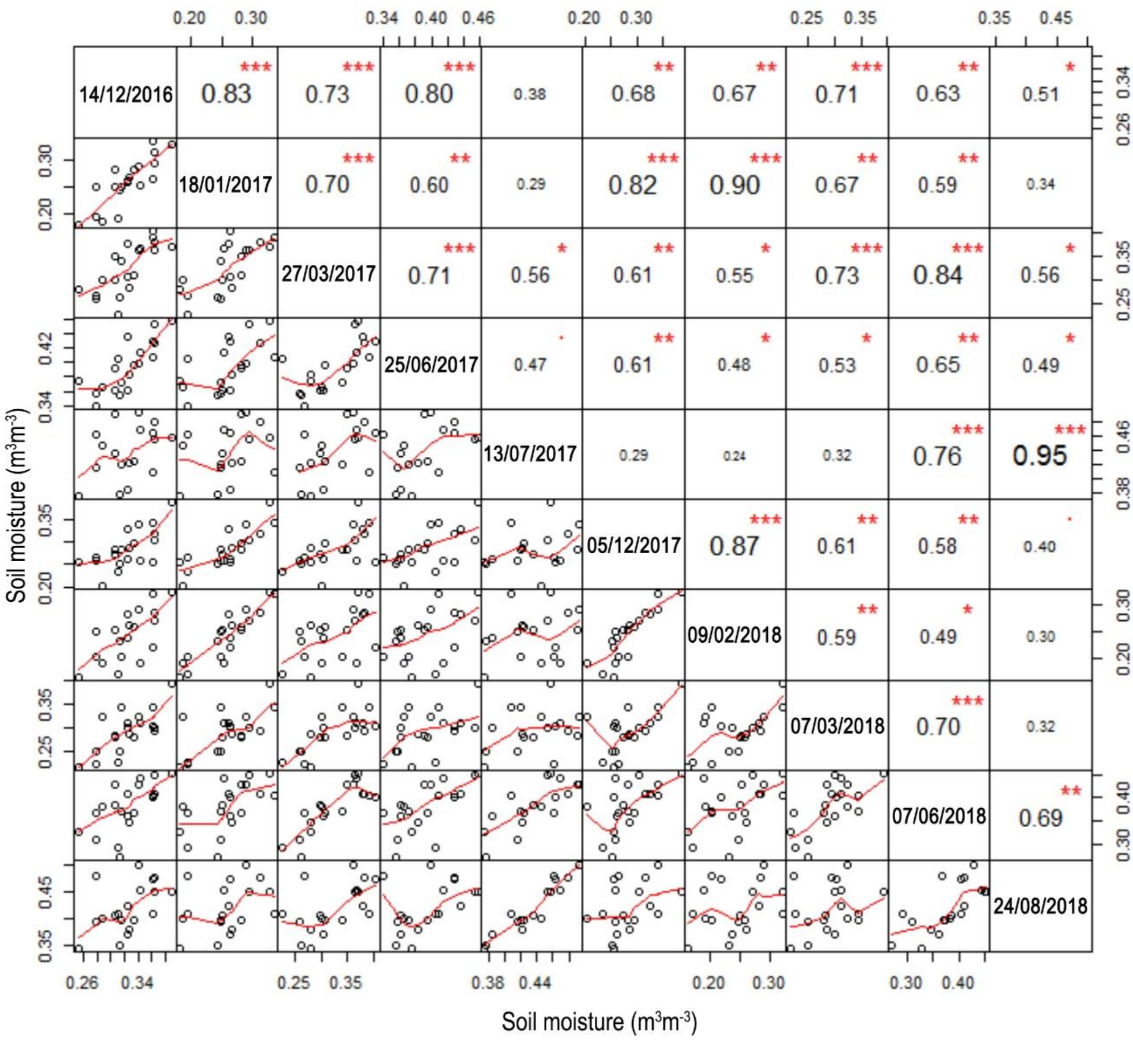

Figure 5.6 Scatterplot matrix with fitted lines and the bivariate correlations with significance values of soil moisture content measured by the AquaCheck probes at 20 microsites at the Patitapu Station. The data pairs display soil moisture values derived by combining the four depths on ten selected dates. (P value legend: 0 '*', 0.001 '**', 0.01 '*', 0.05 '.' 0.1 ' ').**

Similarly to the Spearman's rank correlation analysis results described above, a P value < 0.001 was chosen as the condition to determine if the correlation was insignificant. The significant bivariate correlations, expressed as r ranged between 0.48-0.95 giving the strongest positive correlations when the soil was in the extreme conditions, e.g. wet and the dry stages in Year 1 and Year 2. Similar findings were reported by Hedley and Yule (2009) who found the most obvious temporal stability when the soils were in the dry stage. The lowest and mostly insignificant r values were found if dry and wet patterns were related suggesting that the soil moisture distribution differ highly in these conditions. The transition stages were represented by mainly moderate temporal stability. Significant relationship was dominantly observed between consecutive dates, except if the transition stage in June 2017 and the following wet, and the wet and dry conditions were related.

5.3.4 Spatial characteristics

5.3.4.1 Temporal dynamics of spatial field mean and variance

The relationships between the spatial variance i.e. the CV and SD, and the spatial field mean soil moisture were analysed to assess the spatial variability among the microsites. These parameters were calculated on a daily basis and plotted in Figure 5.7 for each soil depth separately to illustrate the temporal evolution of the spatial variability. Additionally, the evolution of daily total precipitation is also displayed on the top of the chart to be able to link the soil moisture changes to the received rainfall. Visualising the values this way also allowed exploring whether the variance was greater in dry or wet conditions and how its dynamics changed through transition periods from dry to wet conditions and vice versa.

The accumulated rainfall was 1011 mm in Year 1 and 861 mm in Year 2, whereas the long-term. The dry season lasted longer in Year 2 than in Year 1 and the rewetting process in Year 2 was not as quick as it had happened in Year 1 when near-saturated conditions were reached in May.

The spatial mean varied synchronously in all soil depth showing apparent response of soil moisture to the rainfall events. Soil moisture values decreased continuously from the 8 Nov 2016 until mid-January 2017, when the driest day occurred in Year 1. From mid-January, the spatial mean increased until mid-May 2017 when most microsites reached soil moisture levels near saturation. The soil saturation was maintained until the 8 Oct 2017 when another drying cycle started dividing the dataset into two main periods (Year 1 and Year 2). The water stored in the soil was lost considerably faster in Year 1 reaching Year 1's lowest soil water content already in early-December 2017.

During Year 2 summer season the study farm did not receive significant amount of rainfall (a total of 172 mm compared to the 207 mm in Year 1) although evaporation rates were higher due to the elevated air and soil temperature. The summer low and the lowest soil moisture content during the two-years long recording time was reached on the 9 Feb 2018.

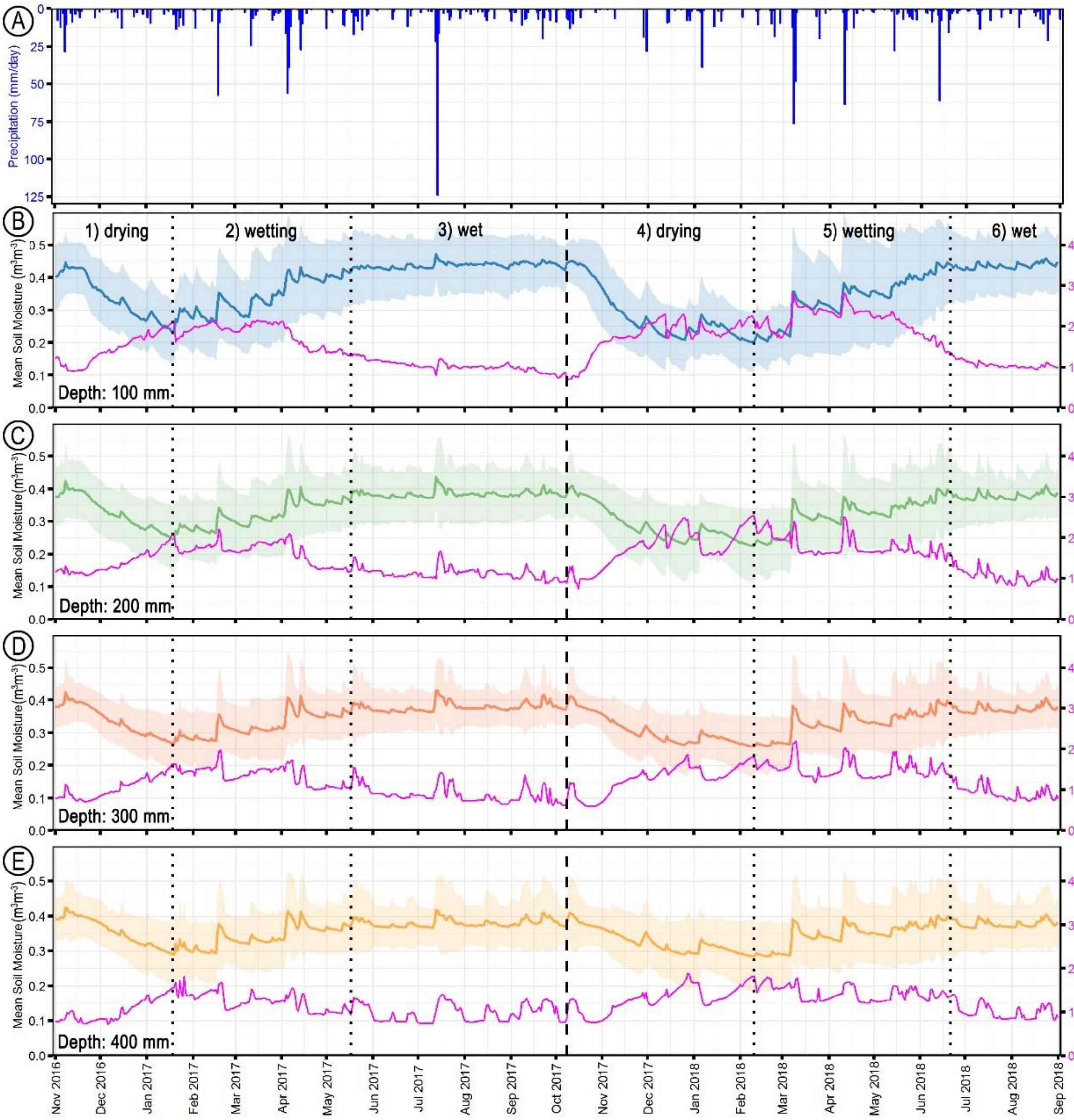

Figure 5.7 Top: Time series of daily precipitation values at the Patitapu Station (A) extracted from the local climate station. The A, B, C, and D plots show the temporal evaluation of daily values of spatial mean (20 probes) soil moisture (shaded areas corresponding to ± 2* standard deviation) and its coefficient of variation (CV) at each depth separately.

Following the dry season, near-saturation conditions occurred relatively late, end June 2018, as opposed to Year 1. This wet stage lasted until the end of the data collection, 31 Aug 2018. The range of the temporal soil moisture change was the largest at the 100 mm depth reaching 0.27 $m^3 m^{-3}$, with a minimum occurring on the 18 Feb 2018 and maximum on the 13 July 2017. The range decreased with depth, reducing to 0.21 $m^3 m^{-3}$ at 200 mm, 0.172 $m^3 m^{-3}$ at 300 mm and 0.14 $m^3 m^{-3}$ at 400 mm depth.

As the near surface layer is exposed to the largest effects of atmospheric forcing, the SD and the CV showed the largest changes depicting more time variance in the spatial pattern behaviour than other parts of the profile. The temporal stability of the spatial variability in the deeper sections of the soil profile were more pronounced as described by the lower SD and CV than in the 100 mm soil layer.

The CV and SD were highest in the dry seasons (Jan-Feb 2017 and Dec 2017-March 2018) and the wetting periods in autumn (Mar-Apr 2017 and Mar-May 2018) in both years. The variability decreased noticeably through the wet stages when soil moisture levels increased to 0.26-0.29 $m^3\ m^{-3}$ at 100 mm soil depth and reached its minimum at the end of the wet seasons. Similar findings were reported by Korres et al. (2015) on various spatial scales in the Ruhr-catchment in Western Germany based on nine different datasets during a two-year measurement period. The minimum CV values were associated with soil conditions just below saturation point (above field capacity) (Fig. 5.7) that was also found by Harter and Zhang (1999) and Owe et al. (1982) in heterogeneous soils in South Dakota, USA. Most studies found that spatial variability decreased with increasing soil moisture content (Famiglietti et al., 1999, Hu et al., 2011, Korres et al., 2013). The CV and SD parameters showed increasing trends during the transition from wet to dry stage, although the values were usually lower than changing from dry to wet state. The differences in CV and SD among sub-periods were the largest in the 100 mm depth, and less significant towards the deeper layers. While the CV line is relatively smooth for the near surface soil, the impact of heavy rainfall events often associated with large peaks in CV and SD in the deeper horizons of the profile.

5.3.4.2 Site-specific temporal soil moisture variability

A 3D visualisation of the research area and the microsite locations with some of their statistical properties are given in Figure 5.8 to describe and quantify the soil moisture variability temporally, spatially and vertically at each microsite and each depth. The boxplots generated from the daily averaged soil moisture readings for the two-year monitoring period represent the soil moisture temporal distribution. In addition, the temporal mean, SD and CV are summarised for each depth to reveal trends along the soil profile. The role of temporal soil moisture distribution is better understood if the soil moisture levels at essential water holding parameters are indicated. Thus, the estimated soil water levels at wilting point, field capacity and saturation were marked on the boxplots at each microsite and at each depth. To compare the soil moisture distribution patterns at various aspects and slope angles, these terrain attributes are also indicated in Figure 5.8.

Considering the theoretical water holding parameters, most soil moisture readings were recorded within the expected range between saturation and permanent wilting point. Concerning the spatial field mean soil moisture (as shown in Fig. 5.7), the soil water state at the

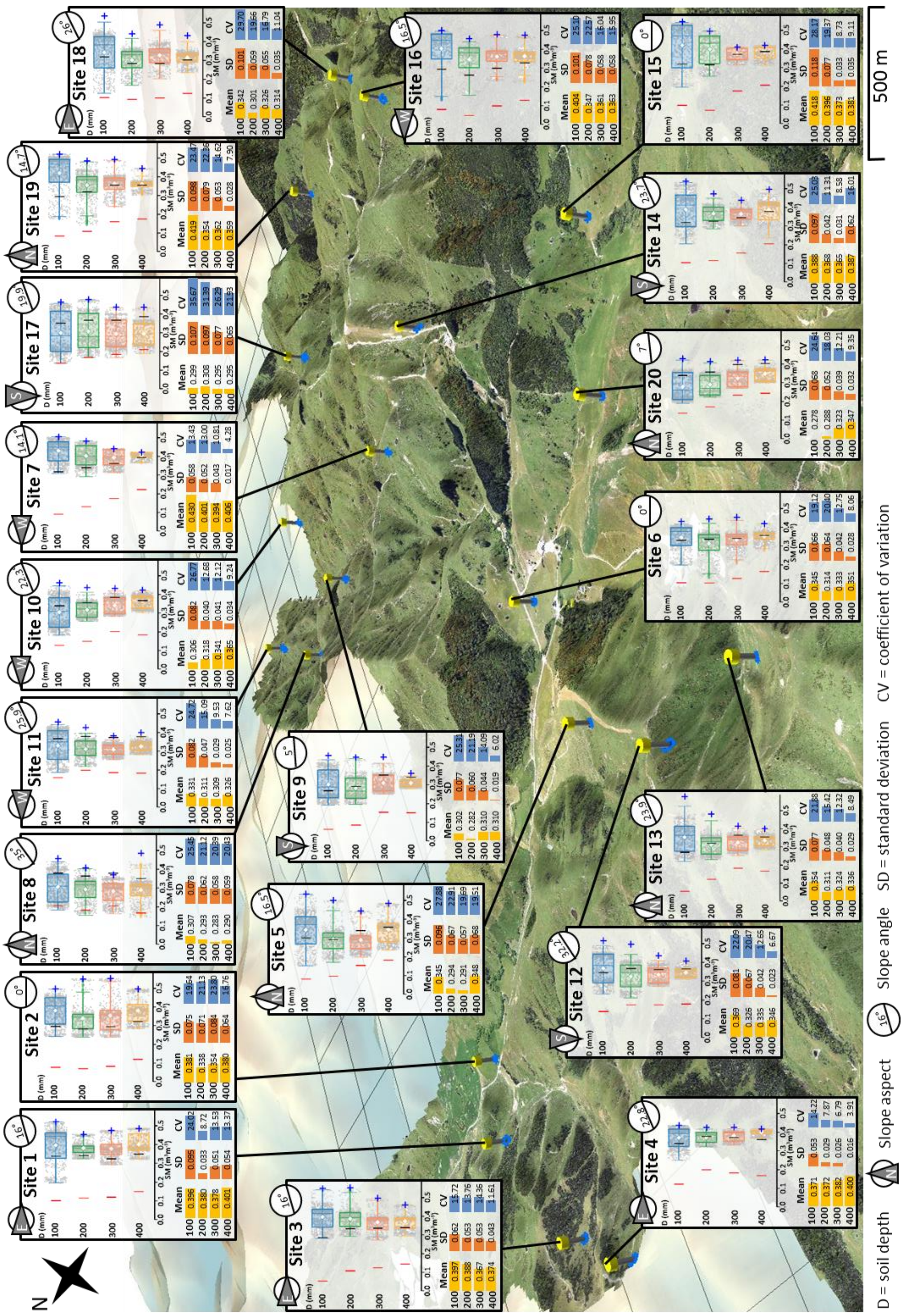

Figure 5.8 Vertical distribution of temporally averaged soil moisture content at the Patitapu Station. The boxplots visually summarises the following statistical parameters: the mean (white rhomboid), the median (line across the box), 25th percentile and 75th percentile as lower and upper hinges and outlying points. The red vertical line indicates theoretical permanent wilting point, the black lines shows theoretical field capacity (Saxton and Rawls, 2006). The blue crosses indicate saturation observed from the sensor readings.

permanent witling point was never reached during the study period. Although, looking at the individual microsites, the measurements obtained at Site 8 and Site 17 showed values at or below permanent wilting point that occurred in the summer of Year 2. In terms of saturation, the estimated values were reached at most microsites along the entire soil profile. In winter, the soils were often saturated and soil moisture levels were often recorded above field capacity, except at microsites that are situated on very steep slopes, (Site 8), at high ridge position (Site 17,) or upper slope position (i.e. Site 11 and Site 20). The microsites located on flat surfaces held soil water above field capacity for the highest number of days. Based on the estimated soil water holding properties, the amount of soil water available for plants decreased with depth in most cases as it was expected mainly due to the increasing portion of the clay fraction with soil depth (Table 5.1).

It is clearly visible, that the range of soil moisture measurements were the largest in the 100 mm horizon, while the deeper sections of the soil profile showed readings in a narrower range indicating less variability and temporally more stable soil water contents in agreement with the findings described previously. Soil moisture measurements on flat and north-facing slopes are generally more spread out, especially at microsites located on moderately steep and steep slopes. However, some of the microsites on strongly rolling and rolling slopes can be characterised with similar, wider spread of soil moisture distribution than we would expect, particularly near the surface. Monitoring stations on west- and east-facing slopes were observed to have similar soil moisture dynamics.

Figure 5.9 presents the rank stability plots for the temporal mean soil moisture, as a function of SD and the CV at each microsite and at each depth considering the entire study period. The microsites are ordered by CV from low to high values to be able to examine the behaviour of each microsite. The differences in spatial soil moisture behaviour at the four depths were analysed by taking into account the data presented in Figure 5.8 and Figure 5.9.

In general, the largest SD and CV values were observed in the 100 mm soil horizon while the lowest values occurred in the 400 mm layer showing an apparent decreasing trend. The lowest SD values occurred at Site 4 (moderately steep, east aspect) at all depths ranging between 0.016-0.053 $m^3 m^{-3}$. Moreover, Site 4 also demonstrated the lowest CV at 200, 300, 400 mm soil depths ranging between 3.9-7.8%. At the 100 mm depth, the minimum CV, 13 %, was represented by Site 7 placed on a rolling, west-facing open slope. Site 17 demonstrated the largest temporal variability at all depths with CV values ranging between 35.7-21.9 % from the near surface layer to the deepest horizon. Near the surface, the wettest location was at Site 7 giving 0.430 $m^3 m^{-3}$

for temporal mean soil water content on a rolling, west-facing open slope, whereas the driest temporal mean soil moisture of 0.278 m^3 m^{-3} was obtained from Site 20 on north-facing, undulating slope but positioned closed to a ridge. Site 8 and Site 9 showed similarly dry conditions to Site 20 at 100 mm soil depth. However, concerning all depths, Site 8 was observed to be the driest location, placed on steep, north-facing slope with mean temporal soil moisture of 0.293 m^3 m^{-3} agreeing with the general expectations in the southern hemisphere.

Deeper in the soil profile, the wettest conditions were recorded also at Site 7 ranging between 0.397-0.406 m^3 m^{-3}. This observation may be explained by the large upslope contributing area of Site 7 and the assumption that west-facing slopes receive more rainfall than the other aspects. Interestingly, the wettest and driest microsites were both situated on the same elevation level at approximately 310 m. The rank of the microsites with respect to their mean and the variability expressed by SD and CV showed significant variation vertically as only Site 17 kept the same rank at all depths.

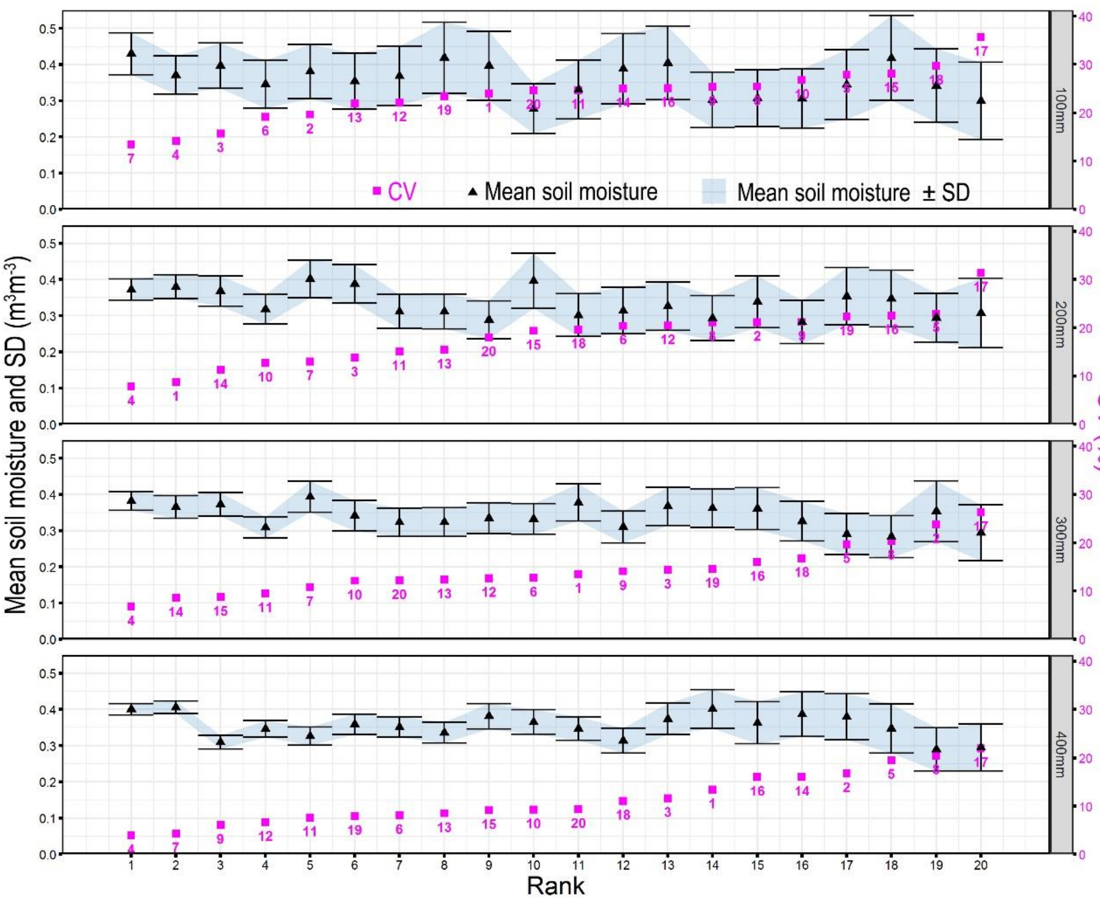

Figure 5.9 Ranked stability of the microsites at the Patitapu Station showing the mean, standard deviation SD and coefficient of variation CV considering the entire study period.

5.3.4.3 Relationship between spatial soil moisture mean and spatial variance

In soil moisture data analysis, it is a widely employed approach to relate SD representing absolute variability and CV (relative variability) to the spatial mean soil water using scatterplots and regression (Brocca et al., 2007, Famiglietti et al., 2008b, Molina et al., 2014). It is applied as one of the most common procedures, including the examination of changes in soil moisture variance with low or high soil water conditions. The results from previous studies have been found contradictory, as some researchers reported decreasing variation with drying (Famiglietti et al., 1998), whereas others observed decreasing variation as the soil was wetting (Hupet and Vanclooster, 2002, Teuling et al., 2007a, Mittelbach and Seneviratne, 2012).

In this section, the relationship between the spatial mean soil moisture, the CV and SD were examined individually during selected sub-periods in each year and in each soil depth (Fig. 5.10). The sub-periods were chosen based on the soil moisture change and seasons to get a better understanding of the correlations and trends with changing soil water conditions. The relatively long observation time allowed a detailed investigation of this relationship. The sub-periods included transition from wet to dry during spring (Nov 2016 and Oct – Nov 2017) and summer (Dec 2016-Jan 2017 and Dec 2017-Feb 2018), dry to wet state during summer (Jan 2017-Febr 2017 and Feb 2018) and autumn (Mar 2017-May 2017 and Mar 2018-May 2018) and wet (Year 1: Jun 2017-Aug 2017 and Jun 2018-Aug 2018) conditions in winter for both years.

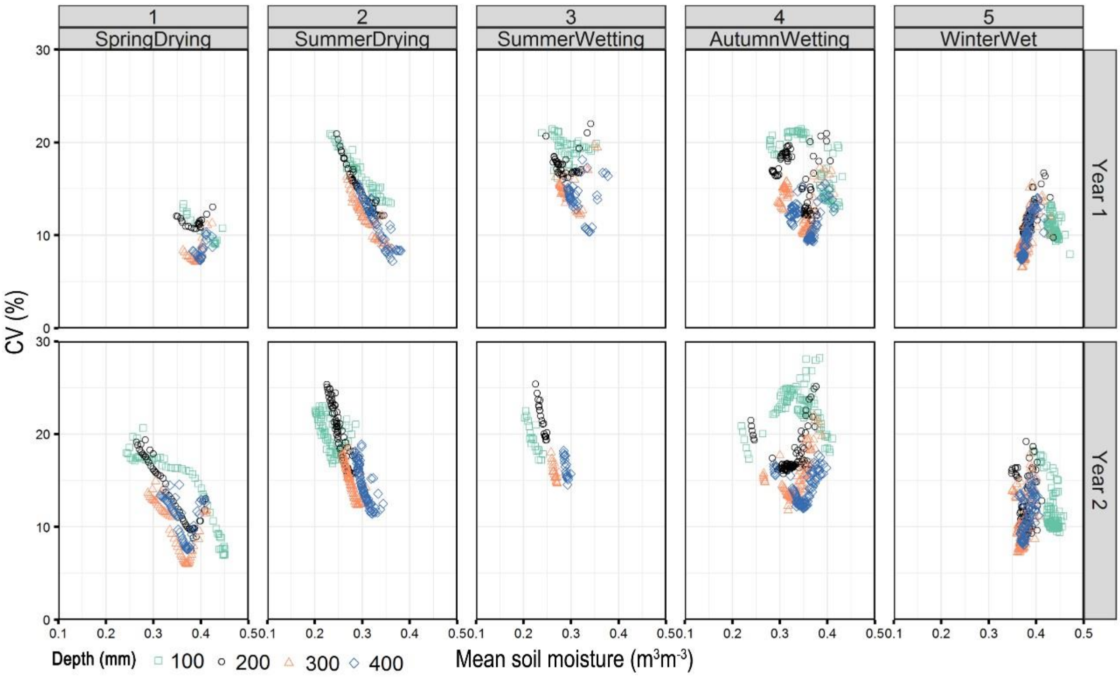

Figure 5.10 Relationship between the spatial daily mean soil moisture and coefficient of variation (CV) in the six selected sub-periods for each year visualised on scatterplots. The dots represent data from twenty microsites and the colours indicates the four monitoring depths.

Figure 5.10 shows a very similar annual soil moisture behaviour during both Year 1 and Year 2. However, the variance was not consistent in the sub-periods and it is clearly not a static property in complex terrain. The relationship varied between CV and the field spatial mean soil moisture with the sub-periods and with the soil depth. The variability was the largest in dry conditions typically below 0.25 $m^3 m^{-3}$ mean soil moisture and in transition from dry stage to the wet stage. The lowest variability occurred in wet conditions, mostly when mean soil moisture levels were over 0.35 $m^3 m^{-3}$.

In our analysis, polynomial fit resulted in increase of the R^2 value in only a few cases, therefore the linear relationships were applied for better comparability (Table 5.5). During the drying down periods and the beginning of the rewetting stage, as the mean soil moisture level declined, the CV values inclined. During autumn, some of the correlations changed direction and were positive but not significant. In winter, positive, significant correlations were observed which was more pronounced in Year 1.

Other researchers also identified a variable relationship between the field mean soil moisture and the CV. The results have been found contradictory, i.e. both increasing and decreasing soil moisture variability with increasing mean soil moisture have been identified (Famiglietti et al., 1998, Vereecken et al., 2014, Gwak and Kim, 2017). The relationship between spatial variability and mean of soil moisture can change depending on a threshold as explained by Pan and Peters-Lidard (2008). Exponentially decreasing CV pattern with increasing mean soil moisture was found by Famiglietti et al. (2008a) and Gao et al. (2011b), while linearly decreasing CV with increasing mean soil moisture was observed by Brocca et al. (2007).

Table 5.5 Values of coefficient of determination (R^2) derived from linear regression between coefficient of variation (CV) and the corresponding spatial mean soil moisture in the five sub-periods for each depth.

	DEPTH	SPRING - DRYING	SUMMER - DRYING	SUMMER - WETTING	AUTUMN - WETTING	WINTER - WET
YEAR 1	100	-0.86	-0.93	-0.04	0.56	-0.21
	200	0.01	-0.93	0.02	0.19	0.45
	300	0.39	-0.88	0.02	0.05	0.44
	400	0.43	-0.88	0.00	0.00	0.79
YEAR 2	100	-0.84	-0.24	-0.78	0.00	-0.40
	200	-0.86	-0.81	-0.94	0.05	0.01
	300	-0.45	-0.69	-0.65	0.32	0.12
	400	-0.17	-0.67	-0.66	0.08	0.41

The significant correlations were mostly negative during the drying in spring and summer at 100 mm soil depth. The correlation dropped drastically in the rewetting stage in summer and autumn in Year 1. In contrast, in Year 2, summer wetting showed high negative R^2 values for every depth. The least significant linear relationships were found during transition towards the wet soil state in both years. Positive, moderate and strong correlations were observed during the wettest conditions in the 200-400 mm soil depth in Year 1, whereas Year 2 showed a slightly different behaviour with technically no considerable correlations in the 200-300 mm soil depth and negative linear relationship in the near surface layer. These results show agreement with the work published by Hedley and Yule (2009) who observed that the soil moisture pattern was most stable during the drying out period in February and March. The CV peaked at 0.35 $m^3 m^{-3}$ during the wetting stage reaching 28% variability and its minimum value was found in the wet conditions giving a CV of 6.5 % in winter.

As a function of spatial soil moisture distribution, daily SD was related to mean field soil moisture (Fig. 5.11), similarly, to how the CV and the mean soil moisture were correlated previously during the same sub-periods. The SD behaved in the same manner as CV in the drying (or descending) periods, while it did not present the same trends in the summer rewetting times. During autumn and winter, the largest variance in SD occurred during the transition from dry to wet stage in autumn. The deeper soil sections were more stable during the entire study period than the soil moisture at 100 mm soil depth. The minimum SD values were found in the drying stage and in winter whereas the peaks occurred in autumn in both years. During drying and wetting periods, parabolic shapes were found, and the spatial variability was more widely scattered within these transition stages.

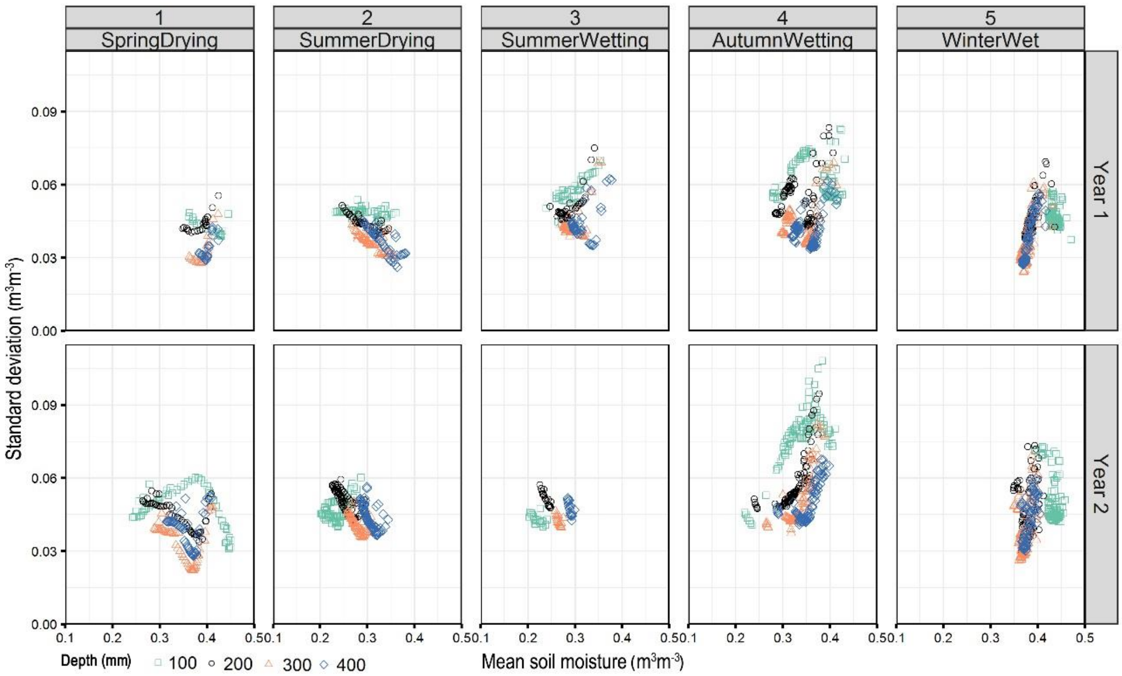

Figure 5.11 Relationship between the spatial mean soil moisture and standard deviation in the six selected sub-periods for each year. The dots represent data from twenty microsites and the colours indicates the four monitoring depths.

Linear regression was used to fit models on the spatial mean soil moisture and the SD. The analysis revealed similar trends to the ones found previously when CV and mean soil moisture were correlated. Only the 100 mm soil depth showed unimodal convex shape during the drying and wetting stages with a maximum soil moisture variability at about 0.35 $m^3 m^{-3}$. Table 5.6 presents the R^2 values between SD and spatial mean soil moisture, showing that significant correlations exist in most cases, although the character of the spatial correlation changed as the soils were drying out and as the soils were rewetting. This behaviour was also presented in other studies reporting that SD increases during drying from a very wet stage until it reaches a specific soil moisture level and then SD decreases as the drying continues (Famiglietti et al., 1998, Harter and Zhang, 1999, Choi et al., 2007). When the soils were drying out, mainly negative correlation was found whereas during the wetting and wet stages the significant correlations were positive.

Table 5.6 Values of coefficient of determination R^2 of derived from linear regression between standard deviation SD and the corresponding spatial mean soil moisture in the five sub-periods.

	DEPTH	SPRING - DRYING	SUMMER - DRYING	SUMMER - WETTING	AUTUMN - WETTING	WINTER - WET
YEAR 1	100	-0.55	-0.07	0.65	0.01	-0.08
	200	0.58	-0.75	0.58	0.01	0.6
	300	0.57	-0.68	0.38	0.1	0.56
	400	0.62	-0.74	0.22	0.19	0.84
YEAR 2	100	-0.01	0.28	-0.24	0.58	-0.27
	200	-0.49	-0.54	-0.87	0.52	0.06
	300	-0.11	-0.39	-0.43	0.63	0.22
	400	0.01	-0.46	-0.54	0.49	0.52

The most disperse data pairs appeared in autumn during the wetting processes with not significant correlations in Year 1. Although, during autumn in Year 2, the results showed moderate to strong positive linear relationships between SD and the mean soil moisture.

Our findings suggest that the relationship between CV, SD and mean soil moisture was not consistent through the two monitoring years and their dependency on the soil's wetness state was apparent. Based on the analysis above, it can be concluded that soil moisture spatial variability was affected by ascending or descending soil wetness change. Even though the analysis considered the linear relationship between mean soil moisture, CV and SD, the theoretical parabolic shape of the relationship, also found by Vereecken et al. (2007), occurred in the drying stages and during wetting. This phenomenon may be explained by the frequent change between drying and wetting events in the sub-periods that resulted in non-linear characteristics. The transition periods generally showed a highly varied spatial distribution while the relationship between mean soil moisture, SD and CV were more evident and significant in the dry and wet stages. Gwak and Kim (2017) evaluated a humid hillslope and found that variability was high in intermediate soil moisture levels and low in extremely dry and wet conditions that partly agrees with our findings. Soil water content variability was high when the soils were dry in a hillslope transect study conducted by of Harter and Zhang (1999). However, Famiglietti et al. (1998) and Hu et al. (2011) reported decreasing variability (expressed as SD) as soil moisture was decreasing that is in disagreement with our results, since we observed mainly increasing spatial variability with decreasing mean soil moisture content.

In an earlier study by Hajdu and Yule (2017) at the Patitapu Station, a 10-day soil moisture measurement period was assessed for spatial variability containing data from six microsites. They reported an inverse relationship between mean soil moisture and CV, i.e. soil moisture distribution was more homogenous with increasing mean soil moisture. It was also observed that the terrain attributes, such as slope angle and aspect had an effect on the soil moisture distribution. The contribution of topographical attributes on spatial soil moisture variability increased as the mean soil moisture decreased especially at the 100 mm soil depth which was also found by Gwak and Kim (2017). The soil moisture patterns in the deeper soil layers were temporally more stable than in the near surface layers that is mainly due to the decreased impact of atmospheric forcing.

5.4 Summary and conclusions

In this chapter, the focus was placed on identifying trends and patterns in the spatiotemporal distribution of soil moisture as these parameters are essential to improve simulations with statistical error modelling for hydrological or agronomical purposes, such as pasture growth forecasts. Temporally dense datasets are rarely available in hill country; thus, a soil moisture time series dataset was collected containing capacitance-based, AquaCheck sensor measurements from 20 spatially distributed locations at four consecutive depths. The nearly two-year long dataset has been examined to quantify temporal and spatial variability as well as temporal stability of soil moisture patterns at Patitapu Station.

It was observed that the soil moisture distribution could be characterised with non-normality on complex terrain. Year 1 and Year 2 showed similarly shaped Kernel density curves in the 200-400 mm soil depths indicating temporal stability in the distribution. Year 2, the drier part of the data collection period, represented larger soil moisture variability than Year 1, although the value and range of CV and SD of soil moisture decreased with soil depth in both years. The range of soil moisture readings were the largest in the 100 mm soil depth while the spread became narrower with increasing soil depth.

The results obtained in the present work show that it is possible to select a station that is representative of the mean water content of the soil in a given area, regardless of scale, from a pre-established network of measuring stations. The temporal stabilities were not entirely consistent at various soil depths; therefore, the depths were combined to select representative microsites. We found that a microsite established on a north-facing, moderately steep and open slope was the most representative of the field mean soil moisture (R^2 of 0.94 and RMSE of 0.021 $m^3\ m^{-3}$) at the study area based on the analysis of four statistical parameters.

We found that CV of soil moisture was the lowest when the soils were near saturation (or above field capacity) showing negligible spatial variability and highest in the descending and ascending transition stages, i.e. drying and rewetting periods. This study did not define specific soil moisture levels to describe dry condition due to the rather arbitrary description of that soil water stage.

In hill country, under the varied macro- and micro-climatic conditions, increasing spatial variability was observed with decreasing mean soil moisture consistently at four soil depth down to 400 mm. The evolution of spatially averaged soil moisture, its SD and CV in time revealed the difference in soil moisture dynamics in the upper and deeper soil layers. The magnitude of the spatial variation of soil moisture was greater near the surface than in the soil layers at 200-400 mm depths indicated by the lower SD and CV than at the 100 mm soil depth. The soil moisture spatial pattern was more temporally stable at very dry and very wet conditions, i.e. when soil water conditions are similar, and soil moisture spatial patterns tended to be less temporally stable when soils are drying down or wetting up.

The temporal stability of the spatial pattern was not maintained between two extreme soil moisture levels (minimum dry and maximum wet), which finding was supported by the Spearman's rank correlation analysis results. Recharging stages were found to carry higher variability than drying periods that might be caused by the varied evaporation, infiltration and runoff rates induced by the complex topography. Consequently, the spatial patterns were dependent on the aspect, slope angle and the topographical position while the effect of soil textural properties were not as significant as most locations have soils falling in the silt loam, silty clay loam texture classes.

North-facing locations, especially on steep and moderately steep slopes tended to be drier and represented more spread-out soil moisture range than the other aspects while microsites on east- and west-facing slopes showed similar soil moisture distributions and trends. In overall, at combined depths, the wettest microsite was located on a west-facing, rolling, open slope with

0.408 $m^3 m^{-3}$ temporal mean soil moisture while the driest microsite was situated on a north-facing, steep slope on a midslope ridge with 0.293 $m^3 m^{-3}$ temporal mean soil moisture.

The differences in soil moisture patterns have been shown and the knowledge of variability is vital to improve our understanding of land-water interactions on complex terrains. The appropriate consideration of the multi-modal nature of soil moisture distribution and the spatiotemporal variability may contribute to the development of more accurate modelling performance in the field of pedological, yield or hydrological applications. Moreover, the small-scale study has the potential to be used to calibrate or validate within pixel average values derived from remote sensing as the role of remotely sensed data in agricultural applications has been increasing. Thus, the within pixel spatial characteristics and variation soil moisture has been of great interest as it is an essential component of the statistical models.

Chapter 6

Modelling of near surface soil moisture using machine learning and multi-temporal Sentinel-1, Sentinel-2, Landsat 7 and Landsat 8 images in New Zealand

6 Chapter 6 - Modelling of near surface soil moisture using machine learning and multi-temporal Sentinel-1, Sentinel-2, Landsat 7 and Landsat 8 images in New Zealand

6.1 Introduction

The demand for accurate, high to medium resolution satellite-derived information for agricultural and land-based predictions is rising steadily (Atzberger, 2013, Roumenina et al., 2015). One critical attribute is the soil moisture that drives many environmental processes and it is considered as an essential input of many numerical simulations related to climate, hydrology and land-surface processes (Seneviratne et al., 2010). Since agricultural productivity is strongly controlled by the soil moisture availability (Martínez-Fernández et al., 2016), the spatial mapping of soil moisture of New Zealand's hilly landscapes is of great interest. The better understanding of these hydrologically complex systems is beneficial for improved farm management to hit productivity targets (e.g. fertiliser, stock and feed budgeting) and to mitigate impacts on climate-related extreme events (e.g. drought).

In hilly and mountainous regions, soil moisture can be characterised by distinctly variable dynamics that is dependent on the spatial scale. The interaction of soil properties, the rugged topography, land cover type and meteorological factors result in high spatiotemporal variability in soil moisture distribution, especially near the surface (Famiglietti et al., 1998, Brocca et al., 2007) as it was also shown in Chapter 5 during the spatial variability and stability analysis. Consequently, the measurement and monitoring of such a variable parameter by traditional techniques is cumbersome especially if there are significant changes in topography. Hence, many different approaches have been developed to retrieve soil moisture from remotely sensed data (Petropoulos et al., 2015, Zhang and Zhou, 2016, Karthikeyan et al., 2017).

Spaceborne microwave remote sensing has been effectively used to sense soil moisture at various scales, although the reliable, global soil moisture products have been only produced at coarse spatial resolution (approx. 25-40 km). Scatterometers and passive microwave sensors have been launched through Soil Moisture Active Passive (SMAP) programme, Aquarius (failed in 2015) and Soil Moisture and Ocean Salinity (SMOS) missions have been providing soil moisture estimations at the continental and global scale (Entekhabi et al., 2010b, Kerr et al., 2010, Mecklenburg et al., 2012, Das et al., 2018). Active microwave sensors showed lower sensitivity to soil moisture, although the product's spatial resolution is higher than the observations obtained by passive microwave methods (Nichols et al., 2011). Among active microwave sensors, the Synthetic Aperture Radar (SAR) instrument has been exploited effectively for monitoring bio-geophysical surface properties including near surface soil moisture (Ulaby et al., 1982b, Baghdadi et al., 2012, Paloscia et al., 2013, Eweys et al., 2017b). The presence of vegetation cover tends to reduce the sensitivity of the SAR signal to soil water content due to the biomass water content and the vegetation structure causing a two-way attenuation effect (Vereecken et al., 2012) described in Chapter 2.

The radar-based soil moisture retrieval methods are built on the physical principle, that the radar backscatter σ^0 (dB) is sensitive to the dielectric constant of the targeted surface, i.e. water content of the imaged bare soil or vegetated terrain (Wagner et al., 2008). Over bare soil, the sensitivity and response of microwave electromagnetic waves to soil moisture changes are well established (Wang, 1980). As a general empirical rule, the presence of free water increases the amount of energy reflected back towards the sensor from the bare soil surface (Dean et al., 1987). However, numerous additional factors have impact on the σ^0 generating an ill-posed challenge in the retrieval processes as the relationship among the interacting target properties is generally characterised by complexity and non-linearity (Ali et al., 2015).

The occurrence of vegetation, the confounding influence of radar configuration, topographical variability, land use heterogeneity, surface roughness and soil parameters (soil texture, soil moisture) are considered as the main driving forces of the σ^0 behaviour in mountainous areas (Ulaby et al., 1978, Luckman, 1998, Wagner et al., 2009a). The topography related effects and distortions are taken into account through geometric and terrain correction, radiometric (topographic) normalisation and speckle reduction as part of the SAR data pre-processing procedure. In mountainous landscapes, the retrieval of soil moisture retrieval using SAR information is very challenging (Pasolli et al., 2015), thus complementary information such as topographical attributes can be included to reduce the remaining contribution of the terrain on the σ^0 (Luckman, 1998, Paloscia et al., 2013) and help establish relations between the response and explanatory variables.

The soil moisture retrieval processes may include data from different radar configurations (incidence angle, polarisation, frequency) to be able to segregate and define the contribution of vegetation, and surface roughness from that of soil (Paloscia et al., 2008, Barrett et al., 2009). Advanced retrieval techniques utilise the main influencing features (vegetation coverage, surface roughness and soil properties) as input parameters to reduce their effects on the radar signal (Barrett et al., 2009, Petropoulos et al., 2015).

The application of optical imagery as well as the fusion of radar and multispectral data demonstrated its capability in accounting for some of these effects, i.e. the vegetation cover, structure and water content of the vegetation (Inglada et al., 2015, Veloso et al., 2017). Over vegetated areas, the combination of SAR and optical data is a preferred approach in near surface soil moisture estimation (Baghdadi et al., 2017). It remains a widely applied approach due to increased temporal coverage of the recently launched multispectral satellites (Bousbih et al., 2017, Gao et al., 2017, Urban et al., 2018). The possibility of using the combination of satellite derived multispectral and SAR data can be limited by cloud cover leading to observation gaps in the time series.

However, the combination of European Space Agency's (ESA) Sentinel missions and the Landsat Data Continuity Mission offers new opportunities in Earth observation, for capturing the dynamics of environmental parameters that has never possible before at an unprecedented spatiotemporal resolution. The Sentinel-1 dedicated radar imaging mission was expected to largely contribute to the mapping of high-resolution, near surface soil moisture (Malenovský et al., 2012). Sentinel-1, Sentinel-2 and Landsat 8 images have been used synergistically by Urban et al. (2018) for drought monitoring and vegetation cover analysis. Gao et al. (2017) attempted to map soil moisture at 100 m resolution using change detection by combining Sentinel-1 and Sentinel-2 observations. However, there has been no attempt made to map soil moisture at even higher resolution, i.e. 20-30 m, to address paddock scale soil moisture retrieval in hilly areas. The advances of the ESA's Sentinel-1 mission made it feasible to capture land surface processes, including soil moisture change without the limitation of daylight and cloud cover. The constellation of two satellites carrying C-band, SAR instruments provides 10 m pixel size multi-looked images with a region-dependent 6-day repeat cycle when both satellites are considered. SAR acquisitions are often preferred over frequently cloudy areas because of their daylight and weather independent characteristics.

Recently, the analysis and use of the ever-increasing number of geospatial datasets and remotely sensed products utilised in monitoring environmental systems have shown significant advancement in their utilisation. Open access data, cloud computing and machine learning allow the integration of large datasets faster and easier than ever before (Hird et al., 2017). Google Earth Engine is one of the cloud-based free service available for computing large geospatial data (Sidhu et al., 2018). GEE is being increasingly used in studies ranging from the field and catchment scale to the country and planetary scale (Clement et al., 2018, Mandal et al., 2018, Van Tricht et al., 2018).

Soil moisture retrieval algorithms are generally divided into two main distinct groups although there are other alternative methods, such as change detection. Theoretical or physical model-based approaches are the first group commonly used for soil moisture estimation by mathematical inversion of the models (Pasolli et al., 2015). The second group collects the techniques that are built on experimental data. However, the target variables and the remote sensing measurements are often related through non-linear functions signal saturation or the non-uniform sensitivity of the signal to physical properties (Haboudane et al., 2004, Twomey, 2013). To capture this complexity, numerous studies investigated the potential of machine learning techniques such as artificial neural networks, support vector regression or Random Forest (Ali et al., 2015). These methods have been successfully applied to exploit information and establish relationships between σ^0, soil-vegetation characteristics and near surface soil moisture (Dawson et al., 1997, Ali et al., 2015, Alexakis et al., 2017, Kumar et al., 2018).

The currently available SAR and optical datasets with fine spatial resolution and frequent over passes have been showing promising results in soil moisture prediction at a temporal scale close to user needs. The currently applied water balance models use low spatial resolution input from the Fundamental Soil Layers often failing to deal with the spatial heterogeneity of soil properties. Considering the variability occurring in hill country terrain, a soil moisture product with 10-30 m pixel size would result in more accurate fertiliser planning and application as well as improved decision-making on pastoral land. Therefore, the main objectives of the present study are to:

1. Implement an ensemble machine learning method to model soil moisture at medium resolution and its temporal evolution during the study period at the Patitapu Station, in the Wairarapa region.
2. Investigate radar signal sensitivity to near surface soil moisture at various spatial resolutions to understand the backscatter behaviour specific to the research area.
3. Combine Sentinel-2, Landsat 7 and Landsat 8 observations to generate a time series of Normalized Difference Vegetation Index (NDVI) for the representation of vegetation presence and to account for its contribution on the radar signal.
4. Contribute to the generation and development of a systematic, spatial soil moisture product for more accurate water balance calculations applied in farm management practices and fertiliser application planning.
5. Provide an insight of the utilisation of a simple, synergetic use of remotely sensed data and topographic attributes in soil moisture modelling in hilly landscapes.

6.2 Materials and methods

6.2.1 Study area

The study was conducted on a 2623 ha hill country property, located in the Wairarapa region of the North Island of New Zealand (40.745020 S, 175.887320 E). The study area is a primarily pastoral farmland mixed with patches of forestry on rolling to steep hills, interspersed with fertile plains. The average annual rainfall is 1050-1127 mm on the property, while elevation ranges from 148-531 m above sea level. The predominant plant communities are ryegrass *(Lolium perenne)* and white clover *(Trifolium repens)* species, while the soils are mainly silty clay loam in texture. The ground-based, in situ soil moisture data collection was limited to relatively homogenous, permanent pasture surfaces on soils with mainly silt loam and silty clay loam texture. Figure 6.1 illustrates the research area on a Sentinel-2 RGB composite (Fig. 6.1 A) on which the ground-based microsites were also displayed. A composite of timely averages (i.e. seasonal mean) of Sentinel-1 σ^0 data in spring, summer and winter (Fig 6.1 B) indicates various land cover types as they exert different responses on the radar signal that is supported by an NDVI product calculated from a Sentinel-2 scene from August 2018 (Fig. 6.1 C).

6.2.2 In situ data sources

6.2.2.1 Ground-based, in situ soil moisture observations

Soil moisture measurements were obtained by 20 capacitance-based, AquaCheck sub-surface probes (AquaCheck Soil Moisture Management, Durbanville, South Africa) arranged into a WSN (Fig. 6.1 A). The WSN deployment has been described previously in detail in Chapter 3 along with the specific terrain and soil properties at each microsite.

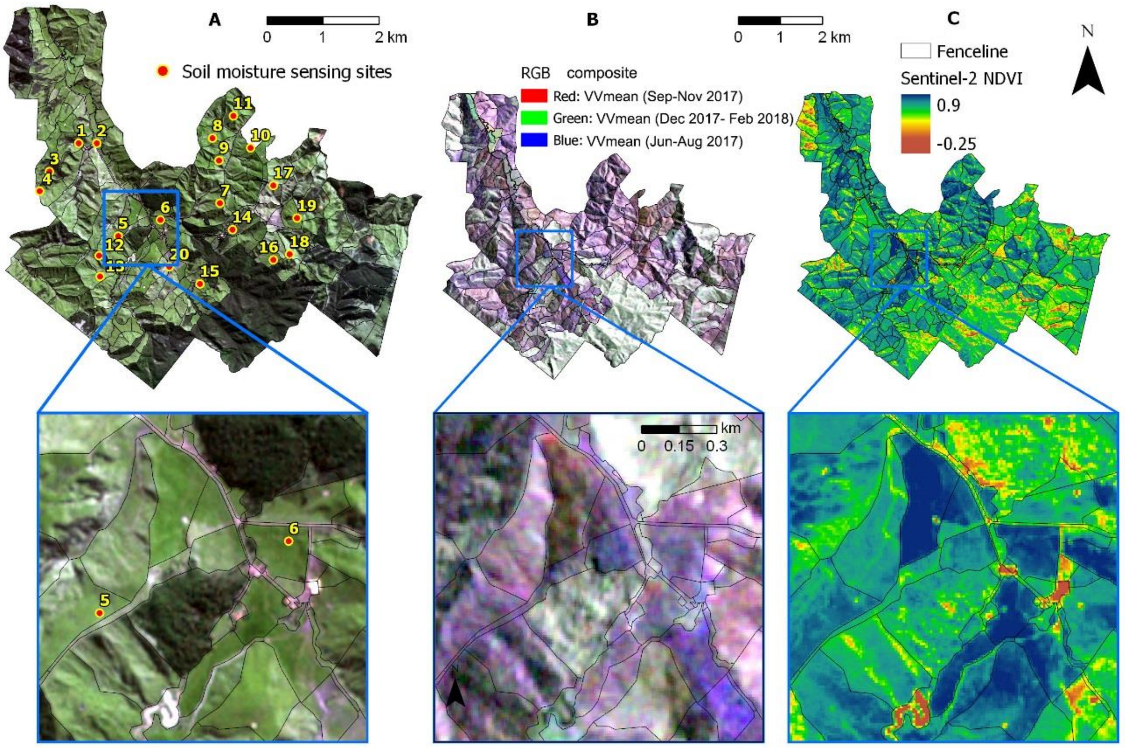

Figure 6.1 The extent of the research area represented by Sentinel-2 multispectral data and Sentinel-1 radar backscatter composite. A: the microsites marked on a cloud free Sentinel-2 optical image. B: VV backscatter data where the red band shows the mean of the VV backscatter during spring (Sept 2017 - Dec 2017), the green band shows the mean of VV backscatter in summer (Dec 2017 - Feb 2018) and the blue band shows the mean of VV backscatter in winter (Jun 2018 - Aug 2018). C: Sentinel-2 NDVI on 24 Aug 2018.

The AquaCheck probe is equipped with moisture sensors spaced at 100, 200, 300, and 400 mm depths, although only the 100 mm readings were utilised in this study. Soil water content was recorded at 15-minute time intervals and the raw sensor readings were converted to volumetric soil moisture (θ_v, m^3 m^{-3}) through sensor-specific calibration functions. The applied calibration formulas were obtained through gravimetric soil moisture measurements considering a wide range of various wetness conditions. More details on the calibration method and sensor accuracy analysis was presented in Chapter 4. To create the reference database, θ_v data was obtained from the WSN at the time stamp that coincided best with the SAR image acquisition.

We note that θ_v measurements at 100 mm depth have their limitations when related to C-band SAR data with typically shallow (few cm) soil penetration (Bruckler et al., 1988, Le Morvan et al., 2008). However, the network is set up on an operating farm where the devices had to be protected against human and animal activity by burying them. Due to the probe design and the sensors' cylindrical shaped sphere of influence, θ_v information was gained from the ~70-130 mm increment and hereafter referred to as near surface θ_v.

6.2.2.2 Terrain attributes

Terrain variables were extracted from a high-resolution (0.2x0.2 m) DSM generated through a structure-from-motion technique (Micheletti et al., 2015) where images were captured using DSLR camera from a fixed wing aircraft. The DSM was smoothed using focal statistics prior to the terrain analysis. Topographical parameters and hydrological metrics, such as slope angle, aspect, SAGA topographic wetness index (SWI), topographic position index (TPI) and terrain ruggedness index (TRI) were derived from the DSM. The process was conducted by the application of the terrain analysis tool sets built in the System for Automated Geoscientific Analysis (SAGA) software (Conrad et al., 2015). The datasets were resampled to 20 m pixel size using bilinear interpolation to ensure integration with the SAR data. The reference terrain information was extracted from the radar pixel footprint overlapping the twenty microsites.

6.2.3 Remote sensing data

6.2.3.1 Data access through Google Earth Engine

Due to the number of images used in the study, the associated processing time and computing power requirements, the remotely sensed information was obtained via the cloud-based Google Earth Engine (GEE) computing platform (Gorelick et al., 2017). GEE offers pre-processed image collections and a unified framework to process large number of images that are stored within Google's cloud computing services. GEE's data manipulation and visualisation toolsets provide unprecedented possibilities for temporal analysis and data extraction from the vast amount of publicly available remote sensing data.

For the purpose of the study, the JavaScript application programming interface was used via the GEE code editor to access, filter, manipulate and extract a variety of the data from the GEE's data catalogue. Our study utilised the publicly accessible, standard Earth science raster datasets, including high-resolution Synthetic Aperture Radar (SAR) images captured by the Sentinel-1 satellites and multispectral scenes acquired by the Sentinel-2, Landsat 7 and Landsat 8 missions. The analysis and modelling tasks were executed on images that satisfied the geometric quality requirements, i.e. GEE's Tier 1 image collection.

6.2.3.2 Overview of the exploited remote sensing images

As the Sentinel-1 SAR imagery is dominantly independent from cloud cover, a relatively dense image collection was generated. Although the research area is covered by Sentinel-2 scenes every 5-10 days, only 21 cloud-free images were available within the study period due to the frequent overcast conditions in New Zealand. The extraction of clear, cloud-free pixel values over all microsites was crucial to build up a representative training dataset. Thus, we investigated the availability of cloud free Landsat 7 and Landsat 8 acquisitions and incorporated them to increase the temporal density of observations in the time series data. Table 6.1 summarises the number of analysed images acquired by various satellite sensors in partly cloudy and cloud free conditions.

Table 6.1 The number of remote sensing images used in this study grouped by cloud cover.

Satellite and sensor			*Total no. of images*
Sentinel 1 / SAR			153
	No. of cloud free images over all microsites	*No. of partly cloudy images*	
Sentinel 2 / MSI	21	18	39
Landsat 7 / ETM+	11	7	18
Landsat 8 / OLI	9	11	20

The multispectral scenes were available in a significantly lower number and only about half of the images were cloud free over all the microsites. Landsat and Sentinel-2 satellites have spectral and spatial similarities so that they could be combined to increase the amount of cloud-free observations (Flood, 2017, Li and Roy, 2017, Skakun et al., 2017, Pastick et al., 2018, Urban et al., 2018). In total, 230 satellite scenes were exploited over a time span of 22 months for the synergistic use of the data to achieve high model training results. Figure 6.2 illustrates the temporal distribution of the remotely sensed images over the study period for the four satellite missions from Nov 2016 to Aug 2018.

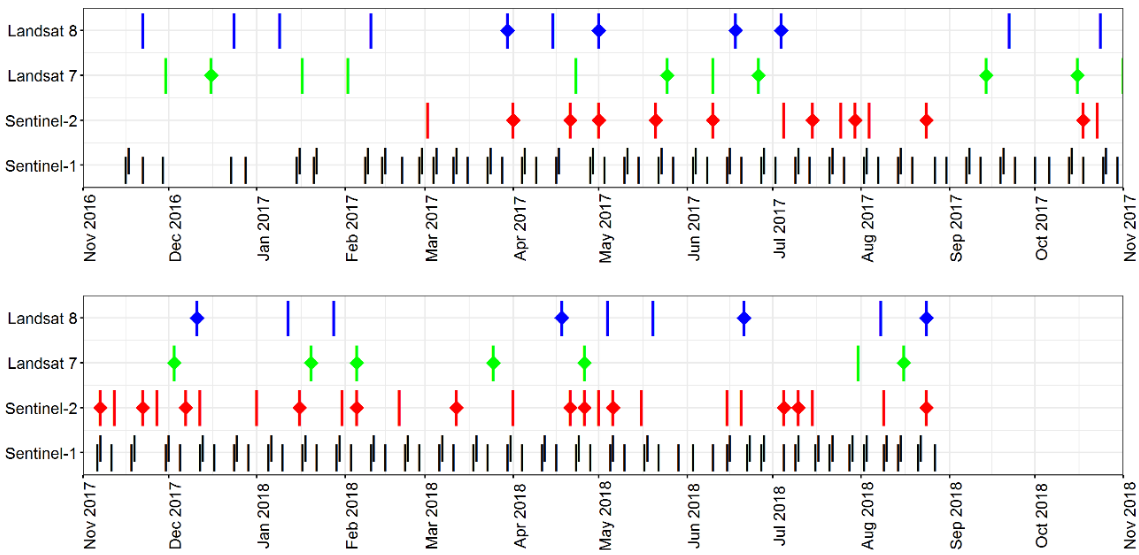

Figure 6.2 Overview of the used satellite data coverage of Sentinel 1 (A/B), Sentinel 2 (A/B), Landsat 7 and Landsat 8 acquisitions over the Patitapu Station between 01/11/2016 and 31/08/2018. The scenes marked with a rhomboid were cloud-free over all the 20 ground-based measurement locations.

6.2.3.3 Radar imagery from the Sentinel-1 mission

The SAR data applied in this study was captured by instruments on board the Sentinel-1A and 1B satellites. The Sentinel-1 constellation is operated by the ESA and the mission is part of the Copernicus program. The Sentinel-1 satellites are mounted with C-band (central frequency of 5.404 GHz) SAR instruments with equivalent configurations. Due to the design of the Sentinel-1 mission, a 6-day repeat cycle can be reached if both satellites are considered providing data in single and dual polarisation modes. The mission provides an all-weather day-and-night supply of SAR imagery with a spatial resolution of 10x10 m after multi-looking.

6.2.3.3.1 The SAR dataset over the study area

Incidence angle (ϑ) and the σ^0 and data were extracted from 153 Level-1, Ground Range Detected (GRD) images acquired in Interferometric Wide swath mode. The GRD products were exploited in the available dual polarisation, i.e. VV (vertical transmit and vertical receive) and VH (vertical transmit and horizontal receive) over the study area. GEE's Sentinel-1 image collection contains images with several different instrument configurations, resolutions obtained by the satellite constellation during both descending (DES) and ascending (ASC) orbits. The attached metadata properties can be used to filter the dataset and generate a homogenous Sentinel-1 image collection. In this project, we kept all the available SAR images to increase the amount of radar data input into the model. Sentinel-1 σ^0 was available at four acquisition modes over the Patitapu Station, i.e. ASC orbits with 34° and 44° ϑ and DES orbits with 30° and 41° ϑ. Considering a specific acquisition mode, the ϑ property found in the metadata barely changed due to the proximity of the microsites and the small extent of the area. Additionally, the SAR data was extracted at 10, 20 and 30 m resolution through GEE for each acquisition mode to investigate the sensitivity of σ^0 to soil moisture depending on ϑ and spatial resolution.

6.2.3.4 Multispectral imagery

6.2.3.4.1 Sentinel-2 mission and available dataset in GEE

The ESA has launched the Sentinel-2 satellite constellation comprising of two identical satellites as part of the Copernicus program. The satellites are equipped with the Multi Spectral Instrument (MSI) providing high to moderate spatial resolution imagery with frequent revisits and similar spectral characteristics to the Landsat family (Drusch et al., 2012). The Sentinel-2 obtains images in 13 spectral bands spanning from visible (VIS) to short wave infrared (SWIR) range, at different spatial resolutions ranging from 10 to 60 m. GEE delivers Sentinel-2, Level 1C data representing orthorectified Top of Atmosphere (TOA) reflectance since June 2015. Additionally, a quality assessment bit mask is added for cloud identification and masking.

6.2.3.4.2 Landsat 7 and 8 mission and datasets in GEE

The Landsat 7 mission, launched in 1999, is equipped with the Enhanced Thematic Mapper Plus instrument (ETM+) collecting information with a 16-day repeat coverage. The ETM+ sensor captures images in seven spectral bands with a spatial resolution of 30-60 m and a panchromatic band with 15 m resolution (USGS, 2018). For the purpose of the study the TOA reflectance image collection was chosen, as Sentinel-2 data is only available in TOA reflectance.

The Landsat 8 mission was launched in 2013 and it captures images every 16 days in an 8-day offset from Landsat 7. The satellite is equipped with the Operational Land Imager (OLI) for multispectral observations. Landsat 8 images are also delivered in calibrated TOA reflectance format by GEE containing 12 bands (USGS, 2018). Most bands have a resolution of 30 m, which have been utilised in the present work. A quality assessment band is provided for every Landsat 7 and 8 products carrying descriptions about observation quality. This band was applied as a per pixel filter to generate cloud-free image collections.

6.2.4 Combination of NDVI and adjustments specific to the study area

6.2.4.1 NDVI calculation

To represent the vegetation cover, NDVI was derived from spectral information captured by the three multispectral satellite missions and combined into one time series following an adjustment process. NDVI has been a widely applied indicator of green vegetation cover (Reviewed by Bannari et al. (1995)). The generic form of NDVI calculation is given as Eq. (6.1).

$$NDVI = \frac{\rho_{NIR} - \rho_{RED}}{\rho_{NIR} + \rho_{RED}} \tag{6.1}$$

Where ρ_{NIR} and ρ_{RED} represents the reflectance in the near-infrared (NIR) and red channels, respectively. Sentinel-2 NDVI was derived based on the Band 8A (NIR) and Band 4 (Red) as the difference between Landsat 8 and Sentinel-2 NDVI were less pronounced when the Band 8A was selected instead of Band 8 (Zhang et al., 2018). The same results were presented by Mandanici and Bitelli (2016) showing that Band 8A should be used when Sentinel-2 NDVI is calculated to be able to compare that to Landsat 8 NDVI. For Landsat 7, the Band 4 (NIR) and Band 3 (Red), while in the case of Landsat 8, Band 5 (NIR) and Band 4 (Red) were selected for NDVI calculation as per Eq. (6.1).

6.2.4.2 Satellite product comparability

In principle, the Sentinel-2 Level 1C TOA, Landsat 7 and Landsat 8 TOA products should provide broadly comparable and complementary observations for most cases. However, small but consistent differences have been found during comparisons of Landsat 7 and Landsat 8 as well as between Sentinel-2 and Landsat products (Flood, 2014, Holden and Woodcock, 2016, Zhu et al., 2016, Flood, 2017). The combination of data from multiple satellites may lead to data discrepancies due to the slight differences between sensor properties and bandwidth (Flood, 2014). Landsat 7 and Landsat 8 are not identical but they exhibit systematic variation between the two sensors that makes them comparable after corrections (Flood, 2014, Holden and Woodcock, 2016). The difference between Landsat 8 and 7 was quantified by Flood (2014) who stated that NDVI values were systematically overestimated by Landsat 8 OLI by about 5% as compared to Landsat 7 ETM+ without adjustment.

NASA released the Harmonized Landsat 8 and Sentinel-2 products and reported the transformation functions for selected areas globally (Claverie et al., 2017), that did not include New Zealand. Zhang et al. (2018) and Flood (2017) also characterised the transformation parameters and found that their results were substantially different from the NASA's published coefficients. Therefore, it was suggested that the adjustment among these satellite products might require coefficients derived on a regional basis.

6.2.4.3 Site-specific NDVI adjustments for Patitapu Station

Consequently, study area specific adjustments were developed and applied locally to the various NDVI products to ensure a better match over the Patitapu Station. The corrections are commonly based on Ordinary Least Square (OLS) linear regressions fitted on co-registered raster datasets captured by different sensors and obtained on the same day or within a given time window (Flood, 2014, Holden and Woodcock, 2016, Flood, 2017, Zhang et al., 2018). The present work followed this method and the broadly accepted OLS technique was employed to generate the specific adjustment formulas.

To develop the correction functions, coincident acquisitions were selected from dominantly cloud free conditions on the same day or within a 3-day window. The cloud mask information was derived from the Quality Assessment bit-mask bands for each satellite products to eliminate cloudy pixels. The 10 m Sentinel-2 bands were spatially resampled to match the 30 m resolution of Landsat scenes. NDVI was derived in GEE and the images with added NDVI bands were exported and co-registered to ensure alignment between corresponding pixels from different scenes. NDVI values were extracted from 5000 randomly generated sampling points distributed over the study area from each image pair. A small portion of the sampled NDVI values was removed due to patches of cloud cover or cloud shadow. To derive transformation functions from Landsat 7 and Landsat 8 NDVI values to Sentinel-2 NDVI, linear models were fitted on the sampled NDVI individually as per Eq. (6.2).

$$NDVI_{S2} = c_0 + c_1 * NDVI_L \tag{6.2}$$

Where, $NDVI_{S2}$ is NDVI derived from Sentinel-2 spectral information and $NDVI_L$ represents NDVI from either Landsat 7 or Landsat 8 images while c_0 and c_1 are the intercept and slope of the fitted models.

6.2.4.4 Filling NDVI gaps in the time series

To create a complete training dataset, a continuous, daily NDVI time series input was generated from the combined, adjusted NDVI data. To derive NDVI values on the days coincident with SAR image acquisitions, a missing value imputation process was applied by the utilisation of the tools offered by *ImputeTS* package (Moritz and Bartz-Beielstein, 2017) in R software environment (R Core Team, 2017). Although there are different algorithms available in ImputeTS, a Kalman filter technique was chosen to improve the temporal consistency of the NDVI time series because it is widely applied algorithm for remotely sensed and in situ data assimilation (de Wit and van Diepen, 2007, Kleynhans et al., 2011). Similarly, the Kalman filter method has been used to create continuous time series of NDVI images by Sedano et al. (2014).

6.2.5 SAR backscatter sensitivity to soil moisture

As the SAR images were obtained in four acquisition configurations in different θ ranges, we investigated the sensitivity of σ^0 to θ_v for each image collection. Under certain circumstances, i.e. constant surface roughness and bare soil surface or negligible amount of vegetation cover, a positive linear relationship can be assumed between these two parameters (Weimann et al., 1998, Quesney et al., 2000, Srivastava et al., 2009). Therefore, a regression analysis was performed to investigate the sensitivity and the linear relationship between σ^0 to θ_v at the microsites. The analysis was conducted at various spatial resolutions to examine which cell size is the most promising for θ_v retrieval and noise reduction.

6.2.6 SAR backscatter normalisation

Due to the significantly different viewing orientation of the ASC and DES orbits, a simplified normalisation process was applied to incorporate all the σ^0 data to the training of the RF regressor. The variance in σ^0 caused by the angular variation was reduced by conducting a broadly used square cosine angle correction technique (Ulaby et al., 1982b, Mladenova et al., 2013, Topouzelis and Singha, 2016). The normalisation method follows Lambert's law for optics and it assumes that the portion of the energy returning to the satellite sensor follows a cosine law and the radiation variability within the observed area is also cosine dependent (Mladenova et al., 2013). The correction approximates the radar response under any given angle from the observed radar backscatter σ_{ϑ}^{0} acquired at ϑ as per the formula provided in Eq. (6.3).

$$\sigma_{\vartheta ref}^{0} = \frac{\sigma_{\vartheta}^{0} \cos^2 \vartheta_{ref}}{\cos^2 \vartheta} \tag{6.3}$$

Where, $\sigma_{\vartheta ref}^{0}$ is the normalised radar response at a selected reference incidence angle ϑ_{ref}. The Sentinel-1 SAR data obtained over the Patitapu Station ranged from approximately 30° to 44° considering all acquisition modes and orbits. Therefore, the mean θ, i.e. 37° was chosen as ϑ_{ref} following the method by Van Tricht et al. (2018) who combined Sentinel-1 and Sentinel-2 imagery for crop mapping.

6.2.7 The proposed methodology

To develop a model that can predict θ_v and to capture the variability at the paddock and sub-paddock scale, at least medium spatial resolution input layers at 10-100 m pixel size (Gao et al., 2010) are required. Although σ^0 is affected by noise and numerous parameters such as the vegetation cover, dielectric properties and the geometrical characteristics (i.e. roughness) of the targeted surface (Ulaby et al., 1978, Ulaby et al., 1982a), it carries information about θ_v. In particular, volume scattering exerts a strong influence on SAR σ^0 by attenuating the signal and reducing its sensitivity to θ_v (Ulaby et al., 1986b). The degree of this effect is highly dependent on the geometrical alignment and characteristics of the vegetation (Karjalainen et al., 2004, Patel et al., 2006). Consequently, these effects need to be incorporated to the θ_v modelling algorithm in some ways to improve the performance of the simulation.

Optical imagery with multispectral characteristics can indicate the presence of vegetation and its temporal evolution through derived indices such as the NDVI. Therefore, NDVI is commonly used to correct for the vegetation effect on the radar signal and to improve the performance of θ_v retrieval algorithms (Alexakis et al., 2017, Gao et al., 2017). It was shown that increasing NDVI resulted in decreasing sensitivity of the radar signal to θ_v (Bousbih et al., 2017). Hence, the integration of radar and multispectral imagery into a time series was implemented to model the temporal and spatial distribution of θ_v. Furthermore, terrain attributes were derived from a DSM to represent some of the radar signal influencing parameters.

The various environmental variables and the nature of the previously described non-linear θ_v retrieval problem required an advanced method. Machine learning techniques represent a selection of techniques that are able to learn from a reference dataset using various learning strategies (Ali et al., 2015). As a typical application of artificial intelligence, a machine learning technique can detect patterns in data without relying on programmed prior rules and relationships. The machine learning algorithms are able to predict or map further data from the automatically recognised trends and relations (Robert, 2014). A great advantage of the machine learning tools are that they have the capability to integrate data from different sources, as the algorithms do not require assumptions regarding the statistical distribution of the given set of predictors (Ali et al., 2015).

The overall modelling task was considered as a complex supervised regression problem built upon a dataset consisting of continuous and categorical variables from various sources. Furthermore, numerical values were expected as model output. Therefore, a non-parametric regression tool, the Random Forest (RF) method was chosen, since this algorithm is capable of simultaneously handling both type of variables and the prediction generates continuous numerical values (Breiman, 2001). The state-of-the-art RF algorithm is fast and does not require as large training datasets as other machine learning approaches such as artificial neural networks (Ali et al., 2015).

RF predicts the final numerical value of a response variable (i.e. θ_v), from several predictor variables (i.e. σ^0, NDVI and terrain attributes) by aggregating the results from multiple independently drawn decision trees (a "regression forest"). RF can overcome the commonly occurring overfitting and training data sensitivity problems by constructing an ensemble of decision trees from randomly selected training samples and variables at each node (Park et al., 2017). The numerous decorrelated trees were constructed from bootstrapped samples from the training data and the variance in the trees was reduced by averaging the results. It was shown that RF was capable of efficient θ_v retrieval under various crops by Kumar et al. (2018). The chosen RF regressor was built on the Breiman's algorithm (Breiman, 2001) and the model was developed and assessed by the utilisation of the *Caret* (Kuhn, 2008) as well as *randomForest* (Liaw and Wiener, 2002) R software packages. The overall model building and assessment procedure is presented in Figure 6.3.

To evaluate the algorithm performance, 22-months' worth of data was used to create validation (25% of the observations) and training data (75% of the observations) subsets, based on pseudo random sample selection. First, the RF model was fine-tuned to achieve the best performance and the results from the Out-Of-Bag error estimation technique were used to assess prediction performance.

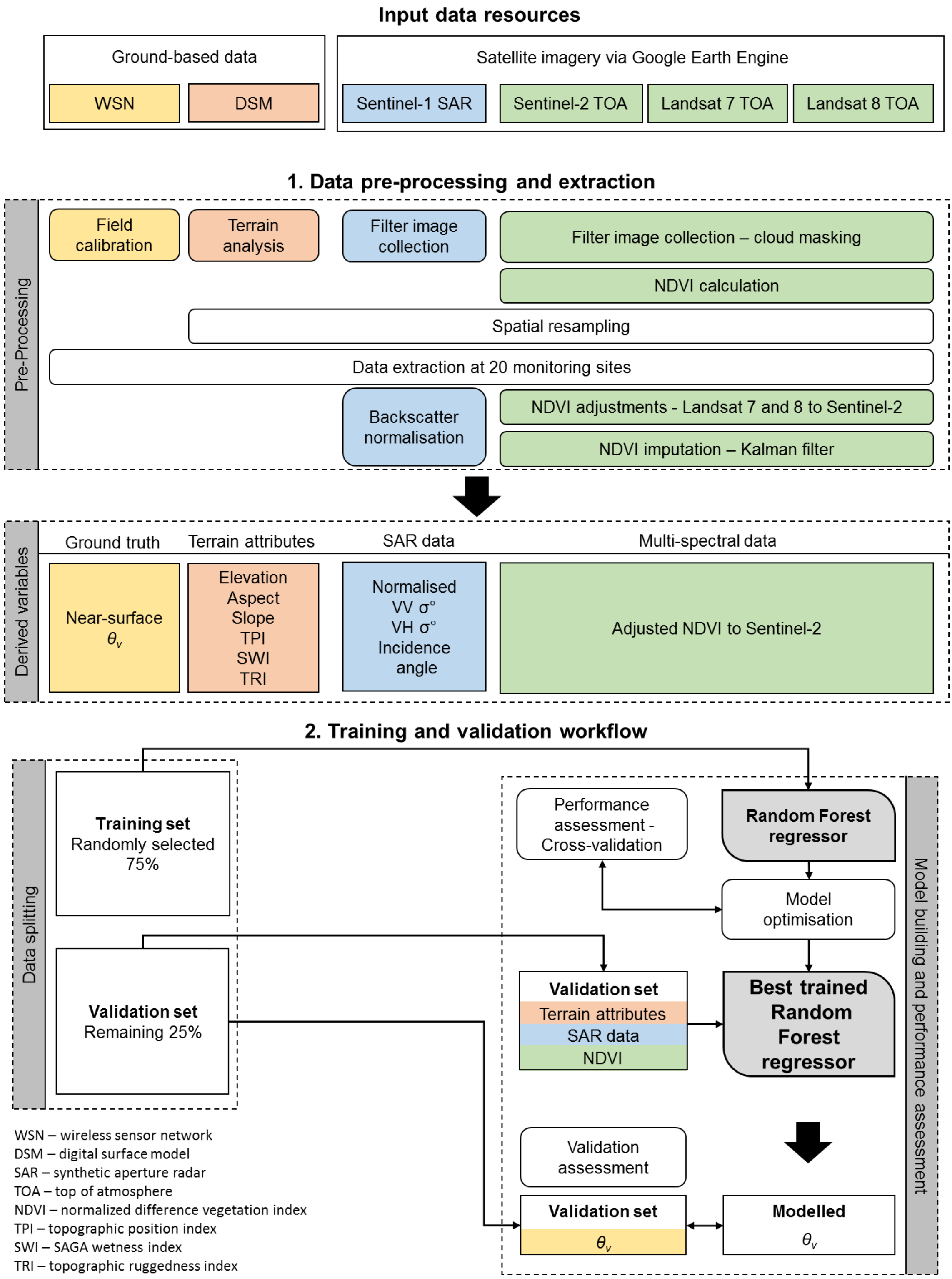

Figure 6.3 Graphical representation of the data pre-processing, extraction as well as the modelling and validation workflow (θ_v – volumetric soil moisture, σ^0 – backscatter coefficient).

The second step included a repeated cross-validation to investigate generalised model stability, predictive accuracy and the difference between Out-Of-Bag error estimations and the cross-validation. Mean Absolute Error (MAE), Root Mean Square Error (RMSE) and adjusted coefficient of determination (R^2) were selected to benchmark the model accuracy and loss functions. As part of the third step, the validation subset was fed into the optimised model and the time series of observed and modelled θ_v were compared at each in situ θ_v monitoring location.

As a last step, we investigated the spatial θ_v mapping capability of the trained RF regressor at the Patitapu Station on selected dates. To derive θ_v spatially, a reference dataset collected by 15 microsites was used for training the RF algorithm. Five microsites were left out and used for a technically independent evaluation of the RF model performance. The validation microsites were chosen to represent various terrain conditions distributed over the farm pastoral areas with different aspect and slope angle conditions. Modelled θ_v values were extracted from eight computed spatial layers and related against corresponding observed θ_v.

6.3 Results and discussion

6.3.1 NDVI adjustment

The derived model parameters and the amount of data used to develop the transformation model for NDVI from Landsat 7 and Landsat 8 to Sentinel-2 are presented in Table 6.2. Strong linear relationships were observed during the model fitting, resulting in an R^2 of 0.85 for Landsat 8 to Sentinel-2 and R^2 of 0.89 for Landsat 7 to Sentinel-2 for NDVI transformations.

Table 6.2 Coefficients for adjusting Landsat 7 and Landsat 8 Normalized difference Vegetation Index (NDVI) to Sentinel 2 NDVI generated over the Patitapu Station.

NDVI conversion	*Intercept c_0*	*Slope c_1*	*R^2*	*No. of pixels / image pairs*
Landsat 8 to Sentinel-2	-0.0307	1.0296	0.85	19425 / 4
Landsat 7 to Sentinel-2	0.0686	0.9565	0.89	24121 / 5

6.3.2 Sensitivity of radar backscatter to soil moisture

C-band SAR data sensitivity to θ_v is dependent on the θ of the radar signal and lower θ showed higher sensitivity to soil water content (Ulaby et al., 1978, Baghdadi et al., 2006). To investigate the difference in SAR data response to θ_v in the multiple acquisition modes, VV and VH σ^0 data were related to θ_v through linear regression analysis as an initial approximation. The correlation was defined at each ground-based microsite between VV and VH σ^0 and θ_v. VH polarisation showed insignificant correlation and sensitivity to θ_v changes compared to the VV σ^0. These findings were confirmed by previous studies observing that VH polarisation is less affected by soil water content than VV (Eweys et al., 2017a, Amazirh et al., 2018). Hence, we provide detailed results only on the VV σ^0 and θ_v relationship by reporting adjusted coefficient of determination (adjusted R^2) values as indicator of the strength of the relationship.

Figure 6.4 depicts the distribution of adjusted R^2 values calculated for four ϑ classes, although the values were grouped by orbit mode and spatial resolution. It was observed that, in general, the 20 m spatial resolution SAR data reached a slightly higher mean adjusted R^2 than the datasets generated at 10 m and 30 m pixel size considering the twenty microsites.

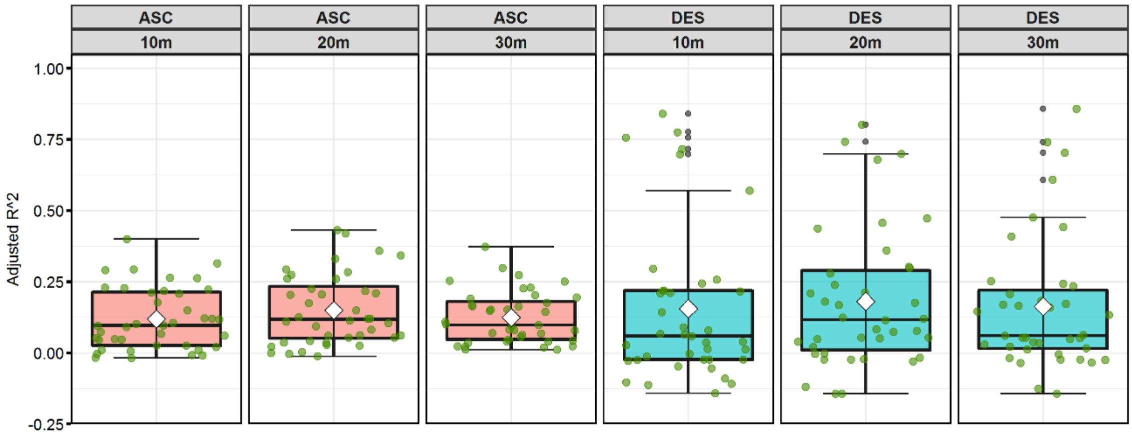

Figure 6.4 Adjusted coefficient of determination (R^2) values of the regression between Sentinel-1A and 1B (SAR) VV backscatter and ground-based volumetric soil moisture for various satellite orbit and spatial resolution combinations (ASC - ascending orbit - Sentinel-1B, DES - descending orbit - Sentinel-1A). The boxplots visually summarise the following statistical parameters: the mean (white rhomboid), the median (line across the box), 25th percentile and 75th percentile as lower and upper hinges and outlying points.

For low ϑ, i.e. DES orbit, some of the microsites showed positive, moderately strong correlation whereas at higher ϑ, i.e. ASC orbit, the strength of the relationship ranged from weak to moderate. It is likely that the application of 10 m pixel size SAR dataset contained more noise than the 20 m data, whereas the 30 m resolution seemed to be too large to represent θ_v due to its highly variable distribution over complex terrain. Therefore, the 20 m spatial resolution was chosen for the Sentinel-1 dataset and the spatial resolution of the modelling and mapping. The lower θ of the DES mode were shown to be better suited for θ_v estimation than high ϑ. According to these results, the prediction could be improved by only using the DES orbit data. However, in this study, the RF algorithm was trained on normalised SAR data, thus the utilisation of various SAR images will help to keep the high temporal resolution and make the model able to process scenes captured in different acquisition modes.

The VV σ^0 was plotted as a function of θ_v for all θ in ASC and DES orbits at 20 m resolution. The linear fit between VV σ^0 and θ_v with shaded confidence regions (0.95) is presented in Figure 6.5. Some of the microsites (i.e. 4, 9, 10, 12, 13 and 20) represented moderate correlations while all the others showed weak or insignificant linear relationship. Although, it was clear that high σ^0 values were related to high θ_v and low σ^0 values were generally associated with dry conditions.

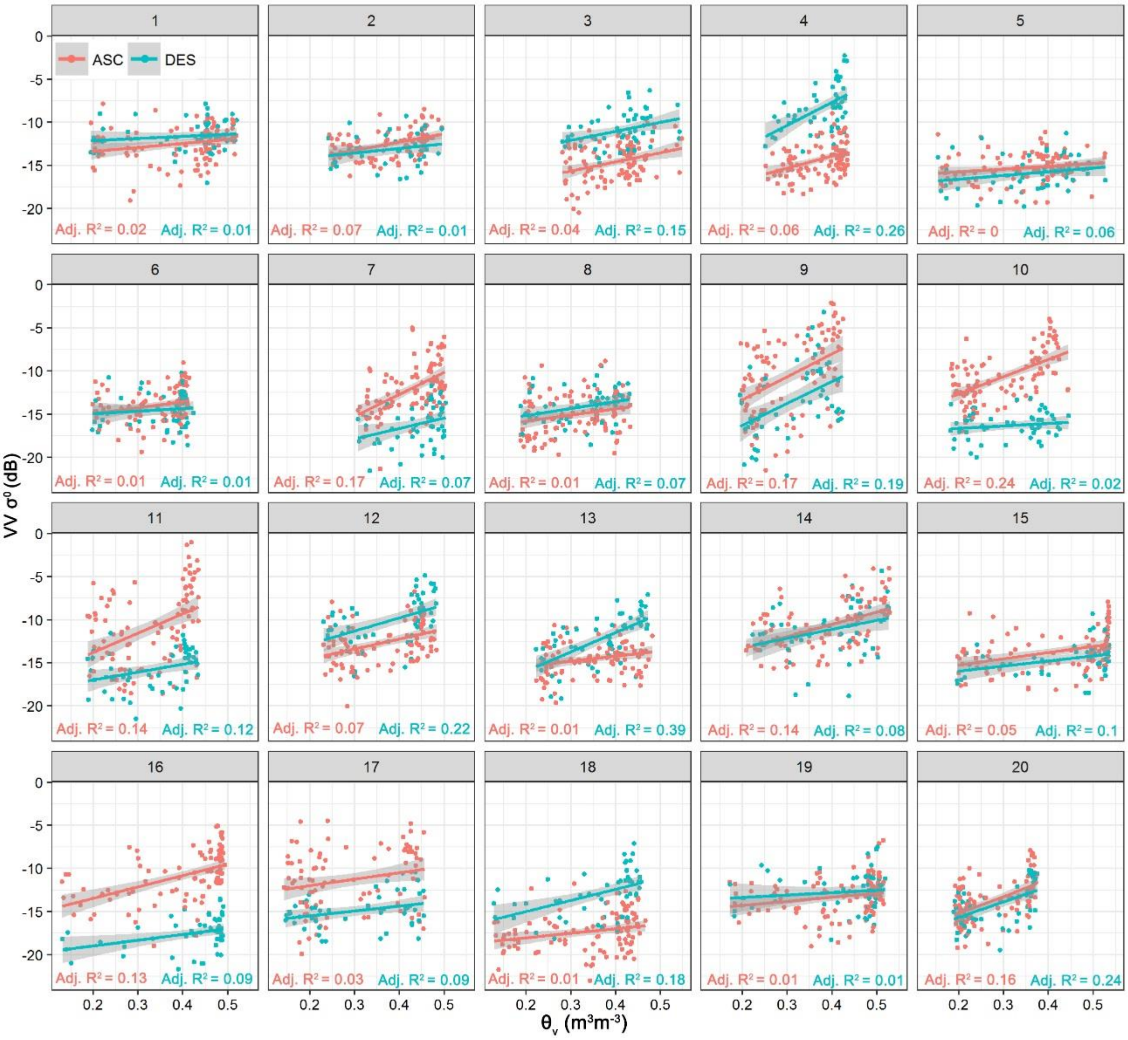

Figure 6.5 Scatterplots illustrating the relationship between VV backscatter (σ^0) at 20 m spatial resolution and near surface soil moisture (θ_v) at the 20 monitoring locations installed at the Patitapu Station coloured by orbit mode. The shaded areas represent the 0.95 confidence regions.

These results suggest that the linear approach was not suitable to derive the $\theta_v$retrieval functions over pastoral surfaces under hill country conditions. The low adjusted R^2 values and the varying slopes of the fitted linear models indicates a large amount of uncertainty which can be attributed to numerous influencing factors, such as speckle noise, vegetation cover, surface roughness and complex terrain generating variable angular responses. According to Baghdadi et al. (2008) the fitted linear models and their coefficients may differ from year to year and on a regional basis requiring frequent calibration. Additionally, the θ_v sensors were located at 70-130 100 mm soil depth that was slightly deeper than the theoretical penetration depth for C-band SAR signal. It was observed that the generation of homogenous image collections by using θ as a filter, achieved higher R^2 values, although the filtering led to significantly reduced temporal SAR observation density.

At a selected location, namely at Site 9, the temporal evolution of normalised SAR data, NDVI, daily total rainfall and daily mean θ_v were plotted together as shown in Figure 6.6. Site 9 is situated on a near high ridge position with relatively homogenous pasture cover and a narrow annual θ_v fluctuation range.

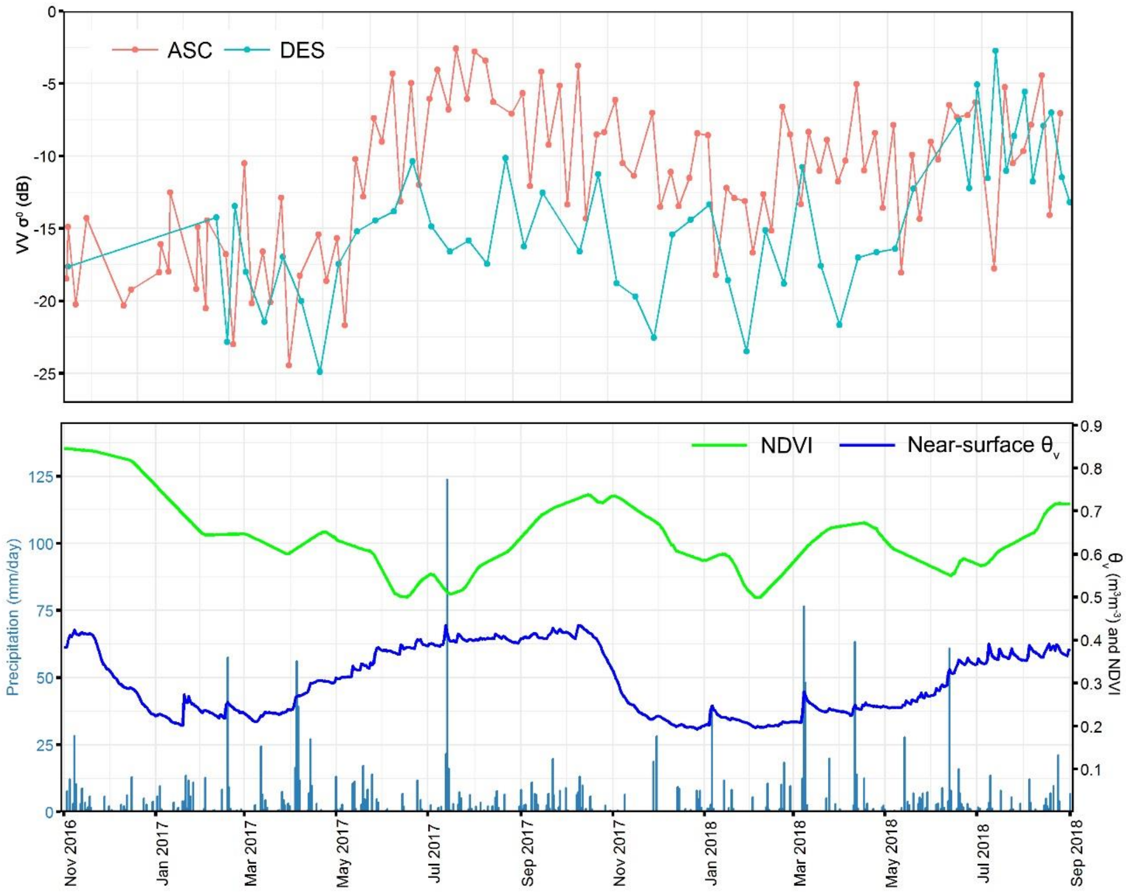

Figure 6.6 Ascending (ASC) and descending (DES) VV backscatter (σ^0) development analogous to daily mean volumetric soil moisture (θ_v) , to daily NDVI derived at Site 9 and total daily rainfall measured by the local weather station during two consecutive years at the Patitapu Station.

Both ASC and DES σ^0 showed recognisable patterns and increasing values with increasing θ_v. During the dry periods, the amount of backscattered energy was low, although the heavy rainfall events seemed to increase the σ^0 values. During Nov 2016 - Jan 2017 period, it was clearly visible that low NDVI was associated with high σ^0 and vice versa suggesting the presence of the vegetation cover effect on the SAR signal (Fig. 6.6). Similar σ^0 behaviour and moderate negative correlations were observed at other locations as well, which are not presented here in detail. Our results demonstrate agreement with other studies confirming that moisture sensitivity of the σ^0 likely to decrease with increasing NDVI (Zribi and Dechambre, 2003, Baghdadi et al., 2008, Gao et al., 2017). The response of σ^0 to θ_v changes was weak, but noticeable despite the fact that the several affecting variables were not considered through the linear approach.

6.3.3 Soil moisture modelling by a Random Forest (RF) ensemble learning method

6.3.3.1 Training accuracy assessment

Initially the RF model was built using the default parameters that include the number of trees to grow (*ntree*) and the number of variables randomly considered at each split (*mtry*). To get the best performance from the algorithm, a fine-tuning process was conducted to examine the model performance with various settings. For this purpose, pseudo randomly sampled training and validation datasets were generated. It was observed that the prediction accuracy decreased if the *mtry* was > 4 for test error assessment and > 4 for the Out-of-Bag error estimates, i.e. training accuracy. Considering the ntree parameter, no significant decrease in error was observed if the ntree was set to > 300. The training error versus *ntree* and the optimisation of *mtry* through the training and test error calculations are shown in Figure 6.7.

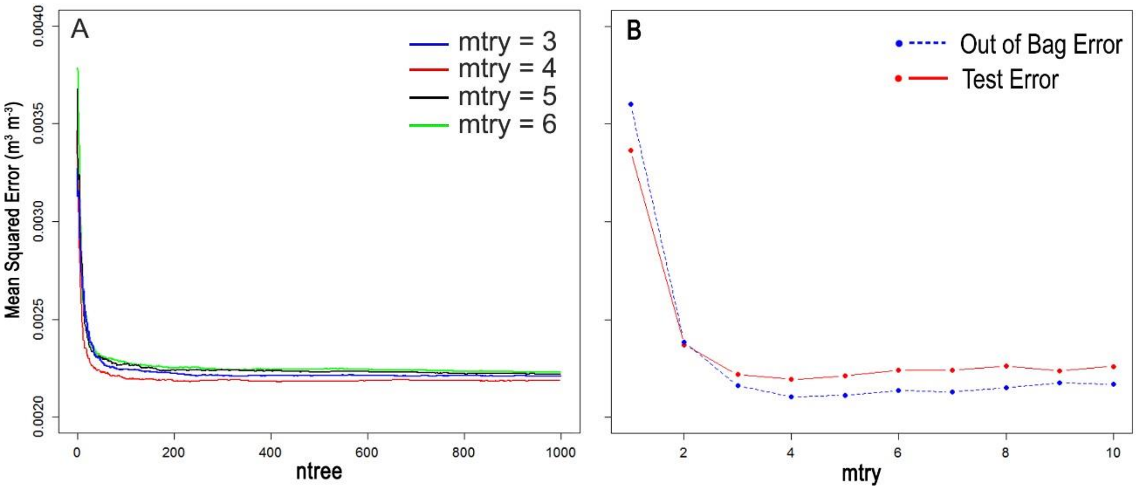

Figure 6.7 Training error evolution through the optimisation of the number of trees (ntree) and the number of variables randomly chosen at each split (mtry) hyperparameters.

Therefore, in the optimised model, the *ntree* was set to 300 and *mtry* to 4. These hyperparameters were implemented during the cross validation of the final RF model. The Out-of-Bag technique resulted in a 0.047 $m^3 m^{-3}$ RMSE and 76% of the variation was explained by the RF model.

The second part of the RF algorithm assessment was based on the MAE, RMSE and R^2 values generated by the five times repeated, 15-fold cross-validation. MAE ranged between 0.026 and 0.038 $m^3 m^{-3}$, RMSE between 0.036 and 0.056 $m^3 m^{-3}$ while the mean R^2 achieved a relatively high value of 0.76. Figure 6.8 presents the θ_v modelling and cross-validation results, including a summary of the mean and the spread of accuracies. These results suggest that the RF algorithm performed generally well in modelling the θ_v regardless of which section of the data population was taken as training set.

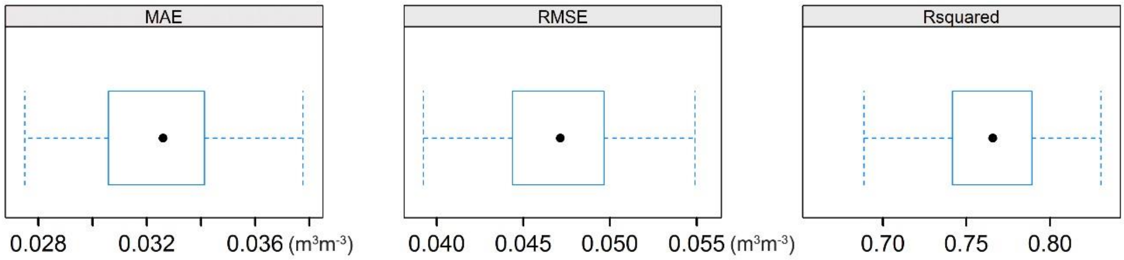

	Min.	1st Qu.	Median	Mean	3rd Qu.	Max.
MAE	0.026	0.030	0.033	0.032	0.034	0.038
RMSE	0.036	0.044	0.047	0.047	0.049	0.056
R^2	0.69	0.74	0.77	0.76	0.79	0.85

Figure 6.8 Statistical summary of the Random Forest modelling performance using five times repeated 15-fold cross-validation.

6.3.3.2 Variable importance

In the RF implementation used in this study, two measures were used for interpreting variable importance as provided and described by Liaw and Wiener (2002). For regression, the mean decrease in accuracy is defined as the mean squared error (MSE) that was estimated based on the prediction error on Out-of-Bag subsets of the data after a variable is permuted. Secondly, the mean decrease in node impurity is described as the total decrease in node impurities from splitting on the variable, averaged over all trees and expressed as residual sum of squares. Figure 6.9 shows the importance of variables for the final dataset based on these two metrics.

Following the previous results from the sensitivity analysis, σ^0 with VV polarisation was more related to θ_v than VH, thus σ^0 with VH configuration was not included in the final set of variables. The introduction of a seasonality component clearly increased the amount of variability explained by the model from 40% to over 77% in case of RF training accuracy. NDVI, SWI, slope angle and VV σ^0 were the most important explanatory variables besides the season while elevation, aspect, TPI and TRI had less influence on the predictions. Concerning the mean decrease in accuracy, VV σ^0 was situated at the bottom of the chart meaning that it had a weak prediction strength. Although VV σ^0 represented a higher ranked position in the total decrease in node impurities. These charts can be used for variable selection for tree-based models and for this study; the variables presented in Fig. 6.x were kept. During the model building, some other variables such as VV/VH ratio, VV and VH difference were left out as they did not improve the prediction accuracy and showed the less important roles than VV σ^0.

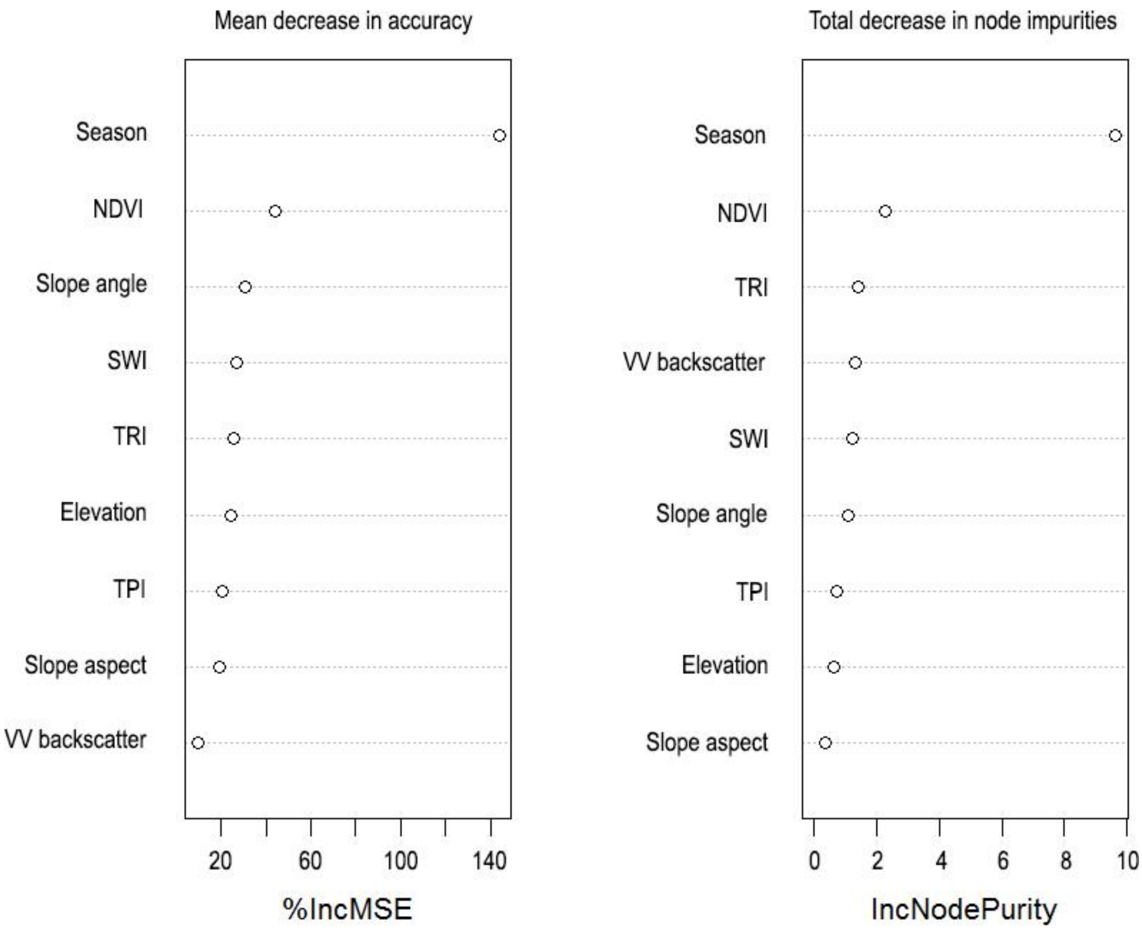

Figure 6.9 The relative importance of variables from the final Random Forest model showing the mean decrease in accuracy (mean square error) and the total decrease in node impurities (as residual sum of squares) as exported from the *randomForest* R package (Liaw and Wiener, 2002).

6.3.3.3 Test accuracy assessment

The optimised, best performing RF model was executed on the test subset and the prediction function was applied to model θ_v. The accuracy of the predicted responses was assessed by fitting linear regression on the modelled θ_v values and the observed θ_v in the validation set. The comparison resulted in 0.046 $m^3\ m^{-3}$ residual standard error and 0.78 adjusted R^2 values at the statistically significant level (P value < 0.001). Figure 6.10 depicts the time series of the in situ θ_v and the modelled θ_v at each sensing location with the imputed NDVI values coinciding with the θ_v observations. The residuals were computed as the difference between observed and modelled θ_v, and shown for each microsite on the right y-axis.

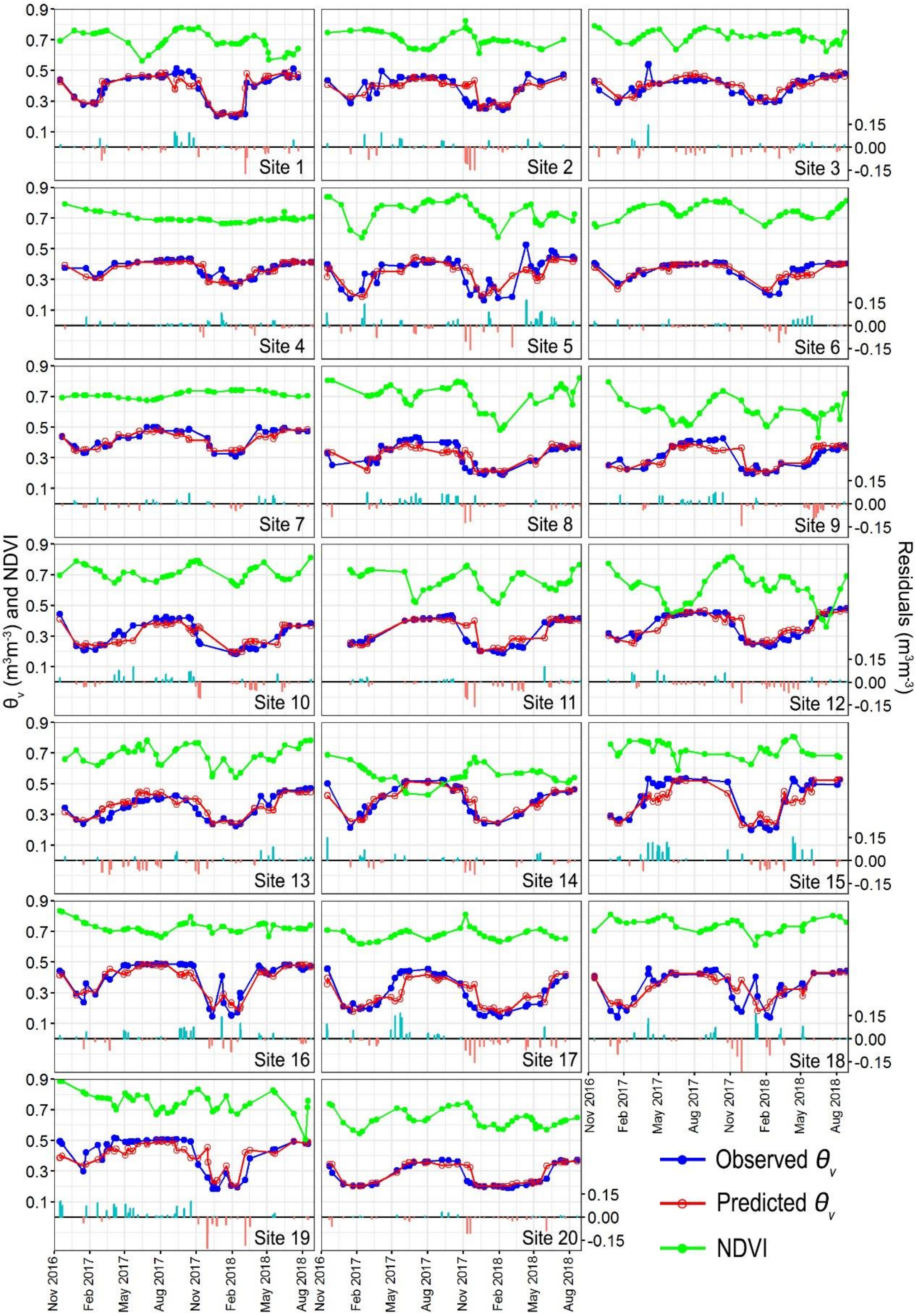

Figure 6.10 Time series of predicted versus observed volumetric water content (θ_v) and the evolution of NDVI at 20 sensing locations. The residuals are shown as columns for each observation pair indicating either overestimation (light red) or underestimation (light blue).

Since the test subset is randomly selected, the analysed time interval varies at the microsites. The general annual trend of θ_v was closely followed by the modelled responses and the closest agreement was found during the wet seasons between Apr-Aug 2017 and Jun-Aug 2018 at every sensing location. Similarly, the algorithm worked well in the dry seasons (December – February) in both years that might be due to the reduced amount of water in the vegetation.

However, significant uncertainty and errors occurred in the θ_v prediction during the transition periods, i.e. during the drying and rewetting stages. Large errors of ~0.06-0.16 $m^3 m^{-3}$ were produced between March-May 2017 dominantly underestimating the real θ_v when the soils were in the ascending period. It was assumed that the generally high errors in autumn were due to the combination of the actual phenological stage of the pasture cover, the increasing amount of water content in the vegetation and the effect of increasing θ_v in the soils. It has been observed in Chapter 5 that this period was characterised by high spatial soil moisture variability that might be reflected in the radar signal.

On the other hand, when the soils were in the descending transition period (Dec 2017 – Jan 2018), i.e. drying out stage, the model typically overestimated the observed θ_v values producing the largest errors. These findings suggest that the vegetation exerted a noticeable impact on the predictions during the drying out period and the errors can be associated with high NDVI values as it is shown in Figure 6.8. The commonly observed high NDVI values of late autumn, late spring - early summer can be associated with the perennial ryegrass-based pastures' strong spring and autumn tillering characteristics resulting in increased herbage accumulation and feed surplus. In autumn, the growth rate is triggered by the soils rewetting stage after the usually dry summer. Consequently, enhanced plant growth rate resulted in increased amount of fresh biomass and vegetation water content, which could lead to elevated σ^0, thus higher modelled θ_v responses.

6.3.4 Spatial modelling and the validation of near surface soil moisture predictions

After selecting the best performing RF model, the algorithm was executed on a spatial dataset of input variables to compute and develop θ_v maps over the research area on selected cloud free days. All available ancillary datasets were co-registered and resampled to 20 m spatial resolution to match the Sentinel-1 and Sentinel-2 images. The land cover was classified based on a hyperspectral raster layer and the non-pasture areas were masked out from the mapping (The classification method is described in more detail in Chapter 3). The previously presented training and testing procedure was applied to the RF model.

The algorithm was fed by the reduced dataset collected from fifteen in situ θ_v monitoring locations. The Out-Of-Bag error estimates of the RF training provided 0.79 adjusted R^2 and 0.045 $m^3 m^{-3}$ RMSE, whereas the test accuracy assessment resulted in 0.78 adjusted R^2 and 0.047 $m^3 m^{-3}$ RMSE. These correlations were statistically significant (P value < 0.001) for both training and test assessment. A summary of the five times repeated, 15-fold cross-validation process is reported in Figure 6.11 providing the accuracy distribution of the performance considering MAE, RMSE and R^2 as quantifying parameters.

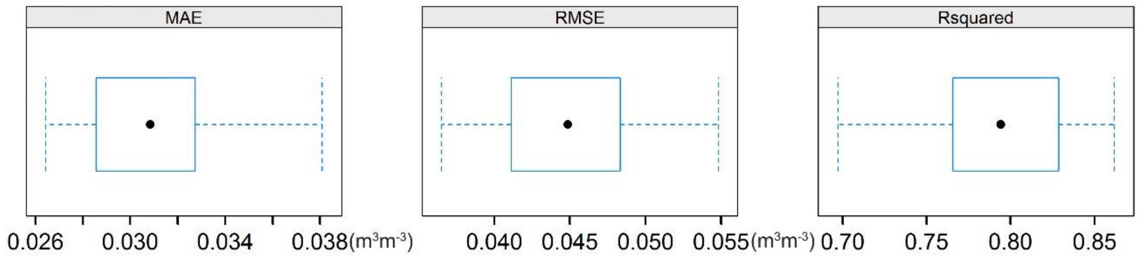

	Min.	*1st Qu.*	*Median*	*Mean*	*3rd Qu.*	*Max.*
MAE	*0.026*	*0.029*	*0.031*	*0.031*	*0.033*	*0.038*
RMSE	*0.037*	*0.041*	*0.045*	*0.045*	*0.048*	*0.055*
R^2	*0.70*	*0.75*	*0.78*	*0.79*	*0.82*	*0.85*

Figure 6.11 Statistical summary of the Random Forest modelling performance using five times repeated 15-fold cross-validation on the reduced reference dataset obtained by 15 ground-based microsites.

A relatively high deviation was observed, which could potentially be reduced by increasing the number of folds and repeats. It was noticed that the model performance trained on the reduced dataset did not drop considerably if compared to the model assessment results considering all of the θ_v monitoring locations (Fig. 6.8). However, the stability of the RF model performance somewhat decreased if executed on the reduced dataset as indicated by the mainly lower minimum and greater maximum values of the statistical parameters.

6.3.4.1 Independent validation of near surface soil moisture predictions

The following analysis aimed to investigate the spatial mapping performance of the proposed method. The evaluation process included the extraction of modelled θ_v values at five selected microsites (Site 3, 5, 6, 9, 16) from a series of eight θ_v maps compared to the observed daily average θ_v obtained from the five microsites on the same days. The linear regression (Fig. 6.12) was executed at each validation microsite separately and for all microsites considered together. The process resulted in a statistically significant correlation (P value < 0.001) with 0.77 adjusted R^2 and 0.048 $m^3 m^{-3}$ RMSE. The relatively high values of these statistical measures suggested that the spatial prediction process was not strongly affected by the lower amount of input data in the case of the five selected validation microsites.

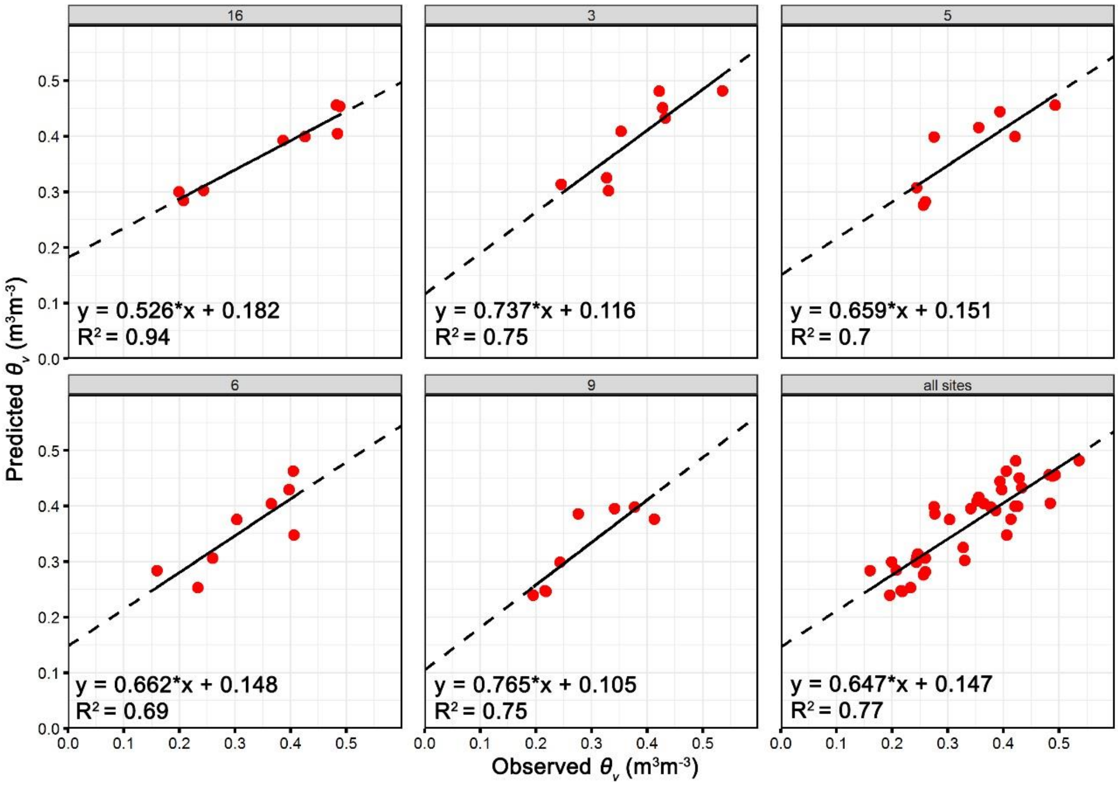

Figure 6.12 Scatterplots and linear model fitting between the observed daily mean volumetric soil moisture (θ_v) from the WSN and the predicted θ_v extracted from eight maps at five microsites and for all microsites considered together.

Table 6.3 lists the acquisition dates of the Sentinel-1 and Sentinel-2 satellite image pairs with basic descriptive statistics computed for each θ_v raster dataset. The image pairs were chosen in a way that the longest time difference between the radar and multispectral acquisition was two days that was considered suitable for the combination of these images.

Table 6.3 Sentinel-1 and Sentinel-2 scene pairs used for spatial soil moisture mapping and basic statistical parameters in $m^3\,m^{-3}$ computed from all the cellular values from each raster layer.

Sentinel-1 SAR	*Sentinel-2 MSI*	*Mean*	*SD*	*Min*	*Max*
22/05/2017	*21/05/2017*	*0.437*	*0.029*	*0.328*	*0.523*
18/10/2017	*18/10/2017*	*0.388*	*0.024*	*0.297*	*0.484*
7/11/2017	*07/11/2017*	*0.387*	*0.023*	*0.292*	*0.486*
05/12/2017	*07/12/2017*	*0.264*	*0.031*	*0.181*	*0.364*
17/01/2018	*16/01/2018*	*0.271*	*0.034*	*0.184*	*0.372*
03/02/2018	*05/02/2018*	*0.252*	*0.029*	*0.175*	*0.374*
06/05/2018	*06/05/2018*	*0.369*	*0.051*	*0.232*	*0.48*
10/07/2018	*10/07/2018*	*0.442*	*0.029*	*0.355*	*0.53*

The temporal distribution of the obtained θ_v maps and their basic statistical values including spatial mean and SD (Table 6.3) was plotted along with the temporal behaviour of the observed daily mean θ_v averaged over 20 microsites (Fig. 6.13). Furthermore, daily spatial θ_v standard deviation, minimum and maximum values extracted from the WSN using all sensors are represented by the ribbons. The dates of the spatial predictions were selected to represent intermediately wet (07/11/2017 and 06/05/2018), dry (05/12/2017, 16/01/2018 and 03/02/2018) and very wet (21/05/2017, 18/10/2017 and 10/07/2018) soil water levels.

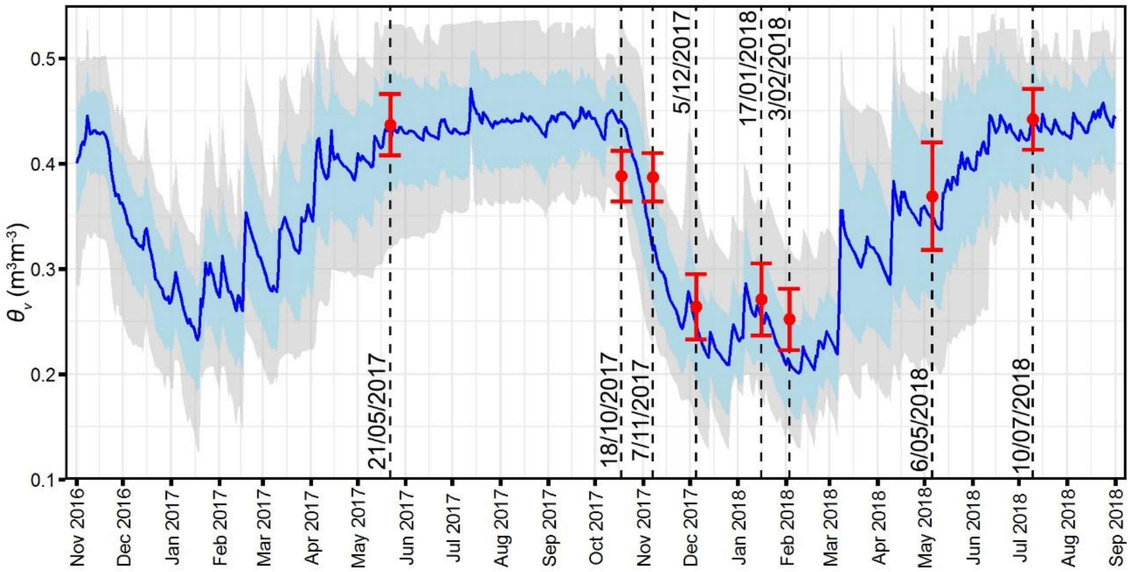

Figure 6.13 Temporal distribution of the modelled soil moisture (θ_v) maps along with the evolution of daily spatial mean θ_v collected by the wireless sensor network. The blue ribbon marks the mean θ_v ± its standard deviation (SD), while the grey ribbon indicates the range between daily minimum and maximum values. The red dots indicate the modelled spatial mean θ_v on the given day marked by vertical dashed lines while the error bars reflect the mean θ_v ± SD.

The θ_v trend was closely followed by the mean values calculated from the modelled maps except in the drying out period during spring in 2017. As it was found previously during the test accuracy assessment (Fig. 6.10), the transition period from wet to dry conditions were associated with significant modelling uncertainty that was reflected in the spatial mapping process.

The θ_v values were considerably overestimated on 11 Nov 2017 giving a mean value of 0.387 m^3 m^{-3} compared to the observed WSN spatial mean of 0.33 m^3 m^{-3}. The phenomena may be explained by the strong influence of vegetation, possibly as a result of the late spring early summer high growth rate and biomass production. In Nov 2017, the soil temperatures increased very quickly triggering the pasture production to a high level (refer to Chapter 7, Figure 7.5), which was followed by further soil warming causing a considerable drop in pasture growth rates. The VV σ^0 values did not decrease in proportion with the dropping θ_v levels. The influence of high NDVI values on C-band VV σ^0 SAR data during summer season was also observed by Oldak et al. (2003) on test microsites with grass cover.

Figure 6.14 illustrates eight θ_v maps under various soil wetness conditions in autumn, spring, summer and winter. The spatially modelled maps during the summer period of 2017-2018 showed close agreement with the mean observed soil moisture values ranging between 0.22-0.25 $m^3 m^{-3}$ that matched with the previously observed trend in the prediction accuracy. The lowest soil water levels were reached on 3 Feb 2018 giving a mean θ_v of 0.252 $m^3 m^{-3}$.

During the rewetting stage in Apr - Jun 2018, the RF algorithm was able to model the θ_v showing a relatively good fit between mean modelled θ_v of 0.369 $m^3 m^{-3}$ and observed θ_v of 0.35 $m^3 m^{-3}$. After the rewetting period, the soils reached saturation in July 2018 and remained at the near saturated level for the rest of the data collection time that is characterised by the lowest spatial variability. The mean θ_v calculated from the predicted map was 0.442 $m^3 m^{-3}$ on 10 July 2018 that was a close match with the observed spatial mean value of 0.448 $m^3 m^{-3}$.

Based on a visual analysis, macro-scale patterns can be recognised on all the eight images that showed good agreement with the expected temporal θ_v evolution during the study period. The spatial θ_v pattern was strongly linked to the various landscape features suggesting the existence of temporal stability in θ_v spatial distribution in support of the results showed in Chapter 5. These observations also indicate the importance of topographical attributes in θ_v patterns with an enhanced influence near the surface due to the meteorological forcing. Those pixels located along the valley floors and flat areas were generally represented by wetter conditions reaching 0.45-0.53 $m^3 m^{-3}$ θ_v in certain cases. It was also apparent that hilltops, ridges and steep hill slopes showed lower θ_v than areas with low altitude and gentle slope angles. The flat areas located along the stream running along the valley bottoms dried out slower than the hill slopes that is clearly visible on the maps (Fig. 6.14).

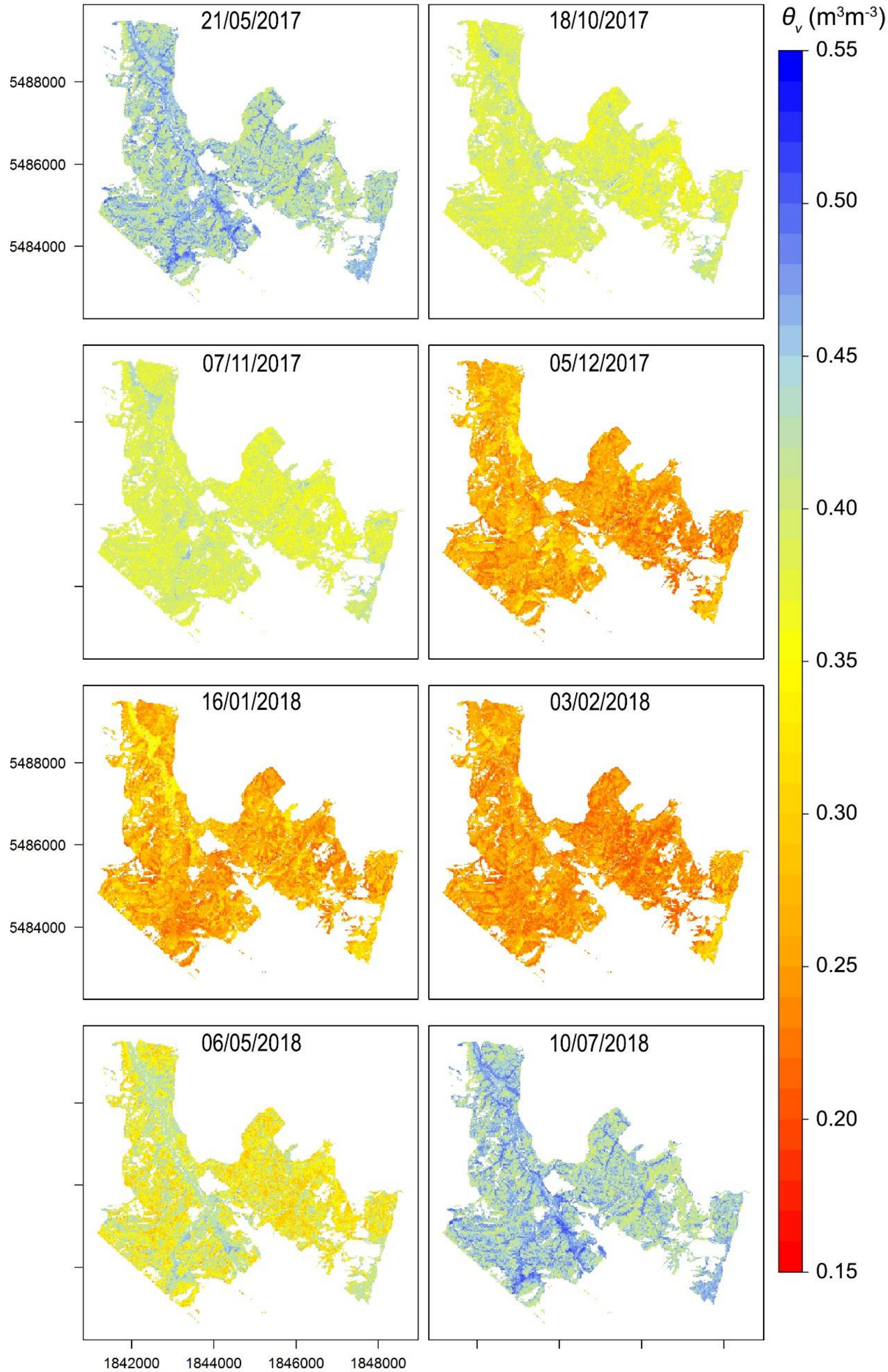

Figure 6.14 Comparison of spatially modelled near-surface volumetric soil moisture (θ_v) under different wetness conditions at the Patitapu Station computed by Random Forest algorithm. Blank areas correspond to the non-pasture surfaces.

Two predicted maps with the two extreme θ_v levels were chosen for further, more detailed illustration and visual comparison. Figure 6.15 (A) presents a smoothed, resampled version of θ_v conditions on 3 Feb 2018 and July 10, 2018 (Fig. 6.15 (B)) using bilinear interpolation overlaid on high-resolution aerial imagery captured in 2017. To emphasize the relief, the terrain is displayed by a 1.7 vertical exaggeration of the elevation surface for easier interpretation and better visualisation. Additionally, a zoomed in view is provided for a closer visual assessment of θ_v patterns over various terrain features and topographic positions.

Based on raster statistics supported by visual examination, the role of slope and aspect was not obvious during the winter season, although the presence of its effect was noticeable during the driest conditions on 3 Feb 2018. Hill slopes facing north were represented by the lowest mean θ_v value of 0.245 $m^3\,m^{-3}$ while the flat areas held the highest amount θ_v at 0.265 $m^3\,m^{-3}$. East facing surfaces were slightly wetter giving 0.26 $m^3\,m^{-3}$ than south and west aspects with 0.251 $m^3\,m^{-3}$ mean θ_v, respectively. The differences in mean θ_v found among various aspect was not extremely significant, it clearly shows agreement with our expectations and previous results (Radcliffe and Lefever, 1981) considering the findings of the spatiotemporal variability analysis in Chapter 5 and the role of aspect discussed in Chapter 2. Aspect can be characterised with a seasonal pattern exerting its effect on θ_v dominantly during the descending transition and in dry periods while its influence is less evident through the rewetting and in wet the stages.

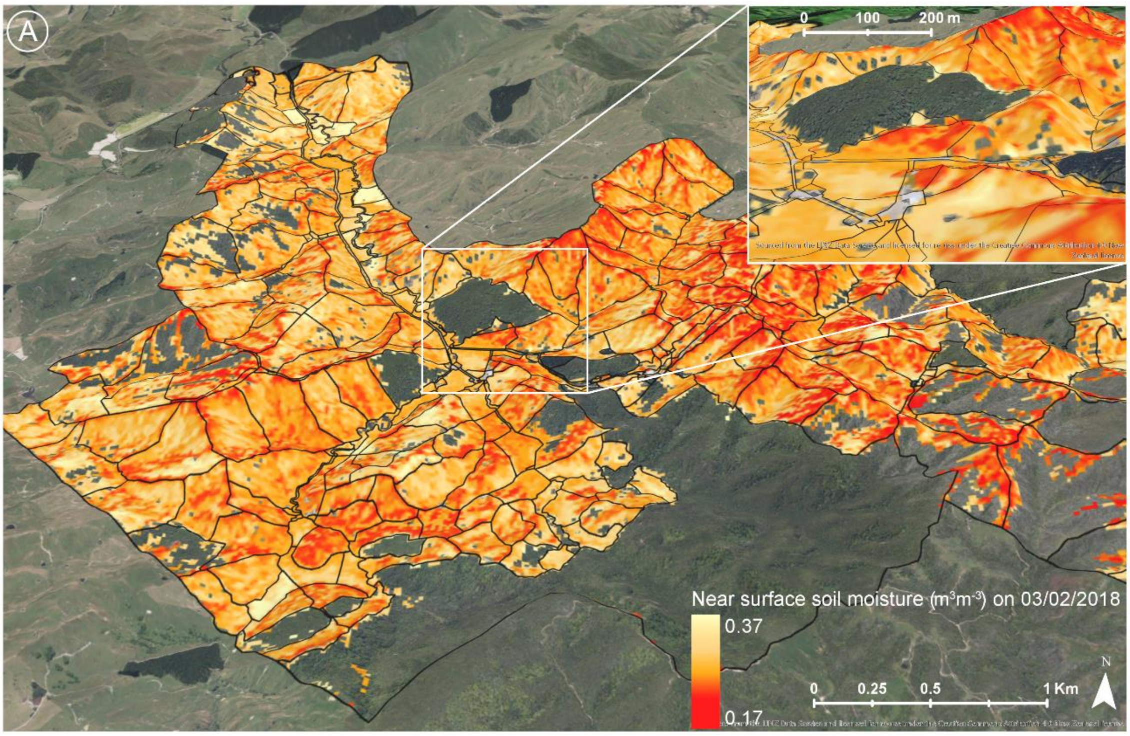

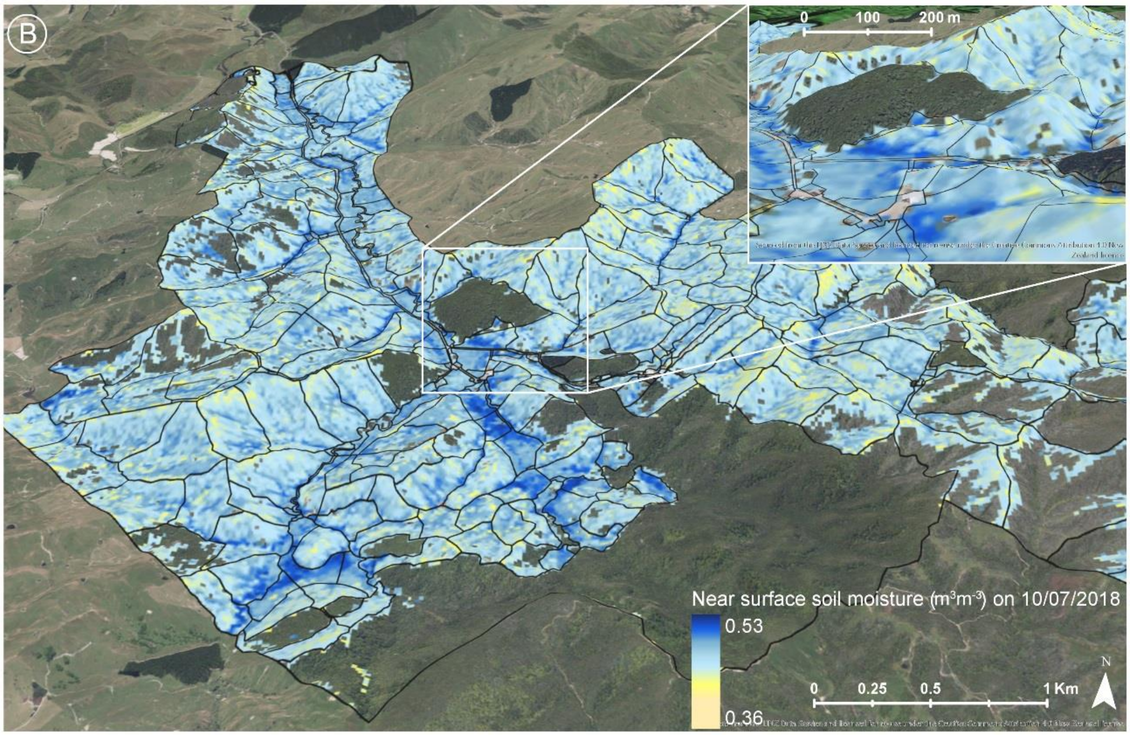

Figure 6.15 Dry (A) soil moisture conditions captured on 03 Feb 2018 and very wet (B), winter obtained on 10 Jul 2018 over pastoral surfaces superimposed on aerial imagery and visualised in 3D with 1.7 vertical exaggeration of the terrain. The insets show a detailed view of a central part of the research area with diverse pastoral landscape features.

Due to the nature of the experiment, the spatial validation was limited and would be further improved by the independent collection of θ_v values on a grid basis. The model was clearly able to predict the θ_v differences between surfaces with various steepness that is one of the main drivers of θ_v distribution in hilly landscapes (Crow et al., 2012b). The pattern seemed to be consistent throughout the year in different θ_v levels.

The approach presented here suggests that the combination of ground-based variables and radar imagery and multispectral data has the capability to generate θ_v products based-on historical training data at relatively high accuracy. The incorporation of terrain information and a seasonal component improved the precision on the θ_v estimates. High-resolution regional or country scale modelling of θ_v is also a possibility since most of the chosen variables can be derived either from the nationally available digital elevation model or from the datasets made available by GEE. The introduction of new parameters and a temporally denser vegetation cover information could improve the simulation accuracy and provide closer agreement during the rewetting and drying out stages of the soils. As the study area is limited to pastoral surfaces, pasture growth measurements could provide information about the biomass, the vegetative stage as well as the water content of the vegetation. However, these measurements are usually carried out at the point like scale, which is not suitable for the spatial modelling of θ_v on complex terrain. Thus, this study highlights the importance of using multisensory data and advanced machine learning methods to deal with the complex relationships among the environmental variables interacting within a hill country pastoral farming system.

As a direction of focus in the future, the trained RF model could be executed on an independent area to examine its potential and the value of the obtained reference dataset by the WSN. Furthermore, the more detailed investigation of the effect of reduced spatial resolution can be a possible future perspective as well as a study that could be based on θ_v prediction as per farm management areas, i.e. paddocks. This sort of approach might be also useful for planning applications and it could reduce the noise in the data, although the method would lose the capability to represent the high θ_v variability within a particular paddock. Further steps could include a classification-based modelling approach that could improve the prediction accuracy by predicting wetness classes rather than absolute θ_v values. The consideration of other terrain attributes related to hydrological processes influencing θ_v distribution such as curvature, convergence index can have a positive impact on the prediction performance. Similarly, other type of vegetation indices such as enhanced vegetation index, normalised difference water index derived from multispectral images may contribute to the improvement of θ_v estimation on a map basis.

6.4 Conclusion

This study explored the application of the Random Forest machine learning method in near surface soil moisture mapping at high spatial resolution (20 m cell size). The chosen regression driven algorithm has proved to be a useful tool in modelling the relationship among SAR data, NDVI, volumetric soil moisture and predictor variables derived from a high-resolution digital surface model. Although, there are discrepancies between the modelled and the observed soil moisture values, the investigated method was considered effective in soil moisture mapping at the farm scale (2600 ha).

The series of estimated maps described the temporal and spatial patterns of near surface soil moisture in a heterogeneous environment showing generally good agreement with observed values. It can be concluded that the synergetic use of remotely sensed and ground-based data has the power for soil moisture retrieval in New Zealand’s hilly landscapes. Since the model is empirical, the proposed method requires historical, long-term field observations and temporally dense remote sensing data in addition to terrain information. In this regard, WSNs will increasingly enable the temporally dense data to be provided to these modelling efforts.

The results revealed that θ_v may be modelled using a machine learning approach with an RMSE below 0.05 $m^3 m^{-3}$ at both the point and the spatial scale over pastoral surfaces with relatively homogenous vegetation cover. The average prediction accuracy during training achieved cross-validated 0.047 $m^3 m^{-3}$ for mean RMSE and 0.77 for mean adjusted R^2 while 0.048 $m^3 m^{-3}$ RMSE and 0.77 R^2 occurred during the independent validation phase. These measures suggest a reasonably high average modelling performance over the 22-month study period.

VV polarized backscatter was more sensitive to soil moisture dynamics than the VH configuration. It was generally observed that VV backscatter increased with increasing soil moisture while the relationship between NDVI and VV backscatter values followed an inverse function. Seasonality, slope angle, NDVI and SAGA wetness index explained more variability than aspect, topographic position and the terrain ruggedness.

While radar data were useful for soil moisture predictions and increased the accuracy, seasonality and NDVI were the most important variables confirming that the synergy of multispectral and radar data has the potential for medium resolution soil moisture mapping in complex landscapes.

We associate the relatively low sensitivity to near surface soil moisture partially with the ground-based sensors located deeper than the potential penetration of depth of SAR signal. The prediction accuracy and model performance could be improved by using a larger number of soil moisture sensors and cover more landscape position and terrain conditions. We propose that data collection from soil sensors installed at the top 5 cm of soil layer could result in better prediction performance. Due to the low number of regular cloud-free optical images over New Zealand, space-borne radar techniques with multiple polarisations will provide potentially more effective tools for monitoring near surface soil moisture for farming applications at regional scale with medium to high spatial resolution.

The systematic incorporation of spatially mapped near-surface soil moisture products may lead to an increase in prediction results of feed surplus and thus to better pasture management and grazing practices. The study can be regarded as an initial investigation of the feasibility of using satellite data for mapping soil moisture at a spatial scale that is practical for multiple farming applications.

Chapter 7

The analysis of topographical effects on pasture production patterns in complex landscapes of New Zealand’s hill country

7 Chapter 7 - The analysis of topographical effects on pasture production in complex landscapes of New Zealand's hill country

7.1 Introduction

There are two major pastoral systems in New Zealand usually referred to as dairy farming (1) mainly situated on lowlands, and sheep and beef farming (2) spanning low-altitude, seasonally dry, steep lands of hilly landscapes with lower fertility soils. The dairy industry produces a considerable fraction of exports from NZ, thus pasture quality, pasture growth rates (PGR) and annual dry matter (DM) production on dairy farms have been studied extensively (Woodward, 2001, Macdonald et al., 2008, Chapman et al., 2009, Dalley and Geddes, 2012).

On the contrary, the number of research programs investigating the dynamic hill country pastoral systems is low compared to lowland pastures despite its importance in the primary sector contributing $7-7.5 billion towards annual exports (Morrison, 2017, Statistics New Zealand, 2018, updated April 2018). The recent growth in the dairy industry has required more land conversion, thus beef and sheep farms are increasingly being dominated by low-fertility areas containing a mixture of flat, rolling, and steep land (Gaukrodger, 2014). However, pastoral hill country farms still occupy a large fraction of agricultural land (4 million ha in the North Island) and holds most of the nation's sheep and beef stock (Keller et al., 2014, Cameron, 2016, Scrimgeour, 2016).

To improve the profitability and resilience of hilly, non-irrigated farming systems, the efficient use of the available resources, including water held by the soil, is crucial to ensure that the quantity and quality of feed will meet stock demand. Sustainable yield maintenance and growth enhancement have been of great interest, especially as a result of recent increased pressure on environment (soil conservation, fertiliser application impacts, nutrient use and climatic volatility) and food production (Scrimgeour, 2016). Consequently, the better understanding of growth distribution, its variability and seasonal patterns may assist in the implementation of more effective land management practices where diverse topography is a key influencing feature.

In general, hill country landscapes are dominated by slopes > 15 ° and located below an altitude of 1000 m (Basher et al., 2008) and demonstrate extremely variable pasture growing characteristics that are influenced by a wide range of factors. The documentation of hill country pasture production is difficult due to the complex interrelationships between terrain attributes (i.e. high local variation in microrelief), pasture composition and structure, uneven grazing management, stock behaviour, soil fertility, soil patterns, and microclimatic parameters (Gillingham, 1973, Lambert and Roberts, 1978, Chapman and Macfarlane, 1985, Bretherton, 2012).

7.1.1 Review of pasture growth studies in New Zealand

Aspect and slope angle are two of the primary topographical factors affecting pasture growth patterns in hill country, which have received early attention with agronomic studies. Pasture yield has been investigated on sunny (northerly) and shady (southerly) faces by several authors, Suckling (1959), Suckling (1975) Bircham and Gillingham (1986), White et al. (1972), Gillingham and Bell (1977) Lambert and Roberts (1978), Radcliffe et al. (1976), Gillingham et al. (1998) and Bretherton (2012) on both unimproved and improved pastures of New Zealand.

Table 7.1 provides a structured summary of the studies completed in hill country, monitoring annual pasture yield accumulation on surfaces with varying aspect and slope angle at various locations in New Zealand. Radcliffe (1982) and Bretherton (2012) also provided a shorter review on previous results on pasture growth accumulation. Furthermore, some of the key findings are explained below to provide details from selected studies comparing mainly north and south aspects. Suckling (1975) and Suckling (1959) observed that there were distinct differences in seasonal yield between northerly and southerly faces (mainly due to temperature differences), so that shady faces were grazed more in summer and sunny faces were grazed more in winter.

In terms of annual pasture production, 25 % more yield was observed on sunny faces if averaged over a 9-year experiment. A field trial carried out by Luscombe (1980) at Ballantrae hill country research station found that north easterly aspects produced more pasture than south west aspects, producing approximately twice as much dry matter. Gillingham (1973) observed that north aspects in steep hill country outperformed the south aspects, yielding 10 % more pasture mainly due to the high winter growth on sunny faces. In contrast, Bretherton (2012) observed similar total pasture production on south and north aspects, although his results indicated that south-facing slopes might yield more pasture during summer and autumn in years with below average soil water content. It should be noted, that there are latitude differences between these two studies and the differences in seasonal rainfall amplitude may play a considerable role. During winter and spring, northern slopes may out-perform southern slopes when soil water content is not a limiting factor. Lambert et al. (2000) monitored pasture growth as part of a long-term experiment and found the highest yield on east-facing slopes, although north-westerly faces produced 7 % more pasture than south-westerly faces.

By investigating the papers listed in Table 7.1, most of the considered studies examined the differences between south- and north-facing slopes, providing little information about the entire slope-aspect spectrum. It is was observed that most of the considered papers found higher yield on north-facing slopes and a few on south-facing slopes. It is apparent, that these findings were not consistent and somewhat controversial. This suggests that regional and local effects on productivity are neither well defined nor fully understood in relation to the terrain, vegetation cover, soil properties, and climatic parameters, agreeing with the conclusions made by Lambert et al. (1983).

Table 7.1 Overview of annual herbage accumulation studies on different aspects and slope angles recorded at various hilly regions of New Zealand using the trim technique.

Aspect with highest yield	Reference	Location	Slope angle (°)	Time of data collection
N	Radcliffe (1971)	Whatawhata, near Hamilton (NI)	0-20, 15-20, 36-40	11/01/1965 – 15/11/1965
		Te Kuiti, near Hamilton (NI)	10, 20	16/07/1969 - 24/06/1970
	Suckling (1959)	Te Awa, near Palmerston North (NI)	varied (easy to steep)	1949 - 1956
	Suckling (1975)	Te Awa, near Palmerston North (NI)	varied (easy to steep)	1951 - 1957
	Radcliffe et al. (1968)	Whatawhata, near Hamilton (NI)	15-20, 25, 36-40, 20	Nov 1964 – Nov 1965
	Gillingham (1973)	Whatawhata, near Hamilton (NI)	steep (aver. 30)	August 1970-July 1973
	Gillingham et al. (1998)	near Waipawa, Hawke's Bay (NI)	15-20, 25-30	1995-1998
	Gillingham et al. (2003)	near Waipawa, Hawke's Bay (NI)	varied (easy to steep)	1995-2002
S	Lambert and Roberts (1978)	Ballantrae, near Woodville (NI)	5-30 (aver. 16)	1972
	White et al. (1972)	Hunua, near Waikari, North Canterbury, (SI)	steep	1970-1971
	Radcliffe (1971)	Coopers Creek, near Oxford (SI)	25-28	12/10/1970-22/06/1971
	Radcliffe (1982)	Coopers Creek, near Oxford (SI)	varied	1973-1976
SW	Radcliffe et al. (1977)	Coopers Creek, Canterbury (SI)	10-20, 20-25	1972-1975
NE	Luscombe (1980)	Ballantrae, near Woodville (NI)	10-15	June 1977 – December 1978
SE	Bircham (1977)	North Wairarapa (NI)	10-20	1975-1976
E	Radcliffe (1971)	Geraldine (SI)	26-33	1970-1971
	Lambert et al. (1983)	Ballantrae, near Woodville (NI)	1-12, 13-25, >26	1971-1981
Insignificant yield differences between N and S				
-	Bretherton (2012)	Alfredton (NI)	20-30	2010-2012

In terms of slope angle, pasture production tend to decrease with increasing slope angle demonstrating a highly significant negative relationship (Gillingham, 1973, Lambert et al., 1983).

The differences in yield are mainly attributed to the greater soil water availability on easier slopes than on steep surfaces (Gillingham et al., 1998, Bretherton, 2012). Additionally, changes in slope can also result in variations in organic matter, soil physical properties, pH, botanical composition and soil fertility due to animal and gravity nutrient transfer from steep slopes towards easier slopes, (Mackay et al., 1999, Lambert et al., 2000, López et al., 2003).

7.1.2 Review of pasture production models

The diverse terrain, grazing management, and the climate-driven characteristics of pasture growth patterns makes spatial and temporal prediction of pasture production difficult; hence, several forecasting models have been developed (Herrero et al., 1998). These models attempt to simulate pasture growth as a function of one or more environmental, soil and/or management variables.

The classic modelling approaches include mechanistic and empirical techniques (Moir et al., 2000, Scott, 2002, Zhang et al., 2005). While mechanistic models are built on theoretical concepts and can be more broadly applied, empirical models are developed using experimental data from a detailed trial work at a specific site and provide higher prediction accuracy over mechanistic models for the particular area (Rickert et al., 2000). Therefore, to determine pasture productivity affecting factors and to evaluate their contributions to spatiotemporal yield distribution, empirical methods are preferred (Zhang et al., 2005).

To identify the key driving factors of pasture production, some pasture growth models are discussed here. Pasture growth simulations are highly dependent on the prediction capability of soil water status (McCall, 1984, Woodward, 2001). Moreover, it is evident that the key component of water balance models is the evapotranspiration (Leenhardt et al., 1995) input that can be estimated by theoretical models (i.e. calculation of potential evapotranspiration) or empirical functions developed locally (i.e. actual evapotranspiration).

The climate driven, soil fertility dependent model developed by Moir et al. (2000) is based on an assumption that pasture growth is proportional to the actual evaporation rate, which is corrected for a site-specific factor indicating soil fertility status. Actual evaporation rate is estimated through a soil water balance as given by Coulter (1973). Moir et al. (2000) attempted to develop a pasture growth model that takes into account the soil fertility as well as the climate as it influences soil water content and evapotranspiration.

Woodward (2001) reported the development of the Pasture Quality model to predict daily growth of various vegetative grasses and dead fractions considering temperature, rainfall and incoming solar radiation. The considered biological processes are dependent on soil water which is calculated by the two-layer model of Scotter et al. (1979). The model was further improved by Woodward et al. (2001) by rewriting it into differential format and modifying the formulas so that available water holding capacity can be added to estimate actual evapotranspiration.

The McCall model (McCall, 1984), later published and described in detail by McCall and Bishop-Hurley (2003), was designed to predict pasture accumulation on grazed dairy pastures of New Zealand by considering pasture growth dynamics, and the effects of climatic and management variables. McCall's simple algorithm mainly requires weather data; therefore, it has been widely applied in farm system models and used in research with ryegrass-dominant pastures. One of the drawbacks is the restricted generalised application due to the requirements for site-specific, empirical data for calibration (Romera et al., 2009).

The pasture prediction models discussed above are mainly applicable for pasture growth simulations on lowlands with deep soils as the model parameters assumed flat surfaces for incoming solar radiation (ISR) and evapotranspiration estimations, and ignored other hydrological processes such as surface runoff, lateral flows and water repellency.

In hill country, only a few in-depth studies have been conducted to develop water balance models for sloping land (Bircham and Gillingham, 1986, Bretherton et al., 2010). These models took into account the terrain effect on ISR and climate variables to calculate potential reference crop evapotranspiration values and then the use of a soil water balance model to obtain actual evapotranspiration. However, using these actual evaporation estimates for modelling hill country water status can introduce uncertainties due to the assumption about rooting depth and unrealistic soil-limited evaporation rates (Bretherton et al., 2010).

Some of the latest commercial models, for example, the Pasture Growth Forecaster (used by Ravensdown Ltd.), have been calibrated for dairy farming conditions (i.e. dominantly high fertility flat land) and modifications were introduced for predictions on sloping land. The Pasture Growth Forecaster is defined as a hybrid model built on the McCall herbage growth model (McCall, 1984) as revised by Romera et al. (2009). To improve this model's accuracy, the soil water balance model of Woodward et al. (2001) was chosen to replace the McCall model (Ogle and Ma, 2015). Recently, improvements have been made by including corrections for slope angle, aspect, and rainfall, to ensure that the algorithm is tuned to the terrain attributes (Ogle et al., 2016). As a result of the changes, the model has become capable of independently calculating the evapotranspiration for an inclined surface based on the Penman-Monteith model as described in Zotarelli et al. (2010).

Certain pasture growth model components rely on empirical parameters that makes the site-specific calibration and model tuning required to achieve better predictive precision (Romera et al., 2009). Model parameterisation can be made more efficient by improving the knowledge of the numerous interrelated factors controlling pasture growth. The purpose of this chapter is to provide a detailed overview of the role of soil parameters, topographic attributes, and the influence of some climatic variables and their interactions within this complex system at the Patitapu Station (the research area) situated in the lower east coast of the North Island. Our study was designed to provide a more detailed analysis regarding pasture productivity than previous studies. Spatial PGR distribution and response patterns were described by relating yield data and environmental parameters recorded between November 2016 and June 2018.

Thus, soil and pasture monitoring microsites were designed and spatially distributed in the research area to sample various pastures on various topographic positions. The microsites were equipped with AquaCheck probes connected using a wireless sensor network (WSN) for long-term, multi-level soil temperature (T_S, °C) and volumetric soil moisture (θ_v, m^3 m^{-3}) measurements. The latter is extremely valuable for the investigation of stored and plant-available water variability within the rooting zone (Hillel, 1998, Nolz, 2013). Pasture yield was measured by the traditional pre-trimmed exclusion cage technique on the grazed areas (Radcliffe et al., 1968). The land surface was represented by a very high-resolution (0.2x0.2 m cell size) digital surface model (DSM) surveyed in 2017 and used for deriving the terrain attributes considered in this chapter.

Ever since the incorporation of precision agriculture techniques was introduced to hill country farming, the variability in pasture production occurring on complex landscapes can be addressed and better understood and the accuracy of yield simulations can be improved. Therefore, the presented study aims to:

1. Utilise the combination of recent WSN technology and classic pasture monitoring methodology assessing the herbage accumulation and PGR response to recorded and derived parameters
2. Capture the differences in PGR in various landscape positions by descriptive and comparative methods, and multivariate statistical analysis.
3. Provide a discussion on PGR variability by isolating the limiting effects of topography, seasonality and soil parameters, on individual sites, as the combinations of these factors could explain a significant amount of the variability in pasture yield in hill country.

7.2 Materials and methods

7.2.1 Research site

The selected research site, the Patitapu Station is situated within the East Coast Hill Country (ECHC) area (40.745020 S, 175.887320 E) of the North Island of New Zealand (Fig. 7.1 (A)). The ECHC region is an extensive section of primarily pastoral farmland and forestry on a mixture of rolling to steep hills, flat terraces prone to summer-autumn soil moisture deficit as well as flooding and heavy storm events. Patitapu Station is recognised as steep hill country terrain with lower fertility soils where drought frequently occurs in summer. The station can be characterised as steeply dissected with a high-density drainage network, and highly variable contour, aspect, soil type, soil fertility, and altitude, and therefore a wide range of micro-climatic conditions.

Pastoral land covers approximately 70% of the 2,623 ha farm, typically experiencing warm, dry summer and wet, mild winter conditions. Rotational grazing, which is in use by most hill country farmers (Osborn and Cowie, 1978) has been adopted at the research area. The microsites were selected from improved, permanent pasture areas under grazing by sheep or sheep and cattle. Although the botanical composition varied between sites, the predominant plant communities were perennial ryegrass (*Lolium perenne L.),* browntop *(Agrostis capillaris)* and Yorkshire fog *(Holcus lanatus)* in combination with white clover (*Trifolium repens)*. These species are commonly found in many of New Zealand's productive pastoral systems (Charlton and Stewart, 1999).

Figure 7.1 (B) illustrates the topography of the research site and its immediate surroundings as well as the locations of the microsites superimposed on a recent aerial imagery (2017) clearly showing native bush and pasture-based land cover types. An example of a microsite with the AquaCheck probe and the pasture sampling locations within a 3 m circle is presented in Figure 7.1 (C).

7.2.2 Fertiliser history

Patitapu Station has been operated and developed by the current owners since 2000, with a relatively poor fertiliser history prior to purchase 19 years ago. Pasture swards have been maintained by regular aerial oversowing, and have been top-dressed to build up soil fertility. The station is divided into management blocks, which receive up to two applications in some years. A maintenance rate is usually applied in November and a capital fertiliser input in February.

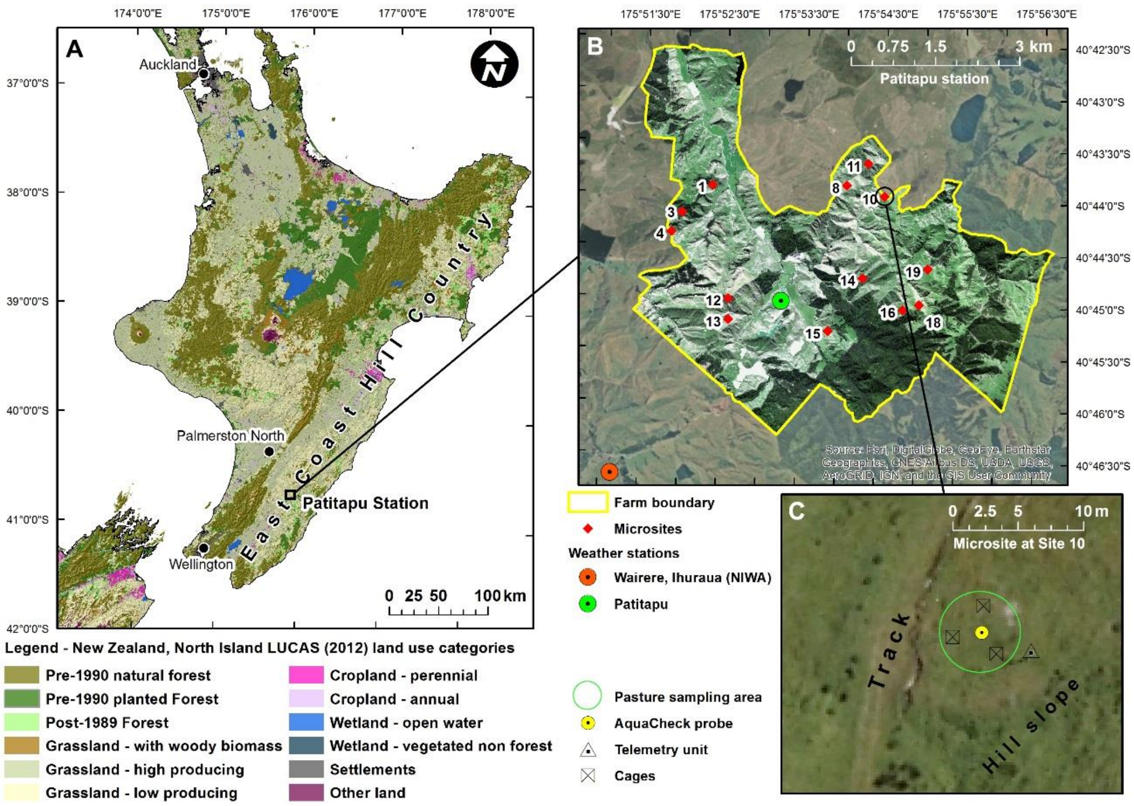

Figure 7.1 Geographical location of the research area (A), the spatial distribution of the 13 microsites and weather station locations (B), and an inset map showing the relative positioning of an AquaCheck probe and the situation of pasture sampling cages (C).

These applications have been mostly superphosphate at 200-300 kg/ha rate with some di-ammonium phosphate added. The microsite locations were chosen from farm blocks that historically received superphosphate at mainly 250 kg/ha. Based on the available fertiliser history, all microsites received similar amount of input. Consequently, the effect of fertiliser amount and products were not included in the analysis, which was due to the lack of spatial and temporal data about the applied products.

7.2.3 Microsite characteristics, sampling design and data collection

7.2.3.1 Microsite characteristics

The thirteen microsite locations were chosen at variable landscape positions i.e. on flat areas, north-, east-, south- and west-facing slopes, with rolling (8-15°), strongly rolling (16-20°), moderately steep (21-25°) and steep (26-35°) slope angle classes following the Land Use Capability slope classification scheme (Lynn et al., 2009). Additionally, they were placed on a range of geomorphological elements, i.e. plains, open slopes, upper slopes and ridges. This study used GIS-assisted methodologies to compute primary (i.e. slope angle, aspect) and secondary or compound (i.e. landform elements) topographic attributes in raster format for the extraction of pixel-based information at the microsites (Fig. 7.2).

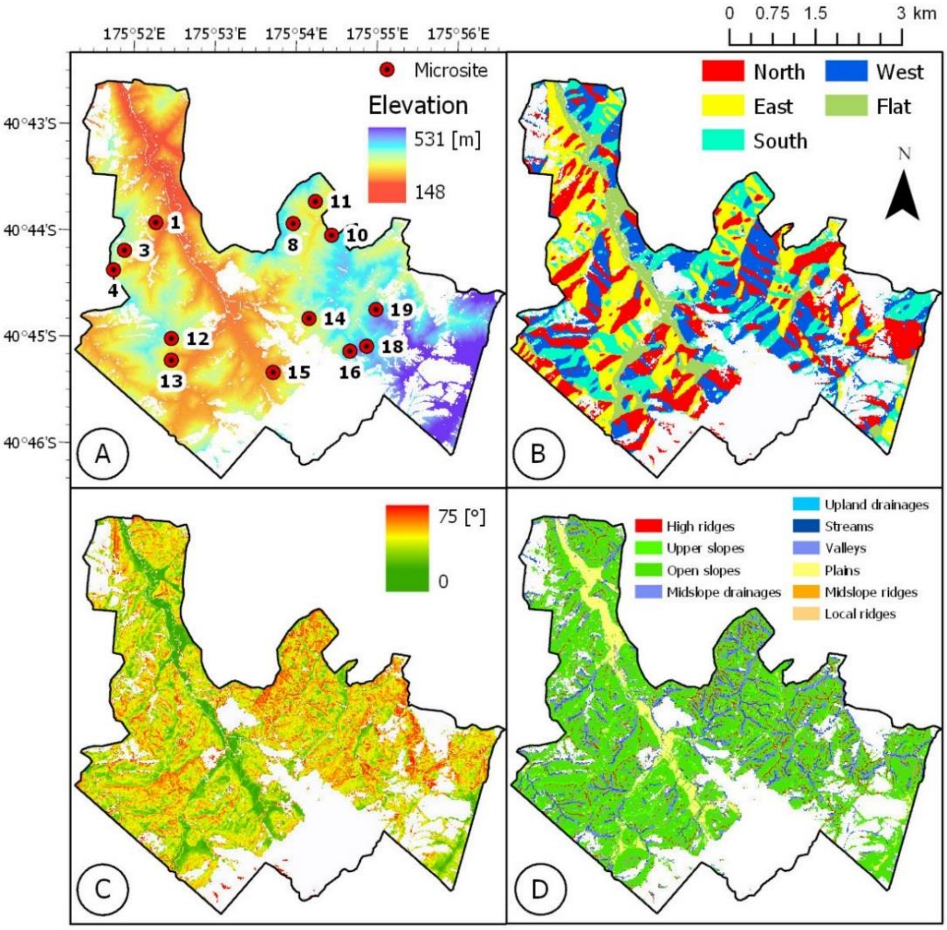

Figure 7.2 Primary and secondary terrain attributes generated from a 5x5m pixel resolution digital terrain model at the Patitapu Station. Elevation (A), aspect (B), slope angle (C) and landform elements (D) are shown. The non-pasture areas within the property have been masked out (white pixels).

Geomorphometric parameters were derived from an originally 0.2x0.2 m pixel size digital surface model (DSM) generated using the novel structure-from-motion photogrammetric technique (Micheletti et al., 2015) in 2017. Overlapping, high-resolution images were captured using a digital camera mounted on a fixed wing aircraft. Following the processing of images taken from multiple angle, a 3-dimensional representation of the land surface can be generated (Fig. 7.2 (A)). Due to the nature of DSM, the natural and built features of the land surface are captured. Therefore, smoothing and resampling techniques were applied to acquire a 5x5 m resolution DSM to represent terrain attributes with mean values for the sampled pasture area.

Firstly, primary geomorphometric attributes such as aspect (Fig. 7.2 (B)) and slope angle (Fig.7.2 (C)) were derived. Secondly, since it is a compound attribute, the landform elements (Fig. 7.2 (D)) were identified based on a landform classification using topographic position index from the hydrologically corrected DSM (Moore et al., 1991). The pre-processing and terrain analysis were executed in the open source SAGA (System for Automated Geoscientific Analysis) GIS software developed by Conrad et al. (2015) and in ArcGIS Pro (Environmental Systems Research Institute, Redlands, California, USA, 2017) environment. Table 7.2 provides information about the microsites' topographical attributes extracted from the generated topographic layers.

Table 7.2 Terrain attributes at the microsites as derived from a 5x5m digital surface model.

Site ID	*Landscape element*	*Slope (in degrees and class)*		*Aspect (in degrees and class)*		*Elevation (m)*
1	Upper slope	13	Rolling	175	South	196.7
3	Open slope	16	Strongly rolling	115	East	249.0
4	Open slope	23	Moderately steep	94	East	279.0
8	Midslope ridge	35	Steep	35	North	307.8
10	Open slope	22	Moderately steep	298	West	318.6
11	Upper slope	26	Steep	257	West	314.8
12	High ridge	32	Steep	178	South	301.8
13	Open slope	23	Moderately steep	22	North	232.8
14	Upper slope	23	Moderately steep	157	South	287.8
15	Plain	-	Flat	-	Flat	196.4
16	Open slope	17	Strongly rolling	283	West	373.6
18	Open slope	26	Steep	46	East	400.7
19	Open slope	14	Rolling	15	North	380.7

The following variables were monitored at each site: above ground-accumulated regrowth, i.e. live herbage, θ_v content and T_s at multiple depth. Data collection started on 1 October 2016 for pasture yield and on the 1 November 2016 for θ_v and T_s due to the time needed for soil settlement after the AquaCheck probe installation. The soil and pasture monitoring was completed on 20 June 2018 due to extremely wet conditions and difficulties in site accessibility. In this chapter, the study period was divided into Year 1 and Year 2 and used to refer to the time intervals of 1 November 2016 - 31 October 2017 and 1 November 2017 - 20 June 2018 hereinafter, respectively.

7.2.3.2 Pasture growth measurement and yield calculation

The growth of the ryegrass-based pastures was measured by the utilisation of the exclosure cage-technique (also known as "rate of growth") described and evaluated by Lynch and Mountier (1954) and Radcliffe (1974a). The application of the method involves the cutting of regrowth of pasture within a standard quadrat over short time intervals from previously trimmed areas protected by exclosure cages. The microsites were selected on relatively uniform vegetation cover to ensure that approximately the same pasture composition was sampled. A detailed description of the technique can be found in Chapter 2.

To measure the accumulated yield, three moveable pasture cages were positioned around the AquaCheck probe. The cages were moved around at 4-6 weeks intervals and placed randomly over freshly trimmed surfaces (down to 10 mm height) avoiding previously trimmed areas, depressions, waterways and other irregularities on the soil surface. An example of a microsite design and the cage relocation procedure is presented in Figure 7.3.

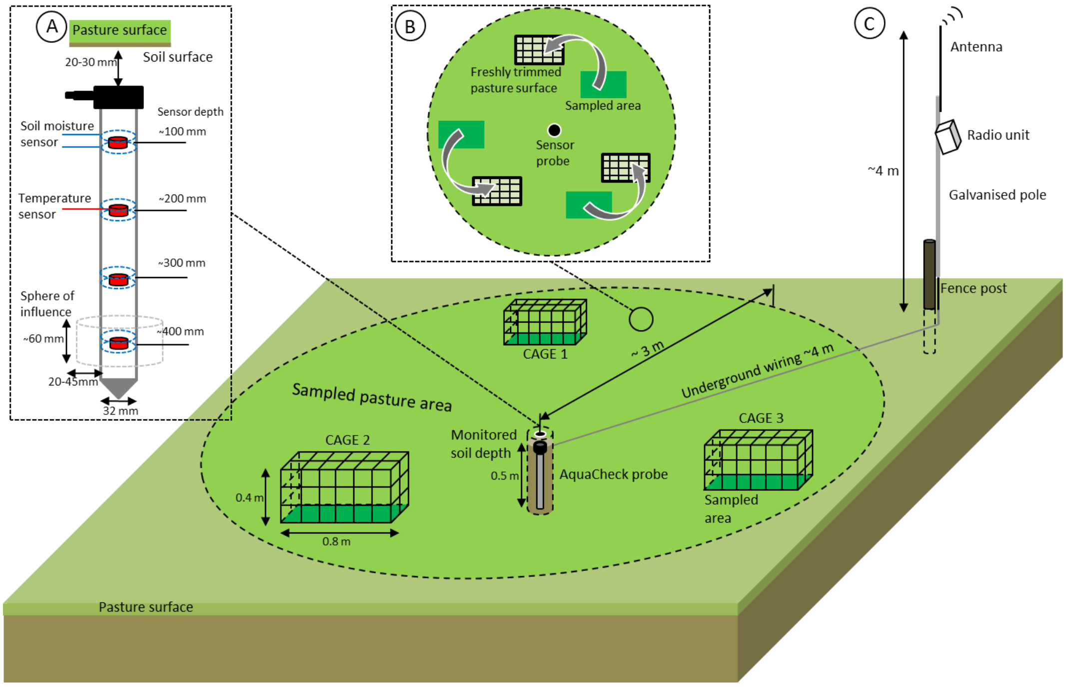

Figure 7.3 Pasture and soil monitoring site (microsite) design with the AquaCheck multisensory probe (A) located in the centre surrounded by the regularly rotated exclosure cages (B) and their position relative to the high range telemetry unit (C).

To derive dry matter (DM) (kg DM/ha) and mean daily pasture growth rate (PGR) (kg DM/ha/day), the collected samples were dried for 48 h in an oven and weighed in the laboratory. At every site, the total herbage accumulation was calculated by averaging the DM data from the three sampled surfaces exclosed by the cages. The mean daily PGR was computed by dividing the total yield by the number of days separating two consecutive cuts.

The primary focus of this study is the variation between spatially distributed microsites and relative differences between various landscape positions rather than absolute values in terms of PGR and accumulated DM. It is noted that the "cage technique" suffer from a number of disadvantages (e.g. micro-variability within the quadrats, inaccuracy related to human errors, the effect of exclusion cage on growth). Despite of these factors, this method was observed to deliver close and consistent approximations of the actual yield (Stephen and Revfeim, 1971) and it is considered as an applicable method if the interest being the examination of relative growth differences (Devantier et al., 1998).

7.2.3.3 Soil moisture and soil temperature monitoring

As water extraction by pasture occurs down to a depth of at least 350 mm in the hill country if the soil is deep enough (Bretherton *et al.*, 2011), a capacitance-based, AquaCheck Sub-surface Probe (AquaCheck Soil Moisture Management, Durbanville, South Africa) was chosen. The probe collected θ_v and T_s readings at four soil depths (100, 200, 300, 400 mm) at 15-minute intervals. The accuracy of the θ_v sensors were improved by calibration following the procedure reported in Chapter 4. The probes were attached to radio-based telemetry units (Tag I.T Technologies Ltd, Hamilton, New Zealand) and arranged into a WSN. The HALO Farm System, an online service developed by Tag I.T is used for monitoring, accessing and visualising the WSN data.

7.2.4 Meteorological data

The Patitapu Station is equipped with a weather station with a 2.5 m mast, and at an elevation of 263 m on an open gently sloping site. The station collects precipitation, minimum and maximum air temperature, net radiation, and wind speed and direction data at 1-hour intervals. The rainfall data is collected at 0.2 mm resolution by a tipping bucket gauge. Rainfall information was aggregated in daily intervals for this study and used for a comparison with historical averages to characterise the study period as compared to the past 65 years. Historical rainfall data (1953-2017) was sourced from the CliFlo web system (https://cliflo.niwa.co.nz/) that contains New Zealand’s National Climate Database. The extracted data was collected by a nearby NIWA climate station at Wairere, Ihuraua, located only 4.5 km from the centre of the research area (Fig. 7.1 (B)).

7.2.5 Soil moisture storage and soil water deficit calculation

As θ_v is not measured continuously with depth, the monitored soil profile was divided into 7 discrete depths around the four sensors. Between each sensor, the trapezoid rule (Rahgozar et al., 2012) of numerical integration was used to approximate the region under the soil water profile curve, and to calculate the amount of stored water (SWS, mm). The SWS represents the total amount of soil water stored in the monitored soil profile, and it does not refer to the plant available water content. It was assumed that θ_v in the top 70 mm layer was similar to the topmost (100 mm) sensor reading due to the lack of sensors in that layer. The daily soil water storage (SWS_d, mm) was calculated for the top 430 mm soil layer (i.e. the sensing limit of the bottom sensor) based on the data from the capacitance sensors as described by Eq. (7.1):

$$SWS_d = \sum_{i=1}^{7} b_i * \theta_{vi} \tag{7.1}$$

The formula above integrates over seven discrete soil layers, where b_i (mm) and θ_{vi} ($m^3 m^{-3}$) are the depth and volumetric water content for soil layer i, respectively. To represent the amount of stored water in the soil during the individual regrowth periods, accumulated soil water storage SWS_a, i.e. the sum of the SWS_d values, was computed taking into account the number of days within the cutting intervals.

Soil water deficit (mm) was computed as the difference between θ_v on a given day at midnight, and field capacity (Woodward et al., 2001). Field capacity was estimated from field-based θ_v data collected by the WSN during the wintertime when water loss due to evapotranspiration was at its minimum. Field capacity was determined following heavy rain events after which the soils were saturated. In most cases, after 1-3 days, the rate of downward movement markedly decreased and the free drainage of excess water was negligible which was indicated by the change in slope on the θ_v curve, marking the transition to field capacity. The transition point was identified by fitting tangential curves on the θ_v curve by using derivatives of a fitted spline function. By taking the intersection of the tangent curves, field capacity values can be obtained.

It is noted, that determining field capacity this way is subjective and heavily rely on visual interpretation of the time stamp when the redistribution virtually ceased. Although, due to the 15 min sensor reading interval, the method should provide adequate field capacity estimates for this study. The concept of field capacity and the questions raised regarding its definition is discussed in Hillel (2003b) and Horne and Scotter (2016).

Theoretical values of permanent wilting point were calculated for each soil depth at each microsite by the Soil Water Characteristics Hydraulic Properties predictive system developed by Saxton and Rawls (2006). Mean field capacity, and permanent wilting point were calculated by averaging over the four soil depths at each microsite.

7.2.6 Heat accumulation

Plant growth is controlled by T_s and air temperature (T_a) dependent on the different requirements of the plant species. In hilly landscapes, T_s distribution is a function of aspect and slope, thus sunny and shady areas, flat, steep, and gentle slopes provide different conditions for active growth (Chapman and Macfarlane, 1985). This means that some species may prefer generally warmer surfaces while others can be efficient with less ISR, although, depending on the season, the plants will also need to tolerate low θ_v levels on sunny aspects.

A popular approach to define the relationship between temperature and plant development is to express the amount of heat as growing degree-days (GDD_d in units of °C) (also known as thermal time) (Arnold and Monteith, 1974, Moot et al., 2000). To investigate the relationship between the temperature change over time and the pasture growth at various topographic positions, daily GDD_d was computed using a canonical function given as per Eq. (7.2) as follows (McMaster and Wilhelm, 1997):

$$GDD_d = \frac{T_{s\,max} + T_{s\,min}}{2} - T_{base} \tag{7.2}$$

Where $T_{s\,max}$ represents the maximum T_s on a given day, $T_{s\,min}$ is the minimum T_s on the same day and T_{base} is the threshold temperature below which the plant does not develop. Since pasture cover at the microsites contained mainly temperate pasture species, an appropriate T_{base} had to be chosen. An appraisal of the available published threshold values, as well as a review provided by Hutchinson et al. (2000) on experimental results in the United Kingdom and New Zealand, 4 °C was selected as T_{base}. In this study, T_s values obtained at 100 mm soil depth were used to calculate GDD_d. Furthermore, annual heat accumulation GDD_a was calculated as the sum of daily mean T_s above a selected T_{base} for a defined period (i.e. Year 1 and Year 2), following the work of Radcliffe (1974b) and Hutchinson et al. (2000).

$$GDD_a = \sum_{Year\ n\ Day\ 1}^{Year\ n\ Day\ last} \left[\frac{T_{s\,max} + T_{s\,min}}{2} - T_{base}\right] \tag{7.3}$$

Annual accumulated heat GDD_a was used to compare the amount of accumulated heat at various terrain positions and microsites for both years ($n = 1, 2$).

7.2.7 Multivariate statistics using multiple factor analysis (MFA)

Statistical factor analysis is an important method in ecological studies and behavioural science in which individuals or observations are described by groups of variables (Escofier and Pagès, 1994, Thanoon et al., 2014). Multiple factor analysis (MFA) is a dedicated tool for studying complex datasets containing continuous and categorical variables provided in a group-based structure (Escofier and Pagès, 1994). Therefore, MFA is considered as a factorial technique that allows the simultaneous investigation of mixed data groups, i.e. a collection of quantitative (numerical) and qualitative (categorical or nominal) variables. MFA is part of the multiblock principle component analysis (PCA) method family and it is often referred to as an extension of PCA to handle qualitative variables (Abdi and Williams, 2010, Abdi et al., 2013). By the application of MFA, the influence of several sets of variables as well as an overview of interdependence between various groups and the typology of individuals described by the whole set of variables can be examined (Pagès, 2014, Thanoon et al., 2014).

With MFA, the variables within a specified group of variables are normalised and then weighted with an attributed value that may be different for each group. This is an essential aspect of MFA, thus variables in a group should be of the same type (Escofier and Pagès, 1994). During this stage of MFA, variables were organised into relevant groups, such as supplementary data (1), pasture growth (2), soil moisture (3), soil temperature (4), climatic variables (5), terrain attributes (6) and seasons (7).

Ultimately, MFA aims to summarise and to simplify the data by reducing the dimensionality of the data set, utilising multivariate statistical data analysis methods, depending on the type of data within a given variable group. MFA is a synthesis of multiple methods, that applies a generalised PCA for quantitative variables and a type of multiple correspondence analysis for qualitative variables (Lê et al., 2008).

For visualisation, biplots (i.e. a generalised scatter plot representing principle components on the axes) and scree plots (i.e. a line segment plot showing a fraction of total variance) were generated for both quantitative and qualitative variables. Biplots are low dimension graphical representations that can reveal the relationship between variables and the correlations between the dimensions by displaying the data in a correlation circle. Although PCA is not designed for time series analysis, it is possible to apply PCA to time series without taking into account the time as variable and considering the daily measurements as individual observations (Zuur et al., 2003).

For the purpose of this study, it was sufficient to use MFA as no temporal dependence was incorporated and the variables observed at the same time were grouped together. The analysis was carried out using the following R software packages: *FactoMineR* for the analysis (Husson et al., 2007) and *factoextra* for data visualisation (Kassambara and Mundt, 2016).

7.2.8 PGR in polar space

An attempt was made to generate a polar-grid-based representation of PGRs using a radial basis interpolation method (i.e. a polar form of spatial interpolation) (Schaback, 2007). This method calculates the PGR values at a high number of points defined by polar coordinate pairs. The Gaussian approximation approach was chosen as interpolation algorithm for constructing a continuous function from discrete data points, i.e. the microsites, defined by aspect and slope angel as polar coordinates. Radial basis function methods are a special case of splines where the generated surface will pass through all of the observed values. The Gaussian method was selected due to its capability to capture trends and highlight local variations better than other techniques, which often fit a 2-dimensional plane to the observations.

The hill plot (Fig. 7.4) approach provides an alternative visualisation option of the results as it includes the compass directions (aspect) on the polar axis and slope angle on the radius axis with steepness decreasing from the centre. These two parameters have been observed to be the dominant terrain attributes influencing pasture communities and production (Radcliffe, 1982, Moir et al., 2000, Bretherton, 2012, Kemp and López, 2016).

A hypothetical hill plot was used to represent the relative position of the microsites in terms of slope angle and aspect (Fig. 7.4). A simplified version of the technique has been used in several studies to depict soil nutrient distribution (Lieffers and Larkin-Lieffers, 1987) and variations in the composition of grassland vegetation when correlated with numerous slope characteristics (Ayyad and Dix, 1964).

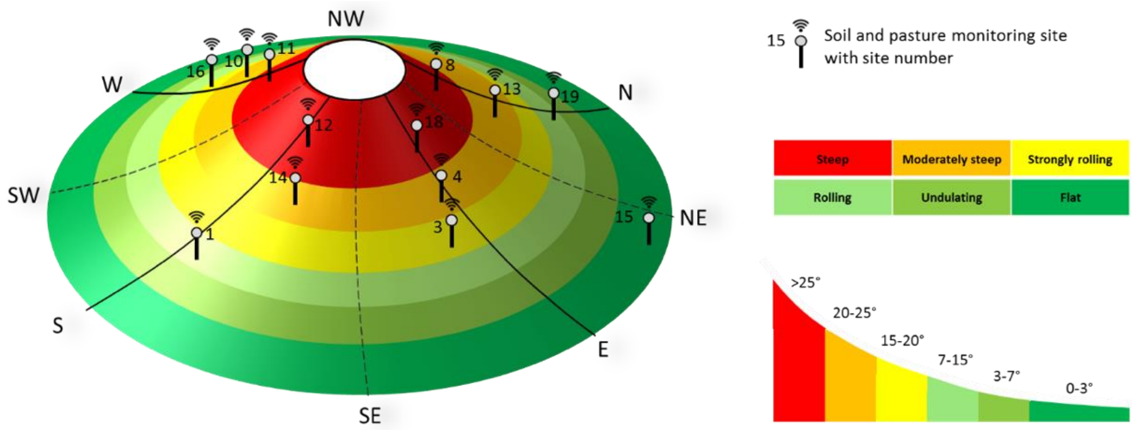

Figure 7.4 An idealised hill plot to illustrate the situation of the microsites as a function of slope angle and aspect used in this study. Slope angle ranges were categorised into six classes following the Land Use Capability (Lynn et al., 2009) slope classification except in the case of the steep category.

7.3 Results and discussion

7.3.1 General description of the evolution of environmental parameters during the study period and the spatial mean pasture production

The theoretical background of DM accumulation and regrowth of perennial ryegrass is well documented, although field measurements can show high variability over different years (Chapman et al., 2012). Climatic parameters, especially temperature, precipitation, and consequently soil moisture are some of the most important determinants of pasture growth on non-irrigated pastoral areas (Baars and Waller, 1979, Harris et al., 1985). An understanding of their limiting effects as well as their temporal patterns within a specific area is essential to realise the full potential to produce pasture. Hence, the measured PGR and the accumulated DM evolution over time was plotted together with climatic data to allow investigation of temporal growth trends (Fig. 7.5).

A comparison was made between the study period and the previous 65 years in terms of rainfall distribution to examine if the years between 2016 and 2018 can be considered as average years and follow the general historical trends (Fig. 7.5 (A)). Additionally, the examination of rainfall characteristics as opposed to the historic mean values of the study site can reveal the dependencies of PGR on the temporal distribution of water supply.

Figure 7.5 (A) presents the time series of available precipitation data collected by the local weather station and the nearest NIWA meteorological station. The annual rainfall of the historical periods ranged from 721 to 1,735 mm with a mean of 1,139 mm over the 65-year period recorded at the Wairere, Ihuraua climate station. Generally, the highest amount of rainfall was received during the winter months while the lowest amount of precipitation occurred in November and from January to March. The three-year mean annual precipitation (2016-2018) was 997 mm at the study site based on data recorded by the local weather station. The total precipitation was 842 mm in 2016, 1,020 mm in 2017 and 1,130 mm in 2018.

Based on the historical precipitation characteristics of the research area it was observed that the monthly total rainfall closely followed the historical mean values in November 2016 - September 2017 while the rest of the year and the summer of 2017-2018 was drier than the historical average (Fig. 7.5 (A)).

The temporal and spatial variability of θ_v at multiple depths were discussed in Chapter 5 in more detail. Fluctuations of θ_v showed close agreement with daily rainfall patterns, with the largest seasonal θ_v amplitude occurring at the 100 mm soil depth (Fig. 7.5. (B)). The 200-400 mm soil depth behaved similarly but displaying less amplitude across seasons. The driest conditions were observed in January and February 2018 dropping to mean θ_v of 0.2 $m^3\,m^{-3}$, whereas the highest mean θ_v levels at 0.45 $m^3\,m^{-3}$ (at near-saturated or saturated conditions) were reached and maintained during most of the winter season triggering erosion, saturation excess runoff, and stream flooding events (for example in July 2017). The driest θ_v= 0.18 $m^3\,m^{-3}$ and wettest θ_v= 0.48 $m^3\,m^{-3}$ soil conditions occurring at the 100 mm soil depth is indicative of higher amplitude responses of the surface soil to meteorological forcing.

During the summer season, the deepest soil sections had the highest θ_v with a gradually increasing difference in θ_v between soil depths from late November 2016 and early November 2017 when the curves crossed each other (Fig. 7.5 (B)). This indicates that the water loss by evapotranspiration in the deeper soil layers occurred slower than at the top of the soil profile.

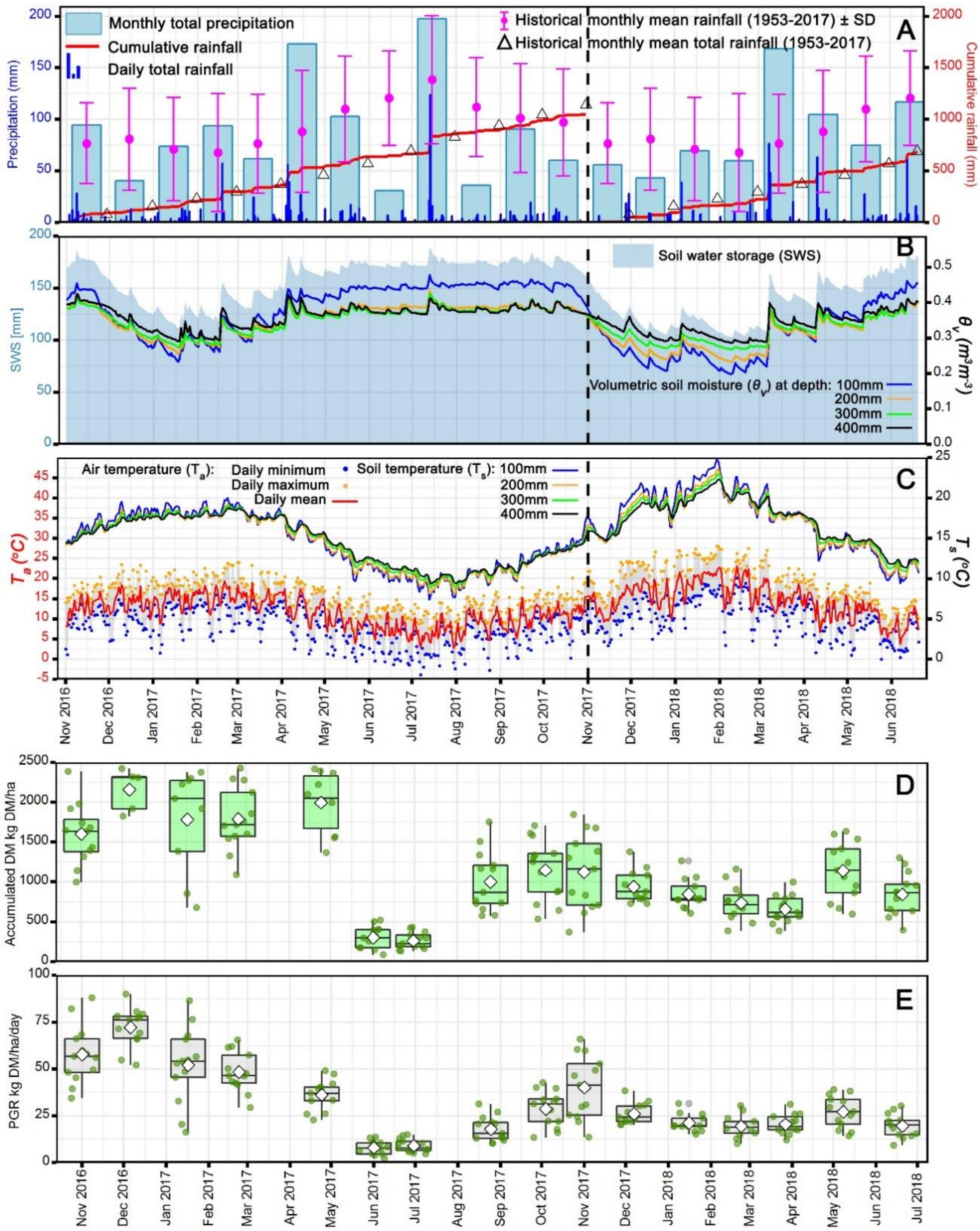

Figure 7.5 Temporal plots of climatic variables obtained from the Patitapu weather station are shown (A and C) along with historic rainfall data extracted from NIWA (A). These parameters include historical monthly mean and monthly total rainfall (1953-2017). Daily total precipitation, cumulative rainfall, and monthly total rainfall are shown in (A) whereas the minimum, maximum and mean daily air temperature (T_a) are presented in (C). Daily spatial mean volumetric soil moisture (θ_v) and total stored water (SWS) in the profile (B) and soil temperature (T_s) (C) were acquired by AquaCheck probes. Dry matter (DM) (D) and mean daily pasture growth rate (PGR) are shown in (E). Each DM and PGR data point represents the average of measurement results from three cages at a single site.

The spatial mean (averaged over all sites) SWS_d reached 190 mm in the 430 mm soil profile during the wettest conditions and the heaviest rainfall events. The lowest SWS_d (100 mm) was related to the long dry season in Year 2 (December 2017 – March 2018), which most likely impacted on PGR. In Year 1, this impact was not observed, even though SWS_d decreased to about 120 mm. Presumably, this level of water stress was not serious enough to significantly impact on PGR levels. SWS_d only reached or approached the calculated values at permanent wilting point at the north- and east-facing steep microsites as it is presented in Figure 5.7 in Chapter 5.

To visually examine the effect of temperature on pasture growth and to better understand the temporal changes in θ_v and SWS_d, T_a and T_s time series obtained from both the local weather station and the WSN are illustrated in Figure 7.5 (C). The T_s spatial mean rose as high as 20 °C in the summer of 2017 and to 25 °C in 2018. This may indicate the considerable difference in the incoming radiation during the dry periods between the two monitored years, although the rate of uptake via evapotranspiration can regulate T_s to a certain extent. According to NIWA, January 2018 was the hottest month on record across the majority of New Zealand and T_s rose above the historic annual average while θ_v levels dropped below average within the ECHC. These trends were also reflected in the climatic data collected at the Patitapu Station.

The coldest days were observed in July and August 2017 with spatial mean T_s dropping to 7 °C at 100 mm soil depth, although at the deepest, 300-400 mm, soil depths it did not fall below 9 °C. The temporal change in T_s was closely followed by T_a reaching a maximum of 28 °C in Feb 2018 and a minimum of -4.8 °C in Jul 2017 (Fig. 7.5 (C)). Winter frosts (< -1 °C) were recorded on 9 days at the Patitapu weather station in 2017.

The DM and PGR values for the perennial ryegrass pasture are represented by boxplots in Figure 7.5 (D) and (E), respectively, to investigate the spatial and temporal variability of pasture growth and to be able to relate the response pattern of yield to the previously described environmental variables. Each boxplot is a graphical rendition of descriptive statistics generated from the 13 microsites linked to the days of samplings. These boxplots visually summarise the following statistical parameters: the mean (white rhomboid), the median (line across the box), 25th percentile and 75th percentile as lower and upper hinges and outlying points. As the regrowth intervals varied in length, the boxplots are distributed accordingly over time.

By visually investigating the pasture productivity charts, it can be concluded that considerable spatial variation exists between the 13 microsites. The recorded DM and calculated PGR values showed the largest variability in spring and summer seasons and the least noticeable differences between sites were measured in winter. In late autumn and winter, the low values of T_s and T_a

inhibited pasture production, although the θ_v levels at near-saturated conditions may also effect yield due to the reduced oxygen diffusion rate and aeration.

It is also apparent that less DM was accumulated through Year 2 than in Year 1 if the overlapping months are considered. In both years, a strong spring - early summer peak was shown in DM production. This peak was lower and appeared slightly earlier, in Year 2, (November 2017) than in Year 1 (December 2016) when the highest PGR were observed during the study period. In Year 2, summer growth was limited by the early dry soil conditions in spring and the length of this period exerted a large impact on yield. The extreme temperature conditions of January 2018 had a strong impact on SWS_d that is reflected by the considerably lower pasture production compared to Year 1 (Fig. 7.4 (D) and (E)). The production window in spring was characterised by increasing temperatures and at this time θ_v was not a growth-limiting factor in Year 1, although it was in Year 2. Our observation shows agreement with the findings of Radcliffe (1982) associating early reduction in PGR with low spring rainfall, as well as and that of Zhang et al. (2005) stating that spring rainfall is one of the most important factors in annual pasture productivity in hill country.

7.3.2 Optimal environmental conditions for pasture growth at Patitapu Station

Concerning the measured growth and the parameters recorded by the Patitapu weather station, the optimal conditions can be defined for the highest yield-producing periods. The widest PGR range of 55-90 kg DM/ha/day was observed when the mean T_a was between 13 and 16°C during the regrowth interval. The T_s at 100 mm soil depth varied in the 15-19 °C optimal temperature window in the highest production periods. In terms of ISR, the pasture was most productive at 5500-6500 WH/m^2 and the variation in PGR between microsites was shown to follow a gradually increasing trend with increasing ISR. This trend was clearly linked to the topographical positions of the sites controlling differences in ISR. The most significant pasture development occurred when cumulative precipitation for a regrowth interval was around 100 mm and the mean θ_v values at 100 mm soil depth ranged between 0.29 and 0.45 m^3 m^{-3}. The highest pasture productivity was reached when SWS_d was between 125 and 175 mm.

Low yield was observed when the mean air temperature dropped below 10 °C, giving the lowest PGR values at 7.5 °C. However, when the mean T_a exceeded 17 °C, the PGR markedly dropped to 10-30 kg DM/ha/day. Similar trend was shown by the T_s; indicating that T_s below 14 °C and above 19 °C were associated with lower PGR values. By looking at only this single parameter, high temperature could potentially be a growth-limiting factor, although it has not been deeply investigated in this study. The changes in T_s have to be examined together with the θ_v levels, which were extremely low during the warm period, taking over the limiting role of grass growth during the summer. The minimum values and the least variation in PGR occurred at 1500-2000 WH/m^2 ISR.

7.3.3 Dry matter accumulation and pasture growth rate trend analysis

7.3.3.1 Total accumulated dry matter

Total pasture production, expressed as accumulated DM, are shown for the period of Nov 2016 - Jun 2018 (individually for Year 1 and Year 2) in Figure 7.6 as a function of aspect and slope angle (flat, rolling, strongly rolling, moderately steep, steep). Pasture yield was most abundant on flat paddocks accumulating 16205 kg DM/ha in Year 1 and 7409 kg DM/ha in Year 2. In Year 1, the lowest amount of accumulated, i.e. cumulative DM was observed on the steep, west-facing microsite which produced 7642 kg DM/ha, while in Year 2 a steep, south-facing microsite produced the least amount of DM yielding 4660 kg DM/ha.

In our study, north-facing slopes produced more DM than south-facing slopes in both years, mirroring the observations of Suckling (1959) and Suckling (1975) sited on sandy loams in hill country near the Ruahine ranges (60 km north of Patitapu Station). It also shows agreement with the findings of Gillingham (1973) conducted on steep lands near Hamilton (350 km north of Patitapu Station). The high productivity levels on north-facing slopes were dominantly due to the better winter growth. On steep slopes, very similar DM accumulation was observed on both south and north aspects, while the largest difference in DM production between north and south aspects occurred on moderately steep slopes in Year 1. Most microsites on east-facing slopes showed very similar results if compared to the sites on the west aspects. These observations can be associated with the ISR input that are expected to be about the same on east and west aspects. Although, the microsite at the steep, east-facing slope produced considerably more DM in Year 1 than the microsite at the steep, west-facing slope. Little difference was observed between east and west in Year 2. West- and east-facing slopes accumulated more herbage yield than the microsites on the south-facing slopes.

These results are somewhat contradictory with the findings of Lambert and Roberts (1978) obtained at a hill country research site located 45 km north of Patitapu Station. They reported that east-facing slopes had higher productivity than north, south and west in the order of decreasing yield potential. White et al. (1972) found that south aspects (shady faces) produced twice as much yield as north aspects in North Canterbury, South Island. Similar results were presented by Radcliffe et al. (1976) showing that 14% more DM was produced on south aspects. Gillingham (1973) and Ledgard et al. (1982) found little difference between annual production rates as a function of aspect. These controversial findings support the evidence of the varying role of aspect effect on DM in different parts of the country that can be related to latitude.

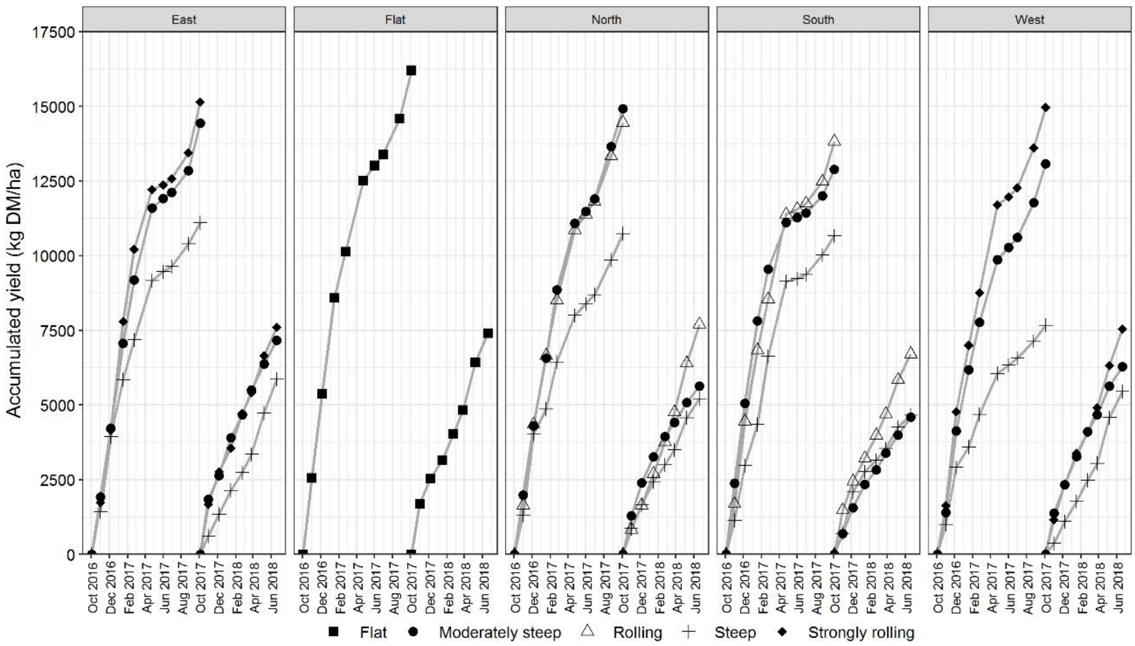

Figure 7.6 Total cumulative yield (kg dry matter (DM)/ha) for perennial ryegrass pasture surfaces as a function of aspect and slope categories between Oct 2016 and Jun 2018.

As expected, the lowest total cumulative DM was observed on steep slopes and DM production tended to decrease as slope angle increased, in agreement with the findings of Gillingham et al. (1998), Bretherton (2012) and Roberts and White (2016). They associated this trend with the diminishing amount of available soil water with increasing slope angle due to decreasing soil depth with increasing slope. The dominant effect of slope angle was also highlighted by Zhang et al. (2005) resulting from their decision-tree approach to pasture productivity modelling in New Zealand. Our observations, and the agreement with previous studies confirm that slope angle and aspect are specific landscape features dominating pasture productivity levels. Furthermore, on the basis of the results presented in Figure 7.6, it can be inferred (from visual inspection) that slope angle had a stronger effect on pasture yield than aspect. This is further investigated by multivariate statistical methods later on in this chapter.

7.3.3.2 Spatial growth patterns and the effect of topography on the pasture growth rate

Annual yield is one of the most important measures of pasture performance, although seasonal variation of PGR is also of great interest due to its impacts on farm management. ECHC areas tend to experience seasonal weather extremes thus prompting an examination of the temporal distribution of pasture production (Fig. 7.7). For improved interpretation of the relationship between PGR variability and topographical attributes, the PGR time series at each microsite was visualised and assessed by considering the aspect and slope angle categories. This information was used together with Figure 7.8 to describe spatial and temporal PGR trends.

The largest variation in pasture production between various microsites occurred during the spring growth and summer periods as indicated by the standard deviation (SD) values of 17-20 kg DM/ha/day. There was little spatial variability in PGR during winter and autumn, with similar SDs ranging between 3-10 kg DM/ha/day in Year 1 and Year 2. A decreasing trend was observed in PGR variability from summer to winter in Year 1, with the lowest PGR values and the lowest SD in June and July 2017. Following the pasture growth rate in winter, the SD values gradually increased and reached a peak in the spring growing period in Year 2 (Nov 2017).

Figure 7.7 shows that the PGR evolution recorded at microsites with steep slope characteristics consistently provided the lowest production values over the study period. Specifically, the west-facing steep slope being the lowest producing location, followed by east and south aspects. Rolling and moderately steep slopes are situated in the middle range, while strongly rolling and flat areas produced the highest DM in Year 1. The spatial pattern of production was not consistent and changed in Year 2, when moderately steep east-facing slopes produced nearly as much DM as flat and strongly rolling east-facing microsites.

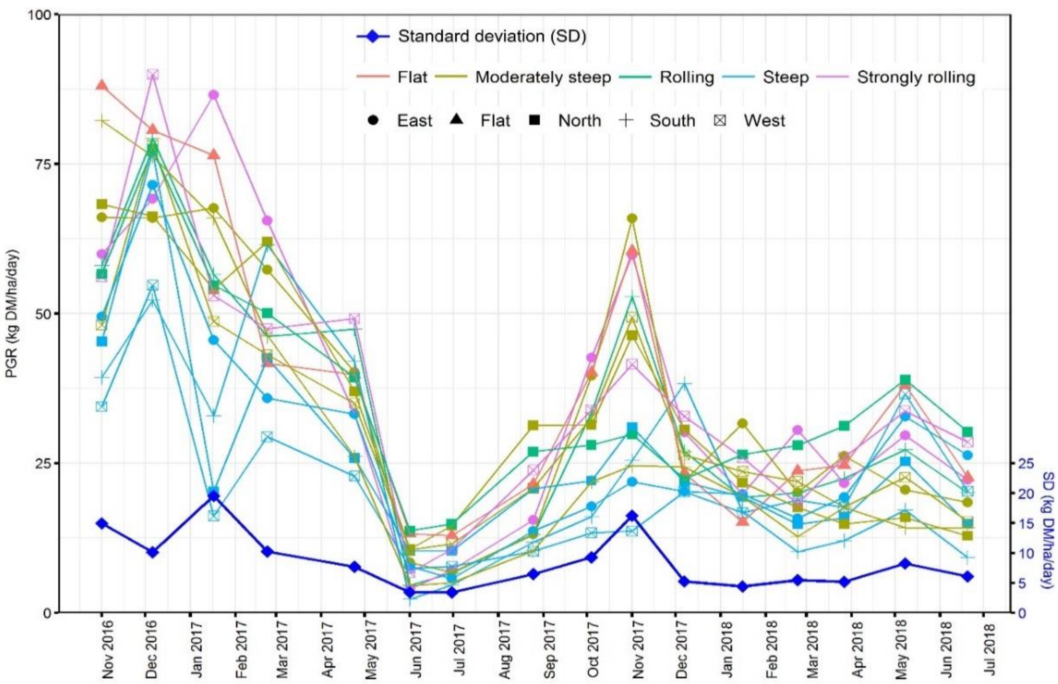

Figure 7.7 Mean daily pasture growth rate (PGR) of different slope and aspect categories of hill country pastures at Patitapu Station between Nov 2016 and Jun 2018 and their standard deviation (SD) over time.

The data presented in Figure 7.7 suggests that the effect of slope angle and aspect has a marked seasonal component and that this relationship changes with growth rates reaching maximum variation during the spring and summer seasons. These results can be linked to the spatial

θ_v variation, which was the highest during the dry seasons and strongly linked to aspect, and the lowest in the wet periods as it was discussed in Chapter 5. This is due to the more divergent ISR differences between north and south aspects over the longer dry periods. The high variation in PGR observed during the dry season can also be partly explained by the difference in GDD_a on various aspects resulting in the warmest conditions on north and the least amount of GDD_a on south.

PGR values were displayed in the polar space to examine the potential patterns of the effect of slope angle and aspect by the aid of a hypothetical hill plot (Fig. 7.8). It is clear that PGR values tended to decrease with increasing slope angle for each aspect category. The effect was present throughout the study period, although the strongest contrast between flat and steep surfaces was observed in spring and summer. The difference in PGR between sites were not as marked in winter.

PGR values ranged between 2.3 and 89.95 kg DM/ha/day, where the minimum and maximum values were measured on a west-facing steep site and a flat paddock, respectively. Greater winter production was observed on northerly aspects than on south-facing aspects and higher summer yield was recorded on the north- and east-facing aspects than at the sites on the west and south aspects. In contrast to the above findings, Lambert (1977) observed, that without the use of fertiliser input, south aspects produced more yield than northerly faces through the year except early summer. Findings by Suckling (1975) showed that pasture production on cooler faces was often greater than that of on warmer slopes in summer on fertilised trials. These various results indicate that regional dependence and latitude are factors to consider, as well as the amplitude of seasonal fluctuations. For example, an increase in slope angle by a degree resulted in a change of PGR in the range of 1.2-2 kg DM/ha/day in spring 2016 and 0.1-0.4 kg DM/ha/day in the winter of 2017.

When examining the relationship between PGR values and aspect, the production difference between aspect classes was less apparent, except for the flat category that exhibited the highest PGR values during the study period. Additionally, production differences between years needs to be examined, as there are other environmental variables, i.e. wind that can influence microclimatic conditions and, therefore, PGR.

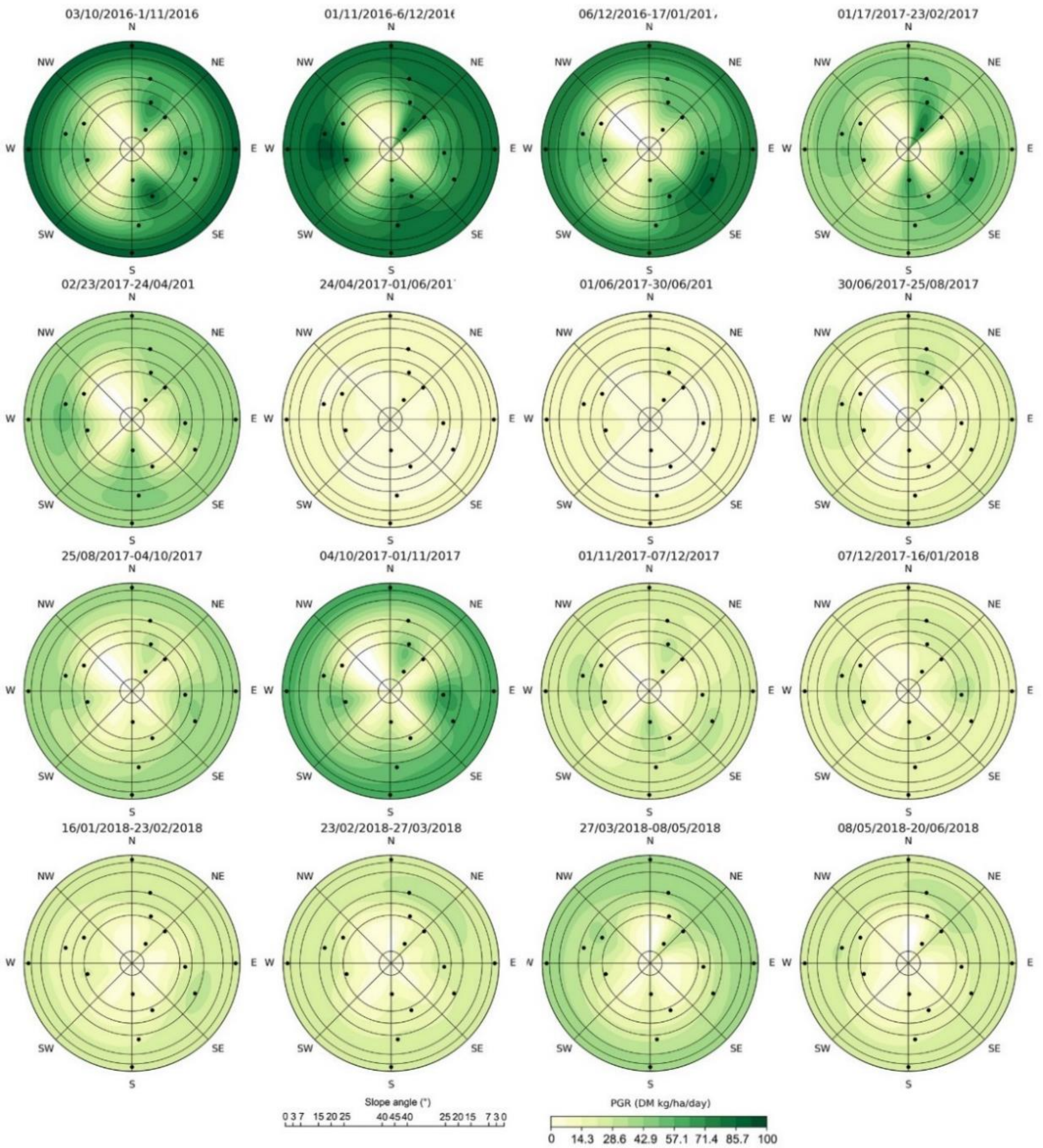

Figure 7.8 Time series of polar plots illustrating pasture growth rate changes dependent on slope angle and aspect. For interpolation, the Gaussian radial basis function approach was chosen. Black dots mark the position of microsites based on their slope angle and aspect attributes.

By using a time series of polar plots (Fig. 7.8), it was expected that any variation caused by the complex topography would be observable. However, the only noteworthy variation was attributed to slope, supporting the previously the observations of other researchers. The influence of other factors may be detected by employing more sampling sites, thereby improving the systematic distribution of the sites in terms of topographic settings.

7.3.4 Heat accumulation as a function of topography

The rate of pasture development is highly influenced by T_S and strong relationships were observed between pasture growth and accumulated heat (Frank and Hofmann, 1989, Hutchinson et al., 2000). Since perennial ryegrass pasture is adapted to temperate climates, cold winter and hot summer conditions limit its growth. Furthermore, the white clover, the companion species of ryegrass, is summer active, and can be less productive and susceptible to dying off in hot, dry conditions. This is clearly reflected by the PGR data presented in Figure 7.5. In this section, the differences in annual heat accumulation, expressed as GDD_a (calculated as per Equation 7.2), between the microsites based on aspect and slope angle was investigated (Fig. 7.9).

In Year 1, the north-facing moderately steep slope reached the greatest annual GDD_a of 4370 °C, while the lowest amount of heat, 3386 °C, was accumulated on a south-facing steep site, i.e. 22.5 % less GDD_a. East- and west-facing, moderately steep slopes behaved very similarly, gathering 3986 °C and 3904 °C, respectively. Steep microsites were represented by slightly less GDD_a than moderately steep microsites, whereas strongly rolling slopes received the lowest amount of incident energy, accumulating 3659 °C on east and 3569 °C on west aspects. At the flat microsite, 3714 °C was recorded placing this aspect in the middle of the GDD_a range observed at Patitapu Station. In Year 2, the moderately steep locations accumulated the highest amount of GDD_a similar to Year 1. The general trends observed with respect to aspect in Year 1 were mostly present in Year 2 as well, although the differences were not as large, due to the shorter monitoring period in Year 2.

It can be seen that moderately steep slopes accumulated the highest amount of heat in most cases in both years, except for the south aspect, where a microsite situated on a rolling slope received the highest amount of heat. North, east, west and south aspects, accumulated heat in decreasing order. In general, moderately steep, steep, flat, strongly rolling and rolling slopes accumulated less heat in decreasing order, except for the south aspect where rolling, moderately steep, and steep slopes exhibited a decreasing trend in GDD_a. The difference in heat accumulation between microsites located on the same aspect started increasing during early autumn in both years indicating the effect of slope angle on ISR.

The energy supply received from the incident radiation, converted/stored as heat, is available for evaporation processes and it heats up the air and soil, thus influencing pasture development (Gillingham and Bell, 1977). The accumulated heat energy is disseminated by evapotranspiration that results an increase in water flow to the pasture root mass from lower depths in dry conditions.

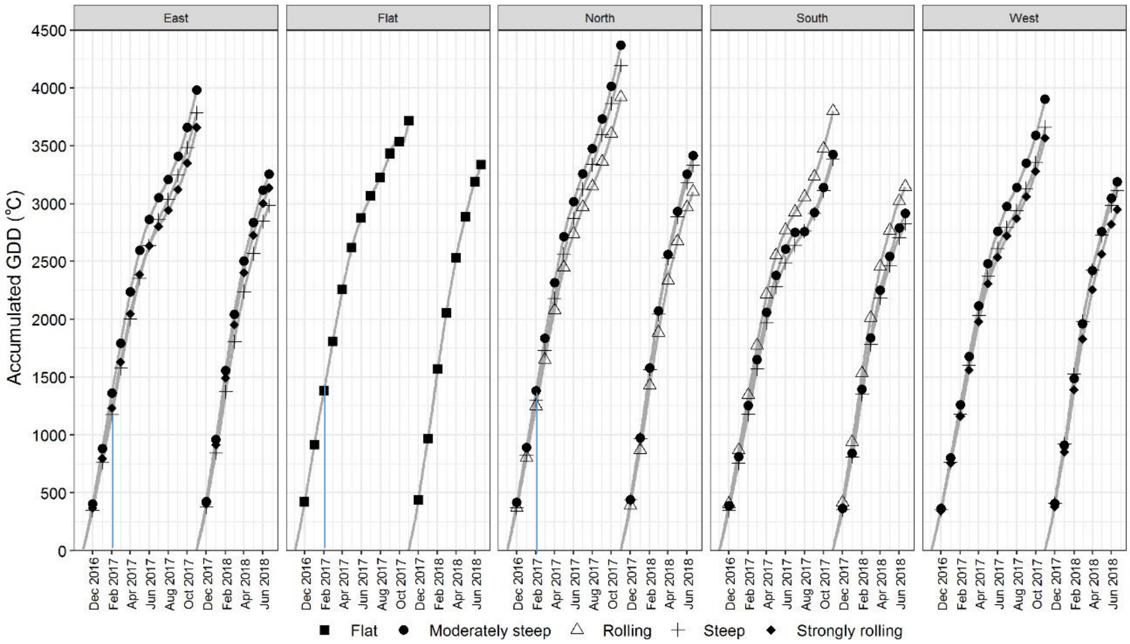

Figure 7.9 Annual accumulated growing degree-days (GDD_a) as a function of aspect and slope angle classes at Patitapu Station plotted separately for Year 1 and Year 2

It is evident that the received heat at a given pasture surface is dependent on its topographical situation (Benseman and Cook, 1969), therefore hill country topography is an important factor in the spatial distribution of received energy, enhancing spatial variation in heat patterns. Consequently, the differences observed with GDD_a would suggest that spatial and temporal variability in PGR would be affected. Our observations are in agreement with the conclusions of several studies (Lambert and Roberts, 1976, Gillingham and Bell, 1977, Radcliffe and Lefever, 1981) where higher evaporation rates were governed by the warmer nature of north-facing slopes than south-facing slopes with various slope angles.

7.3.5 The influence and interaction of soil water content and soil temperature on pasture growth rate

In hill country, θ_v levels can range between the two soil moisture extremes, therefore pasture production needs to cope with θ_v stress in dry, hot conditions as well as saturated conditions during winter when the plants are relatively dormant. The temporal pattern of θ_v deficit is indicative of the amount of plant available water (PAW) throughout the study period. This variable was plotted along with PGR and GDD_d to provide a better understanding of pasture response patterns at each microsite (Fig. 7.10).

In the winter of 2017, θ_v soil conditions were very wet, at near-saturated levels. At this time, GDD_d values were very low, resulting in low to negligible PGR at most microsites. During late spring and summer, PGR can be limited by θ_v availability. The PGRs at this time were much lower in Year 2; most likely due to the early and quick GDD_d rise during spring, which, in turn, is dependent on the amount of ISR. This led towards a significantly warmer summer period than in Year 1, causing a greater soil water deficit and reduced yield. During the longer dry period of Year 2, the highest θ_v deficit was reached at most microsites, reducing their PGR. Steeper slopes suffered from less effective rewetting due to slope angle and the earlier onset of soil water repellency (Bretherton et al., 2018). These factors, coupled with the lower amount of stored water in the shallower soil profiles, resulted in more severe and extended periods of θ_v deficits for these slopes.

In Year 1, although θ_v levels were decreasing from the end of November until the greatest soil moisture deficit in January 2017, there was still sufficient moisture for the production of relatively high amounts of pasture. A steady decline in PGR can be seen at most microsites from November 2016 until June 2017. Medium PGR values at 40-50 kg DM/ha/day were recorded while the water storage was refilling and approaching field capacity at the beginning of April 2017, when GDD_d started decreasing.

Due to the combined effects of these two variables, PGR reached a minimum in May 2017. A contrasting observation occurred in Year 2 after the long dry summer as GDD_d was decreasing and the amount of θ_v stored was increasing during autumn. Leaf growth recommenced and higher PGR values were observed. A rapid decrease in GDD_d was experienced both in May 2017 and May 2018, resulting in a decrease in PGR. Subsequently, for both years, the soil water content was at or exceeded field capacity, thus providing ideal θ_v conditions for growth. However, the limiting role of GDD_d was becoming more prominent at this time, resulting in low winter growth.

A study undertaken by Parfitt et al. (1985) indicated that ryegrass pasture growth was significantly limited when soil water deficit reached 50 mm, and then ceased at 140 mm on undulating terrain supporting silt loam soils. We observed that the PGR values noticeably decreased at 30-45 mm soil water deficit at most microsites in both years. It is likely then, that the 50 mm soil water deficit suggested by Parfitt et al. (1985) threshold is an acceptable approximation of the level at which the PGR is significantly limited, although our study would suggest that ryegrass/white clover pasture growth would begin to decrease at soil water deficit levels around 30-45 mm. We note that the field capacity values used in this study are estimations from the field-based θ_v data, which can have effect on these results.

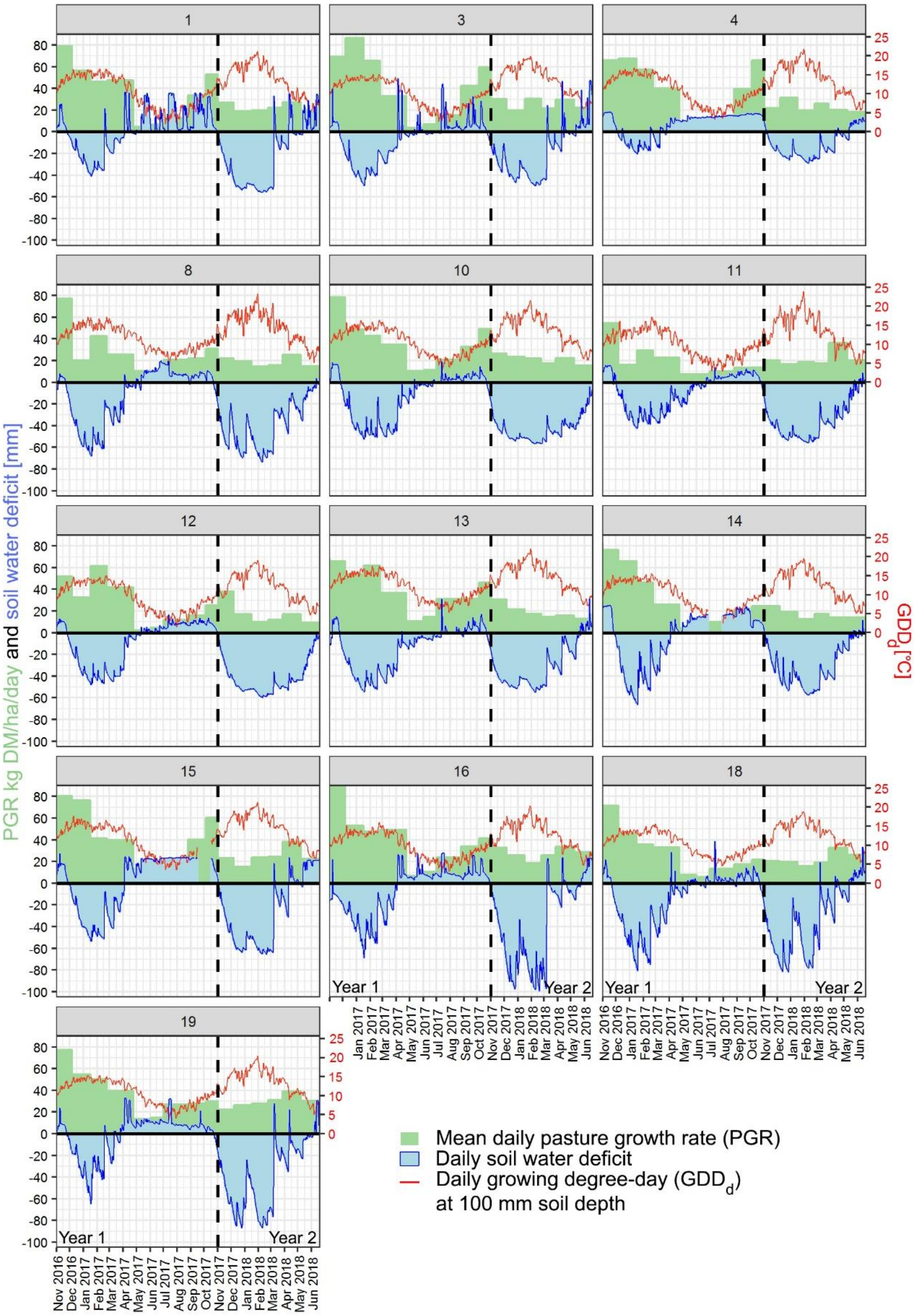

Figure 7.10 The pattern of mean daily pasture growth rate, daily soil water deficit and growing degree-days (GDD_d) at each microsite. The black horizontal line marks the position of field capacity estimated for each microsite based on in situ soil moisture (θ_v) measurements.

In this study, the annual pattern of θ_v has clearly affected plant growth. These patterns are in agreement with the studies of Bretherton et al. (2011) and Bircham and Gillingham (1986). There are many environmental components affecting PGR, causing variability in yield over complex landscapes. The amount of PAW in the soils is one of the primary factors improving pasture resilience (and hence productivity) and is influenced by effective infiltration, which, in turn, is dependent on of slope position (i.e. altitude above channel lines and altitude below ridge lines), shape (i.e. convexity) and slope angle and aspect (Lieffers and Larkin-Lieffers, 1987).

It was earlier demonstrated (Fig. 7.10) that during summer, pasture growth decreased with decreasing θ_v despite the adequate temperature conditions. In contrast, in autumn and winter, GDD_d was the main growth-limiting factor. θ_v and T_s variables at 100 mm depth were observed to explain most of the variation of the autumn yield in Hawkes Bay by Baars and Waller (1979). This implies that there were times, when specific soil moisture and temperature conditions prevailed, when the dominance of these two variables was inverted. Accordingly, in late autumn and winter, and despite sufficient PAW, plant growth slowed down due to temperature limitations.

There are periods when these limiting effects overlap, such as late autumn, so that pasture growth is severely constrained. During late spring and early summer, when both soil moisture and soil temperature are non-limiting, pasture production is relatively unconstrained.

7.3.6 Multivariate statistical analysis

In this study, a large amount of sensory data has been presented in a descriptive manner, primarily because the relationship between environmental variables and pasture production has been difficult to quantify and interpret. Accordingly, a multivariate approach, such as MFA, is likely to be an applicable and suitable method in order to examine the interdependence and correlation amongst groups of observed variables. MFA looks for the common structures in either all of the groups or in some of them and derives an integrated picture of the observations and the relationships (Abdi and Valentin, 2007).

Most of the literature has examined the effect of a single soil attribute (López et al., 2003) on pasture yield, despite the fact that herbage production is a result of a compound interaction of several elements. In our ensuing analysis, the following input variables were considered, and arranged into groups according to their quantitative or qualitative nature (Table 7.3). The MFA labels listed in Table 7.3 will be used to tag the results of the analysis in this section.

Table 7.3 An overview of the various input variables used in the multiple factor analysis (MFA). The variables are arranged into groups based on their type. The corresponding group and variable labels, and variable types as they were used in the MFA are shown in the right.

Description	*[Group Labels]* - variable type [Variable labels]
Group 1 - supplementary variables: ▪ location reference ▪ date of cuts	***[Origin]* - qualitative** ▪ [SiteID] ▪ [Date]
Group 2 - variable related to pasture growth: ▪ Mean daily pasture growth rate	***[PGR]* - quantitative** ▪ [PGR]
Group 3 - variables describing soil moisture levels: ▪ Soil moisture at four depths ▪ Accumulated soil water storage	***[Moisture]* - quantitative** ▪ [SM100, SM200, SM300, SM400] ▪ [AccSWS]
Group 4 - variables describing soil temperature and accumulated heat: ▪ Soil temperature at four depths ▪ Accumulated growing degree-days	***[Temperature]* - quantitative** ▪ [T100, T200, T300, T400] ▪ [AccGDD]
Group 5 - climatic variables: ▪ Total accumulated rainfall ▪ Rainfall frequency [> 2mm]	***[Rainfall]* - qualitative** ▪ [TotRain] ▪ [RainFq]
Group 6 - terrain attributes: ▪ Slope angle ▪ Aspect ▪ Landscape element	***[Terrain]* - qualitative** ▪ [Slo] ▪ [Asp] ▪ [LandScEl]
Group 7 - seasonality: ▪ Seasons	***[Season]*- qualitative** ▪ [Season]

A comparative MFA was performed separately on Year 1 and Year 2 in terms of PGR, soil moisture and soil temperature conditions. As a first step, the MFA algorithm standardises the input variables, balancing their influence to avoid the over-contribution of variable groups with the strongest structure and largest variance. This step is necessary to make these groups comparable (Abdi and Valentin, 2007). Secondly, the normalised datasets are merged to generate a unique matrix. Then, this matrix was analysed in multidimensional (global) space resulting in coordinates (factor scores) which were represented by points. To be able to compare Year 1 and Year 2, the analysis was completed over the same months for Year 1 that were present in Year 2. The MFA was executed on a total of 156 observations (78 per year).

7.3.6.1 Inter-dependence between groups and quantitative variables

Table 7.4 summarises the Eigen roots and Eigen vectors obtained from the MFA for both years and reflects how much of the total inertia (i.e. a measure of the total variance or dispersion) is explained by each dimension (or factor), i.e. a collection of reference information about a measureable variable (Sourial et al., 2010). In MFA, there are the same number of factors as there are variables and each factor captures a portion of the total variance within the year under investigation. Eigenvalues of the correlation matrix that are greater than one, explained more variance than a single variable. Based on the Kaiser criterion (Kaiser, 1960), only those dimensions that satisfied the "eigenvalue-greater-than-one rule" were retained (i.e. the first five dimension in this study). This is a popular approach due to its simplicity and ease of implementation (Braeken and van Assen, 2017). The variables of the supplementary group (Group 1) containing point IDs and location information were not considered during the generation of factor scores and the computation of contribution.

Table 7.4 Summary of the multiple factor analysis (MFA) results including Eigenvalues and the explained variance for each dimension for Year 1 and Year 2. *Dim.* – dimension.

Dimension	Eigenvalue	Variance (%)	Cumulative variance (%)
	Year 1		
Dim.1	3.7	24.7	24.7
Dim.2	2.5	17	41.8
Dim.3	2.3	15.4	57.1
Dim.4	1.2	8.2	65.4
Dim.5	1.1	7.2	72.6
	Year 2		
Dim.1	3.5	24.1	24.1
Dim.2	2.2	15.3	39.4
Dim.3	2.0	13.7	53.1
Dim.4	1.3	8.7	61.8
Dim.5	1.0	7.0	68.8

The analysis showed that the groups of *Moisture*, *Temperature*, *Rainfall*, *Terrain* and *Season* explained a significant portion of the variability through the first five dimensions explaining 72.6 % and 68.8 % of the total variability for Year 1 and Year 2, respectively. The *Dim.1* and *Dim.2* accounted for 41.8 % of the variability for Year 1 and 39.4 % for Year 2.

The contribution of each group (i.e. the variation of squared loadings) and the correlation (R^2) to the corresponding dimensions or components can be used to assess the importance of a group and the inter-relationships with other groups. The contribution results were converted to percentage values and presented in Table 7.5. Similar contribution trends were observed for both years, although the values changed from Year 1 to Year 2 indicating that the importance of groups might change from year to year or season to season. The larger the percent contribution value, the more a variable group contributed to the given dimension. Some of the groups, such as *Rainfall*, *Season* can be considered as multi-dimensional groups because of their contribution to several dimensions.

Table 7.5 The percentage contribution and correlation of each group of variables to the five dimensions are shown for Year 1 and Year 2 as obtained by the multiple factor analysis.

	Percentage contribution (%)					*Correlation (R^2)*				
	Dim.1	*Dim.2*	*Dim.3*	*Dim.4*	*Dim.5*	*Dim.1*	*Dim.2*	*Dim.3*	*Dim.4*	*Dim.5*
Group	***Year 1***									
PGR	16.44	11.25	0.57	1.49	0.26	0.78	0.53	0.11	0.14	0.05
Moisture	9.99	13.23	9.68	3.65	7.89	0.63	0.59	0.68	0.42	0.29
Temperature	23.00	0.52	4.28	4.71	0.38	0.92	0.13	0.37	0.28	0.08
Rainfall	26.38	36.97	43.07	78.58	5.43	0.99	0.97	0.99	0.98	0.24
Terrain	0.21	1.10	0.24	2.00	82.88	0.11	0.20	0.09	0.16	0.95
Season	23.99	36.94	42.16	9.58	3.17	0.94	0.97	0.98	0.34	0.18
	Year 2									
PGR	1	15.9	0	27.94	1.19	0.19	0.60	0.00	0.60	0.11
Moisture	19.93	0.47	0.19	11.64	0.74	0.84	0.44	0.07	0.39	0.10
Temperature	25.64	0.33	0.45	2.52	2	0.95	0.18	0.18	0.20	0.16
Rainfall	26.75	41.31	49.67	14.39	69.6	0.98	0.96	1.00	0.46	0.85
Terrain	0.46	0.86	0.02	35.83	25.81	0.17	0.17	0.02	0.74	0.52
Season	26.24	41.13	49.67	7.69	0.66	0.96	0.96	1.00	0.31	0.08

A graphical illustration of the results is provided in Figure 7.11 for comparison between the two years by focusing on the first two, principle dimensions. Figure 7.11 (A) and (B) present the map of supplementary or origin (in green) and active variable groups (in red) based on the coordinates of the groups that allow visualising the distance between tables. The position of the groups in the MFA showed quite clearly that the Dim.1 was highly related to *Temperature, Moisture, Season* and *PGR* in Year 1. In Year 2, *Temperature, Moisture, Season* and *Rainfall* were characterised as the highest contributing groups for *Dim.1*, whereas the *Dim.2* was mostly related to *Rainfall, Season* and to a lower extent to *PGR*.

Figure 7.11 (C) and (D) depict the scree plots of $\cos^2$ for *Dim.1*, that indicates the importance of a component (or dimension) for a given observation (Abdi and Williams, 2010). For inter-correlated quantitative dependent variables, $\cos^2$ indicates the contribution of a component to the squared distance of the observation to the origin. Large values of $\cos^2$ suggest high component importance for a given observation. In Year 1 *Temperature* and *PGR* were the most important groups, while the *Temperature* and *Moisture* groups had the highest $\cos^2$ values and considerably higher importance was observed in Year 2 than in Year 1.

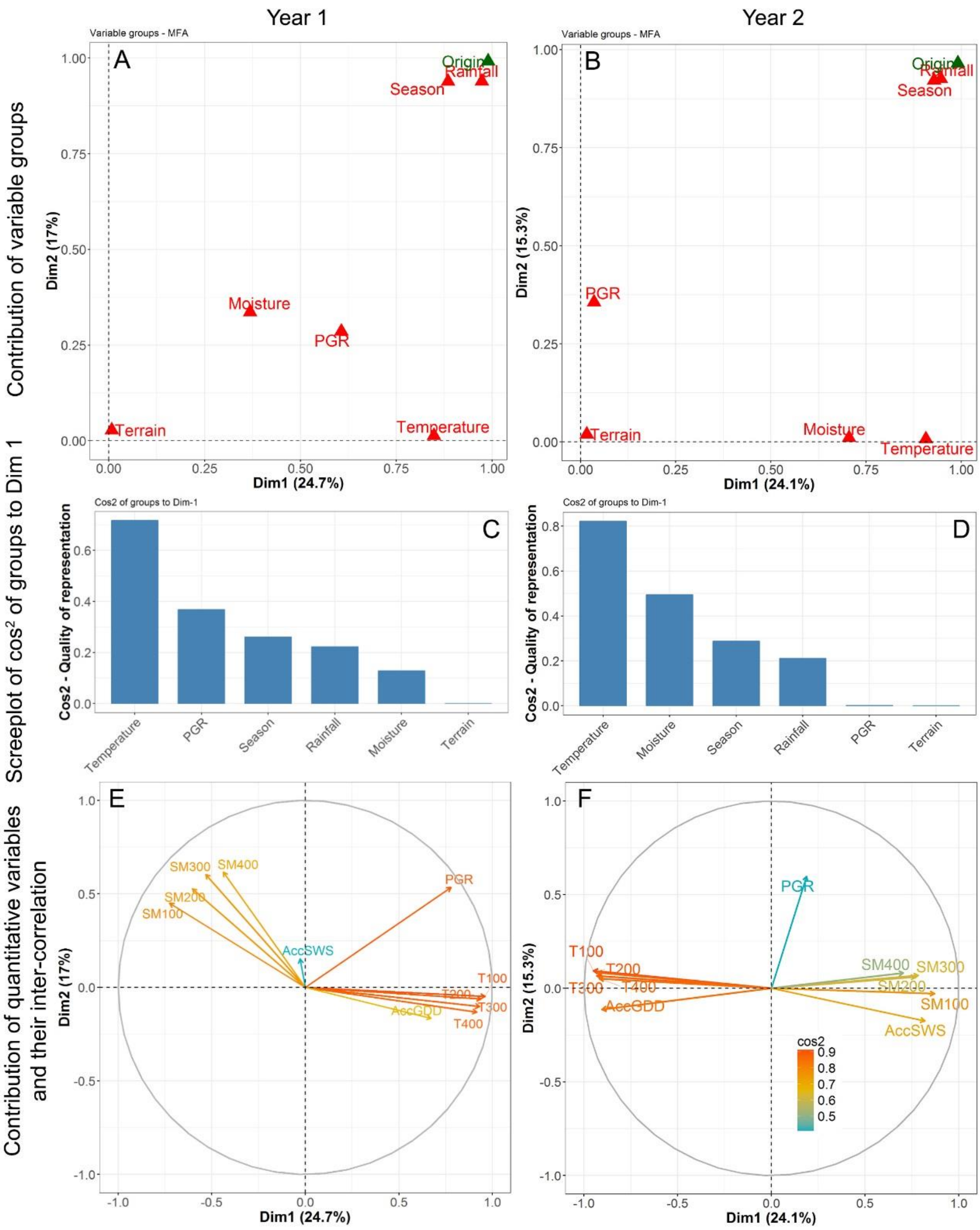

Figure 7.11 Graphical representation of MFA with the map of tables showing the individual groups and their position along the Dimension 1 and 2 axes (A and B). The bar plots depict the contributions of each variable group to the Dimensions 1 and 2 (C and D). The correlation circle of quantitative variables (coloured by cos²) illustrates the inter correlation between variables and Dimensions 1 and 2 (E and F).

By analysing the correlation circle of quantitative variables (Fig. 7.11 (E) and (F)), it is clear that *Moisture* and *Temperature* groups were highly related to each other (negative correlation) and strongly correlated with *Dim.1*. The *PGR* variable was more closely related (positive correlation) to *Temperature* in Year 1 than in Year 2. Within the *Moisture* groups, *SM100* was negatively correlated to *PGR* in Year 1. In contrast, *Moisture* was more closely correlated with *PGR* in Year 2 with an indication of positive correlation along the *Dim.1* axis.

On the basis of cos^2 values, the most important variables were the *SM100* and *T100*. Even though *AccSWS* did not show high importance, it was negatively correlated to *PGR* while *AccGDD* showed indication of positive correlation to *PGR* in Year 1. In Year 2, these relationships were found not to be significant showing near orthogonal positions between *PGR*, *AccSWS,* and *AccGDD*. The correlation of quantitative variables and their statistical significance (i.e. P value) are reported in Table 7.6 for *Dim.1* and *Dim.2* for both years. This represents the basis of the correlation circle map presented in Figure 7.11 (E) and Figure 7.11 (F).

Table 7.6 Significant correlations between quantitative variables and principle dimensions obtained by the multiple factor analysis for Year 1 and Year 2. If the P value is < 0.001 the relationship is considered significant (***).

	Year 1				***Year 2***			
Dimension	Variable	R^2	P value	Signific.	Variable	R^2	P value	Signific.
Dim.1	T100	0.96	0.000	***	SM100	0.87	0.000	***
	T200	0.94	0.000	***	AccSWS	0.82	0.000	***
	T300	0.93	0.000	***	SM300	0.78	0.000	***
	T400	0.92	0.000	***	SM200	0.77	0.000	***
	PGR	0.77	0.000	***	SM400	0.70	0.000	***
	AccGDD	0.67	0.000	***	AccGDD	-0.90	0.000	***
	AccSWS	-0.12	0.000	***	T400	-0.92	0.000	***
	SM400	-0.44	0.000	***	T200	-0.93	0.000	***
	SM300	-0.53	0.000	***	T300	-0.93	0.000	***
	SM200	-0.6	0.000	***	T100	-0.95	0.000	***
	SM100	-0.73	0.000	***				
Dim.2	PGR	0.53	0.000	***	PGR	0.60	0.000	***
	SM300	0.60	0.000	***				
	SM400	0.61	0.000	***				
	SM200	0.52	0.000	***				
	SM100	0.44	0.000	***				
	AccGDD	-0.34	0.000	***				

7.3.6.2 The effect of terrain-related qualitative variables

Figure 7.12 shows the individual observations with confidence ellipses and the centroids of selected qualitative variables, such as *Slo, Asp, LandScEl* and *Season* for Year 1 and Year 2 separately. The variables contained in the *Terrain* group were strongly correlated along the *Dim. 4* and *Dim.5* axes. Therefore, these axes were used to visualise the role of these groups to help understand the diversity of the observations induced by the tables within this group. Individuals, i.e. observations, with similar characteristics are displayed close to each other on the factor map (Fig. 7.12). The applied MFA highlighted general tendencies in the role of terrain attributes.

A number of the centroids in Figure 7.12 of the qualitative variables are close to the origin, i.e. *Asp* in Year 1, suggesting that its effect was not significant. In Year 2, the separation observed along the *Dim.5* axis suggested that the *Asp* variable was characterised with a slightly more dominant role than in Year 1. Individuals with horizontal aspects clearly differed from all the other aspects as indicated by higher coordinates along the *Dim.4* and *Dim.5* axes. In both years, the effect of *Slo* was more apparent than the influence of *Asp*. The centroids of the *Slo* and *LandScEl* categories were more widely distributed across the length of the *Dim.4* axis in Year 2 axis, *Dim.5* in Year 1, indicating that the variability found in these dimension was more closely associated with these variables. Steep and rolling slopes were placed at the low and high end of the *Dim.4* and *Dim.5* axes. This supports our previous findings regarding the considerable contribution of slope angle to the variability that can be related to the observed decreasing trend of PGR with increasing slope angle.

The position of the microsites in the landscape, represented by the *Landscape element (LandScEl*) variable, had a discriminative effect, suggesting a considerable contribution to the total annual variance, especially in both years. Upper slope, open slope (i.e. slope section between upper and lower slopes) and ridge landform elements (Weiss, 2001) were located at the lowest and highest positions of the range *LandScEl* along *Dim.5* in Year 1 and *Dim.4* in Year 2. The impact caused by *LandScEl* may be related to the varying soil types, soil moisture conditions, and nutrient content dependence on slope position, i.e. its distance from the hilltops and ridges.

The previously observed role of θ_v and T_s on pasture production was supported by the results of this analysis. In Year 1, θ_v was not a limiting factor and the relationship between θ_v and PGR was not significant. In contrast, the PGR was more related to T_s in Year 1. In Year 2, due to the long dry period (December 2017 – March 2018), the PGR was more closely correlated to the θ_v variables, confirming our earlier statement that θ_v availability limited pasture production during Year 2. However, T_s was still the most dominant factor explaining the highest amount of variability in PGR in Year 2.

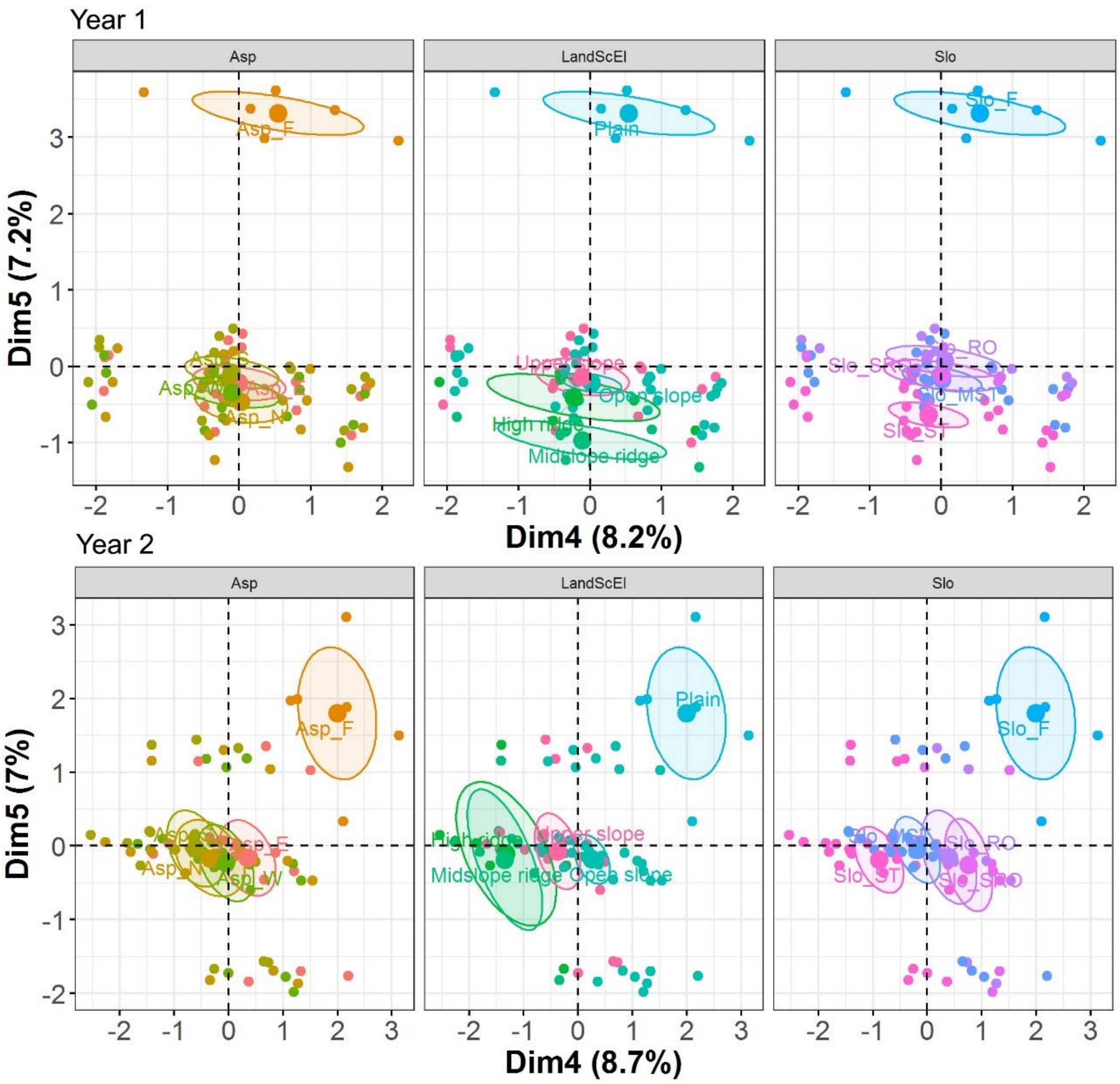

Figure 7.12 Ordination of the individual observations on factor maps and the projection of centroids with confidence ellipsoids calculated by MFA. The individuals were colour coded according to the variables of the *Terrain* group, i.e. aspect, landscape elements and slope angle classes for Year 1 and Year 2.

7.4 Summary and conclusions

The main terrain-related determinant of the spatial variability in PGR was the slope angle. A combination of visual interpretation and multivariate statistical methods (MFA) helped determine the effect of variable topography on the variation in pasture production. The application of MFA allowed analysis of multiple dataset tables containing both quantitative and qualitative variables. As a result, the observed PGR values were strongly associated with landscape elements, i.e. the geomorphological position of the microsites, while aspect played a less important role as physiographic factor. However, the importance of aspect changed with seasonal analysis and its influence on PGR variation increased with increasing ISR and accumulated heat, and thus with increasing T_s. Due to the complexity of the soil-water- plant-terrain-climate system, numerous factors contributed to the variation found in PGR values.

Seasonal temperatures and moisture regimes varied markedly between different micro-environments induced by topographical diversity. In terms of temperature, the highest yield (55-90 kg DM/ha/day) was observed at a mean T_a ranging between 13 and 16 °C, with T_s at 100 mm soil depth ranging between 15-19 °C. The influence of terrain was most significant during the late spring and summer periods when high ISR values were prevalent. The importance of terrain attributes in explaining pasture yield variability dropped during cold, wet seasons, and also when large precipitation events occurred in autumn.

The terrain attributes under consideration exerted significant influences on soil moisture values, which were observed to be less variable as the mean soil water content increased. An inverse relationship between mean soil moisture and slope angle was also observed, suggesting that microsites on steep slopes became drier earlier, held less water, and re-wetted later than gentle sloping land.

These hill country farms are iconic platforms of New Zealand's meat and wool industry, and will remain so for the foreseeable future. Although non-irrigated farming is unable to control many of the studied environmental factors, once the spatial and temporal effect of these factors on pasture production are quantified, farm management practices can be implemented to improve pasture production and profitability. However, accurate measurement of pasture growth is a challenging task in hill country due to the complex terrain, representative sampling, and access during adverse weather conditions in winter.

The conclusions drawn in this chapter may allow hill country pastoral farmers to use their lands to their higher potential especially in spring and autumn and these findings may contribute to the solution of currently relevant management issues to the farmer of today. Deeper knowledge on pasture growth is essential to effectively setting stocking rates and realistic production targets. It is also crucial for the driving of farming practices, such as feed budgeting, planning of calving, seasonal pasture management and drying off dates.

Chapter 8

GENERAL DISCUSSION AND CONCLUSIONS

This chapter begins with a brief summary of the key concepts and motivation behind the thesis. It also introduces the scopes that govern the discussion section. Afterwards, the chapter presents the main findings of this thesis relevant to each scope. The discussion places a strong focus on the implications and practical applications that can be considered based on the findings this study. Limitation and future perspectives are given for the various methods used in each chapter. The chapter ends with the list of main conclusions and recommendation for future work.

8 Chapter 8 - General Discussion and Conclusions

8.1 Brief summary of the key concepts

New Zealand's pastoral agriculture faces significant challenges, including the ever-increasing pressure on profit margins, the need for sustainable future farming and more efficient, enhanced productivity due to the growing food demand (FAO, 2011) while reducing the destructive impacts on the environment. Furthermore, the already evident changes in climate and its trends will have a strong impact on agriculture with an increasing likelihood of more frequent heat waves and more intense, extreme precipitation events (Howden et al., 2007, Pachauri et al., 2014). These issues have led to a strong conviction that the monitoring of yield affecting parameters is necessary to accomplish future production targets in non-irrigated hill country pastoral systems (Atzberger, 2013).

These challenges need to be addressed not only regionally but also at the smaller scales, ensuring a more coherent adaptation of pastoral farming systems to the potential changes. One of the key concepts that makes facing these challenges in agricultural productivity in New Zealand's hilly landscapes cumbersome is the presence of high spatiotemporal environmental variability. In hill country pastures, much variability exists at the farm and within the management units (i.e. paddocks) as well as at both macro- and micro-topographical levels that has been investigated by numerous studies (Harris et al., 1985, Scott et al., 1985, López et al., 2003, Chapman et al., 2009). Although, the farming related issues caused by these challenging factors and decision making in land management have been usually targeted by the "averaging approach" (Kerr, 2016).

Recent advancements in precision agriculture, computing technologies, machine learning supported statistical methods, data analytics, in situ sensor development, global positioning systems, digital representations of the terrain and satellite imagery opened up new vistas in supporting decisions (Schellberg et al., 2008). These innovative methods allow researchers, agronomists and farmers to address numerous problems imposed by the diverse, rugged environmental conditions. The latest digital technologies are reshaping the ways of describing complex landscapes and interrelations existing in this environment. The modern agricultural industry utilises advanced technical solutions that are able to provide more accurate, denser datasets, containing a high number of variables (for instance mass, volume, temperature, relative humidity, etc.) at higher spatial resolution than traditional approaches (Cox, 2002). However, several traditional, classic methods, such as ground-based soil moisture measurements, are still used for validation and performance assessment of the modern techniques and modelling approaches (De Lannoy et al., 2006).

Consequently, the joint use of some of these methods are progressively being employed to support farmers' decision making related to farming activities, land management and the use of optimal type and amount of inputs. Attempts have been made to quantify and incorporate the variability and the effects of environmental parameters on yield into fertiliser planning applications, pasture growth simulations and forecasts to achieve better returns. These aims led to the ultimate goal of the current hill country development programs focusing on the improvement of resilience and production efficiency while reducing the environmental pressure induced by fertiliser applications.

Agricultural production is highly dependent on soil moisture (θ_v, $m^3\ m^{-3}$), which is one of the primary environmental factors controlling pasture yield in hill country (Davis et al., 1994, Woodward et al., 2001, Bittelli, 2011). Soil water content is considered as a highly variable environmental parameter both spatially and temporally (Brocca et al., 2007) which is further complicated by the sloping nature of the land (Gillingham, 1973) resulting in significant variability in pasture growth.

These concepts guide the motivation behind this thesis that aims to contribute to the knowledge generated around the role, variability and potential monitoring methods of near surface and root-zone θ_v in hill country pastoral systems. In addition, the objectives included the development of a better understanding of the main driving factors of pasture production, such as soil temperature (T_s, °C) and terrain attributes in hilly landscapes for better parameterisation of pasture models. Based on the given background the discussion is structured around four main scopes, which are defined as follows:

1. The need for accurate θ_v and T_s monitoring at the farm scale and the importance of site-specific sensor calibration.
2. The quantification and description of the spatiotemporal behaviour of θ_v patterns on hilly terrain.
3. Extending the dimensions: moving from the point-scale θ_v observations to the spatial mapping over the research area.
4. The investigation and quantification of pasture growth driving factors on hilly terrains with a special focus on topographic attributes.

8.2 The study area

The study is conducted on a 2600 ha predominantly beef and sheep farm situated in the Wairarapa region, on the East Coast of the North Island (shown in Fig 3.1). In terms of terrain, rolling to steep hills dominate the landscape interspersed with some flat terraces (Fig. 8.1).

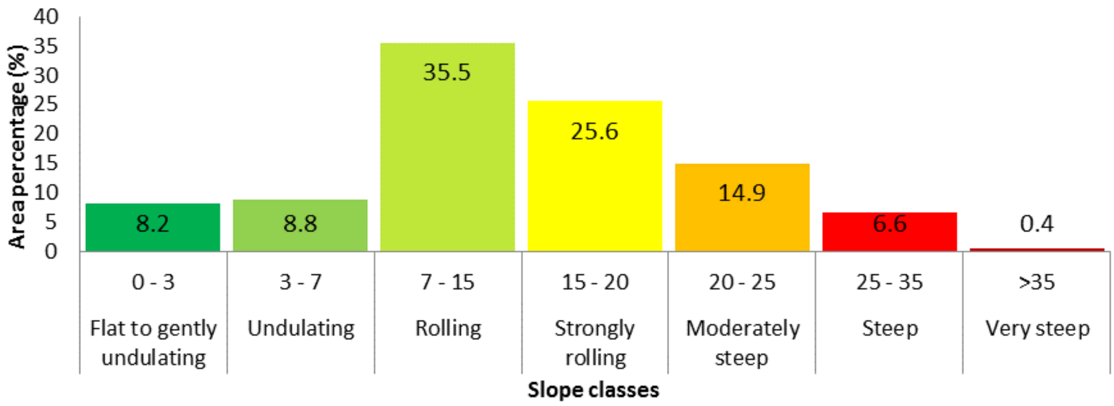

Figure 8.1 Slope category distribution of the Patitapu Station based on LUC (Lynn et al., 2009) slope categories derived from an 8m digital elevation model (LINZ, 2012).

The significant environmental heterogeneity was described early by Murray (1982), stating that "The Wairarapa region tends to extremes, too wet, too windy, too dry, too hot or too cold, all this between seasons and over longer years". Therefore, the chosen research area is a typical representation of the diverse, pastoral hill country environment closely satisfying the description of the hypothetical hill country farm by Kerr (2016). Hence, the farm, Patitapu Station, is considered suitable for carrying out this study and the research area selection is supported by the observed spatial and temporal variability in θ_v, T_s and pasture growth during the study.

8.3 The first scope – Accurate and representative monitoring of soil water and temperature in the rooting zone

Since the collection of θ_v information is highly challenging in hill country, the available datasets are rare, and the sensors are often not calibrated to the site-specific soil conditions. Therefore, the first scope of the study is to collect accurate multi-depth θ_v data with high temporal resolution from spatially distributed locations to represent the rugged terrain conditions. Here, the following research questions were raised:

a) How to collect θ_v from spatially distributed positions?

b) How to select the location of the microsites to represent typical hill country conditions?

c) What type of sensor and sensing depth would be ideal for the purpose of the study?

d) How to calibrate, assess and validate the sensor performance?

8.3.1 The WSN concept and deployment

The traditional θ_v determination methods or θ_v readings at a single location would not have been sufficient for the purpose of the study considering the amount and richness of the data needed. Hence, a smart environmental monitoring approach utilising WSN technology (Rawat et al., 2014) is chosen for systematic data collection. The deployed WSN implements a multihop (i.e. mesh topology) communication paradigm between sensor nodes, a relay node and the gateway, whereas a 3G mobile network provides data transmission between the gateway and a remote server. The near-real time data access is managed via a web interface operated by HALO Farm Systems, TAG I.T. Technologies Ltd (Hamilton, New Zealand).

The WSN deployment and the microsite localisation posed a series of three-dimensional problems concerning the highly variable terrain. Some of these were the natural and manmade objects obstructing line-of-sight visibility, the relatively long distances, and the vertical differences between microsites. The microsite localisation was guided by a two-step, conditional decision approach taking into account several GIS layers through a geomorphometrical analysis of the terrain. The candidate and the final microsite locations were selected by satisfying a set of criteria including topographical attributes, soil types, inter-visibility, vegetation type, farm management plans and equipment protection.

The microsites were equipped with AquaCheck multi-depth sensor probes (AquaCheck Soil Moisture Management, Durbanville, South Africa). The probes were set to collect T_s readings and capacitance-based θ_v data at 15-min intervals at four soil depths (70-130, 170-230, 270-330 and 370-430 mm). The sensor type was chosen considering the completely subsurface-based operation design, the robust, tube-like shape (meaning easier installation), as well as the broad compatibility with telemetry units. The length of the probe was determined by the hill country soil characteristics and the 400 mm probe covers most of the soil profile that is used for plant water uptake, which occurs down to at least 350 mm soil depth according to Bretherton et al. (2010).

The financial resources allowed the installation of 20 AquaCheck sensor probes. The probes were spatially distributed on flat surfaces and on sloping land classified based on five slope angle and four aspect categories following mostly the LUC (Lynn et al., 2009) slope classes (Fig. 8.1).

8.3.2 Data gaps and WSN operation

The WSN operated mostly perfectly during the study period, although we experienced some weaknesses regarding the power support at the gateway and certain sensor nodes, which was attributed to the recharging performance of the solar panels on specific aspects and slopes. As it is shown in Figure 8.2, the power issues occurred mainly in winter on flat areas (Site 2, 15 and 6), on a south-facing, moderately steep slope (Site 14) and a south-facing strongly rolling slope (Site 17). If the battery voltage decreased below the 2.8-3.2 V ranges, the battery was manually recharged and replaced since they were not able to recover from the flat stage.

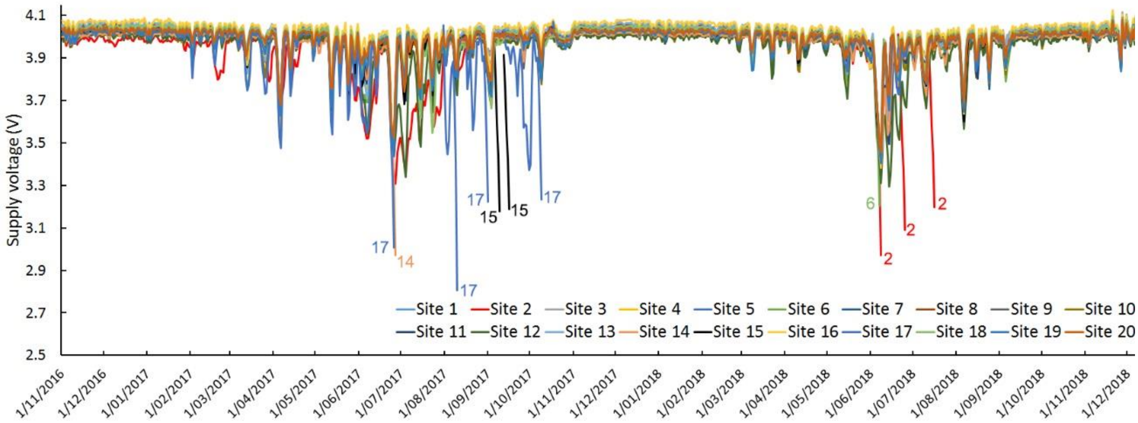

Figure 8.2 Temporal evolution of power supply (Volt) for each sensor node with drops in the wintertime at several microsites. The microsite IDs of the low performing locations are indicated. The lower end of the numbered lines indicates the moment when the battery went flat and the communication was lost temporarily.

The shadow produced by the hilly landscape, and the lower incoming solar radiation on south-facing aspect that may explain some of the reasons behind the insufficient charging. This could be avoided by shadow detection as part of the WSN planning procedure. On the other hand, due to the self-healing, flexible communication protocol, Site 6 often transmitted significantly larger amount of data packages, operating as a relay node, than the other microsites because of its central position close to the gateway (Fig. 3.12).

During the study, the communication layouts revealed that the sensor nodes, more specifically the radio units, were able to send data packages to other nodes situated much farther, than the recommended maximum radio range of 1.7 km. It was observed that some of the nodes located 3.5-4 km (in line-of-sight) distance from each other could establish data transmission. These findings should be taken into account if these devices are installed either on flat or hilly terrain, which may improve the usefulness, and versatility of these instruments in the future, and provide more flexibility for the microsite localisation.

8.3.3 Sensor calibration, performance and accuracy

The deployed WSN allows data collection in an automated manner with high temporal resolution that provides a more effective way to monitor θ_v, than other classic methods such as time domain reflectometry, gravimetric techniques, neutron probes (Brocca et al., 2007). The most essential components of the WSN is the connected AquaCheck sensor probe that utilises the capacitance technique (Topp et al., 1980) to measure the surrounding soil's apparent dielectric constant. The frequency domain based readings can be related to θ_v (Dean et al., 1987, Mittelbach et al., 2012).

Soil dielectric constant is mainly the function of θ_v, although other factors, such as soil bulk density, clay content and organic matter have been observed to have an influence on the dielectric properties (Topp et al., 1980, Roth et al., 1990). Due to the physical principles behind the capacitance technique (and other dielectric techniques), the sensor readings are sensitive to the above mentioned and several other soil properties that needs to be taken into account (Robinson et al., 1994, Mittelbach et al., 2012, Fares et al., 2016).

Therefore, the AquaCheck sensors require either laboratory- or field-based calibrations to convert the raw sensor readings to as accurate θ_v observations as possible. Most manufacturers provide calibration formulas for common and generic soil types, which may or may not achieve sufficient measurement accuracy for agronomic or scientific purposes. Thus, in this study, for the first time, the globally utilised, industry leading AquaCheck sensors and their factory calibrations were evaluated in New Zealand's hill country soils. Furthermore, new site-specific calibration formulas were generated and assessed.

The calibration and evaluation was based on thermo-gravimetric soil water measurements (Schmugge et al., 1980) taken between dry and wet soil water states by collecting 400 reference soil samples. The soil particle size analyses revealed that most of the probes are placed in silt loam or silty clay loam soils as per the USDA classification (USDA, 1999), although soil texture changed at several microsites along the soil profile and the clay content markedly increased with increasing soil depth (Fig. 8.3).

The same increasing trend occurred for bulk density in contrast to the organic matter that generally decreased moving downwards the soil profile. Concerning these trends in the soil properties, it is likely, that discrepancies would occur in sensor measurement accuracy varying not only between microsites but also vertically between shallow depths and the deeper soil sections.

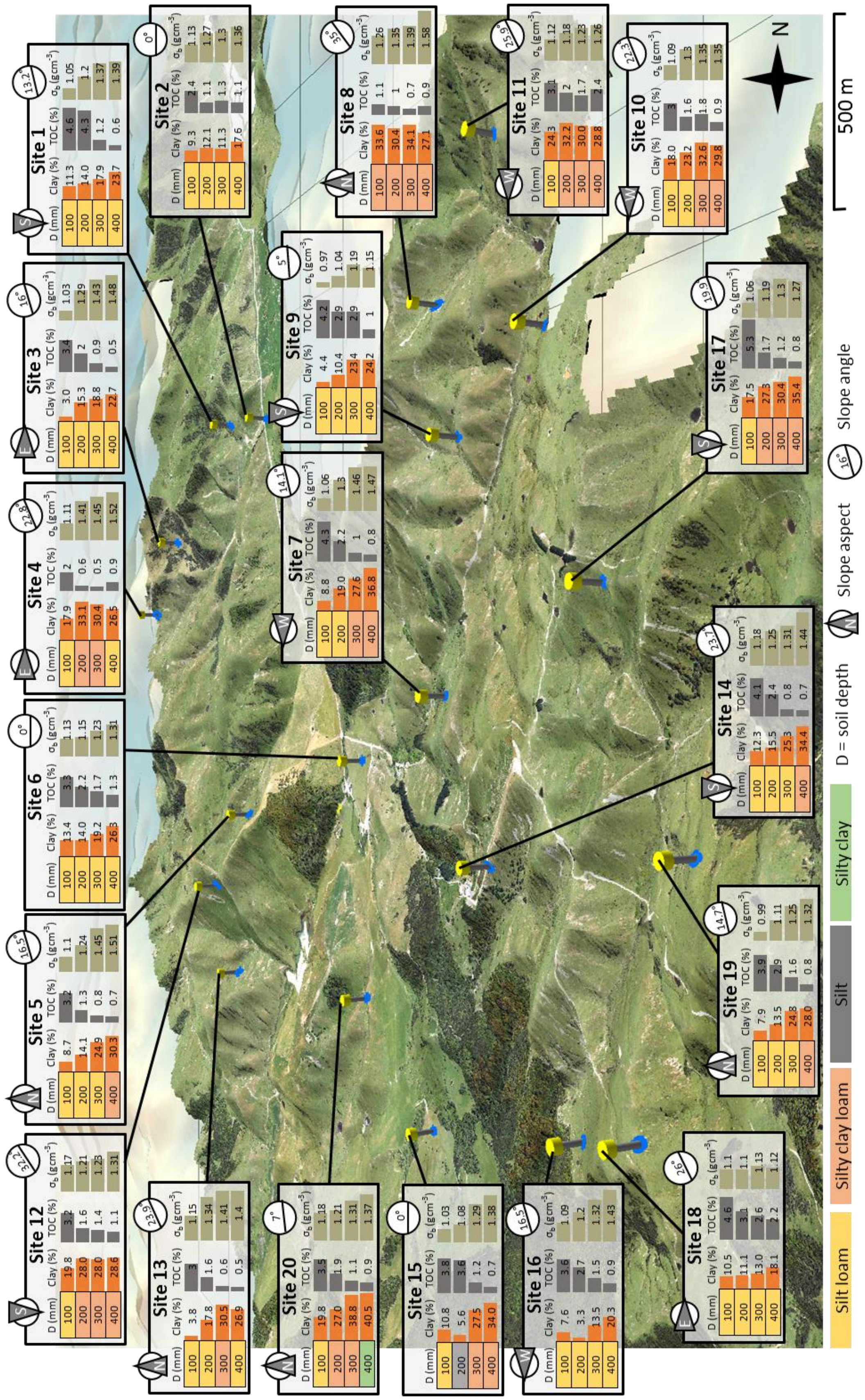

Figure 8.3 A 3D view of the Patitapu Station and the spatial distribution of microsites equipped with AquaCheck probes. Soil texture is indicated by colour codes based the USDA soil classification (USDA, 1999), the portion of clay content (%), total organic matter (TOC, %), bulk density (σ_b, gcm^{-3}) are shown for each microsite and each depth along with aspect and slope information.

To date, little is known about the performance of the standard, manufacturer provided AquaCheck calibration formulas despite the importance of these products in the worldwide soil moisture sensor market. These reasons triggered the idea of assessing the manufacturer-provided equations as compared to the reference θ_v as well as the generation of new site-specific calibration formulas. Nolz (2013) found that AquaCheck sensors within a single probe performed differently during a comparison to EnviroSCAN probes. Thus, the custom calibration process specific to the research area was carried out at three different levels, i.e. farm (Level 1), probe (Level 2) and individual sensors (Level 3), which can be reproduced in other regions depending on the available soil information and the required accuracy for the chosen utilisation.

Our results showed that the application of the factory-provided equation designed for silt loam soils markedly underestimated the true θ_v by a mean RMSE of 0.106 $m^3\,m^{-3}$. A root mean square difference of 0.163 $m^3\,m^{-3}$ was observed by Singh et al. (2018) when AquaCheck sensors were assessed in loamy soils against neutron probe measurements. These measurement errors were rather too large for most purposes, thus the need for soil-specific formulas for AquaCheck sensors was also confirmed by our findings.

A single, linear farm-specific calibration formula (Level 1) noticeably reduced the errors resulting in a mean RMSE of 0.039 $m^3\,m^{-3}$ and mean R^2 of 0.58. This improvement was outperformed by the probe- or microsite-specific (Level 2) calibration giving a mean RMSE of 0.029 $m^3\,m^{-3}$. The lowest mean RMSE, 0.19 $m^3\,m^{-3}$ was achieved by the sensor-specific (Level 3) calibration indicating a substantially increased sensor accuracy.

The error distribution was not uniform, overestimation occurred in dry conditions while underestimation tended to take place in wet soils. The effect of clay content, bulk density and organic matter on sensor accuracy was significant (P value < 0.001) that could be minimised by the sensor-specific calibration which considers the changes in soil properties with depth.

The created equations may be applicable in soils with similar characteristics, since the procedure can be employed by any users for either irrigation scheduling or informing farming on non-irrigated lands. Conserving freshwater on irrigated soils is one of the top concerns of our age that can be addressed by the application of soil-specific sensor calibrations and increased accuracy, thereby improving water use efficiency.

Based on the number of sensors, the achieved measurement accuracy and the identified soil properties, the established WSN satisfies the requirements of the International Soil Moisture Network (ISMN) (Dorigo et al., 2011a). In addition, the ISMN primarily accepts θ_v measurements that are made at least in the top soil layer (< 10 cm) and preferably also in the root zone (Dorigo et al., 2013). Depending on the decision from the project funders, the WSN may become part of the ISMN as the first data provider from New Zealand in the international context. The collected dataset should be applicable for validating products retrieved from land-surface models or remote sensing applications at various spatiotemporal scales.

From a New Zealand centred perspective, the WSN at Patitapu Station and similar networks can provide calibration or ground truth opportunities for emerging, primarily agriculture-focussed satellite missions in New Zealand, e.g. the one coordinated by the Centre for Space Science Technology in Alexandra (CSST, 2018). In the near future, one of the main goals of the upcoming projects is to develop high-resolution θ_v products for better irrigation management and more efficient pasture production in hill country as well as for hazard management and forestry applications.

The sensor accuracy could potentially be further improved by the collection of more reference samples. Another possibility is the application of a non-linear calibration approach that would consider the saturation effect on the top end of the θ_v levels. An investigation on the impact of other affecting factors, such as T_s, could result in slight improvements. Even though the AquaCheck probes are equipped with a built in T_s correction function, there has not been any assessment published about its performance to date.

8.4 The second scope - The quantification of spatiotemporal behaviour of soil moisture patterns in hill country

The soil moisture spatiotemporal variability is an important attribute for studying the variable infiltration and lateral redistribution rates, land - atmosphere interactions, hydrologic, geomorphic, biologic, pedogenic processes as well as for predicting soil profile wetting and drying between rainfall events (Western et al., 1998, da Silva et al., 2001, Western et al., 2004, Teuling and Troch, 2005, Bolten et al., 2010). In general, most predictions have to be provided along with their uncertainty, because the statistical error models utilise the quantified spatial characteristics as an essential parameter (Lakhankar et al., 2010). Soil moisture variability is known to be scale dependent and this makes its investigation crucial for numerous applications. The improvement of soil water sampling schemes (Warrick, 1980), the understanding of environmental aspects of the water cycle, and pasture growth patterns on sloping land from the small (sub-catchment) to the large scale (regional), rely on the parameters describing variability (Teuling and Troch, 2005, Hu et al., 2010).

In the global context, near-surface θ_v values are derived from advanced microwave remote sensing over large areas, although these products average the spatial heterogeneity in θ_v within the sensor footprint (Famiglietti et al., 1999, Brocca et al., 2009). An image pixel, i.e. the sensor footprint, might overlap a mixture of flat and hilly landscapes. Hence, the derived mean value masks the underlying θ_v spatial variation and not able to provide practically useful information for hill country farming. For instance, one of the globally available θ_v products generated by NASA and USDA provides surface θ_v using a data assimilation approach (Bolten et al., 2010) at approximately 27.8x21.1 km (0.25x0.25°) over the North Island (Fig. 8.4).

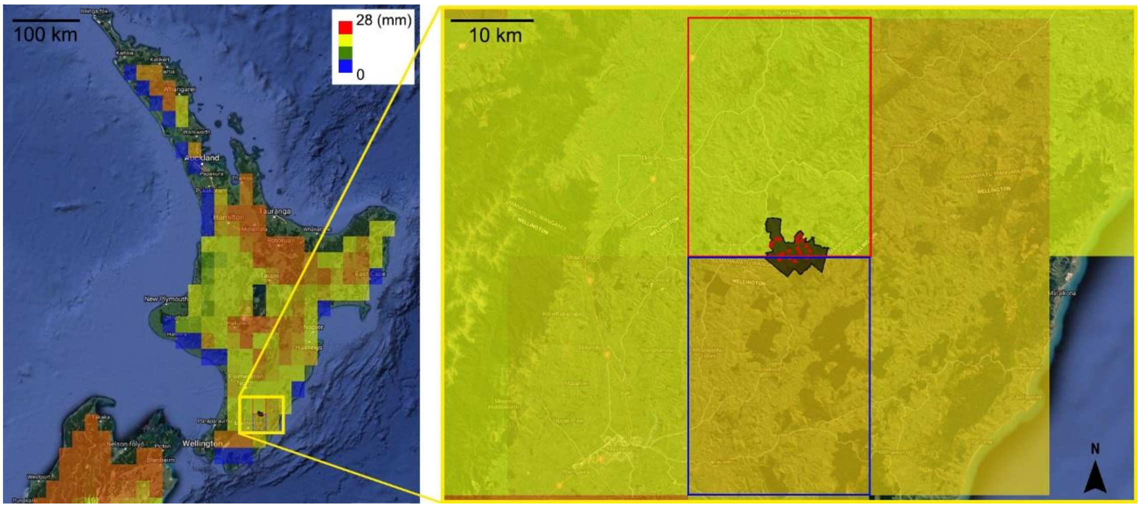

Figure 8.4 NASA-USDA global soil moisture data at 0.25x0.25° spatial resolution over the lower North Island of New Zealand. The Patitapu Station, the overlapping pixels and the sensor locations (red dots) are marked in the figure that was derived from Google Earth Engine showing surface soil moisture conditions on 18 April 2018.

Little is known about the spatiotemporal behaviour of θ_v in complex landscapes (Molina et al., 2014) and this is particularly true in New Zealand. To our knowledge, this is the first study to document the θ_v variability over the extent scale of approximately 14 km^2 at the Patitapu Station, using high temporal resolution in situ measurements. The collection of a temporally dense dataset was made possible due to the advances of the deployed WSN.

It is noted that the number of sensors used in this study would not be sufficient to completely characterise the variation within such a large pixel (see Fig 8.4). Although, the conducted analysis can give a better parameterisation of the spatiotemporal behaviour of θ_v at a smaller scale than studies of the past decades. Due to the high number of implications of this type of multi-depth θ_v datasets, the statistical properties of the observed θ_v quantities are fundamental to characterise the θ_v patterns within the rooting zone (da Silva et al., 2001, Brocca et al., 2007).

The spatial resolution of global and regional θ_v products is generally increasing; thereby future missions with improved resolution will potentially be able to use the Patitapu WSN or a similarly designed monitoring network to estimate variation within a pixel or validate the mean value with better accuracy.

The purpose of Chapter 5 is to describe a small scale field investigation of θ_v variability through the application of various statistical techniques based on point measurements, which have the advantage of easier interpretation than remotely sensed data (Western et al., 1998). This approach raised questions within the second scope of this thesis, addressed by the items below:

a) Descriptive statistics of the collected soil moisture data
b) Soil moisture spatiotemporal variability and temporal stability at multiple depths
c) Finding the representing microsite and the spatial mean of the area
d) Site-specific temporal soil moisture characteristics and trends along the root zone

8.4.1 Descriptive statistics and data distribution

This part of the study aimed to analyse the θ_v data collected at the 20 microsites over four depths, to determine its statistical properties and investigate its spatial structure as well as its relation to topography. At the Patitapu Station, the annual temporal θ_v distribution can be characterised with negative skewness and with non-normality that agrees with the findings of Brocca et al. (2007) and Famiglietti et al. (1999). These authors carryed out studies on silty loam soils and defined non-normal distribution on terrains with significant relief. The temporal variance of θ_v and its range decreased with increasing depth. The 100- and 200-mm soil depths demonstrated the greatest values of standard deviation (SD) as expected due to the higher sensitivity to the changes in the climatic parameters and meteorological forcing. Firstly, θ_v data distribution around the mean value is important for remote sensing applications to quantify within pixel variability (Charpentier and Groffman, 1992). Secondly, persistent wet spots or extremely dry areas might introduce uncertainties e.g. into pasture growth simulations or hydrological models.

By the investigation of the Kernel density curves, characteristic peaks were identified at θ_v of 0.35 $m^3 m^{-3}$ at 200 mm depth and 0.42 $m^3 m^{-3}$ at 400 mm depth that were repeated annually (during the 2-year study period) indicating the persistence of higher temporal stability in the θ_v distribution deeper in the soil profile.

8.4.2 Time-stability analysis to identify the most representative microsite

In practice, the determination of the spatial θ_v mean in the root zone and the identification of the most representative monitoring locations are essential for soil water management decisions, particularly in watersheds situated on rugged terrain (Hu et al., 2010, Gao et al., 2011a).

Furthermore, this analysis is useful for the evaluation of low spatial resolution remote sensing products as a pixel is represented by a derived mean θ_v value for the overlapping area that can be complex. By the help of time-stability analysis, the representative microsites can be chosen more efficiently at various scales if a new WSN deployment is the primary objective.

Utilising the various statistical measures introduced by Vachaud et al. (1985) such as the mean relative difference (MRD) and its standard deviation (SDRD) the number of monitoring sites necessary to describe the θ_v characteristics of a given area can be reduced (Vachaud et al., 1985, Wagner et al., 2008). Our results indicate that the spatial field mean θ_v can be obtained with an R^2 of 0.94 and an RMSE of 0.021 $m^3 m^{-3}$ using a single representative microsite on north-facing aspect, situated on a moderately steep (23.9°) open slope. It is assumed; that the simultaneous utilisation of data from the four most representative microsites, i.e. Site 6, Site 10, Site 12 and Site 13 would be optimal to describe the mean θ_v in these mixed landscapes. This is because they represent flat areas, west-facing open slopes, north-facing mid-slopes and south-facing steep slopes (see Fig. 5.2 in Chapter 5).

8.4.3 Time stability of soil moisture spatial patterns

Cumulative probability density functions and frequency distribution analysis demonstrated that topographical attributes exert their effect on the θ_v temporal stability. Site 1, Site 8, Site 15 and Site 6 could keep their rank between two extreme θ_v levels and various slope angle and aspect classes tended to move along the cumulative probability curve, suggesting the influence of the landscape. The examination of Spearman's rank correlation coefficients (r_s) and their significance confirmed that θ_v spatial patterns between extremely dry and wet conditions were not maintained resulting in insignificant relationships with low r_s of 0.24-0.39. However, two wet days (in different years) with θ_v levels at or above field capacity were significantly and highly correlated (r_s= 0.91, P value < 0.001). θ_v patterns on two dry days (in different years) behaved analogously showing strong correlation (r_s= 0.88, P value < 0.001). The θ_v spatial patterns were significantly correlated (P value < 0.001) with relatively high r_s values in the drying out phase and not so much during rewetting, which was also found by Kachanoski and Jong (1988). Furthermore, in hill country, the relationship became weaker by time within one sub-period.

The outcome of the time stability analysis also suggested that the θ_v spatial distribution was stable in dry and wet conditions and it can be preserved from one timestamp to another to a certain extent depending on the stage of θ_v change. As the spatial organisation of θ_v exhibits temporal stability, it is possible to describe an area through carefully selected, limited number of microsites, thereby reducing the cost of data collection and field campaigns. Moreover, since the spatial patterns are time dependent, the defined θ_v spatial distribution and its temporal stability could be applied in management as they also reflect the influence of soil properties and landscape attributes (da Silva et al., 2001).

8.4.4 Temporal dynamics of spatial field mean and its variance

The statistical analysis of spatiotemporal dynamics of the field mean θ_v included the calculation of absolute variability, i.e. SD, and relative variability, i.e. coefficient of variation (CV). The daily CV showed the highest values during the dry seasons of the study period. Thus, the spatial variability under this climate and humid climates in general, was greater when the soils are dry. In general, the spatial SD and CV decrease with increasing wetness conditions and the rewetting (ascending) stages show the highest SD values in the top layer. The CV tend to drop once the mean θ_v levels have reached 0.35 $m^3\,m^{-3}$ and CV values decline to the minimum at 0.45 $m^3\,m^{-3}$. The temporal difference in SD is noticeable but not that prominent in the deeper layers and the variance of θ_v decreases with soil depth.

8.4.5 Relationship between spatial soil moisture mean and spatial variance

Relating SD, i.e. absolute variability and CV, i.e. relative variability to the spatial mean θ_v using scatterplots and regression is a common procedure to characterise variability and the influence of wetness conditions (Bell et al., 1980, Brocca et al., 2007, Famiglietti et al., 2008b, Molina et al., 2014). There is no consensus in the literature on the relationship between mean θ_v, SD and CV due to the scale dependency and the numerous influencing factors. Consequently, the role of vegetation, soil properties, wetness conditions, topographical attributes and climatic variables are not fully understood, and its characterisation requires research at various scales.

In this study, both increasing and decreasing variability (expressed by SD and CV) with increasing mean θ_v occured depending on the soil wetness. The variability showed dependence on the sub-periods and seasons, i.e. whether the land was dry, drying out, rewetting or wet, meaning that variance was non-consistent in these landscapes. This indicates that the role and importance of controlling factors on θ_v variation change with time. During dry conditions, the influence of terrain attributes (i.e. aspect, slope angle, elevation, etc.) take over the control on θ_v variation while the soil properties (i.e. soil texture, especially clay content) play more important role on the θ_v patterns (Famiglietti et al., 1998, Harter and Zhang, 1999, Choi et al., 2007).

8.4.6 Site-specific temporal soil moisture variability

The microsite-specific spatiotemporal analysis helps to identify the wettest and driest microsites and reveal the different features of the shallower and deeper soil layers. If all depths were averaged, the wettest location was situated on a west-facing rolling open slope at Site 7 and the driest position was a north-facing, steep midslope ridge at Site 8. The second wettest location was Site 15 located on a flat paddock and the third wettest was Site 1 installed on an upper part of a south-facing, rolling slope. The second driest topographic position was at Site 17, a south-facing strongly rolling surface, located on a high ridge landscape element, while the third driest location was Site 9 installed on an undulating slope near a high ridge.

The range of θ_v measurements were the largest in the 100 mm soil depth, while the deeper sections of the soil profile showed a narrower θ_v range indicating less variability and temporally more stable soil water contents with increasing soil depth. Site 4, an east-facing moderately steep location with silt loam and silty clay loam soils represented the lowest θ_v ranges in time all over the four depths. In contrast, the widest temporal θ_v range varied among depths and microsites, although the 100 mm soil depth at an east-facing steep slope (Site 18) showed the largest difference between minimum and maximum θ_v.

8.4.7 Future work

As a recommendation for further work, the daily averaged θ_v data could be subjected to geospatial and geostatistical analysis that are a frequently used techniques to characterise θ_v spatial organisation and spatial autocorrelation (Western and Blöschl, 1999, Brocca et al., 2007, Famiglietti et al., 2008b, Molina et al., 2014). Although, the fact, that the variogram-based analysis defines the variance as a function of distance between microsites might pose some issues due to the non-grid-based distribution of the microsites. The highly varied topography within two microsites would question the usefulness of this kind of analysis approach at the small scale in hill country.

Furthermore, the temporally dense dataset could be used to estimate the shortest or the ideal sampling interval to describe the temporal trends, which could reduce the amount of data and optimise the sampling scheme for different seasons or drying and recharging sub-periods as also suggested by Molina et al. (2014).

8.5 The third scope - Extending the dimensions: moving from the point-scale soil moisture observations to the spatial mapping

Remote sensing applications with frequent revisit time are broadly and increasingly applied in agriculture for the monitoring of growth patterns and temporally changing variables that influence yield (i.e. θ_v, T_s, etc.) (Atzberger, 2013). θ_v is a crucial parameter in agricultural production and it is part of many environmental systems (Seneviratne et al., 2010). Therefore, the mapping of its distribution on a spatial and temporal basis is subject to research globally at various scales. Remote sensing has the potential to highlight the θ_v patterns dominantly caused by the variability in soil properties, land cover, climate and the terrain (Kong et al., 2011). However, the generation of highly accurate, high- to medium-resolution θ_v products on an operational manner, particularly over vegetated areas has been posing challenges over the last four decades.

In New Zealand, the frequent cloud cover further complicates the generation of systematic remotely sensed θ_v products. Therefore, the use of active and passive microwave-based satellite products would be preferred to create θ_v maps in all weather conditions. Although, the currently applied methods and missions (e.g. SMAP and SMOS) have some considerable limitations, such as the complex signal interpretation and low spatial resolution (approx. 3x3 km and 40x40 km depending on the latitude) that is far too coarse for addressing the sub-farm variability. In contrast, multi-spectral Earth observation satellites are able to provide θ_v estimates at higher resolution, although the image acquisition is cloud dependent.

The present study aims to explore the utilisation of an emerging synergy-based technique for θ_v mapping. The proposed method takes advantage of the combination of radar and optical satellite images, the digital representation of the terrain, GIS-based platforms, and a modern ensemble learning statistical method (i.e. the Random Forest).

Despite the importance of θ_v data in pasture production models, current algorithms use low-resolution estimates of θ_v input into their water balance equations. As a result, the currently used simulations do not yet adequately represent the spatial and temporal variability of θ_v in hill country. The proposed approach can be potentially used to provide θ_v information for more intelligent pastoral farming at an improved spatial resolution (i.e. paddock scale, ideally under 40x40 m) that is to be of actual use to the farmer and pasture yield predictions.

In addition, Chapter 6 also aims to contribute to the better understanding of the issues emerging around the θ_v retrieval from satellite images on hilly terrain. Moreover, it evaluates the accuracy of the generated spatial θ_v predictions near the surface by the aid of calibrated, ground-based measurements. These issues, the need for θ_v monitoring and the introduced advantages of remote sensing raised the following points:

a) Synergetic use of various satellite products to increase temporal coverage of θ_v maps
b) Usage of a cloud-based platform for pre-processed, remotely sensed data access
c) Investigation of SAR data and θ_v relationship over pastoral surfaces and complex terrain
d) Spatial prediction of a medium resolution θ_v product at various wetness conditions

e) Testing the prediction accuracy and validating the spatial θ_v maps

8.5.1 Obtaining remote sensing data via Google Earth Engine

Obtaining and downloading remote sensing imagery captured by various satellites for a nearly two-year period is a time-consuming task. It requires a large amount of storage and computing power for executing the several pre-processing steps on varying data formats. Free software environments and toolboxes are made available for the pre-processing, such as the SNAP (SNAP, 2018) but they require the building of processing chains and large memory capacity as well as processor performance. Moreover, the data preparation procedure may vary slightly depending on the products. Therefore, to generate a consistent and extendable dataset, the Google Earth Engine (GEE), a cloud-based, geospatial computing platform was utilised in this study (Gorelick et al., 2017). Data extraction through GEE and its web-based programming interface can produce systematic and consistent products from pre-processed images without downloading the images to the personal computer (Fig. 8.5). Thus, GEE allows users to visualize, manipulate and analyse a large number of satellite scenes rapidly. In this study, pixel-based data extraction at the microsites was conducted from Sentinel-1, Sentinel-2, Landsat 7 and Landsat 8 image collections via the GEE platform.

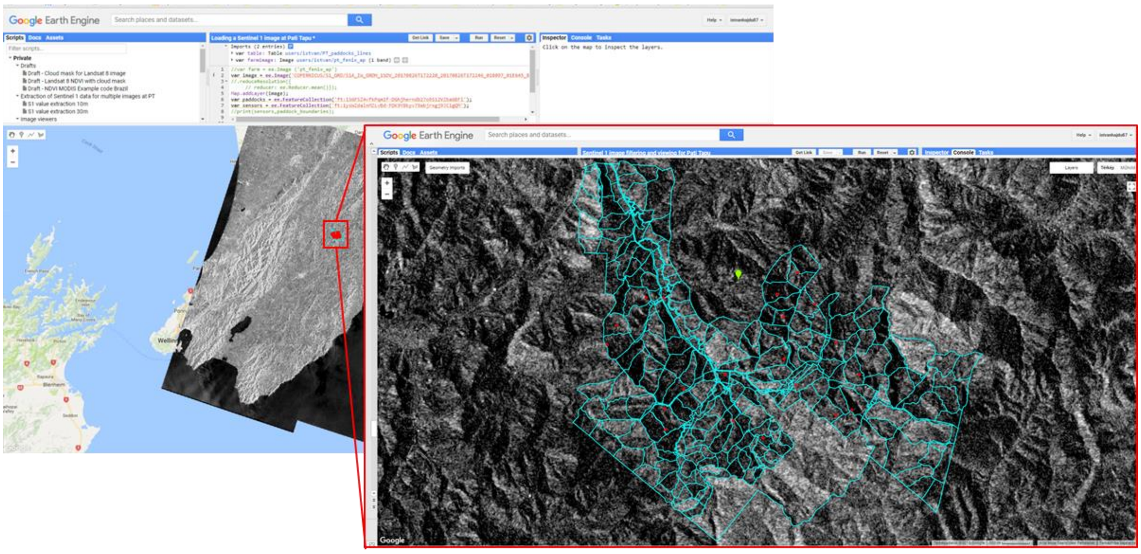

Figure 8.5 Components of Google Earth Engine programming interface and a 10x10 m resolution Sentinel-1 SAR image (26/08/2017) over the Patitapu Station with fence lines and microsites (red dots).

8.5.2 Soil moisture retrieval from radar images – relevant issues over vegetated surface

The linear nature of the relationship between the radar backscatter coefficient (σ^0) and θ_v over bare soil surfaces has been observed by many studies (Le Hégarat-Mascle et al., 2002, Zribi et al., 2005, Le Morvan et al., 2008). High θ_v content results in high backscattered energy towards the sensor and low θ_v conditions cause low σ^0 values, thus reflecting more energy away from the sensor (Dean et al., 1987). However, the most pronounced problems with radar-based θ_v retrieval is the complexity of the backscattering mechanisms from the targeted surface with vegetation cover, which is even more enhanced over hilly terrains (Pasolli et al., 2015). Over vegetation, the σ^0 represents the total backscattered energy from the vegetation, the soil and the interaction occurring between these two components within a resolution cell, determining its electromagnetic response. Additionally, the heterogeneous terrain, the sensor parameters (i.e. frequency, polarisation, and incidence angle), the amount of vegetation, its geometric and structural features and the soil surface characteristics (i.e. roughness, dielectric properties, soil properties) further complicate the interaction processes and its interpretation. Consequently, these factors need to be accounted for to reduce their effects on σ^0 (Barrett et al., 2009, Petropoulos et al., 2015) and to disaggregate the impact of the θ_v.

Due to the multiple contribution of these factors, a so-called variable equifinality problem exists, meaning that various combinations of target characteristics might result in very similar σ^0 values (Beven and Freer, 2001). Hence, the θ_v retrieval from radar images is considered as an ill-posed problem (Ali et al., 2015). One of the other shortcomings of the satellite-derived θ_v products is the shallow effective depth (0-5 cm) that is dependent on the SAR operational frequency, the wetness conditions, the vegetation characteristics and soil physical properties (Barrett et al., 2009). C-band radars, such as Sentinel-1 has a penetration depth of approximately 2-5 cm in dry conditions and only a couple of cm in wet conditions (Bruckler et al., 1988). Longer wavelengths, such as L-band would be optimal for θ_v retrieval with low incidence angles (Ulaby et al., 1986c).

Surface roughness is one of the major determinants of the signal response, which cannot be differentiated easily and there are no simple procedures to account for its effect (Altese et al., 1996, Barrett et al., 2009). Generally, radar sensitivity to surface roughness increases with increasing incidence angle and increasing degree of roughness results in elevated σ^0. Although, its effect is dependent on the wavelength (Ulaby and Batlivala, 1976, Ulaby et al., 1982b, Sano et al., 1998, Wagner et al., 2007, Baghdadi and Zribi, 2016).

8.5.3 Synergetic use of satellite data and terrain attributes

Several theoretical and physical models have been used to retrieve θ_v. In this study, the potential application of an empirical technique was investigated. The presented work used a time series of in situ θ_v measurements recorded by the Patitapu WSN as reference and training data. Various variables were obtained through a proper pixel-based extraction from satellite images and DSM derived GIS layers at the microsites. The ground-based θ_v measurements, the corresponding variables and derived indices were fed into the Random Forest (RF) algorithm for the generation of an optimised θ_v prediction model.

An image collection of 153 scenes was created from the Sentinel-1 SAR, C-band imagery to utilise the weather independent, systematic and temporally dense features of the σ^0 over the pastoral land. To address the degree of vegetation coverage and its spatiotemporal pattern, an adjusted NDVI was developed, since it is a broadly used indicator of phenological variations and biomass changes (Sun et al., 2016). To increase the temporal coverage and to create a daily time series of adjusted NDVI at 20x20 m resolution over the research area, a total of 77 Sentinel-2, Landsat 7 and Landsat 8 multi spectral images were used for data extraction. The geospatial layers, i.e. slope angle, aspect, SAGA topographic wetness index, topographic position index and terrain ruggedness indices, were derived from a high-resolution DSM to represent some of the hydrological metrics, terrain attributes and surface ruggedness.

8.5.4 Results and accuracy

The Landsat 7 and Landsat 8 NDVI values were adjusted to the Sentinel-2 NDVI, to generate more cloud free images over the study area, and to use the 20x20 m pixel size of Sentinel-2 images in the modelling. Strong linear relationship was observed between Landsat 7 and Sentinel-2 NDVI (0.85 R^2) as well as between Landsat 8 and Sentinel-2 NDVI (0.89 R^2) making them comparable and complementary observations.

During the examination of σ^0 sensitivity to near surface θ_v, VV polarisation showed more promising correlations than VH. The VV σ^0 at 20x20 m spatial resolution demonstrates adjusted R^2 of 0-0.5 for ascending orbits and adjusted R^2 of -0.13-0.8 for descending orbits. This indicated that lower incidence angles of the descending orbit can result in stronger relationships over pasture cover. At the microsites located on sensor-facing land surfaces, i.e. east and north aspects, tended to demonstrate higher R^2 values, while flat microsites and microsites facing away from the SAR sensor, i.e. south- and west-facing aspects show lower R^2. This could suggest that the relation between the terrain and the sensing parameters affect the θ_v sensitivity despite of the terrain correction steps taken during pre-processing. GEE uses the Shuttle *Radar* Topography Mission's 30x30 m resolution DEM for correction, which might be too low resolution for the rugged hill country landscapes. This could be potentially improved by applying a higher resolution elevation product generated for the specific region under investigation.

The examination of the temporal trends between normalised σ^0, NDVI, daily total rainfall and daily θ_v revealed that the θ_v sensitivity of the σ^0 likely to decrease with increasing NDVI in agreement with previous studies (Zribi and Dechambre, 2003, Baghdadi et al., 2008, Gao et al., 2017). C-band signal can penetrate vegetation better if the vegetation is drier, which usually means lower NDVI values. This partly explains the noticeable response of σ^0 to the dry conditions in agreement with Brown et al. (1992). It can be concluded that over grass cover, linearly relating near surface θ_v and σ^0 does not provide reliable correlation strength at the targeted spatial resolution. Although, the utilisation of a homogenous image collection from the descending orbit type could improve the correlation with reduced temporal resolution.

8.5.5 Random Forest modelling

To investigate the potential use of different machine learning techniques, several algorithms, such as Random Forest (RF), Cubist (*cubist*), Bagged Cart (*bagging*), Cart (*cart*), Generalised Boosted modelling (*gbm*), k-Nearest Neighbours (knn), Lasso and Elastic-Net Regularized Generalized Linear Models (*glmnet*), Support Vector Machine (*svm*) and Logistic regression (*logistic*) were executed on the reference dataset with default hyperparameters (Fig. 8.6).

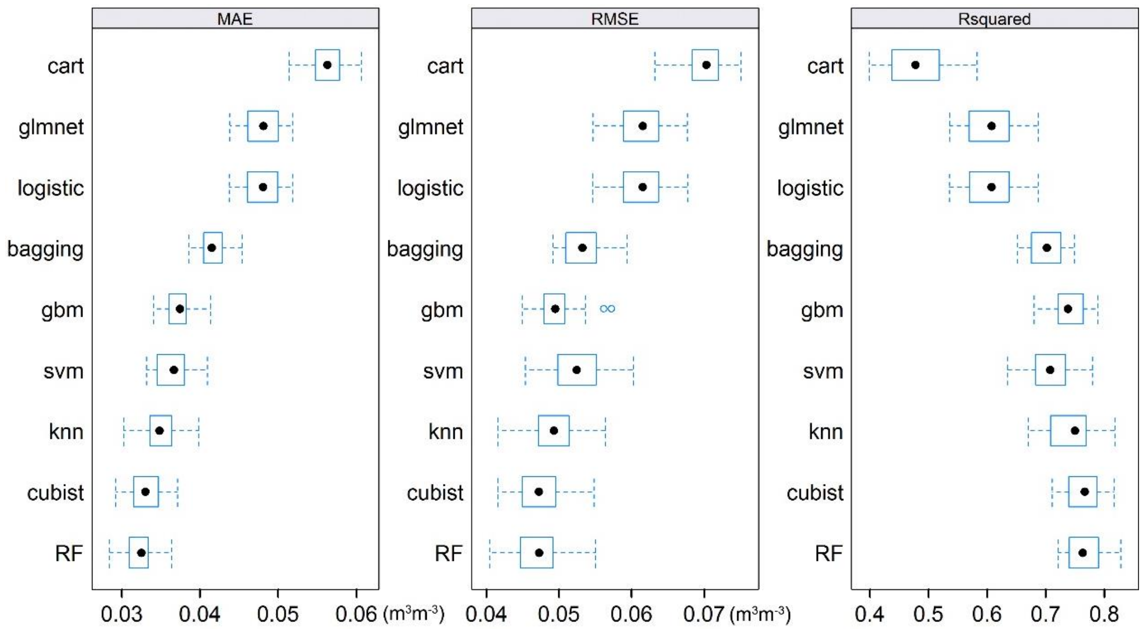

Figure 8.6 Comparisons between several machine learning algorithms for soil moisture modelling using the *caret* R package (Kuhn, 2008) and default hyperparameters.

The RF model achieved the best results concerning RMSE, MAE and R^2 as the accuracy and correlation measures, therefore the RF approach was chosen for this study. The final RF model (hyperparameters: *mtry* = 4, *ntree* = 300) was able to predict near-surface θ_v with an average accuracy of 0.047 $m^3\,m^{-3}$ and R^2 of 0.76 retrieved from the repeated cross-validation process. The RF performed generally well regardless of which section of the data population was used for model training. The most important variables were the seasonality, NDVI and slope angle while the σ^0 data provided less contribution to the prediction than it was expected. Without the addition of seasons, the importance rank of the variables changes and σ^0 represented a highly important position along with NDVI in the θ_v prediction, although it resulted in a significant drop in the percentage of explained variation (40%). The development of RF models for each season could be a potential way to increase the accuracy and the amount of explained variation.

Using only the test dataset (randomly selected 25 % of the observations), θ_v predictions agreed well with the observed θ_v values at the point scale. An RMSE of 0.046 $m^3 m^{-3}$ and 0.078 R^2 supported the statistically significant (P value < 0.001) good fit and indicated that the modelling accuracy of RF algorithm was satisfactory. During winter and summer, i.e., in the wet and dry seasons the modelled θ_v values closely followed the observed θ_v, while significant errors (0.06-0.16 $m^3 m^{-3}$) occurred during drying and rewetting periods. Typically, overestimations were found during the drying out period and underestimations took place in the rewetting stage, which might be related to the high spatial variability of θ_v in these seasons observed in Chapter 5. Moreover, these errors can be linked to the increased pasture herbage accumulation confirmed by the pasture growth trends and the elevated NDVI values. It is likely that enhanced plant growth resulted in increased vegetation water content, and the higher amount of fresh biomass due to the strong spring and autumn tillering could lead to elevated σ^0, thus higher modelled θ_v responses.

Concerning the spatial modelling performance with a reduced training dataset (15 microsites) and 5 microsites used for independent validation, the RF model was still able to estimate θ_v at the same accuracy level. The correlation between modelled and observed θ_v varied between 0.69-0.94 with a mean of 0.77 R^2 and mean RMSE of 0.048 $m^3 m^{-3}$.

The predicted spatial θ_v maps reflected the expected θ_v patterns at the macro-scale. Valley bottoms and flat surfaces were dominantly represented by higher θ_v content while ridges and hilltops showed lower θ_v and dry conditions could be observed on steep slopes. The effect of aspect was noticeable giving lower θ_v on north-facing slopes (in dry seasons). Additionally, the general temporal trend was closely followed by the mean θ_v values calculated for the eight predicted maps individually.

It can be concluded, that the RF algorithm is a powerful predictor of near-surface θ_v using environmental covariates and remote sensing data, and it can produce outputs with acceptable accuracy for most agriculture related applications. Data fusion and long time series carries the strength of machine learning, and the flexible features of non-parametric techniques allow the extension of the number of variables. Due to the prime importance of water management issues around the world and the increasing role of agricultural yield monitoring, more and more satellite missions are being lunched carrying microwave-based sensors, leading towards the "golden age" of θ_v research. The quality of θ_v predictions can be improved by the combination of data from various instruments operating in a range of domains of the electromagnetic spectrum as it was also stated by Rodríguez-Fernández et al. (2019).

8.5.6 Limitations

The RF algorithm may suggest a "black box" approach for a researcher, although the models can be described by complex mathematical functions. In case of regression, RF does not predict beyond the range in the training data therefore a longer study period, covering extremely dry conditions would be required for wider θ_v range in the training dataset. Additionally, the generated RF model is only valid on the area used for training. Despite of the considerable progress made in θ_v retrieval in the last few decades, there is no universal technique for generalised application over various surfaces at various spatial scales. Increasing the amount of training data has the potential for model improvement. Other machine learning methods could be run on the existing dataset, such as the artificial neural networks, which is one of the earliest statistical learning algorithms that can outperform classic regression techniques.

Another direction could be the prediction of biomass from radar imagery through the non-parametric RF method as it was also suggested by Ali et al. (2015). One of the concerns in satellite-based θ_v retrieval is the shallow penetration depth in case of SAR (0-5 cm). This study used measurements from the soil depth of 7-13 cm as the probes must be protected from farming activates and stock but several studies compared satellite-based water content estimations to 10 cm or soil profile measurements (Matthias et al., 2004).

8.5.7 Implications of near surface soil moisture spatial maps in New Zealand

It is assumed that a more advanced version of this machine learning approach would only be useful for refining existing water balance models rather than producing an independent θ_v product. Another limiting factor is the latency of the satellite image products as timing can be crucial for farmers. This is a critical issue in globally available remotely sensed θ_v data due to the relatively long computing and delivery time (i.e. days).

To model the root zone θ_v from the spatial near surface estimations, an additional processing step would be needed. Root zone water dynamics is of the highest interest for water balance calculations and decision making for farming activities. Promising results have been achieved for root zone θ_v modelling from near surface θ_v estimations by Bezerra et al. (2013) over homogenous area and Ford et al. (2014) in the USA.

In New Zealand, a modified two-layer water balance model (similar to the one by Woodward et al. (2001)) on a GIS basis could utilise the near surface θ_v data to model root zone conditions or to validate and adjust predictions as often as possible. Incorporating actual $\theta_v$values would potentially have a significant positive impact on the simulation accuracy, especially during the transition periods when the highest spatial θ_v variability occurs. The relationship between near surface θ_v and the deeper sections show seasonal variations in correlation (Wu and Dickinson, 2004) and it has also been observed in this study (Fig. 8.7). Dry periods and wet periods tended to show high correlation, although in different directions. Slightly lower R values could be seen for the drying out and dry periods than in very wet, winter seasons. The correlations drastically dropped during autumn, i.e. in the rewetting stage.

The water balance model should take into account the increasing persistence of θ_v patterns with increasing soil depth (as observed in Chapter 5) at least in the top 45 cm soil layer in hill country.

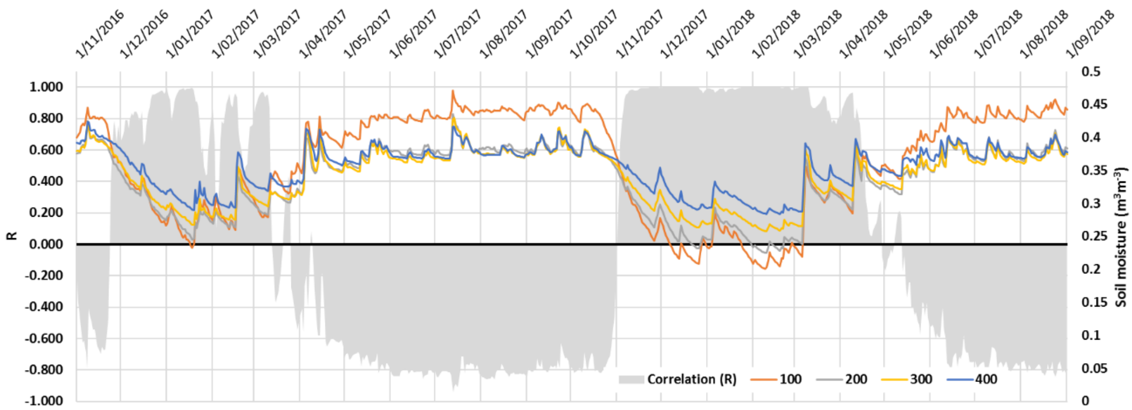

Figure 8.7 Temporal evolution of daily correlation values (expressed as R) between soil moisture and soil depth (shaded area) and the time series of volumetric soil moisture content at four depths (mm).

8.6 The fourth scope - The investigation and quantification of the driving factors of pasture growth on hilly terrains

The monitoring of hill country pastures is difficult as they span over low-altitude steep lands representing diverse environmental characteristics with complex interrelationships between the present soil, vegetation cover, management and climatic parameters (Gillingham, 1973, Lambert and Roberts, 1978, Chapman and Macfarlane, 1985, Bretherton, 2012). On the account of the challenges in pasture growth documentation, and the difficulties caused by the rugged conditions, the interaction between the numerous environmental variables are not fully understood yet. Pasture predictions are made to aid in land management decisions and fertiliser application planning. The models are usually subject to validation against empirical data, which is problematic due to the lack of appropriate pasture growth information (Woodward, 2001).

Thus, periodic pasture growth observations at various topographic positions are highly valuable and needed for validating yield forecasts as well as for model training and parameter adjustments. On New Zealand's non-irrigated hill country farms, the matching of seasonal feed demands of the stock and the seasonal pattern of pasture productivity highly effects the amount and timing of silage to be purchased (Woodward, 2001). The better understanding of the spatiotemporal variability of pasture growth patterns is of great interest that can assist in the usage of more effective land management practices in areas where diverse topography is a major concern. While previous studies dominantly investigated the pasture productivity difference between north and south aspects, the presented work considers the north, east, south and west aspects, flat areas and five slope categories.

Chapter 7 aims to develop a clearer picture of the issues emerging around the pasture productivity and vegetation response patterns on hilly terrain. Moreover, it evaluates the role of various terrain parameters on the rate of growth and investigates the main limiting factors and their dynamics through a nearly two-year study period.

These issues and the need for pasture growth monitoring raised the following questions:

a) Is it possible to capture the spatiotemporal variability in pasture productivity?

b) Can we quantify the impact of static topographical attributes on spatial pasture growth patterns?

c) Is it feasible to isolate the effect of θ_v and T_s, and their intermittent temporal behaviour?

d) How could these findings be used for better parameterisation of pasture forecasts and what differences they could make?

8.6.1 The methodological summary

This part of the study utilises 13 selected microsites for collecting multi-depth θ_v and T_s information as well as herbage accumulation and attempts to assess the pasture productivity response to the monitored variables, climatic parameters and the derived topographical attributes. This experiment combines the use of the deployed WSN, with the AquaCheck probes and a classic pasture growth monitoring method, i.e. the cage technique (Radcliffe et al., 1968) and GIS-derived terrain attributes through and empirical approach including multivariate statistics. Additionally, a theoretical hill plot is used to visualise the effect of slope angle and aspect on pasture growth rates (PGR) and dry matter (DM) production. It also allows the investigation of pasture growth as a function of soil wetness conditions at four depths, the water stored in the soil profile, and the accumulated heat.

8.6.2 Pasture growth trends, optimal growth conditions and limiting factors

The temporal evolution of PGR is related to θ_v and T_s conditions (Fig. 8.8). The stored soil water levels dropped considerably (to 100 mm) in the second year following a long dry season spanning through late spring and summer that limited the PGR (Fig. 8.8 (A)). The spatial mean T_s rose as high as 20 °C in the summer of 2017 and 25 °C in 2018 indicating the considerable difference in the amount of received heat (Fig. 8.8 (B)). The limiting role of θ_v and T_s change through the seasons and governs pasture production. Figure 8.8 (D) depicts the alternating limiting effect of θ_v and T_s during the two-year period, without taking into account the influence of fertiliser applications.

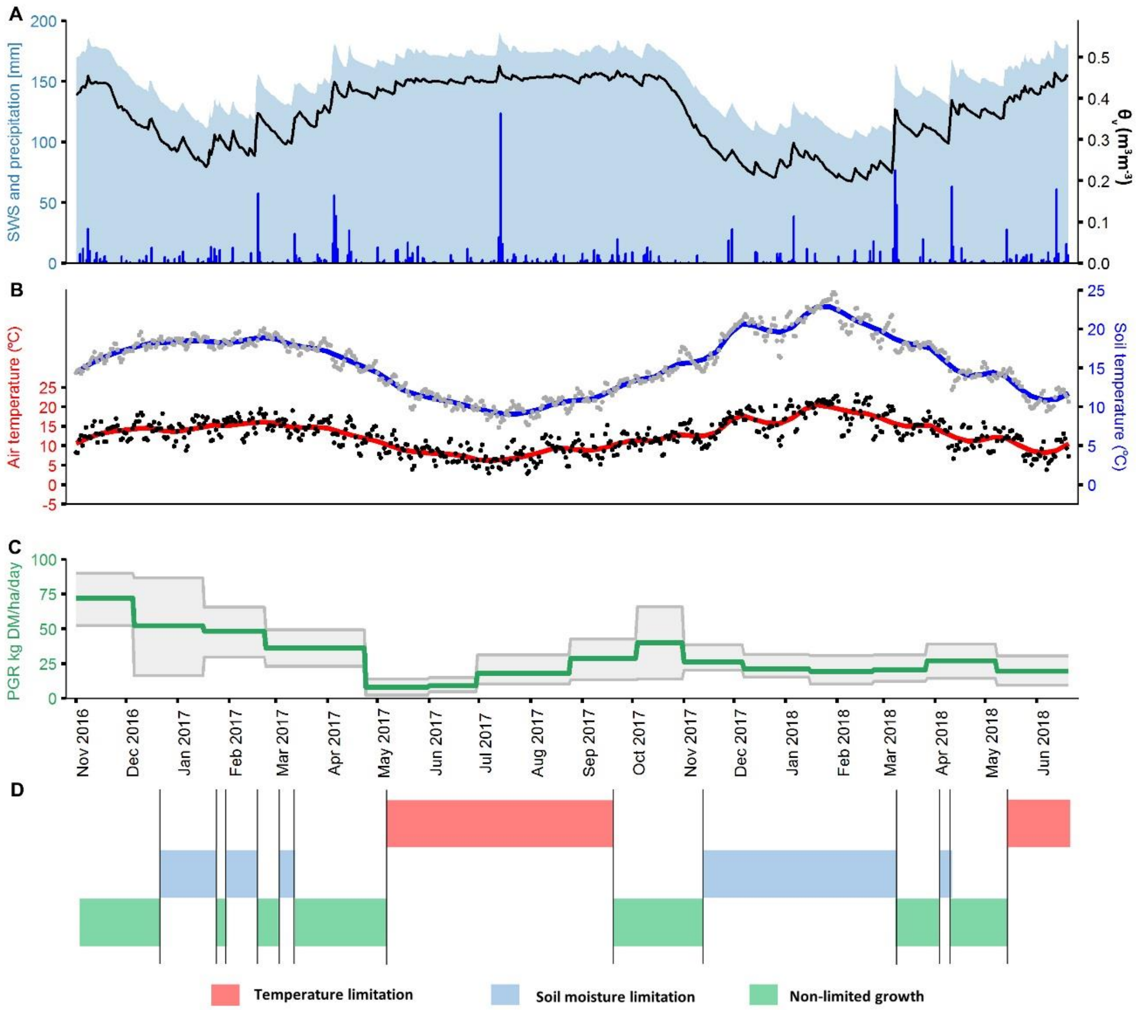

Figure 8.8 The temporal evolution of soil water content at 100 mm soil depth and soil water storage in the monitored soil profile (A). The changes in air and soil temperature at 100 mm soil depth are shown in (B) while the annual distribution of pasture growth rate (PGR) is depicted in (C). The changing limiting role of soil moisture and temperature on PGR is illustrated during a nearly 2-year period (D).

At the Pati Tapu station, the highest PGR values can be observed typically in November and December (Fig. 8.8 (C)). Based on the nearly two-year dataset, the highest pasture production occurs if the

- Spatial mean soil water storage deficit is < 35-45 mm
- Cumulative precipitation for the observed 4-6-week growth interval is approx. 100 mm
- Spatial mean θ_v is 0.29-0.45 $m^3 m^{-3}$ at 100 mm soil depth
- Spatial mean T_s is 15-19 °C at 100 mm soil depth
- Air temperature is 13-16 °C and
- The incoming solar radiation is 5500-6500 WH/m^2.

The early dry soil conditions beginning in late spring of 2017 in the second year exerted its limiting effect on pasture productivity levels in agreement with the findings of Radcliffe (1982) and Zhang et al. (2005). They impressed that spring rainfall is one of the most important factors in annual pasture productivity in hill country.

The recognised non-limited growth periods can be used for optimising farming activity patterns and a longer time series could reveal the temporal shifts of the high producing periods which is most likely to be related to the changing trends in climate. Furthermore, these time intervals may be used for timing nitrogen fertiliser applications in order to achieve higher production response without the limitations of θ_v and temperature on PGR (Lambert et al., 2012).

During these ideal conditions, the pasture clearly reflects the soil fertility parameters enabling the examination of the spatial patterns of soil fertility characteristics and the effect of added fertilisers. The application of high-resolution, airborne hyperspectral imagery is an emerging method for hill country pasture monitoring with the capability of linking spectral reflectance to several biophysical and biochemical properties of pasture quality and soil (Pullanagari et al., 2018). Identifying these optimal periods can help in planning the ground-based sampling for the calibration or validation of remote sensing observations and soil nutrient content mapping.

8.6.3 Spatial pasture growth variation and the role of topography

Even though the presence of environmental heterogeneity in hill country is obvious, the quantitative assessment of variations is essential for investigating the strength and dynamics of farm management effecting factors. It is clear, that considerable spatial variation exists between the microsites' pasture productivity. The differences are associated with the topographical positions described by slope angle, aspect, landscape element and elevation. These features have a significant control on the seasonal temperature and available θ_v conditions affecting the plant growth.

In terms of aspect, the sunnier, warmer north aspects are generally drier while the shadier, cooler south aspects are wetter. At the Patitapu Station, north-facing slopes are more productive than south-facing slopes mainly due to the better winter growth and the approximately 22.5 % more accumulated heat on north aspects enhancing pasture development. East-facing slopes are slightly more productive than west-facing surfaces concerning summer yield and the steep east-facing slopes are significantly more productive than steep west-facing slopes. Steep west- and south-facing slopes produce the lowest amount of yield while strongly rolling and flat surfaces are the areas with the highest productivity.

Based on the findings of the comparative and multivariate statistical analysis, slope angle is the most important factor governing PGR and DM. As the slope angle increases, the amount of yield declines which is in agreement with previous studies by Gillingham et al. (1998), Bretherton (2012), Roberts and White (2016) and Zhang et al. (2005). Aspect exerts its effect on PGR, although it is not as significant as that of slope angle. In winter, the PGR spatial variation is low, while in summer the difference in pasture production on various terrain positions is remarkably more expressed. Hence, the degree of slope angle and aspect influences can be associated with a temporal parameter and seasonality since these features control the distribution patterns of energy supply, i.e. the accumulated heat as well as the stored soil water (Gillingham and Bell, 1977).

The geomorphometrical settings, i.e. the situation of a given point in terms of landscape elements, are strongly associated with PGR and accumulated DM. Consequently, this study suggests that landscape elements should be considered as input variable in the pasture growth forecasting models based on the role of upslope contributing area as a predictor of θ_v patterns in wet conditions (Famiglietti et al., 1998, Western et al., 1999). A geomorphometrical analysis of a given terrain provide useful GIS layers that could be incorporated into algorithms predicting pasture growth on a spatial basis.

These results might become an integral part of grazing management and it was already suggested by Lambert and Roberts (1978) that slope angle and aspect variability should be considered during decision making in farm management. Although, considering aspect in grazing might not be feasible on highly broken hill country farms. On the other hand, it might be beneficial to include the effect of aspect into the management plan, land subdivision and fertiliser applications (Lambert and Roberts, 1978).

In hill country, fertiliser requirements are dependent on slope angle and aspect features and soil types (Lambert et al., 1983, Gillingham et al., 1999). Therefore, the findings of this chapter might contribute to the better planning of variable rate input applications and to reduce over and under fertilising. Moreover, following the findings of this study might enable farmers to adjust their grazing and achieve a more even grazing pattern.

8.6.4 Limitations of the dataset and methods

The number of microsites and the number of cages were restricted due to a limited resource, time constrains, and microsite access issues. A greater number of microsites could cover more slope angle and aspect classes and could provide an improved dataset as far as the terrain variables are concerned. The microsites were not replicated and the variation between the cuts from the three cages at each microsite was not considered during the analysis. Therefore, the pasture growth information presented in this study is not suitable for spatial interpolation since it only represents the specific topographic and soil conditions at a given location.

The effect of management practices and fertiliser applications were also not considered in this study. The assumption was made that every microsite received the same type of management and fertiliser treatment. PGR may have been affected by the timing of the pasture cuts. In this study, 4-6-week harvest intervals were chosen as a compromise to simulate sheep grazing. The timing of harvests was strongly limited by weather conditions and farm operations. The microsite distribution was primarily planned for θ_v observations to study the potential of remote sensing applications on spatial θ_v mapping. Therefore, their locations could have been tailored differently for the specific examination of pasture productivity.

Additionally, the length of the study and the difference between the “years” can be considered as another limitation. Longer periods could potentially provide more robust conclusions. It should be noted that the amount of precipitation may not be evenly distributed within the property extent. The minimum, maximum and mean distance between the Patitapu weather station and microsites were 0.34, 2.9 and 1.8 km, respectively. Hence, measuring rainfall accumulation at each microsite could have significantly improved the assessment.

8.6.5 Future perspectives

The findings suggest that the spatial distribution patterns of pasture growth need to be investigated regionally and locally, as the generalisation of the trends is cumbersome due the environmental variability. The generalisation of the role of topographical factors in pasture production has not been fully developed. Concerning the labour-intensive pasture growth measurements, the limitations of the point-like information, remote sensing will become the main tool for spatial pasture growth mapping. Due to the sensitivity of radar signal to the amount of vegetation present, the Sentinel-1 SAR imagery and future SAR missions have the potential to be the basis of pasture growth mapping. An experiment that considers the pasture growth within the satellite footprint with various pixel sizes may be used for calibration of radar signal for the direct estimation of DM and temporal change in PGR.

8.7 General conclusions

Ultimately, the monitoring and quantitative description of the environmental factors and their effect on pasture productivity might enable the hill country farming sector to produce more pasture on the same area and use the inputs more efficiently. The achieved results and the findings of this thesis can be summarised as follows:

- The field-based calibration is essential for accurate θ_v measurements if capacitance sensors are used.
- The application of an automated θ_v monitoring technique is capable of collecting useful datasets to define spatiotemporal θ_v variability and temporal stability.
- The lack of currently available, temporally dense θ_v, T_s and pasture productivity datasets in hill country enhances the value and usefulness of the collected data throughout this experiment.
- A θ_v dataset containing information from spatially distributed locations at the farm-scale can be used to extend point-scale observations to the spatial extent. Machine learning approaches can provide high training and test accuracy on a map basis.
- The synergetic use of radar (SAR) and multispectral satellite imagery can contribute towards the improvement of locally generated θ_v products at a spatial resolution that is practical for farm management.
- The applied Random Forest machine learning technique showed promising predictions for spatial, near surface θ_v mapping.
- The generated terrain information, pasture growth and climatic datasets may be a valuable dataset for testing out and validating pasture growth simulations.
- While slope angle is the most important terrain attribute influencing pasture productivity levels, aspect and landscape elements are also parameters to consider along with the associated seasonality component.

- θ_v and T_s at 100 mm soil depths were the most important for the pasture growth, showing the strongest correlations, although their role changes with seasons.
- Based on the observed spatiotemporal variability, the need for improved θ_v monitoring is critical to support fertiliser applications, farmers and in general decision making in hill country farm management.

8.7.1 Recommendation for future research

The number of WSNs is continuously increasing, as the long-term records of θ_v are fundamental for understanding how the climate change affects the water cycle as well as agricultural productivity (Seneviratne et al., 2010, Dorigo et al., 2011c). Despite the growing number of sensor networks, the resolution of θ_v measurements is still relatively coarse globally, and regionally (Dorigo et al., 2014).

Therefore, a potential future research direction could include the deployment of a regional or country scale θ_v and T_s monitoring network using latest, and more affordable sensors. The collected data could also be useful for climatic studies, better weather predictions and validating remote sensing products. The research could involve farmers, who would voluntarily upload the data and receive information and data access in return using subscription-based online surfaces. At this stage, the knowledge between generations and farmers is given by extension; hence, this kind of collaboration may improve the recognition of the values of scientific research and data collection by the growers and bring closer the scientific and farming communities. If they are willing to take up technology, willing to engage and be part of the innovation system, the relationship between scientific research and practical implications could be significantly improved. Thus, ultimately, this collaboration would lead to better wealth and more sustainable growth in hill country farming.

Appendix

DRC 16 forms

Appendix

DRC 16

MASSEY UNIVERSITY
GRADUATE RESEARCH SCHOOL

STATEMENT OF CONTRIBUTION
DOCTORATE WITH PUBLICATIONS/MANUSCRIPTS

We, the candidate and the candidate's Primary Supervisor, certify that all co-authors have consented to their work being included in the thesis and they have accepted the candidate's contribution as indicated below in the *Statement of Originality*.

Name of candidate:	ISTVAN HAJDU
Name/title of Primary Supervisor:	IAN YULE
Name of Research Output and full reference: manuscript - about to be submitted	
In which Chapter is the Manuscript /Published work:	Chapter 5
Please indicate:	
• The percentage of the manuscript/Published Work that was contributed by the candidate:	70%
and	
• Describe the contribution that the candidate has made to the Manuscript/Published Work:	
The candidate collected and analysed the dataset using several statistical methods and reported these results. The candidate will be named as first author.	
For manuscripts intended for publication please indicate target journal:	
Journal of Hydrology	
Candidate's Signature:	Istvan Hajdu
Date:	27/02/2020
Primary Supervisor's Signature:	for Yule
Date:	27/02/2020.

(This form should appear at the end of each thesis chapter/section/appendix submitted as a manuscript/ publication or collected as an appendix at the end of the thesis)

GRS Version 4– January 2019

DRC 16

MASSEY UNIVERSITY
GRADUATE RESEARCH SCHOOL

STATEMENT OF CONTRIBUTION
DOCTORATE WITH PUBLICATIONS/MANUSCRIPTS

We, the candidate and the candidate's Primary Supervisor, certify that all co-authors have consented to their work being included in the thesis and they have accepted the candidate's contribution as indicated below in the *Statement of Originality*.

Name of candidate:	ISTVAN HAJDU
Name/title of Primary Supervisor:	IAN YULE
Name of Research Output and full reference: manuscript about to be submitted	
In which Chapter is the Manuscript /Published work:	Chapter 6
Please indicate:	
• The percentage of the manuscript/Published Work that was contributed by the candidate:	90%
and	
• Describe the contribution that the candidate has made to the Manuscript/Published Work:	
The candidate chose and investigated new remote sensing techniques and the supervisors provided feedback. The candidate will be the first author on the paper.	
For manuscripts intended for publication please indicate target journal:	
Remote Sensing	
Candidate's Signature:	Istvan Hajdu
Date:	27/02/2020
Primary Supervisor's Signature:	Ian Yule
Date:	27/02/2020.

(This form should appear at the end of each thesis chapter/section/appendix submitted as a manuscript/ publication or collected as an appendix at the end of the thesis)

GRS Version 4– January 2019

Appendix

DRC 16

MASSEY UNIVERSITY
GRADUATE RESEARCH SCHOOL

STATEMENT OF CONTRIBUTION
DOCTORATE WITH PUBLICATIONS/MANUSCRIPTS

We, the candidate and the candidate's Primary Supervisor, certify that all co-authors have consented to their work being included in the thesis and they have accepted the candidate's contribution as indicated below in the *Statement of Originality*.

Name of candidate:	ISTVAN HAJDU
Name/title of Primary Supervisor:	IAN YULE.
Name of Research Output and full reference: manuscript about-to-be-submitted	
In which Chapter is the Manuscript /Published work:	Chapter 7
Please indicate:	
• The percentage of the manuscript/Published Work that was contributed by the candidate:	90%
and	
• Describe the contribution that the candidate has made to the Manuscript/Published Work:	
The candidate completed the work along with the supervisor's suggestions and feedback. The candidate will be marked as first author.	
For manuscripts intended for publication please indicate target journal:	
Plant and Soil	
Candidate's Signature:	Istvan Hajdu
Date:	27/02/2020
Primary Supervisor's Signature:	Ian Yule.
Date:	27/02/2020.

(This form should appear at the end of each thesis chapter/section/appendix submitted as a manuscript/ publication or collected as an appendix at the end of the thesis)

GRS Version 4– January 2019

References

References

ABDI, H. & VALENTIN, D. 2007. Multiple factor analysis (MFA). *Encyclopedia of measurement and statistics*, 1-14.

ABDI, H. & WILLIAMS, L. J. 2010. Principal component analysis. *Wiley interdisciplinary reviews: computational statistics,* 2**,** 433-459.

ABDI, H., WILLIAMS, L. J. & VALENTIN, D. 2013. Multiple factor analysis: principal component analysis for multitable and multiblock data sets. *Wiley Interdisciplinary reviews: computational statistics,* 5**,** 149-179.

ABDOLLAHZADEH, S. & NAVIMIPOUR, N. J. 2016. Deployment strategies in the wireless sensor network: A comprehensive review. *Computer Communications,* 91-92**,** 1-16. Available: https://doi.org/10.1016/j.comcom.2016.06.003

ADAMCHUK, V. & ROSSEL, R. V. 2010. Development of on-the-go proximal soil sensor systems. *Proximal soil sensing.* Springer.

AGRI OPTICS, N. Z. 2017. *AquaCheck Products* [Online]. Available: https://www.agrioptics.co.nz/portfolio/aquacheck/ [Accessed 29/01/2018 2018].

AHMAD, S., KALRA, A. & STEPHEN, H. 2010. Estimating soil moisture using remote sensing data: A machine learning approach. *Advances in Water Resources,* 33**,** 69-80. Available: https://doi.org/10.1016/j.advwatres.2009.10.008

AKYILDIZ, I. F., SU, W., SANKARASUBRAMANIAM, Y. & CAYIRCI, E. 2002. Wireless sensor networks: a survey. *Computer Networks,* 38**,** 393-422. Available: http://dx.doi.org/10.1016/S1389-1286(01)00302-4

AL-TURJMAN, F. M., HASSANEIN, H. S. & IBNKAHLA, M. A. 2013. Efficient deployment of wireless sensor networks targeting environment monitoring applications. *Computer Communications,* 36**,** 135-148. Available: https://doi.org/10.1016/j.comcom.2012.08.021

ALBERGEL, C., DE ROSNAY, P., GRUHIER, C., MUÑOZ-SABATER, J., HASENAUER, S., ISAKSEN, L., KERR, Y. & WAGNER, W. 2012. Evaluation of remotely sensed and modelled soil moisture products using global ground-based in situ observations. *Remote Sensing of Environment,* 118**,** 215-226. Available: http://dx.doi.org/10.1016/j.rse.2011.11.017

ALBERTSON, J. D. & KIELY, G. 2001. On the structure of soil moisture time series in the context of land surface models. *Journal of Hydrology,* 243**,** 101-119. Available: https://doi.org/10.1016/S0022-1694(00)00405-4

ALEXAKIS, D. D., MEXIS, F.-D. K., VOZINAKI, A.-E. K., DALIAKOPOULOS, I. N. & TSANIS, I. K. 2017. Soil Moisture Content Estimation Based on Sentinel-1 and Auxiliary Earth Observation Products. A Hydrological Approach. *Sensors (Basel, Switzerland),* 17**,** 1455. Available: 10.3390/s17061455

ALI, I., GREIFENEDER, F., STAMENKOVIC, J., NEUMANN, M. & NOTARNICOLA, C. 2015. Review of Machine Learning Approaches for Biomass and Soil Moisture Retrievals from Remote Sensing Data. *Remote Sensing,* 7**,** 15841.

ALTESE, E., BOLOGNANI, O. & MANCINI, M. 1996. Retrieving Soil Moisture Over Bare Soil from ERS 1 Synthetic Aperture Radar Data: Sensitivity Analysis Based on a Theoretical Surface Scattering Model and Field Data. *Water Resources Research,* 32**,** 653-661. Available: doi:10.1029/95WR03638

AMADOR, J. A., GÖRRES, J. H. & SAVIN, M. C. 2005. Role of soil water content in the carbon and nitrogen dynamics of Lumbricus terrestris L. burrow soil. *Applied Soil Ecology,* 28**,** 15-22.

AMAZIRH, A., MERLIN, O., ER-RAKI, S., GAO, Q., RIVALLAND, V., MALBETEAU, Y., KHABBA, S. & ESCORIHUELA, M. J. 2018. Retrieving surface soil moisture at high spatio-temporal resolution from a synergy between Sentinel-1 radar and Landsat thermal data: A study case over bare soil. *Remote Sensing of Environment,* 211**,** 321-337. Available: https://doi.org/10.1016/j.rse.2018.04.013

ANDERSON, M. C., NORMAN, J. M., MECIKALSKI, J. R., OTKIN, J. A. & P., K. W. 2007. A climatological study of evapotranspiration and moisture stress across the continental United States based on thermal remote sensing: 1. Model formulation. *Journal of Geophysical Research: Atmospheres,* 112. Available: doi:10.1029/2006JD007506

ANGUELA, T. P., ZRIBI, M., BAGHDADI, N. & LOUMAGNE, C. 2010. Analysis of Local Variation of Soil Surface Parameters With TerraSAR-X Radar Data Over Bare Agricultural Fields. *IEEE Transactions on Geoscience and Remote Sensing,* 48**,** 874-881. Available: 10.1109/TGRS.2009.2028019

ANNE, N. J. P., ABD-ELRAHMAN, A. H., LEWIS, D. B. & HEWITT, N. A. 2014. Modeling soil parameters using hyperspectral image reflectance in subtropical coastal wetlands. *International Journal of Applied Earth Observation and Geoinformation,* 33**,** 47-56. Available: https://doi.org/10.1016/j.jag.2014.04.007

AQUACHECK, P. L. 2008. AquaCheck probe instruction manual.

ARNOLD, S. M. & MONTEITH, J. L. 1974. Plant Development and Mean Temperature in a Teesdale Habitat. *Journal of Ecology,* 62**,** 711-720. Available: 10.2307/2258951

ATTEMA, E., DAVIDSON, M., FLOURY, N., LEVRINI, G., ROSICH, B., ROMMEN, B. & SNOEIJ, P. Sentinel-1 ESA's New European Radar Observatory. 7th European Conference on Synthetic Aperture Radar, 2-5 June 2008 2008. 1-4.

ATTEMA, E. P. W. & ULABY, F. T. 1978. Vegetation modeled as a water cloud. *Radio science,* 13**,** 357-364.

ATZBERGER, C. 2013. Advances in remote sensing of agriculture: Context description, existing operational monitoring systems and major information needs. *Remote sensing,* 5**,** 949-981.

AUBERT, M., BAGHDADI, N. N., ZRIBI, M., OSE, K., HAJJ, M. E., VAUDOUR, E. & GONZALEZ-SOSA, E. 2013. Toward an Operational Bare Soil Moisture Mapping Using TerraSAR-X Data Acquired Over Agricultural Areas. *IEEE Journal of Selected Topics in Applied Earth Observations and Remote Sensing,* 6**,** 900-916. Available: 10.1109/JSTARS.2012.2220124

AYYAD, M. A. G. & DIX, R. L. 1964. An Analysis of a Vegetation--Microenvironmental Complex on Prairie Slopes in Saskatchewan. *Ecological Monographs,* 34**,** 421-442. Available: 10.2307/2937071

BAARS, J. & WALLER, J. Effects of temperature on pasture production. Proceedings of the Agronomy Society of New Zealand, 1979. 101-104.

BAGHDADI, N., AUBERT, M., CERDAN, O., FRANCHISTÉGUY, L., VIEL, C., MARTIN, E., ZRIBI, M. & DESPRATS, J. F. 2007. Operational Mapping of Soil Moisture Using Synthetic Aperture Radar Data: Application to the Touch Basin (France). *Sensors (Basel, Switzerland),* 7**,** 2458-2483.

REFERENCES

BAGHDADI, N., CERDAN, O., ZRIBI, M., AUZET, V., DARBOUX, F., EL HAJJ, M. & KHEIR, R. B. 2008. Operational performance of current synthetic aperture radar sensors in mapping soil surface characteristics in agricultural environments: application to hydrological and erosion modelling. *Hydrological Processes,* 22**,** 9-20. Available: doi:10.1002/hyp.6609

BAGHDADI, N., CRESSON, R., POTTIER, E., AUBERT, M., MEHREZ, M., JACOME, A. & BENABDALLAH, S. 2012. A Potential Use for the C-Band Polarimetric SAR Parameters to Characterize the Soil Surface Over Bare Agriculture Fields. *IEEE Transactions on Geoscience and Remote Sensing,* 50**,** 3844-3858. Available: 10.1109/TGRS.2012.2185934

BAGHDADI, N., EL HAJJ, M., ZRIBI, M. & BOUSBIH, S. 2017. Calibration of the Water Cloud Model at C-Band for Winter Crop Fields and Grasslands. *Remote Sensing,* 9**,** 969.

BAGHDADI, N., GAULTIER, S. & KING, C. 2002. Retrieving surface roughness and soil moisture from synthetic aperture radar (SAR) data using neural networks. *Canadian Journal of Remote Sensing,* 28**,** 701-711. Available: 10.5589/m02-066

BAGHDADI, N., HOLAH, N. & ZRIBI, M. 2006. Soil moisture estimation using multi-incidence and multi-polarization ASAR data. *International Journal of Remote Sensing,* 27**,** 1907-1920. Available: 10.1080/01431160500239032

BAGHDADI, N. & ZRIBI, M. 2016. *Microwave Remote Sensing of Land Surfaces: Techniques and Methods*, Elsevier.

BANNARI, A., MORIN, D., BONN, F. & HUETE, A. R. 1995. A review of vegetation indices. *Remote Sensing Reviews,* 13**,** 95-120. Available: 10.1080/02757259509532298

BÁRDOSSY, A. & LEHMANN, W. 1998. Spatial distribution of soil moisture in a small catchment. Part 1: geostatistical analysis. *Journal of Hydrology,* 206**,** 1-15. Available: http://dx.doi.org/10.1016/S0022-1694(97)00152-2

BARRETT, B. W., DWYER, E. & WHELAN, P. 2009. Soil moisture retrieval from active spaceborne microwave observations: An evaluation of current techniques. *Remote Sensing,* 1**,** 210-242.

BARRETT, P. D., LAIDLAW, A. S. & MAYNE, C. S. 2004. An evaluation of selected perennial ryegrass growth models for development and integration into a pasture management decision support system. *The Journal of Agricultural Science,* 142**,** 327-334. Available: 10.1017/S0021859604004289

BASHER, L. R., BOTHA, N., DODD, M. B., DOUGLAS, G. B., LYNN, I., MARDEN, M., MCLVOR, I. R. & SMITH, W. 2008. Hill country erosion: a review of knowledge on erosion processes, mitigation options, social learning and their long-term effectiveness in the management of hill country erosion. *Landcare Research Contract Report: LC0708/081*.

BAUMANN, F., HE, J.-S., SCHMIDT, K., KUHN, P. & SCHOLTEN, T. 2009. Pedogenesis, permafrost, and soil moisture as controlling factors for soil nitrogen and carbon contents across the Tibetan Plateau. *Global Change Biology,* 15**,** 3001-3017. Available: doi:10.1111/j.1365-2486.2009.01953.x

BAYER, T., WINTER, R. & SCHREIER, G. 1991. Terrain influences in SAR backscatter and attempts to their correction. *IEEE Transactions on Geoscience and Remote Sensing,* 29**,** 451-462. Available: 10.1109/36.79436

BEEF + LAMB New Zealand. 2017. *Annual report 2016-2017*. Wellington. Available: www.beeflambnz.com.

BEEGLE, D. B., CARTON, O. & BAILEY, J. 2000. Nutrient management planning: justification, theory, practice. *Journal of Environmental Quality,* 29**,** 72-79.

BEHARI, J. 2006. *Microwave dielectric behaviour of wet soils*, Springer Science & Business Media.

BELL, K. R., BLANCHARD, B., SCHMUGGE, T. & WITCZAK, M. 1980. Analysis of surface moisture variations within large-field sites. *Water Resources Research,* 16**,** 796-810.

BENSEMAN, R. & COOK, F. 1969. Solar radiation in New Zealand-standard year and radiation on inclined slopes. *New Zealand Journal of Science,* 12**,** 696-&.

BERTOLDI, G., DELLA CHIESA, S., NOTARNICOLA, C., PASOLLI, L., NIEDRIST, G. & TAPPEINER, U. 2014. Estimation of soil moisture patterns in mountain grasslands by means of SAR RADARSAT2 images and hydrological modeling. *Journal of Hydrology,* 516**,** 245-257. Available: http://dx.doi.org/10.1016/j.jhydrol.2014.02.018

BEVEN, K. & FREER, J. 2001. Equifinality, data assimilation, and uncertainty estimation in mechanistic modelling of complex environmental systems using the GLUE methodology. *Journal of Hydrology,* 249**,** 11-29. Available: https://doi.org/10.1016/S0022-1694(01)00421-8

BEVEN, K. J. & KIRKBY, M. J. 1979. A physically based, variable contributing area model of basin hydrology / Un modèle à base physique de zone d'appel variable de l'hydrologie du bassin versant. *Hydrological Sciences Bulletin,* 24**,** 43-69. Available: 10.1080/02626667909491834

BEZERRA, B. G., SANTOS, C. A. C. D., SILVA, B. B. D., PEREZ-MARIN, A. M., BEZERRA, M. V. C., BEZERRA, J. R. C. & RAO, T. V. R. 2013. Estimation of soil moisture in the root-zone from remote sensing data. *Revista Brasileira de Ciência do Solo,* 37**,** 596-603.

BIRCHAM, J. S. 1977. Grazing management for the improvement of browntop pastures in hill country: A programme. *Proceedings of the New Zealand Grassland Association,* 38**,** 87-93.

BIRCHAM, J. S. & GILLINGHAM, A. G. 1986. A soil water balance model for sloping land. *New Zealand Journal of Agricultural Research,* 29**,** 315-323. Available: 10.1080/00288233.1986.10426988

BITTELLI, M. 2011. Measuring soil water content: A review. *HortTechnology,* 21**,** 293-300.

BLONQUIST, J. M., JONES, S. B. & ROBINSON, D. A. 2005. Standardizing Characterization of Electromagnetic Water Content Sensors: Part 2. Evaluation of Seven Sensing Systems. *Vadose Zone Journal,* 4**,** 1059-1069. Available: 10.2136/vzj2004.0141

BLONQUIST JR, J. M., JONES, S. B. & ROBINSON, D. A. 2005. A time domain transmission sensor with TDR performance characteristics. *Journal of Hydrology,* 314**,** 235-245. Available: https://doi.org/10.1016/j.jhydrol.2005.04.005

BLUETT, S. J., MATTHEW, C., BISHOP-HURLEY, G. J., HASLETT, S. J. & HODGSON, J. 1998. The relationship between herbage mass and pasture accumulation rate in winter. *New Zealand Journal of Agricultural Research,* 41**,** 299-305. Available: 10.1080/00288233.1998.9513314

BODYCOMB, J. 2013. *How to select the best refractive index*. Horiba Scientific.

BOGENA HEYE R., HUISMAN JOHAN A., GÜNTNER ANDREAS, HÜBNER CHRISTOF, KUSCHE JÜRGEN, JONARD FRANÇOIS, VEY SIBYLLE & VEREECKEN HARRY 2015. Emerging methods for noninvasive sensing of soil moisture dynamics from field to catchment scale: a review. *Wiley Interdisciplinary Reviews: Water,* 2**,** 635-647. Available: doi:10.1002/wat2.1097

REFERENCES

BOGENA, H. R., HERBST, M., HUISMAN, J. A., ROSENBAUM, U., WEUTHEN, A. & VEREECKEN, H. 2010. Potential of Wireless Sensor Networks for Measuring Soil Water Content Variability. *Vadose Zone Journal,* 9**,** 1002-1013. Available: 10.2136/vzj2009.0173

BOGENA, H. R., HUISMAN, J. A., OBERDÖRSTER, C. & VEREECKEN, H. 2007. Evaluation of a low-cost soil water content sensor for wireless network applications. *Journal of Hydrology,* 344**,** 32-42. Available: https://doi.org/10.1016/j.jhydrol.2007.06.032

BÖHNER, J., KÖTHE, R., CONRAD, O., GROSS, J., RINGELER, A. & SELIGE, T. 2001. Soil regionalisation by means of terrain analysis and process parameterisation. *Soil classification,* 2003.

BOJINSKI, S., VERSTRAETE, M., PETERSON, T. C., RICHTER, C., SIMMONS, A. & ZEMP, M. 2014. The Concept of Essential Climate Variables in Support of Climate Research, Applications, and Policy. *Bulletin of the American Meteorological Society,* 95**,** 1431-1443. Available: 10.1175/bams-d-13-00047.1

BOLTEN, J. D., CROW, W. T., ZHAN, X., JACKSON, T. J. & REYNOLDS, C. A. 2010. Evaluating the utility of remotely sensed soil moisture retrievals for operational agricultural drought monitoring. *IEEE Journal of Selected Topics in Applied Earth Observations and Remote Sensing,* 3**,** 57-66.

BOUMAN, B. A. M. & HOEKMAN, D. H. 1993. Multi-temporal, multi-frequency radar measurements of agricultural crops during the Agriscatt-88 campaign in The Netherlands. *International Journal of Remote Sensing,* 14**,** 1595-1614. Available: 10.1080/01431169308953988

BOUSBIH, S., ZRIBI, M., LILI-CHABAANE, Z., BAGHDADI, N., EL HAJJ, M., GAO, Q. & MOUGENOT, B. 2017. Potential of Sentinel-1 Radar Data for the Assessment of Soil and Cereal Cover Parameters. *Sensors,* 17**,** 2617.

BRAEKEN, J. & VAN ASSEN, M. A. L. M. 2017. An empirical Kaiser criterion. *Psychological Methods,* 22**,** 450-466. Available: 10.1037/met0000074

BRAUN, A. & HOCHSCHILD, V. 2017. Potential and Limitations of Radar Remote Sensing for Humanitarian Operations. *GI_Forum 2017,* 1**,** 228-243.

BREIMAN, L. 2001. Random Forests. *Machine Learning,* 45**,** 5-32. Available: 10.1023/a:1010933404324

BRETHERTON, M., HORNE, D., SUMANASENA, H. A., JEYAKUMAR, P. & SCOTTER, D. 2018. Repellency-induced runoff from New Zealand hill country under pasture: A plot study. *Agricultural Water Management,* 201**,** 83-90. Available: https://doi.org/10.1016/j.agwat.2018.01.013

BRETHERTON, M., SCOTTER, D. R., HORNE, D. J. & HEDLEY, M. J. 2011. *Water Uptake by Hill Country Pasture - More than You think*. Fertilizer and Lime Research Centre, Massey University.

BRETHERTON, M. R. 2012. *An investigation into repellency-induced runoff and its consequences in a New Zealand hill country pasture system: a thesis submitted in partial fulfilment of the requirements for the degree of Doctor of Philosophy in Soil Science, Massey University.*

BRETHERTON, M. R., SCOTTER, D. R., HORNE, D. J. & HEDLEY, M. J. 2010. Towards an improved understanding of the soil water balance of sloping land under pasture. *New Zealand Journal of Agricultural Research,* 53**,** 175-185. Available: 10.1080/00288233.2010.482957

BROCCA, L., CIABATTA, L., MASSARI, C., CAMICI, S. & TARPANELLI, A. 2017. Soil Moisture for Hydrological Applications: Open Questions and New Opportunities. *Water,* 9**,** 140.

BROCCA, L., MELONE, F., MORAMARCO, T. & MORBIDELLI, R. 2009. Soil moisture temporal stability over experimental areas in Central Italy. *Geoderma,* 148**,** 364-374. Available: https://doi.org/10.1016/j.geoderma.2008.11.004

BROCCA, L., MELONE, F., MORAMARCO, T., WAGNER, W. & HASENAUER, S. 2010a. ASCAT soil wetness index validation through in situ and modeled soil moisture data in central Italy. *Remote Sensing of Environment,* 114**,** 2745-2755. Available: https://doi.org/10.1016/j.rse.2010.06.009

BROCCA, L., MELONE, F., MORAMARCO, T., WAGNER, W., NAEIMI, V., BARTALIS, Z. & HASENAUER, S. 2010b. Improving runoff prediction through the assimilation of the ASCAT soil moisture product. *Hydrology and Earth System Sciences,* 14**,** 1881-1893.

BROCCA, L., MORBIDELLI, R., MELONE, F. & MORAMARCO, T. 2007. Soil moisture spatial variability in experimental areas of central Italy. *Journal of Hydrology,* 333**,** 356-373. Available: http://dx.doi.org/10.1016/j.jhydrol.2006.09.004

BRONICK, C. J. & LAL, R. 2005. Soil structure and management: a review. *Geoderma,* 124**,** 3-22. Available: https://doi.org/10.1016/j.geoderma.2004.03.005

BROWN, R. J., MANORE, M. J. & POIRIER, S. 1992. Correlations between X-, C-, and L-band imagery within an agricultural environment. *International Journal of Remote Sensing,* 13**,** 1645-1661. Available: 10.1080/01431169208904218

BRUCKLER, L., WITONO, H. & STENGEL, P. 1988. Near surface soil moisture estimation from microwave measurements. *Remote Sensing of Environment,* 26**,** 101-121. Available: http://dx.doi.org/10.1016/0034-4257(88)90091-0

BURATTI, C., CONTI, A., DARDARI, D. & VERDONE, R. 2009. An Overview on Wireless Sensor Networks Technology and Evolution. *Sensors,* 9**,** 6869.

BURT, T. P. & BUTCHER, D. P. 1985. Topographic controls of soil moisture distributions. *Journal of Soil Science,* 36**,** 469-486. Available: doi:10.1111/j.1365-2389.1985.tb00351.x

CALVET, J. C., WIGNERON, J. P., WALKER, J., KARBOU, F., CHANZY, A. & ALBERGEL, C. 2011. Sensitivity of Passive Microwave Observations to Soil Moisture and Vegetation Water Content: L-Band to W-Band. *IEEE Transactions on Geoscience and Remote Sensing,* 49**,** 1190-1199. Available: 10.1109/TGRS.2010.2050488

CAMERON, D. 2016. Sustaining the productivity of New Zealand's hill country – A land manager's view. *Hill Country – Grassland Research and Practice Series,* 16**,** 151-156.

CAMPS-VALLS, G. & BRUZZONE, L. 2009. *Kernel methods for remote sensing data analysis*, John Wiley & Sons.

CAMPS-VALLS, G., TUIA, D., BRUZZONE, L. & BENEDIKTSSON, J. A. 2014. Advances in Hyperspectral Image Classification: Earth Monitoring with Statistical Learning Methods. *IEEE Signal Processing Magazine,* 31**,** 45-54. Available: 10.1109/MSP.2013.2279179

CARSEY, F. D. 1992. *Microwave remote sensing of sea ice*, American Geophysical Union.

CASSEL, D. & NIELSEN, D. 1986. Field capacity and available water capacity. *Methods of Soil Analysis: Part 1—Physical and Mineralogical Methods***,** 901-926.

CHAI, T. & DRAXLER, R. R. 2014. Root mean square error (RMSE) or mean absolute error (MAE)?–Arguments against avoiding RMSE in the literature. *Geoscientific model development,* 7**,** 1247-1250.

REFERENCES

CHANASYK, D. S. & NAETH, M. A. 1996. Field measurement of soil moisture using neutron probes. *Canadian Journal of Soil Science,* 76**,** 317-323. Available: 10.4141/cjss96-038

CHANDLER, D. G., SEYFRIED, M., MURDOCK, M. & MCNAMARA, J. P. 2004. Field Calibration of Water Content Reflectometers This research was sponsored by NASA Grant Number NAG5-7537 and the Utah Agricultural experiment Station, Utah State University, Logan, UT. UAES journal paper number 7550. *Soil Science Society of America Journal,* 68**,** 1501-1507. Available: 10.2136/sssaj2004.1501

CHAPMAN, D. & MACFARLANE, M. 1985. Pasture growth limitations in hill country and choice of species. *Using Herbage Cultivars. Grassland Research and Practice Series,* 3**,** 25-29.

CHAPMAN, D. F., CULLEN, B. R., JOHNSON, I. R. & BECA, D. 2009. Interannual variation in pasture growth rate in Australian and New Zealand dairy regions and its consequences for system management. *Animal Production Science,* 49**,** 1071-1079. Available: https://doi.org/10.1071/AN09054

CHAPMAN, D. F., THARMARAJ, J., AGNUSDEI, M. & HILL, J. 2012. Regrowth dynamics and grazing decision rules: further analysis for dairy production systems based on perennial ryegrass (Lolium perenne L.) pastures. *Grass and Forage Science,* 67**,** 77-95. Available: 10.1111/j.1365-2494.2011.00824.x

CHARLESWORTH, P. 2005. Soil water monitoring. *Irrigation Insights*.

CHARLTON, J. & STEWART, A. Pasture species and cultivars used in New Zealand-a list. Proceedings of the conference-New Zealand Grassland Association, 1999. 147-166.

CHARPENTIER, M. A. & GROFFMAN, P. M. 1992. Soil moisture variability within remote sensing pixels. *Journal of Geophysical Research: Atmospheres,* 97**,** 18987-18995. Available: doi:10.1029/92JD00882

CHAUDHARI, P. R., AHIRE, D. V., AHIRE, V. D., CHKRAVARTY, M. & MAITY, S. 2013. Soil bulk density as related to soil texture, organic matter content and available total nutrients of Coimbatore soil. *International Journal of Scientific and Research Publications,* 3**,** 1-8.

CHAUHAN, S., SRIVASTAVA, H. & PATEL, P. 2017. *IMPROVED PARAMETERIZATION OF WATER CLOUD MODEL FOR HYBRID-POLARIZED BACKSCATTER SIMULATION USING INTERACTION FACTOR*. Available: 10.5194/isprs-archives-XLII-4-W2-61-2017

CHEN, B., DING, Y. G. & LIU, J. M. 2005. The Soil moisture Prediction Model Experiment Research of The Climatic Humid Zone. *Scientia Meteorological Sinica,* 25**,** 231-237.

CHEN, S. W., LI, Y. Z., WANG, X. S., XIAO, S. P. & SATO, M. 2014. Modeling and Interpretation of Scattering Mechanisms in Polarimetric Synthetic Aperture Radar: Advances and perspectives. *IEEE Signal Processing Magazine,* 31**,** 79-89. Available: 10.1109/MSP.2014.2312099

CHEN, X.-Z., CHEN, S.-S., ZHONG, R.-F., SU, Y.-X., LIAO, J.-S., LI, D., HAN, L.-S., LI, Y. & LI, X. 2012. A semi-empirical inversion model for assessing surface soil moisture using AMSR-E brightness temperatures. *Journal of hydrology,* 456**,** 1-11.

CHOI, M. & HUR, Y. 2012. A microwave-optical/infrared disaggregation for improving spatial representation of soil moisture using AMSR-E and MODIS products. *Remote Sensing of Environment,* 124**,** 259-269. Available: http://dx.doi.org/10.1016/j.rse.2012.05.009

CHOI, M., JACOBS, J. M. & COSH, M. H. 2007. Scaled spatial variability of soil moisture fields. *Geophysical Research Letters,* 34.

CLAVERIE, M., MASEK, J. G., JU, J. & DUNGAN, J. L. 2017. Harmonized Landsat-8 Sentinel-2 (HLS) Product User's Guide. *National Aeronautics and Space Administration (NASA): Washington, DC, USA*.

CLEMENT, M. A., KILSBY, C. G. & MOORE, P. 2018. Multi-temporal synthetic aperture radar flood mapping using change detection. *Journal of Flood Risk Management,* 11**,** 152-168. Available: doi:10.1111/jfr3.12303

COMEGNA, V. & BASILE, A. 1994. Temporal stability of spatial patterns of soil water storage in a cultivated Vesuvian soil. *Geoderma,* 62**,** 299-310. Available: https://doi.org/10.1016/0016-7061(94)90042-6

CONRAD, O., BECHTEL, B., BOCK, M., DIETRICH, H., FISCHER, E., GERLITZ, L., WEHBERG, J., WICHMANN, V. & BÖHNER, J. 2015. SAGA, System for automated geoscientific analyses (SAGA) v. 2.1. 4. *Geoscientific Model Development,* 8**,** 1991.

COPERNICUS OPEN ACCESS HUB. 2018. *Copernicus Open Access Hub* [Online]. Available: https://scihub.copernicus.eu/ [Accessed 09/29/2018 2018].

COSH, M. H., JACKSON, T. J., BINDLISH, R. & PRUEGER, J. H. 2004. Watershed scale temporal and spatial stability of soil moisture and its role in validating satellite estimates. *Remote Sensing of Environment,* 92**,** 427-435. Available: http://dx.doi.org/10.1016/j.rse.2004.02.016

COSH, M. H., JACKSON, T. J., MORAN, S. & BINDLISH, R. 2008. Temporal persistence and stability of surface soil moisture in a semi-arid watershed. *Remote Sensing of Environment,* 112**,** 304-313.

COULTER, J. 1973. *A water balance assessment of New Zealand rainfall*, New Zealand Meteorological Service.

COX, S. 2002. Information technology: the global key to precision agriculture and sustainability. *Computers and Electronics in Agriculture,* 36**,** 93-111. Available: https://doi.org/10.1016/S0168-1699(02)00095-9

CRONJE, R. & MOSTERT, P. A holistic approach to improve litchi orchard management in South Africa. III International Symposium on Longan, Lychee, and other Fruit Trees in Sapindaceae Family 863, 2008. 433-436.

CROW, W. T., BERG, A. A., COSH, M. H., LOEW, A., MOHANTY, B. P., PANCIERA, R., DE ROSNAY, P., RYU, D. & WALKER, J. P. 2012a. Upscaling sparse ground-based soil moisture observations for the validation of coarse-resolution satellite soil moisture products. *Reviews of Geophysics,* 50**,** n/a-n/a. Available: 10.1029/2011RG000372

CROW, W. T., BERG, A. A., COSH, M. H., LOEW, A., MOHANTY, B. P., PANCIERA, R., ROSNAY, P., RYU, D. & WALKER, J. P. 2012b. Upscaling sparse ground-based soil moisture observations for the validation of coarse-resolution satellite soil moisture products. *Reviews of Geophysics,* 50. Available: 10.1029/2011RG000372

CSST. 2018. *Annual report 2017 / 2018*. Alexandra, Central Otago, New Zealand: Centre for Space Science Technology.

DA SILVA, A. P., NADLER, A. & KAY, B. D. 2001. Factors contributing to temporal stability in spatial patterns of water content in the tillage zone. *Soil and Tillage Research,* 58**,** 207-218. Available: https://doi.org/10.1016/S0167-1987(00)00169-0

DALLEY, D. & GEDDES, T. Pasture growth and quality on Southland and Otago dairy farms. Proceedings of the New Zealand Grassland Association, 2012. 237-241.

REFERENCES

DAS, K. & PAUL, P. K. 2015a. Present status of soil moisture estimation by microwave remote sensing. *Cogent Geoscience,* 1**,** 1084669. Available: 10.1080/23312041.2015.1084669

DAS, K. & PAUL, P. K. 2015b. Soil moisture retrieval model by using RISAT-1, C-band data in tropical dry and sub-humid zone of Bankura district of India. *The Egyptian Journal of Remote Sensing and Space Science,* 18**,** 297-310. Available: https://doi.org/10.1016/j.ejrs.2015.09.004

DAS, N. N., ENTEKHABI, D., DUNBAR, R. S., COLLIANDER, A., CHEN, F., CROW, W., JACKSON, T. J., BERG, A., BOSCH, D. D., CALDWELL, T., COSH, M. H., COLLINS, C. H., LOPEZ-BAEZA, E., MOGHADDAM, M., ROWLANDSON, T., STARKS, P. J., THIBEAULT, M., WALKER, J. P., WU, X., O'NEILL, P. E., YUEH, S. & NJOKU, E. G. 2018. The SMAP mission combined active-passive soil moisture product at 9 km and 3 km spatial resolutions. *Remote Sensing of Environment,* 211**,** 204-217. Available: https://doi.org/10.1016/j.rse.2018.04.011

DAVIS, J., VALENTINE, I., KEMP, P. & CAMPBELL, B. A comparative study of the resistance and resilience of hill country pasture species exposed to water deficit stress. Proceedings of the Annual Conference. Agronomy Society of New Zealand, 1994. 15-20.

DAWSON, M. S., FUNG, A. K. & MANRY, M. T. 1997. A robust statistical-based estimator for soil moisture retrieval from radar measurements. *IEEE Transactions on Geoscience and Remote Sensing,* 35**,** 57-67. Available: 10.1109/36.551934

DE LANNOY, G. J., VERHOEST, N. E., HOUSER, P. R., GISH, T. J. & VAN MEIRVENNE, M. 2006. Spatial and temporal characteristics of soil moisture in an intensively monitored agricultural field (OPE3). *Journal of Hydrology,* 331**,** 719-730.

DE ROSNAY, P., GRUHIER, C., TIMOUK, F., BAUP, F., MOUGIN, E., HIERNAUX, P., KERGOAT, L. & LEDANTEC, V. 2009. Multi-scale soil moisture measurements at the Gourma meso-scale site in Mali. *Journal of Hydrology,* 375**,** 241-252. Available: https://doi.org/10.1016/j.jhydrol.2009.01.015

DE WIT, A. J. W. & VAN DIEPEN, C. A. 2007. Crop model data assimilation with the Ensemble Kalman filter for improving regional crop yield forecasts. *Agricultural and Forest Meteorology,* 146**,** 38-56. Available: https://doi.org/10.1016/j.agrformet.2007.05.004

DEAN, T. J., BELL, J. P. & BATY, A. J. B. 1987. Soil moisture measurement by an improved capacitance technique, Part I. Sensor design and performance. *Journal of Hydrology,* 93**,** 67-78. Available: https://doi.org/10.1016/0022-1694(87)90194-6

DESMET, P. & GOVERS, G. 1996. A GIS procedure for automatically calculating the USLE LS factor on topographically complex landscape units. *Journal of soil and water conservation,* 51**,** 427-433.

DEVANTIER, B., LAMBERT, M., BROOKES, I. & HAWKINS, C. Measuring production of continuously grazed hill pastures. PROCEEDINGS OF THE CONFERENCE-NEW ZEALAND GRASSLAND ASSOCIATION, 1998. 157-160.

DIAS, P., ROQUE, W., C. FERREIRA, E. & SIQUEIRA DIAS, J. A. 2011. *Proposal of a novel heat dissipation soil moisture sensor*.

DINGMAN, S. L. 2002. *Physical hydrology,* Upper Saddle River, NJ., Prentice Hall.

DOBRIYAL, P., QURESHI, A., BADOLA, R. & HUSSAIN, S. A. 2012. A review of the methods available for estimating soil moisture and its implications for water resource management. *Journal of Hydrology,* 458-459**,** 110-117. Available: https://doi.org/10.1016/j.jhydrol.2012.06.021

DOBSON, M. C. & ULABY, F. T. 1986. Active Microwave Soil Moisture Research. *IEEE Transactions on Geoscience and Remote Sensing,* GE-24**,** 23-36. Available: 10.1109/TGRS.1986.289585

DOBSON, M. C., ULABY, F. T., HALLIKAINEN, M. T. & EL-RAYES, M. A. 1985. Microwave dielectric behavior of wet soil-Part II: Dielectric mixing models. *IEEE Transactions on Geoscience and Remote Sensing***,** 35-46.

DORIGO, W. & DE JEU, R. 2016. Satellite soil moisture for advancing our understanding of earth system processes and climate change. *International Journal of Applied Earth Observation and Geoinformation,* 48**,** 1-4. Available: http://dx.doi.org/10.1016/j.jag.2016.02.007

DORIGO, W., OEVELEN, P., WAGNER, W., DRUSCH, M., MECKLENBURG, S., ROBOCK, A. & JACKSON, T. 2011a. A New International Network for in Situ Soil Moisture Data. *Eos, Transactions American Geophysical Union,* 92**,** 141-142. Available: 10.1029/2011EO170001

DORIGO, W., WAGNER, W., HOHENSINN, R., HAHN, S., PAULIK, C., XAVER, A., GRUBER, A., DRUSCH, M., MECKLENBURG, S. & OEVELEN, P. V. 2011b. The International Soil Moisture Network: a data hosting facility for global in situ soil moisture measurements. *Hydrology and Earth System Sciences,* 15**,** 1675-1698.

DORIGO, W., XAVER, A., VREUGDENHIL, M., GRUBER, A., HEGYIOVA, A., SANCHIS-DUFAU, A., ZAMOJSKI, D., CORDES, C., WAGNER, W. & DRUSCH, M. 2013. Global automated quality control of in situ soil moisture data from the International Soil Moisture Network. *Vadose Zone Journal,* 12.

DORIGO, W. A., GRUBER, A., DE JEU, R. A. M., WAGNER, W., STACKE, T., LOEW, A., ALBERGEL, C., BROCCA, L., CHUNG, D., PARINUSSA, R. M. & KIDD, R. 2015. Evaluation of the ESA CCI soil moisture product using ground-based observations. *Remote Sensing of Environment,* 162**,** 380-395. Available: https://doi.org/10.1016/j.rse.2014.07.023

DORIGO, W. A., REIMER, C., CHUNG, D., PARINUSSA, R. M., MELZER, T., WAGNER, W., DE JEU, R. A. M. & KIDD, R. 2014. Soil Moisture. *In:* BLUNDEN, J. & ARNDT, D. S. (eds.) *State of the Climate in 2014.* Bulletin of the American Meteorological Society (BAMS).

DORIGO, W. A., WAGNER, W., HOHENSINN, R., HAHN, S., PAULIK, C., XAVER, A., GRUBER, A., DRUSCH, M., MECKLENBURG, S. & OEVELEN, P. V. 2011c. The International Soil Moisture Network: a data hosting facility for global in situ soil moisture measurements. *Hydrology and Earth System Sciences,* 15**,** 1675-1698.

DOUGILL, A. J., HEATHWAITE, A. L. & THOMAS, D. S. G. 1998. Soil water movement and nutrient cycling in semi-arid rangeland: vegetation change and system resilience. *Hydrological Processes,* 12**,** 443-459. Available: doi:10.1002/(SICI)1099-1085(19980315)12:3<443::AID-HYP582>3.0.CO;2-N

DRUSCH, M., DEL BELLO, U., CARLIER, S., COLIN, O., FERNANDEZ, V., GASCON, F., HOERSCH, B., ISOLA, C., LABERINTI, P., MARTIMORT, P., MEYGRET, A., SPOTO, F., SY, O., MARCHESE, F. & BARGELLINI, P. 2012. Sentinel-2: ESA's Optical High-Resolution Mission for GMES Operational Services. *Remote Sensing of Environment,* 120**,** 25-36. Available: https://doi.org/10.1016/j.rse.2011.11.026

DRUSCH, M. & VITERBO, P. 2007. Assimilation of Screen-Level Variables in ECMWF's Integrated Forecast System: A Study on the Impact on the Forecast Quality and Analyzed Soil Moisture. *Monthly Weather Review,* 135**,** 300-314. Available: 10.1175/mwr3309.1

REFERENCES

DUGUA, C. R. & PIETRONIRO, A. 2005. *Remote sensing in northern hydrology: measuring environmental change*, American Geophysical Union.

EKANAYAKE, J. C. & HEDLEY, C. B. 2018. Advances in Information Provision from Wireless Sensor Networks for Irrigated Crops. *Wireless Sensor Network,* Vol.10No.04**,** 23. Available: 10.4236/wsn.2018.104004

EL EMARY, I. M. M. & RAMAKRISHNAN, S. 2014. Wireless Sensor Networks: From Theory to Applications. Taylor & Francis, CRC Press, New York.

ENGMAN, E. T. The potential of SAR in hydrology. Geoscience and Remote Sensing Symposium, 1994. IGARSS '94. Surface and Atmospheric Remote Sensing: Technologies, Data Analysis and Interpretation., International, 8-12 Aug 1994 1994. 283-285 vol.1.

ENTEKHABI, D., NJOKU, E. G., NEILL, P. E., KELLOGG, K. H., CROW, W. T., EDELSTEIN, W. N., ENTIN, J. K., GOODMAN, S. D., JACKSON, T. J. & JOHNSON, J. 2010a. The soil moisture active passive (SMAP) mission. *Proceedings of the IEEE,* 98**,** 704-716.

ENTEKHABI, D., NJOKU, E. G., O'NEILL, P. E., KELLOGG, K. H., CROW, W. T., EDELSTEIN, W. N., ENTIN, J. K., GOODMAN, S. D., JACKSON, T. J. & JOHNSON, J. 2010b. The soil moisture active passive (SMAP) mission. *Proceedings of the IEEE,* 98**,** 704-716.

ENTIN, J. K., ROBOCK, A., VINNIKOV, K. Y., HOLLINGER, S. E., LIU, S. & NAMKHAI, A. 2000. Temporal and spatial scales of observed soil moisture variations in the extratropics. *JOURNAL OF GEOPHYSICAL RESEARCH,* 105**,** 11865-11877.

ESA, E. S. A. 2018a. *Acquisition Segments - Sentinel-1 - Sentinel Online* [Online]. Available: https://sentinel.esa.int/web/sentinel/missions/sentinel-1/observation-scenario/acquisition-segments [Accessed 09/29/2018 2018].

ESA, E. S. A. 2018b. Copernicus, observing the Earth: Overview.

ESA, E. S. A. 2018c. *User Guides - Sentinel-1 SAR - Acquisition Modes - Sentinel Online* [Online]. Sentinel Online. Available: https://sentinel.esa.int/web/sentinel/user-guides/sentinel-1-sar/acquisition-modes [Accessed 09/29/2018 2018].

ESA, E. S. A. 2018d. *User Guides - Sentinel-1 SAR - Product Types and Processing Levels - Sentinel Online* [Online]. Available: https://sentinel.esa.int/web/sentinel/user-guides/sentinel-1-sar/product-types-processing-levels [Accessed 09/29/2018 2018].

ESCH, T., ÜREYEN, S., ZEIDLER, J., METZ–MARCONCINI, A., HIRNER, A., ASAMER, H., TUM, M., BÖTTCHER, M., KUCHAR, S., SVATON, V. & MARCONCINI, M. 2018. Exploiting big earth data from space – first experiences with the timescan processing chain. *Big Earth Data,* 2**,** 36-55. Available: 10.1080/20964471.2018.1433790

ESCOFIER, B. & PAGÈS, J. 1994. Multiple factor analysis (AFMULT package). *Computational Statistics & Data Analysis,* 18**,** 121-140. Available: https://doi.org/10.1016/0167-9473(94)90135-X

ESHEL, G., LEVY, G. J., MINGELGRIN, U. & SINGER, M. J. 2004. Critical Evaluation of the Use of Laser Diffraction for Particle-Size Distribution Analysis. *Soil Science Society of America Journal,* 68**,** 736-743. Available: 10.2136/sssaj2004.7360

EUROPEAN SPACE AGENCY. 2012. *The electromagnetic spectrum* [Online]. ESA. Available: http://sci.esa.int/education/50368-the-electromagnetic-spectrum/ [Accessed 15/05/2018 2018].

EVANS, D. A., WILLIARD, K. W. & SCHOONOVER, J. E. 2016. Comparison of terrain indices and landform classification procedures in low-relief agricultural fields. *Journal of Geospatial Applications in Natural Resources,* 1**,** 1.

EVANS, I. S. 1972. General geomorphometry, derivatives of altitude, and descriptive statistics. *Spatial analysis in geomorphology***,** 17-90.

EVETT, S. 2000a. Exploits and endeavours in soil water management and conservation using nuclear techniques. *Nuclear techniques in integrated plant nutrient, water and soil management,* 16**,** 151.

EVETT, S. 2000b. Some aspects of time domain reflectometry, neutron scattering and capacitance methods for soil water content measurement. *FAO/IAEA Division of Nuclear Techniques in Food and Agriculture. Comparison of Soil Water Measurement using the Neutron Scattering, Time Domain Reflectometry, and Capacitance Methods. IAEA-TECDOC-1137***,** 5-49.

EVETT, S. & PARKIN, G. 2005. Advances in soil water content sensing. *Vadose Zone Journal,* 4**,** 986-991.

EVETT, S. & STEINER, J. 1995. Precision of neutron scattering and capacitance type soil water content gauges from field calibration. *Soil Science Society of America Journal,* 59**,** 961-968.

EWEYS, O. A., ELWAN, A. A. & BORHAM, T. I. 2017a. Retrieving topsoil moisture using RADARSAT-2 data, a novel approach applied at the east of the Netherlands. *Journal of Hydrology,* 555**,** 670-682. Available: https://doi.org/10.1016/j.jhydrol.2017.10.048

EWEYS, O. A., ESCORIHUELA, M. J., VILLAR, J. M., ER-RAKI, S., AMAZIRH, A., OLIVERA, L., JARLAN, L., KHABBA, S. & MERLIN, O. 2017b. Disaggregation of SMOS Soil Moisture to 100 m Resolution Using MODIS Optical/Thermal and Sentinel-1 Radar Data: Evaluation over a Bare Soil Site in Morocco. *Remote Sensing,* 9**,** 1155.

FABRE, S., BRIOTTET, X. & LESAIGNOUX, A. 2015. Estimation of Soil Moisture Content from the Spectral Reflectance of Bare Soils in the 0.4–2.5 µm Domain. *Sensors,* 15**,** 3262.

FAMIGLIETTI, J. S., DEVEREAUX, J. A., LAYMON, C. A., TSEGAYE, T., HOUSER, P. R., JACKSON, T. J., GRAHAM, S. T., RODELL, M. & OEVELEN, P. J. 1999. Ground-based investigation of soil moisture variability within remote sensing footprints During the Southern Great Plains 1997 (SGP97) Hydrology Experiment. *Water Resources Research,* 35**,** 1839-1851. Available: doi:10.1029/1999WR900047

FAMIGLIETTI, J. S., RUDNICKI, J. W. & RODELL, M. 1998. Variability in surface moisture content along a hillslope transect: Rattlesnake Hill, Texas. *Journal of Hydrology,* 210**,** 259-281. Available: http://dx.doi.org/10.1016/S0022-1694(98)00187-5

FAMIGLIETTI, J. S., RYU, D., BERG, A. A., RODELL, M. & JACKSON, T. J. 2008a. Field observations of soil moisture variability across scales. *Water Resources Research,* 44. Available: 10.1029/2006WR005804

FAMIGLIETTI, J. S., RYU, D., BERG, A. A., RODELL, M. & JACKSON, T. J. 2008b. Field observations of soil moisture variability across scales. *Water Resources Research,* 44**,** n/a-n/a. Available: 10.1029/2006WR005804

FAO, F. A. A. O. O. T. U. N. 2011. *Global Strategy to Improve Agricultural and Rural Statistics*. Rome, Italy: FAO. Report number: 56719-GB.

FARES, A., AWAL, R. & BAYABIL, H. K. 2016. Soil Water Content Sensor Response to Organic Matter Content under Laboratory Conditions. *Sensors (Basel, Switzerland),* 16**,** 1239. Available: 10.3390/s16081239

REFERENCES

FENNESSY, P., GLENNIE, S. & MCCORKINDALE, A. 2016. Innovations behind the farm gate that will influence performance of hill farming. *Grassland Research and Practice Series,* 16**,** 15-20.

FERRARA, G. & FLORE, J. A. 2003. Comparison Between Different Methods for Measuring Transpiration in Potted Apple Trees. *Biologia Plantarum,* 46**,** 41-47. Available: 10.1023/a:1022301931508

FERRAZZOLI, P., PALOSCIA, S., PAMPALONI, P., SCHIAVON, G., SOLIMINI, D. & COPPO, P. 1992. Sensitivity of microwave measurements to vegetation biomass and soil moisture content: a case study. *IEEE Transactions on Geoscience and Remote Sensing,* 30**,** 750-756. Available: 10.1109/36.158869

FISHER, P., AUMANN, C., CHIA, K., O'HALLORAN, N. & CHANDRA, S. 2017. Adequacy of laser diffraction for soil particle size analysis. *PLOS ONE,* 12**,** e0176510. Available: 10.1371/journal.pone.0176510

FLOOD, N. 2014. Continuity of Reflectance Data between Landsat-7 ETM+ and Landsat-8 OLI, for Both Top-of-Atmosphere and Surface Reflectance: A Study in the Australian Landscape. *Remote Sensing,* 6**,** 7952.

FLOOD, N. 2017. Comparing Sentinel-2A and Landsat 7 and 8 Using Surface Reflectance over Australia. *Remote Sensing,* 9**,** 659.

FORD, J. P., PLAUT, J. J., WEITZ, C. M., FARR, T. G., SENSKE, D. A., STOFAN, E. R., MICHAELS, G., PARKER, T. J. & FULTON, D. Guide to Magellan image interpretation. Guide to Magellan Image Interpretation, 1993.

FORD, T. W., HARRIS, E. & QUIRING, S. M. 2014. Estimating root zone soil moisture using near-surface observations from SMOS. *Hydrol. Earth Syst. Sci.,* 18**,** 139-154. Available: 10.5194/hess-18-139-2014

FRANCIS, C. F., THORNES, J. B., ROMERO DIAZ, A., LOPEZ BERMUDEZ, F. & FISHER, G. C. 1986. Topographic control of soil moisture, vegetation cover and land degradation in a moisture stressed mediterranean environment. *CATENA,* 13**,** 211-225. Available: https://doi.org/10.1016/S0341-8162(86)80014-5

FRANK, A. B. & HOFMANN, L. 1989. Relationship among Grazing Management, Growing Degree-Days, and Morphological Development for Native Grasses on the Northern Great Plains. *Journal of Range Management,* 42**,** 199-202. Available: 10.2307/3899472

FRASER, D. S. & VESELY, E. T. 2011. Connecting North Island hill country farmers nutrient requirements with soil mapping units. *In:* RESEARCH, L. (ed.). Fertilizer and Lime Research Centre Workshop.

FREEMAN, A. & DURDEN, S. L. 1998. A three-component scattering model for polarimetric SAR data. *IEEE Transactions on Geoscience and Remote Sensing,* 36**,** 963-973. Available: 10.1109/36.673687

FRIEDMAN, S. P. 1998. A saturation degree-dependent composite spheres model for describing the effective dielectric constant of unsaturated porous media. *Water Resources Research,* 34**,** 2949-2961.

FRIENDLY, M., MONETTE, G. & FOX, J. 2013. Elliptical insights: understanding statistical methods through elliptical geometry. *Statistical Science,* 28**,** 1-39.

GABRIEL, J. L., LIZASO, J. I. & QUEMADA, M. 2010. Laboratory versus field calibration of capacitance probes. *Soil Science Society of America Journal,* 74**,** 593-601.

GALLANT, J. C. & WILSON, J. P. 2000. Primary Topographic Attributes. *In:* WILSON, J. P. & GALLANT, J. C. (eds.) *Terrain Analysis—Principles and Applications.* New York: Wiley.

GAO, F., MASEK, J. G., WOLFE, R. E. & HUANG, C. 2010. *Building a consistent medium resolution satellite data set using moderate resolution imaging spectroradiometer products as reference*, SPIE.

GAO, Q., ZRIBI, M., ESCORIHUELA, M. & BAGHDADI, N. 2017. Synergetic Use of Sentinel-1 and Sentinel-2 Data for Soil Moisture Mapping at 100 m Resolution. *Sensors,* 17**,** 1966.

GAO, X., WU, P., ZHAO, X., SHI, Y. & WANG, J. 2011a. Estimating spatial mean soil water contents of sloping jujube orchards using temporal stability. *Agricultural Water Management,* 102**,** 66-73. Available: https://doi.org/10.1016/j.agwat.2011.10.007

GAO, X., WU, P., ZHAO, X., SHI, Y., WANG, J. & ZHANG, B. 2011b. Soil moisture variability along transects over a well-developed gully in the Loess Plateau, China. *CATENA,* 87**,** 357-367. Available: http://dx.doi.org/10.1016/j.catena.2011.07.004

GAO, X., WU, P., ZHAO, X., WANG, J. & SHI, Y. 2014. Effects of land use on soil moisture variations in a semi-arid catchment: implications for land and agricultural water management. *Land Degradation & Development,* 25**,** 163-172. Available: 10.1002/ldr.1156

GAO, Z., XU, X., WANG, J., YANG, H., HUANG, W. & FENG, H. 2013. A method of estimating soil moisture based on the linear decomposition of mixture pixels. *Mathematical and Computer Modelling,* 58**,** 606-613. Available: https://doi.org/10.1016/j.mcm.2011.10.054

GARDNER, C. M., ROBINSON, D., BLYTH, K. & COOPER, J. D. 2000. Soil water content. *Soil analysis: physical methods***,** 1-74.

GARDNER, W. & KIRKHAM, D. 1952. DETERMINATION OF SOIL MOISTURE BY NEUTRON SCATTERING. *Soil Science,* 73**,** 391-402.

GARDNER, W. H. 1986. Water content. *Methods of Soil Analysis: Part 1—Physical and Mineralogical Methods***,** 493-544.

GAUKRODGER, L. 2014. The next step: intensification of East Coast hill country farming.

GEE, G. W. & BAUDER, J. W. 1986. Particle-Size Analysis. *In:* KLUTE A. (ed.) *Methods of Soil Analysis, Part 1. Physical and Mineralogical Methods.* 2nd ed.: American Society of Agronomy/Soil Science Society of America, Madison, WI.

GHASEMI, A. & ZAHEDIASL, S. 2012. Normality Tests for Statistical Analysis: A Guide for Non-Statisticians. *International Journal of Endocrinology and Metabolism,* 10**,** 486-489. Available: 10.5812/ijem.3505

GILLINGHAM, A., GRAY, M. & SMITH, D. Pasture responses to phosphorus and nitrogen fertilisers on dry hill country. PROCEEDINGS OF THE CONFERENCE-NEW ZEALAND GRASSLAND ASSOCIATION, 1998. 135-140.

GILLINGHAM, A., MABER, J., MORTON, J. & TUOHY, M. Precise aerial fertiliser application on hill country. PROCEEDINGS OF THE CONFERENCE-NEW ZEALAND GRASSLAND ASSOCIATION, 1999. 221-226.

GILLINGHAM, A., SHEATH, G., GRAY, M. & WEBBY, R. 2003. Management and nitrogen fertiliser options for increased pasture productivity in dryland hill systems. *Legumes for dryland pastures. Grassland Research and Practice Series***,** 43-50.

GILLINGHAM, A. G. Influence of physical factors on pasture growth on hill country. Proceedings of the New Zealand Grassland Association, 1973. 77-85.

REFERENCES

GILLINGHAM, A. G. & BELL, L. D. 1977. Effect of aspect and cloudiness on grass and soil temperatures at a hill site in Raglan County. *New Zealand Journal of Agricultural Research,* 20**,** 37-44. Available: 10.1080/00288233.1977.10427299

GOETZ, A. F. H., VANE, G., SOLOMON, J. E. & ROCK, B. N. 1985. Imaging Spectrometry for Earth Remote Sensing. *Science,* 228**,** 1147-1153. Available: 10.1126/science.228.4704.1147

GÓMEZ-PLAZA, A., ALVAREZ-ROGEL, J., ALBALADEJO, J. & CASTILLO, V. M. 2000. Spatial patterns and temporal stability of soil moisture across a range of scales in a semi-arid environment. *Hydrological Processes,* 14**,** 1261-1277. Available: 10.1002/(SICI)1099-1085(200005)14:7<1261::AID-HYP40>3.0.CO;2-D

GOOGLE EARTH ENGINE. 2018a. *Platform – Google Earth Engine* [Online]. @GoogleEarth. Available: https://earthengine.google.com/platform/ [Accessed 09/29/2018 2018].

GOOGLE EARTH ENGINE. 2018b. *Sentinel-1 Algorithms* [Online]. Available: https://developers.google.com/earth-engine/sentinel1 [Accessed 09/29/2018 2018].

GORELICK, N., HANCHER, M., DIXON, M., ILYUSHCHENKO, S., THAU, D. & MOORE, R. 2017. Google Earth Engine: Planetary-scale geospatial analysis for everyone. *Remote Sensing of Environment*. Available: https://doi.org/10.1016/j.rse.2017.06.031

GRAY, D., REID, J., KEMP, P., BROOKES, I., HORNE, D., KENYON, P., MATTHEW, C., MORRIS, S. & VALENTINE, I. 2004. Controlling pasture quality on hill country-key decisions and techniques. *Agronomy New Zealand,* 34**,** 73-82.

GRAYSON, R. B. & WESTERN, A. W. 1998. Towards areal estimation of soil water content from point measurements: time and space stability of mean response. *Journal of Hydrology,* 207**,** 68-82. Available: https://doi.org/10.1016/S0022-1694(98)00096-1

GRAYSON, R. B., WESTERN, A. W., CHIEW, F. H. S. & BLÖSCHL, G. 1997. Preferred states in spatial soil moisture patterns: Local and nonlocal controls. *Water Resources Research,* 33**,** 2897-2908. Available: 10.1029/97WR02174

GREACEN, E. L. 1981. Soil water assessment by the neutron method.

GREATER WELLINGTON REGIONAL COUNCIL. 2012. *Air, land and water in the Wellington region - state and trends* [Online]. Wellington: Greater Wellington Regional Council. Available: http://www.gw.govt.nz/assets/Our-Environment/Environmental-monitoring/Environmental-Reporting/Eastern-Wairarapa-Hills-low-res.pdf [Accessed 15/10/2016 2016].

GROSSMAN, R. & REINSCH, T. 2002. *Methods of Soil Analysis: Part 4 Physical Methods,* Madison, WI, Soil Science Society of America. Available: 10.2136/sssabookser5.4

GUBER, A. K., GISH, T. J., PACHEPSKY, Y. A., VAN GENUCHTEN, M. T., DAUGHTRY, C. S. T., NICHOLSON, T. J. & CADY, R. E. 2008. Temporal stability in soil water content patterns across agricultural fields. *CATENA,* 73**,** 125-133. Available: https://doi.org/10.1016/j.catena.2007.09.010

GUISAN, A., WEISS, S. B. & WEISS, A. D. 1999. GLM versus CCA spatial modeling of plant species distribution. *Plant Ecology,* 143**,** 107-122. Available: 10.1023/a:1009841519580

GUPTA, V. & JANGID, R. 2011. Microwave response of rough surfaces with auto-correlation functions, RMS heights and correlation lengths using active remote sensing. *92.40. Lg; 78.20. Ci*.

GWAK, Y. & KIM, S. 2017. Factors affecting soil moisture spatial variability for a humid forest hillslope. *Hydrological Processes,* 31**,** 431-445. Available: doi:10.1002/hyp.11039

HABOUDANE, D., MILLER, J. R., PATTEY, E., ZARCO-TEJADA, P. J. & STRACHAN, I. B. 2004. Hyperspectral vegetation indices and novel algorithms for predicting green LAI of crop canopies: Modeling and validation in the context of precision agriculture. *Remote Sensing of Environment,* 90**,** 337-352. Available: https://doi.org/10.1016/j.rse.2003.12.013

HAGHIGHI, F., GORJI, M. & SHORAFA, M. 2010. A study of the effects of land use changes on soil physical properties and organic matter. *Land Degradation & Development,* 21**,** 496-502. Available: 10.1002/ldr.999

HAHN, S., REIMER, C., VREUGDENHIL, M., MELZER, T. & WAGNER, W. 2017. Dynamic Characterization of the Incidence Angle Dependence of Backscatter Using Metop ASCAT. *IEEE Journal of Selected Topics in Applied Earth Observations and Remote Sensing,* 10**,** 2348-2359. Available: 10.1109/JSTARS.2016.2628523

HAJDU, I. & YULE, I. 2017. Application of a Wireless Sensor Network for Multi-Depth Soil Moisture Monitoring at Farm Scale in New Zealand's Hill Country. *Advances in Animal Biosciences,* 8**,** 412-417. Available: 10.1017/S2040470017000450

HAJDU, I., YULE, I., BRETHERTON, M., SINGH, R. & HEDLEY, C. 2019. Field performance assessment and calibration of multi-depth AquaCheck capacitance-based soil moisture probes under permanent pasture for hill country soils. *Agricultural Water Management,* 217**,** 332-345. Available: https://doi.org/10.1016/j.agwat.2019.03.002

HAJNSEK, I., JAGDHUBER, T., SCHON, H. & PAPATHANASSIOU, K. P. 2009. Potential of Estimating Soil Moisture Under Vegetation Cover by Means of PolSAR. *IEEE Transactions on Geoscience and Remote Sensing,* 47**,** 442-454. Available: 10.1109/TGRS.2008.2009642

HALDER, S., GHOSAL, A. & BIT, S. D. 2011. A pre-determined node deployment strategy to prolong network lifetime in wireless sensor network. *Computer Communications,* 34**,** 1294-1306. Available: https://doi.org/10.1016/j.comcom.2011.01.004

HARRIS, A., CHU, A., BURGESS, R. & BROCK, J. 1985. Limitations to production and choice of species in finishing pastures. *Using herbage cultivars. Grassland research and practice series (3)***,** 53-57.

HARTER, T. & ZHANG, D. 1999. Water flow and solute spreading in heterogeneous soils with spatially variable water content. *Water Resources Research,* 35**,** 415-426. Available: doi:10.1029/1998WR900027

HAWLEY, M. E., JACKSON, T. J. & MCCUEN, R. H. 1983. Surface soil moisture variation on small agricultural watersheds. *Journal of Hydrology,* 62**,** 179-200.

HE, B., XING, M. & BAI, X. 2014. A Synergistic Methodology for Soil Moisture Estimation in an Alpine Prairie Using Radar and Optical Satellite Data. *Remote Sensing,* 6**,** 10966.

HEADY, H. F. 1957. Effect of Cages on Yield and Composition in the California Annual Type. *Rangeland Ecology & Management/Journal of Range Management Archives,* 10**,** 175-177.

HEATHMAN, G. C., LAROSE, M., COSH, M. H. & BINDLISH, R. 2009. Surface and profile soil moisture spatio-temporal analysis during an excessive rainfall period in the Southern Great Plains, USA. *CATENA,* 78**,** 159-169. Available: https://doi.org/10.1016/j.catena.2009.04.002

HÉBRARD, O., VOLTZ, M., ANDRIEUX, P. & MOUSSA, R. 2006. Spatio-temporal distribution of soil surface moisture in a heterogeneously farmed Mediterranean catchment. *Journal of Hydrology,* 329**,** 110-121. Available: https://doi.org/10.1016/j.jhydrol.2006.02.012

REFERENCES

HEDLEY, C., EKANAYAKE, J. & ROUDIER, P. Wireless soil moisture sensor networks for precision irrigation scheduling. Workshop abstracts, advanced nutrient management: Gains from the past-goals for the future, 2012. 85.

HEDLEY, C. B. & YULE, I. J. 2009. A method for spatial prediction of daily soil water status for precise irrigation scheduling. *Agricultural Water Management,* 96**,** 1737-1745. Available: https://doi.org/10.1016/j.agwat.2009.07.009

HERRERO, M., DENT, J. & FAWCETT, R. 1998. The plant/animal interface in models of grazing systems. *Agricultural Systems Modeling and Simulation***,** 495-542.

HEWITT, A. E. 2010. *New Zealand soil classification*, Manaaki Whenua Press. Available: 10.7931/DL1-LRSS-1-2010

HILLEL, D. 1998. *Environmental Soil Physics,* San Diego, CA, Academic Press.

HILLEL, D. 2003a. 19 - Plant Uptake of Soil Moisture. *Introduction to Environmental Soil Physics (First).* Burlington: Academic Press. Available: https://doi.org/10.1016/B978-012348655-4/50020-4

HILLEL, D. 2003b. *Introduction to environmental soil physics*, Elsevier.

HIRD, J., DELANCEY, E., MCDERMID, G. & KARIYEVA, J. 2017. Google Earth Engine, Open-Access Satellite Data, and Machine Learning in Support of Large-Area Probabilistic Wetland Mapping. *Remote Sensing,* 9**,** 1315.

HODGSON, J., CAMERON, K., CLARK, D., CONDRON, L., FRASER, T., HEDLEY, M., HOLMES, C., KEMP, P., LUCAS, R. & MOOT, D. 2005. New Zealand's pastoral industries: efficient use of grassland resources. *In:* REYNOLDS, S. & FRAME, J. (eds.) *Grasslands: Developments, Opportunities, Perspectives. Rome and Enfield, New Hampshire: Food and Agriculture Organization of the United Nations and Science Publishers, Inc.* Enfield, USA: Science Publishers, Inc.

HOEKSTRA, P. & DELANEY, A. 1974. Dielectric properties of soils at UHF and microwave frequencies. *Journal of Geophysical Research,* 79**,** 1699-1708. Available: doi:10.1029/JB079i011p01699

HOLDEN, C. E. & WOODCOCK, C. E. 2016. An analysis of Landsat 7 and Landsat 8 underflight data and the implications for time series investigations. *Remote Sensing of Environment,* 185**,** 16-36. Available: https://doi.org/10.1016/j.rse.2016.02.052

HOLMES, C. W., WILSON, G. F., MACKENZIE, D., FLUX, D., BROOKES, I. & DAVEY, A. 1987. *Milk production from pasture*, Butterworths of New Zealand Ltd.

HOOGENDOORN, C. J., NEWTON, P. C. D., DEVANTIER, B. P., ROLLE, B. A., THEOBALD, P. W. & LLOYD-WEST, C. M. 2016. Grazing intensity and micro-topographical effects on some nitrogen and carbon pools and fluxes in sheep-grazed hill country in New Zealand. *Agriculture, Ecosystems & Environment,* 217**,** 22-32. Available: https://doi.org/10.1016/j.agee.2015.10.021

HORIBA SCIENTIFIC. 2017. *A guidebook to particle size analysis* [Online]. Horiba Instruments, Inc. Available: https://www.horiba.com/fileadmin/uploads/Scientific/.../PSA/PSA_Guidebook.pdf [Accessed 21/11/2017 2017].

HORNACEK, M., WAGNER, W., SABEL, D., TRUONG, H. L., SNOEIJ, P., HAHMANN, T., DIEDRICH, E. & DOUBKOVA, M. 2012. Potential for High Resolution Systematic Global Surface Soil Moisture Retrieval via Change Detection Using Sentinel-1. *IEEE Journal of Selected*

Topics in Applied Earth Observations and Remote Sensing, 5**,** 1303-1311. Available: 10.1109/JSTARS.2012.2190136

HORNE, D. J. & SCOTTER, D. R. 2016. The available water holding capacity of soils under pasture. *Agricultural Water Management,* 177**,** 165-171. Available: http://dx.doi.org/10.1016/j.agwat.2016.07.012

HOWDEN, S. M., SOUSSANA, J.-F., TUBIELLO, F. N., CHHETRI, N., DUNLOP, M. & MEINKE, H. 2007. Adapting agriculture to climate change. *Proceedings of the National Academy of Sciences,* 104**,** 19691. Available: 10.1073/pnas.0701890104

HOWELL, T. A. 2001. Enhancing water use efficiency in irrigated agriculture. *Agron J,* 93**,** 281-289.

HU, W., SHAO, M., HAN, F. & REICHARDT, K. 2011. Spatio-temporal variability behavior of land surface soil water content in shrub- and grass-land. *Geoderma,* 162**,** 260-272. Available: https://doi.org/10.1016/j.geoderma.2011.02.008

HU, W., SHAO, M., HAN, F., REICHARDT, K. & TAN, J. 2010. Watershed scale temporal stability of soil water content. *Geoderma,* 158**,** 181-198.

HU, W., SHAO, M., WANG, Q. & REICHARDT, K. 2009. Time stability of soil water storage measured by neutron probe and the effects of calibration procedures in a small watershed. *CATENA,* 79**,** 72-82. Available: https://doi.org/10.1016/j.catena.2009.05.012

HU, W., TALLON, L. K., BISWAS, A. & SI, B. C. 2013. Time stability of soil water content. *Advances in Agrophysical Research.* InTech.

HUANG, Y., WU, C., DONG, J., ZHANG, Y. & CHENG, L. 2013. A Sensor Redeployment Approach Based on Energy-balanced in Wireless Sensor Network. *JOURNAL OF INFORMATION &COMPUTATIONAL SCIENCE,* 10**,** 9-16.

HUISMAN, J. A., SNEPVANGERS, J. J. J. C., BOUTEN, W. & HEUVELINK, G. B. M. 2002. Mapping spatial variation in surface soil water content: comparison of ground-penetrating radar and time domain reflectometry. *Journal of Hydrology,* 269**,** 194-207. Available: https://doi.org/10.1016/S0022-1694(02)00239-1

HUPET, F. & VANCLOOSTER, M. 2002. Intraseasonal dynamics of soil moisture variability within a small agricultural maize cropped field. *Journal of Hydrology,* 261**,** 86-101. Available: https://doi.org/10.1016/S0022-1694(02)00016-1

HUSSON, F., JOSSE, J., LÊ, S. & MAZET, J. 2007. Factor analysis and data mining with R. *The FactoMineR Package*.

HUTCHINSON, G., RICHARDS, K. & RISK, W. Aspects of accumulated heat patterns (growing degree-days) and pasture growth in Southland. PROCEEDINGS OF THE CONFERENCE-NEW ZEALAND GRASSLAND ASSOCIATION, 2000. 81-86.

INGLADA, J., ARIAS, M., TARDY, B., HAGOLLE, O., VALERO, S., MORIN, D., DEDIEU, G., SEPULCRE, G., BONTEMPS, S., DEFOURNY, P. & KOETZ, B. 2015. Assessment of an Operational System for Crop Type Map Production Using High Temporal and Spatial Resolution Satellite Optical Imagery. *Remote Sensing,* 7**,** 12356.

JACOBS, J. M., MOHANTY, B. P., HSU, E.-C. & MILLER, D. 2004. SMEX02: Field scale variability, time stability and similarity of soil moisture. *Remote Sensing of Environment,* 92**,** 436-446.

JACQUES, D., MOHANTY, B., TIMMERMAN, A. & FEYEN, J. 2001. Study of time dependency of factors affecting the spatial distribution of soil water content in a field-plot. *Physics and*

Chemistry of the Earth, Part B: Hydrology, Oceans and Atmosphere, 26**,** 629-634. Available: https://doi.org/10.1016/S1464-1909(01)00060-0

JAGDHUBER, T., HAJNSEK, I., BRONSTERT, A. & PAPATHANASSIOU, K. P. 2013. Soil Moisture Estimation Under Low Vegetation Cover Using a Multi-Angular Polarimetric Decomposition. *IEEE Transactions on Geoscience and Remote Sensing,* 51**,** 2201-2215. Available: 10.1109/TGRS.2012.2209433

JENSEN, J. R. 2009. *Remote sensing of the environment: An earth resource perspective 2/e*, Pearson Education India.

JIA, Y.-H. & SHAO, M.-A. 2013. Temporal stability of soil water storage under four types of revegetation on the northern Loess Plateau of China. *Agricultural Water Management,* 117**,** 33-42. Available: https://doi.org/10.1016/j.agwat.2012.10.013

JOHNSON, A. I. 1962. Methods of measuring soil moisture in the field. *U.S. Geol. Survey Water-Supply Paper***,** 25.

JOHNSON, I. R., LODGE, G. M. & WHITE, R. 2003. *The Sustainable Grazing Systems Pasture Model: Description, philosophy and application to the SGS National Experiment*. Available: 10.1071/EA02213

JONES, S. B., BLONQUIST, J., ROBINSON, D., RASMUSSEN, V. P. & OR, D. 2005. Standardizing Characterization of Electromagnetic Water Content SensorsPart 1. Methodology. *Vadose Zone Journal,* 4**,** 1048-1058.

JONES, S. B., WRAITH, J. M. & OR, D. 2002. Time domain reflectometry measurement principles and applications. *Hydrological processes,* 16**,** 141-153.

JOSEPH, A. T., VELDE, R. V. D., NEILL, P. E. O., LANG, R. H. & GISH, T. 2008. Soil Moisture Retrieval During a Corn Growth Cycle Using L-Band (1.6 GHz) Radar Observations. *IEEE Transactions on Geoscience and Remote Sensing,* 46**,** 2365-2374. Available: 10.1109/TGRS.2008.917214

JUDD, T., THOMSON, N. & MCCALLUM, D. Pasture management and pasture species for improved dry matter production in south Taranaki. Proceedings of the New Zealand Grassland Association, 1990. 109-112.

JULIEN, M., KHANZAIB, J., FRANÇOIS, J., MOHAMMADREZA, M., PHUONGANH, T. & SÉBASTIEN, L. 2011. Advanced Ground-Penetrating Radar for Soil Moisture Retrieval. *Multiscale Hydrologic Remote Sensing.* CRC Press. Available: doi:10.1201/b11279-4

10.1201/b11279-4

KACHANOSKI, R. G. & JONG, E. 1988. Scale dependence and the temporal persistence of spatial patterns of soil water storage. *Water Resources Research,* 24**,** 85-91. Available: doi:10.1029/WR024i001p00085

KAISER, H. F. 1960. The Application of Electronic Computers to Factor Analysis. *Educational and Psychological Measurement,* 20**,** 141-151. Available: 10.1177/001316446002000116

KALEITA, A. L., M.C., H. & TIAN, L. F. Field-scale surface soil moisturepatterns and their relationship to topographic indices. Transactions of the ASABE, 2007. 557-564.

KARJALAINEN, M., KAARTINEN, H., HYYPPÄ, J., LAURILA, H. & KUITTINEN, R. The use of Envisat alternating polarization SAR images in agricultural monitoring in comparison with radarsat-1 SAR images. Proceedings of the ISPRS Congress, Istanbul, Turkey, 2004. 12-23.

KARTHIKEYAN, L., PAN, M., WANDERS, N., KUMAR, D. N. & WOOD, E. F. 2017. Four decades of microwave satellite soil moisture observations: Part 1. A review of retrieval algorithms. *Advances in Water Resources,* 109**,** 106-120. Available: https://doi.org/10.1016/j.advwatres.2017.09.006

KASHIF, G. M., TIRUSEW, A., W., K. M. & MAC, M. 2006. SOIL MOISTURE PREDICTION USING SUPPORT VECTOR MACHINES1. *JAWRA Journal of the American Water Resources Association,* 42**,** 1033-1046. Available: doi:10.1111/j.1752-1688.2006.tb04512.x

KASSAMBARA, A. & MUNDT, F. 2016. Factoextra: extract and visualize the results of multivariate data analyses. *R package version,* 1.

KELLER, E., BAISDEN, W., TIMAR, L., MULLAN, B. & CLARK, A. 2014. Grassland production under global change scenarios for New Zealand pastoral agriculture. *Geoscientific Model Development,* 7**,** 2359-2391.

KEMP, P. D. & LÓPEZ, I. F. 2016. Hill country pastures in the southern North Island of New Zealand: an overview. *Hill country - Grassland Research and Practice Series,* 16**,** 289-298.

KENNY, G. J. 2001. *Climate Change: Likely Impacts on New Zealand Agriculture: a Report Prepared for the Ministry of the Environment as Part of the New Zealand Climate Change Programme*, Ministry for the Environment.

KERKEZ, B., GLASER, S. D., BALES, R. C. & MEADOWS, M. W. 2012. Design and performance of a wireless sensor network for catchment-scale snow and soil moisture measurements. *Water Resources Research,* 48**,** n/a-n/a. Available: 10.1029/2011WR011214

KERR, G. A. 2016. Why a hill country symposium? *Hill Country – Grassland Research and Practice Series,* 16**,** 7-10.

KERR, Y. H., WALDTEUFEL, P., WIGNERON, J.-P., DELWART, S., CABOT, F., BOUTIN, J., ESCORIHUELA, M.-J., FONT, J., REUL, N. & GRUHIER, C. 2010. The SMOS mission: New tool for monitoring key elements ofthe global water cycle. *Proceedings of the IEEE,* 98**,** 666-687.

KERR, Y. H., WALDTEUFEL, P., WIGNERON, J.-P., MARTINUZZI, J., FONT, J. & BERGER, M. 2001. Soil moisture retrieval from space: The Soil Moisture and Ocean Salinity (SMOS) mission. *IEEE transactions on Geoscience and remote sensing,* 39**,** 1729-1735.

KETTLER, T. A., DORAN, J. W. & GILBERT, T. L. 2001. Simplified Method for Soil Particle-Size Determination to Accompany Soil-Quality Analyses Journal Series no. 13277 of the Agric. Res. Div., Univ. of Nebraska, Lincoln, NE. *Soil Science Society of America Journal,* 65**,** 849-852. Available: 10.2136/sssaj2001.653849x

KEYS, W. S. 1990. *Borehole geophysics applied to ground-water investigations*, US Department of the Interior, US Geological Survey.

KHEDRI, E., HASANLOU, M. & TABATABAEENEJAD, A. 2017. ESTIMATING SOIL MOISTURE USING POLSAR DATA: A MACHINE LEARNING APPROACH. *International Archives of the Photogrammetry, Remote Sensing & Spatial Information Sciences,* 42.

KIENZLE, S. 2004. The Effect of DEM Raster Resolution on First Order, Second Order and Compound Terrain Derivatives. *Transactions in GIS,* 8**,** 83-111. Available: 10.1111/j.1467-9671.2004.00169.x

KIRKHAM, M. B. 2014. *Principles of soil and plant water relations*, Academic Press.

KIZITO, F., CAMPBELL, C. S., CAMPBELL, G. S., COBOS, D. R., TEARE, B. L., CARTER, B. & HOPMANS, J. W. 2008. Frequency, electrical conductivity and temperature analysis of a low-cost capacitance soil moisture sensor. *Journal of Hydrology,* 352**,** 367-378. Available: https://doi.org/10.1016/j.jhydrol.2008.01.021

KLEYNHANS, W., OLIVIER, J. C., WESSELS, K. J., SALMON, B. P., BERGH, F. V. D. & STEENKAMP, K. 2011. Detecting Land Cover Change Using an Extended Kalman Filter on MODIS NDVI Time-Series Data. *IEEE Geoscience and Remote Sensing Letters,* 8**,** 507-511. Available: 10.1109/LGRS.2010.2089495

KONG, X., DORLING, S. & SMITH, R. 2011. Soil moisture modelling and validation at an agricultural site in Norfolk using the Met Office surface exchange scheme (MOSES). *Meteorological Applications,* 18**,** 18-27. Available: 10.1002/met.197

KORNELSEN, K. C. & COULIBALY, P. 2013. Advances in soil moisture retrieval from synthetic aperture radar and hydrological applications. *Journal of Hydrology,* 476**,** 460-489. Available: http://dx.doi.org/10.1016/j.jhydrol.2012.10.044

KORRES, W., REICHENAU, T. G., FIENER, P., KOYAMA, C. N., BOGENA, H. R., CORNELISSEN, T., BAATZ, R., HERBST, M., DIEKKRÜGER, B., VEREECKEN, H. & SCHNEIDER, K. 2015. Spatio-temporal soil moisture patterns – A meta-analysis using plot to catchment scale data. *Journal of Hydrology,* 520**,** 326-341. Available: https://doi.org/10.1016/j.jhydrol.2014.11.042

KORRES, W., REICHENAU, T. G. & SCHNEIDER, K. 2013. Patterns and scaling properties of surface soil moisture in an agricultural landscape: An ecohydrological modeling study. *Journal of Hydrology,* 498**,** 89-102. Available: http://dx.doi.org/10.1016/j.jhydrol.2013.05.050

KUHN, M. 2008. Caret package. *Journal of statistical software,* 28**,** 1-26.

KUMAR, K., HARI PRASAD, K. S. & ARORA, M. K. 2012. Estimation of water cloud model vegetation parameters using a genetic algorithm. *Hydrological Sciences Journal,* 57**,** 776-789. Available: 10.1080/02626667.2012.678583

KUMAR, P., PRASAD, R., CHOUDHARY, A., GUPTA, D. K., MISHRA, V. N., VISHWAKARMA, A. K., SINGH, A. K. & SRIVASTAVA, P. K. 2018. Comprehensive evaluation of soil moisture retrieval models under different crop cover types using C-band synthetic aperture radar data. *Geocarto International***,** 1-20. Available: 10.1080/10106049.2018.1464601

KURUCU, Y., SANLI, F. B., ESETLILI, M. T., BOLCA, M. & GOKSEL, C. 2009. Contribution of SAR images to determination of surface moisture on the Menemen Plain, Turkey. *International Journal of Remote Sensing,* 30**,** 1805-1817. Available: 10.1080/01431160802639764

LAKHANKAR, T., GHEDIRA, H., TEMIMI, M., SENGUPTA, M., KHANBILVARDI, R. & BLAKE, R. 2009. Non-parametric methods for soil moisture retrieval from satellite remote sensing data. *Remote Sensing,* 1**,** 3-21.

LAKHANKAR, T., JONES, A. S., COMBS, C. L., SENGUPTA, M., VONDER HAAR, T. H. & KHANBILVARDI, R. 2010. Analysis of large scale spatial variability of soil moisture using a geostatistical method. *Sensors (Basel, Switzerland),* 10**,** 913-932. Available: 10.3390/s100100913

LAL, R. & SHUKLA, M. K. 2004. *Principles of soil physics*, CRC Press.

LAMBERT, M. The influence of aspect on pasture environment. Proc NZ Grassl Assoc Conf, 1977.

LAMBERT, M. & LITHERLAND, A. A practitioner's guide to pasture quality. Proceedings of the conference-new zealand grassland association, 2000. 111-116.

LAMBERT, M., ROBERTS, A. & MORTON, J. 2012. Nitrogen use on hill country: Lessons from the national wise use of nitrogen focus farm project. *Advanced nutrient management: gains from the pastgoals for the future. Eds. Currie LD*.

LAMBERT, M. & ROBERTS, E. 1976. Aspect differences in an unimproved hill country pasture: I. Climatic differences. *New Zealand journal of agricultural research,* 19**,** 459-467.

LAMBERT, M. G., CLARK, D. A., GRANT, D. A., COSTALL, D. A. & FLETCHER, R. H. 1983. Influence of fertiliser and grazing management on North Island moist hill country. *New Zealand Journal of Agricultural Research,* 26**,** 95-108. Available: 10.1080/00288233.1983.10420958

LAMBERT, M. G., CLARK, D. A., MACKAY, A. D. & COSTALL, D. A. 2000. Effects of fertiliser application on nutrient status and organic matter content of hill soils. *New Zealand Journal of Agricultural Research,* 43**,** 127-138. Available: 10.1080/00288233.2000.9513414

LAMBERT, M. G. & ROBERTS, E. 1978. Aspect differences in an unimproved hill country pasture: II. Edaphic and biotic differences. *New Zealand Journal of Agricultural Research,* 21**,** 255-260. Available: 10.1080/00288233.1978.10427407

LANDCARE RESEARCH. 2017. *Fundamental Soil Layers - New Zealand Soils Portal* [Online]. Landcare Research Informatics and Soil and Landscape. Available: https://soils.landcareresearch.co.nz/soil-data/fundamental-soil-layers/ [Accessed 23/11/2017 2017].

LANDVISION LTD. 2009. *Pati Tapu Station Whole Farm Plan*. Palmerston North: Horizons Regional Council.

LANG, S. 2015. *Future challenges and opportunities for hill country farming on the East Coast*. Lincoln University New Zealand.

LE HÉGARAT-MASCLE, S., ZRIBI, M., ALEM, F., WEISSE, A. & LOUMAGNE, C. 2002. Soil moisture estimation from ERS/SAR data: Toward an operational methodology. *IEEE Transactions on Geoscience and Remote Sensing,* 40**,** 2647-2658.

LE MORVAN, A., ZRIBI, M., BAGHDADI, N. & CHANZY, A. 2008. Soil moisture profile effect on radar signal measurement. *Sensors,* 8**,** 256-270.

LÊ, S., JOSSE, J. & HUSSON, F. 2008. FactoMineR: an R package for multivariate analysis. *Journal of statistical software,* 25**,** 1-18.

LEDGARD, S., GILLINGHAM, A. & SHEATH, G. 1982. Pasture responses to nitrogen fertiliser on hill country as influenced by topographic, soil and pasture properties. *New Zealand journal of agricultural research*.

LEE, J.-S. 1981. Speckle analysis and smoothing of synthetic aperture radar images. *Computer Graphics and Image Processing,* 17**,** 24-32. Available: https://doi.org/10.1016/S0146-664X(81)80005-6

LEE, J. M. & BEGG, J. G. C. 2002. *Geology of the Wairarapa area,* Lower Hutt, New Zealand, Institue of Geological & Nuclear Sciences Limited.

LEENHARDT, D., VOLTZ, M. & RAMBAL, S. 1995. A survey of several agroclimatic soil water balance models with reference to their spatial application. *European Journal of Agronomy,* 4**,** 1-14. Available: https://doi.org/10.1016/S1161-0301(14)80012-9

LEIB, B. G., JABRO, J. D. & MATTHEWS, G. R. 2003. Field evaluation and performance comparison of soil moisture sensors. *Soil Science,* 168**,** 396-408.

REFERENCES

LEKSHMI, S., SINGH, D. N. & SHOJAEI BAGHINI, M. 2014. A critical review of soil moisture measurement. *Measurement,* 54**,** 92-105. Available: https://doi.org/10.1016/j.measurement.2014.04.007

LI, B. & RODELL, M. 2013. Spatial variability and its scale dependency of observed and modeled soil moisture over different climate regions. *Hydrol. Earth Syst. Sci.,* 17**,** 1177-1188. Available: 10.5194/hess-17-1177-2013

LI, F. Y., SNOW, V. O. & HOLZWORTH, D. P. 2011. Modelling the seasonal and geographical pattern of pasture production in New Zealand. *New Zealand Journal of Agricultural Research,* 54**,** 331-352. Available: 10.1080/00288233.2011.613403

LI, J. & ROY, D. 2017. A Global Analysis of Sentinel-2A, Sentinel-2B and Landsat-8 Data Revisit Intervals and Implications for Terrestrial Monitoring. *Remote Sensing,* 9**,** 902.

LIANCOURT, P., SHARKHUU, A., ARIUNTSETSEG, L., BOLDGIV, B., HELLIKER, B. R., PLANTE, A. F., PETRAITIS, P. S. & CASPER, B. B. 2012. Temporal and spatial variation in how vegetation alters the soil moisture response to climate manipulation. *Plant and Soil,* 351**,** 249-261. Available: 10.1007/s11104-011-0956-y

LIAW, A. & WIENER, M. 2002. Classification and regression by randomForest. *R news,* 2**,** 18-22.

LIEFFERING, M., NEWTON, P., LI, F. & VIBART, R. 2012. Hill country sheep and beef: Impacts and adaptation to climate change In: Enhanced climate change impact and adaptation evaluation: A comprehensive analysis of New Zealand's land-based primary sectors [Clark, A., Nottage, R. *Ministry for Primary Industries, New Zealand***,** 145-188.

LIEFFERS, V. J. & LARKIN-LIEFFERS, P. A. 1987. Slope, aspect, and slope position as factors controlling grassland communities in the coulees of the Oldman River, Alberta. *Canadian Journal of Botany,* 65**,** 1371-1378. Available: 10.1139/b87-189

LIEVENS, H. & VERHOEST, N. E. C. 2011. On the Retrieval of Soil Moisture in Wheat Fields From L-Band SAR Based on Water Cloud Modeling, the IEM, and Effective Roughness Parameters. *IEEE Geoscience and Remote Sensing Letters,* 8**,** 740-744. Available: 10.1109/LGRS.2011.2106109

LILLESAND, T., KIEFER, R. W. & CHIPMAN, J. 2014. *Remote sensing and image interpretation*, John Wiley & Sons.

LIN, G. F., CHEN, G. R., WU, M. C. & CHOU, Y. C. 2009. Effective forecasting of hourly typhoon rainfall using support vector machines. *Water Resources Research,* 45. Available: doi:10.1029/2009WR007911

LIN, H. 2006. Temporal Stability of Soil Moisture Spatial Pattern and Subsurface Preferential Flow Pathways in the Shale Hills Catchment. *Vadose Zone Journal,* 5**,** 317-340. Available: 10.2136/vzj2005.0058

LINN, D. M. & DORAN, J. W. 1984. Effect of water-filled pore space on carbon dioxide and nitrous oxide production in tilled and nontilled soils 1. *Soil Science Society of America Journal,* 48**,** 1267-1272.

LINZ 2012. New Zealand 8m digital elevation model (DEM). Sourced from the LINZ Data Service and licensed by LINZ for re-use under the Creative Commons Attribution 4.0 International licence.: LINZ.

LINZ 2017. New Zealand 10m satellite imagery (Sentinel-2). Sourced from the LINZ Data Service and licensed by LINZ for re-use under the Creative Commons Attribution 4.0 International licence.: LINZ.

LIU, C. & SHI, J. 2016. Estimation of Vegetation Parameters of Water Cloud Model for Global Soil Moisture Retrieval Using Time-Series L-Band Aquarius Observations. *IEEE Journal of Selected Topics in Applied Earth Observations and Remote Sensing,* 9**,** 5621-5633. Available: 10.1109/JSTARS.2016.2596541

LIU, Y. Y., PARINUSSA, R., DORIGO, W. A., DE JEU, R. A., WAGNER, W., VAN DIJK, A., MCCABE, M. F. & EVANS, J. 2011. Developing an improved soil moisture dataset by blending passive and active microwave satellite-based retrievals. *Hydrology and Earth System Sciences,* 15**,** 425.

LIU, Z., LI, P. & YANG, J. 2017. Soil Moisture Retrieval and Spatiotemporal Pattern Analysis Using Sentinel-1 Data of Dahra, Senegal. *Remote Sensing,* 9**,** 1197.

LIU, Z., WANG, Y., YU, P., TIAN, A., WANG, Y., XIONG, W. & XU, L. 2018. Spatial Pattern and Temporal Stability of Root-Zone Soil Moisture during Growing Season on a Larch Plantation Hillslope in Northwest China. *Forests,* 9**,** 68.

LÓPEZ, I. F., LAMBERT, M. G., MACKAY, A. D. & VALENTINE, I. 2003. The influence of topography and pasture management on soil characteristics and herbage accumulation in hill pasture in the North Island of New Zealand. *Plant and Soil,* 255**,** 421-434. Available: 10.1023/a:1026062502566

LUCKMAN, A. J. 1998. The effects of topography on mechanisms of radar backscatter from coniferous forest and upland pasture. *IEEE Transactions on Geoscience and Remote Sensing,* 36**,** 1830-1834. Available: 10.1109/36.718651

LUNT, I. A., HUBBARD, S. S. & RUBIN, Y. 2005. Soil moisture content estimation using ground-penetrating radar reflection data. *Journal of Hydrology,* 307**,** 254-269. Available: https://doi.org/10.1016/j.jhydrol.2004.10.014

LUSCOMBE, P. C. 1980. Seasonal nitrogen deficiency in hill country pastures. *New Zealand Journal of Experimental Agriculture,* 8**,** 117-122. Available: 10.1080/03015521.1980.10426245

LV, L., LIAO, K., LAI, X., ZHU, Q. & ZHOU, S. 2016. Hillslope soil moisture temporal stability under two contrasting land use types during different time periods. *Environmental Earth Sciences,* 75**,** 560. Available: 10.1007/s12665-015-5238-1

LYNCH, P. & MOUNTIER, N. 1954. Cutting techniques in grassland experiments. *New Zealand journal of science and technology 36A***,** 375-385.

LYNN, I., MANDERSON, A., PAGE, M., HARMSWORTH, G., EYLES, G., DOUGLAS, G., MACKAY, A. & NEWSOME, P. 2009. Land Use Capability Survey Handbook–a New Zealand handbook for the classification of land. *Hamilton: AgResearch*.

MA, B. L. & HERATH, A. W. 2016. Timing and rates of nitrogen fertiliser application on seed yield, quality and nitrogen-use efficiency of canola. *Crop and Pasture Science,* 67**,** 167-180. Available: 10.1071/CP15069

MACDONALD, K. A., PENNO, J. W., LANCASTER, J. A. S. & ROCHE, J. R. 2008. Effect of Stocking Rate on Pasture Production, Milk Production, and Reproduction of Dairy Cows in Pasture-Based Systems. *Journal of Dairy Science,* 91**,** 2151-2163. Available: https://doi.org/10.3168/jds.2007-0630

MACKAY, A., LAMBERT, M. & BARKER, D. 1999. Effect of intensification of livestock farming on the physical properties of a hill soil. *Best soil management practices for production (Eds Currie LD, Hedley MJ, Horne DJ, Loganathan P), Fertilizer and Lime Research Centre, Massey University, Palmerston North, New Zealand***,** 311-315.

REFERENCES

MACKAY, A., WEDDERBURN, M. & LAMBERT, M. Sustainable management of hill land. Proceedings of the New Zealand Grassland Association, 1993. New Zealand Grassland Association., 170-176.

MACKAY, A. D. 2008. Impacts of intensification of pastoral agriculture on soils: Current and emerging challenges and implications for future land uses. *New Zealand Veterinary Journal,* 56**,** 281-288. Available: 10.1080/00480169.2008.36848

MAHDAVI, S., MAGHSOUDI, Y. & AMANI, M. 2017. *Effects of changing environmental conditions on synthetic aperture radar backscattering coefficient, scattering mechanisms, and class separability in a forest area*. Available: 10.1117/1.JRS.11.036015

MAJONE, B., VIANI, F., FILIPPI, E., BELLIN, A., MASSA, A., TOLLER, G., ROBOL, F. & SALUCCI, M. 2013. Wireless Sensor Network Deployment for Monitoring Soil Moisture Dynamics at the Field Scale. *Procedia Environmental Sciences,* 19**,** 426-435. Available: https://doi.org/10.1016/j.proenv.2013.06.049

MALENOVSKÝ, Z., ROTT, H., CIHLAR, J., SCHAEPMAN, M. E., GARCÍA-SANTOS, G., FERNANDES, R. & BERGER, M. 2012. Sentinels for science: Potential of Sentinel-1, -2, and -3 missions for scientific observations of ocean, cryosphere, and land. *Remote Sensing of Environment,* 120**,** 91-101. Available: https://doi.org/10.1016/j.rse.2011.09.026

MALTESE, A., BATES, P. D., CAPODICI, F., CANNAROZZO, M., CIRAOLO, G. & LA LOGGIA, G. 2013. Critical analysis of thermal inertia approaches for surface soil water content retrieval. *Hydrological Sciences Journal,* 58**,** 1144-1161. Available: 10.1080/02626667.2013.802322

MANDAL, D., KUMAR, V., BHATTACHARYA, A., RAO, Y. S., SIQUEIRA, P. & BERA, S. 2018. Sen4Rice: A Processing Chain for Differentiating Early and Late Transplanted Rice Using Time-Series Sentinel-1 SAR Data With Google Earth Engine. *IEEE Geoscience and Remote Sensing Letters***,** 1-5. Available: 10.1109/LGRS.2018.2865816

MANDANICI, E. & BITELLI, G. 2016. Preliminary comparison of Sentinel-2 and Landsat 8 Imagery for a combined use. *Remote Sensing,* 8**,** 1014.

MARK, D. M. 1975. Geomorphometric Parameters: A Review and Evaluation. *Geografiska Annaler: Series A, Physical Geography,* 57**,** 165-177. Available: 10.1080/04353676.1975.11879913

MARSH, R. 1978. Effect of exclosure cages on growth rate of pastures at different times of the year. *New Zealand Journal of Experimental Agriculture,* 6**,** 115-117. Available: 10.1080/03015521.1978.10426025

MARTÍNEZ-FERNÁNDEZ, J. & CEBALLOS, A. 2003. Temporal stability of soil moisture in a large-field experiment in Spain. *Soil Science Society of America Journal,* 67**,** 1647-1656.

MARTÍNEZ-FERNÁNDEZ, J. & CEBALLOS, A. 2005. Mean soil moisture estimation using temporal stability analysis. *Journal of Hydrology,* 312**,** 28-38. Available: https://doi.org/10.1016/j.jhydrol.2005.02.007

MARTÍNEZ-FERNÁNDEZ, J., GONZÁLEZ-ZAMORA, A., SÁNCHEZ, N., GUMUZZIO, A. & HERRERO-JIMÉNEZ, C. M. 2016. Satellite soil moisture for agricultural drought monitoring: Assessment of the SMOS derived Soil Water Deficit Index. *Remote Sensing of Environment,* 177**,** 277-286. Available: https://doi.org/10.1016/j.rse.2016.02.064

MASSARI, C., BROCCA, L., MORAMARCO, T., TRAMBLAY, Y. & DIDON LESCOT, J.-F. 2014. Potential of soil moisture observations in flood modelling: Estimating initial conditions and correcting rainfall. *Advances in Water Resources,* 74**,** 44-53. Available: https://doi.org/10.1016/j.advwatres.2014.08.004

MATEJOVIC, I. 1993. Determination of carbon, hydrogen, and nitrogen in soils by automated elemental analysis (dry combustion method). *Communications in Soil Science and Plant Analysis,* 24**,** 2213-2222. Available: 10.1080/00103629309368950

MATSON, P. A., PARTON, W. J., POWER, A. G. & SWIFT, M. J. 1997. Agricultural Intensification and Ecosystem Properties. *Science,* 277**,** 504-509. Available: 10.1126/science.277.5325.504

MATTHIAS, D., F., W. E., H., G. & ARIANE, T. 2004. Soil moisture retrieval during the Southern Great Plains Hydrology Experiment 1999: A comparison between experimental remote sensing data and operational products. *Water Resources Research,* 40. Available: doi:10.1029/2003WR002441

MATTIA, F., TOAN, T. L., PICARD, G., POSA, F. I., ALESSIO, A. D., NOTARNICOLA, C., GATTI, A. M., RINALDI, M., SATALINO, G. & PASQUARIELLO, G. 2003. Multitemporal C-band radar measurements on wheat fields. *IEEE Transactions on Geoscience and Remote Sensing,* 41**,** 1551-1560. Available: 10.1109/TGRS.2003.813531

MATULA, S., BÁŤKOVÁ, K. & LEGESE, W. 2016. Laboratory Performance of Five Selected Soil Moisture Sensors Applying Factory and Own Calibration Equations for Two Soil Media of Different Bulk Density and Salinity Levels. *Sensors,* 16**,** 1912.

MCANENEY, K. & JUDD, M. 1983. Pasture production and water use measurements in the central Waikato. *New Zealand journal of agricultural research,* 26**,** 7-13.

MCANENEY, K. J. & NOBLE, P. F. 1976. Estimating solar radiation on sloping surfaces. *New Zealand Journal of Experimental Agriculture,* 4**,** 195-202. Available: 10.1080/03015521.1976.10425869

MCCALL, D. G. 1984. *A systems approach to research planning for North Island hill country : a thesis presented in partial fulfilment of the requirements for the degree of Doctor of Philosophy.* Doctor of Philosophy (Ph.D.) Doctoral, Massey University.

MCCALL, D. G. & BISHOP-HURLEY, G. J. 2003. A pasture growth model for use in a whole-farm dairy production model. *Agricultural Systems,* 76**,** 1183-1205. Available: https://doi.org/10.1016/S0308-521X(02)00104-X

MCLAREN, R. G. & CAMERON, K. C. 1996. *Soil Science: Sustainable Production and Environmental Protection,* Auckland, New Zealand, Oxford University Press.

MCMASTER, G. S. & WILHELM, W. W. 1997. Growing degree-days: one equation, two interpretations. *Agricultural and Forest Meteorology,* 87**,** 291-300. Available: https://doi.org/10.1016/S0168-1923(97)00027-0

MECKLENBURG, S., DRUSCH, M., KERR, Y. H., FONT, J., MARTIN-NEIRA, M., DELWART, S., BUENADICHA, G., REUL, N., DAGANZO-EUSEBIO, E., OLIVA, R. & CRAPOLICCHIO, R. 2012. ESA's Soil Moisture and Ocean Salinity Mission: Mission Performance and Operations. *IEEE Transactions on Geoscience and Remote Sensing,* 50**,** 1354-1366. Available: 10.1109/TGRS.2012.2187666

MICHELETTI, N., CHANDLER, J. H. & LANE, S. N. 2015. Structure from motion (SFM) photogrammetry.

MILLER, B. A. & SCHAETZL, R. J. 2012. Precision of soil particle size analysis using laser diffractometry. *Soil Science Society of America Journal,* 76**,** 1719-1727.

REFERENCES

MINAR, J. & EVANS, I. S. 2008. Elementary forms for land surface segmentation: The theoretical basis of terrain analysis and geomorphological mapping. *Geomorphology,* 95**,** 236-259.

MINASNY, B. & MCBRATNEY, A. B. 2006. A conditioned Latin hypercube method for sampling in the presence of ancillary information. *Computers & Geosciences,* 32**,** 1378-1388. Available: https://doi.org/10.1016/j.cageo.2005.12.009

MINASNY, B. & MCBRATNEY, A. B. 2018. Limited effect of organic matter on soil available water capacity. *European Journal of Soil Science,* 69**,** 39-47. Available: doi:10.1111/ejss.12475

MING, P., XITIAN, C., W., C. N., DARA, E. & F., W. E. 2016. An initial assessment of SMAP soil moisture retrievals using high-resolution model simulations and in situ observations. *Geophysical Research Letters,* 43**,** 9662-9668. Available: doi:10.1002/2016GL069964

MINISTRY FOR PRIMARY INDUSTRIES 2018. Situation and Outlook for Primary Industries 2016. New Zealand Government Ministry for Primary Industries, Wellington.

MINISTRY FOR THE ENVIRONMENT. 2012. *Land-Use and Carbon Analysis System: Satellite imagery interpretation guide for land-use classes*

interpretation guide for land-use classes (2nd. Wellington: Ministry for the Environment.

MITTELBACH, H., CASINI, F., LEHNER, I., TEULING, A. J. & SENEVIRATNE, S. I. 2011. Soil moisture monitoring for climate research: Evaluation of a low-cost sensor in the framework of the Swiss Soil Moisture Experiment (SwissSMEX) campaign. *Journal of Geophysical Research: Atmospheres,* 116**,** n/a-n/a. Available: 10.1029/2010JD014907

MITTELBACH, H., LEHNER, I. & SENEVIRATNE, S. I. 2012. Comparison of four soil moisture sensor types under field conditions in Switzerland. *Journal of Hydrology,* 430-431**,** 39-49. Available: https://doi.org/10.1016/j.jhydrol.2012.01.041

MITTELBACH, H. & SENEVIRATNE, S. I. 2012. A new perspective on the spatio-temporal variability of soil moisture: Temporal dynamics versus time-invariant contributions. *Hydrology and Earth System Sciences,* 16**,** 2169-2179.

MLADENOVA, I. E., JACKSON, T. J., BINDLISH, R. & HENSLEY, S. 2013. Incidence Angle Normalization of Radar Backscatter Data. *IEEE Transactions on Geoscience and Remote Sensing,* 51**,** 1791-1804. Available: 10.1109/TGRS.2012.2205264

MLADENOVA, I. E., JACKSON, T. J., NJOKU, E., BINDLISH, R., CHAN, S., COSH, M. H., HOLMES, T. R. H., DE JEU, R. A. M., JONES, L., KIMBALL, J., PALOSCIA, S. & SANTI, E. 2014. Remote monitoring of soil moisture using passive microwave-based techniques — Theoretical basis and overview of selected algorithms for AMSR-E. *Remote Sensing of Environment,* 144**,** 197-213. Available: https://doi.org/10.1016/j.rse.2014.01.013

MOHANTY, B. P., COSH, M. H., LAKSHMI, V. & MONTZKA, C. 2017. Soil Moisture Remote Sensing: State-of-the-Science. *Vadose Zone Journal,* 16. Available: 10.2136/vzj2016.10.0105

MOHANTY, B. P. & SKAGGS, T. H. 2001. Spatio-temporal evolution and time-stable characteristics of soil moisture within remote sensing footprints with varying soil, slope, and vegetation. *Advances in Water Resources,* 24**,** 1051-1067. Available: https://doi.org/10.1016/S0309-1708(01)00034-3

MOIR, J., SCOTTER, D., HEDLEY, M. & MACKAY, A. 2000. A climate-driven, soil fertility dependent, pasture production model. *New Zealand Journal of Agricultural Research,* 43**,** 491-500.

MOLINA, A. J., LATRON, J., RUBIO, C. M., GALLART, F. & LLORENS, P. 2014. Spatio-temporal variability of soil water content on the local scale in a Mediterranean mountain area (Vallcebre, North Eastern Spain). How different spatio-temporal scales reflect mean soil water content. *Journal of Hydrology,* 516**,** 182-192. Available: https://doi.org/10.1016/j.jhydrol.2014.01.040

MONAGHAN, R. M., HEDLEY, M. J., DI, H. J., MCDOWELL, R. W., CAMERON, K. C. & LEDGARD, S. F. 2007. Nutrient management in New Zealand pastures— recent developments and future issues. *New Zealand Journal of Agricultural Research,* 50**,** 181-201. Available: 10.1080/00288230709510290

MOORE, I. D., BURCH, G. J. & MACKENZIE, D. H. 1988. Topographic effects on the distribution of surface water and the location of ephemeral gullies. *American Society of Agricultural and Biological Engineers,* 31**,** 1098-1107. Available: 10.13031/2013.30829

MOORE, I. D., GRAYSON, R. B. & LADSON, A. R. 1991. Digital terrain modelling: A review of hydrological, geomorphological, and biological applications. *Hydrological Processes,* 5**,** 3-30. Available: 10.1002/hyp.3360050103

MOOT, D., MILLS, A., LUCAS, D. & SCOTT, W. 2009. Country Pasture/Forage Resource Profiles New Zealand. *Publishing Policy and Support Branch, Office of Knowledge Exchange, Research and Extension, Food and Agriculture Organization of the United Nations (FAO), Viale delle Terme di Caracalla, Rome, Italy*.

MOOT, D. J., SCOTT, W. R., ROY, A. M. & NICHOLLS, A. C. 2000. Base temperature and thermal time requirements for germination and emergence of temperate pasture species. *New Zealand Journal of Agricultural Research,* 43**,** 15-25. Available: 10.1080/00288233.2000.9513404

MORAN, M. S., MCELROY, S., WATTS, J. M. & PETERS LIDARD, C. D. 2006. Radar remote sensing for estimation of surface soil moisture at the watershed scale. *Modeling and Remote Sensing Applied in Agriculture (US and Mexico)***,** 91-106.

MORAN, M. S., PETERS-LIDARD, C. D., WATTS, J. M. & MCELROY, S. 2004. Estimating soil moisture at the watershed scale with satellite-based radar and land surface models. *Canadian Journal of Remote Sensing,* 30**,** 805-826. Available: 10.5589/m04-043

MOREIRA, A., PRATS-IRAOLA, P., YOUNIS, M., KRIEGER, G., HAJNSEK, I. & PAPATHANASSIOU, K. P. 2013. A tutorial on synthetic aperture radar. *IEEE Geoscience and remote sensing magazine,* 1**,** 6-43.

MORITZ, S. & BARTZ-BEIELSTEIN, T. 2017. imputeTS: Time Series Missing Value Imputation. *The R Journal.* 2.6 ed.

MORRISON, J. 2017. *The Pastoral Industry Forage Discussion Document*.

MPI, M. O. P. I. 2018. *Situation and outlook for primary industries, March 2018*. Wellington, New Zealand: Ministry of Primary Industries.

MUÑOZ-CARPENA, R., SHUKLA, S. & MORGAN, K. 2004. *Field devices for monitoring soil water content*, University of Florida Cooperative Extension Service, Institute of Food and Agricultural Sciences, EDIS.

MURO, J., CANTY, M., CONRADSEN, K., HÜTTICH, C., NIELSEN, A., SKRIVER, H., REMY, F., STRAUCH, A., THONFELD, F. & MENZ, G. 2016. Short-Term Change Detection in Wetlands Using Sentinel-1 Time Series. *Remote Sensing,* 8**,** 795.

MURRAY, K. 1982. The Place of Soil Conservation in Hill Country. *Hill Country Potential, 4th National Conference of the Society of Farm Management***,** 85-90.

MURRAY, R. I., YULE, I. J. & GILLINGHAM, A. G. 2007. Developing variable rate application technology: Modelling annual pasture production on hill country. *New Zealand Journal of Agricultural Research,* 50**,** 41-52. Available: 10.1080/00288230709510281

REFERENCES

MURUNGU, F. S., CHIDUZA, C., MUCHAONYERWA, P. & MNKENI, P. N. S. 2011. Mulch effects on soil moisture and nitrogen, weed growth and irrigated maize productivity in a warm-temperate climate of South Africa. *Soil and Tillage Research,* 112**,** 58-65. Available: https://doi.org/10.1016/j.still.2010.11.005

NAGELMÜLLER, S., KIRCHGESSNER, N., YATES, S., HILTPOLD, M. & WALTER, A. 2016. Leaf Length Tracker: a novel approach to analyse leaf elongation close to the thermal limit of growth in the field. *Journal of Experimental Botany,* 67**,** 1897-1906. Available: 10.1093/jxb/erw003

NATIONAL ACADEMIES OF SCIENCES, E. & MEDICINE 2015. *A Strategy for Active Remote Sensing Amid Increased Demand for Radio Spectrum,* Washington, DC, The National Academies Press. Available: doi:10.17226/21729

NICHOLS, S., ZHANG, Y. & AHMAD, A. 2011. Review and evaluation of remote sensing methods for soil-moisture estimation. *Journal of Photonics for Energy***,** 028001-028001-17. Available: 10.1117/1.3534910

NIEMANN, K. O. & EDGELL, M. C. R. 1993. Preliminary analysis of spatial and temporal distribution of soil moisture on a deforested slope. *Physical Geography,* 14**,** 449-464. Available: 10.1080/02723646.1993.10642491

NIWA CLIFLO. 1953-2017. *National Climate Database (CliFlo)* [Online]. Available: https://cliflo.niwa.co.nz/ [Accessed 02/10/2016 2016].

NJOKU, E. G. & ENTEKHABI, D. 1996. Passive microwave remote sensing of soil moisture. *Journal of Hydrology,* 184**,** 101-129. Available: https://doi.org/10.1016/0022-1694(95)02970-2

NOBORIO, K. 2001. Measurement of soil water content and electrical conductivity by time domain reflectometry: a review. *Computers and Electronics in Agriculture,* 31**,** 213-237. Available: https://doi.org/10.1016/S0168-1699(00)00184-8

NOLZ, R. 2013. *Performance assessment of selected devices for monitoring soil water balance components with respect to agricultural water management.* Dr. nat. techn, University of Natural Resources and Life Sciences.

NOTARNICOLA, C., ANGIULLI, M. & POSA, F. 2008. Soil moisture retrieval from remotely sensed data: Neural network approach versus Bayesian method. *IEEE Transactions on Geoscience and Remote Sensing,* 46**,** 547-557.

NYBERG, L. 1996. Spatial variability of soil water content in the covered catchment at Gårdsjön, Sweden. *Hydrological Processes,* 10**,** 89-103.

OCHSNER, T. E., COSH, M. H., CUENCA, R. H., DORIGO, W. A., DRAPER, C. S., HAGIMOTO, Y., KERR, Y. H., NJOKU, E. G., SMALL, E. E., ZREDA, M. & LARSON, K. M. 2013. State of the Art in Large-Scale Soil Moisture Monitoring. *Soil Science Society of America Journal,* 77**,** 1888-1919. Available: 10.2136/sssaj2013.03.0093

OGILVY, J. A. & MERKLINGER, H. M. 1991. Theory of Wave Scattering from Random Rough Surfaces. *The Journal of the Acoustical Society of America,* 90**,** 3382-3382. Available: 10.1121/1.401410

OGLE, G., LING, H. & LARKIN, R. 2016. *Addition of new slope and aspect equations*. Ravensdown Ltd.: Ravensdown Ltd.

OGLE, G. & MA, S. 2015. *Calibrating the Pasture Growth Forecaster's soil fertility*. Ravensdown Fertiliser.

OLARIU, S. & STOJMENOVIC, I. Design Guidelines for Maximizing Lifetime and Avoiding Energy Holes in Sensor Networks with Uniform Distribution and Uniform Reporting.

Proceedings IEEE INFOCOM 2006. 25TH IEEE International Conference on Computer Communications, April 2006 2006. 1-12.

OLDAK, A., JACKSON, T. J., STARKS, P. & ELLIOTT, R. 2003. Mapping near-surface soil moisture on regional scale using ERS-2 SAR data. *International Journal of Remote Sensing,* 24**,** 4579-4598. Available: 10.1080/0143116031000070463

OSBORN, W. & COWIE, J. Review of Manawatu farming. Proceedings of the New Zealand Grassland Association, 1978.

OUCHI, K. 2013. Recent Trend and Advance of Synthetic Aperture Radar with Selected Topics. *Remote Sensing,* 5**,** 716.

OWE, M., JONES, E. B. & SCHMUGGE, T. J. 1982. Soil moisture variation patterns observed in Hand County, South Dakota. *JAWRA Journal of the American Water Resources Association,* 18**,** 949-954. Available: 10.1111/j.1752-1688.1982.tb00100.x

OYEOGBE, A., OLUWASEMIRE, K. O. & G.E, A. 2012. *Modelling soil water characteristics of an inland valley soil*.

OZER, M., ORHAN, M. & ISIK, N. S. 2010. Effect of particle optical properties on size distribution of soils obtained by laser diffraction. *Environmental & Engineering Geoscience,* 16**,** 163-173.

PACHAURI, R. K., ALLEN, M. R., BARROS, V. R., BROOME, J., CRAMER, W., CHRIST, R., CHURCH, J. A., CLARKE, L., DAHE, Q. & DASGUPTA, P. 2014. *Climate change 2014: synthesis report. Contribution of Working Groups I, II and III to the fifth assessment report of the Intergovernmental Panel on Climate Change*, IPCC.

PACHEPSKY, Y., RADCLIFFE, D. E. & SELIM, H. M. 2003. *Scaling methods in soil physics*, CRC press.

PAGÈS, J. 2014. *Multiple factor analysis by example using R*, Chapman and Hall/CRC.

PALOSCIA, S., PAMPALONI, P., PETTINATO, S. & SANTI, E. 2008. A Comparison of Algorithms for Retrieving Soil Moisture from ENVISAT/ASAR Images. *IEEE Transactions on Geoscience and Remote Sensing,* 46**,** 3274-3284. Available: 10.1109/TGRS.2008.920370

PALOSCIA, S., PETTINATO, S., SANTI, E., NOTARNICOLA, C., PASOLLI, L. & REPPUCCI, A. 2013. Soil moisture mapping using Sentinel-1 images: Algorithm and preliminary validation. *Remote Sensing of Environment,* 134**,** 234-248. Available: http://dx.doi.org/10.1016/j.rse.2013.02.027

PALTINEANU, I. C. & STARR, J. L. 1997. Real-time Soil Water Dynamics Using Multisensor Capacitance Probes: Laboratory Calibration. *Soil Science Society of America Journal,* 61**,** 1576-1585. Available: 10.2136/sssaj1997.03615995006100060006x

PAN, F. & PETERS-LIDARD, C. D. 2008. On the Relationship Between Mean and Variance of Soil Moisture Fields1. *JAWRA Journal of the American Water Resources Association,* 44**,** 235-242. Available: doi:10.1111/j.1752-1688.2007.00150.x

PAN, Z., ARRITT, R. W., GUTOWSKI JR, W. J. & TAKLE, E. S. 2001. Soil moisture in a regional climate model: simulation and projection. *Geophysical research letters,* 28**,** 2947-2950.

PARFITT, R. L., JOE, E. N. & COOK, F. J. 1985. Water use and pasture growth on Judgeford silt loam. *New Zealand Journal of Agricultural Research,* 28**,** 387-392. Available: 10.1080/00288233.1985.10430443

PARK, S., IM, J., PARK, S. & RHEE, J. 2017. Drought monitoring using high resolution soil moisture through multi-sensor satellite data fusion over the Korean peninsula. *Agricultural and*

Forest Meteorology, 237-238**,** 257-269. Available: https://doi.org/10.1016/j.agrformet.2017.02.022

PARVIN, N. & DEGRÉ, A. 2016. Soil-specific calibration of capacitance sensors considering clay content and bulk density. *Soil Research,* 54**,** 111-119. Available: https://doi.org/10.1071/SR15036

PASOLLI, L., NOTARNICOLA, C., BERTOLDI, G., BRUZZONE, L., REMELGADO, R., GREIFENEDER, F., NIEDRIST, G., CHIESA, S. D., TAPPEINER, U. & ZEBISCH, M. 2015. Estimation of Soil Moisture in Mountain Areas Using SVR Technique Applied to Multiscale Active Radar Images at C-Band. *IEEE Journal of Selected Topics in Applied Earth Observations and Remote Sensing,* 8**,** 262-283. Available: 10.1109/JSTARS.2014.2378795

PASOLLI, L., NOTARNICOLA, C., BRUZZONE, L., BERTOLDI, G., DELLA CHIESA, S., HELL, V., NIEDRIST, G., TAPPEINER, U., ZEBISCH, M., DEL FRATE, F. & VAGLIO LAURIN, G. 2011. Estimation of Soil Moisture in an Alpine Catchment with RADARSAT2 Images. *Applied and Environmental Soil Science,* 2011. Available: 10.1155/2011/175473

PASTICK, N., WYLIE, B. & WU, Z. 2018. Spatiotemporal Analysis of Landsat-8 and Sentinel-2 Data to Support Monitoring of Dryland Ecosystems. *Remote Sensing,* 10**,** 791.

PATEL, P., SRIVASTAVA, H. S., PANIGRAHY, S. & PARIHAR, J. S. 2006. Comparative evaluation of the sensitivity of multi-polarized multi-frequency SAR backscatter to plant density. *International Journal of Remote Sensing,* 27**,** 293-305. Available: 10.1080/01431160500214050

PEACOCK, J. M. 1975. Temperature and Leaf Growth in Lolium perenne. III. Factors Affecting Seasonal Differences. *Journal of Applied Ecology,* 12**,** 685-697. Available: 10.2307/2402182

PEARCE, P., FEDAEFF, N., MULLAN, B., SOOD, A., BELL, R., TAIT, A., COLLINS, D. & ZAMMIT, C. 2017. *Climate change and variability - Wellington Region*. Auckland: National Institute of Water & Atmospheric Research Ltd. (NIWA). Report number: 2017066AK.

PENG, Z., TIAN, F., HU, H., ZHAO, S., TIE, Q., SHENG, H., DARNAULT, C. & LU, H. 2016. Spatial Variability of Soil Moisture in a Forest Catchment: Temporal Trend and Contributors. *Forests,* 7**,** 154.

PENNA, D., BROCCA, L., BORGA, M. & DALLA FONTANA, G. 2013. Soil moisture temporal stability at different depths on two alpine hillslopes during wet and dry periods. *Journal of Hydrology,* 477**,** 55-71. Available: https://doi.org/10.1016/j.jhydrol.2012.10.052

PETERS, A. J., WALTER-SHEA, E. A., JI, L., VINA, A., HAYES, M. & SVOBODA, M. D. 2002. Drought monitoring with NDVI-based standardized vegetation index. *Photogrammetric engineering and remote sensing,* 68**,** 71-75.

PETROPOULOS, G. P. 2013. *Remote sensing of energy fluxes and soil moisture content*, CRC Press.

PETROPOULOS, G. P., GRIFFITHS, H. M., DORIGO, W., XAVER, A. & GRUBER, A. 2014. Surface Soil Moisture Estimation: Significance, Controls, and Conventional Measurement Techniques. *In:* PETROPOULOS, G. P. (ed.) *Remote Sensing of Energy Fluxes and Soil Moisture Content.*

PETROPOULOS, G. P., IRELAND, G. & BARRETT, B. 2015. Surface soil moisture retrievals from remote sensing: Current status, products & future trends. *Physics and Chemistry of the Earth, Parts A/B/C,* 83–84**,** 36-56. Available: http://dx.doi.org/10.1016/j.pce.2015.02.009

PETTITT, A. N. & MCBRATNEY, A. B. 1993. Sampling Designs for Estimating Spatial Variance Components. *Journal of the Royal Statistical Society. Series C (Applied Statistics),* 42**,** 185-209. Available: 10.2307/2347420

PHILLIPS, R., EKEN, M. & RUNDQUIST, B. A topographic framework for estimating spatial variation in hill country grasslands. Hill Country Symposium. Grassland Research and Practice Series, 2016. 119-126.

PIERDICCA, N., CASTRACANE, P. & PULVIRENTI, L. 2008. Inversion of electromagnetic models for bare soil parameter estimation from multifrequency polarimetric SAR data. *Sensors,* 8**,** 8181-8200.

PORPORATO, A., D'ODORICO, P., LAIO, F., RIDOLFI, L. & RODRIGUEZ-ITURBE, I. 2002. Ecohydrology of water-controlled ecosystems. *Advances in Water Resources,* 25**,** 1335-1348. Available: https://doi.org/10.1016/S0309-1708(02)00058-1

POST, W. M. & KWON, K. C. 2000. Soil carbon sequestration and land-use change: processes and potential. *Global change biology,* 6**,** 317-327.

PRICE, J. C. 1977. Thermal inertia mapping: A new view of the Earth. *Journal of Geophysical Research,* 82**,** 2582-2590. Available: doi:10.1029/JC082i018p02582

PULLANAGARI, R. R., KERESZTURI, G. & YULE, I. 2018. Integrating Airborne Hyperspectral, Topographic, and Soil Data for Estimating Pasture Quality Using Recursive Feature Elimination with Random Forest Regression. *Remote Sensing,* 10**,** 1117.

PULLANAGARI, R. R., KERESZTURI, G., YULE, I. J. & GHAMISI, P. Assessing the performance of multiple spectral–spatial features of a hyperspectral image for classification of urban land cover classes using support vector machines and artificial neural network. 2017. SPIE, 22.

QIU, Y., FU, B., WANG, J. & CHEN, L. 2001a. Soil moisture variation in relation to topography and land use in a hillslope catchment of the Loess Plateau, China. *Journal of Hydrology,* 240**,** 243-263. Available: http://dx.doi.org/10.1016/S0022-1694(00)00362-0

QIU, Y., FU, B., WANG, J. & CHEN, L. 2001b. Spatial variability of soil moisture content and its relation to environmental indices in a semi-arid gully catchment of the Loess Plateau, China. *Journal of Arid Environments,* 49**,** 723-750. Available: http://dx.doi.org/10.1006/jare.2001.0828

QUESNEY, A., LE HÉGARAT-MASCLE, S., TACONET, O., VIDAL-MADJAR, D., WIGNERON, J. P., LOUMAGNE, C. & NORMAND, M. 2000. Estimation of Watershed Soil Moisture Index from ERS/SAR Data. *Remote Sensing of Environment,* 72**,** 290-303. Available: https://doi.org/10.1016/S0034-4257(99)00102-9

R CORE TEAM 2017. R: A language and environment for statistical computing. Vienna, Austria: R Foundation for Statistical Computing.

RADCLIFFE, J. 1974a. Seasonal distribution of pasture production in New Zealand: I. Methods of measurement. *New Zealand journal of experimental agriculture,* 2**,** 337-340.

RADCLIFFE, J. E. Cutting techniques for pasture yields on hill country. Proceedings of the New Zealand Grassland Association, 1971. 91-103.

RADCLIFFE, J. E. 1974b. Seasonal distribution of pasture production in New Zealand. *New Zealand Journal of Experimental Agriculture,* 2**,** 341-348. Available: 10.1080/03015521.1974.10427693

REFERENCES

RADCLIFFE, J. E. 1982. Effects of aspect and topography on pasture production in hill country. *New Zealand Journal of Agricultural Research,* 25**,** 485-496. Available: 10.1080/00288233.1982.10425211

RADCLIFFE, J. E., DALE, W. R. & VIGGERS, E. 1968. Pasture production measurements on hill country. *New Zealand Journal of Agricultural Research,* 11**,** 685-700. Available: 10.1080/00288233.1968.10422447

RADCLIFFE, J. E., JOHNSTONE, P. D. & YOUNG, S. R. 1977. Survival and growth of introduced grasses in Canterbury hill pastures. *New Zealand journal of experimental agriculture,* 5**,** 129-135.

RADCLIFFE, J. E. & LEFEVER, K. R. 1981. Aspect influences on pasture microclimate at Coopers Creek, North Canterbury. *New Zealand Journal of Agricultural Research,* 24**,** 55-56. Available: 10.1080/00288233.1981.10420871

RADCLIFFE, J. E., YOUNG, S. & CLARKE, D. Effects of sunny and shady aspect on pasture yield, digestibility and sheep performance in Canterbury. Proceedings of the New Zealand Grassland Association, 1976. 66-77.

RAHGOZAR, M., SHAH, N. & ROSS, M. 2012. Estimation of Evapotranspiration and Water Budget Components Using Concurrent Soil Moisture and Water Table Monitoring. *ISRN Soil Science,* 2012**,** 15. Available: 10.5402/2012/726806

RAHIMZADEH-BAJGIRAN, P., BERG, A. A., CHAMPAGNE, C. & OMASA, K. 2013. Estimation of soil moisture using optical/thermal infrared remote sensing in the Canadian Prairies. *ISPRS Journal of Photogrammetry and Remote Sensing,* 83**,** 94-103. Available: https://doi.org/10.1016/j.isprsjprs.2013.06.004

RAWAT, P., SINGH, K. D., CHAOUCHI, H. & BONNIN, J. M. 2014. Wireless sensor networks: a survey on recent developments and potential synergies. *The Journal of Supercomputing,* 68**,** 1-48. Available: 10.1007/s11227-013-1021-9

REES, W. G. 2013. *Physical principles of remote sensing*, Cambridge university press.

REFSGAARD, J. C. 2001. Towards a formal approach to calibration and validation of models using spatial data. *Spatial patterns in catchment hydrology: observations and modelling***,** 329-354.

REYNOLDS, S. G. 1970. The gravimetric method of soil moisture determination Part III An examination of factors influencing soil moisture variability. *Journal of Hydrology,* 11**,** 288-300. Available: http://dx.doi.org/10.1016/0022-1694(70)90068-5

RICKERT, K. G., STUTH, J. W. & MCKEON, G. M. 2000. Modeling pasture and animal production. *In:* MANNETJE, L. & JOONES, R. M. (eds.) *Field and laboratory methods for grassland and animal production research.* Wallingofrd, UK: CAB International.

RIEGER, W. 1998. A phenomenon-based approach to upslope contributing area and depressions in DEMs. *Hydrological Processes,* 12**,** 857-872. Available: 10.1002/(SICI)1099-1085(199805)12:6<857::AID-HYP659>3.0.CO;2-B

ROBBINS, N. E. & DINNENY, J. R. 2018. Growth is required for perception of water availability to pattern root branches in plants. *Proceedings of the National Academy of Sciences,* 115**,** E822-E831. Available: 10.1073/pnas.1710709115

ROBERT, C. 2014. Machine learning, a probabilistic perspective. Taylor & Francis.

ROBERTS, A. H. C. & WHITE, M. D. 2016. From there to where? Past, present and future soil fertility management on hill country farms. *Hill Country – Grassland Research and Practice Series,* 16**,** 127-136.

ROBERTSON, B., BROWN, J., MCDONALD, T. & JAKSONS, P. 2013. BAS: Balanced acceptance sampling of natural resources. *Biometrics,* 69**,** 776-784.

ROBINSON, D., CAMPBELL, C., HOPMANS, J., HORNBUCKLE, B., JONES, S. B., KNIGHT, R., OGDEN, F., SELKER, J. & WENDROTH, O. 2008a. Soil moisture measurement for ecological and hydrological watershed-scale observatories: A review. *Vadose Zone Journal,* 7**,** 358-389.

ROBINSON, D. A., ABDU, H., LEBRON, I. & JONES, S. B. 2012. Imaging of hill-slope soil moisture wetting patterns in a semi-arid oak savanna catchment using time-lapse electromagnetic induction. *Journal of Hydrology,* 416-417**,** 39-49. Available: https://doi.org/10.1016/j.jhydrol.2011.11.034

ROBINSON, D. A., BELL, J. P. & BATCHELOR, C. H. 1994. Influence of iron minerals on the determination of soil water content using dielectric techniques. *Journal of Hydrology,* 161**,** 169-180. Available: https://doi.org/10.1016/0022-1694(94)90127-9

ROBINSON, D. A., CAMPBELL, C. S., HOPMANS, J. W., HORNBUCKLE, B. K., JONES, S. B., KNIGHT, R., OGDEN, F., SELKER, J. & WENDROTH, O. 2008b. Soil Moisture Measurement for Ecological and Hydrological Watershed-Scale Observatories: A Review All rights reserved. No part of this periodical may be reproduced or transmitted in any form or by any means, electronic or mechanical, including photocopying, recording, or any information storage and retrieval system, without permission in writing from the publisher. *Vadose Zone Journal,* 7**,** 358-389. Available: 10.2136/vzj2007.0143

ROBINSON, D. A., JONES, S. B., WRAITH, J. M., OR, D. & FRIEDMAN, S. P. 2003. A Review of Advances in Dielectric and Electrical Conductivity Measurement in Soils Using Time Domain Reflectometry. *Vadose Zone Journal,* 2**,** 444-475. Available: 10.2113/2.4.444

ROBOCK, A., VINNIKOV, K. Y., SRINIVASAN, G. & ENTIN, J. K. 2000a. The global soil moisture data bank. *Bulletin of the American Meteorological Society,* 81**,** 1281.

ROBOCK, A., VINNIKOV, K. Y., SRINIVASAN, G., ENTIN, J. K., HOLLINGER, S. E., SPERANSKAYA, N. A., LIU, S. & NAMKHAI, A. 2000b. The Global Soil Moisture Data Bank. *Bulletin of the American Meteorological Society,* 81**,** 1281-1299.

RODELL, M. 2012. Satellite Gravimetry Applied to Drought Monitoring. *Remote Sensing of Drought: Innovative Monitoring Approaches***,** 261.

RODELL, M., HOUSER, P. R., JAMBOR, U., GOTTSCHALCK, J., MITCHELL, K., MENG, C.-J., ARSENAULT, K., COSGROVE, B., RADAKOVICH, J., BOSILOVICH, M., ENTIN, J. K., WALKER, J. P., LOHMANN, D. & TOLL, D. 2004. The Global Land Data Assimilation System. *Bulletin of the American Meteorological Society,* 85**,** 381-394. Available: 10.1175/bams-85-3-381

RODRIGEZ-ITURBE, I. 2000. Ecohydrology: A hydrologic perspective of climate-soil-vegetation dynamies. *Water Resources Research,* 36**,** 3-9. Available: doi:10.1029/1999WR900210

RODRÍGUEZ-FERNÁNDEZ, N., AL BITAR, A., COLLIANDER, A. & ZHAO, T. 2019. Soil Moisture Remote Sensing across Scales. Multidisciplinary Digital Publishing Institute.

RODRÍGUEZ-ITURBE, I. & PORPORATO, A. 2007. *Ecohydrology of water-controlled ecosystems: soil moisture and plant dynamics*, Cambridge University Press.

RODRIGUEZ-ITURBE, I., D'ODORICO, P., PORPORATO, A. & RIDOLFI, L. 1999. On the spatial and temporal links between vegetation, climate, and soil moisture. *Water Resources Research,* 35**,** 3709-3722. Available: 10.1029/1999WR900255

ROMANO, N. 2014. Soil moisture at local scale: Measurements and simulations. *Journal of Hydrology,* 516**,** 6-20. Available: http://dx.doi.org/10.1016/j.jhydrol.2014.01.026

REFERENCES

ROMER, K. & MATTERN, F. 2004. The design space of wireless sensor networks. *IEEE Wireless Communications,* 11**,** 54-61. Available: 10.1109/MWC.2004.1368897

ROMERA, A., BEUKES, P., CLARK, D., CLARK, C. & TAIT, A. 2013. Pasture growth model to assist management on dairy farms: testing the concept with farmers. *Grassland Science,* 59**,** 20-29.

ROMERA, A. J., BEUKES, P., CLARK, C., CLARK, D., LEVY, H. & TAIT, A. 2010. Use of a pasture growth model to estimate herbage mass at a paddock scale and assist management on dairy farms. *Computers and Electronics in Agriculture,* 74**,** 66-72. Available: https://doi.org/10.1016/j.compag.2010.06.006

ROMERA, A. J., MCCALL, D. G., LEE, J. M. & AGNUSDEI, M. G. 2009. Improving the McCall herbage growth model. *New Zealand Journal of Agricultural Research,* 52**,** 477-494. Available: 10.1080/00288230909510529

ROTH, K., SCHULIN, R., FLÜHLER, H. & ATTINGER, W. 1990. Calibration of time domain reflectometry for water content measurement using a composite dielectric approach. *Water Resources Research,* 26**,** 2267-2273.

ROUMENINA, E., ATZBERGER, C., VASSILEV, V., DIMITROV, P., KAMENOVA, I., BANOV, M., FILCHEV, L. & JELEV, G. 2015. Single- and Multi-Date Crop Identification Using PROBA-V 100 and 300 m S1 Products on Zlatia Test Site, Bulgaria. *Remote Sensing,* 7**,** 13843.

ROWNTREE, P. R. & BOLTON, J. A. 1983. Simulation of the atmospheric response to soil moisture anomalies over Europe. *Quarterly Journal of the Royal Meteorological Society,* 109**,** 501-526. Available: 10.1002/qj.49710946105

RÜDIGER, C., WESTERN, A. W., WALKER, J. P., SMITH, A. B., KALMA, J. D. & WILLGOOSE, G. R. 2010. Towards a general equation for frequency domain reflectometers. *Journal of Hydrology,* 383**,** 319-329. Available: https://doi.org/10.1016/j.jhydrol.2009.12.046

RUDNICK, D. R. & IRMAK, S. 2014. Spatial and Temporal Maize Soil Water Extraction (Depletion) Dynamics: Part I. Development and Evaluation of a Soil Water Extraction Model. *Transactions of the ASABE,* 57**,** 431. Available: https://doi.org/10.13031/trans.57.10253

RUDNICK, D. R., LO, T., SINGH, J., WERLE, R., MUÑOZ-ARRIOLA, F., SHAVER, T., BURR, C. A. & DORR, T. J. 2018. Reply to comments on "Performance assessment of factory and field calibrations for electromagnetic sensors in a loam soil". *Agricultural Water Management,* 203**,** 272-276. Available: https://doi.org/10.1016/j.agwat.2018.02.036

RYŻAK, M. & BIEGANOWSKI, A. 2011. Methodological aspects of determining soil particle-size distribution using the laser diffraction method. *Journal of Plant Nutrition and Soil Science,* 174**,** 624-633. Available: 10.1002/jpln.201000255

SABAGHY, S., WALKER, J. P., RENZULLO, L. J. & JACKSON, T. J. 2018. Spatially enhanced passive microwave derived soil moisture: Capabilities and opportunities. *Remote Sensing of Environment,* 209**,** 551-580. Available: https://doi.org/10.1016/j.rse.2018.02.065

SABINS, F. F. 2007. *Remote sensing: principles and applications*, Waveland Press.

SANO, E. E., HUETE, A. R., TROUFLEAU, D., MORAN, M. S. & VIDAL, A. 1998. Relation between ERS-1 synthetic aperture radar data and measurements of surface roughness and moisture content of rocky soils in a semiarid rangeland. *Water Resources Research,* 34**,** 1491-1498. Available: 10.1029/98WR00032

SANTI, E., PALOSCIA, S., PETTINATO, S., NOTARNICOLA, C., PASOLLI, L. & PISTOCCHI, A. 2013. Comparison between SAR Soil Moisture Estimates and Hydrological Model Simulations over the Scrivia Test Site. *Remote Sensing,* 5**,** 4961.

SATALINO, G., MATTIA, F., DAVIDSON, M. W. J., THUY LE, T., PASQUARIELLO, G. & BORGEAUD, M. 2002. On current limits of soil moisture retrieval from ERS-SAR data. *IEEE Transactions on Geoscience and Remote Sensing,* 40**,** 2438-2447. Available: 10.1109/TGRS.2002.803790

SAXTON, K., RAWLS, W. J., ROMBERGER, J. & PAPENDICK, R. 1986. Estimating generalized soil-water characteristics from texture 1. *Soil Science Society of America Journal,* 50**,** 1031-1036.

SAXTON, K. E. & RAWLS, W. J. 2006. Soil water characteristic estimates by texture and organic matter for hydrologic solutions. *Soil science society of America Journal,* 70**,** 1569-1578.

SAXTON, K. E. & WILLEY, P. H. 2005. The SPAW model for agricultural field and pond hydrologic simulation. *Watershed Models. CRC Press, Boca Raton, FL. Doi,* 10**,** 401-422.

SCHABACK, R. 2007. A practical guide to radial basis functions. *Electronic Resource,* 11**,** 1-12.

SCHELLBERG, J., HILL, M. J., GERHARDS, R., ROTHMUND, M. & BRAUN, M. 2008. Precision agriculture on grassland: Applications, perspectives and constraints. *European Journal of Agronomy,* 29**,** 59-71. Available: https://doi.org/10.1016/j.eja.2008.05.005

SCHMUGGE, T. & JACKSON, T. 1994. Mapping surface soil moisture with microwave radiometers. *Meteorology and Atmospheric Physics,* 54**,** 213-223.

SCHMUGGE, T. J., JACKSON, T. J. & MCKIM, H. L. 1980. Survey of methods for soil moisture determination. *Water Resources Research,* 16**,** 961-979. Available: 10.1029/WR016i006p00961

SCHMUGGE, T. J., KUSTAS, W. P., RITCHIE, J. C., JACKSON, T. J. & RANGO, A. 2002. Remote sensing in hydrology. *Advances in Water Resources,* 25**,** 1367-1385. Available: https://doi.org/10.1016/S0309-1708(02)00065-9

SCHNEIDER, K., HUISMAN, J. A., BREUER, L., ZHAO, Y. & FREDE, H. G. 2008. Temporal stability of soil moisture in various semi-arid steppe ecosystems and its application in remote sensing. *Journal of Hydrology,* 359**,** 16-29. Available: https://doi.org/10.1016/j.jhydrol.2008.06.016

SCHWARTZ, R. C., EVETT, S. R. & LASCANO, R. J. 2018. Comments on "J. Singh et al., Performance assessment of factory and field calibrations for electromagnetic sensors in a loam soil" [Agric. Water Manage. 196 (2018) 87–98]. *Agricultural Water Management,* 203**,** 236-239. Available: https://doi.org/10.1016/j.agwat.2018.02.029

SCOTT, D. 2002. Sustainability of New Zealand high-country pastures under contrasting development inputs. 8. Modelling sheep carrying capacity. *New Zealand Journal of Agricultural Research,* 45**,** 151-163. Available: 10.1080/00288233.2002.9513505

SCOTT, D., KEOGHAN, J. M., COSSENS, G. G., MAUNSELL, L. A., FLOATE, M. J. S., WILLS, B. J. & DOUGLAS, G. 1985. Limitations to pasture production and choice of species. *In:* BURGESS, R. E. & BROCK, J. L. (eds.) *Using Herbage Cultivars.* 3rd ed. Palmerston North: New Zealand Grassland Association.

SCOTTER, D., CLOTHIER, B. & TURNER, M. 1979. The soil water balance in a fragiaqualf and its effect on pasture growth in central New Zealand. *Soil Research,* 17**,** 455-465.

SCRIMGEOUR, F. 2016. Pathways ahead for New Zealand hill country farming. *JNZ Grassl,* 78**,** 73-82.

SEDANO, F., KEMPENEERS, P. & HURTT, G. 2014. A Kalman filter-based method to generate continuous time series of medium-resolution NDVI images. *Remote Sensing,* 6**,** 12381-12408.

REFERENCES

SENEVIRATNE, S. I., CORTI, T., DAVIN, E. L., HIRSCHI, M., JAEGER, E. B., LEHNER, I., ORLOWSKY, B. & TEULING, A. J. 2010. Investigating soil moisture–climate interactions in a changing climate: A review. *Earth-Science Reviews,* 99**,** 125-161. Available: https://doi.org/10.1016/j.earscirev.2010.02.004

SERRARENS, D., MACINTYRE, J. L., HOPMANS, J. W. & BASSOI, L. H. 2000. Soil moisture calibration of TDR multilevel probes. *Scientia Agricola,* 57**,** 349-354.

SEYFRIED, M. S. & MURDOCK, M. D. 2001. Response of a New Soil Water Sensor to Variable Soil, Water Content, and Temperature. *Soil Science Society of America Journal,* 65**,** 28-34. Available: 10.2136/sssaj2001.65128x

SHADBOLT, N. & MARTIN, S. 2005. *Farm Management in New Zealand*, Oxford University Press.

SHARKOV, E. A. 2003. *Passive microwave remote sensing of the Earth: physical foundations*, Springer Science & Business Media.

SHARMA, D., VERMA, S. & SHARMA, K. 2013a. Network Topologies in Wireless Sensor Networks: A Review 1.

SHARMA, H., SHUKLA, M. K., BOSLAND, P. W. & STEINER, R. 2017. Soil moisture sensor calibration, actual evapotranspiration, and crop coefficients for drip irrigated greenhouse chile peppers. *Agricultural Water Management,* 179**,** 81-91. Available: https://doi.org/10.1016/j.agwat.2016.07.001

SHARMA, S., KUMAR, D. & KISHORE, K. 2013b. Wireless Sensor Networks-A Review on Topologies and Node Architecture. *International Journal of Computer Sciences and Engineering,* 1**,** 19-25.

SHEATH, G. W. & BOOM, R. C. 1985. Effects of November–April grazing pressure on hill country pastures 3. Interrelationship with soil and pasture variation. *New Zealand Journal of Experimental Agriculture,* 13**,** 341-349. Available: 10.1080/03015521.1985.10426102

SHEINER, L. B. & BEAL, S. L. 1981. Some suggestions for measuring predictive performance. *Journal of Pharmacokinetics and Biopharmaceutics,* 9**,** 503-512. Available: 10.1007/bf01060893

SHI, Z. H., ZHU, H. D., CHEN, J., FANG, N. F. & AI, L. 2012. Spatial heterogeneity of soil moisture and its relationships with environmental factors at small catchment level. *Chinese Journal of Applied Ecology,* 23**,** 889-895.

SHOSHANY, M., SVORAY, T., CURRAN, P. J., FOODY, G. M. & PEREVOLOTSKY, A. 2000. The relationship between ERS-2 SAR backscatter and soil moisture: Generalization from a humid to semi-arid transect. *International Journal of Remote Sensing,* 21**,** 2337-2343. Available: 10.1080/01431160050029620

SHUKLA, M. K. 2013. *Soil physics: An introduction*, CRC Press.

SIDHU, N., PEBESMA, E. & CÂMARA, G. 2018. Using Google Earth Engine to detect land cover change: Singapore as a use case. *European Journal of Remote Sensing,* 51**,** 486-500. Available: 10.1080/22797254.2018.1451782

SILVERMAN, B. W. 1986. *Density estimation for statistics and data analysis,* London, Chapman and Hall.

SINGH, J., LO, T., RUDNICK, D. R., DORR, T. J., BURR, C. A., WERLE, R., SHAVER, T. M. & MUÑOZ-ARRIOLA, F. 2018. Performance assessment of factory and field calibrations for electromagnetic sensors in a loam soil. *Agricultural Water Management,* 196**,** 87-98. Available: https://doi.org/10.1016/j.agwat.2017.10.020

SKAKUN, S., VERMOTE, E., ROGER, J.-C. & FRANCH, B. 2017. Combined use of Landsat-8 and Sentinel-2A images for winter crop mapping and winter wheat yield assessment at regional scale. *AIMS geosciences,* 3**,** 163.

SLEUTEL, S., DE NEVE, S., SINGIER, B. & HOFMAN, G. 2007. Quantification of organic carbon in soils: a comparison of methodologies and assessment of the carbon content of organic matter. *Communications in Soil Science and Plant Analysis,* 38**,** 2647-2657.

SMITH, M., ALLEN, R. & PEREIRA, L. 1998. Revised FAO methodology for crop-water requirements. *Management of nutrients and water in rainfed arid and semi-arid areas, proceedings of a consultants meeting.* Vienna: INTERNATIONAL ATOMIC ENERGY AGENCY.

SNAP, S. A. P. 2018. *Science toolbox exploitation platform* [Online]. ESA. Available: http://step.esa.int/main/download/ [Accessed 09/29/2018 2018].

SONNEVELD, M. P. W., BACKX, M. A. H. M. & BOUMA, J. 2003. Simulation of soil water regimes including pedotransfer functions and land-use related preferential flow. *Geoderma,* 112**,** 97-110. Available: http://dx.doi.org/10.1016/S0016-7061(02)00298-7

SOURIAL, N., WOLFSON, C., ZHU, B., QUAIL, J., FLETCHER, J., KARUNANANTHAN, S., BANDEEN-ROCHE, K., BÉLAND, F. & BERGMAN, H. 2010. Correspondence analysis is a useful tool to uncover the relationships among categorical variables. *Journal of clinical epidemiology,* 63**,** 638-646. Available: 10.1016/j.jclinepi.2009.08.008

SPERAZZA, M., MOORE, J. N. & HENDRIX, M. S. 2004. High-resolution particle size analysis of naturally occurring very fine-grained sediment through laser diffractometry: research methods papers. *Journal of Sedimentary Research,* 74**,** 736-743.

SPERRY J. S., HACKE U. G., OREN R. & COMSTOCK J. P. 2002. Water deficits and hydraulic limits to leaf water supply. *Plant, Cell & Environment,* 25**,** 251-263. Available: doi:10.1046/j.0016-8025.2001.00799.x

SRIVASTAVA, H. S., PATEL, P., SHARMA, Y. & NAVALGUND, R. R. 2009. Large-Area Soil Moisture Estimation Using Multi-Incidence-Angle RADARSAT-1 SAR Data. *IEEE Transactions on Geoscience and Remote Sensing,* 47**,** 2528-2535. Available: 10.1109/TGRS.2009.2018448

STACHEDER, M., KOENIGER, F. & SCHUHMANN, R. 2009. New Dielectric Sensors and Sensing Techniques for Soil and Snow Moisture Measurements. *Sensors (Basel, Switzerland),* 9**,** 2951-2967. Available: 10.3390/s90402951

STATISTICS New Zealand. 2015. *Agricultural Production Statistics: June 2015 (final)* [Online]. Statistics NZ. Available: http://www.stats.govt.nz/browse_for_stats/industry_sectors/agriculture-horticulture-forestry/AgriculturalProduction_final_HOTPJun15final.aspx [Accessed 15/10/2016 2016].

STATISTICS New Zealand 2018, updated April 2018. Environmental-economic accounts: 2018 (corrected). Stats NZ Tatauranga Aotearoa, Wellington, New Zealand.

STAVI, I., UNGAR, E. D., LAVEE, H. & SARAH, P. 2008. Grazing-induced spatial variability of soil bulk density and content of moisture, organic carbon and calcium carbonate in a semi-arid rangeland. *CATENA,* 75**,** 288-296. Available: https://doi.org/10.1016/j.catena.2008.07.007

STEPHEN, R. & REVFEIM, K. A comparison of three pasture measurement techniques. Proceedings of the New Zealand Grassland Association, 1971. 76-82.

REFERENCES

SUCKLING, F. E. T. 1959. Pasture management trials on unploughable hill country at Te Awa. II. Results for 1951-57. *New Zealand Journal of Agricultural Research,* 2**,** 488-543. Available: 10.1080/00288233.1959.10418033

SUCKLING, F. E. T. 1975. *Pasture management trials on unploughable hill country at Te Awa. III. Results for 1959-69*. Available: 10.1080/00288233.1959.10418033

SUGGATE, R. P., STEVENS, G. R. & TE PUNGA, M. T. 1978. *The Geology of New Zealand*, EC Keating, Govt. Printer.

SULEBAK, J. R., TALLAKSEN, L. M. & ERICHSEN, B. 2000. Estimation of areal soil moisture by use of terrain data. *Geogr. Ann,* 82**,** 89-105.

SUN, C., LIU, Y., ZHAO, S., ZHOU, M., YANG, Y. & LI, F. 2016. Classification mapping and species identification of salt marshes based on a short-time interval NDVI time-series from HJ-1 optical imagery. *International Journal of Applied Earth Observation and Geoinformation,* 45**,** 27-41. Available: https://doi.org/10.1016/j.jag.2015.10.008

TAPLEY, B. D., BETTADPUR, S., RIES, J. C., THOMPSON, P. F. & WATKINS, M. M. 2004. GRACE Measurements of Mass Variability in the Earth System. *Science,* 305**,** 503.

TEULING, A., UIJLENHOET, R., HURKMANS, R., MERLIN, O., PANCIERA, R., WALKER, J. & TROCH, P. 2007a. *Dry-end surface soil moisture variability during NAFE'06*. Available: 10.1029/2007GL031001

TEULING, A. J., HUPET, F., UIJLENHOET, R. & TROCH, P. A. 2007b. Climate variability effects on spatial soil moisture dynamics. *Geophysical Research Letters,* 34. Available: 10.1029/2006GL029080

TEULING, A. J. & TROCH, P. A. 2005. Improved understanding of soil moisture variability dynamics. *Geophysical Research Letters,* 32**,** n/a-n/a. Available: 10.1029/2004GL021935

THANOON, T. Y., ADNAN, R. & SAFFARI, S. E. Multiple factor analysis with continuous and dichotomous variables. AIP Conference Proceedings, 2014. AIP, 926-933.

THOMA, D., MORAN, M., BRYANT, R., COLLINS, C. H., RAHMAN, M. & SKIRVIN, S. Comparison of two methods for extracting surface soil moisture from C-band radar imagery. IGARSS 2004. 2004 IEEE International Geoscience and Remote Sensing Symposium, 20-24 Sept. 2004 2004. 827-830.

TOAN, T. L., BEAUDOIN, A., RIOM, J. & GUYON, D. 1992. Relating forest biomass to SAR data. *IEEE Transactions on Geoscience and Remote Sensing,* 30**,** 403-411. Available: 10.1109/36.134089

TOMLINSON, A. I. & SANSOM, J. 1994. *Temperature normals for New Zealand for the period 1961 to 1990*, NIWA Wellington, New Zealand.

TOPOUZELIS, K. & SINGHA, S. 2016. *Incidence angle Normalization of Wide Swath SAR Data for Oceanographic Applications*. Available: 10.1515/geo-2016-0029

TOPP, G. C., DAVIS, J. L. & ANNAN, A. P. 1980. Electromagnetic determination of soil water content: Measurements in coaxial transmission lines. *Water Resources Research,* 16**,** 574-582. Available: 10.1029/WR016i003p00574

TORRES, R., SNOEIJ, P., GEUDTNER, D., BIBBY, D., DAVIDSON, M., ATTEMA, E., POTIN, P., ROMMEN, B., FLOURY, N., BROWN, M., TRAVER, I. N., DEGHAYE, P., DUESMANN, B., ROSICH, B., MIRANDA, N., BRUNO, C., L'ABBATE, M., CROCI, R., PIETROPAOLO, A., HUCHLER, M. & ROSTAN, F. 2012. GMES Sentinel-1 mission. *Remote Sensing of Environment,* 120**,** 9-24. Available: https://doi.org/10.1016/j.rse.2011.05.028

TOSELLI, F. 1987. *Applications of Remote Sensing to Agrometeorology: Proceedings of a Course held at the Joint Research Centre of the Commission of the European Communities in the Framework of the Ispra-Courses, Ispra, Varese, Italy, 6–10 April 1987*, Springer Science & Business Media.

TOWNSEND, C. & ARMS, S. 2005. Wireless Sensor Networks: Principles and Applications. *In:* WILSON, J. S. (ed.) *Sensor Technology Handbook.* 1st ed. Burlington, MA, USA: Elsevier/Newnes.

TRENBERTH, K. E., DAI, A., VAN DER SCHRIER, G., JONES, P. D., BARICHIVICH, J., BRIFFA, K. R. & SHEFFIELD, J. 2013. Global warming and changes in drought. *Nature Climate Change,* 4**,** 17. Available: 10.1038/nclimate2067

TSHEKO, R. & SAVAGE, M. 2005. Calibration of a frequency-domain reflectometer for determining soil-water content in a clay loam soil. *Water SA,* 32**,** 37-42.

TULINA, A. S., SEMENOV, V. M., ROZANOVA, L. N., KUZNETSOVA, T. V. & SEMENOVA, N. A. 2009. Influence of moisture on the stability of soil organic matter and plant residues. *Eurasian Soil Science,* 42**,** 1241-1248. Available: 10.1134/s1064229309110064

TWOMEY, S. 2013. *Introduction to the mathematics of inversion in remote sensing and indirect measurements*, Elsevier.

ULABY, F., MOORE, R. & FUNG, A. 1982a. Microwave remote sensing: Active and passive. Volume 2-Radar remote sensing and surface scattering and emission theory.

ULABY, F. T. & BATLIVALA, P. P. 1976. Optimum radar parameters for mapping soil moisture. *IEEE Transactions on Geoscience Electronics,* 14**,** 81-93.

ULABY, F. T., BATLIVALA, P. P. & DOBSON, M. C. 1978. Microwave Backscatter Dependence on Surface Roughness, Soil Moisture, and Soil Texture: Part I-Bare Soil. *IEEE Transactions on Geoscience Electronics,* 16**,** 286-295. Available: 10.1109/TGE.1978.294586

ULABY, F. T., DUBOIS, P. C. & VAN ZYL, J. 1996. Radar mapping of surface soil moisture. *Journal of Hydrology,* 184**,** 57-84. Available: https://doi.org/10.1016/0022-1694(95)02968-0

ULABY, F. T., KOUYATE, F., BRISCO, B. & WILLIAMS, T. H. L. 1986a. Textural Infornation in SAR Images. *IEEE Transactions on Geoscience and Remote Sensing,* GE-24**,** 235-245. Available: 10.1109/TGRS.1986.289643

ULABY, F. T., MOORE, R. & FUNG, A. 1986b. *Microwave Remote Sensing: Active and Passive, Vol. III, From Theory to Applications*.

ULABY, F. T., MOORE, R. K. & FUNG, A. K. 1981. Microwave remote sensing: Active and passive. volume 1-microwave remote sensing fundamentals and radiometry.

ULABY, F. T., MOORE, R. K. & FUNG, A. K. 1982b. *Microwave remote sensing: active and passive. Vol. 2, Radar remote sensing and surface scattering and emission theory*, Addison-Wesley Reading, MA.

ULABY, F. T., MOORE, R. K. & FUNG, A. K. 1986c. *Microwave Remote Sensing, Active and Passive, Volume I, Microwave Remote Sensing Fundamentals and Radiometry*, Reading, MA: Addison-Wesley.

ULLMANN, T., SCHMITT, A. & JAGDHUBER, T. 2016. Two Component Decomposition of Dual Polarimetric HH/VV SAR Data: Case Study for the Tundra Environment of the Mackenzie Delta Region, Canada. *Remote Sensing,* 8**,** 1027.

URBAN, M., BERGER, C., MUDAU, T., HECKEL, K., TRUCKENBRODT, J., ONYANGO ODIPO, V., SMIT, I. & SCHMULLIUS, C. 2018. Surface Moisture and Vegetation Cover Analysis for Drought

Monitoring in the Southern Kruger National Park Using Sentinel-1, Sentinel-2, and Landsat-8. *Remote Sensing,* 10**,** 1482.

USDA 1999. *Soil Taxonomy A basic system of soil classification for making and interpreting soil surveys,* United States Department of Agriculture - Natural Resources Conservation Service, U.S. Government Printing Office.

USGS. 2018. *Landsat Missions* [Online]. Available: www.landsat.usgs.gov [Accessed 04/12/2018].

VACHAUD, G., PASSERAT DE SILANS, A., BALABANIS, P. & VAUCLIN, M. 1985. Temporal Stability of Spatially Measured Soil Water Probability Density Function1. *Soil Science Society of America Journal,* 49**,** 822-828. Available: 10.2136/sssaj1985.03615995004900040006x

VAN BYSTERVELDT, A. & CHRISTIE, R. Dairy farmer adoption of science demonstrated by a commercially focused demonstration farm. Proceedings of the 3rd Australasian dairy science symposium'.(Eds DF Chapman, DA Clark, KL Macmillan, DP Nation) pp, 2007. 535-540.

VAN GROENIGEN, J. W., SIDERIUS, W. & STEIN, A. 1999. Constrained optimisation of soil sampling for minimisation of the kriging variance. *Geoderma,* 87**,** 239-259.

VAN TRICHT, K., GOBIN, A., GILLIAMS, S. & PICCARD, I. 2018. Synergistic Use of Radar Sentinel-1 and Optical Sentinel-2 Imagery for Crop Mapping: A Case Study for Belgium. *Remote Sensing,* 10**,** 1642.

VANDERLINDEN, K., VEREECKEN, H., HARDELAUF, H., HERBST, M., MARTÍNEZ, G., COSH, M. H. & PACHEPSKY, Y. A. 2012. Temporal Stability of Soil Water Contents: A Review of Data and Analyses. *Vadose Zone Journal,* 11. Available: 10.2136/vzj2011.0178

VARBLE, J. L. & CHÁVEZ, J. L. 2011. Performance evaluation and calibration of soil water content and potential sensors for agricultural soils in eastern Colorado. *Agricultural Water Management,* 101**,** 93-106. Available: https://doi.org/10.1016/j.agwat.2011.09.007

VELOSO, A., MERMOZ, S., BOUVET, A., LE TOAN, T., PLANELLS, M., DEJOUX, J.-F. & CESCHIA, E. 2017. Understanding the temporal behavior of crops using Sentinel-1 and Sentinel-2-like data for agricultural applications. *Remote Sensing of Environment,* 199**,** 415-426. Available: https://doi.org/10.1016/j.rse.2017.07.015

VERDONE, R., DARDARI, D., MAZZINI, G. & CONTI, A. 2010. *Wireless sensor and actuator networks: technologies, analysis and design*, Academic Press.

VEREECKEN, H., HUISMAN, J. A., BOGENA, H., VANDERBORGHT, J., VRUGT, J. A. & HOPMANS, J. W. 2008. On the value of soil moisture measurements in vadose zone hydrology: A review. *Water Resources Research,* 44. Available: 10.1029/2008WR006829

VEREECKEN, H., HUISMAN, J. A., PACHEPSKY, Y., MONTZKA, C., VAN DER KRUK, J., BOGENA, H., WEIHERMÜLLER, L., HERBST, M., MARTINEZ, G. & VANDERBORGHT, J. 2014. On the spatio-temporal dynamics of soil moisture at the field scale. *Journal of Hydrology,* 516**,** 76-96. Available: https://doi.org/10.1016/j.jhydrol.2013.11.061

VEREECKEN, H., KAMAI, T., HARTER, T., KASTEEL, R., HOPMANS, J. & VANDERBORGHT, J. 2007. Explaining soil moisture variability as a function of mean soil moisture: A stochastic unsaturated flow perspective. *Geophysical Research Letters,* 34.

VEREECKEN, H., WEIHERMÜLLER, L., JONARD, F. & MONTZKA, C. 2012. Characterization of Crop Canopies and Water Stress Related Phenomena using Microwave Remote Sensing Methods: A Review. *Vadose Zone Journal,* 11. Available: 10.2136/vzj2011.0138ra

VERHOEST, N. E. C., LIEVENS, H., WAGNER, W., ÁLVAREZ-MOZOS, J., MORAN, M. S. & MATTIA, F. 2008. On the Soil Roughness Parameterization Problem in Soil Moisture Retrieval of Bare Surfaces from Synthetic Aperture Radar. *Sensors (Basel, Switzerland),* 8**,** 4213-4248. Available: 10.3390/s8074213

VERMEESCH, P. 2012. On the visualisation of detrital age distributions. *Chemical Geology,* 312-313**,** 190-194. Available: https://doi.org/10.1016/j.chemgeo.2012.04.021

VISCONTI, F., DE PAZ, J. M., MARTÍNEZ, D. & MOLINA, M. J. 2014. Laboratory and field assessment of the capacitance sensors Decagon 10HS and 5TE for estimating the water content of irrigated soils. *Agricultural Water Management,* 132**,** 111-119. Available: https://doi.org/10.1016/j.agwat.2013.10.005

VIVONI, E. R., GEBREMICHAEL, M., WATTS, C. J., BINDLISH, R. & JACKSON, T. J. 2008. Comparison of ground-based and remotely-sensed surface soil moisture estimates over complex terrain during SMEX04. *Remote Sensing of Environment,* 112**,** 314-325. Available: https://doi.org/10.1016/j.rse.2006.10.028

VOOREND, W., LOOTENS, P., NELISSEN, H., ROLDÁN-RUIZ, I., INZÉ, D. & MUYLLE, H. 2014. LEAF-E: a tool to analyze grass leaf growth using function fitting. *Plant Methods,* 10**,** 37. Available: 10.1186/1746-4811-10-37

WAGNER, W., BLÖSCHL, G., PAMPALONI, P., CALVET, J.-C., BIZZARRI, B., WIGNERON, J.-P. & KERR, Y. 2007. Operational readiness of microwave remote sensing of soil moisture for hydrologic applications. *Hydrology Research,* 38**,** 1-20. Available: 10.2166/nh.2007.029

WAGNER, W., HAHN, S., KIDD, R., MELZER, T., BARTALIS, Z., HASENAUER, S., FIGA-SALDAÑA, J., DE ROSNAY, P., JANN, A. & SCHNEIDER, S. 2013. The ASCAT soil moisture product: A review of its specifications, validation results, and emerging applications. *Meteorologische Zeitschrift,* 22**,** 5-33.

WAGNER, W., LEMOINE, G. & ROTT, H. 1999a. A Method for Estimating Soil Moisture from ERS Scatterometer and Soil Data. *Remote Sensing of Environment,* 70**,** 191-207. Available: http://dx.doi.org/10.1016/S0034-4257(99)00036-X

WAGNER, W., NOLL, J., BORGEAUD, M. & ROTT, H. 1999b. Monitoring soil moisture over the Canadian Prairies with the ERS scatterometer. *IEEE Transactions on Geoscience and Remote Sensing,* 37**,** 206-216. Available: 10.1109/36.739155

WAGNER, W., PATHE, C., DOUBKOVA, M., SABEL, D., BARTSCH, A., HASENAUER, S., BLÖSCHL, G., SCIPAL, K., MARTÍNEZ-FERNÁNDEZ, J. & LÖW, A. 2008. Temporal Stability of Soil Moisture and Radar Backscatter Observed by the Advanced Synthetic Aperture Radar (ASAR). *Sensors (Basel, Switzerland),* 8**,** 1174-1197. Available: 10.3390/s80201174

WAGNER, W., R. DE JEU & OEVELEN, P. V. Towards MultiSource Global Soil Moisture Datasets for Unravelling Climate Change Impacts on Water Resources. Electronic Proceedings of the 33rd International Symposium on Remote Sensing of the Environm ent (ISRSE), 4-8 May 2009 2009a Stresa, Italy.

WAGNER, W., SABEL, D., DOUBKOVA, M., BARTSCH, A. & PATHE, C. The potential of Sentinel-1 for monitoring soil moisture with a high spatial resolution at global scale. Symposium of Earth Observation and Water Cycle Science, 2009b.

WALKER, J. P., WILLGOOSE, G. R. & KALMA, J. D. 2004. In situ measurement of soil moisture: a comparison of techniques. *Journal of Hydrology,* 293**,** 85-99. Available: https://doi.org/10.1016/j.jhydrol.2004.01.008

REFERENCES

WANG, J. R. 1980. The dielectric properties of soil-water mixtures at microwave frequencies. *Radio Science,* 15, 977-985. Available: 10.1029/RS015i005p00977

WANG, L. & QU, J. J. 2009. Satellite remote sensing applications for surface soil moisture monitoring: A review. *Frontiers of Earth Science in China,* 3, 237-247. Available: 10.1007/s11707-009-0023-7

WARDLE, P. 1991. *Vegetation of New Zealand*, CUP Archive.

WARNER, T. A., FOODY, G. M. & NELLIS, M. D. 2009. *The SAGE handbook of remote sensing*, Sage Publications.

WARRICK, A. 1980. Spatial variability of soil physical properties in the field. *Application of soil physics.*, 319-344.

WEIMANN, A., VON SCHONERMARK, M., SCHUMANN, A., JORN, P. & GUNTHER, R. 1998. Soil moisture estimation with ERS-1 SAR data in the East-German loess soil area. *International Journal of Remote Sensing,* 19, 237-243. Available: 10.1080/014311698216224

WEISS, A. Topographic position and landforms analysis. Poster presentation, ESRI user conference, San Diego, CA, 2001.

WENDROTH, O., NAMBUTHIRI, S. & WALTON, R. J. 2013. Accounting for Soil Spatial Variability in Soil Water Capacitance Probe Calibration. *Vadose Zone Journal,* 12. Available: 10.2136/vzj2012.0182

WESTERN, A., GRAYSON, R. B., BLÖSCHL, G. & WILSON, D. J. 2003. *Spatial Variability of Soil Moisture and Its Implications for Scaling*. Available: 10.1201/9780203011065.ch8

WESTERN, A. W. & BLÖSCHL, G. 1999. On the spatial scaling of soil moisture. *Journal of Hydrology,* 217, 203-224. Available: https://doi.org/10.1016/S0022-1694(98)00232-7

WESTERN, A. W., BLÖSCHL, G. & GRAYSON, R. B. 1998. How well do indicator variograms capture the spatial connectivity of soil moisture? *Hydrological Processes,* 12, 1851-1868. Available: doi:10.1002/(SICI)1099-1085(19981015)12:12<1851::AID-HYP670>3.0.CO;2-P

WESTERN, A. W., GRAYSON, R. B. & BLÖSCHL, G. 2002. Scaling of Soil Moisture: A Hydrologic Perspective. *Annual Review of Earth and Planetary Sciences,* 30, 149-180. Available: 10.1146/annurev.earth.30.091201.140434

WESTERN, A. W., GRAYSON, R. B., BLÖSCHL, G., WILLGOOSE, G. R. & MCMAHON, T. A. 1999. Observed spatial organization of soil moisture and its relation to terrain indices. *Water Resources Research,* 35, 797-810. Available: 10.1029/1998WR900065

WESTERN, A. W., ZHOU, S.-L., GRAYSON, R. B., MCMAHON, T. A., BLÖSCHL, G. & WILSON, D. J. 2004. Spatial correlation of soil moisture in small catchments and its relationship to dominant spatial hydrological processes. *Journal of Hydrology,* 286, 113-134. Available: http://dx.doi.org/10.1016/j.jhydrol.2003.09.014

WHITE, J. G. H., MEIJER, G. & LANGER, R. H. M. Oversowing grasses on sunny and shady faces. Proceedings of the New Zealand Grassland Association, 1972. 139-146.

WILLMOTT, C. J. 1982. Some comments on the evaluation of model performance. *Bulletin of the American Meteorological Society,* 63, 1309-1313.

WILSON, D. J., WESTERN, A. W. & GRAYSON, R. B. 2004. Identifying and quantifying sources of variability in temporal and spatial soil moisture observations. *Water Resources Research,* 40. Available: 10.1029/2003WR002306

WILSON, D. J., WESTERN, A. W., GRAYSON, R. B., BERG, A. A., LEAR, M. S., RODELL, M., FAMIGLIETTI, J. S., WOODS, R. A. & MCMAHON, T. A. 2003. Spatial distribution of soil moisture over 6 and 30 cm depth, Mahurangi river catchment, New Zealand. *Journal of Hydrology,* 276, 254-274. Available: http://dx.doi.org/10.1016/S0022-1694(03)00060-X

WILSON, J. P. & GALLANT, J. C. 2000. *Terrain analysis: principles and applications*, John Wiley & Sons.

WOODWARD, S. J. R. 2001. Validating a model that predicts daily growth and feed quality of New Zealand dairy pastures. *Environment International,* 27, 133-137. Available: https://doi.org/10.1016/S0160-4120(01)00073-3

WOODWARD, S. J. R., BARKER, D. J. & ZYSKOWSKI, R. F. 2001. A practical model for predicting soil water deficit in New Zealand pastures. *New Zealand Journal of Agricultural Research,* 44, 91-109. Available: 10.1080/00288233.2001.9513464

WU, W. & DICKINSON, R. E. 2004. Time Scales of Layered Soil Moisture Memory in the Context ofLand–Atmosphere Interaction. *Journal of Climate,* 17, 2752-2764. Available: 10.1175/1520-0442(2004)017<2752:tsolsm>2.0.co;2

YANG, F., ZHANG, G.-L., YANG, J.-L., LI, D.-C., ZHAO, Y.-G., LIU, F., YANG, R.-M. & YANG, F. 2014. Organic matter controls of soil water retention in an alpine grassland and its significance for hydrological processes. *Journal of Hydrology,* 519, 3086-3093. Available: https://doi.org/10.1016/j.jhydrol.2014.10.054

YICK, J., MUKHERJEE, B. & GHOSAL, D. 2008. Wireless sensor network survey. *Computer Networks,* 52, 2292-2330. Available: http://dx.doi.org/10.1016/j.comnet.2008.04.002

YOUNIS, S. M. Z. & IQBAL, J. 2015. Estimation of soil moisture using multispectral and FTIR techniques. *The Egyptian Journal of Remote Sensing and Space Science,* 18, 151-161. Available: http://dx.doi.org/10.1016/j.ejrs.2015.10.001

ZAZUETA, F. S. & XIN, J. 1994. Soil moisture sensors. *Soil Science,* 73, 391-401.

ZETTL, J. D., HUANG, M., BARBOUR, S. L. & SI, B. C. 2015. Density-dependent calibration of multisensor capacitance probes in coarse soil. *Canadian Journal of Soil Science,* 95, 331-336. Available: 10.4141/cjss-2015-021

ZHANG, B., VALENTINE, I. & KEMP, P. 2005. Modelling the productivity of naturalised pasture in the North Island, New Zealand: a decision tree approach. *Ecological Modelling,* 186, 299-311. Available: http://dx.doi.org/10.1016/j.ecolmodel.2004.12.016

ZHANG, D. & ZHOU, G. 2016. Estimation of Soil Moisture from Optical and Thermal Remote Sensing: A Review. *Sensors,* 16, 1308.

ZHANG, H. K., ROY, D. P., YAN, L., LI, Z., HUANG, H., VERMOTE, E., SKAKUN, S. & ROGER, J.-C. 2018. Characterization of Sentinel-2A and Landsat-8 top of atmosphere, surface, and nadir BRDF adjusted reflectance and NDVI differences. *Remote Sensing of Environment,* 215, 482-494. Available: https://doi.org/10.1016/j.rse.2018.04.031

ZHAO, W. & LI, Z.-L. 2013. Sensitivity study of soil moisture on the temporal evolution of surface temperature over bare surfaces. *International Journal of Remote Sensing,* 34, 3314-3331. Available: 10.1080/01431161.2012.716532

ZHAO, Y., PETH, S., WANG, X. Y., LIN, H. & HORN, R. 2010. Controls of surface soil moisture spatial patterns and their temporal stability in a semi-arid steppe. *Hydrological Processes,* 24, 2507-2519. Available: 10.1002/hyp.7665

ZHU, Q., SCHMIDT, J., LIN, H. & SRIPADA, R. 2009. Hydropedological processes and their implications for nitrogen availability to corn. *Geoderma,* 154, 111-122.

REFERENCES

ZHU, Z., FU, Y., WOODCOCK, C. E., OLOFSSON, P., VOGELMANN, J. E., HOLDEN, C., WANG, M., DAI, S. & YU, Y. 2016. Including land cover change in analysis of greenness trends using all available Landsat 5, 7, and 8 images: A case study from Guangzhou, China (2000–2014). *Remote Sensing of Environment,* 185**,** 243-257. Available: https://doi.org/10.1016/j.rse.2016.03.036

ZOTARELLI, L., DUKES, M. & MORGAN, K. 2010. Interpretation of soil moisture content to determine soil field capacity and avoid over-irrigating sandy soils using soil moisture sensors. *University of Florida Cooperation Extension Services, AE460*.

ZOU, B., ZHANG, Y., CAO, N. & NGHIA, P. 2015. *A Four-Component Decomposition Model for PolSAR Data Using Asymmetric Scattering Component*. Available: 10.1109/JSTARS.2014.2380151

ZRIBI, M., BAGHDADI, N., HOLAH, N. & FAFIN, O. 2005. New methodology for soil surface moisture estimation and its application to ENVISAT-ASAR multi-incidence data inversion. *Remote Sensing of Environment,* 96**,** 485-496. Available: https://doi.org/10.1016/j.rse.2005.04.005

ZRIBI, M. & DECHAMBRE, M. 2003. A new empirical model to retrieve soil moisture and roughness from C-band radar data. *Remote Sensing of Environment,* 84**,** 42-52. Available: https://doi.org/10.1016/S0034-4257(02)00069-X

ZUUR, A., TUCK, I. & BAILEY, N. 2003. Dynamic factor analysis to estimate common trends in fisheries time series. *Canadian journal of fisheries and aquatic sciences,* 60**,** 542-552.